



UNIVERSITAT POLITÈCNICA
DE CATALUNYA
BARCELONATECH

Doctoral Thesis:

Influence of ambient temperature on building monitoring in urban areas during the construction of tunnels for transportation

Author:

Zengzeng Lian

Advisors:

Dr. Josep A. Gili-Ripoll

Dra. M^a Amparo Nuñez-Andrés

December 2015

UNIVERSITAT POLITÈCNICA DE CATALUNYA

Department of Geotechnical Engineering and Geo-Sciences

Geomatics Engineering Research Group (EGEO)

Abstract

A large number of underground works are under construction in several big cities around the world (London, Paris, Amsterdam, Beijing, Shanghai, Chicago, Caracas, Mexico D.F., and Riad, for instance): railway tunnels, water supplies and other kinds of underground structures. In the last decade several underground infrastructures have been designed and constructed in the city of Barcelona, Spain, as well; e.g. the new line 9 of the city underground and the city junction for the High Velocity train that links Madrid and Barcelona with France.

During the construction, intensive monitoring is becoming an increasingly common practice in order to guarantee the safety of the people, buildings and other infrastructures on the surface. Among others, the Robotic Total Stations (RTS) play an important role in the task.

In these monitoring works, some "Thermal Effects" have occasionally appeared in the graphs, between winter/summer and day/night situation. Sometimes this undesirable noise has produced discussion among the infrastructure actors.

As this effect has not been adequately studied so far, the present PhD aims to improve the basic knowledge and the current practice in the building monitoring in urban areas during underground works when the scene is affected by temperature changes.

To characterize and, eventually, to correct the aforementioned influence of the "environmental variables", a computer simulation program has been implemented. The code can simulate the movement of the buildings when the temperature changes, and proves that the thermal influence on structure deformation monitoring cannot be ignored in the practice.

The PhD work has taken advantage of an experimental monitoring area built at the UPC Campus Nord (Barcelona, Spain) within an I+D project, with Robotic Total Stations and other sensors (temperature, tilt, levelling, insolation and other meteorological data), acquiring data during two years and a half. The fieldwork and data processing have been used to improve and adjust the numerical simulation model.

Several approaches have been tested with the program. Strategies D, B and K permit us, respectively, to simulate the standard monitoring practice, to "fully" filter the thermal effect, and to filter it while preserving the building's own movements.

Apart from helping in the mitigation of the quoted influence, these results may eventually facilitate the improvement of the present monitoring practices..

Resumen

Un gran número de trabajos subterráneos están en marcha en diversas ciudades del mundo (London, Paris, Amsterdam, Beijing, Shanghai, Chicago, Caracas, Mexico D.F., Riad, entre otras): túneles para FFCC y Metro, suministros, otras obras. En la última década varias infraestructuras subterráneas han afectado al Área Metropolitana de Barcelona: la línea 9 de metro y el paso del AVE Madrid-Barcelona-Francia entre otras. Durante la construcción de estas obras, la monitorización intensiva se está convirtiendo en práctica habitual para garantizar la seguridad de la gente, de los edificios y de otras construcciones en superficie. Entre otras técnicas, las Estaciones Totales Robotizadas juegan un papel importante en este cometido.

De manera ocasional, en estos trabajos de auscultación han aparecido en las gráficas diarias o anuales unas oscilaciones espurias atribuibles a “Efecto Térmico”. En algunos momentos ese ruido no deseado ha producido ciertos problemas entre los actores presentes en la Obra Pública. Como este efecto no ha sido adecuadamente estudiado hasta ahora, esta Tesis pretende abundar en el conocimiento de su naturaleza, y mejorar la práctica habitual de la monitorización de edificios en zonas urbanas afectadas por obras subterráneas cuando los cambios de temperatura puedan influir.

Un programa de simulación ha sido desarrollado para caracterizar y corregir la citada influencia de dichas ‘variables ambientales’. El código puede simular el movimiento de los edificios cuando cambia su temperatura, y ha servido para comprobar que los cambios térmicos pueden influir a un nivel que no puede ser ignorado en la práctica de la auscultación de precisión.

La Tesis ha aprovechado una zona experimental a escala real que se estableció en el Campus Nord de la UPC dentro de un proyecto I+D, en la que Estaciones Totales Robotizadas y otros sensores (termómetros, clinómetros, niveles, piranómetros y estaciones meteorológicas) han estado suministrando mediciones durante unos dos años y medio. Los datos de campo y su procesamiento han servido para mejorar el código numérico y para ajustar sus variables.

Con el programa se han establecido varios escenarios. Las estrategias D, B y K permiten simular la práctica habitual de la monitorización, y filtrar totalmente (al menos en teoría) o parcialmente el ‘Efecto Térmico’. Los resultados obtenidos, aparte de ayudar a mitigar la presencia no deseada de la firma térmica en los resultados de la auscultación, tras posteriores investigaciones podrán mejorar las prácticas actuales en la monitorización de edificios.

Acknowledgements

My sincere thanks are given to all the people who have contributed and given their support to the success of this scientific project and who gave me three wonderful and unforgettable years in Barcelona.

There is an old sentence in China, which is “One day for the supervisor, lifelong for father”. So, my gratitude goes first to my supervisors **Prof. Dr. Josep A. Gili Ripoll** and **Dr. M^a Amparo Nuñez Andrés**. Thank you for giving me this opportunity to participate in the doctor program. I want to say “thank you” to them, for their patient guiding and unreserved help throughout my whole PhD study. Their help not only stay in science, but also in life. What is more, I really appreciate Prof. Gili and his wife for their so much help to my family when my son was born. And also give my thanks to Dr. Amparo for her lovely gift to my son. I will remember all of this in my life.

I would express my grateful thanks to Dr. Nieves Lantada for providing valuable advises and comments during my PhD period.

I would like to thank my UPC colleagues and friends——Dr. Marcel, Dr. Carol and Albert, and many PhD students including Sonia, Roger, Clara, Mauricio, Isturitz, Manuel, Basar and etc. for their care and help. I would like to thank Prof. Suarez (CIMNE) for license of ED-Tridim software.

I want to thank my Chinese friends in Barcelona, Liang Wang, Hongyang Xu, Fuqiang Zhai, Lei Wang, Siming Yu, Enhao Li, Xiaoyun Dong, Xiaomin Zhao, Zhishan Luo, Tian Tian, Yu Liu, Yu Zhang, Zhongbo Hu, Chun Feng, Bin Li etc. Because of you, I do not feel lonely in Spain.

Thanks to my two landlords: Mr. Ignacio, for his kindly concerns and lovely gift (typical catalan cookies); and Mr. Juanjo, for showing me the old photos he took in China in 1980s and sharing the stories happened behind the photos. Both of them are lovely and kindness people.

I also want to thank my second hometown, the city of Barcelona, which gives me many good memories. Quoting a sentence from the souvenir—I love you, Barcelona.

I appreciate to the China Scholarship Council (CSC) for providing the financial support through the China Scholarship Council- Universitat Politècnica De Catalunya Joint Program and scholarship. I also appreciate the funding support and data sharing from SOLDATA and the Centre for the Development of Industrial Technology (CDTI), and the Geoterm Project. I also acknowledge the UPC Servei de Patrimoni and Servei de Manteniment and Coordinació C. Nord. Without these support, I could not finish this work.

Lastly, I would like to express my gratitude to my parents and young sister for their never ending support. I also want to give my special thanks to my loved wife and my son for loving me and supporting me all the time. 感谢我生命中的你们。

Contents

1	Introduction	1
1.1	Motivations	1
1.2	PhD Objectives	4
1.3	Work Outline.....	4
2	Structure Health Monitoring in urban areas—State of the art and current practice	7
2.1	Structure Health Monitoring methods in civil engineering	7
2.1.1	Robotic Total Stations (RTS)	9
2.1.2	Global Positioning System (GPS)	13
2.1.3	Terrestrial Laser scanning (TLS).....	19
2.1.4	Ground Based-SAR	26
2.1.5	Sensors.....	29
2.2	Environmental factors to be considered in SHM	32
2.2.1	Thermal influence.....	33
2.2.2	Wind influence	38
2.2.3	Traffic influence	39
2.2.4	Relative humidity influence.....	40
2.3	Current practice in building monitoring during underground works	42
3	Modeling the behavior of buildings and monitoring systems when subjected to Thermal Effects	51
3.1	Conceptual model	51
3.2	Implementation of the conceptual model	54
3.3	Modeling the movements of building subjected to external actions	58
3.3.1	Elastic deformation of structures	58
3.3.2	Thermal effects	62
3.3.3	Stiffness matrix method.....	63
3.3.4	Description of the program.....	64
3.4	Least square adjustment by indirect observations equations	73
3.4.1	Least square adjustment principle	74
3.4.2	Distance correction	75

3.4.3	Blunder detection.....	75
3.4.4	Description of the program.....	75
4	Experimental work Test area Campus Nord UPC	81
4.1	Area selection process.....	81
4.2	Overall design of the systems and sensors	82
4.3	System and sensors installation	85
4.4	Data acquisition processes.....	90
4.5	Data continuity/availability of final filtered data.....	95
4.5.1	RTS data availability	95
4.5.2	Temperature and insolation data availability.....	97
5	Matching the Model with real world results	117
5.1	Sensitivity analysis	117
5.1.1	Sensitivity to horizontal angle—H	118
5.1.2	Sensitivity to zenith angle-V	120
5.1.3	Sensitivity to distance--d	122
5.1.4	Conclusions about the sensitivity analysis	124
5.2	Real monitoring results obtained with the standard system in the Campus Nord test area.....	124
5.2.1	K2M control points movement.....	126
5.2.2	A6-RTS movement.....	138
5.2.3	Temperature and Insolation evolution.....	143
5.2.4	Relationship between temperature and movements	150
5.3	Numerical simulation of the standard monitoring system--- approach D	151
5.3.1	Input data	152
5.3.2	Main steps of approach D.....	164
5.3.3	Approach D results and analysis	167
5.4	Comparing the real monitoring results with the simulated ones (approach D).....	192
5.4.1	Comparing the RTS real monitoring results with the simulated ones (approach-D).....	192

5.4.2	Comparing the Control Points real monitoring results with the simulated ones (approach-D)	195
6	Formulation of the strategy to consider thermal effects in building monitoring	205
6.1	Introduction	205
6.2	Approach B	211
6.2.1	Main step steps of approach B	211
6.2.2	Running time	213
6.2.3	Approach B's results	213
6.2.4	Compare approach B's results with GW	225
6.3	Approach K	238
6.3.1	Main steps of approach K	238
6.3.2	Running time	241
6.3.3	Approach K's results	241
6.3.4	Comparison and analysis between approach-K and GW	253
6.4	Overview	264
7	Conclusions and future work	265
7.1	Conclusions	265
7.2	Future works	267
	References	269
	Annexes	279
A.I	Raw data of the least square adjustment test example in chapter 3.4.4	281
A.II	Results of the least square adjustment test example in chapter 3.4.4	290
A.III	Distance correction steps	295
A.IV	Computing Approximation Coordinates in the Resection Problem	298
A.V	Least Square Adjustment Principle	301
A.VI	Error Equations Linearization Using Taylor's Theorem	304
A.VII	W. Baarda test method	308
A.VIII	Ellipse of Error	310

A.IX	Local Stiffness Matrix for 3D Beam Elements	315
A.X	Transformation from local to global coordinates (3D structures)	318
A.XI	Thermal Effect Modelling Program	320
XI.1	Implementation Language and computer.....	320
XI.2	Structure model program code.....	322
XI.3	Calculate the forces on each node of the structure program code	354
XI.4	Least square adjustment program code.....	377
XI.5	Functions.....	388
XI.6	Simulate reference points' observation data.....	397
XI.7	Simulate control points' observation data.....	422

1 Introduction

The continuous growth of the world population plus other socioeconomic reasons result in a heavy concentration around city areas. There, the high density of inhabitants per square kilometer, traffic congestion and air pollution demand the construction of new transportation infrastructures such as metropolitan lines, commercial centers and parking lots. Most of the new developments are completely or partly underground. These kinds of constructions involve deep excavations or tunneling near the buildings.

In the past decade several underground infrastructures have been designed and constructed in the city of Barcelona, Spain, e.g. the new line 9 of the underground and the city junction for the High Velocity train that links Madrid and Barcelona with France. Other big underground lines have been constructed or are under construction in other parts of the world: London (Jubilee Line; Cross-rail), Amsterdam (new rail access), Paris (new railway links), Riad (underground), Shanghai, New Delhi, Singapore, and Hong Kong, among other places. During these huge constructions, the safety of the buildings and people on the surface has been guaranteed using a variety of monitoring systems and devices. In some locations, the effect of the so-called “thermal influence” on the monitoring systems has surfaced. This PhD Thesis deals with the characterization, measurement and correction of this unwanted influence. The present chapter presents the motivation and the objectives of this research. At the end of the chapter, the content of the work is outlined.

1.1 Motivations

The best way to promote sustainable urban development and environmental protection in cities consists of developing and utilizing the underground space (Fu 2006). Hence, a large number of underground works are under construction in urban areas around the world: railway tunnels, water supply, drainage, power and gas pipes, cable lines for communication, and other kinds of underground structures (Cong 2004).

The new developments under the city affect the heritage to a large extent. Old and recent buildings are close to the work areas. Any underground excavation will disturb the balance of the original stress, causing its redistribution and leading to overburden movement and deformation, which impact on the surface structures, especially urban buildings (Zhu 2010).

In most of the cities mentioned earlier, the security of the buildings and people on the surface has been guaranteed using several monitoring systems and devices. Despite the monitoring deployed, in some cases accidents have happened: a section of the subway in Los Angeles collapsed in 1995, forming a sinkhole in Hollywood Boulevard (Eric Lichtblau and Simon 1995); in 2005, a diversion tunnel of the Barcelona L5 underground buckled during construction (about 1000 inhabitants lost their homes, and more than 10000 were temporarily evacuated) (Aroca 2005, Centre 2005); in 2007, Sao Paulo Line 4 subway (the longest in South America) suffered a deadly collapse (Lehman 2007); in 2009, Cologne's historical archive (enclosing records dating as far back as 922) caved in due to the construction of an underground railway line (Matthias Bartsch, Andrea Brandt et al. 2009); in 2013, four buildings fell into a ten meter hole near the construction of a new underground train station in Guangzhou, one of China's biggest cities (Telegraph 2013).

These unfortunate events highlight even more the importance of monitoring during the construction of new developments near elements at risk. Aware of the potentially serious consequences, the authorities responsible for the management of the projects contract a variety of systems to monitor the stability of the structures and buildings in order to ensure the safety of the people and equipment.

This surveillance task is mostly carried out with Automatic Total Stations (also known as Robotic Total Stations, RTS). They are surveying instruments combining a theodolite (with Automatic Target Recognition) and electronic distance measurement, which can be operated remotely (Cook 2006). Other techniques have also been used, such as extensometers, inclinometers, precision leveling, GPS, clinometers and other sensors spread on the surface, in the ground and inside the tunnel itself.

During the monitoring that is carried out around the new tunnel lines, some thermal effects appear occasionally in the graphs. Even in latitudes like Barcelona, we may

experience great temperature variation due to the direct sun insolation (see for example (Schwarz, Valdemarin et al. 2011) and (Abad 2013)) (Figure 1.1). It is a fact that during the Barcelona L9 construction, this undesirable thermal effect produced some serious discussion between the Owner of the works (Generalitat de Catalunya-GISA), the engineering company responsible for the monitoring systems, and the enterprise that construct the tunnels.

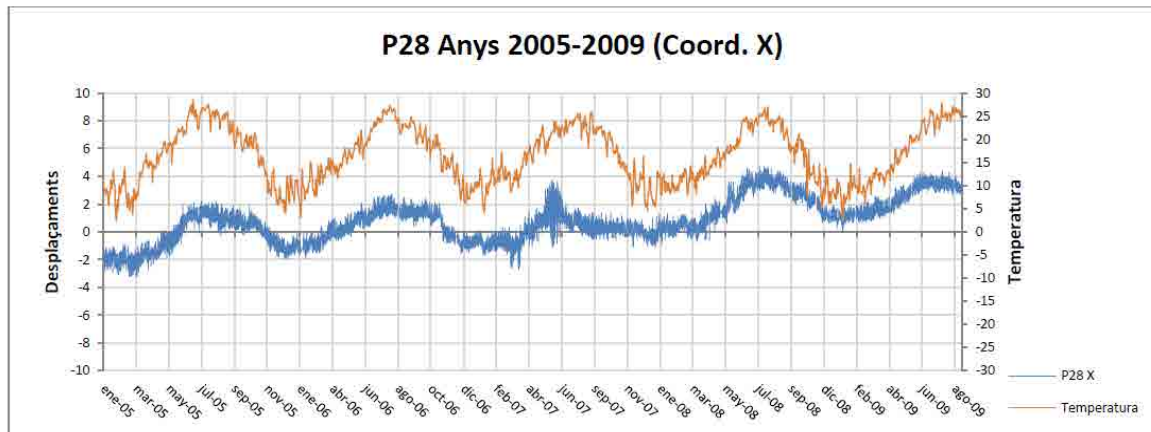


Figure 1.1 X displacements (mm) and temperature (°C) evolution versus time, years 2005-2009, prism P28, Barcelona L9 underground construction, near Ciutat de la Justícia (Abad 2013).

We have several examples that evidence the influence of the environmental variables (mainly temperature changes) on the measurements carried out by the monitoring systems (RTS and other sensors). Hence, the monitoring graphs include the part of the displacement which is caused by the influence of the environment. If we want to know the component of the displacement that is a direct consequence of the influence of the tunnelling works, it is necessary to model or assess the component that is related with the environmental factors. This later component has not been adequately studied so far (Gili, Lantada et al. 2013).

Let us consider that the total deformation observed is the sum of the deformation from the tunnelling and the deformation from environmental or thermal factors, and that the temperature is the main factor influencing the building's deformation. Therefore, if we want to monitor the risk associated with the construction work, it is necessary to model the influence of the temperature and to subtract it. This PhD thesis aims to facilitate the

understanding of the aforementioned ‘thermal effect’ and, eventually, the mitigation of the quoted influence.

1.2 PhD Objectives

The **main objective** of this PhD is to improve the basic knowledge and the current practice in the building monitoring in the urban areas during underground works when the scene is affected by temperature changes.

This main objective can be divided in several **particular** ones:

- 1) To assess the extent and pattern of the deformation of the buildings when subjected to a variation in the temperature due to direct sun insolation. This will be done through the redundant instrumentation of an experimental building;
- 2) To set up a complete numerical model of the structure's behaviour when the temperature field changes. This tool will permit us to compare and match the theoretical deformation with the real behaviour;
- 3) The best strategy to cope with the thermal influence will be identified and proposed in order to develop an approach suitable for application to the current practice in urban monitoring.

1.3 Work Outline

After chapter one, the work done in the thesis consists of 5 chapters plus conclusions, references and annexes. The outline of this dissertation is as follows:

Chapter 1 states the motivation and the objectives of the thesis. This chapter is a brief introduction of the research objectives that have been attempted to achieve in the thesis.

Chapter 2 is a State of the Art review about the monitoring methods in geotechnical engineering projects, the environmental factors that influence the structure health monitoring, and the current practice in building monitoring during underground works.

Chapter 3 concentrates on the steps and process needed to set up a model to investigate the environment's influence on the structure deformation monitoring. There, the methods for structure computations are used to link the thermal action over the building to its deformation. In order to match real deformation data with the computer results, Least Square Adjustment is reviewed and applied. A series of numerical simulation tests have been implemented in order to prove the model is reasonable and in accordance with the hypothesis.

Chapter 4 describes the experimental work test area which includes area selection process, overall design of the systems and installation. On the monitored buildings, some devices have been installed, including Robotic Total Station (RTS), sensors (for collecting temperature data, insolation, leveling, etc.), prisms, one meteorological station (for collecting air temperature, air pressure, wind speed and direction, rainfall), etc.

Chapter 5 presents the process to match the model with the real world results. In this chapter, there are four parts. The first includes a sensitivity analysis to test the robustness of the monitoring results in front of some small measurement errors. In the second part, the Campus Nord monitoring results are presented as an overview. The real thermal influence on the structure deformation monitoring practice is shown. The third and fourth parts present the monitoring of the K2M building with the “standard approach” monitoring versus a numerical simulation.

Chapter 6 further investigates the behavior of the test building when taking into account the thermal effect. Two new approaches have been tested here. Both filter the thermal effect up to a point; the difference is that the first one also filters the movement of the test building, whereas the second one preserves this residual movement. Nonetheless, the two approaches further prove that thermal change has an important influence on the structure deformation monitoring and it is worth correcting it.

Finally, Chapter 7 summarizes the main conclusions on the achievements of this thesis and proposes some future research work.

Some additional data are given in the Annexes.

2 Structure Health Monitoring in urban areas—State of the art and current practice

The state of the art has been structured as follows: in the first part, we include the references that describe the monitoring devices and methods used at present to measure the deformation of urban infrastructures (such as buildings, etc.) when a new public work is carried out, for instance, RTS, GPS and so on. In the second section, we have collected the environment factors that influence structures, which are thermal changes, wind action, traffic and humidity. Finally, in the last section, the current practice that deals with the direct measurement of movements of structures during the construction of underground works is presented.

2.1 Structure Health Monitoring methods in civil engineering

Structural deformation monitoring is the systematic measurement and tracking of the alteration in the shape or dimensions of a structure as a result of stresses induced by applied loads and other actions. Deformation monitoring consists of 1) data capturing and logging; 2) computation and analysis of the raw data; 3) predictive maintenance and alarming (when necessary).

Structural deformation monitoring is a mandatory task to evaluate the structure safety of the structure. Qualitative and non-continuous methods have largely been used to evaluate the capacity of structures to serve their intended purpose. Deformation monitoring systems provide a proactive control of hazards related to a possible change or failure of a structure. Policyholders can reduce risk exposure before and during construction and throughout the lifecycle of the structure. Hence, they can decrease the insurance premium(Cook 2006).

Structure health monitoring methods in geotechnical engineering depend mainly on the measuring devices or sensors. Based on this fact, SHM methods can be divided into four categories. The first is geodetic devices to measure geo-referenced displacements or movements in one monitored area. Generally, geodetic monitoring solution is a network which consists of three parts: a reference network with several witness and stable points, which must be out of the expected deformation area; observation points where geodetic instruments are set up to measure the reference points and object points; and object points located on the monitored object or area. The instruments used for SHM include Total Station or Robotic Total Station (RTS), Global Position System (GPS), Terrestrial Laser Scanning (TLS) and so on. The second category is geotechnical measuring devices to measure the non-georeferenced displacements or movements and related environmental effects or conditions. The devices are independent modules with sensors to collect data. The sensors include a strain sensor, extensometer, tiltmeter, accelerometer, temperature sensor, humidity sensor, anemometer and so on. In one monitoring system, some sensors will be combined and integrated into one overall solution to measure the relative data about the monitored object. The third category is the geophysical measuring devices to measure soil parameters and conditions, which are electrical resistivity of the soil, seismic survey, etc. The fourth category is remote sensing devices to measure geo-referenced displacements or movements without being in contact with the object. The remote sensing devices obtain deformation images about the monitored object from an aircraft or spacecraft platform. The instruments include Synthetic Aperture Radar (SAR), Light Detection And Ranging (LiDAR) and optical cameras. Depending on the monitored object, different kinds of devices may be combined into one system to monitor structure health.

In this review, we list the sensors or systems that work from the surface and measure surface point. These include mainly geodetic measuring devices and geotechnical measuring devices. This kind of systems is also known as “geomatics monitoring”. We exclude from our review the other type of sensors/systems that are known as “geotechnical instrumentation” and include inclinometers, extensometer, piezometers, pressure cells, etc.

Nowadays, the methods used for structure deformation monitoring are mainly Robotic Total Station (RTS), GPS, some sensors (such as temperature sensor, etc.) and so on. In this section, some applications based on those commonly used methods are introduced.

2.1.1 Robotic Total Stations (RTS)

RTS is a new generation of total station which has been used in various civil engineering projects in the past decades, especially in the area of structure health monitoring. The areas where the RTS have been used continue to expand (Cosser, Roberts et al. 2003, Cook 2006, Walker, Hitchcock et al. 2006, Psimoulis and Stiros 2007, Xu and Hu 2009, Stiros and Psimoulis 2010, Zarikas, Gikas et al. 2010, Schwarz, Valdemarin et al. 2011, Afeni 2012, Koo, Brownjohn et al. 2012, Lantada, Núñez et al. 2012, Stiros and Psimoulis 2012, Afeni and Cawood 2013, Psimoulis and Stiros 2013). An overview on the application of the RTS by some researchers follows. It includes bridge deformation monitoring, slope monitoring and monitoring the impact of tunnel construction on existing infrastructure.

The basic principle of RTS is that they emit a narrow infrared or laser beam which is reflected back by a specific reflector and is received back to the RTS. Once taught the location of a reflector, the RTS returns to re-determine the location of that prism during each monitoring cycle. This course allows surveying the location of the reflector in 3D polar coordinates and they measure independently: (i) the distance between the reflector and the RTS; (ii) the angle of the line of sight relative to the vertical axis; (iii) the horizontal angle of the line of sight relative to a selected reference horizontal direction. Based on these polar coordinates, 3D coordinates of the reflector in a selected coordinates system can be automatically calculated. Those final results can be computed to one millimeter accuracy for distances up to a kilometer in favorable conditions (Stiros and Psimoulis 2010).

a) Bridge deformation monitoring

Bridges are classical targets in structural deformation monitoring, and RTS have been used in the testing (Cosser, Roberts et al. 2003, Psimoulis and Stiros 2007, Xu and Hu 2009, Koo, Brownjohn et al. 2012, Stiros and Psimoulis 2012, Psimoulis and Stiros

2013). In this section, several case studies are introduced based on the available references.

Koo (Koo, Brownjohn et al. 2012) installed the RTS (Leica TCA1201M) on the Tamar Bridge in Plymouth, UK (Figure 2.1, a 335m span suspension bridge opened in 1961) to monitor the displacements of the bridge. The results indicated that RTS were a useful way to monitor the movement of structures, and to correlate them with the temperature and wind. Structural temperature leading to thermal expansion of the deck, main cables and additional stays was shown to be a major factor in global deformation, whereas vehicle loading and wind are usually secondary factors. At the same time, there are still some challenges that need to be solved. For instance, how to interpret the load and response data prior to diagnosing normal service behavior; and, secondly, to identify possible performance anomalies.

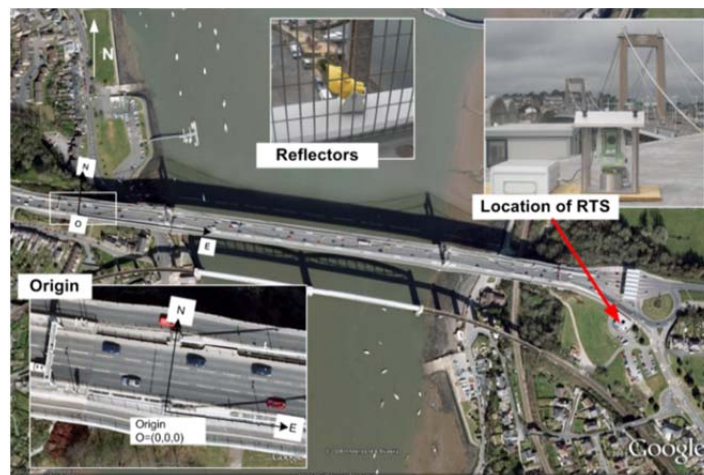


Figure 2.1 RTS monitoring system at the Tamar Bridge(Koo, Brownjohn et al. 2012).

Based on the RTS (Leica 1201) measurements along the Gorgopotamos Bridge, a short-span, historical bridge in central Greece, Stiros and Psimoulis (Stiros and Psimoulis 2012, Psimoulis and Stiros 2013) concluded that 1) RTS can be used to measure absolute displacements of short-span bridges, i.e. relative to a reference system independent of the structure; 2) the result meets the requirement of bridge deformation monitoring. Furthermore, they also deem that RTS is a powerful tool for structural health monitoring, that it can be used for monitoring stiff structures and its accuracy and range of application may increase in the future with a new generation of RTS, with the adaptation of more sophisticated filtering techniques, and, possibly, with fusion with

accelerometers and other sensors. The Figure 2.2 shows the Gorgopotamos Railway Bridge and in the foreground the RTS used for the measurements.

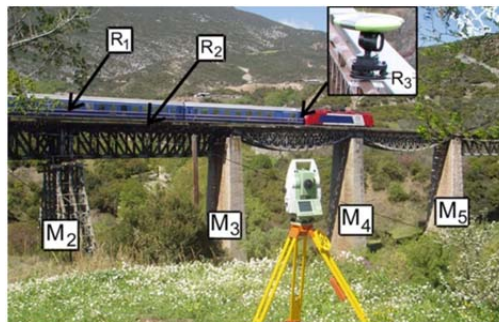


Figure 2.2 The Gorgopotamos Railway Bridge and in the foreground the RTS used for the measurements (Stiros and Psimoulis 2012).

Cosser (Cosser, Roberts et al. 2003) conducted a test on the Wilford Suspension Bridge in Nottingham, including the use of a servo-driven Leica TCA2003 RTS measuring angles and distances at a 1 Hz data rate. After the bridge trial, they concluded that it is possible to measure slow dynamic deformation using RTS, and that the measured displacements matched the result obtained with GPS, when the amplitude of these movements is at the highest approximately 0.1m.

What is more, Xu Chang and Hu Qunge (Xu and Hu 2009) measured the dynamic characteristics of cable-stayed bridges with RTS (Leica TCA2003). Kinematic elevation data were acquired by using precise trigonometric leveling method with the automatic tracking mode with a 3 Hz acquisition rate. The results presented herein are encouraging, and show the potentiality of RTS in dynamic deformation monitoring.

b) Slope monitoring

In the mountains or other special areas, such as open pit mining area, it is very important to ensure the safe of the slopes. In this section, the method of using RTS to monitor the slopes is introduced. Afeni and Cawood (Afeni and Cawood 2013) used the RTS to monitor the slopes in a mining area and discussed the various challenges in open pit mines in their studies. These challenges include: 1) the dusty environment of the area, caused by drilling, blasting and haulage operations, 2) the weather condition, such as heavy rainfall and mist. They propose possible ways to overcome these drawbacks: the RTS system should be complemented by other monitoring techniques, for instance, GPS,

radar, laser scanning and geotechnical instrumentation, such as a piezometer and extensometer, Figure 2.3 shows the base pillar and a reference prism.

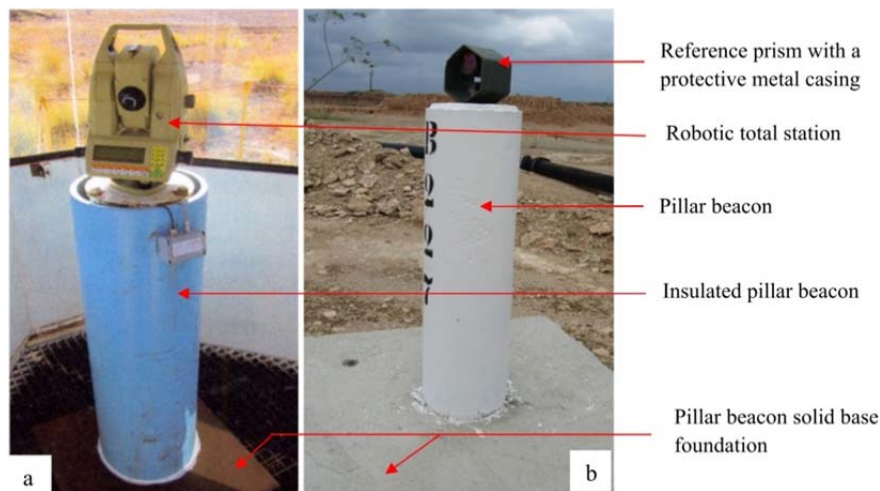


Figure 2.3 (a) RTS on a base pillar; (b) reference prism on top of a concrete cylinder (Afeni and Cawood 2013).

c) Monitoring the impact of tunnel construction on existing infrastructure

In order to ensure the safety of the existing infrastructure around tunnel construction, it is necessary to monitor the condition of the structures. RTS is one of useful method to do this task. Walker (Walker, Hitchcock et al. 2006) used RTS (Leica TCA1800) combined with tiltmeters, electrolevels, in-place-tiltmeters, manually-read tiltmeters, borehole extensometers and precise leveling surveys to monitor the impact of a tunnel (the 1200m Airside Road Tunnel) which was constructed in London Clay beneath Heathrow Airport pathways. The monitoring team utilized an independent server and network which allowed the interconnection of several instrument data-loggers. Instrument readings were collected remotely and/or manually and were incorporated into specifically designed databases for the various project stages. The gathered data was displayed in near real time and, in order to share monitoring data between team members at various locations, data was published hourly to the internet using a 'lite' version of the monitoring package. Figure 2.4 shows a Leica RTS mounted on a custom-made bracket under a beam.



Figure 2.4 The Leica TCA1800 RTS mounted in the TBM shaft (Walker, Hitchcock et al. 2006).

Other dynamic monitoring applications can be found in other fields, such as oceanography. Stiros and Psimoulis (Stiros and Psimoulis 2010) utilized RTS for the accurate determination of near shore wave characteristics by setting-up the RTS in a stable position on the coast and aiming at a passive reflector mounted on a small moored buoy (Figure 2.5). The method can be used not only for small waves with results of exceptional quality, but also for large waves. This study indicates that RTS is an effective, simple, and low-cost method to measure the wave propagation in near-coastal zones.

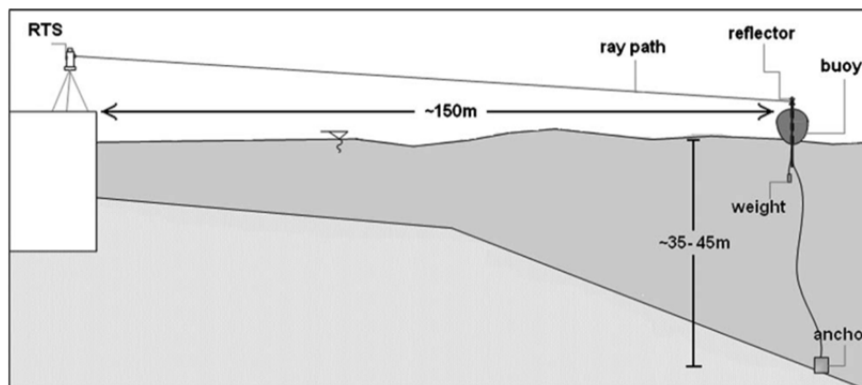


Figure 2.5 Diagram describing the instrumentation used in the experiments reported by (Stiros and Psimoulis 2010).

2.1.2 Global Positioning System (GPS)

Since the decade of the 1970's, when its implementation started, the Global Positioning System (GPS) has been applied in the areas of navigation, surveying and geodesy

among others. The GPS can provide location and time information in any weather conditions, anywhere on or near the Earth where there is an unobstructed line of sight to four or more GPS satellites.

There are three parts for GPS: satellites orbiting the Earth, control and monitoring stations on Earth and GPS receivers. The satellite transmits its current time and positions (x_i, y_i, z_i) to the GPS receivers on Earth. The position of the GPS receiver is calculated using the theory of triangulation using and based on the known position of satellites overhead to determine the position of a GPS receiver pair on Earth. The minimum number of required satellites to solve all the system unknowns is four. If there are more available satellites, a more accurate position for the GPS receiver can be obtained.

With the development of GPS technology, this system has provided a new monitoring method that has been applied in a wide variety of fields (Yi, Li et al. 2012), especially for measuring the displacements of civil structures.

a) Monitoring the high-rise structures

Monitoring the deformation of high-rise structures is an important task for the designer, the constructor and the manager. It seems that Lovse (Lovse, Teskey et al. 1995) firstly introduced GPS technology into the deformation monitoring for the high-rise structure. Since then, more and more users and researcher worked in this field, gaining positive results. GPS technology provides an excellent way to study the displacement of high-rise structures, for instance.

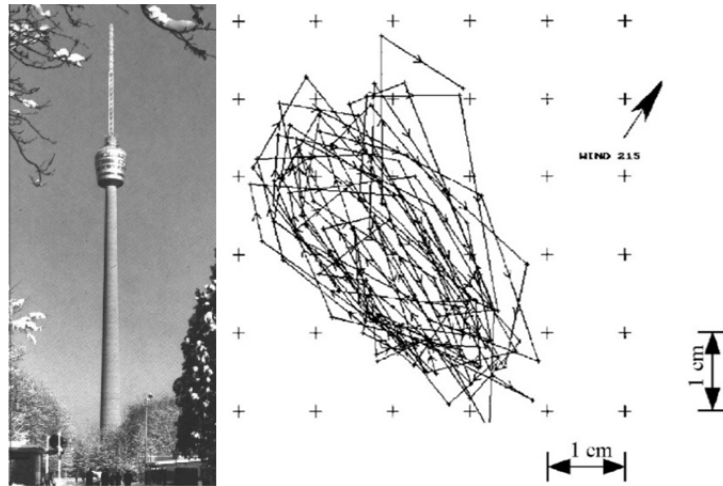


Figure 2.6 Stuttgart TV-tower and its movement during 2-min (Breuer, Chmielewski et al. 2002).

In this work, Breuer (Breuer, Chmielewski et al. 2002) described the use of Global Positioning System (GPS) technology to monitor the static, quasi-static and dynamic deformations of long-period structures. He also described the way in which the Stuttgart TV Tower (Figure 2.6) was monitored using static and kinematic GPS modes. The movement of Stuttgart TV tower resembles an ellipse whose maximum displacement values are approximately equal to 4cm and 2.5cm when the wind velocity is 7m/s. The results clearly demonstrate that the GPS procedure allows us to collect displacement data which could be used to determine the displacement thresholds of the tower and/or to examine the changes of vibration characteristics (Breuer, Chmielewski et al. 2008).

Xiaojing Li and Linlin Ge (Li, Ge et al. 2006) conducted a full-scale tall structural experiment (108-m-high steel tower in Tokyo) where they monitored the movement of the structure as shown in Figure 2.7. They used the GPS and accelerometer sensors by exploiting the complementary characteristics between them. The results agree with each other very well, although the static and quasi-static components are missing from the accelerometer-derived results. Redundancy has therefore been achieved in the monitoring system.

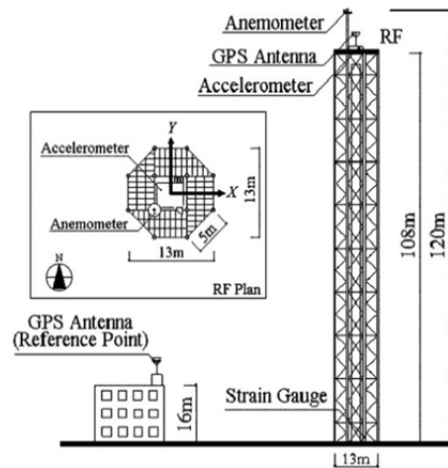


Figure 2.7 The experimental setup for a 108-m-high steel tower in Tokyo (Li, Ge et al. 2006).

Celebi (Celebi and Sanli 2002) used the permanent deployment of GPS units (Leica MC1000) for continuous dynamic real-time monitoring of a tall building in San Francisco. The results show that GPS monitoring of long-period structures provide sufficiently accurate measurements of relative displacements which are within the margin of error specified by the manufacturer (less than 1cm in horizontal, less than 2cm in vertical); so, the dynamic characteristics of vibrating systems can be accurately identified. Figure 2.8 shows the general schema of the GPS deployment.

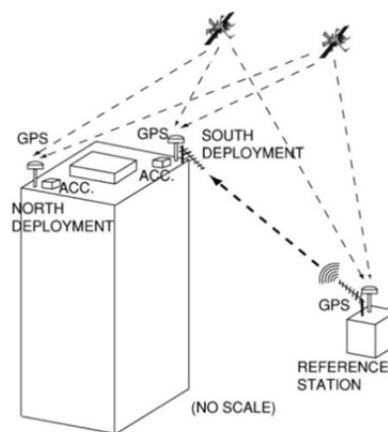


Figure 2.8 Schematic of the GPS deployment in a 34-story San Francisco skyscraper (Celebi and Sanli 2002).

Apart from the previous examples, other researchers' achievements have also proved that the GPS can be used in displacement monitoring. Seco (Seco, Tirapu et al. 2007) monitored a 30-m concrete building (Pamplona, Spain); Park (Park, Sohn et al. 2008)

measured a 234-m mixed-use building in Korea; Ogaja (Ogaja, Wang et al. 2003) monitored the 280-m tall Republic Plaza (Singapore); P. Zhang monitored the Guangzhou New TV Tower, which is a concrete-steel composite structure with a total height of 600 m (Zhang, Xia et al. 2012); similar to (Kijewski-Correa and Kochly 2007).

b) Monitoring the bridges

Bridge monitoring programs have historically been implemented for the purpose of understanding and eventually calibrating models of the load–structural–response chain (Brownjohn 2007). As previously stated, bridges are important structures in our society, so their safety has to be ensured; especially for the modern long-span suspension bridges. GPS technology has also been used in bridge monitoring.

Watson (Watson, Watson et al. 2007) used three Leica System 300 GPS receivers with AT302+gp antennas to monitor the structural movement of a cable-stayed bridge over the River Tamar in northern Tasmania, Australia. Observed displacement was compared with predicted deflections derived from numerical modeling. Results show that GPS is successful in quantifying both thermally induced bridge displacements and high frequency transient motion caused by vehicle loading. At the same time, it was also proved that the GPS is a valuable observational tool for monitoring structures. Figure 2.9 shows the schematic view of Batman Bridge and the instrumentation location.

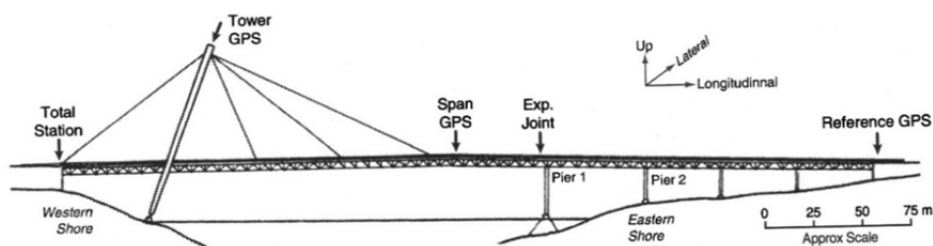


Figure 2.9 Schematic view of Batman Bridge with the location of the instruments, as viewed from south (Watson, Watson et al. 2007).

Psimoulis (Psimoulis, Pytharouli et al. 2008) utilized the GPS (Topcon Javad Legacy E receivers and Legacy-H antennas) to measure the displacement of a long suspension bridge (the Gorgopotamos Bridge in Central Greece), a steel railway bridge consisting of three sets of steel and stone masonry pylons with a spacing of approximately 30m with a steel truss deck (Figure 2.10). The outcome of this study indicated that GPS is

suitable for the identification of dynamic characteristics of even relatively rigid civil engineering structures excited by various loads (wind, traffic, earthquakes, etc.). The displacement, however, must be above the level of uncertainty specified by the method (around 5mm). An excitation frequency of 0.46Hz and a smaller peak slightly above 3 Hz, reflecting the main modal frequency of the span can be identified as shown in Figure 2.11-b.

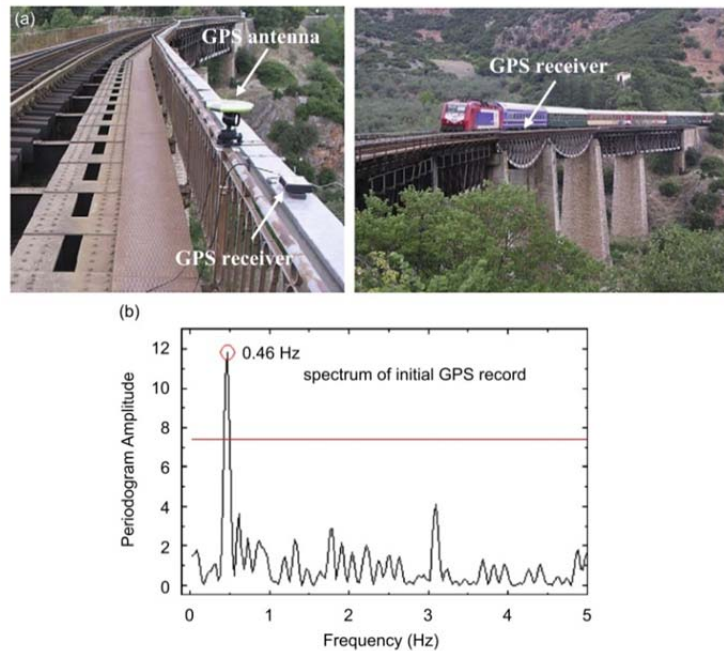


Figure 2.10 (a) A GPS receiver recording the response of the Gorgopotamos Bridge (Greece) while a train was circulating over it; (b) Spectrum of vertical displacements derived from the measurements (Psimoulis, Pytharouli et al. 2008).

The use of GPS for monitoring bridges deformation has been explained by many other authors, including Guo (Guo, Xu et al. 2005) , Roberts (Roberts, Meng et al. 2004) and Moschas (Moschas and Stiros 2011), etc.

c) Slope Monitoring

GPS has also been used for slope monitoring to precisely determine the 3-D coordinates of moving points. The GPS slope monitoring is usually performed using repeated campaigns (Malet, Maquaire et al. 2002). Gili (Gili, Corominas et al. 2000) used the GPS in static and kinematic method to monitor the movement of the landslide of Vallcebre, Eastern Pyrenees (Spain) over a period of 26 months. The results achieved

had a precision ranging from 12 to 16 mm in the horizontal plane and from 18 to 24 mm in elevation. Malet (Malet, Ulrich et al. 2011) installed several GPS receivers on active landslides for the near-real time characterization of displacement; the processing is fully automated, from the data acquisition on-site to the data transmission and storage on local servers, to the processing and the diffusion of the information through relevant graphs and reports.

2.1.3 Terrestrial Laser scanning (TLS)

Terrestrial laser scanning (TLS) is a ground-based technique to measure the position and dimension of objects in the three-dimensional space. A laser beam is emitted from a laser light source and used to scan the surface of surrounding objects in a raster-wise manner. The instrument used to direct those laser beams into varying directions is called ‘laser scanner’ (Boehler, Bordas Vicent et al. 2003, Fröhlich and Mettenleiter 2004).

Terrestrial Laser scanning provides a new method for structure deformation monitoring tasks, a fast and easy way to acquire every kind of structure’s geometric data, from building, bridge, beam, objects, machines and so on (Boehler, Bordas Vicent et al. 2003, Fröhlich and Mettenleiter 2004, Gordon, Lichti et al. 2004, Slob and Hack 2004, Gordon, Lichti et al. 2005, Alba, Fregonese et al. 2006, Schneider 2006, Tsakiri, Lichti et al. 2006, Park, Lee et al. 2007, Monserrat and Crosetto 2008, Zogg and Ingensand 2008, Mosalam, Takhirov et al. 2014). Each point is represented by a coordinate in 3D space (X, Y and Z, relative to the scanner’s position) and the reflected intensity (i) of the laser beam. Based on this kind of data, the 3D shape of any object or environment can be determined and analyzed (Slob and Hack 2004).

Advantages of using TLS in structural health monitoring include (1) no in situ instrumentation of sensors, (2) no difficulties reaching structures or structural members, (3) independence of natural light sources, and (4) no wiring cost. However, no model currently exists for measuring placements and deformed shapes of a structure using TLS (Park, Lee et al. 2007). In view of above mentioned advantages of TLS, the following section describes a number of applications which can show the possible benefits of using TLS as a technique in structure health monitoring practice and research.

a) Bridge deformation monitoring

In order to obtain a reliable basis for the evaluation of the fatigue resistance and to refine the analytical models, Zogg and Ingensand took a load tests by TLS on the Felsenau viaduct, a 33-year-old long span bridge made of concrete and one of the most remarkable bridge structures in Switzerland (Imager 5006 by Zoller+Froehlich). The bridge has a length of 1116 m and traverses the Aare valley at a height of up to 60 m (as shown in Figure 2.11).



Figure 2.11 Overview of Felsenau viaduct(Zogg and Ingensand 2008).

Two tanks with an approximate weight of 54 tons each were used to load the cantilever slabs following the four main steps in the procedure of the load test: initial measurement, loading P1 with one tank, loading P2 with two tanks, final measurements P3 without any load. The time of recovery is about 30 minutes(Zogg and Ingensand 2008).

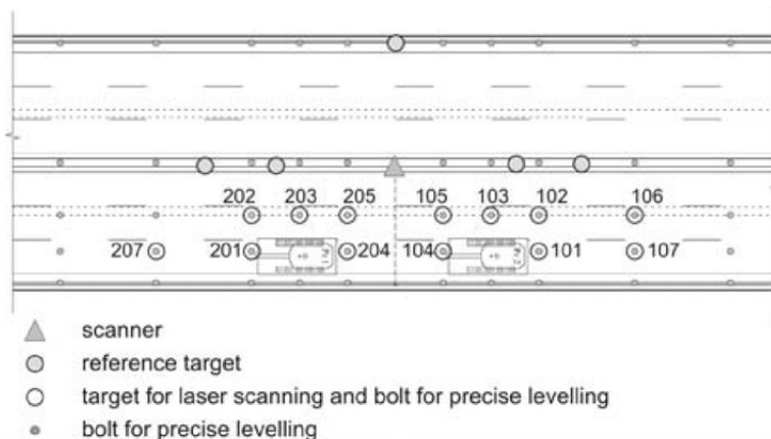


Figure 2.12 Measurement setup for terrestrial laser scanner and targets for TLS and precise levelling(Zogg and Ingensand 2008).

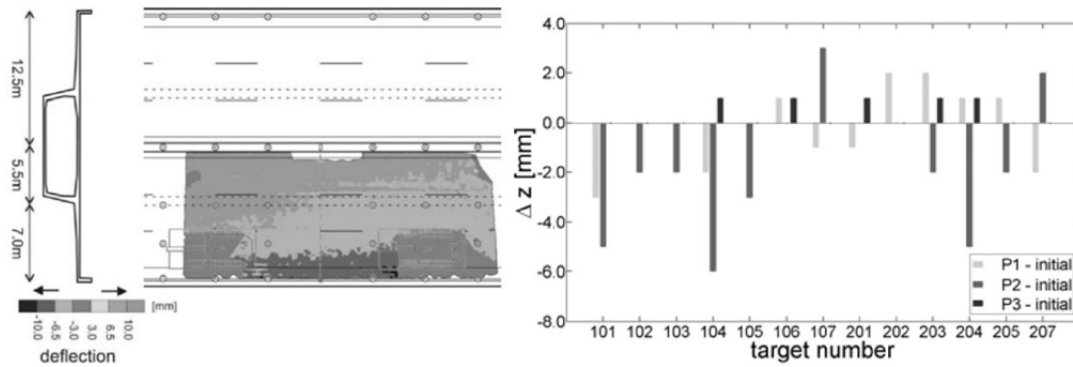


Figure 2.13 Left: Deflections of cantilever slabs detected by terrestrial laser scanner; Right: Vertical displacements of sphere between different loadings and initial situation measured by terrestrial laser scanner imager 5006(Zogg and Ingensand 2008).

As shown in Figure 2.13-left, the deflections of the outer side of the cantilever slabs are detectable and the maximum deflection is around 20 mm. The results for the comparison between the initial situation and loading situation P1 are similar, but the sizes of the residuals are smaller. The influence of the different loadings on the resulting deflections can be clearly distinguished. Figure 13-right shows the vertical displacement (Δz). The largest residuals can be detected for the targets 104 and 204 (Figure 2.12), which were located close to the loads on the outer side of the cantilever slabs. The mean values of the residuals are calculated to -0.2 mm for the differences between situation P1 and the initial situation (standard deviation: 1.6 mm), -1.7 mm for P2 and initial (standard deviation: 2.7 mm), and 0.4 mm for P3 and initial (standard deviation: 0.5 mm). From this bridge loading experiment, it can be seen that TLS is a very fast acquisition method and does not require deployment of any targets on the object. In addition, TLS is suitable for detecting deformations within the mm-range.

Mosalam et al.(Mosalam, Takhirov et al. 2014) used TLS (HDS laser scanner by Leica Geosystems, Inc.) to conduct a bridge damage assessment in Port-au-Prince after the Haiti earthquake. The bridge was scanned from two different positions called Station 1 and Station 2 (Figure 2.14 and 2.15). As shown in Figure 2.16 and Figure 2.17, the damage of the bridge can be shown by color map based on the TLS's point clouds. They show clearly identifiable damage with residual deformation of the surface. Finally, the results show that the residual inclination is about 0.21° and 0.19° in clockwise direction for the east and middle sections, respectively. On the other hand, the residual inclination of the west section is about 0.28° in the opposite (counter clock) direction.



Figure 2.14 Coarse scan from Station 1 for the bridge(Mosalam, Takhirov et al. 2014).

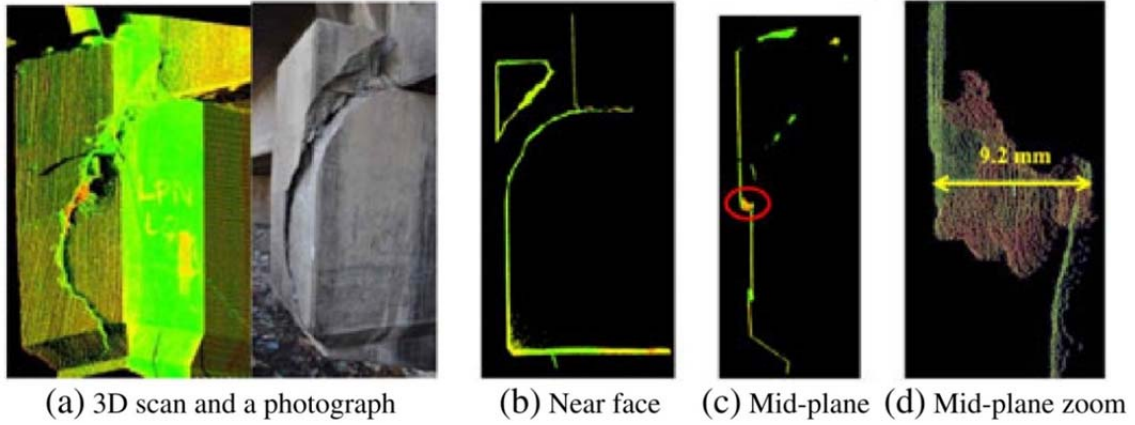


Figure 2.15 Fine scan from Station 2 for north–west shear key of the bridge(Mosalam, Takhirov et al. 2014).

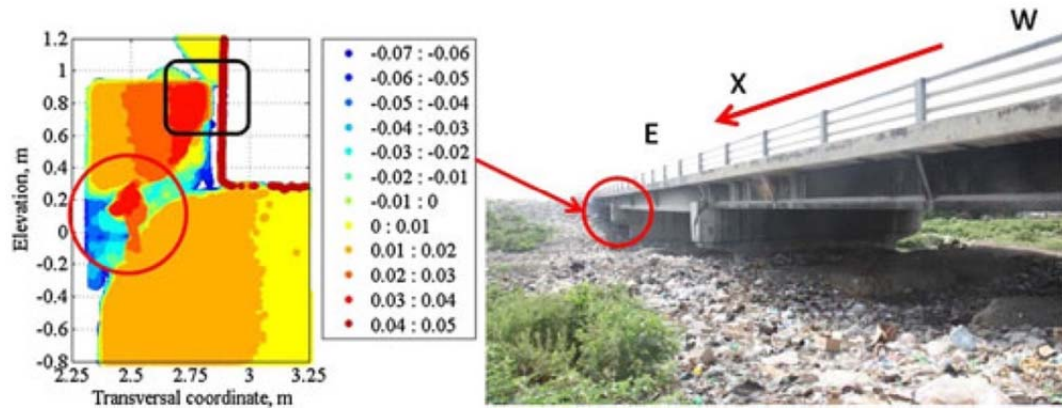


Figure 2.16 Color map of the damage in north–east key(Mosalam, Takhirov et al. 2014).

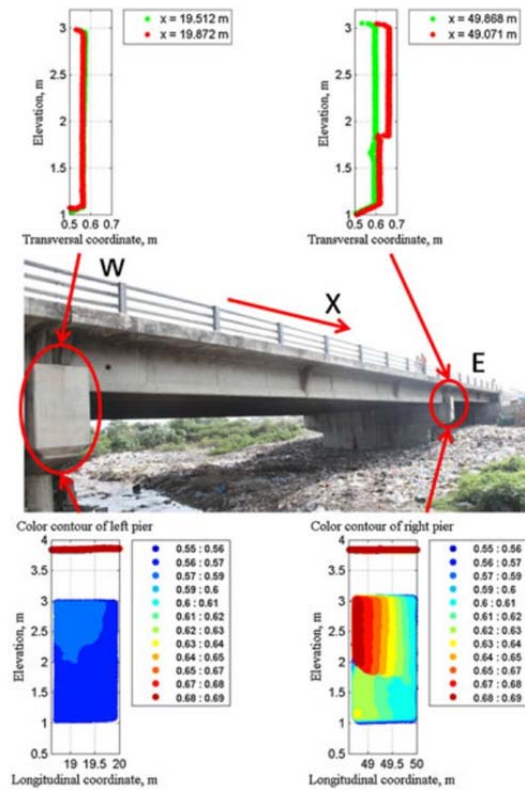


Figure 2.17 Damage of the south–east and no damage of the south–west shear keys(Mosalam, Takhirov et al. 2014).

b) Dam deformation monitoring

Dam deformation monitoring is also an important aspect for the application of TSL (Laserscanner Riegl LMS-Z420i). Several researchers have studied this field. Schneider applied Terrestrial Laser Scanning to water dams(Schneider 2006) and Alba et al.(Alba, Fregonese et al. 2006) used it to monitor the displacement of a large dam which is an arc gravity structure featuring 136 m of height and 381 m of length at the crest in Italy (as shown in Figure 2.18).

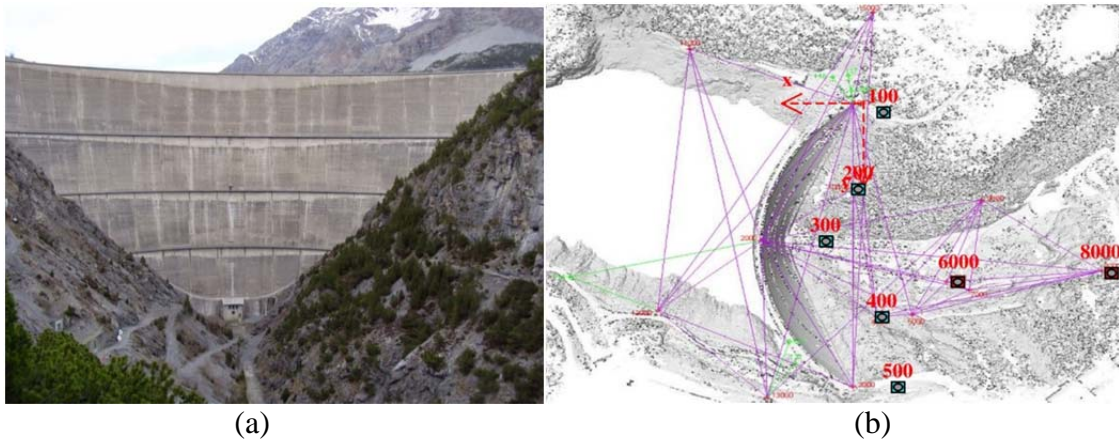


Figure 2.18 (a) Downstream face of the monitored dam; (b) Layout of the geodetic network reporting laser scanner stand-points(Alba, Fregonese et al. 2006).

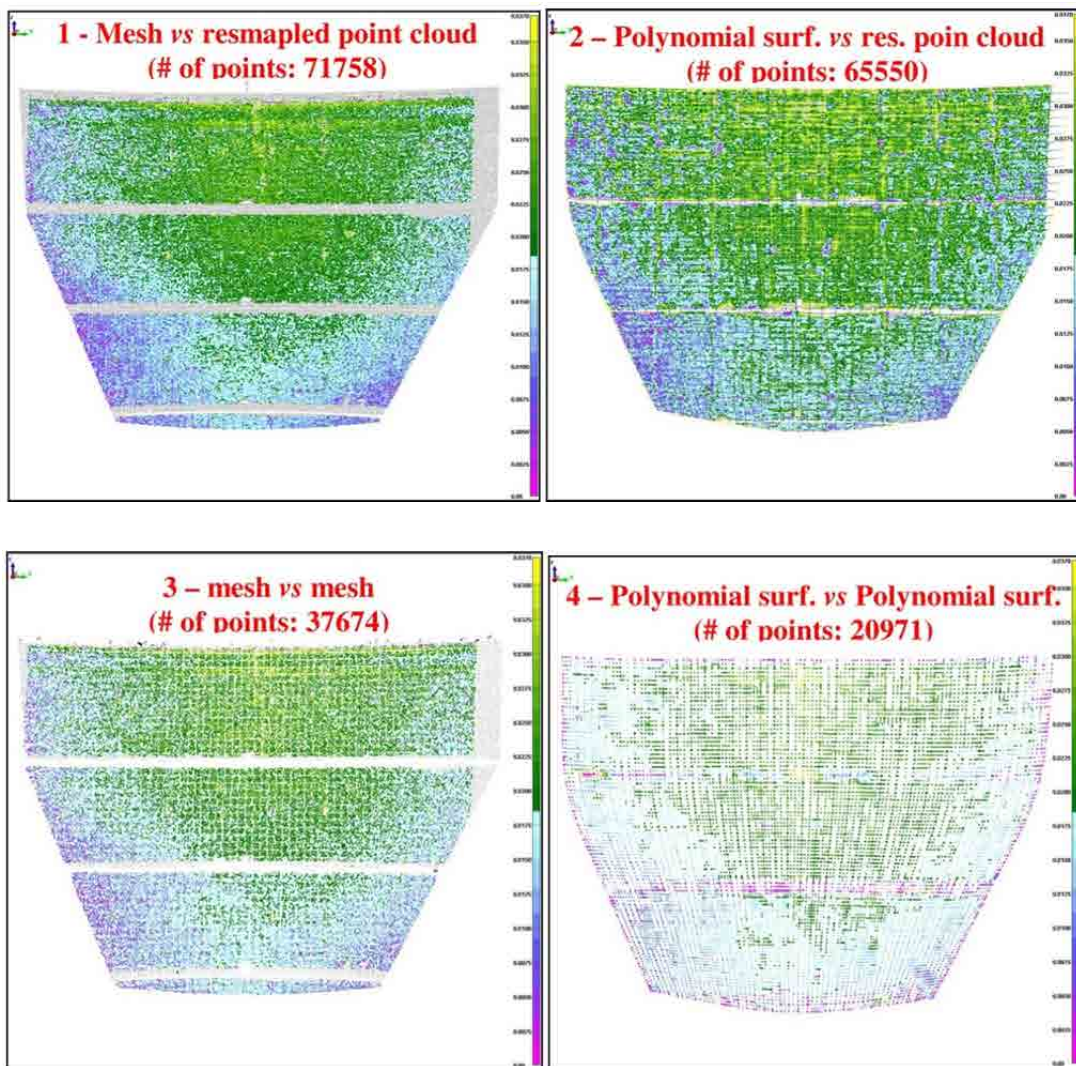


Figure 2.19 Maps of deformation evaluated by comparing different kinds of surface derived from scan acquired from station 8000 in Oct. 2005 and May 2006(Alba, Fregonese et al. 2006).

Figure 2.19 shows the color maps of deformations on the portion of the dam scanned from station 8000 at different times using different kinds of surfaces for comparisons. The results clearly show that the use of TLS technique may make an important contribution to the deformation analysis of large dams.

c) Building deformation monitoring

As for the application of TLS on building deformation monitoring, there are very few studies. Mosalam et al. (Mosalam, Takhirov et al. 2014) also used TLS (HDS laser scanner by Leica Geosystems, Inc.) to do a damage assessment with a building in downtown Port-au-Prince after the Haiti earthquake. Figure 2.20 shows that the vector connecting the corners of the cross-sections of a particular column at the two elevations of the two horizontal slices was assumed to represent the residual deflection of that column. The shown percentage drift was estimated from the ratio of this residual deflection of each column to the difference in elevation between the two slices, Figure 2.21, indicating a significant twist of the building as reflected by a rotated and translated bottom slice with respect to the top slice.

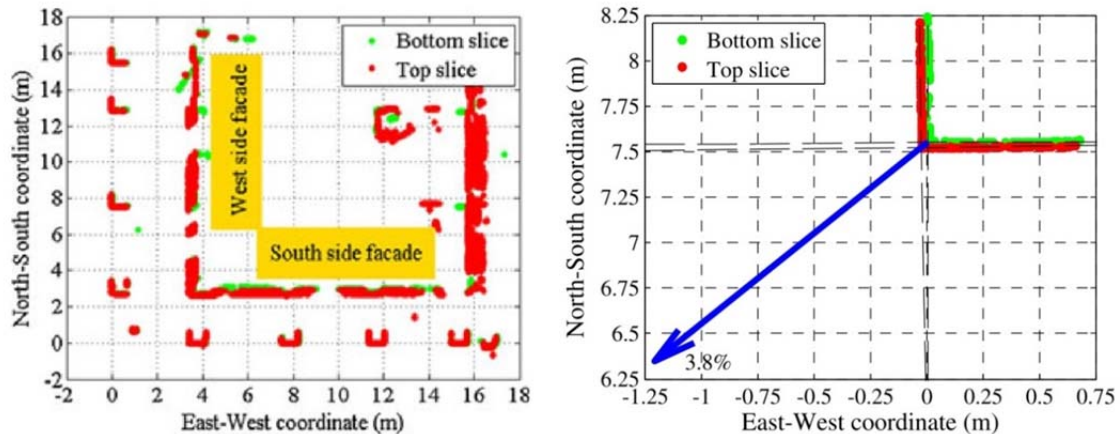


Figure 2.20 Example of drift calculation for one of the Asscotia Hotel columns; Left: horizontal slices of the first story at two elevations; Right: zoomed view of 2nd column on west side from the south–west corner with drift vector shown (amplification factor =40) (Mosalam, Takhirov et al. 2014).

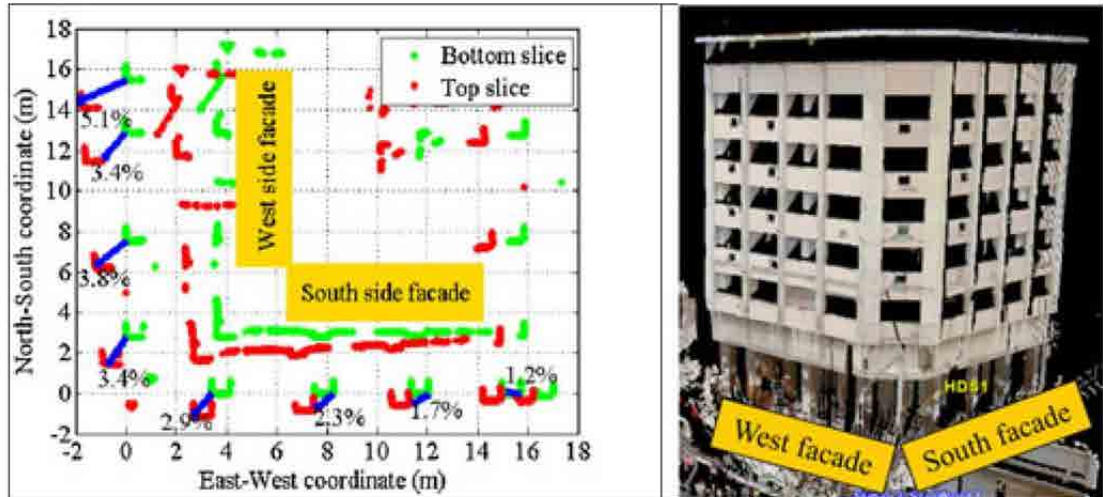


Figure 2.21 Columns drift vectors of Hotel Asscotia as they relate to point cloud registration (amplification factor=40)(Mosalam, Takhirov et al. 2014).

2.1.4 Ground Based-SAR

The Ground Based-SAR(GBSAR) is a radar-based terrestrial remote sensing imaging system(Tarchi, Rudolf et al. 1999). It consists of a radar sensor that emits and receives a burst of microwaves, repeating this operation while the sensor is moving along a rail track(Bernardini, Ricci et al. 2007). The working principle is that the radar transmits a modulated signal that enables detecting separately the displacements of different targets at different distances from the radar head, provided that they are spaced more than the resolution of the radar(Pieraccini 2013).

The precision of the GBSAR deformation estimates ranges from sub-millimeters to a few millimeters: this depends on the characteristics of the target and the wavelength. It can be used for a wide range of applications for detection of movement (structure or terrain monitoring)(Farina, Leoni et al. , Tarchi, Rudolf et al. 1999, Tarchi, Rudolf et al. 2000, Tarchi, Casagli et al. 2003, Antonello, Casagli et al. 2004, Pieraccini, Luzi et al. 2004, Leva, Rivolta et al. 2005, Bernardini, Ricci et al. 2007, Cuevas, Monserrat et al. 2011, Reale, Fornaro et al. 2011, Gernhardt and Bamler 2012, Lantada, Núñez et al. 2012, Zhou, Hu et al. 2012, Fornaro, Reale et al. 2013, Pieraccini 2013, Tapete, Casagli et al. 2013, Tomás, Cano et al. 2013, Ciampalini, Bardi et al. 2014, Crosetto, Monserrat et al. 2014, Monserrat, Crosetto et al. 2014, Talich, Glöckner et al. 2014) . In this section, we briefly review the main GBSAR applications.

a) Building deformation monitoring

Building deformation monitoring is one of important GBSAR application and some researchers have done many applications about building deformation monitoring (Tarchi, Rudolf et al. 2000, Pieraccini, Luzi et al. 2004, Lantada, Núñez et al. 2012, Tapete, Casagli et al. 2013). N. Lantada used IBIS-S (by IDS company, Ku-band (16.6-16.9 GHz)) to measure the building deformation under the thermal changes(Lantada, Núñez et al. 2012). The monitored building is an eight stories reinforced concrete (Figure 2.22-left). The results show that the thermal changes influence the building's behavior and GBSAR can be applied to building deformation monitoring practice (Figure 2.22-right).

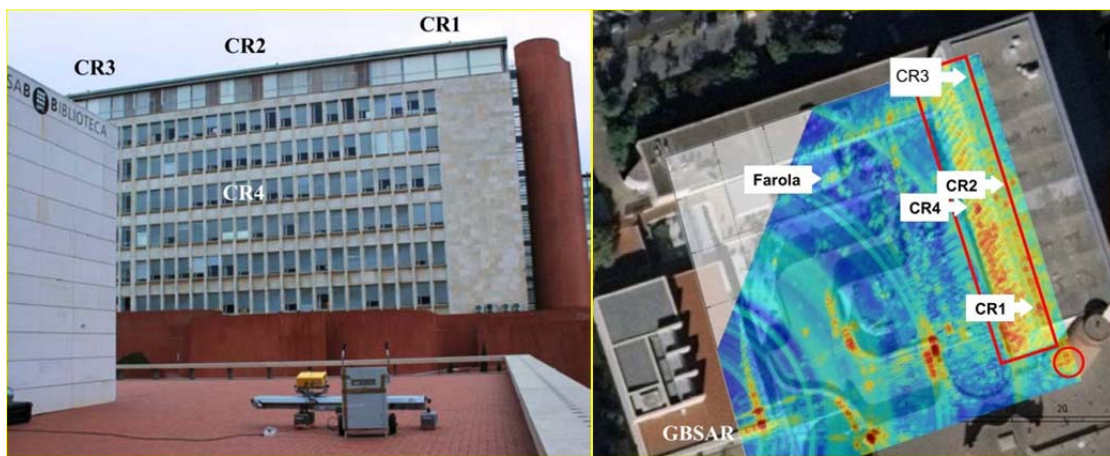


Figure 2.22 IBIS-S radar and the building (left) and the image of GBSAR(right)(Lantada, Núñez et al. 2012).

b) Slope monitoring

The monitoring of slope instability is another major GBSAR application. Farina used IBIS-M system (by IDS company) for slope monitoring within an open pit mines at Minera Yanacocha in Peru (Farina, Leoni et al.). The test results show that IBIS-M is able to significantly improve the performance of slope monitoring radar by providing higher spatial resolution, longer working distances and faster acquisition time. Thus, this innovative system would be used for slope monitoring within open pit mines.

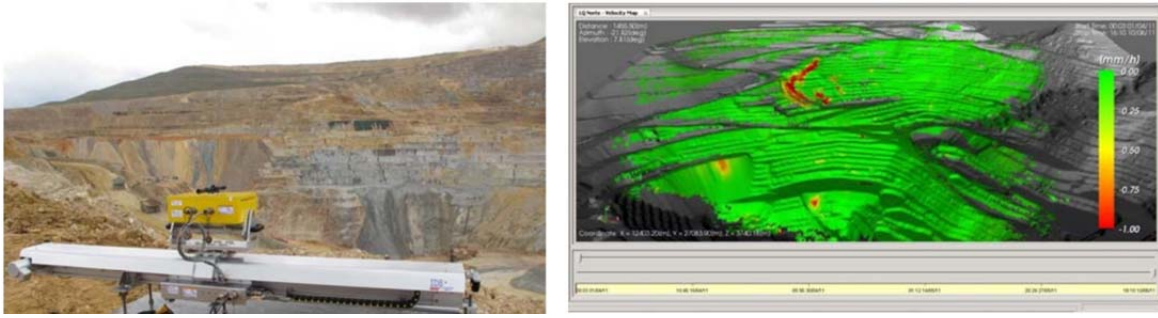


Figure 23 Set-up of an IBIS-M (left) and the monitoring results (right)(Farina, Leoni et al.)

Except that, other researchers also taken several experiments about the GBSAR in slope monitoring, including Leva et al.(Leva, Nico et al. 2003, Leva, Rivolta et al. 2005), Tarchi et al.(Tarchi, Casagli et al. 2003), Herrera et al.(Herrera, Fernández-Merodo et al. 2009), Intrieri et al.(Intrieri, Di Traglia et al. 2013), Iglesias et al (Iglesias, Mallorqui et al. 2015), etc.

c) Dam deformation monitoring

Other important GBSAR application is dam deformation monitoring (Alba, Bernardini et al. 2008, Talich, Glöckner et al. 2014). Alba et al measure the daily deformations of an arch-gravity dam (Alta Valtellina, Italy) by a non-contact GBSAR sensor, IBIS-L (by IDS company) which is a Ku-band (16.6-16.9 GHz) radar sensor designed for the simultaneous monitoring of the response of several points belonging to a large structure, providing for each point the between two different epochs(Alba, Bernardini et al. 2008). The test results highlight very good performance of this sensor coupled with the SAR technique in the measurement of slow movements, if compared with standard monitoring instruments. The global behavior of measured displacements and a quality check based on a comparison to readings from a coordinatometer have enhanced an accuracy of this GBSAR system under ± 1 mm. Figure 2.24 show the IBIS-L and test results.

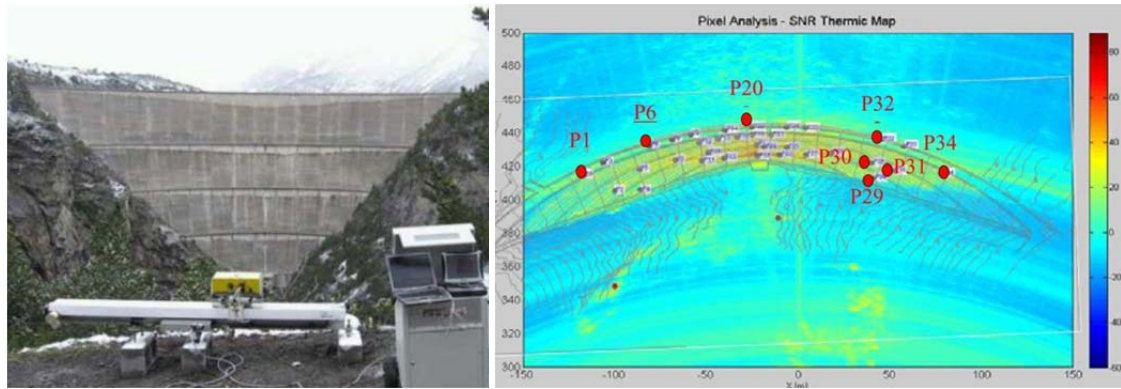


Figure 2.24 IBIS-L (left) and location of tracked points on the dam downstream face with a coherence $\rho > 0.99$ (right)(Alba, Bernardini et al. 2008).

2.1.5 Sensors

Structure health monitoring requires the careful collection and analysis of the measurements from a number of sources. As environmental factors are very important for the structure's behavior, it is necessary to collect the data of temperature, humidity, strain and solar radiation using different sensors. Depending on the aim of the monitoring, sensors are selected by the project manager. At present, the sensors have mainly been used in monitoring the conditions and environment of structures. Some achievements in this field can be found in (Hampshire and Adeli 2000, Peeters and De Roeck 2001, Hill and Sippel 2002, Casas and Cruz 2003, Van der Auweraer and Peeters 2003, Li, Li et al. 2004, Wu, Wang et al. 2004, Xia, Hao et al. 2006, Catbas, Susoy et al. 2008, Yigit, Inal et al. 2008, Brownjohn, Magalhaes et al. 2010, Xu, Chen et al. 2010, Yuen and Kuok 2010, Mosavi, Sedarat et al. 2011, Yi, Li et al. 2011, Chae, Yoo et al. 2012, Morris, Wang et al. 2012, Xia, Chen et al. 2012, Zhang, Xia et al. 2012, Grosso and Lanata 2013, Park, Shin et al. 2013, Unzu, Nazabal et al. 2013, Xia, Zhang et al. 2014, Ye, Su et al. 2014).

Unzu (Unzu, Nazabal et al. 2013) utilized 6 KNX sensors, 20 fiber optic strain sensors, 10 temperature sensors and 1 accelerometer to evaluate the behavior of a new building cladding system in real time and under service conditions during one year. The sensors were connected remotely through a 3G Internet connection. The results of the experiment indicated that 1) panels reached temperatures higher than the outside temperature, 2) the top floor suffered a higher temperature and deformation, 3) the temperature rose higher in the panels in the south side of the building than other sides

from 17.00 to 10.00. From the data gathered, it was concluded that there exists a lineal relationship between deformation and temperature. Unfortunately, no clear relationship or mathematical model was established. Figure 2.25 shows the sensor distribution and the system’s hardware scheme.

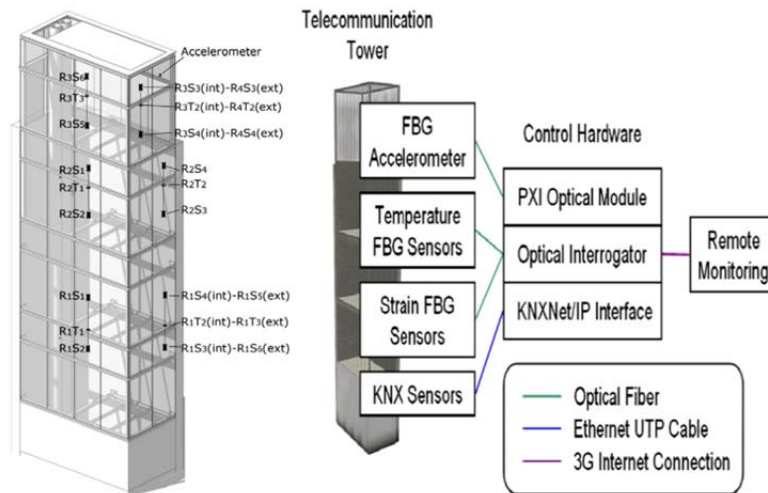


Figure 2.25 The sensor distribution and the system’s hardware scheme (Unzu, Nazabal et al. 2013).

Chae(Chae, Yoo et al. 2012) used a wireless sensor system with forty-five sensors of five different types to monitor the health of a suspension bridge in Korea. ZigBee (IEEE 802.15.4) is used for short-distance communications among sensors and Code Division Multiple Access (CDMA) for long-distance wireless communications with remote locations (showed in Figure 2.26). A data logger is integrated into a sensor and ZigBee into a one-channel data logger that combines a sensor, logger and digital communication module to allow the adding or replacing a sensor with ease. Figure 2.26 shows the u-Node (Sensor+A/D Converter+ZigBeeModule+Battery) and the Star-Type and Mesh-Type Networks.

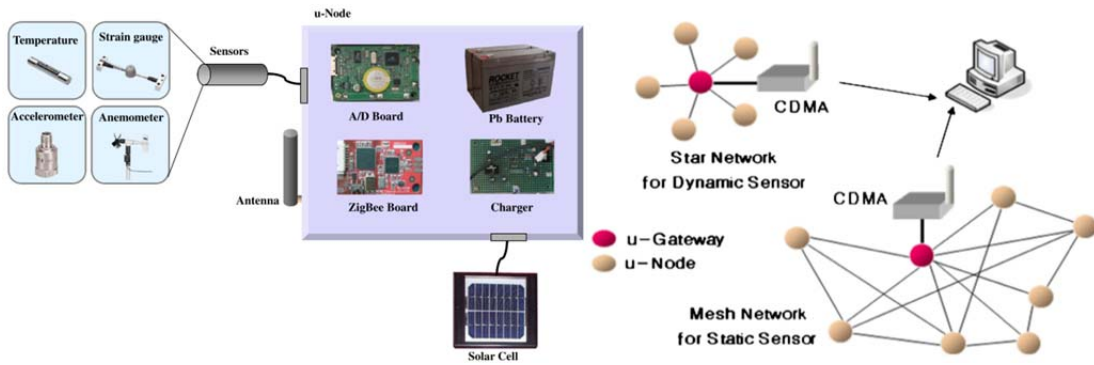


Figure 2.26 The u-Node and the Star-Type and Mesh-Type Networks(Chae, Yoo et al. 2012).

Moreover, Bennett(Bennett, Soga et al. 2010) also used the wireless sensor network in two field case studies involving networks deployed for structural monitoring in the Prague Metro and the London Underground. The wireless sensor network hardware consisted of three modules: radio modules (MICAz boards made by Crossbow); a crackmeter module (Figure 2.27), incorporates two linear potentiometric displacement transducers (LPDTs), one across the joint/crack under observation and one as a control, and two relative humidity and temperature sensors; an inclinometer module (Figure 2.27) containing two Sensirion digital humidity and temperature sensors that monitor the internal and external environment. The two trials demonstrate the feasibility and advantages of wireless sensing in the underground environment, but further investigation is needed to evaluate its long-term performance.

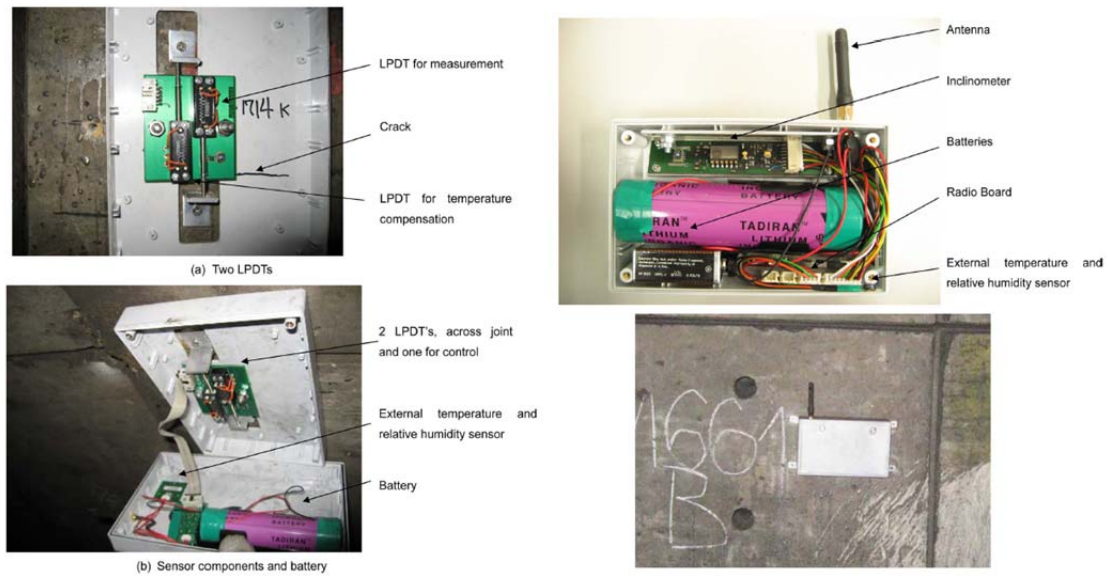


Figure 2.27 Crackmeter module (left) and Inclinator module (right)(Bennett, Soga et al. 2010).

Finally, we can consider the use of the meteorological station. Typically, this kind of units can measure: sun insolation, wind (speed, direction), pressure, temperature, humidity, and precipitation (rain gauge).

2.2 Environmental factors to be considered in SHM

The constructed heritage (infrastructures such as buildings, tunnels, power plants ports and offshore premises, constructions such as buildings, factories, monuments, and others) are part of modern society. It is therefore very important to ensure their safety. The risk associated with a given construction depends on the potential hazards around it and on the vulnerability of the construction itself as well as of the elements inside it (people, goods). Details such as the use (public or private), the location, the singularity, etc., determine the risk level of the construction. Structures at risk should be inspected, monitored and maintained regularly. The so-called Structural Health Monitoring programs may even be established by law. The effectiveness of the maintenance and inspection programs is only as good as their timely ability to reveal problematic performance, hence the trend to supplement limited and intermittent inspection procedures by continuous, online, real-time and automated systems (Brownjohn 2007).

As anticipated in the Introduction, the action of the environmental variables on constructions might play an important role in the structure health monitoring. The effect of the environment may be related with the change in variables such as temperature, humidity and wind etc. In practice, these factors change with time. Therefore, in order to understand the environmental effects, it is necessary to take into account the impact of thermal, humidity and wind conditions around the structure during the process of structure health monitoring.

2.2.1 Thermal influence

The behavior of the structure is influenced by temperature changes introduced mainly by sun radiation; cooling and heating may be considered as well. The thermal expansion law and Young's modulus make the behavior fairly linear within the range of normal ambient temperature (Yuen and Kuok 2010) .

The strain caused by a change in temperature from T_0 in the reference configuration to T in the current configuration is called thermal strain, and it can be expressed by the linear relation,

$$\boldsymbol{\varepsilon}_{thermal} = \alpha(T - T_0) \tag{2.1}$$

where $\varepsilon_{thermal}$ is the thermal strain in the linear theory and α is the dilatation coefficient.

In a linear constrained situation, the force $F_{thermal}$ caused by the temperature change (ΔT) can be estimated as:

$$\mathbf{F}_{thermal} = EA\alpha\Delta T \tag{2.2}$$

where E is Young's modulus and A is the area of a given structural element (a beam or a pillar for instance).

Temperature is one of the most significant factors affecting structural displacements. Almost every structure experiences movement due to changes in the temperature (Grinzato, Bison et al. 2002, Xia, Hao et al. 2006, Brownjohn, Worden et al. 2009, Li,

Li et al. 2010, Xu, Chen et al. 2010, Cuevas, Monserrat et al. 2011, Mananjara 2011, López, Tapia et al. 2012, Xia, Chen et al. 2012, Zhang, Xia et al. 2012), although the movement is generally small.

Zhang (Zhang, Xia et al. 2012) used the GPS and sensors to monitor displacement of the Guangzhou TV Tower (GZNTVT, in China, a 454m high concrete and steel structure) due to the influence of the temperature. The Figure 2.28 shows the displacement of the predicted and GPS-measured temperature-induced displacements at intervals of 0.5 hour. It was observed that the predicted displacement track has the same pattern of west-north-east-south as the GPS-measured path. The maximum predicted displacements towards west and north occurred around 10:30 am and 2:30 pm, respectively, which are a little different from that GPS-measured. The maximum predicted displacement towards west is about 10.2 cm, which is 1.3 cm larger than the GPS-measured displacement. While the maximum predicted displacement towards north is about 4.6 cm, which is 2.5cm smaller than the GPS-measured displacement. The daily maximum shift distance of the predicted and GPS-measured in the north-south direction are approximately 10.3 cm and 9.1cm. The daily maximum shift distance of the predicted and GPS-measured in the east-west direction are approximately 7.6 cm and 10.7 cm. From this reference results, it can be estimated that the accuracy of GPS is around 1cm. This will prevent the use of GPS in the monitoring of medium or low buildings.

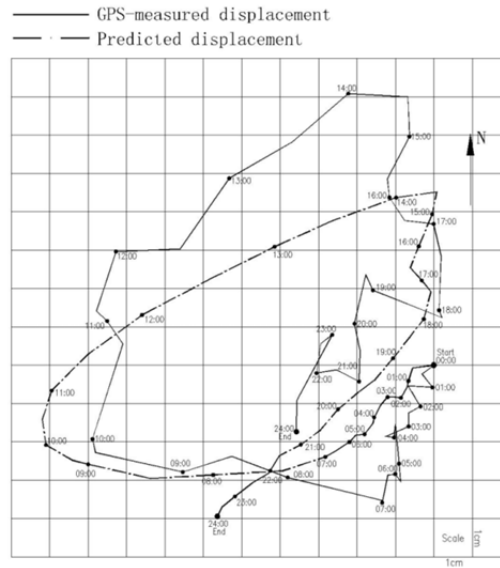


Figure 2.28 Predicted and GPS-measured temperature-induced displacement track at top of inner structure of GZNTVT in China (Zhang, Xia et al. 2012).

Figure 2.29 shows the deformation of the tower caused by heat stress (Tamura, Matsui et al. 2002). The day used for analysis was one with calm and fine weather. Each black dot means 1 h averaged data. Before sunrise, the top of the tower did not move. However, after sunrise, the tower moved to NW direction by about 4 cm. Top of the tower moved in an almost circular shape in the daytime, and returned to zero point after sunset.

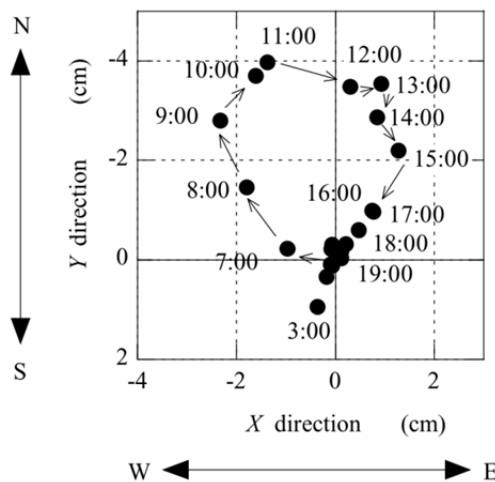


Figure 2.29 Deformation of the tower caused by heat stress(Tamura, Matsui et al. 2002).

Schwarz(Schwarz, Valdemarin et al. 2011) measured the displacement of a water tower through a full scale-test. In Figure 2.30, the daily movement of the water tower due to

the sun rotation can be appreciated. This behavior confirms again the impact of differential temperature on buildings. However, the authors did not set up a model for deformation caused by temperature.

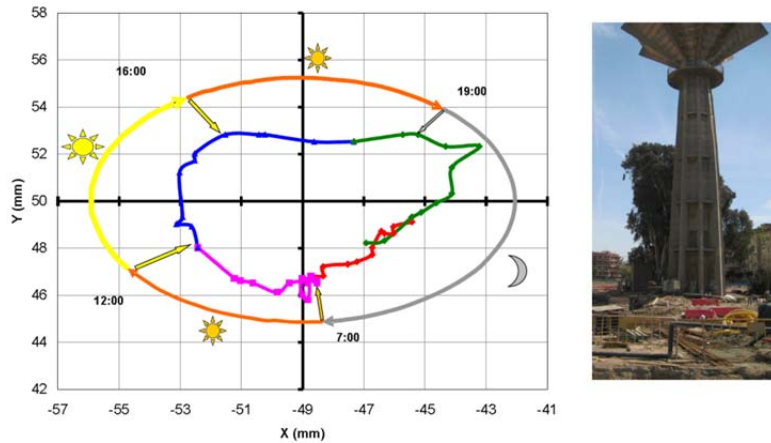


Figure 2.30 Daily movement of a water tower due to sunshine on the structure (Schwarz, Valdemarin et al. 2011).

James MW Brownjohn et al.(Brownjohn, Worden et al. 2009) studied thermal effects on performance on Tamar Bridge, which is a 335m-span suspension bridge in southwest UK (shown in Figure 2.31). They installed a dual monitoring system in the Bridge, which can provide valuable static and dynamic performance data at a range of sample rates.



Figure 2.31 Tamar Bridge, Plymouth, UK(Brownjohn, Worden et al. 2009).

Their results, supported by detailed numerical modeling, proved that temperature is the main factor responsible for the structural behavior. Compare with other effects on the bridge e.g. wind and traffic, thermal effects have apparently dominated the performance,

with significant variations in bridge deck frequency (in excess of 20%) and smaller but clearly diurnal variations in tensions of the 16 additional stays cables. Figure 2.32 shows the variation in tensions in additional stay groups with the temperature over a one-month period, also for September 2007. The relationships vary between the months; some positive correlations switch to negative. Zooming in on a single day shows the relationship to be other than linear, and either having a more complex relationship with temperature or being affected by other parameters(Brownjohn, Worden et al. 2009).

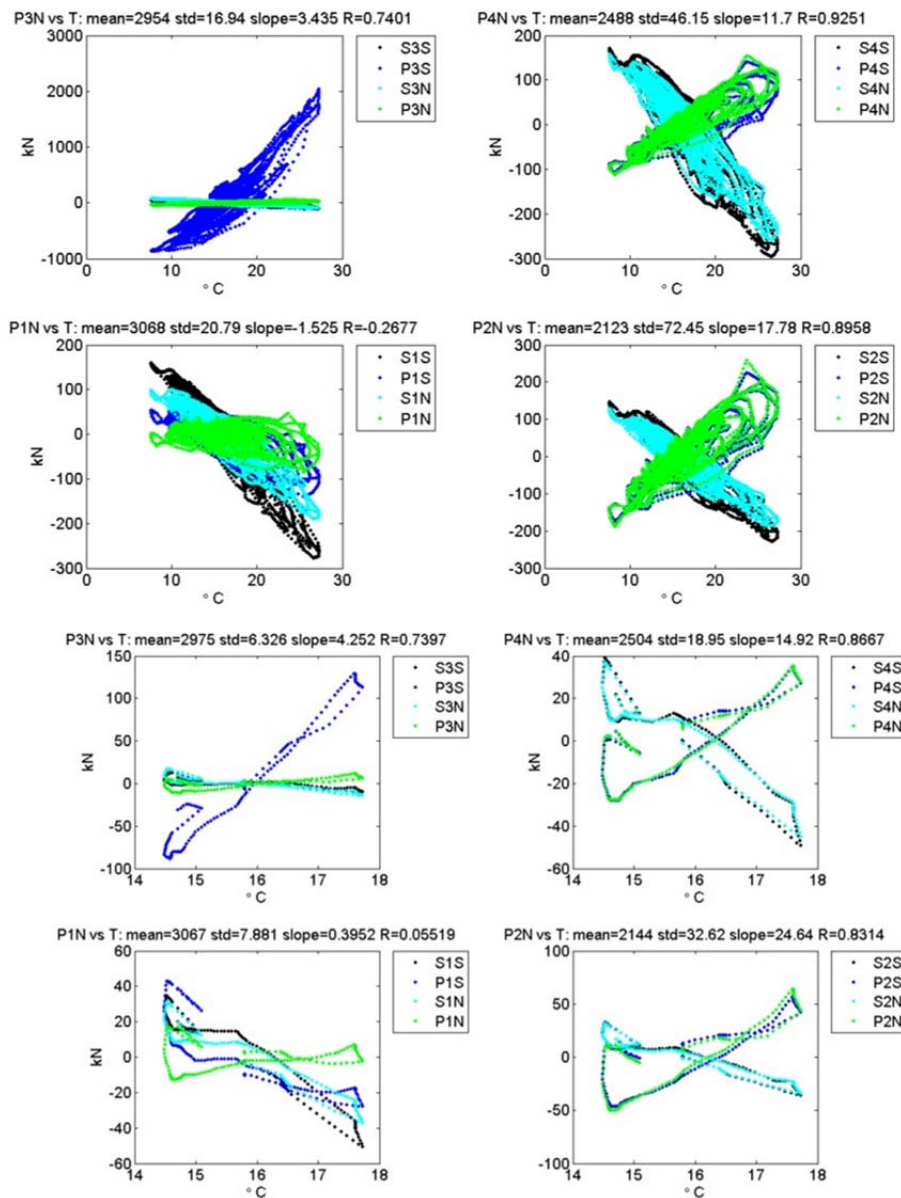


Figure 2.32 Relationships of tensions, frequencies and temperatures of additional stays
Upper set is for Sept 2007, lower set is for 7th July 2007(Brownjohn, Worden et al. 2009).

2.2.2 Wind influence

Wind influence is the wind loads on the structure that result from the movement of the air against the obstructing surfaces. It is particularly significant for tall buildings. Wind effects induce forces, vibrations, and in some cases instabilities in the overall structure as well as its non-structural components. The effects depend on the wind speed, mass density of the air (related to its temperature and humidity), location and geometry of the structure, and dynamic characteristics of the system (West and Geshwindner 2002).

The wind load on the structure is directly related to the velocity pressure q , which is given by

$$q = \frac{\rho V^2}{2} \quad 2.3$$

where ρ is the mass density of air and V is the wind velocity.

The basic wind pressure at a standard height of 30 ft is given by

$$q_s = 0.00256V^2 \quad 2.4$$

where q_s is in pounds per square foot.

In addition to the mechanical action of the wind, an indirect effect must be considered: the air in contact with the building may cool the façades subjected to direct sun insolation.

Wind is another significant factor that affects the displacement of the structure, especially for the high-rise structures and in areas where wind is strong. There are some results that illustrate the structure's behavior under different wind conditions (Breuer, Chmielewski et al. 2002, Tamura, Matsui et al. 2002, Ogaja, Wang et al. 2003, Kijewski-Correa and Kochly 2007, Breuer, Chmielewski et al. 2008, Park, Sohn et al. 2008, Xie and Gu 2009, Li, Li et al. 2010).

By analyzing the representative wind speed data, Koo (Koo, Brownjohn et al. 2012) learned that the significant vertical response is only triggered when the wind speed exceed 13 m/s (Figure 2.33).

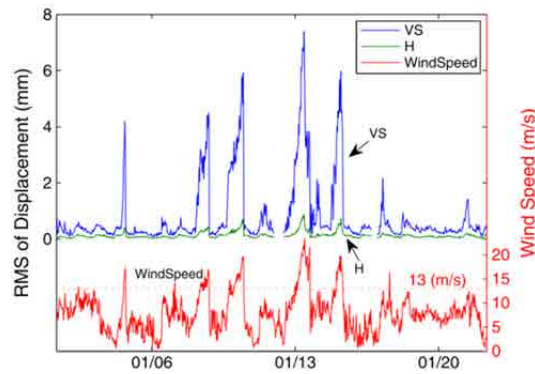


Figure 2.33 Deck displacement and wind speed according to (Koo, Brownjohn et al. 2012).

Finally, Figure 2.34 depicts data points of the movements of the Stuttgart TV tower during 2-min measurements carried out in 1999 with a wind velocity of 7 m/s (Breuer, Chmielewski et al. 2002). The sampling rate was 1Hz (1 value per second). This figure shows a typical, elliptical movement of the TV tower where the cross-wind displacement is approximately equal to 4 cm and the along-wind displacement is equal to 2.5 cm.

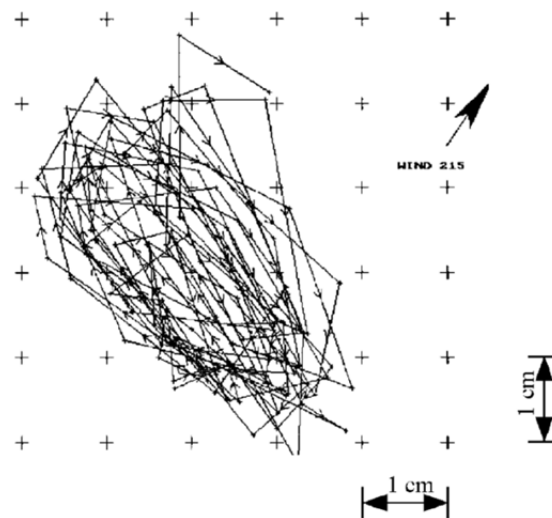


Figure 2.34 Data points during 2-min measurements of the movements of Stuttgart TV tower (the measuring point was 155m above the ground level)(Breuer, Chmielewski et al. 2002).

2.2.3 Traffic influence

Traffic load mainly includes the effects of vehicles and people on the object, and it is dynamic. For bridges, traffic load is a very important factor, especially for bridge design and safe evaluation. Some researchers have obtained results of traffic load effects by

monitoring traffic loads on bridges (Bailey and Bez 1994, Getachew 2003, James 2003, Karoumi, Wiberg et al. 2005, O'Connor and O'Brien 2005).

R. Karoumi et al.(Karoumi, Wiberg et al. 2005) monitored a railway bridge using a cost-effective method to assess the actual traffic load on the bridge, which was built in 2003 and has a span of 14.4m. Figure 2.35 shows that the monitored frequencies close to these may be identified in the analysis of the free vibration part of a measured acceleration signal obtained from a crossing.

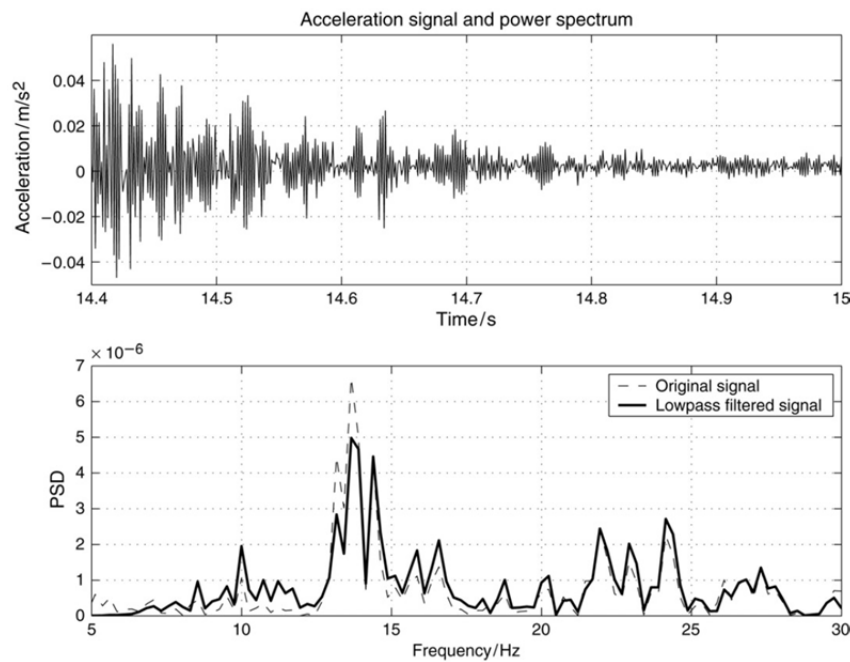


Figure 2.35 Free vibration signal shortly after the train has crossed the bridge and the corresponding frequencies(Karoumi, Wiberg et al. 2005).

2.2.4 Relative humidity influence

Relative humidity is the ratio of the amount of water vapor in the air at a specific temperature to the maximum amount that the air could hold at that temperature, expressed as a percentage. Relative humidity is important because the more moisture that's already in the air, the lower the rate at which water will evaporate and the less moisture that the air can hold. A relative humidity of 100% means the air cannot contain any more water vapor at that temperature, whereas a relative humidity of 50% means that the air only has only half as much water vapor as it can hold at the current

temperature. For some kinds of structures, it is a very important factor in the monitoring, such as, concrete, wood, and so on.

For the concrete, there is a relationship between humidity, temperature and mechanical properties. For instance, concrete will become stiffer if wet. Humidity tends to exhibit positive correlation with the ambient temperature in normal circumstances. Hence, humidity is also a factor for structural deformation monitoring; although the practical importance of this variable is modest according to what is reported in the literature.

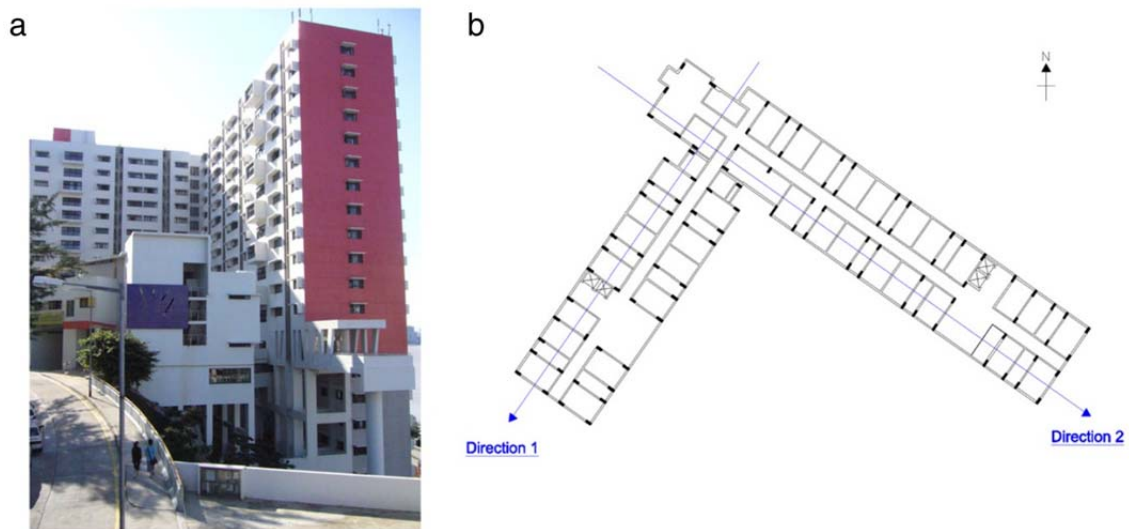


Figure 2.36 (a) Side view and (b) floor plan of the East Asia Hall(Yuen and Kuok 2010).

Ka-Veng Yuan and Sin-chi Kuok(Yuen and Kuok 2010) took one-year daily measurement on a 22-story reinforced concrete building (Figure 2.36) to quantify the modal frequency fluctuation induced by change in ambient conditions, such as temperature and humidity. Their measurements confirm that there is a high correlation between the modal frequencies and the ambient conditions. In addition, the Timoshenko beam model is considered to construct the modal frequency–ambient condition model. Explicit consideration of the ambient temperature as well as the relative humidity is necessary. This work is helpful for future structure health monitoring.

2.3 Current practice in building monitoring during underground works

In recent years, there have been more and more underground projects being instigated, frequently in urban areas in order to maximize space use to save surface land. For example, the most typical project in a city is tunnel construction to deal with the increasing congestion problem for public transportation. Those underground works will inevitably be accompanied by movement of the ground around them. Any underground excavation will break the balance of the original stress underground, causing its redistribution and leading to overburden movement and deformation, which will impact on any surface structures, especially buildings. At the ground surface these movements manifest themselves in what is called a ‘subsidence basin’ or ‘settlement trough’. In case of ground transverse to the axis of the tunnel approximates closely a normal Gaussian distribution curve, which is an idealization that has considerable mathematical advantages. So it becomes a more important task to monitor the health of the surrounding or overlying structures and services during the period of constructing. Many engineers and researchers have spent a lot of time on this task in order to finish it successfully (Boscardin and Cording 1989, ZC, Liao et al. 1994, Urbain 1997, Law 2001, Franzius 2003, Centis and Giacomini 2004, Bhalla, Yang et al. 2005, Kontogianni and Stiros 2005, van der Poel, Gastine et al. 2006, Berkelaar, Huisman et al. 2007, de Rienzo, Oreste et al. 2008, Standing and Burland 2008, Chen, Zhu et al. 2011, Hisatake 2011, Mananjara 2011, Ghorbani, Sharifzadeh et al. 2012, Salimi, Esmaeili et al. 2013, Zhang, Chen et al. 2013, Zhang, Wu et al. 2014).

Ground settlement induced by underground construction may have a serious influence to the adjacent buildings. These influences mainly come from two aspects, vertical displacement and horizontal displacement. Figure 2.37 shows diagrammatically the surface settlement trough above an advancing tunnel.

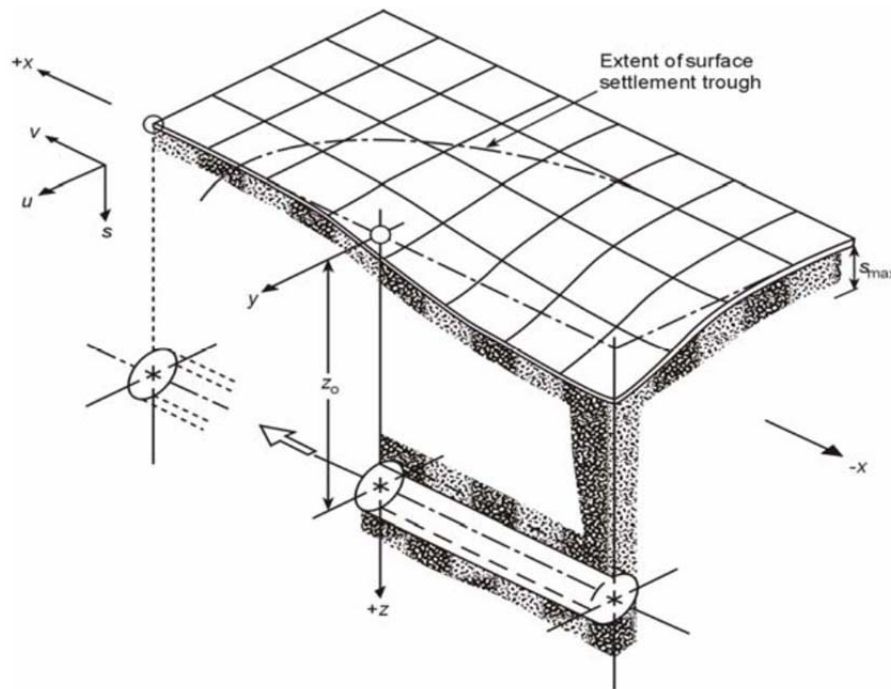


Figure 2.37 Surface settlement above an advancing tunnel(Franzius 2003).

Boscardin and Cording(Boscardin and Cording 1989) studied the impact of construction-related ground movements on surface buildings and utilities during the planning and execution of underground construction. Figure 2.38 shows the general building responses to an underground tunnel excavation: settlements, diagonal strains, horizontal strains, rigid body rotations or tilts, and angular distortions. The two buildings were located at two different areas in the settlement trough: Building I, located nearer the center of the final ground surface settlement trough was in the zone of compression and showed very little final lateral extension; Building II was located near the edge of the ground surface settlement trough in the zone of lateral extension and sustained a larger final lateral extension. Consequently, if we want to obtain the real data for the ground surface settlement, it is necessary to set the reference points sufficiently far from the settlement trough.

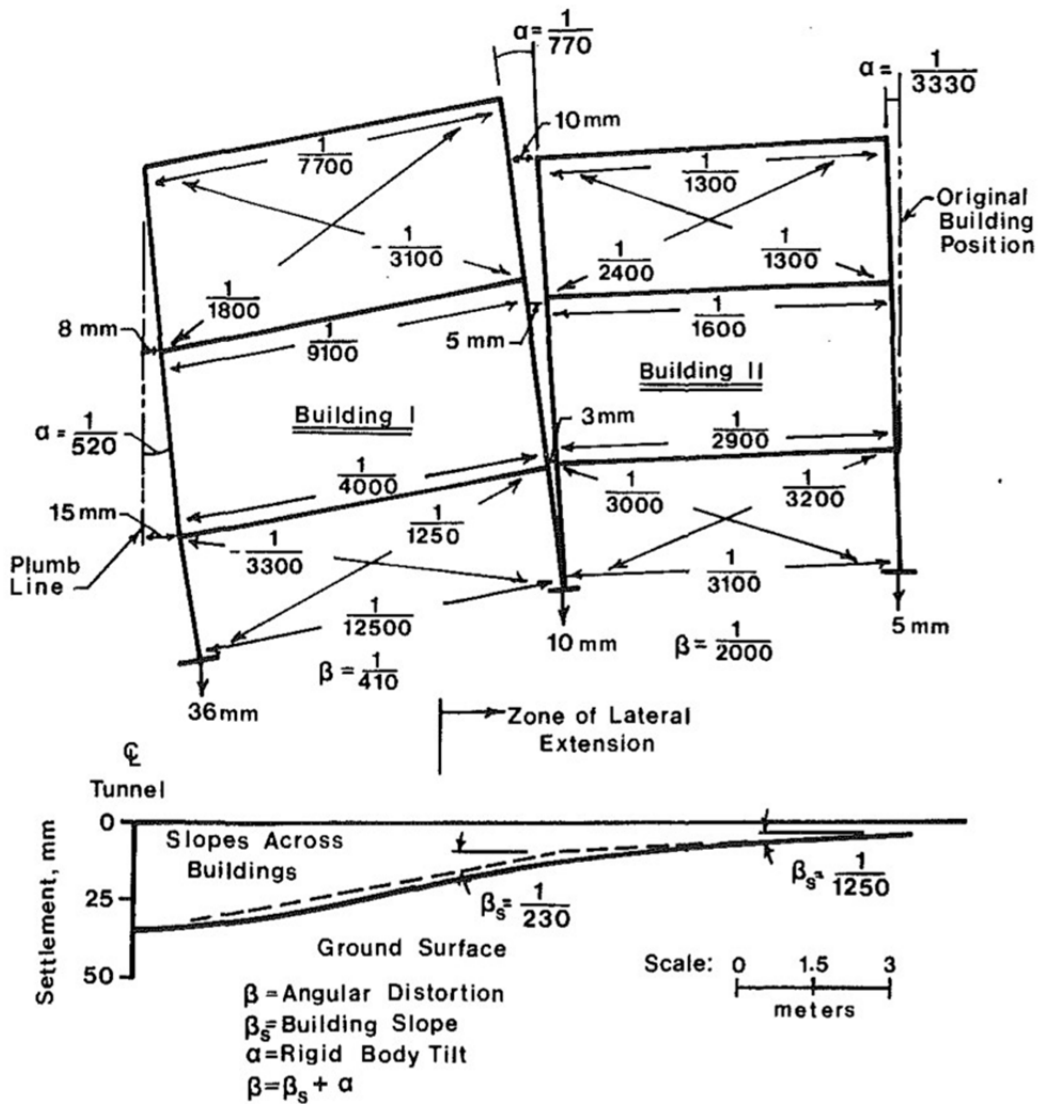


Figure 2.38 Example of building response to tunnel excavation(Boscardin and Cording 1989).

Centis and Giacomini analysed the relevant issues during the excavation of about 6km of tunnel using two EPB Tunnel Boring Machines for the Oporto Light Metro Project(Centis and Giacomini 2004). Figure 2.39 shows the project in field which is at Aliados station and the EPB Shield.



Figure 2.39 TBM breakthrough at Aliados station(left) and 8.7m diameter Herreknecht S-160 EPB Shield after assembly(Centis and Giacomini 2004).

Throughout all the construction phases, the surface displacement was monitored in real time with programmed theodolites. Figure 2.40 shows the whole process of settlement envelop along tunnel axis from Pk 2+340 to Pk 2+350. The settlement took place from the drilling phase until the phase of grouting, when the displacement increased. Later the curves fall dramatically in the phase of TBM. Finally the curves show gently fluctuation.

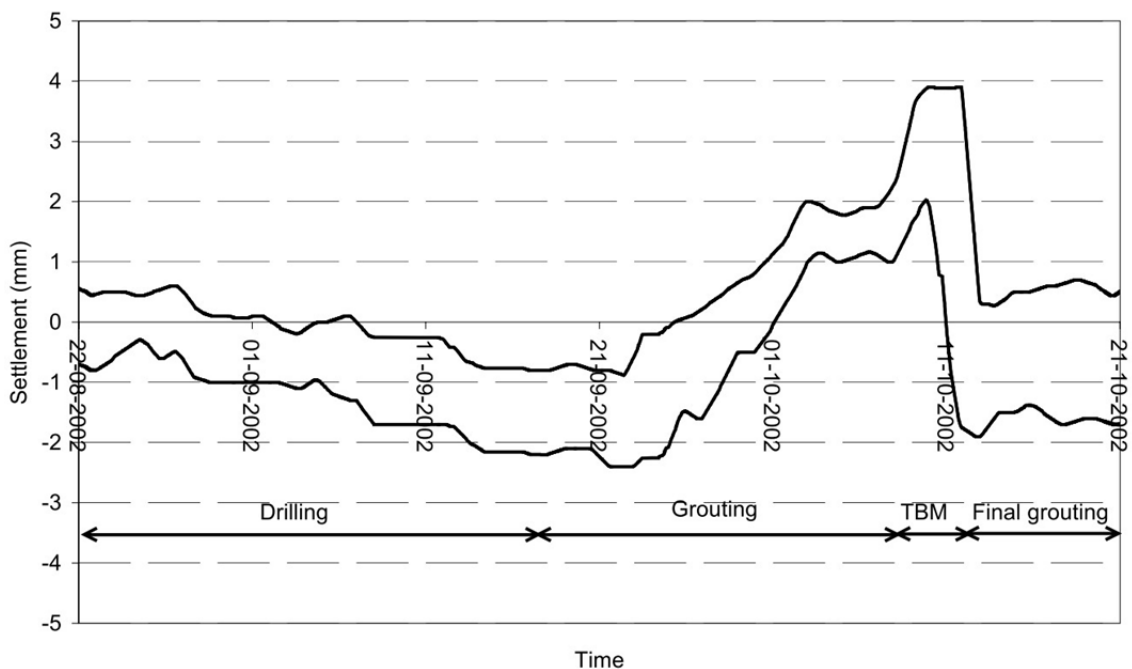


Figure 2.40 Real time monitoring: settlement envelop along tunnel axis from Pk 2+340 to Pk 2+350(Centis and Giacomini 2004).

Jamie and John have done some work on the effect of the temperature on the building measurement under construction of tunneling(Standing and Burland 2008). They used tape extensometer measurements to measure strain and settlement of the building's lower basement. The horizontal strains at slab level that developed along the length of the building during the construction of the two running tunnels have been isolated by a careful selection of a set of base readings, chosen from 17/01/1995. By choosing this date as a datum, the strains caused by thermal changes can be assumed to be almost negligible. Figure 2.41 shows the settlements, corresponding strains and changes in temperature along two sections of the tunnels.

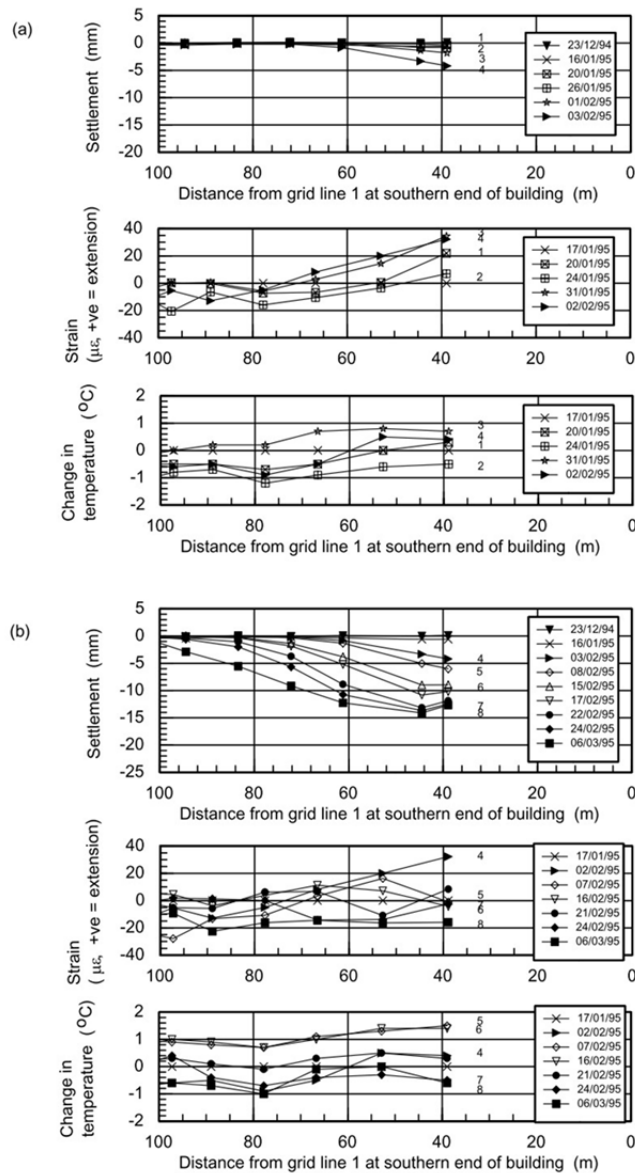


Figure 2.41 Precise levelling and taping data: settlements, horizontal strains and temperature changes in spans along inner Waterloo (eastern) side of Elizabeth house with taping data referenced to 17.01.1995 for construction of (a) westbound and (b) eastbound running tunnels(Standing and Burland 2008).

Similarly, Ghorbani et al. studied the tunneling effect during the construction of the Niayesh tunnel (Tehran, Iran)(Ghorbani, Sharifzadeh et al. 2012). In order to collect data from all the instruments, a unique database system was recommended. This system can collect data from all the instruments and compose and pre-process it and finally provide results in Web, SMS and Email format and give alerts and alarms in necessary cases. In the intelligent and continuous building monitoring system, there are Automatic Total Stations, dual axis inclinometers, a crack meter and GPS, and all data are automatically collected in database, processed and send to the client, consultant, etc. The main source of 3D information is provided by the position of the monitoring reflectors or mini-prism installed permanently on each building. The overall automatic monitoring and database system can be seen in Figure 2.42.

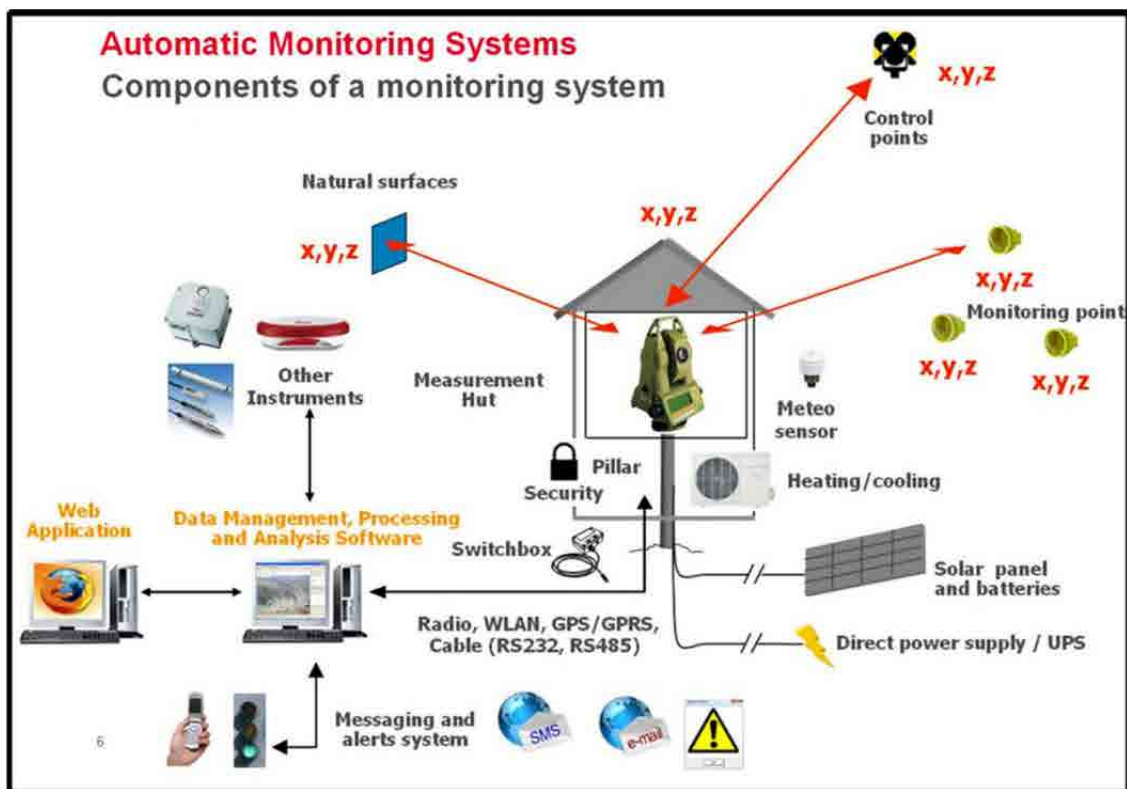


Figure 2.42 Automatic Monitoring Systems(Ghorbani, Sharifzadeh et al. 2012).

Figure 2.43 is the surface settlement graph of Km.0+836 of Southern tunnel, which shows that the system can successfully monitor the Niayesh project to record the ground behavior real time. As seen in Figure 2.43, in the Niayesh project, 40, 45 and 50mm surface settlement values have been defined as alert, alarm and action levels respectively. From this figure, we can see that after top heading in the northern drift of

the tunnel, the rate of surface settlement increased and reached to action level. All the excavations in this area were stopped and remedial measures using soil nailing and closing the temporary invert in the settlement zone were adopted. After these actions, the rate of the settlement decreased and reached stable behavior.

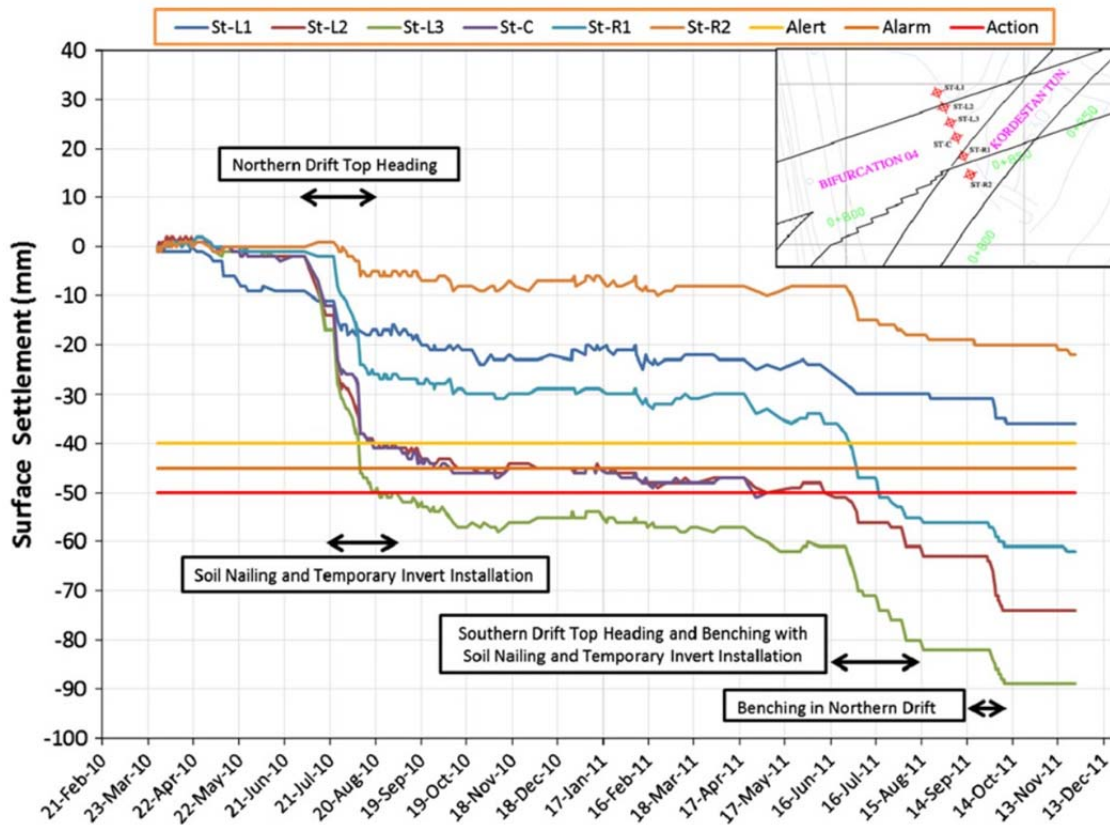


Figure 2.43 Surface settlement graph(Ghorbani, Sharifzadeh et al. 2012).

In order to get the thermal influence in extreme heat conditions, Mananjara(Mananjara 2011) set up an experiment on a sensitive building and deploy a real-time monitoring system to monitor the ground movement vibration and water in the vicinity of the structure to ensure that there is no detrimental impact upon the structure. Figure 2.44 illustrates the recorded movements of a theodolite in millimeters against the temperature in degrees over a one-year period. The pattern of the measured movements does not follow a cycle and the seasonal variation of the temperature has little effect on the measured data Figure 2.45 shows the relationship between the measured temperature and crackmeter data. It indicates that temperature has little influence on the sensor and the structure also does not appear to respond significantly to the change in temperature.

This study is helpful to understand the behavior of the structure and the influence of the temperature.

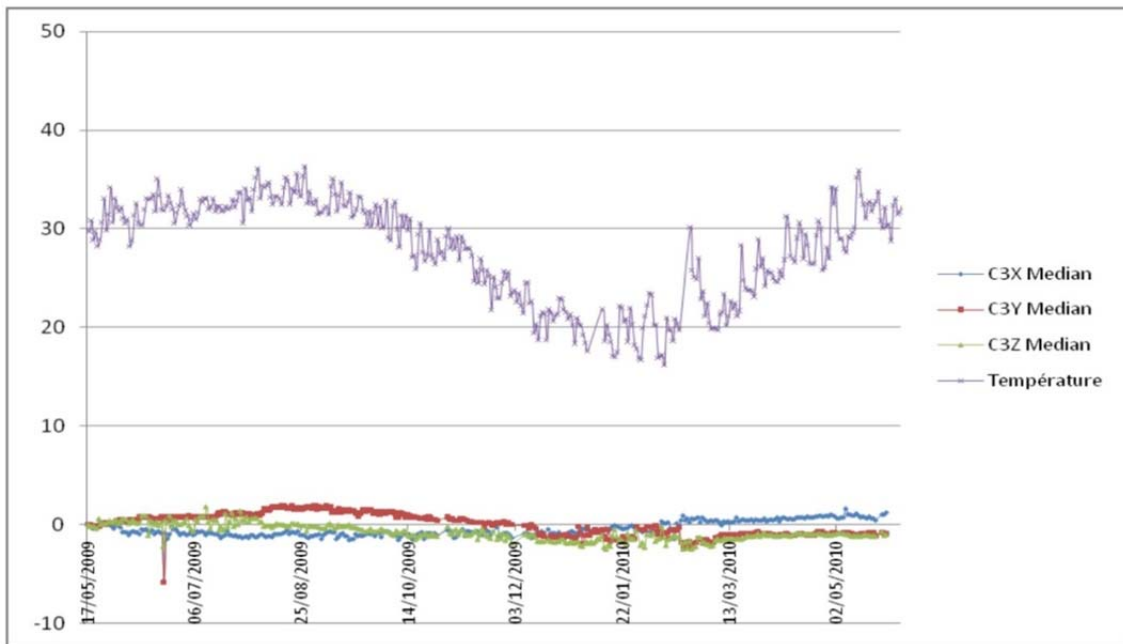


Figure 2.44 Movements of CYCLOPS in X, Y and Z in millimeters and temperature in degrees(Mananjara 2011).

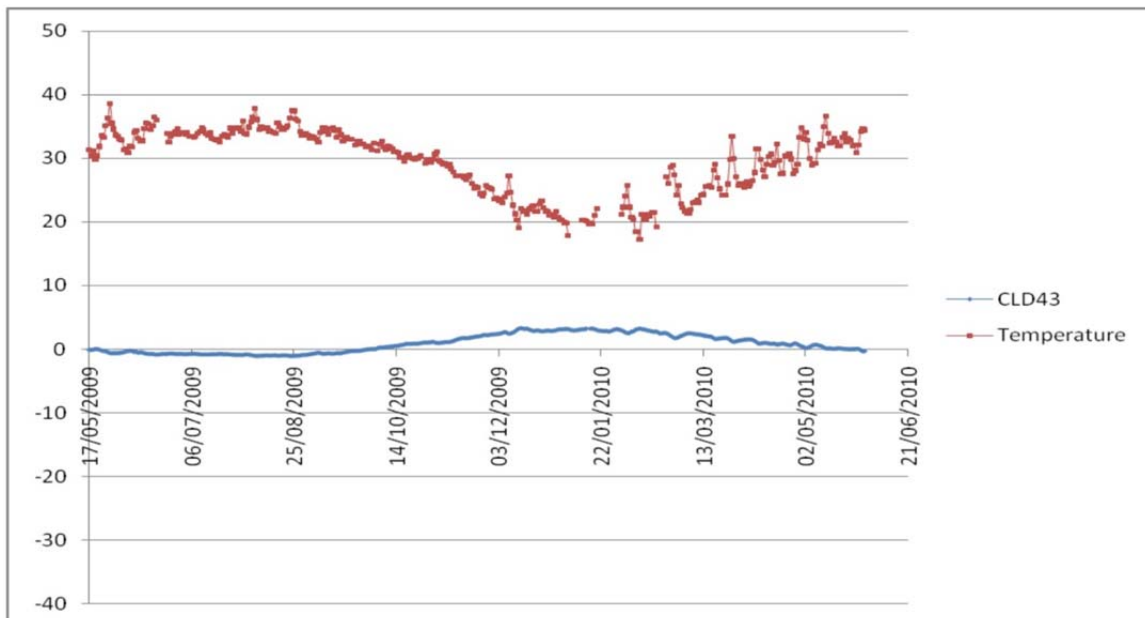


Figure 2.45 Data retrieved from a crack meter installed across a construction joint(Mananjara 2011).

3 Modeling the behavior of buildings and monitoring systems when subjected to Thermal Effects

One of the major challenges in structural deformation monitoring engineering today is to be able to obtain the precise structure deformation values about the monitored object. If we want to do that, it is essential to know the ambient conditions of the structure, such as thermal change, solar insolation etc., and to be able to quickly evaluate the real condition of the structure after an external event, for instance, underground tunneling. However, the values collected from the RTS or another measurement do not only include the influence of external events, but also the influence of environmental load such as thermal change. Therefore, it will become more important to know the environmental impact if we want to get a real deformation value of the structure after an external event.

In this chapter, a model will be set up to investigate the environmental influence on the structural deformation monitoring by simulating the impact of thermal change on the structure base on the Matlab software.

3.1 Conceptual model

As introduced in the section 2.2, the structure health monitoring is influenced by the environmental variables, especially in urban areas during civil engineering construction. The observed displacement ($M_{observed}$) of the surface structure contents the deformation due to the external event and the deformation due to environmental factors (shown in the Equation 3.1).

$$M_{observed} = M_{external\ event} + M_{thermal} + \varepsilon \quad 3.1$$

where $M_{external\ event}$ is the displacement from external event, such as tunnel excavation; $M_{thermal}$ is the displacement due to thermal change; ε is the others influences in the observed value.

In order to ensure that the civil engineering infrastructure maintains a safe condition, it is an indispensable task to distinguish the ambient interference from abnormal variation of the structural properties. As we know that the temperature change is the most influence factor for the structure deformation monitoring compare with other environmental factors, hence it is necessary to assess the extent and pattern of the deformation of the buildings when subjected to variation of the temperature due to direct solar insolation.

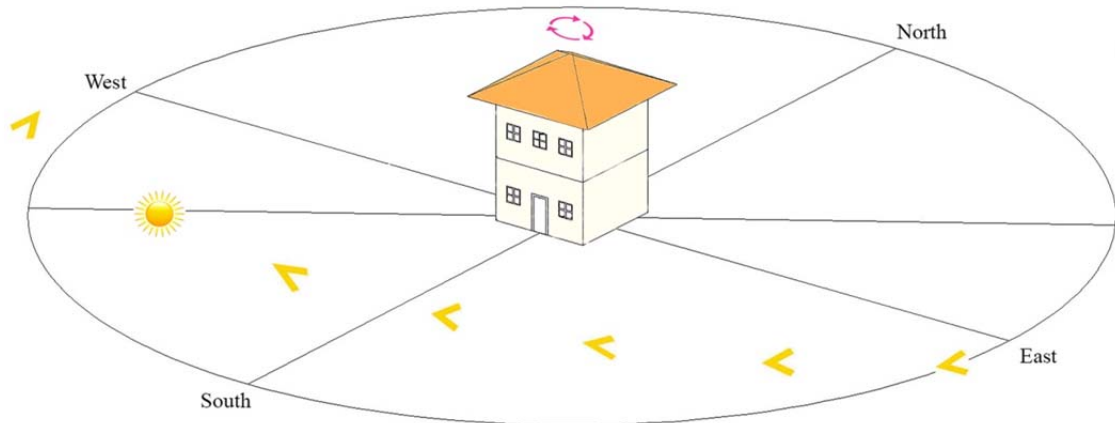


Figure 3.1 One day's movement of a building under temperature and insolation change.

Figure 3.1 shows one day's movement of building under the temperature and insolation change. In this graph, each façade of the building suffers different insolation at different times of the day, which leads to an increase in the temperature on each façade. As for this kind of phenomenon, some researchers (Breuer, Chmielewski et al. 2008,

Brownjohn, Worden et al. 2009, Schwarz, Valdemarin et al. 2011, Zhang, Xia et al. 2012) have conducted experiments to prove that the temperature and insolation change have a great deal of influence on structure deformation.

There are two parts in the concept model. One part is the numerical modeling of the structure, and the other is data post-processing to calculate and adjust the raw observation data (angles and distance) to obtain the displacement of RTS and prisms. The use of numerical modeling enables the quantification of the temperature and insolation effect under daily change during the process of building deformation monitoring. The Least Square Adjustment method has been used to adjust the synthetic raw observation data.

The use of synthetic model based on the real scale building and real temperature and insolation change during one time period allows us to determine the effect of thermal change on the buildings. The building models need to be set up. For the purpose of improving the knowledge of the term $M_{thermal}$, an experimental building has been selected as the monitoring object. This building was over-instrumented, allowing us to build a model that explains the deformation of the building when subjected to real temperature changes. At least one year of data has been gathered: of ambient temperature, insolation, inclination, relative humidity and movements of prisms and RTS.

In real practice, it is necessary to remove the thermal movement ($M_{thermal}$) from the observed value ($M_{observed}$) if we want to get the real movement ($M_{corrected}$) which comes from the external event, such as tunneling. Equation 3.2 illustrates this relationship.

$$\mathbf{M}_{corrected} = \mathbf{M}_{observed} - \mathbf{M}_{thermal} = \mathbf{M}_{external\ event} + \boldsymbol{\varepsilon} \quad 3.2$$

After filtering the thermal movement value from observed value, the final corrected value can be obtained.

Figure 3.2 shows a synthetic example for this computing over the period of one day. In this figure, the blue curve is the assumed observed movement, and the red curve is the

assumed thermal movement. After applying the Equation 3.2 to these two types of movement values, the corrected value has been calculated as shown in green curve in Figure 3.2. From the results shown in the figure, it can be seen that the corrected movements is more stable than the observed movement values after the thermal movements are filtered from the observed movement values.

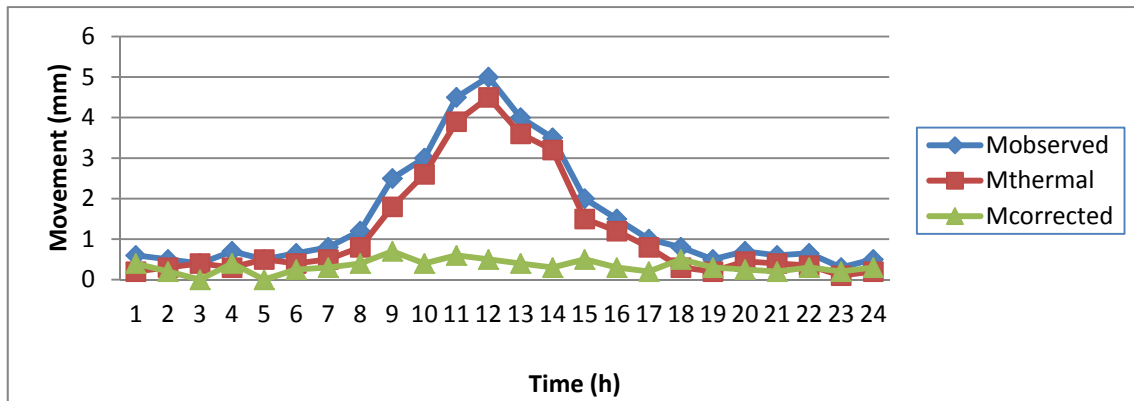


Figure 3.2 A synthetic example showing the thermal correction process following Equation 3.2.

3.2 Implementation of the conceptual model

The Equation 3.2 shows the way to reduce the influence of thermal change from the raw displacement data during the structure health monitoring. However, the aim of the thesis is to improve the standard practice in monitoring an urban area during tunneling. So the idea is to correct the raw data of Δx , Δy , Δz , the standard systems which enterprises deliver to their customers, in order to get better results, i.e. total station monitoring.

On one hand, it is necessary to compute the movements of every element (building) in the area of monitoring around the Total Station, i.e. a program has to be built (numerical code) to compute that. The structure computation and numerical program are introduced in section 3.3. On the other hand, a key step in the RTS monitoring is the least square adjustment of the synthetic raw measurements data to obtain the final movement of RTS and prisms, and to demonstrate that the ideas are right, and that the correction of Equation 3.2 is possible. To do this, real scenarios and real data need to be analyzed. In several real sites the ‘Temperature effect’ has had a role (an influence) in the

3 Modeling the behavior of buildings and monitoring systems when subjected to Thermal Effects

monitoring system and results (Brownjohn, Worden et al. 2009, Schwarz, Valdemarin et al. 2011). Figure 3.3 shows the water tower's daily movement induced by temperature change. This figure clearly shows the tower moves with the day and night alternatively, and the reason is the thermal change during the whole day.

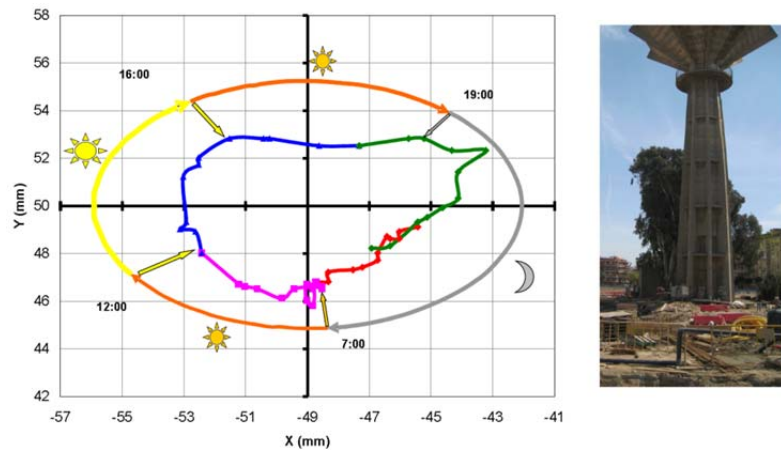


Figure 3.3 Daily movement of a water tower (Schwarz, Valdemarin et al. 2011).

Unfortunately, at this site we do not have enough data to prove how the temperature has influenced the results. The relation cause-effect is not well-established. For this reason, the research project “thermal effect” (between SOLDATA and UPC) has built an experimental area in the Campus Nord (UPC, Barcelona). This area, around Omega & K2M buildings, is described in chapter 4.

In this area, 3 RTS had been installed to surveying prisms attached to the buildings. Other values have been monitored over time: changes in the inclination of several pillars of the structure (with clinometers), the inside and outside temperatures in the same pillars, air temperature, humidity, wind, rainfall (Meteorological Station) and insolation over the façade (insolation cells also known as pyrometers).

The high degree of redundancy of the observables will permit the modeling of the deformation due to the thermal effects, as long as the structural modeling of the building itself is subjected to the recorded temperature changes.

The huge amount of available data will permit the testing of several strategies to mitigate the influence of the temperature changes over the final values of the building deformation.

The flowchart of Figure 3.4 shows the main steps to implement the model. There are two parts in the general process, which are the structure model and data post-processing. The Figure 3.4 shows the procedure to follow in order to build and adjust the model for the building's behavior in the part of the structure model, as well as to use the least square adjustment method to process the synthetic observation data (angles and distance) in the part of data post-processing.

In section 3.3.4, we set up one simple building model to calculate the thermal movement of the building, and in section 3.4.4, the least square adjustment has been programmed in code. During these processes in section 3.3.4 and 3.4.4, the model has been improved little by little, step by step, in order to bring the model to the real behavior of the buildings in the test area. After that, the model will be applied to the real case of our field study as shown in chapter 5.

In the proposed methodology, it is necessary to simulate the deformation of the target, but also the building where the RTS and the reference prisms are simulated.

The comparison between the model and the real results in the test area is presented in chapter 5. After the demonstration of the model, the improved strategy to be used in the monitoring that takes into account thermal effects is explained in chapter 6.

3 Modeling the behavior of buildings and monitoring systems when subjected to Thermal Effects

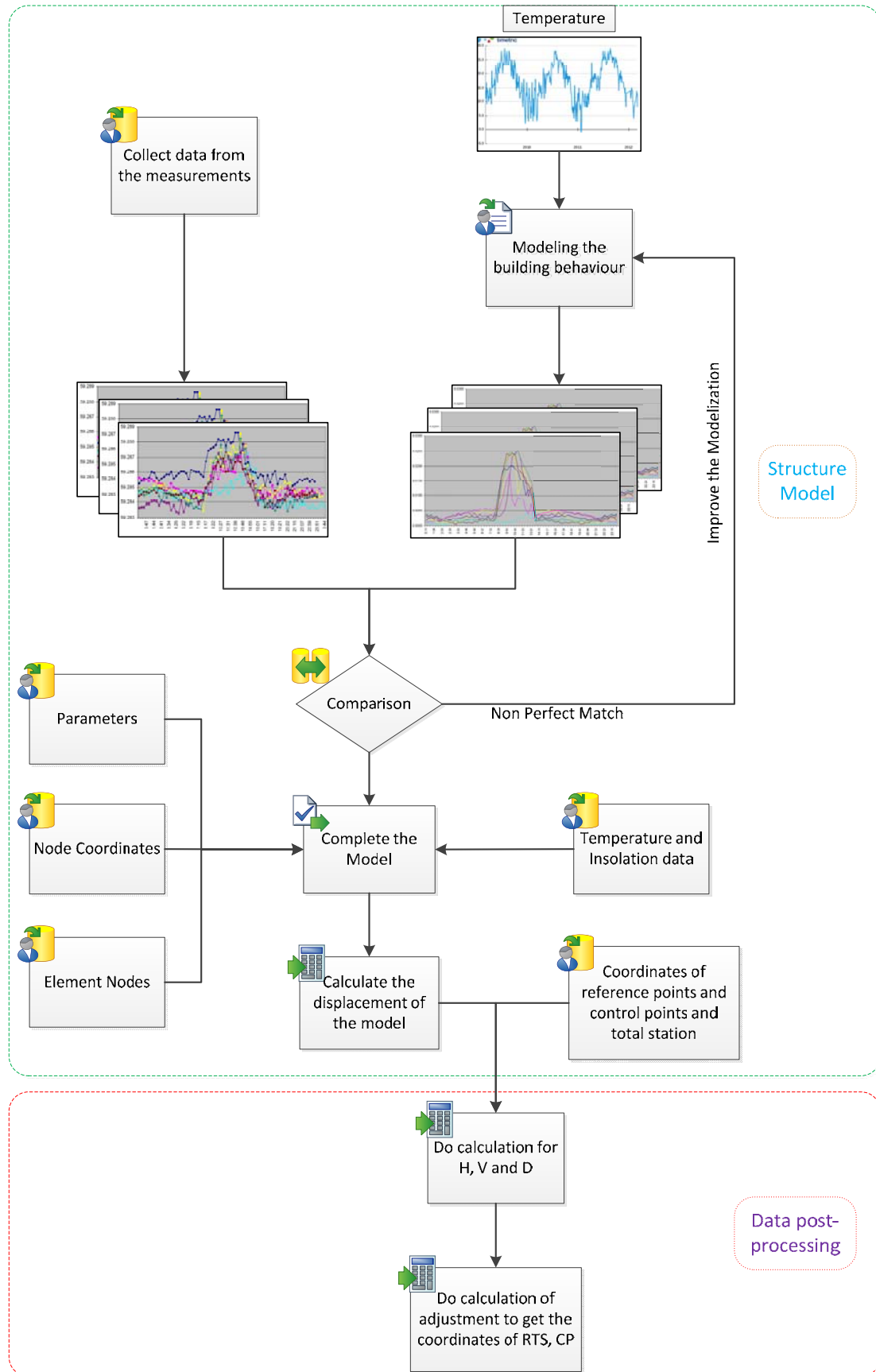


Figure 3.4 Flowchart showing the implementation of the conceptual model.

3.3 Modeling the movements of building subjected to external actions

As a consequence of the procedure outlined in Figure 3.4, it is necessary to compute the theoretical movements of given points of the buildings involved in the monitoring network when the external factors change. We envisage changes in the forces applied to the building (loads, winds etc.), but our analysis will mainly focus on the change in the thermal conditions endured by the pillars and the beams. The theory of the dilatation of the materials (section 3.3.2) states that the structure of the building will deform as a consequence of the expansion of its materials. In this section, a way will be established to compute the displacements of the nodes of a structure when it is subjected to a given field of changes in the temperature. As the deformation is relatively small, it has been supposed that the deformation remains in the elastic regime (section 3.3.1), and the whole compatibility problem will be solved using the well-known Stiffness Matrix Method to solve a 3D framed structure (section 3.3.3 and 3.3.4). Finally, in section 3.3.5 and 3.3.6, the displacement will be transformed into a global reference system in order to relate the changes to the real buildings in the scene.

3.3.1 Elastic deformation of structures

When a load is applied to a metal or other structural material, it will cause the material to change shape. This change in shape is called deformation. A temporary shape change that is self-reversing after the force is removed, allowing the object to return to its original shape, is called elastic deformation.

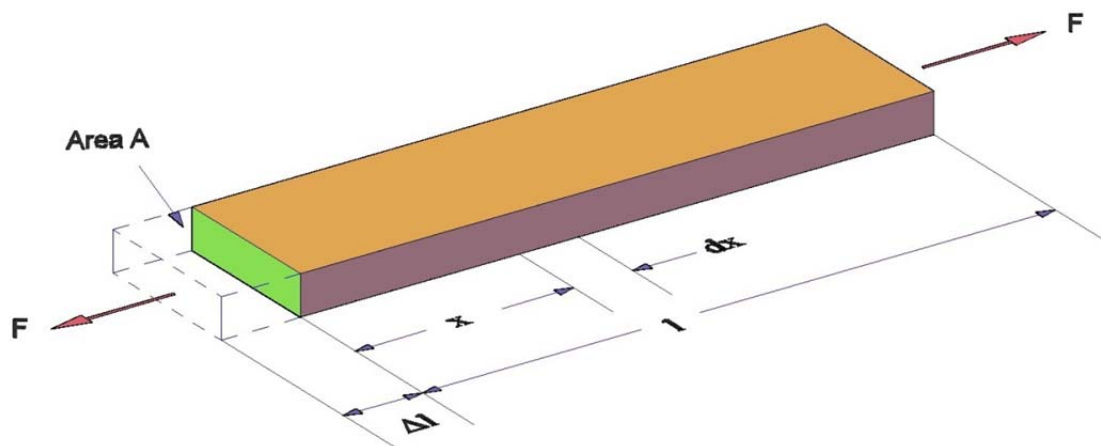


Figure 3.5 Deformation of a beam subjected to an axial load F .

3 Modeling the behavior of buildings and monitoring systems when subjected to Thermal Effects

Consider the member shown in Figure 3.5, which is of length l , has a cross-sectional area A , and is subjected to the axial force F . The stress is defined as the force per unit area. Representing this stress by σ , we thus have

$$\sigma = \frac{F}{A} \quad 3.3$$

The strain is given by the change in length per unit length. If we represent strain by ϵ , we then have

$$\epsilon = \frac{\Delta l}{l} \quad 3.4$$

where Δl is the change in length or the deformation that accompanies the force F .

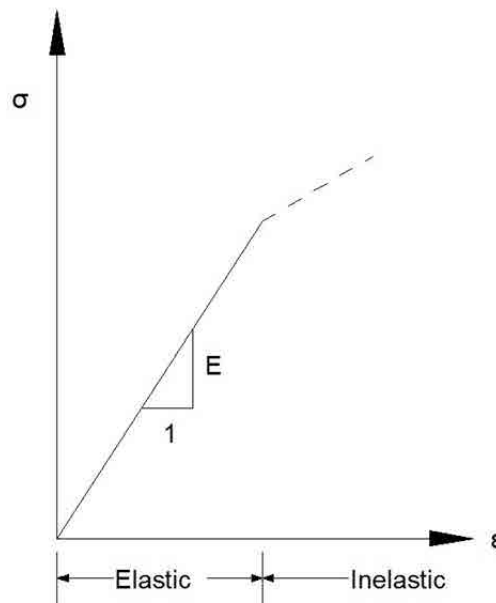


Figure 3.6 Stress-strain diagram.

For a linearly elastic material, if stress is plotted as ordinate against strain as abscissa, we have the linear relationship shown in Figure 3.6. For any given strain, there is a unique stress given by the relationship

$$\sigma = E\epsilon \quad 3.5$$

where E is Young's modulus or the modulus of elasticity. This modulus is a known material property which can be determined from an appropriate test procedure. Some interesting values for E are: 30GPa for High-strength concrete, 200GPa for steel, 190-210GPa for wrought iron and 11GPa for oak wood.

In the theory presented here, the terrain deformations have been considered small enough to guarantee that the deformations will remain in the elastic range.

Substituting, we obtain:

$$F = \frac{EA}{l} \Delta l \quad 3.6$$

or

$$F = k_a \Delta l \quad 3.7$$

The well-known Hook's law, where k_a , the axial stiffness, is defined as

$$k_a = \frac{EA}{l} \quad 3.8$$

If we want to start introducing the Stiffness Matrix Method, let us consider the beam in Figure 3.5 as one element of the structure linking the two end nodes (Figure 3.7).

Now the member-end forces and displacement are separately identified $-F_1$ and δ_1 at end 1, and F_2 and δ_2 at end 2.

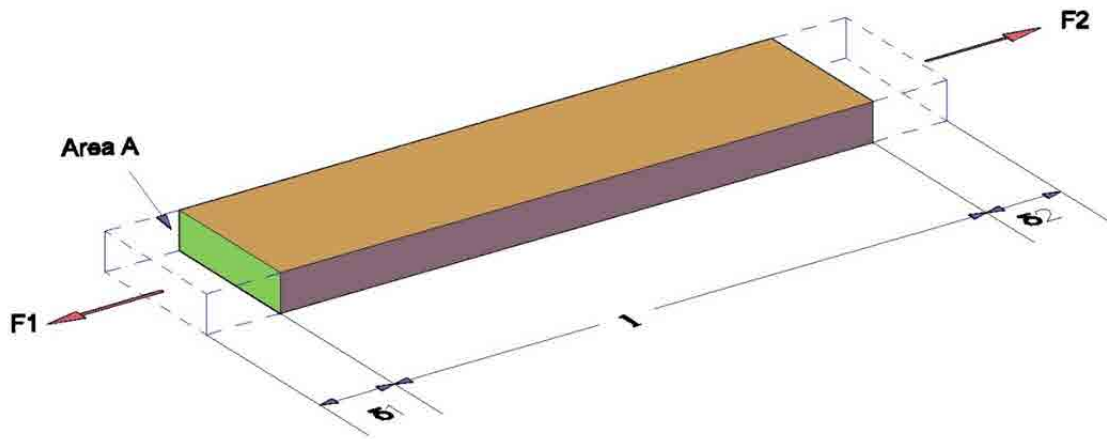


Figure 3.7 Member-end forces and displacements.

Comparing Figure 3.5 and Figure 3.7, it is clear that $F = F_1 = F_2$ and $\Delta l = \delta_1 + \delta_2$. Substitution of these relationships into Equation 3.6, shows:

$$F = F_1 = \frac{EA}{l} \Delta l = \frac{EA}{l} \delta_1 + \frac{EA}{l} \delta_2 \quad 3.9$$

$$F = F_2 = \frac{EA}{l} \Delta l = \frac{EA}{l} \delta_1 + \frac{EA}{l} \delta_2 \quad 3.10$$

The subsequent translation into matrix form leads to:

$$\begin{bmatrix} F_1 \\ F_2 \end{bmatrix} = \begin{bmatrix} \frac{EA}{l} & \frac{EA}{l} \\ \frac{EA}{l} & \frac{EA}{l} \end{bmatrix} \begin{bmatrix} \delta_1 \\ \delta_2 \end{bmatrix} \quad 3.11$$

In an abbreviated form, this equation can be expressed as

$$\{F\} = [k]_a \{\delta\} \quad 3.12$$

where $\{F\}$ and $\{\delta\}$ are the member-end force and displacement vectors, respectively, and $[k]_a$ is the member axial stiffness matrix. Equation 3.12 is the two-dimensional equivalent of Equation 3.7 and the individual elements of $[k]_a$ are in terms of EA/l , which reflects the axial stiffness of the member as it is defined by Equation 3.8.

3.3.2 Thermal effects

Under normal conditions, most concrete structures are subjected to a range of temperature imposed by environmental conditions. Their behavior is strongly influenced by the temperature change which comes from sun radiation, and the thermal expansion varies linearly within the range of normal ambient temperature. If one beam within the structure is subjected to an increase or decrease in length due to thermal changes, then it is necessary to use the thermal strain equation to obtain the solution.

If a structure member of length L is subjected to a temperature increases ΔT , the member will undergo an increase in length of

$$\Delta L = \alpha \Delta T L \quad 3.13$$

where α is the coefficient of thermal expansion. Some interesting values of α for some structural materials are ($10^{-6} \text{ }^\circ\text{C}^{-1}$): 12 for concrete, 11 to 13 for steel, 10.8 for carbon steel and 10.1 to 17.3 for stainless steel.

The strain caused by a change in temperature from T_0 in the reference configuration to T in the current configuration is called thermal strain, $\epsilon_{\text{thermal}}$, and it can be expressed by the linear relation,

$$\epsilon_{\text{thermal}} = \frac{\Delta L}{L} = \alpha(T - T_0) \quad 3.14$$

In linear situations, the force F_{thermal} that will produce the same strain as the change of temperature ΔT can be calculated (using Equation 3.4 & 3.6) as:

$$F_{\text{thermal}} = EA\alpha\Delta T \quad 3.15$$

This force will be used as the mechanical equivalence of the thermal effect in order to compute the deformation of the structure.

3.3.3 Stiffness matrix method

At present, for frame structures made up of bars, beams and columns, whether statically determinate or indeterminate, most computer structural analysis is performed using the stiffness matrix method. This method yields the displacement and forces directly, whereas with others (as with the flexibility method) the displacement is not obtained directly. Furthermore, it is generally easier to formulate the necessary matrices for the computer operations using the stiffness method. Once this is done, the computer calculations can be performed efficiently. Separating out the load and displacement terms, we could write the simultaneous equations as a matrix equation:

$$\{\mathbf{External\ loads}\} = [\mathbf{Stiffness\ coefficients}] \times \{\mathbf{Node\ displacements}\} \quad 3.16$$

where the curly brackets denote a column vector (that is, an $n \times 1$ matrix, where n is the number of degrees of freedom) and the square brackets denote a square ($n \times n$) matrix. Solution then requires the inversion of the *stiffness matrix* to obtain the unknown displacements, which can be done very efficiently by computer. This approach is known as the stiffness matrix method, and can be summarized as follows:

- (a) Formulate the stiffness matrix for each member, relating forces and displacements at the member local stiffness matrix.
- (b) Assemble the local matrices using conditions of equilibrium and compatibility at the joints to give a global stiffness matrix for the entire structure.

$$\{\mathbf{F}\} = [\mathbf{k}]\{\mathbf{\delta}\} \quad 3.17$$

- (c) Invert the stiffness matrix and hence determine the unknown displacements.

$$\{\mathbf{\delta}\} = [\mathbf{k}]^{-1}\{\mathbf{F}\} \quad 3.18$$

- (d) Apply the boundary conditions by substituting the corresponding prescribed nodal displacement values in the global system of equations. This results in the

elimination of the row and the column corresponding to the prescribed degree of freedom, reducing the global system of equations.

- (e) Substitute back into the local matrix equations (a) to find the member forces.
- (f) When the displacement is known, the external and internal forces in the structure can be calculated using the force-displacement relations for each member. The support reactions are obtained through the equations of equilibrium, which were not considered in the reduced system. Given the nodal displacements, it is possible to calculate the reactions at the supports by

$$\mathbf{f} = [\mathbf{k}] * \{\boldsymbol{\delta}\} \quad 3.19$$

In the annex section A.IX and A.X, there is more information about how the local stiffness matrix (a) is formulated.

3.3.4 Description of the program

a. Flowchart of the main steps of the numerical code to compute the structure

In the process of running the program to calculate the displacement, there are mainly three computing parts: calculating the stiffness matrix, the forces on each node of the structure model, and the final displacement of the structure. Here, we will use the software of MATLAB (2013a) to create the numerical model to calculate the movement of buildings (the code can be seen in the Annex A.XI). The process developed in the program is shown in the flowchart (Figure 3.8). The first step is input data, which are the properties of the model's elements (such as E, G and so on), node coordinates, elements' node number, the real temperature data and the boundary conditions of the model. The second step is to calculate the stiffness matrix based on the input data. After solving the system of equations, the last step is to output the results that are the displacement of each node in the model.

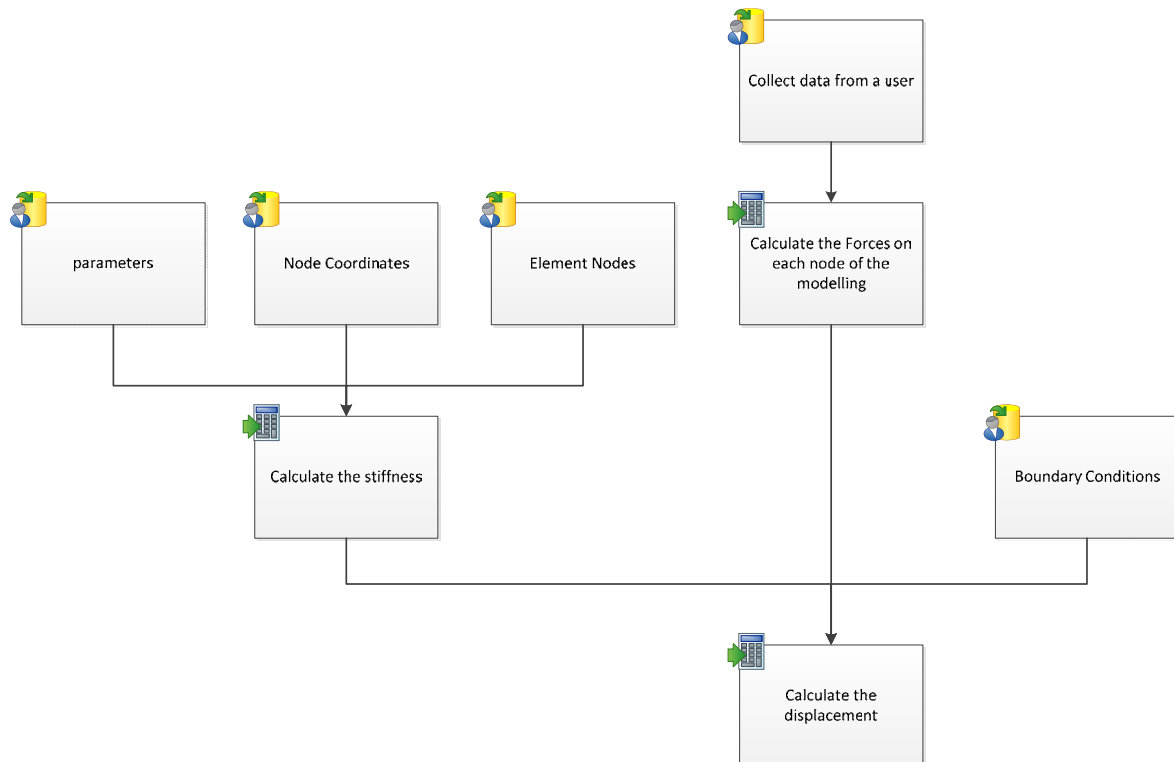


Figure 3.8 Flowchart of the structure modelling.

b. Running example

(1) Input example file

In order to show the functions of the model program, a simple example has been programmed. There are five kinds of input files, which are the temperature, node coordinates, element nodes, parameters and boundary conditions.

In this example, the program calculates eight epochs' data using the same parameters for every element of the structure (Table 3.3). The beams and columns are the same size in the section area, which is 30cm by 30cm. The data of the temperature, which we got from the weather station in Campus-Nord of UPC, is from the first day of September in 2013 (Figure 3.9). The frequency to observe the temperature is every three hours. The model is a simple two-story structure, and its size is 5m*5m*8m and the height of each floor is 4m. There are 8 beams and 8 columns in total and 12 nodes (Figure 3.10). The inside temperature stays the same, at 21 degrees. For the boundary condition, we fix the basement node in X, Y and Z, which means the node in the basement cannot be moved in X, Y and Z directions.

3 Modeling the behavior of buildings and monitoring systems when subjected to Thermal Effects

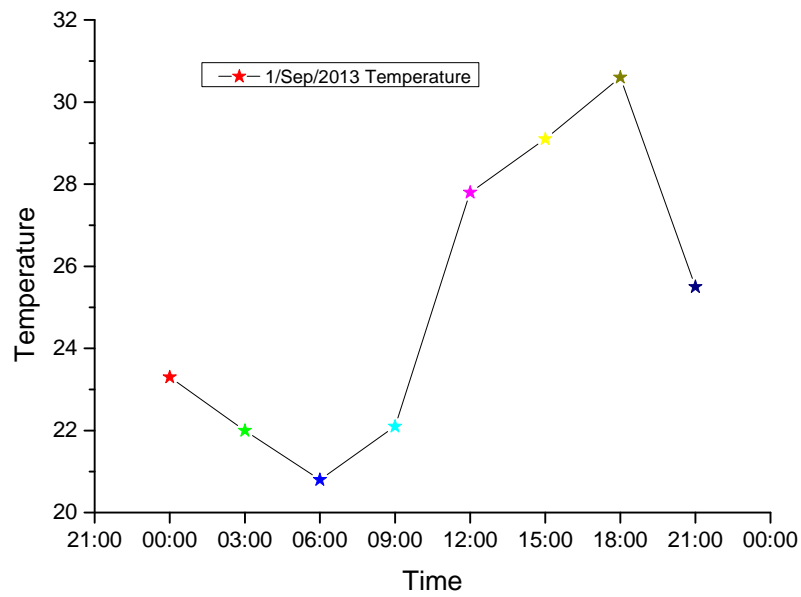


Figure 3.9 Temperatures on 1st September 2013.

Table 3.3 Parameters of the building.

E (N/m ²)	Area (m ²)	I _y (m ⁴)	I _z (m ⁴)	G (N/m ²)	J (m ⁴)
3.00E+10	0.09	6.75E-04	6.75E-04	7.50E+09	1.35E-03

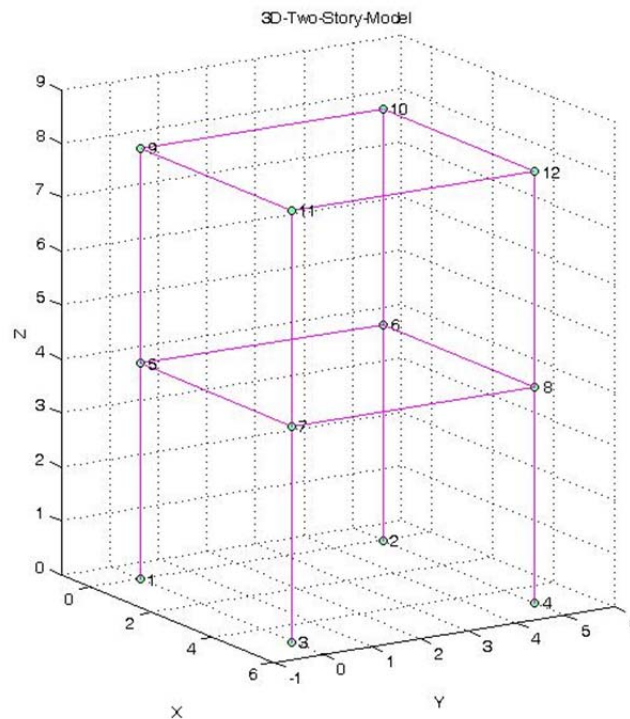


Figure 3.10 Two stories building model.

(2) Typical running time

In total, the running time of the two-story model to calculate eight epochs' data is only 5.02 seconds.

(3) Output example results

There are 8 results graphs that have been drawn based on the result data. In this simple model, the results that have been drawn in Figure 3.11 and Figure 3.12 indicate that the node in the corner has the same displacement trend in X, Y and Z, for example, node-6 and node-10, from 6:00 clock to 18:00 clock, the node goes down in X-direction, however, in Y-direction it goes up. For the rest of the time, the node goes up in X-direction and falls in Y-direction.

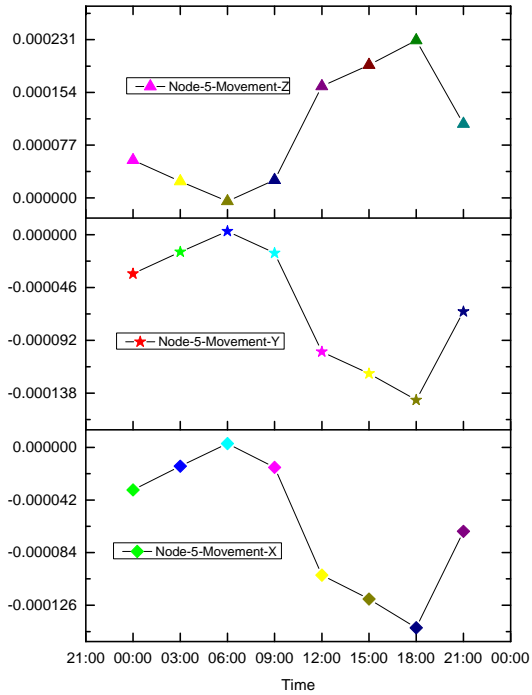
Figure 3.11 indicates that node-5 and node-6, as well as node-7 and node-8, have the same development trend in X direction. As for the pair of node-5 and node-7, and node-6 and node-8, these follow the tendency in Y-direction. In the direction of Z, all of the

nodes have the same movement track which is the value of Z: every node goes down when the temperature falls.

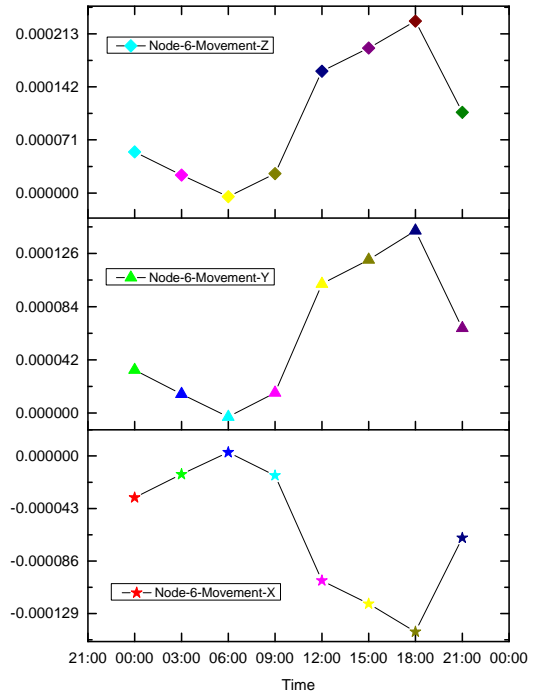
Similarly, Figure 3.12 shows very similar results to Figure 3.11, with node-9 and-10, and node-11 and node-12, behaving the same way in X. In addition, node-9 and node-11, and node-10 and node-12 also have the same trend in Y. For the Z direction, every node shows the same movement track which is the value of Z: every node goes down when the temperature falls.

Figure 3.13 and 3.14 are the results shown in 3D at the different epochs from an overall perspective. Based on the results above, it can be seen that the movement of every node of the structure gets the maximum or minimum value when the temperature reaches the lowest or highest degree. When the temperature falls, the structure moves towards the center of the structure, for instance, the structure expands outward from epoch 6:00 to epoch 18:00. During this time, the temperature rises from 20.8 degrees at 6:00am to 30.6 degrees at 18:00pm. In contrary, when the temperature falls in the night, the structure shrinks toward the center of the building.

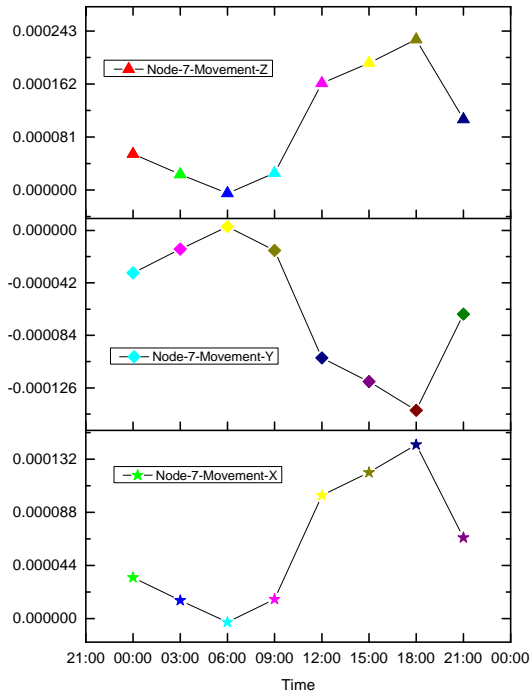
3 Modeling the behavior of buildings and monitoring systems when subjected to Thermal Effects



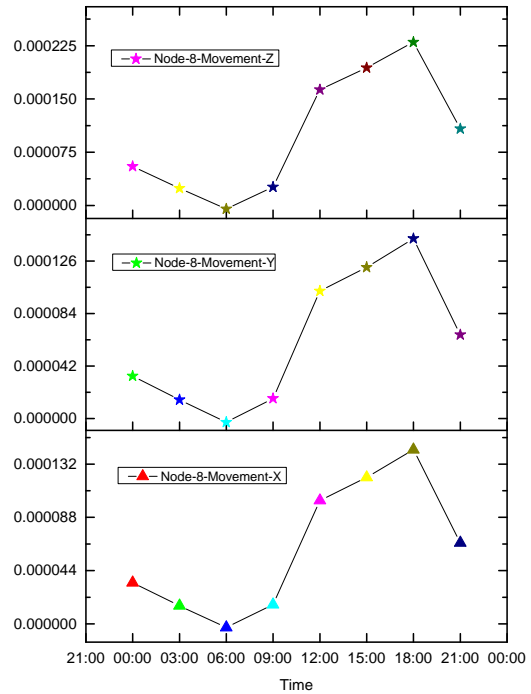
(a)



(b)



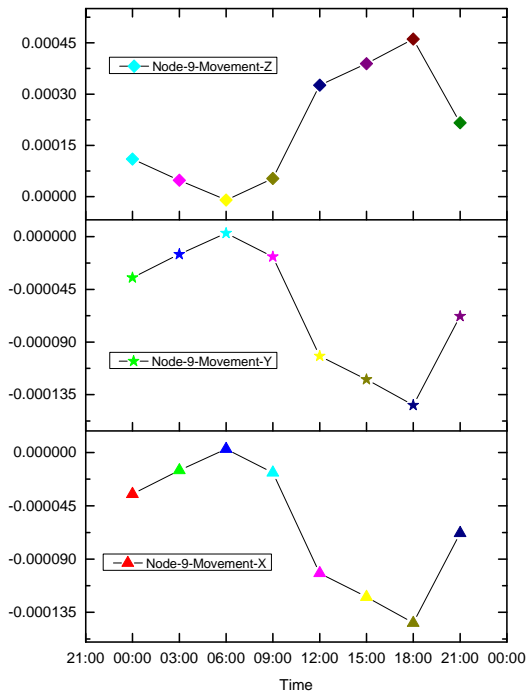
(c)



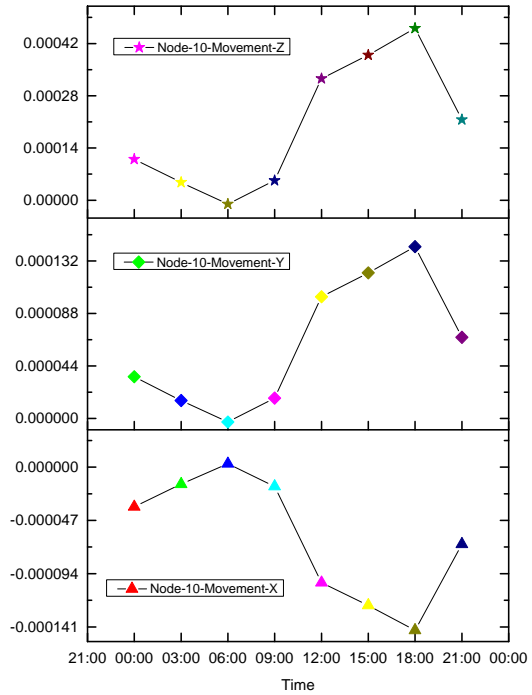
(d)

Figure 3.11 a-Node 5 movement; b- Node 6 movement; c- Node 7 movement; d- Node 8 movement.

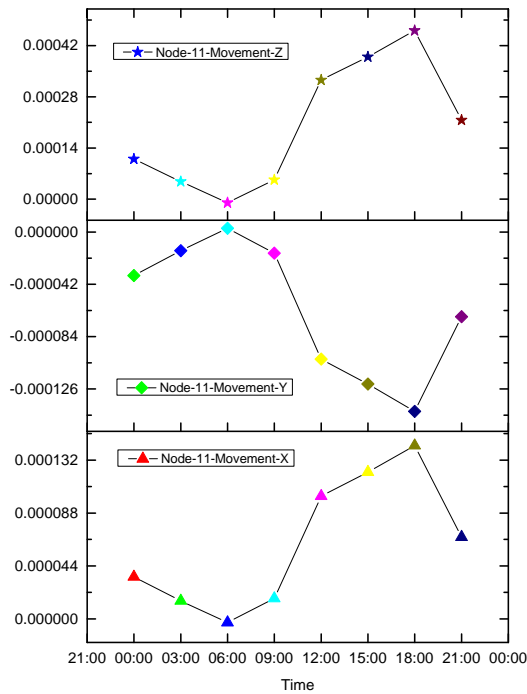
3 Modeling the behavior of buildings and monitoring systems when subjected to Thermal Effects



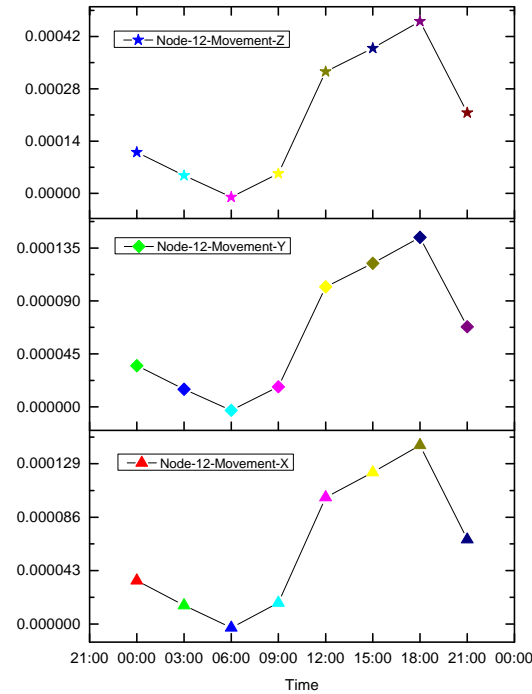
(a)



(b)



(c)



(d)

Figure 3.12 a-Node 9 movement; b- Node 10 movement; c- Node 11 movement; d- Node 12 movement.

3 Modeling the behavior of buildings and monitoring systems when subjected to Thermal Effects

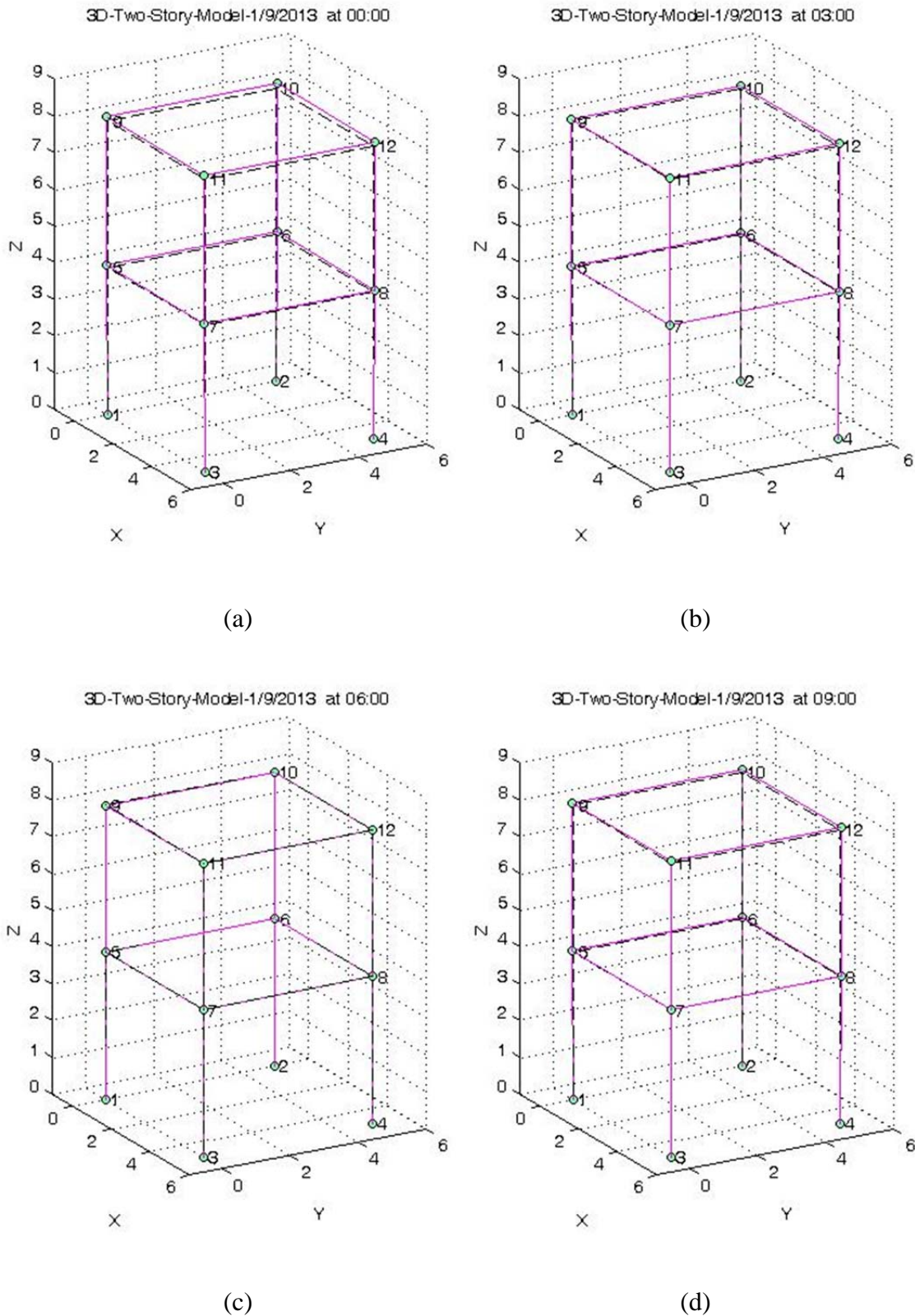


Figure 3.13 a-model result at 00:00; b- model result at 03:00; c- model result at 06:00; d- model result at 09:00.

3 Modeling the behavior of buildings and monitoring systems when subjected to Thermal Effects

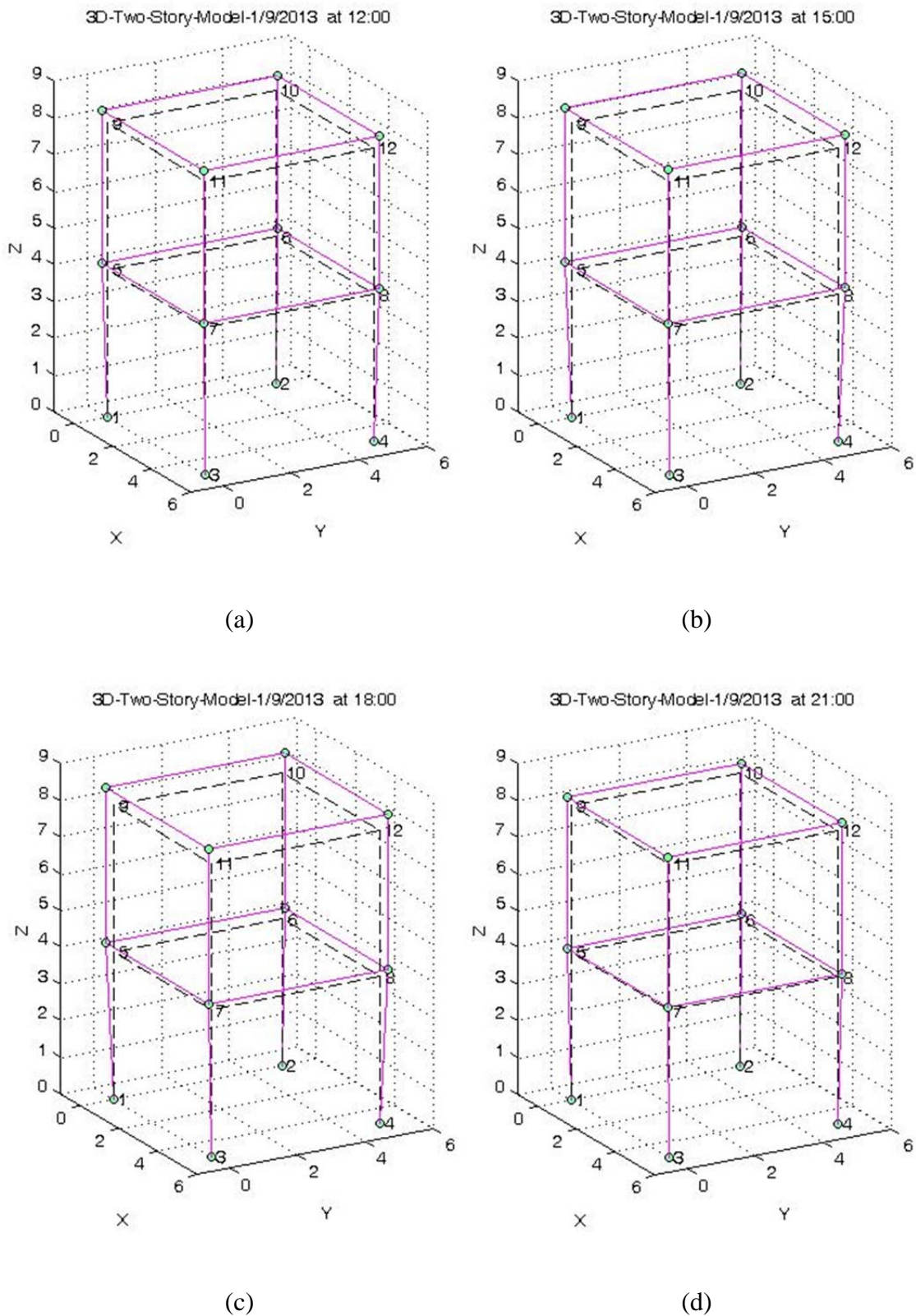


Figure 3.14 a-model result at 12:00; b- model result at 15:00; c- model result at 18:00; d- model result at 21:00.

3.4 Least square adjustment by indirect observations equations

Like intersection, resection is suitable for locating an occasional station and is especially well adapted to inaccessible terrain. In the monitoring of buildings, the resection is used to check or update the coordinates of the base point at the beginning of each epoch of measurement after measuring the reference prisms. Figure 3.15 shows the position of the RTS on a building whose coordinates will be obtained after the observation and adjustment to the reference prisms which are marked with a red dot on the nearby buildings.

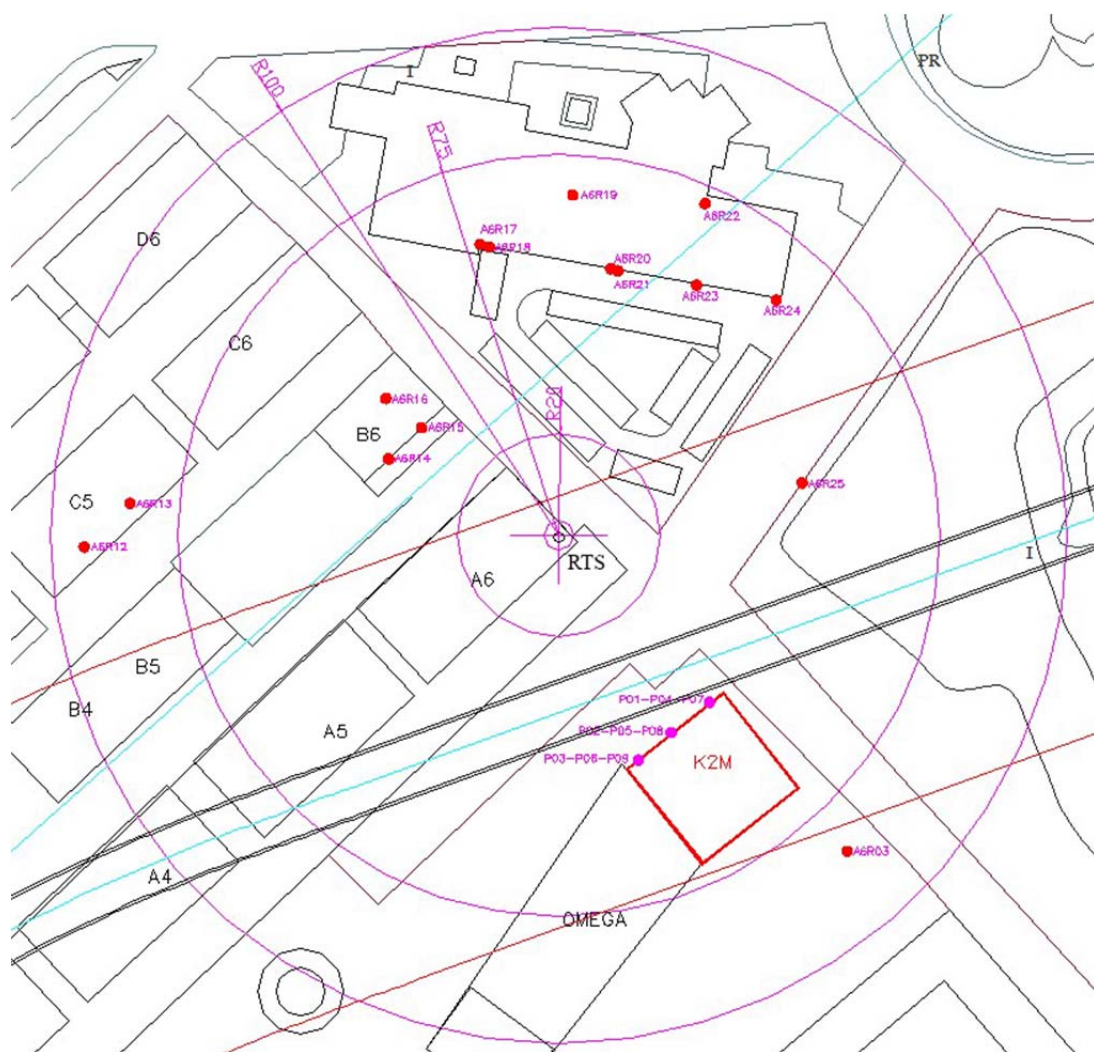


Figure 3.15 Example of a monitoring setup around a RTS.

Inverse resection is a method to determine the unknown plane position of an occupied station by observing theodolite (or Total Station) directions to three or more given

points whose coordinates are known. Directions to three points are the minimum requirement; a unique solution is obtained. If there are more than three known points available or if we also measure distance to these references, redundant observations are available and the coordinates of the unknown point can be calculated using the least squares method. This computation requires the formation of a set of observation equations that yield "normal equations" that are solved for the best estimates of the coordinates of the resected point. Since the observation equations are a linearized approximation, the least squares solution process is iterative. In the case that the initial coordinates are sufficient, a unique iteration is necessary. That is, approximate values are assumed, corrections computed and previous values updated; the process is repeated until the corrections become negligible. In the following sections, the main points of the resection computation (and the program developed to undertake it) have been described.

3.4.1 Least square adjustment principle

Least square adjustment (LSA) is a model for the solution of an overdetermined system of equations based on the principle of least squares of observation residuals. Thus its core is least square. As we know, the sum of the squares of residuals must be minimized in order to obtain the most probable values, as shown in Equation 3.20:

$$\sum v^2 = v_1^2 + v_2^2 + v_3^2 + \dots + v_n^2 = \mathbf{minimum} \quad 3.20$$

In the process of LSA, when the measured angle or distance equation is not linear, it is necessary to linearize the equations using Taylor's theorem. In Annex A.V and A.VI, there is more information about the LSA and the steps followed to linearize the measured angle or distance equations.

What is more, the distance correction based on the change in environment conditions (section 3.4.2) and blunder detection (section 3.4.3) have been introduced into the program as well.

3.4.2 Distance correction

When measuring distances, there is always a change in environment conditions which influence the accuracy of the results (Afeni 2011). At the same time, it is also one source of error. In order to correct the distance, the Barrel and Sears equations have been introduced into the program to correct the measurement data. The correction of the measurement or gross distance D is done with each RTS data from the weather station associated. The formula of the corrected distance D_{corr} is the Barrel and Sears. The data from the weather station are: dry temperature ($^{\circ}C$), pressure (mbar) and relative humidity (%). As for the equations and steps for the distance correction, more information can be found in Annex A.III.

3.4.3 Blunder detection

In the practice of surveying works, it is impossible for the data sets to be free of blunders (Kowalczyk and Rapinski 2014). Blunders are those errors that occur rarely and have identifiable causes (Schwarz and Kok 1993, Junhuan 2005). The aim of blunder detection is to look for blunders in a set of observations and remove them from the data set. The method of Baarda test (Baarda 1968) has been introduced into the program to detect the outliers in observations. This program uses the same criterion for rejection of blunders as Amer (Amer 1979) and Harvey (Harvey 1994), which is 3.29 as the rejection level. The equations that have been used in the program are shown in Annex A.VII.

3.4.4 Description of the program

a. Flowchart of the main steps of the least square adjustment

The LSA program consists of two parts: one is horizontal data adjustment, and the other is height data adjustment. In the first part, the approximate coordinates of the RTS (upper left box in the flowchart) are estimated to solve a resection problem, and the raw data have to be introduced into the program after pre-processing to adjust the format of the data, and then the program calculates the coefficient matrix (\mathbf{B}), weight matrix (\mathbf{P}) and vector of numeric terms (\mathbf{I}). The weight matrix depends on the instrument's distance measuring accuracy and angle measuring accuracy. Based on these matrixes, the vector

of residuals (V) and the vector of 'unknowns' (xy), which are corrections to the approximate coordinates, can be calculated. Later, the W-Baarda has been introduced into the program to deal with the error data and to compute the primary coordinates of RTS. After that an iteration of W-Baarda has been introduced to filter the error data and then re-compute the final coordinates (X and Y) of RTS. The second part follows a similar procedure to calculate matrixes like B , P and I . The difference to the first part is that the simulated angle and distance equations for the height data adjustment are linear. This way, the two matrixes of V and z (the same as xy) can be obtained. After these computation, the final coordinate (Z) of RTS is obtained. After the adjustment the coordinates for the RTS are obtained and the coordinates for the control points can be obtained by a direct computation with the raw data. After the two main steps, the final coordinates of the control points can be obtained. The flowchart of the main steps of the LSA is illustrated in Figure 3.16.

3 Modeling the behavior of buildings and monitoring systems when subjected to Thermal Effects

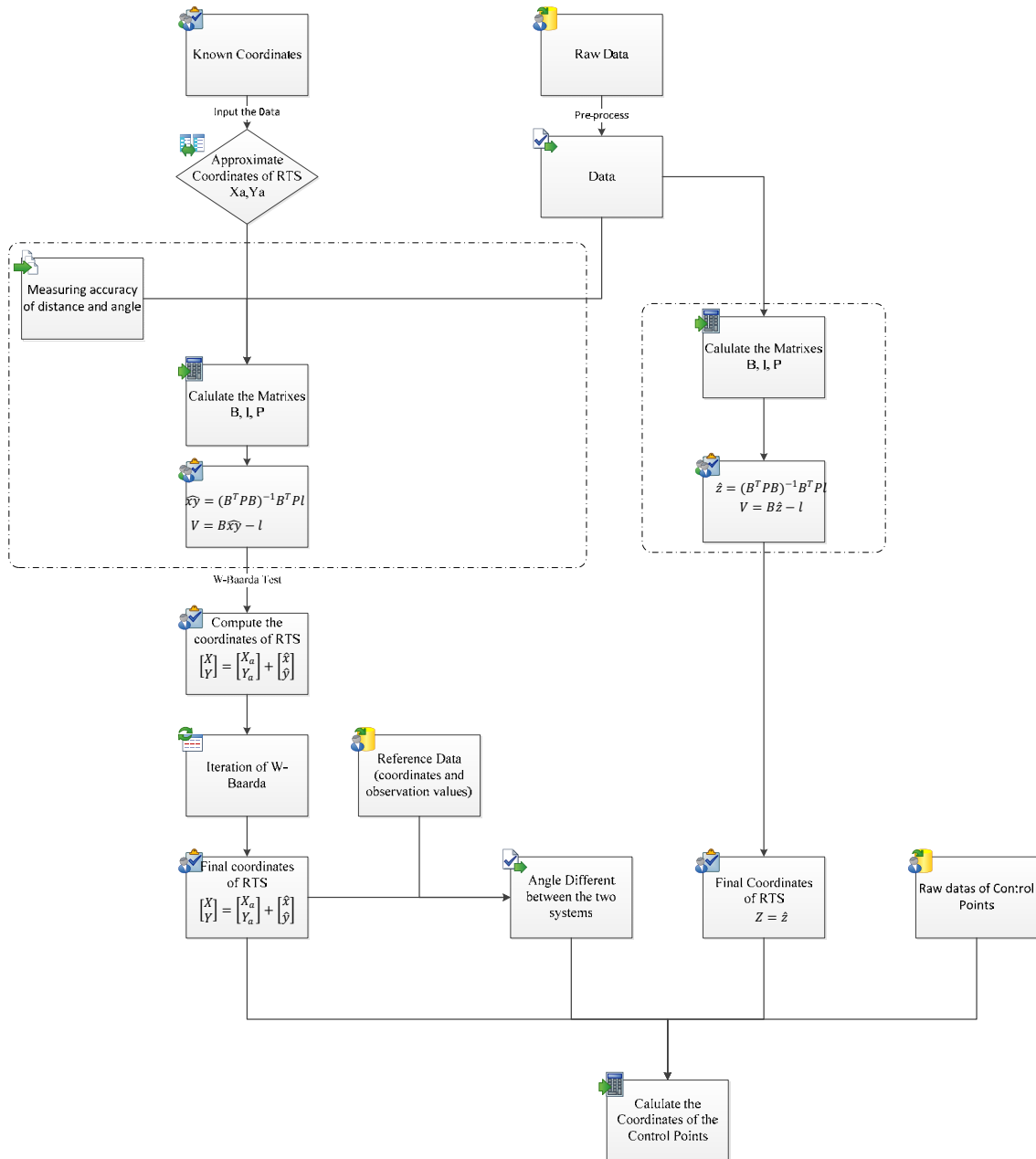


Figure 3.16 Flowchart of the least square adjustment.

b. Running example

As a simple example of the work done by the LSA program, a full set of data has been enclosed in Annex A.I.

(1) Input example file

Eight epoch's data have been selected to test the least square adjustment program. In this program, we need the reference point raw data (from Table 1 to 8 in Annex A.I) and control point raw data (from Table 9 to 16 in Annex A.I), which contain the H (horizontal angle), V (vertical angle), L (distance) and the coordinates of X, Y and Z. There are 13 reference points and 9 control points.

(2) Typical running time

In this example, it took 0.3190 seconds for the eight epoch's data to obtain the final coordinates of the control points.

(3) Output example results (data and graphs)

After the computing, the results have been obtained (from the Table 1 to 10 in Annex A.II), which include the evolution of the coordinates in different epochs. In order to make the analysis easier, the trend curve graphs have been drawn. From the Figure 3.17, it can be seen that the RTS is moving as the time passes. For the X and Y, these keep the same movement trend, where they reach the peak point at 6:00am and the bottom point at 18:00pm. Compare with X and Y, Z shows a totally opposite trend, reaching the lowest point at 6:00am and the highest point at 18:00pm. From Figure 3.18 it can be seen that the 9 control point move similarly and follow the same pattern during the one day period. As for X and Y, all of the control points show the opposite movement compare with RTS, and they have the same displacement trend with Z. Both the control points and the RTS follow the same trend in Z.

This kind of results proves that the structure moves with the thermal change. The influence of thermal change on the structure is a factor that cannot be neglected in the structure health monitoring practice.

3 Modeling the behavior of buildings and monitoring systems when subjected to Thermal Effects

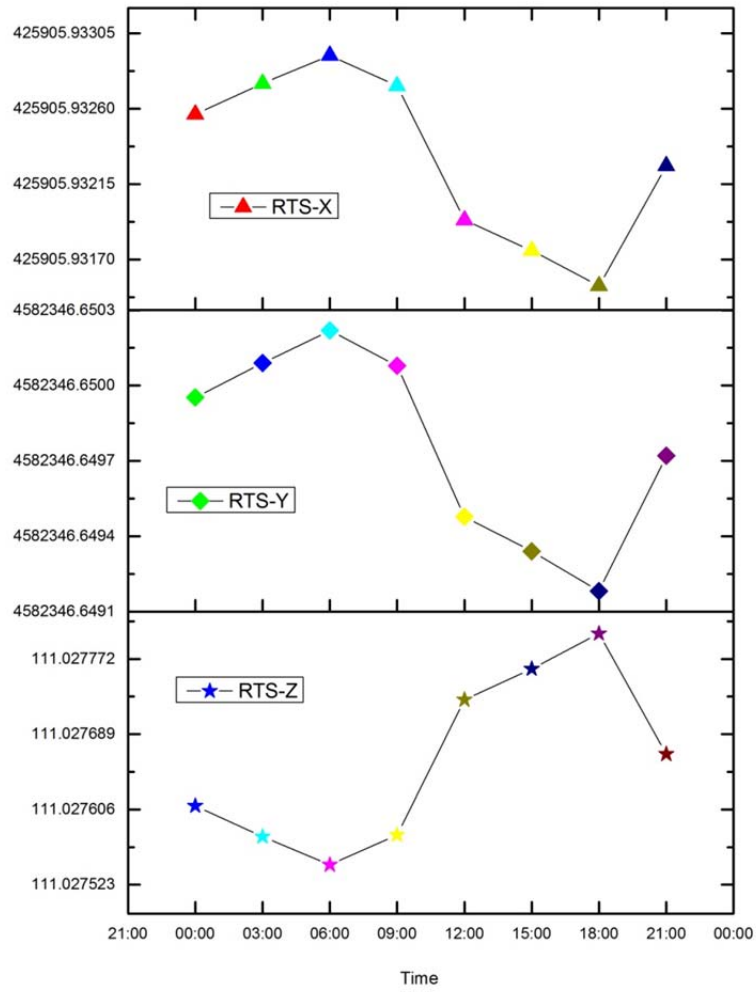


Figure 3.17 RTS movement.

3 Modeling the behavior of buildings and monitoring systems when subjected to Thermal Effects

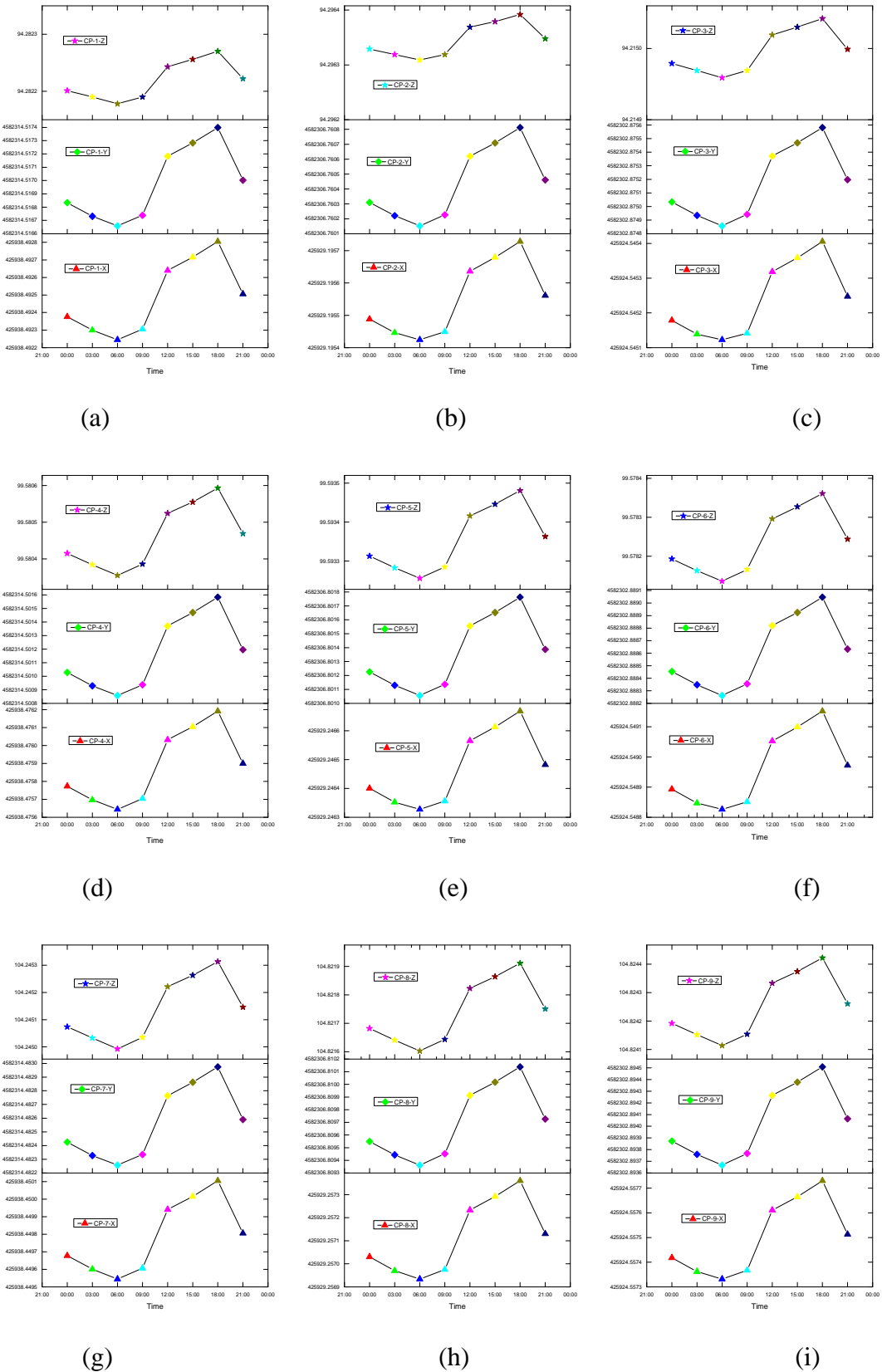


Figure 3.18 The movement of the control points. a-control point-1, b-control point 2, c-control point-3, d-control point-4, e-control point-5, f-control point-6, g-control point-7, h-control point-8, i-control point-9.

4 Experimental work Test area

Campus Nord UPC

This chapter mainly focuses on the experimental work test area, which includes the area selection process, overall design of the systems, and installation. It also includes the data acquisition and preliminary analysis of the temperature and insolation. This work will provide the basic for the follow-up work.

4.1 Area selection process

The biggest advantage of RTS is that it can provide real-time, continual and automatic monitoring of the objective with high accuracy. However, there are some requirements for the monitoring area based on the characteristics of RTS. RTS requirements for the area are as followed.

Lines of sight: It is necessary to keep the lines of sight clear between RTS and the prisms, so the RTS requires a suitable vantage point.

Power supply: For long-term monitoring, Un-interruptible Power Supply (UPS) is a necessary measure against power cuts at the RTS during reading cycles.

Sight distance: For high accuracy displacement monitoring, the sight distance between RTS and the prisms should be as short as possible.

In our project, we considered several possible buildings as candidates for the experiment. Finally, the Omega building (Campus Nord of the UPC, Barcelona, Spain) was selected for practical reasons (as shown in Figure 4.1). In particular, the two extremes of the Omega were instrumented and studied: the “K2M” and the “SO bloc”.



Figure 4.1 Plan of the monitoring network.

4.2 Overall design of the systems and sensors

The selection and the instrumentation of a building that serves as a real experiment is a key point in the development of the general concept presented above. This is a real-scale experiment that use a building which will not be affected in the near future by any public work, so $\delta_{tunneling} = 0$. Thus, $\delta_{observed}$ will be equal to $\delta_{thermal}$, i.e., the movement of the building will be determined purely by environmental causes.

This building was “over-instrumented”; which means that we installed a number of instruments and sensors well beyond the standard practice in building monitoring during tunnel construction. Therefore, we had a certain redundancy that permit us to observe the behavior of the building better and that also allowed the creation and the tuning of the phenomenological model.

In the full-scale experiment, we used 3 RTS to measure the building displacement, and some different kinds of sensors to survey the temperature, wind, air pressure, insolation, inclinometer and so on. All of the data will be sent to the database via the internet, and the users can manage the building’ state in real time (as shown in the Figure 4.2). In the database the raw data will be checked and filtered, prior to using the real data to adjust the model.

4 Experimental work Test area Campus Nord UPC

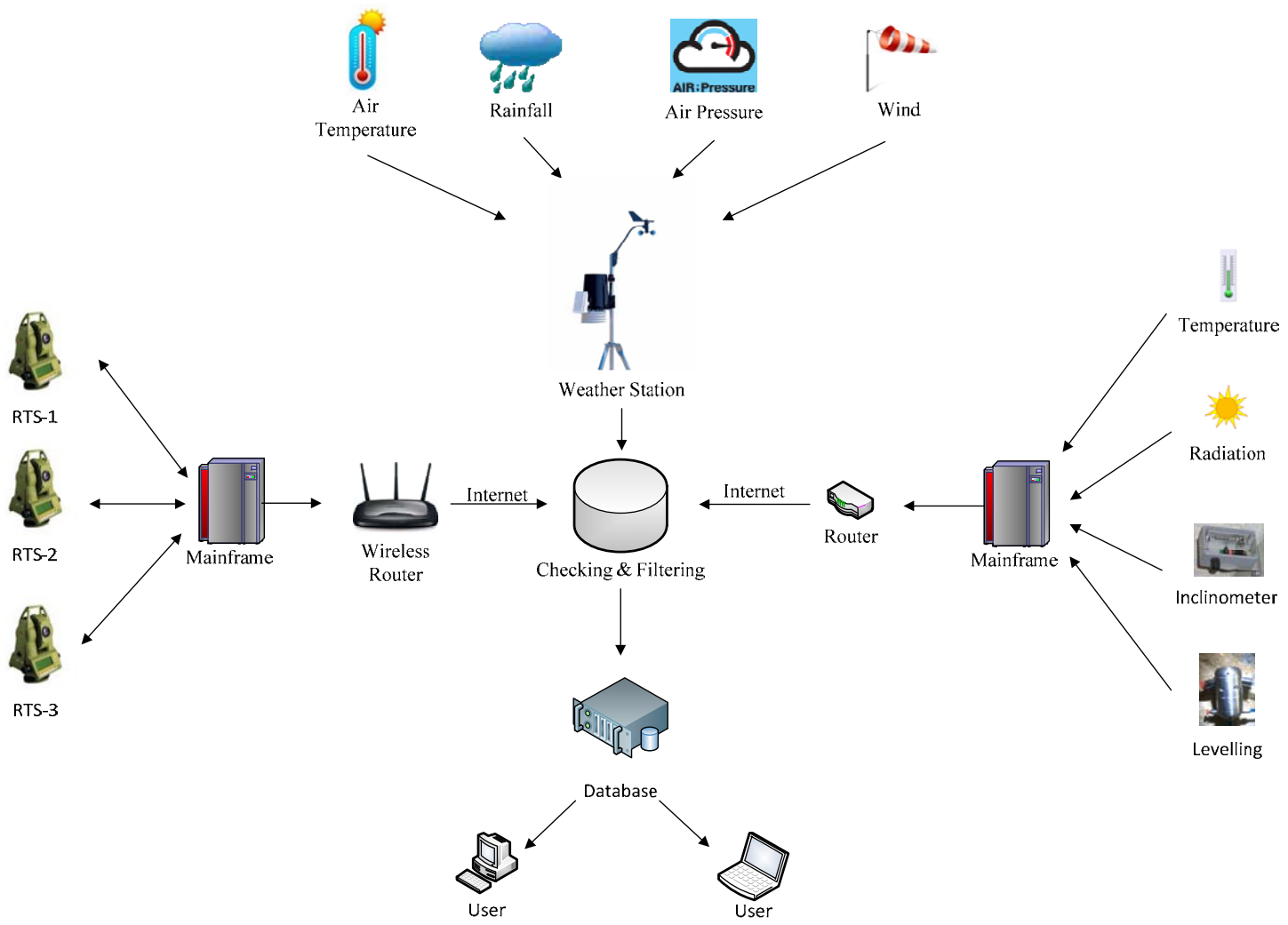


Figure 4.2 Overall experiment design flowchart of the systems.

4.3 System and sensors installation

In the experimental buildings, the monitoring systems consist of RTS, thermometers, inclinometers, insolation sensors, levelling and meteorological data (air pressure, air temperature, wind speed and direction, rainfall). All of the instruments are managed by Geoscope software designed by SOLDATA company and used for real-time data management.

In the communication aspect, all the sensors are wired to a central data logger point. Some Wi-Fi routers permit the linking of the RTS with the central data logger; from there, the data can be transmitted via the internet network to the main Database.

The economic and technical help of the SOLDATA Company has been of paramount importance for the installation of the aforementioned devices. The K2M and SO Bloc buildings were equipped in 2013.

a) Robotic Total Station (RTS)

Robotic Total Stations (RTS) are a comparatively recent monitoring instrument, which have been widely used in various civil engineering areas to measure the movement of structures and slopes in the last decades (Cosser, Roberts et al. 2003, Walker, Hitchcock et al. 2006, Stiros and Psimoulis 2010, Afeni and Cawood 2013). As we know, RTS allow the operator to drive the instrument from a distance via remote control with the specific software to acquire the 3D coordinates of the monitoring points. This eliminates the need for an assistant staff member as the system aims the prism reflector automatically, 24 hours a day.

The basic principle of RTS is that they emit a narrow infrared or laser beam which is reflected back by a specific reflector and is received by the RTS. Once taught the location of a reflector, the RTS returns to re-determine the location of that prism during each monitoring cycle. This course allows surveying the location of the reflector in 3D polar coordinates and they measure independently: (i) the distance between the reflector and the RTS; (ii) the angle of the line of sight relative to the vertical axis; (iii) the horizontal angle of the line of sight relative to a selected reference horizontal direction. Based on these polar coordinates, 3D coordinates of the reflector in a selected coordinates system can be automatically calculated. Those final

results can be computed to one millimeter accuracy for distances up to a kilometer in favorable conditions (Stiros and Psimoulis 2010).

Around the Omega building, we used three RTS (Leica TCA2003 and Leica TCA1800) to monitoring the building's deformation. The features of the RTS are Lens augmentation: 30 x; Angular precision: ± 0.15 mgon; Distance precision: $\pm (1\text{mm} + 1\text{ppm})$; Working distances in the experimental area: 5 to 150 m; Rotation speed: 45°/s. Figure 4.3 indicates a typical operating Robotic Total Stations (RTS) in our experiment. We use the prism as the reflector for control and reference (Figure 4.4).



Figure 4.3 Example of RTS installed on A6-building (left) and N2-building (right) in UPC Nord Campus.



Figure 4.4 Prisms on the K2M building.

b) Sensors

In order to obtain more information about the monitoring object building, we installed

- Temperature sensor (Trademark: HERTEN; Model: Pt-100; Dimensions: 6cm long, 6mm diameter. Silicon cable with 3 wires; Range: -50°C to $+180^{\circ}\text{C}$; Precision: $\pm 0,15^{\circ}\text{C}$);
- Insolation sensor (Trademark: Apogee Instruments, distributed by Campbell Scientific; Model: Silicon Pyranometer CS300; Accuracy: $\pm 5\%$ for daily total radiation; Long-term stability: $<2\%$ per year; Operating temperature: -40° to $+55^{\circ}\text{C}$; Measurement range: 0 to 2000 W/m^2 (full sunlight 1000 W/m^2); Light spectrum waveband: 300 to 1100 nm; Dimensions: 2.4cm diameter, 2.75 cm height);
- Inclometers (Trademark: Slope Indicator; Model: EL tilt sensor, Range: ± 40 arc minutes; Resolution: 1 arc second; Repeatability: ± 3 arc seconds; Operating Temperature: -20 to $+50^{\circ}\text{C}$; Dimensions: 125 x 80 x 59 mm);
- Levelling sensors (Trademark: Position Control GmbH; Model: PC 500; Accuracy: up to $\pm 1\text{mm}$; Repeatability: 0.02 mm for single measurements; Range of vertical movement between pots (pressure sensors): 200 m; Number of pressure sensors deployed in our case: 6).

The pictures from Figure 4.5 to Figure 4.8 show the above-mentioned sensors.



Figure 4.5 Temperature sensors.



Figure 4.6 Inclinometers.



Figure 4.7 Insolation sensor.



Figure 4.8 Levelling sensor.

c) Weather Station

In order to learn know the environment conditions, a weather station was installed on the top of K2M building to collect data about air temperature and pressure, wind speed and direction,

as well as rainfall (Figure 4.9). The variables under measurement and their precision are: rainfall (0.25mm), Temperature (0.1°C), pressure (0.1hPa), wind direction (7°) and speed (0.1m/s). In total, there are four different instruments in the station, a thermometer for measuring air temperature, a barometer for measuring atmospheric pressure, anemometer for measuring wind speed and direction, and a rain gauge for measuring liquid precipitation over a set period of time. All of the data were automatically collected and transferred to the database via internet.



Figure 4.9 Weather station on K2M building.

d) Geoscope software

Geoscope software, a GIS Web software development platform, is an excellent tool developed by Soldata Company that can process any type of data obtained from data-loggers, sensors and files along with real-time acquisition of data. It is a user-friendly application that shows the position and the state of all the installed sensors in real time, whilst also allowing easy access to the historical values stored in the database (as shown in Figure 4.10). It is an open database system that has advanced alarm functions to keep track of recording times.

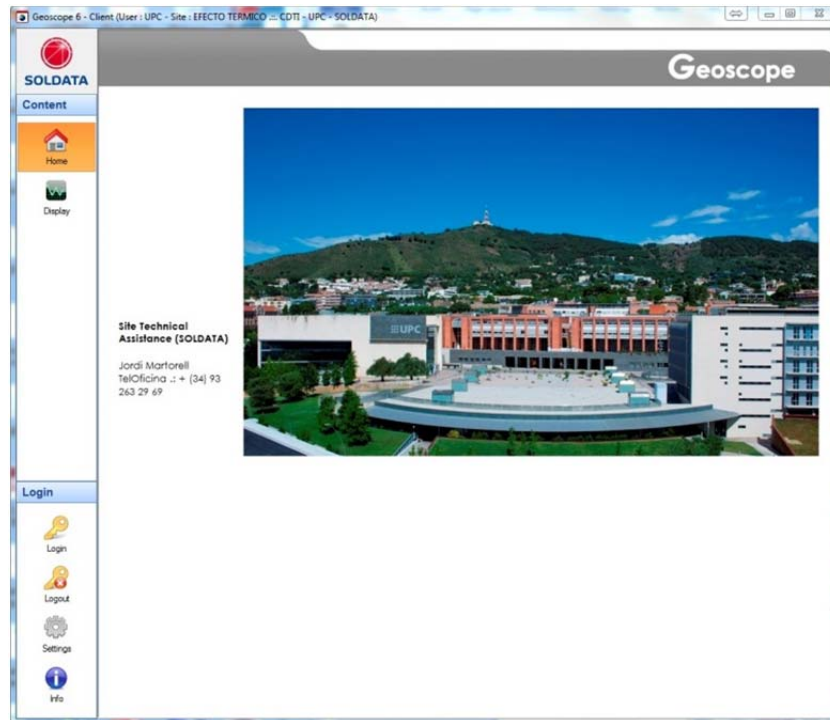


Figure 4.10 Geoscope Web window.

4.4 Data acquisition processes

All of the data, including the prisms' coordinates, temperature, insolation and incline, will be acquired automatically, and they will be transferred to the database via the internet. During this course, there is an important part which is data check and filtering to dislodge unqualified data. The procedure will be continued for a long period of time (one year at least). Finally, all of the data will be shown in Geoscope software. Through this software, the displacement of the control point, insolation, temperature, inclinometer etc. can be indexed. What is more, the data from weather station' data can also be displayed in Geoscope. The user can manage those data by Geoscope software, which is very convenient.

Figure 4.11 to 4.13 show the distribution of the prisms and sensors on three facades of K2M building. From these views, any sensor can be selected and its data may be displayed and/or downloaded.

Figure 4.11 describes the distribution of the prisms and sensors on northeast façade of K2M building. On this façade, there are two prisms as control points on the top of K2M building measured by A6 RTS, and three pairs of temperature sensors for measuring the outside

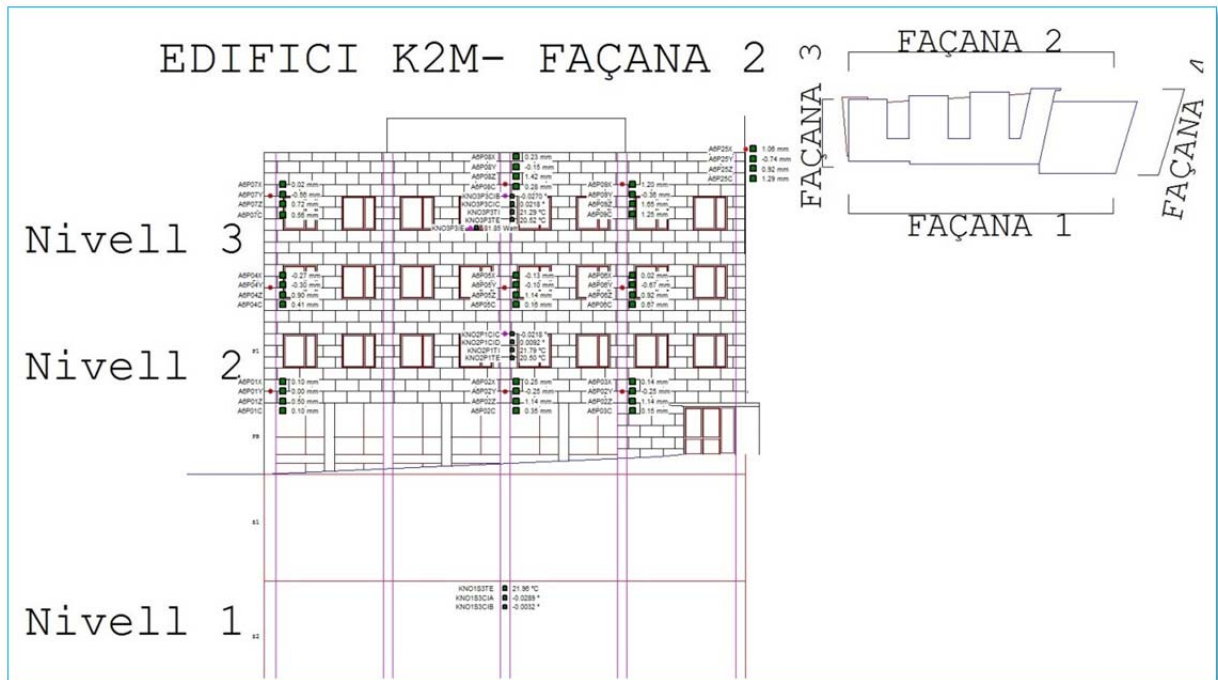


Figure 4.12 Northwest façade of K2M building.

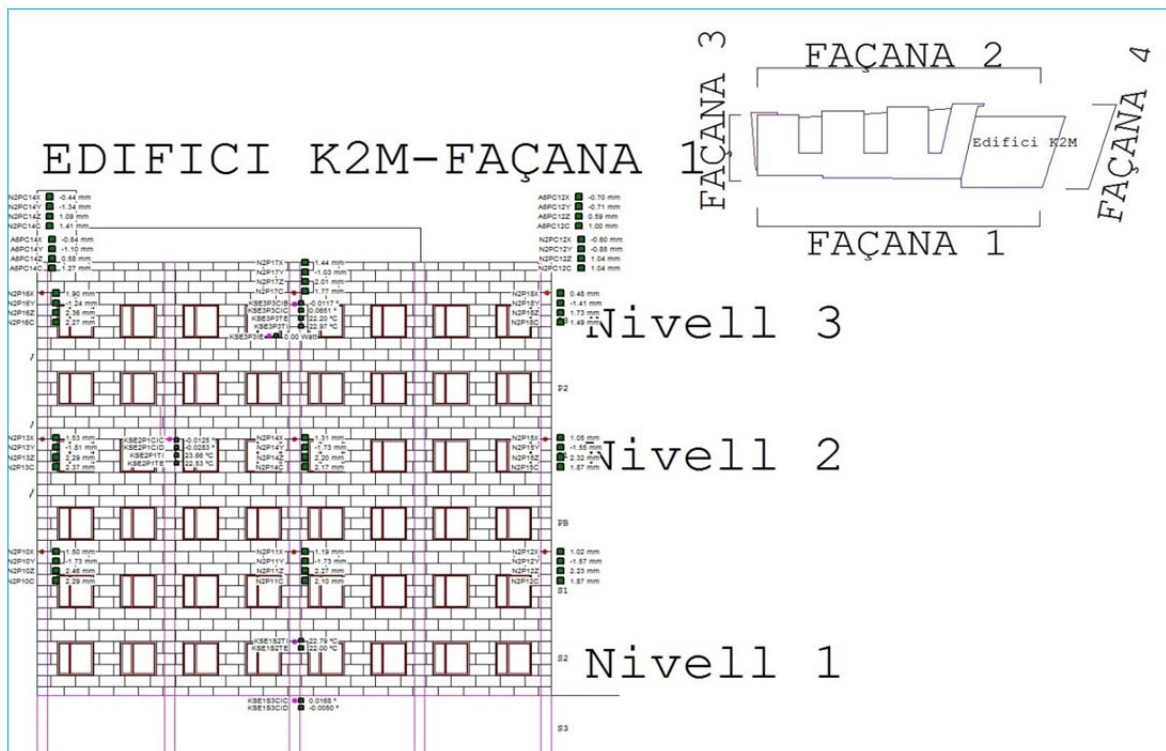


Figure 4.13 Southeast façade of K2M building.

Figure 4.14 to 4.16 show the Bloque SO building, which also has three facades, and the three are equipped. Figure 4.14 displays the distribution of prisms and sensors on the southwest façade of Bloque SO building. As can be seen from the graph, there are 11 prisms, 1 insolation sensor, 3 temperature sensors for measuring the inside temperature of building, and 3 pairs of inclinometers. Figure 4.15 show the distribution of prisms and sensors on the northwest façade of Bloque SO building. As is shown in Figure 4.15, there are 10 prisms, 1 insolation sensor, 3 temperature sensors for recording the inside temperature data and 3 pairs of inclinometers. Figure 4.16 illustrates the distribution of the prisms and sensors on the southeast façade of Bloque SO building. From Figure 4.16, it can be seen that there are 10 prisms distributed on the southeast façade, 1 insolation sensor, 3 pairs of inclinometers on three different floors and 3 temperature sensors to collecting the inside temperature data of Bloque SO building. In sum, there are 31 prisms, 3 insolation sensors, 9 temperature sensors for surveying the inside temperature data, and 9 pairs of inclinometers evenly distributed on the Bloque SO building.

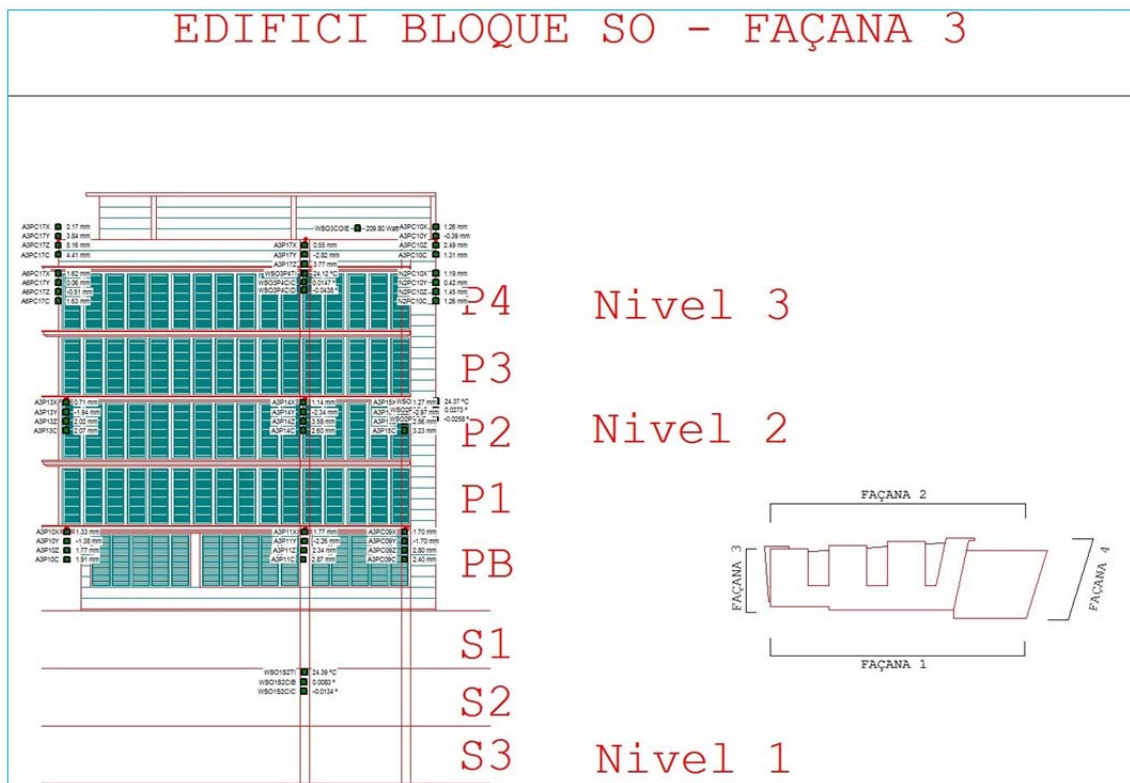


Figure 4.14 Southwest façade of Bloque SO building.

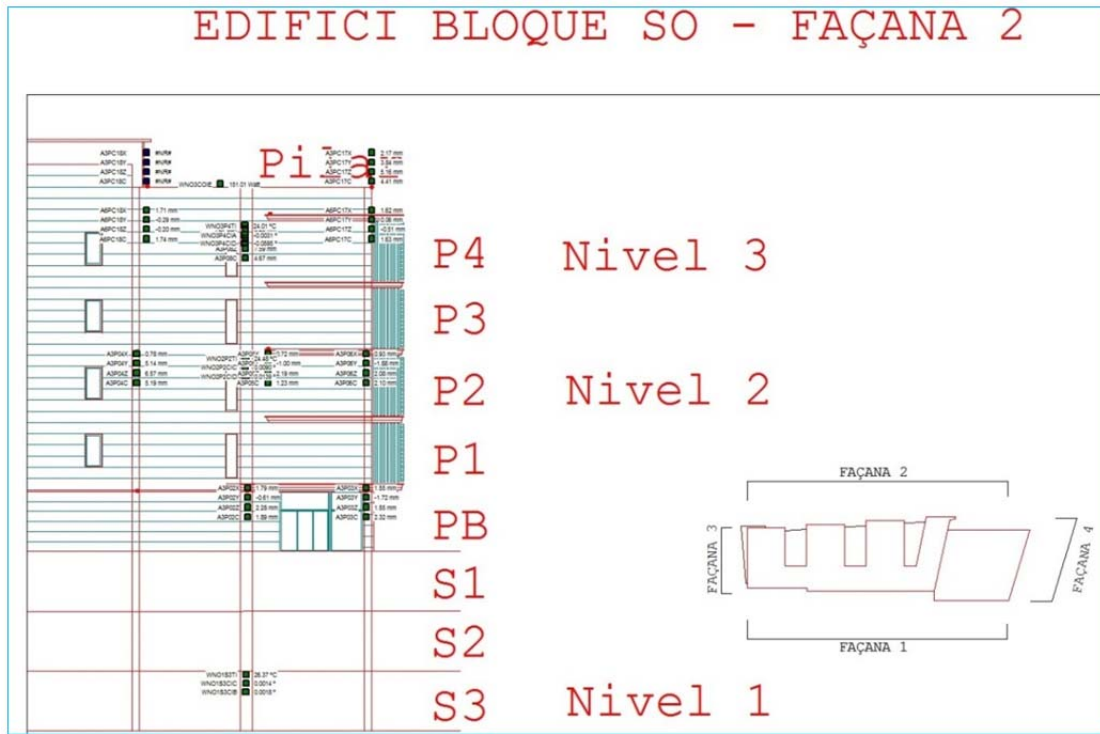


Figure 4.15 Northwest façade of Bloque SO building.

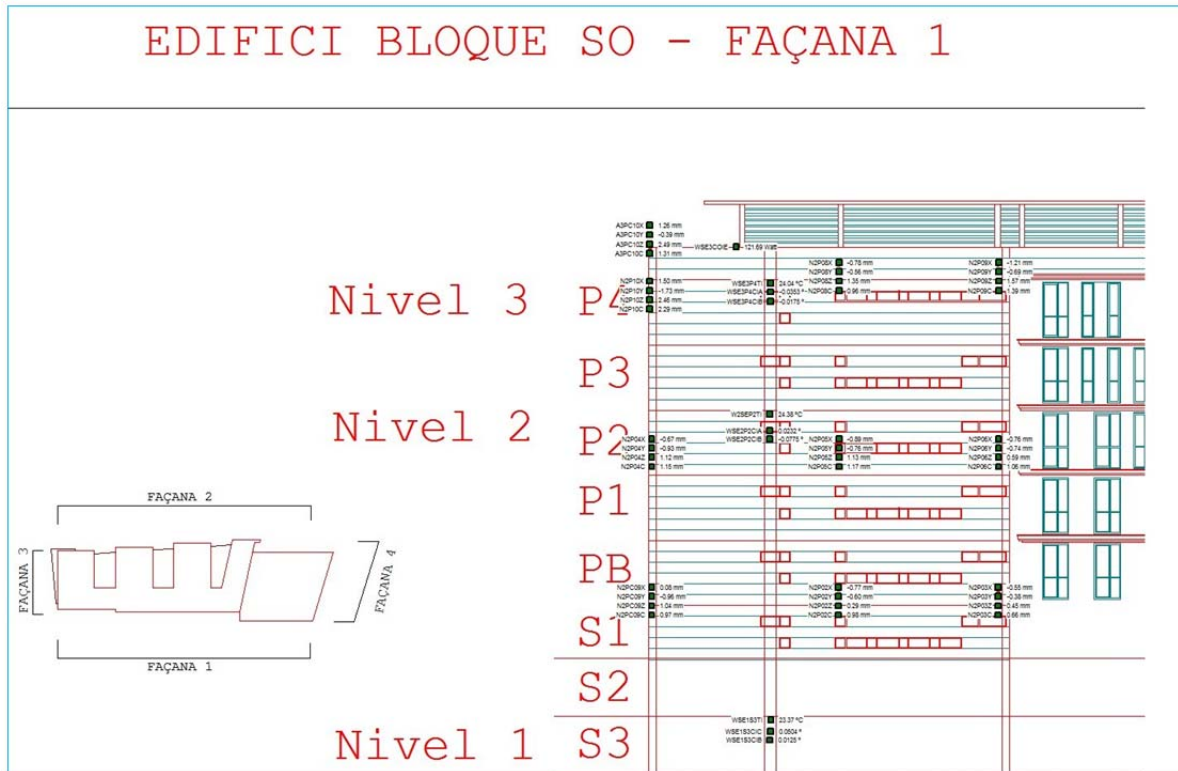


Figure 4.16 Southeast façade of Bloque SO building.

4.5 Data continuity/availability of final filtered data

4.5.1 RTS data availability

In the field monitoring, it is very hard to obtain continual data over a long period time. It means there are some epochs without data because of various reasons, such as power cuts, RTS disorder or inoperativeness. So it is very important to know the data continuity to select the best period for study and analysis.

From the Figure 4.17 to 4.19, it can be seen that the data starts on 12th July 2013, and ends on 28th January 2014, which is about half a year. The figures display the data continuity of the reference point prisms, control point prism and company prism, which is used for adjustment. In those figures, there are some gaps. Generally, there are two reasons, one is a power cut, during which we used a battery to support the RTS; however, the battery is only able to power the system for a limited number of hours. The other reason is that the RTS stop working because it is broken.

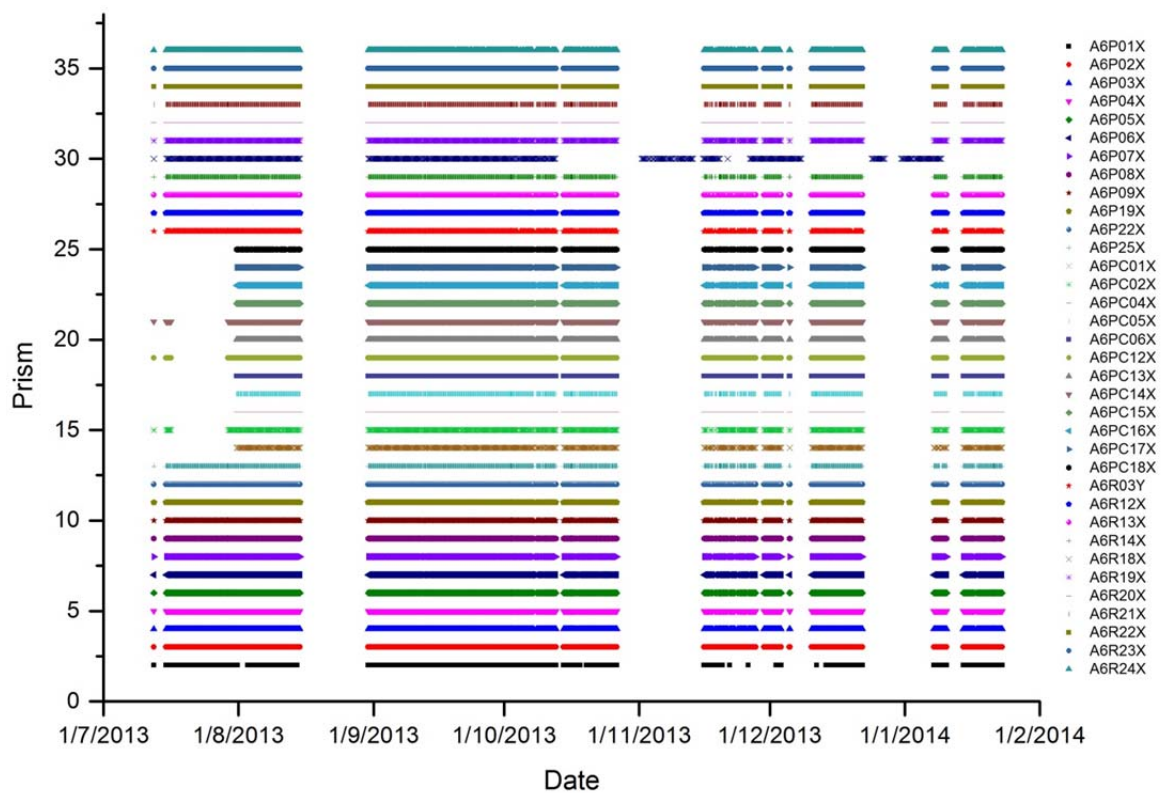


Figure 4.17 A6 RTS availability of final filtered data.

4 Experimental work Test area Campus Nord UPC

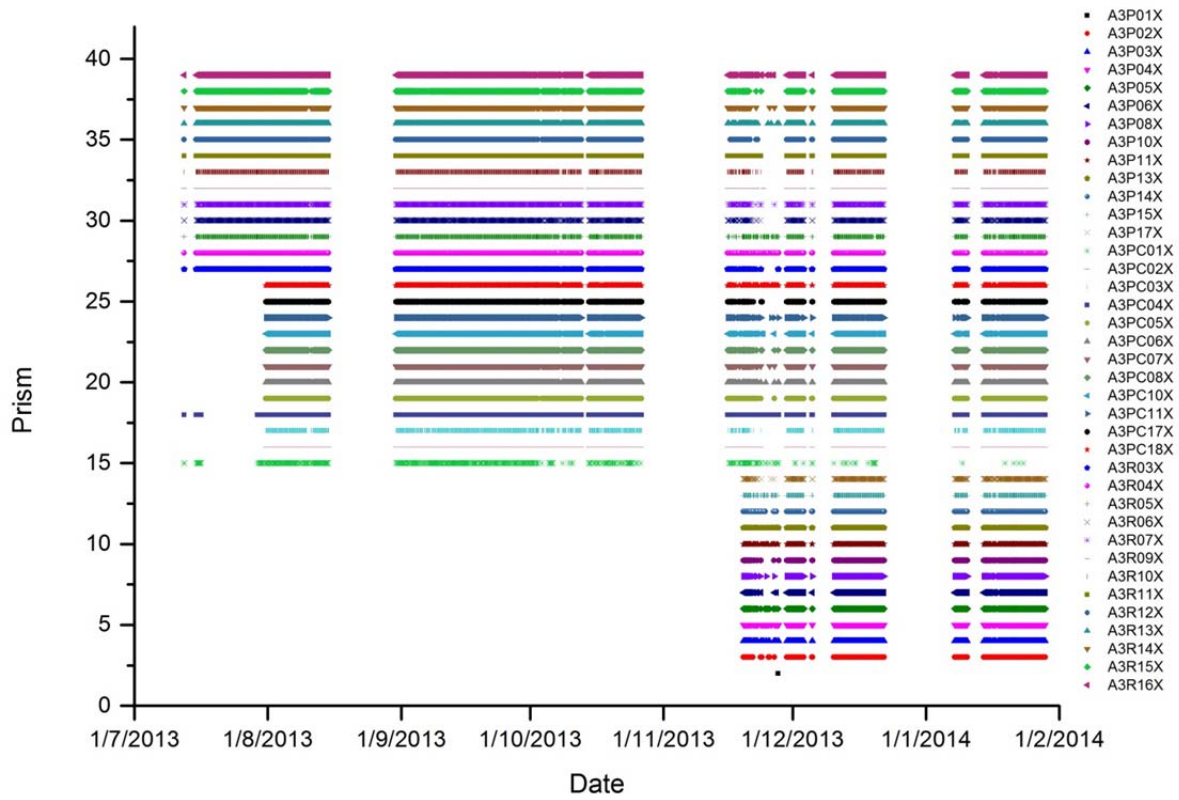


Figure 4.18 A3 RTS availability of final filtered data.

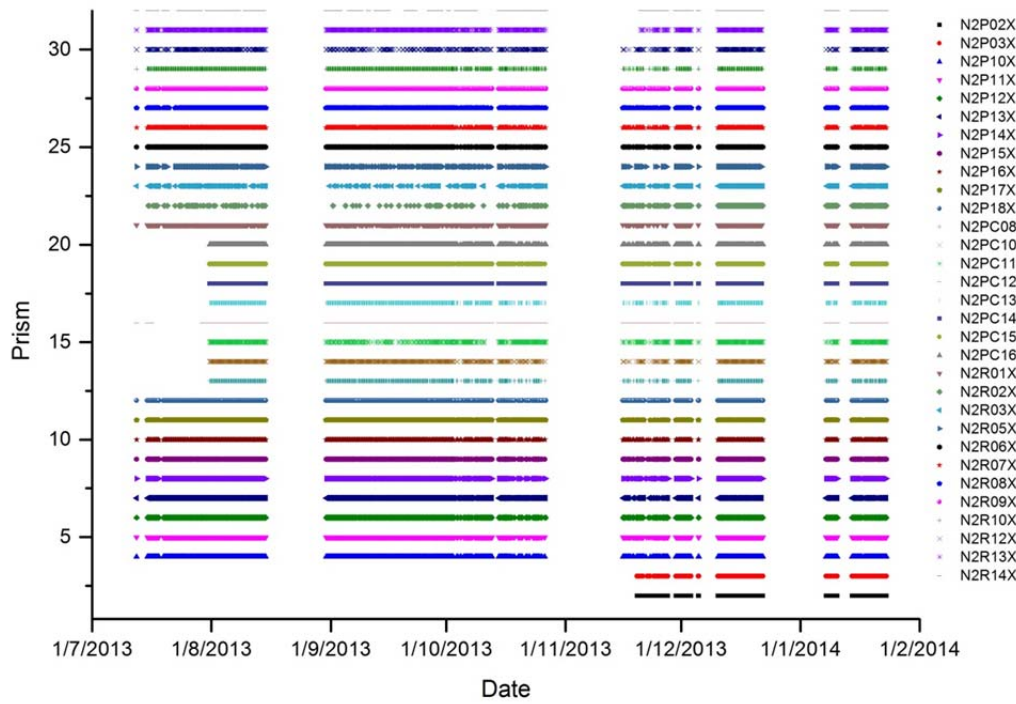


Figure 4.19 N2 RTS availability of final filtered data.

For A3 station, there is no data during the period from 12th July 2013 to 7th January 2014 for some control points. This is because some control point prisms had not been installed on the building in the start stage. The situation is the same for N2 station regarding two control prisms.

After discussion and careful consideration, the period from 1st September 2013 to 15th October 2013 was selected, and used for the following study. One reason is that this time period continued longer than others, totaling 45 days. Another reason to select this period is that there is a good temperature contrast in October.

4.5.2 Temperature and insolation data availability

In order to simulate the behavior of the building under the ambient conditions, it is necessary to know the values of and changes in temperature and insolation around the building. To do this, we installed 17 temperature sensors and 3 insolation sensors on the K2M building to get the temperature and insolation distribution (Table 4.1).

Table 4.1 Temperature and Insolation Sensors Distribution(K2M).

Sensor	Facade				Floor			
	SE	NE	NO	Total	1st	2nd	3rd	Total
Temperature	6	6	5	17	5	6	6	17
Insolation	1	1	1	3	0	0	3	3

(1) Temperature

Temperature is one of the most important factors that affect the building's deformation. The building's behavior is strongly influenced by the temperature change. The Figures (from Figure 4.20 to 4.25) show the temperature changes over the year of 2013 on the three façades (Façade-SE, Façade-NE and Façade-NO) of the K2M building. There are nine sensors to observe the outside temperature data and eight sensors to obtain the inside temperature data.

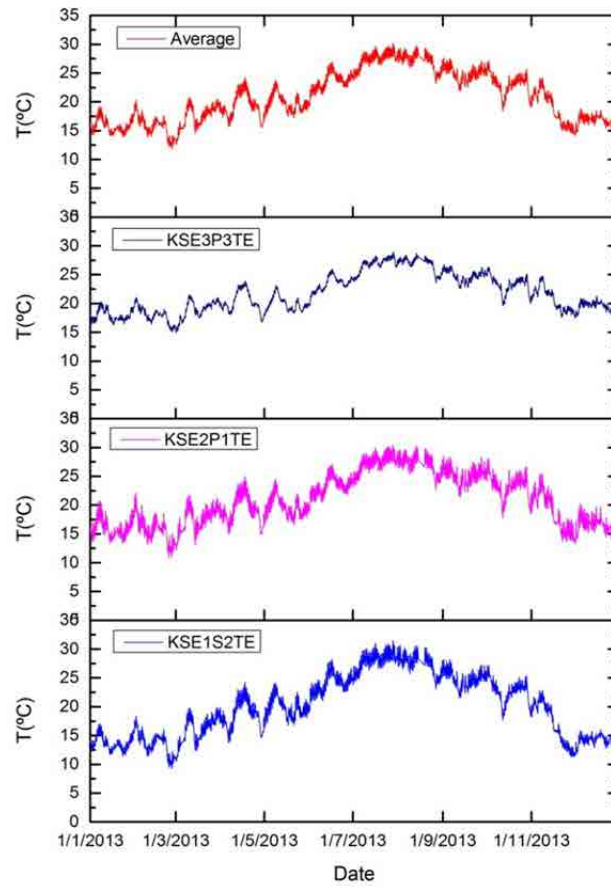


Figure 4.20 Outside temperature variation on the Facade-SE (K2M).

According to this outside temperature graph (Figure 4.20), it can be seen that July and August were the hottest two months, and February and March the coldest. The three curves also follow the same trend. There is an interesting phenomenon: the curve of KSE3P3TE looks smoother than other two. In other words, the curve becomes smoother from the floor-S2 to floor-P3. As for the outside temperature of the building, the daily temperature change on the top floor is smaller than on the basement.

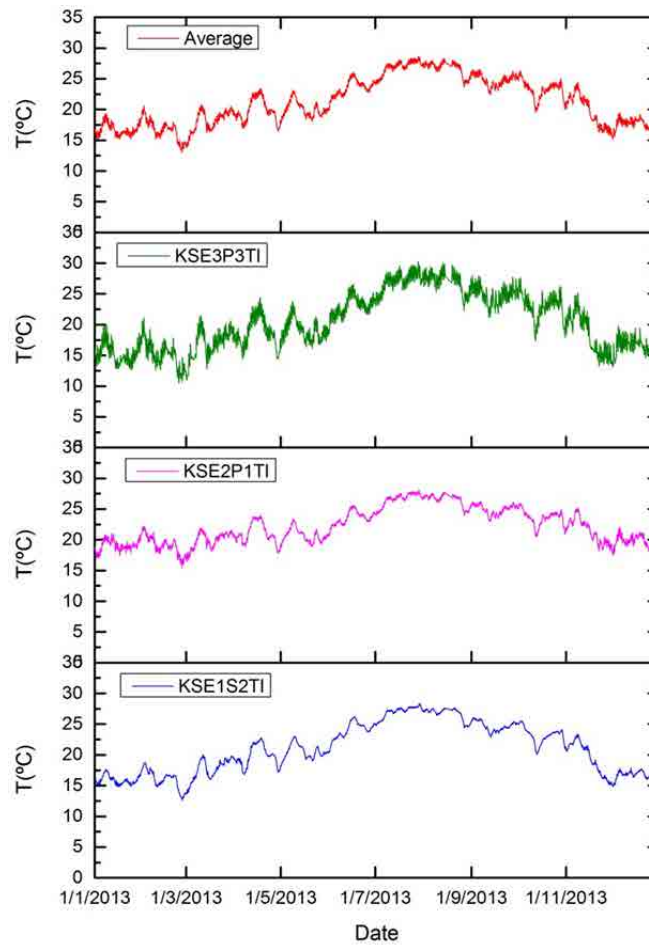


Figure 4.21 Inside temperature variation on the Facade-SE (K2M).

Compare with the curve of the outside-temperature (Figure 4.20), the appearance of the curve of the inside temperature (Figure 4.21) is a different. The higher the floor, the sharper the curve. This means that the inside temperature changed more gently within day and night on the lowest floor-S2. Generally, the trend of inside temperature curve is the same as the outside temperature curve.

4 Experimental work Test area Campus Nord UPC

Table 4.2 Temperature variation on the Facade-SE (K2M).

			January	February	March	April	May	June	July	August	September	October	November	December
Outside	KSE3P3TE	Max	20.71	21.08	21.47	23.9	23.11	25.97	28.94	28.76	26.75	26.31	24.76	21.3
		Min	16.26	15.04	14.93	16.78	17.93	19.7	23.78	23.58	22.54	19.52	17.6	17.43
		Mean	17.99	17.88	18.97	20.38	19.93	23.39	26.84	26.83	24.82	23.32	20.72	19.61
	KSE2P1TE	Max	21.74	22.13	21.7	24.99	24.46	27.09	30.39	30.29	28.52	28.13	25.38	20.33
		Min	13.32	10.9	12.25	14.95	16.5	19.11	23.11	22.57	21.42	17.87	13.53	13.24
		Mean	16.11	15.65	17.53	19.34	19.73	23.39	27.38	27.12	25.15	23.33	18.75	16.63
	KSE1S2TE	Max	17.71	18.41	19.94	24.32	24.08	28.26	31.44	30.7	28.22	27.18	22.88	16.08
		Min	11.38	9.25	10.52	13.73	16.33	19.24	23.81	23.07	21.53	17.75	11.25	11.48
		Mean	13.74	13.53	16	18.71	19.86	24.05	28.11	27.46	24.85	22.68	17.01	14.15
Inside	KSE3P3TI	Max	19.99	21.25	21.48	24.43	23.79	26.67	30.28	30.04	27.98	27.66	25.16	19.88
		Min	15.18	10.50	10.96	14.41	16.03	18.48	22.94	22.26	21.20	17.32	13.26	13.09
		Mean	16.85	15.01	16.89	18.81	19.11	23.05	27.12	26.99	24.82	22.97	18.32	16.56
	KSE2P1TI	Max	22.07	22.20	21.91	23.95	23.39	25.64	28.08	27.77	26.23	25.93	25.16	22.02
		Min	16.97	15.41	16.48	17.78	18.76	20.73	23.99	23.97	22.97	20.43	17.84	17.52
		Mean	19.16	19.04	19.92	21.09	20.69	23.54	26.62	26.46	24.96	23.59	21.42	19.76
	KSE1S2TI	Max	18	18.80	19.98	22.73	23.01	26.26	28.33	27.66	26.05	25.58	23.44	17.91
		Min	14.83	12.65	13.56	16.78	18.20	20.34	24.76	24.37	22.85	20.10	14.98	14.82
		Mean	15.96	15.96	17.62	19.87	20.56	24.01	27.01	26.62	24.68	23.16	19.41	16.77

From this table, we can obtain more exact values to know how the temperature changed outside and inside on the facade-SE over the whole year of 2013.

Regarding the outside temperature, the three observation points reached the peak points in July, namely 28.94 °C at KSE3P3TE point, 30.39 °C at KSE2P1TE point and 31.44 °C at KSE1S2TE point. On the other hand, the two observation points, KSE1S2TE and KSE2P1TE, reached the bottom at 9.25 °C and 10.9 °C respectively in the same month of February. However, the point of KSE2P1TE hit the lowest point in March. At the same time, there is another important value-mean monthly; it can also indicate the temperature change trend in the year of 2013. The mean monthly temperature of the three surveying points varied from 17.88 °C to 26.84 °C at KSE3P3TE, from 15.65 °C to 27.38 °C at KSE2P1TE and from 13.53 °C to 28.11 °C at KSE1S2TE.

As for the inside temperature, it is clearly warmer than the outside. At the KSE3P3TI surveying point, the value varied from 10.5 °C in February to 30.28 °C in July, and its mean monthly temperature changed from 15.01 °C in February to 27.12 °C in July; at the KSE2P1TI surveying point, the value varied from 15.41 °C in February to 28.08 °C in July, and its mean monthly temperature changed from 19.04 °C in February to 26.62 °C in July; at the KSE1S2TI surveying point, the value varied from 12.65 °C in February to 28.33 °C in July, and its mean monthly temperature changed from 15.96 °C in February to 27.01 °C in July.

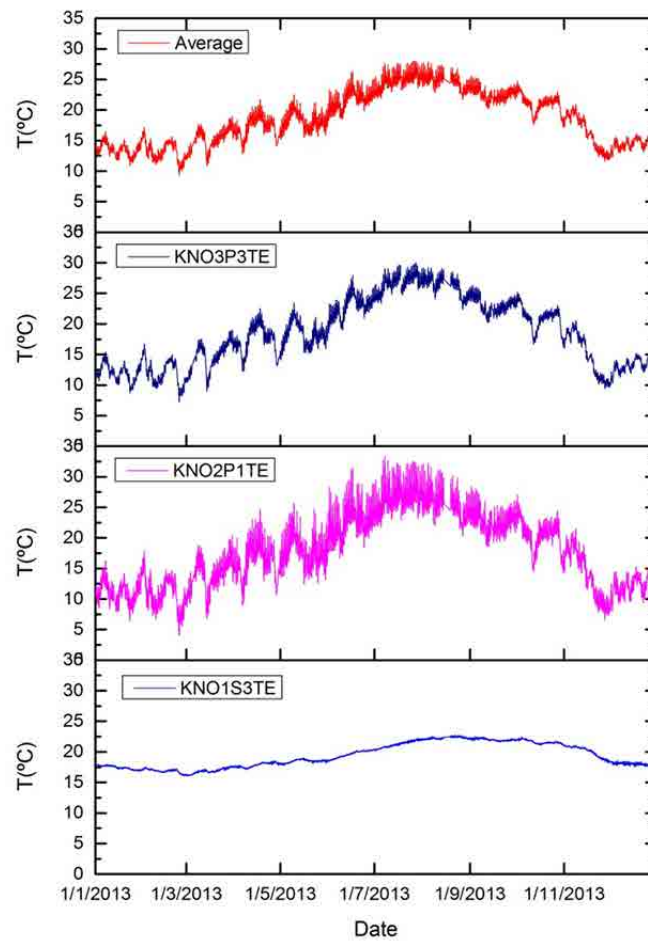


Figure 4.22 Outside temperature variation on the Facade-NO (K2M).

Figure 4.22 shows the outside temperature variable on the facade-NO during the year of 2013. The curve of KNO1S3TE is the smoothest one. The reason is its location underground, so the temperature change was less sharp. Apart from that, its overall range is very narrow. The average temperature trend is similar to the two outside surveying points (KNO3P3TE and KNO2P1TE). The curve of KNO2P1TE is the sharpest compared with the others, and it shows the biggest difference. There are several reasons for it, with the wind being the main one. The wind speed is different on different floors, and the wind is an important factor influencing the temperature changes even if the building is not particularly high.

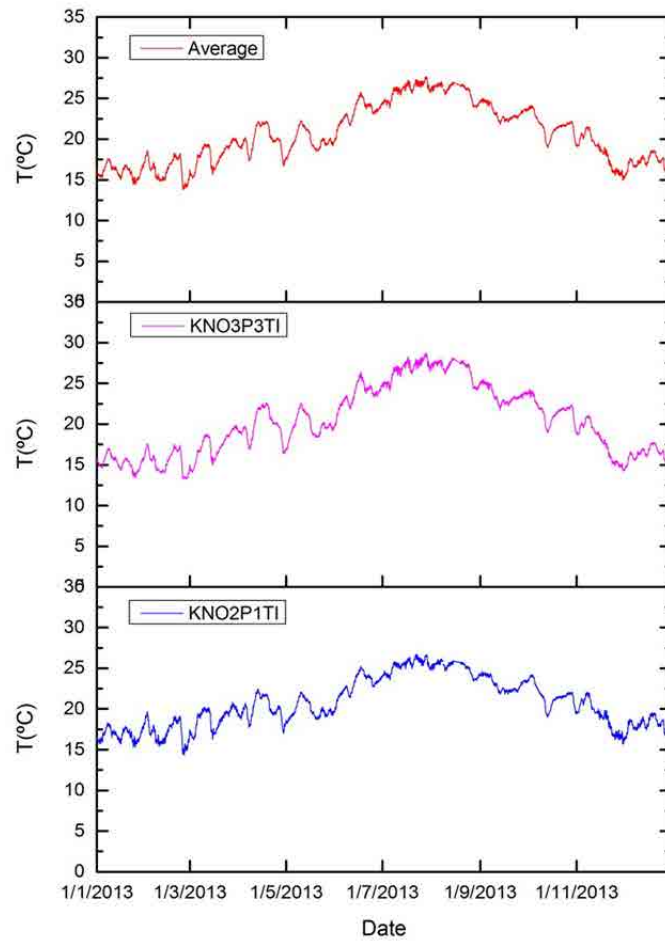


Figure 4.23 Inside temperature variation on the Facade-NO (K2M).

Figure 4.23 illustrates the change in the inside temperature on the facade-NO in 2013. The trends of the three lines are alike, and all of the lines are very smooth.

4 Experimental work Test area Campus Nord UPC

Table 4.3 Temperature variation on the Facade-NO (K2M).

			January	February	March	April	May	June	July	August	September	October	November	December
Outside	KNO3P3TE	Max	15.68	16.7	18.98	22.57	23.5	27.98	30.05	29.23	26.24	25.24	20.57	15.23
		Min	8.67	7.25	9.05	12.22	14.09	18.49	23.36	22.37	20.14	16.26	9.43	9.91
		Mean	12.13	11.89	14.6	17.37	18.3	22.9	26.76	26.25	23.01	20.95	14.95	12.93
	KNO2P1TE	Max	16.66	17.83	20.51	24.75	25.63	31.42	33.39	32.15	28.43	27.07	21.46	15.22
		Min	6.42	4.05	6.74	8.95	12.43	16.65	21.71	20.31	18.57	14.22	6.5	7.98
		Mean	11.2	10.65	13.83	16.21	17.77	22.59	26.59	25.6	22.56	20.41	13.87	11.78
	KNO1S3TE	Max	18.02	17.5	17.72	18.52	19	20.41	22.26	22.79	22.52	22.51	21.14	18.63
		Min	16.81	16.06	16.03	17.07	17.77	18.42	20.08	21.92	21.61	20.89	18.12	17.28
		Mean	17.44	16.88	16.89	17.84	18.48	19.61	21.23	22.28	22	21.62	20.02	17.99
Inside	KNO3P3TI	Max	17.01	17.60	19.91	22.69	22.59	26.38	28.74	28.17	25.50	24.32	21.08	17.77
		Min	13.39	13.24	14.04	16.31	16.89	19.84	24.10	24.15	21.71	18.93	14.22	14.28
		Mean	15.29	15.39	17.34	19.87	19.84	23.65	26.77	26.74	23.56	21.63	17.87	16.26
	KNO2P1TI	Max	19.17	19.71	20.82	22.46	22.06	25.24	26.74	26.18	24.59	24.22	22.08	19.54
		Min	15.3	14.38	16.21	16.97	18.18	19.94	23.55	23.37	21.81	18.98	15.63	16.09
		Mean	16.9	17.09	18.80	20.02	19.89	23.08	25.39	25.07	23.01	21.62	19.08	18.00

Table 4.3 displays more values than Figure 4.22 and Figure 4.23. This table has two sections, one about the outside temperature variable over the year, and the other about the inside temperature.

Regarding the outside temperature, we can see that the temperature changed most violently at KNO2P1TE point, where the temperature varied between 4.05 °C in February and 33.39 °C in July, and its mean monthly temperature changed from 10.65 °C in February to 26.59 °C in July. At KNO3P3TE point, the outside temperature changed from 7.25 °C in February to 30.05 °C in July, and its mean monthly temperature varied between 11.89 °C in February and 26.76 °C in July; at KNO1S3TE point, the temperature changed from 16.03 °C in February to 22.79 °C in July, and its mean monthly temperature varied between 11.89 °C in February and 26.76 °C in July.

As for the inside temperature, at KNO3P3TI point, the temperature changed from 13.24 °C in February to 28.74 °C in July, and its mean monthly temperature varied between 15.29 °C in January and 26.77 °C in July; at KNO2P1TI point, the temperature changed from 14.38 °C in February to 26.74 °C in July, and its mean monthly temperature varied between 16.9 °C in January and 25.39 °C in July.

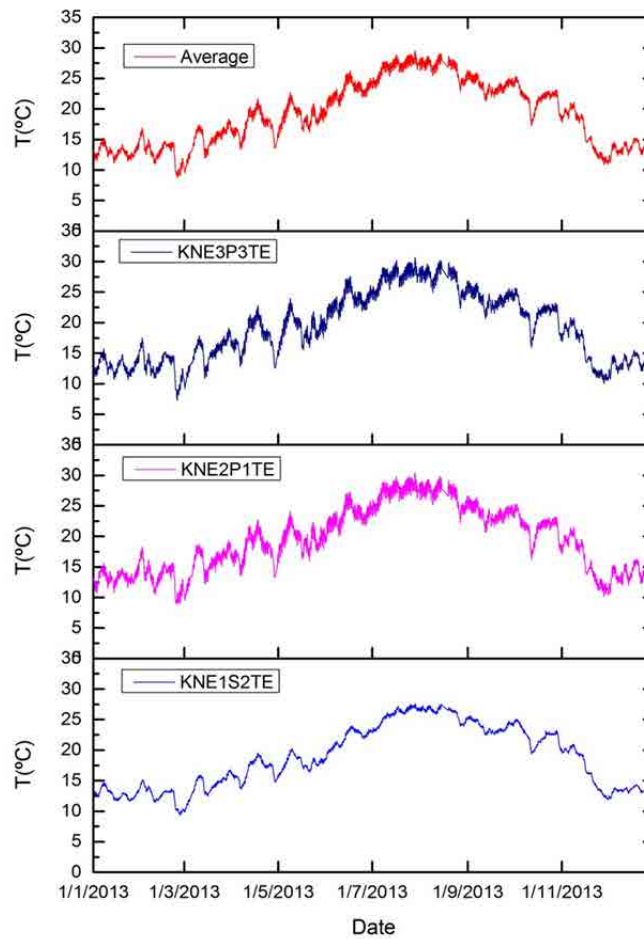


Figure 4.24 Outside temperature variation on the Facade-NE (K2M).

From Figure 4.24, it can be seen that the trend of the outside temperature on the façade-NE is similar to facade-SE and facade-NO. Compared with the curves of KNE3P3TE and KNE2P1TE, the curve of KNE1S2TE is gentler. In addition, the overall range of KNE1S2TE is also smaller. This is because it faces a higher wall, and there is a lack of air renewal and solar insolation.

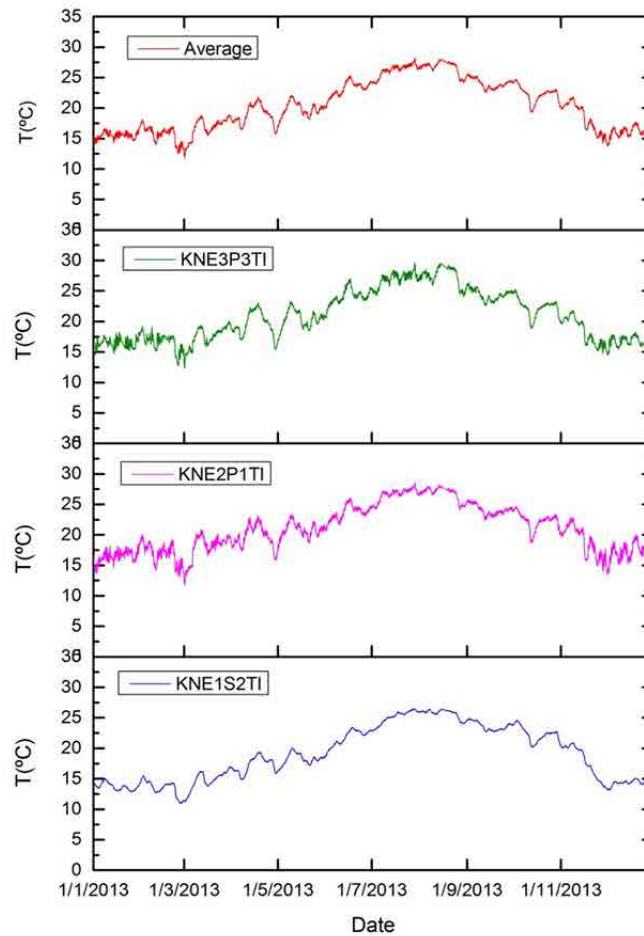


Figure 4.25 Inside temperature variation on the Facade-NE (K2M).

Similarly, Figure 4.25 also shows the same trend of the inside temperature on the Facade-NE as the other two. As with the outside temperature, the curve of KNE1S2TI's variable scope is narrower than KNE3P3TI and KNE2P1TI. The average curve has the same trend with the curves of three monitoring points.

4 Experimental work Test area Campus Nord UPC

Table 4.4 Temperature variation on the Facade-NE (K2M).

			January	February	March	April	May	June	July	August	September	October	November	December
Outside	KNE3P3TE	Max	16.77	17.46	19.1	22.81	23.93	27.58	30.61	30.18	26.81	25.74	20.88	15.47
		Min	10.62	7.32	9.26	12.55	14.56	18.9	23.58	22.24	20.72	15.92	10.05	10.54
		Mean	13.04	12.79	14.97	17.59	19.24	23.7	27.59	27.24	23.97	21.43	15.42	13.22
	KNE2P1TE	Max	17.68	18.28	19.34	22.76	24.1	27.32	30.39	29.81	26.58	25.33	21.54	16.29
		Min	10.71	8.9	9.54	13.22	15.72	19.17	23.27	22.18	20.65	16.19	10.16	10.43
		Mean	13.42	13.34	15.61	17.91	19.7	23.56	27.42	26.93	23.81	21.5	16.04	13.75
	KNE1S2TE	Max	14.72	15.14	16.86	19.57	20.25	24.02	27.6	27.49	25.65	25.11	20.97	14.33
		Min	11.64	9.29	9.82	13.69	15.56	18.54	22.87	23.9	22.45	19.4	11.93	11.88
		Mean	12.86	12.46	14.09	16.74	17.98	21.97	25.75	26.11	23.84	22.26	17.06	13.42
Inside	KNE3P3TI	Max	18.56	19.11	20.05	23.08	23.26	27.03	29.60	29.56	26.44	25.27	21.82	18.36
		Min	14.57	12.76	12.30	15.37	16.85	20.53	24.22	24.02	22.59	18.87	14.72	14.47
		Mean	16.48	16.62	17.51	19.62	20.43	24.13	26.98	27.35	24.38	22.29	18.40	16.52
	KNE2P1TI	Max	19.59	20.17	20.90	23.16	23.31	26.10	28.55	28.28	25.87	24.66	22.90	20.14
		Min	13.67	13.06	11.73	15.89	17.64	20.60	24.15	24.09	22.45	18.63	14.02	13.55
		Mean	16.52	16.85	18.01	19.75	20.84	23.64	26.63	26.71	24.11	22.26	18.92	17.10
	KNE1S2TI	Max	14.97	15.47	16.99	19.38	20.05	23.45	26.48	26.41	24.87	24.51	20.87	15.08
		Min	12.82	10.90	11.22	14.82	16.33	18.72	22.77	23.99	22.66	20.20	13.33	13.16
		Mean	13.73	13.46	14.74	17.26	18.28	21.75	25.06	25.59	23.64	22.29	17.86	14.30

Table 4.4 shows the outside temperature and inside temperature change on the facade-NE in 2013.

The outside temperature, at KNE3P3TE point, reaches its peak of 30.61 °C in July, and hits the bottom of 7.32 °C in February. Its mean monthly temperature ranged from 12.79 °C in February to 27.59 °C in July; at the KNE2P1TE surveying point, the value varied from 8.9 °C in February to 30.39 °C in July, and its mean monthly temperature changed from 13.34 °C in February to 27.42 °C in July; at the KNE1S2TE observation point, the number ranged between 9.29 °C in February and 27.6 °C in July, and its mean monthly temperature ranged from 12.46 °C in February to 26.11 °C in August.

On the other hand, the inside temperature is clearly higher than the outside. At the KNE3P3TI monitoring point, the value changed from 12.30 °C in March to 29.60 °C in July, and its mean monthly temperature varied from 16.48 °C in January to 27.35 °C in August; at the KNE2P1TI surveying point, the value varied from 11.73 °C in March to 28.55 °C in July, and its mean monthly temperature changed from 16.52 °C in January to 26.71 °C in August; at the KNE1S2TI point, the range of the value located between 10.9 °C in February to 26.48 °C in July, and its mean monthly temperature changed from 13.46 °C in February to 25.59 °C in August.

(2) Insolation

Insolation (short for incident or incoming solar radiation) is a measure of solar radiation energy received on a given surface area and recorded during a given time. It is also called solar irradiation and expressed as "hourly irradiation" if recorded during an hour, or "daily irradiation" if recorded during a day.

Insolation is a short way to describe incoming solar radiation. Radiation from the sun is the driving force that creates all the weather on Earth. The layers of the atmosphere filter out some of the most harmful types of electromagnetic radiation. The remaining radiation that reaches the surface of Earth is commonly known as insolation.

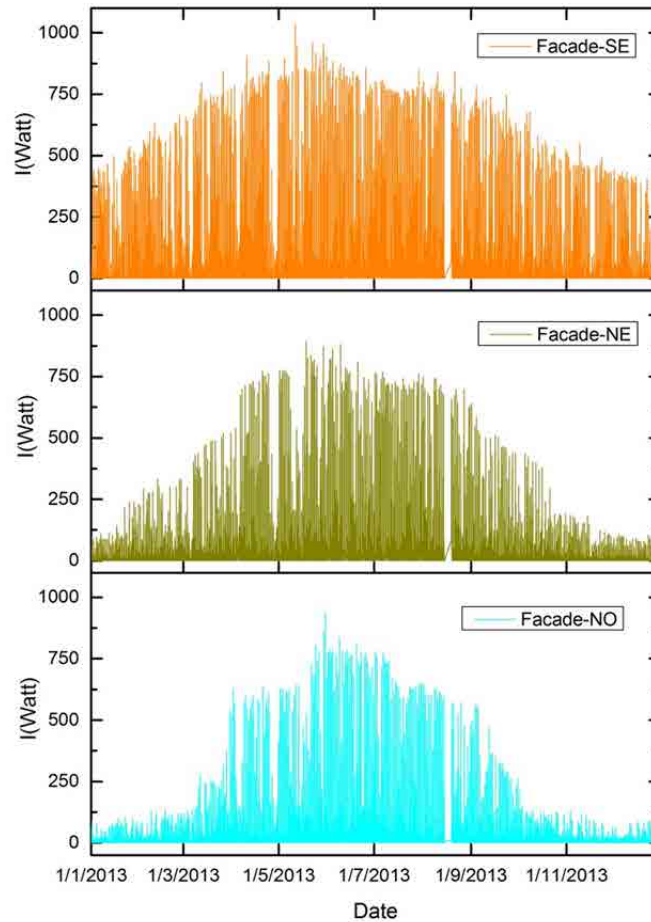


Figure 4.26 Insolation variable.

This bar chart in Figure 4.26 describes the insolation distribution on the three different facades of the K2M building in 2013. From the chart, we can see that the middle part of the three bar charts is more prominent than the two ends, because the insolation is stronger in summer than winter. Among the three facades, which are facade-SE, NE and NO, the facade-SE best absorbs the insolation from the sun, because of its direction of south-east. This is the reason why its insolation is stronger on the two ends of the bar chart than that of facade-NE and NO. The insolation of facade-NO comes mainly from objective reflection, because there is no direct insolation from the sun. What is more, it is an interesting phenomenon that the insolation values are similar during the months of June, July and August. This indicates that this area has very strong insolation in summer whatever the facade if face the sun or not.

(3) Relationship between air temperature and insolation

The sun supplies essentially all the energy that drives most of the atmospheric processes on Earth. Insolation is the amount of solar radiation that reaches the earth's surface through shortwaves.

As Earth revolves around the Sun, locations on the surface may undergo seasonal changes in air temperature because of annual variations in the intensity of insolation. Variations in insolation are primarily controlled by changes in the intensity and duration of received solar insolation which are driven by variations in day length and angle of incidence. The discussion below focuses on how changes in insolation can affect monthly air temperatures in our monitoring location.

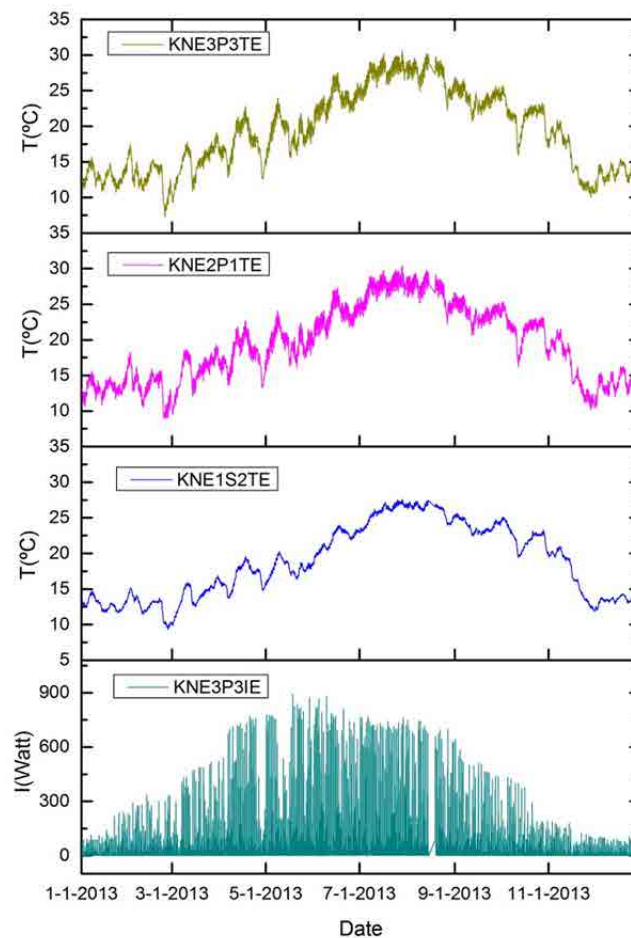


Figure 4.27 Outside temperature and insolation on the facade NE.

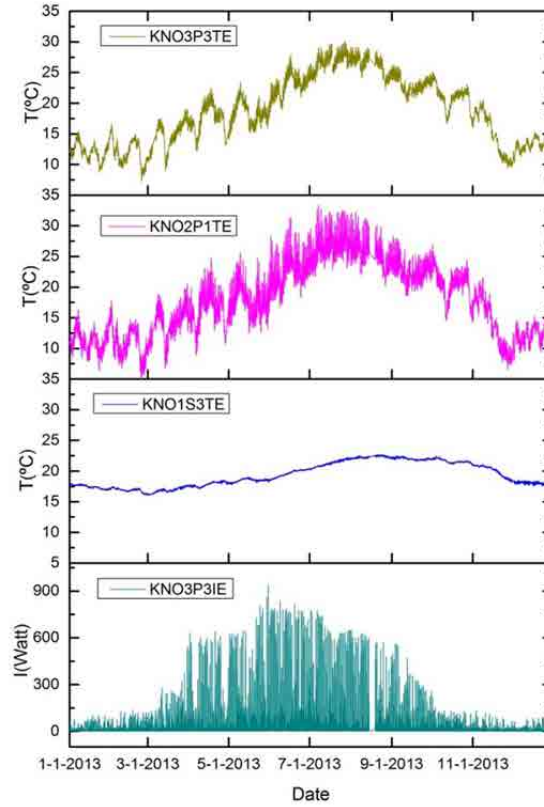


Figure 4.28 Outside temperature and insolation on the facade NO.

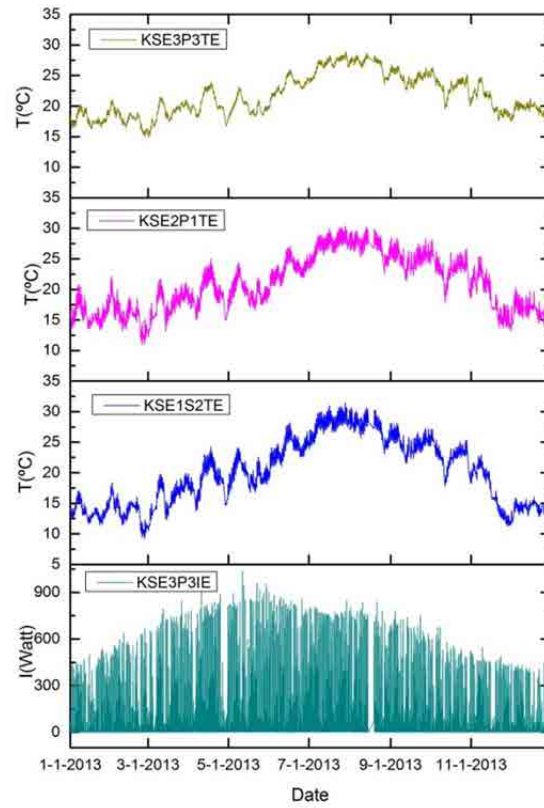


Figure 4.29 Outside temperature and insolation on the facade SE.

From the three figures of Figure 4.27 to 4.29, we can see that there is a close connection between the outside temperature and insolation. When the insolation is strong, the outside temperature rises. In other words, the temperature increases when the insolation increases. It is very obvious that the building's surface temperature goes up with the insolation falling from November to March on the three facades. During this period, the façade-SE's temperature is the highest and the facade-NO is the lowest. Similarly, when the insolation reaches its yearly peak in July, the temperature also hits the highest degree on the three facades.

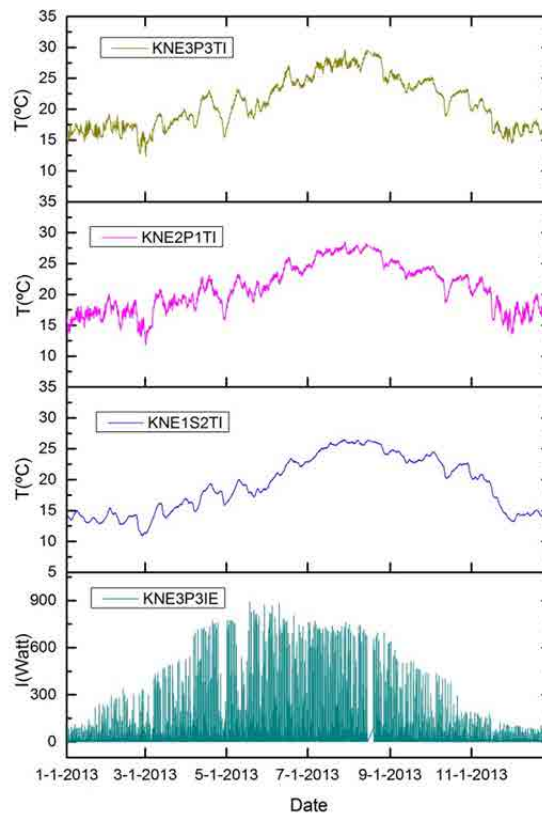


Figure 4.30 Inside temperature and insolation on the facade NE.

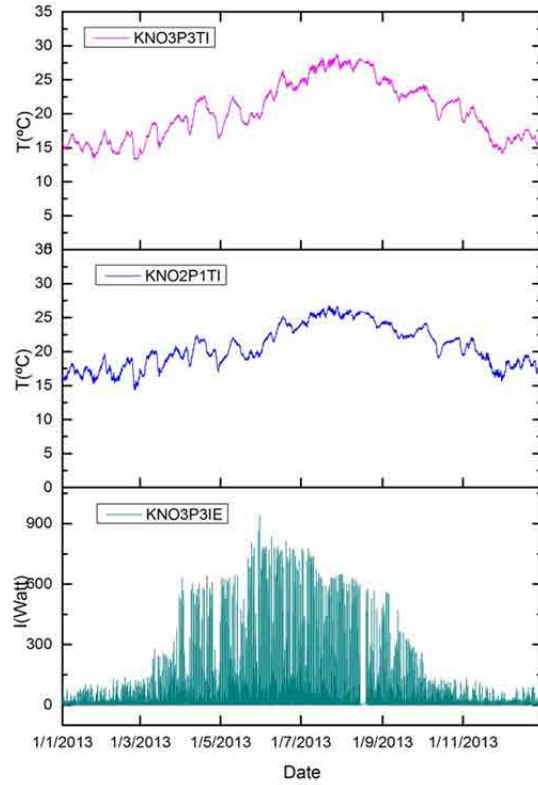


Figure 4.31 Inside temperature and insolation on the facade NO.

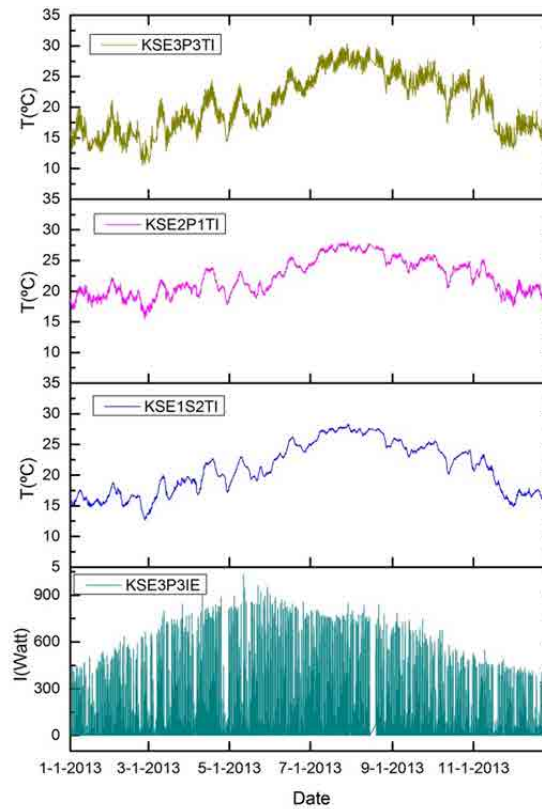


Figure 4.32 Inside temperature and insolation on the facade SE.

From the three figures of Figure 4.30 to 4.32, it can be seen that the inside temperature changes with the season. This does not have a direct relationship with the insolation. There are some significant factors, such as air conditioning and heating, which influence the change in the inside temperature. That is why the temperature is lower inside than outside in summer, and higher in winter.

5 Matching the Model with real world results

In chapter 3, it have been explained how buildings deform when subjected to thermal changes. The structure and numerical methodology to model this behavior has been outlined. In chapter 4, the experimental area has been described. In this chapter, we face the challenge of matching the observed behavior of the test area buildings with the deformations forecast by our conceptual model stating from temperature measurements.

The structure of the chapter 5 is as follows: In section 5.1, a sensitivity analysis is carried out. It investigates how small errors in the measurements (horizontal angle, zenith angle and distances) will influence the results. In the second section, the direct or standard results (obtained with the monitoring system in the Campus Nord test area) are presented. The main features of these results are outlined and the physical explanations of the monitoring system behavior are given. In section 5.3, a numerical simulation of the full scene is carried out in order to demonstrate the aforementioned physical explanations. Finally, in the last section, the direct results and the simulated ones are compared, and several conclusions are derived.

5.1 Sensitivity analysis

RTS is a precision instrument that can measure horizontal and zenith angles and distance automatically. The raw surveying data consist of the horizontal angle (H), zenith or vertical angle (V) and distance (d) between the target and the RTS. In this section, the sensitivity of RTS X, Y and Z coordinates to horizontal angle, zenith angle and distance has been studied. This sensitivity analysis is interesting in order to know how robust the results are in front of some unavoidable measurement errors.

In order to explore the sensitivity of the coordinates, the raw data is changed artificially. A series of tests have been done. The base situation for all the sensitivity analyses has been the same: the computation of the X, Y and Z coordinates of the center of the Total Station, done through an Inverse Resection from the measurements (angles and distances) to the reference prisms. The actual measurements during one given day (1st September 2013) have been used. As the RTS measured each 3h, we have 8 epochs to appreciate the difference in the RTS X, Y and Z coordinates introduced by the artificial change in the selected observable. In order to enhance the effects of the horizontal angle and zenith angle, they have been increased by 0.01g on the reference points R14, R28 and R27; the distance has been increased by 1mm on the reference points R14, R28 and R27. For each observable, there are three different tests: in the first one, only the value for R14 is changed; in the second, the values for R14 and R28 are changed; in the third, the values for R14, R28 and R27 are changed. Later, the original result and the three test results have been compared.

5.1.1 Sensitivity to horizontal angle—H

The measurement of angles is one of the most important tasks in surveying and construction. Horizontal angles are used to determine bearings and directions in control surveys, for locating detail when mapping and for setting out all types of structure. Angles are usually measured using either a theodolite or a total station. In the GeoscopeWeb system (introduced in section 4.3), the horizontal angle and zenith angle can be observed by the RTS. The horizontal angle in the raw data file from GeoscopeWeb is the angle between the zero direction in the horizontal circle of the RTS and the line of sight to the target. The horizontal angle ranges from 0 gon to 400 gons.

Figure 5.1 presents the sensitivity of coordinates X, Y and Z when we introduce small changes in the horizontal angle (0.01g). From the results, it can be concluded that coordinates X and Y are very sensitive to changes in the horizontal angle. On the other hand, coordinate Z is almost unaffected by the changes in the horizontal angle.

5 Matching the Model with real world results

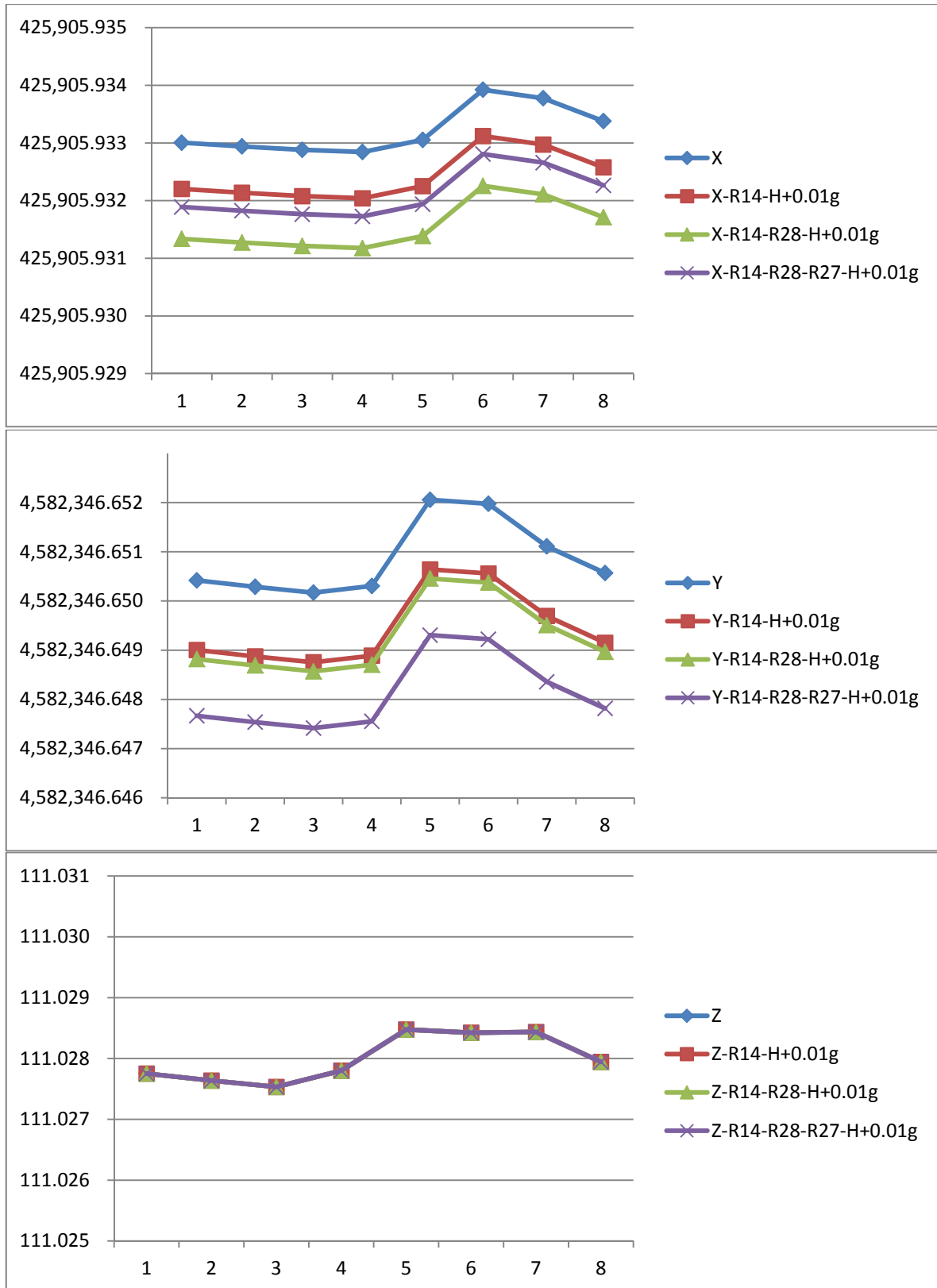


Figure 5.1 Sensitivity to horizontal angle: Evolution of the X, Y Z coordinate of the RTS when a 0.01g change is introduced in one, two or three horizontal angle measurements along the 8 epochs of a given day. Then coordinates (vertical axe) are expressed in m.

5.1.2 Sensitivity to zenith angle-V

The zenith angle is the angle in the vertical planes between the direction vertically above the instrument (zenith angle=0 gon) and the line of sight. The range of the zenith angle is from 0 gon to 200 gon for sights with the telescope in the direct position; and from 200 to 400 for the inverse position; a direct horizontal sight, for instance, corresponds to a 100 gon zenith angle. Zenith angles are used when determining the heights of points by trigonometrical methods, and also to calculate horizontal distances from slope distances.

Figure 5.2 shows four curves for different tests with one, two or three zenith angles perturbed with a small variation (0.01g). It can be seen that the zenith angle has a great influence on the Z coordinate. However, for X and Y, the results are quite similar with the original.

In this section, the sensitivity of the zenith angle change 0.01g in three different tests to the coordinates of X, Y and Z has been studied. When comparing the results seen in Figure 5.2 with those in Figure 5.1, it is clear that X and Y are sensitive to the horizontal angle, whereas Z is sensitive to the zenith angle.

5 Matching the Model with real world results

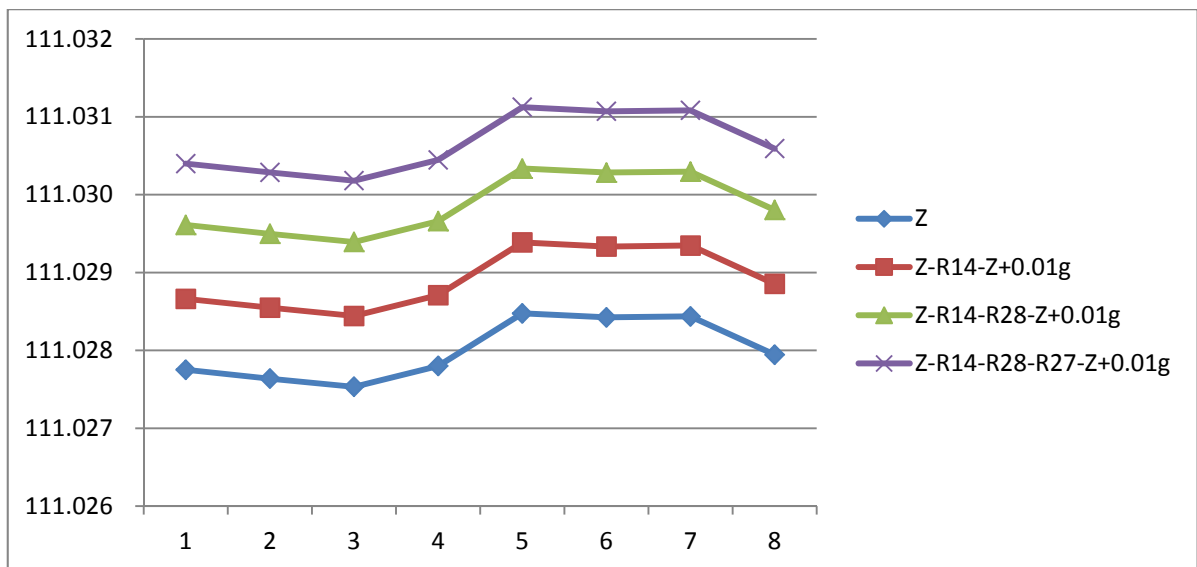
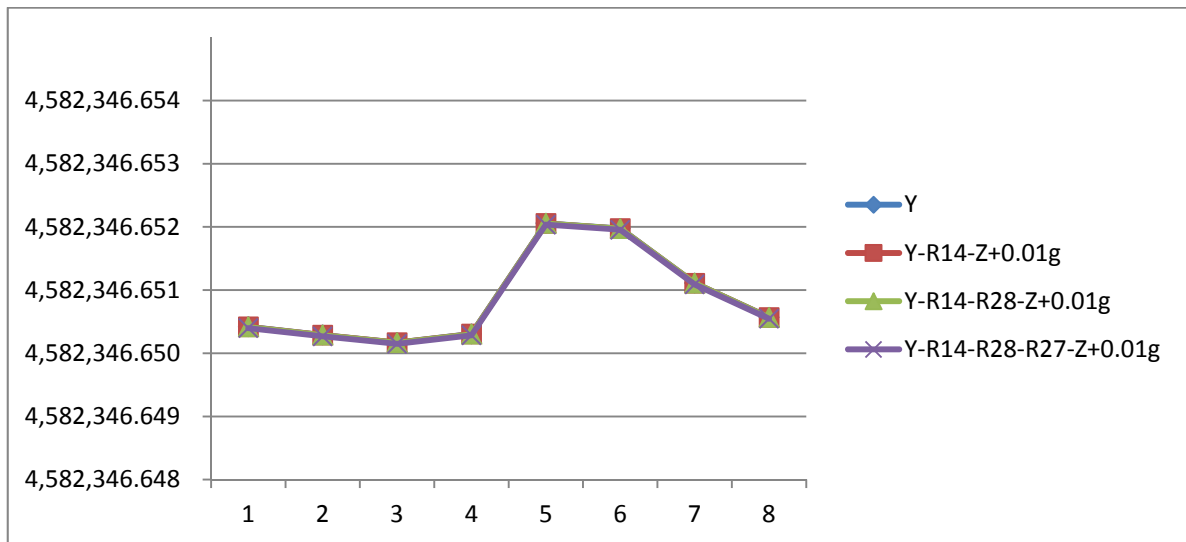
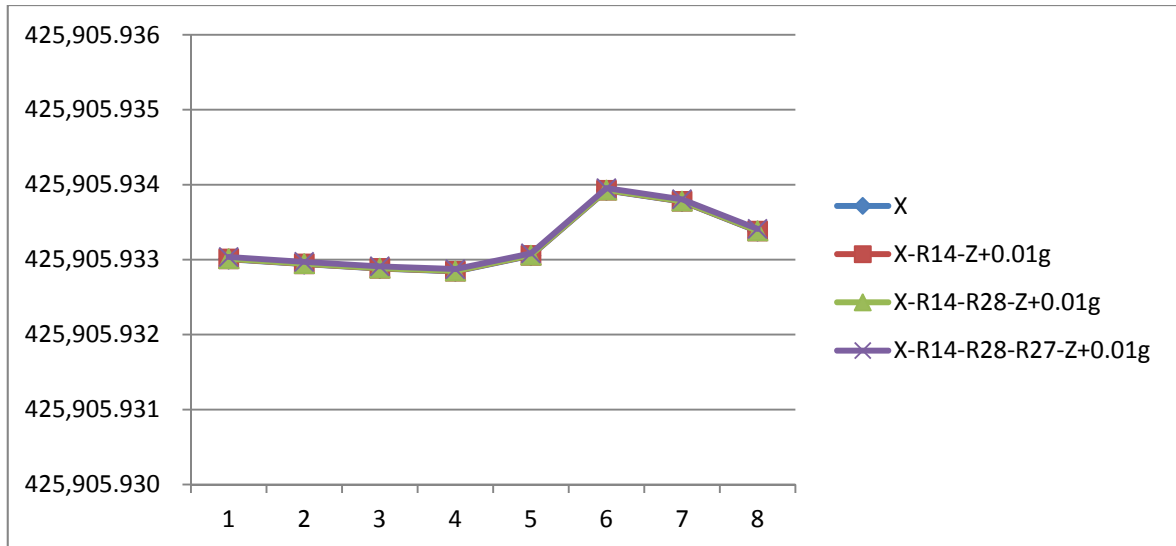


Figure 5.2 Sensitivity to zenith angle: Evolution of the X, Y Z coordinate of the RTS when a 0.01g change is introduced in one, two or three zenith angle measurements along the 8 epochs of a given day. Then coordinates (vertical axe) are expressed in m.

5.1.3 Sensitivity to distance--d

The distance is defined as the length between the RTS and the target. Here there are three different test schemes to test the sensitivity of the distance to the final result: an increase of 1mm on one reference point (R14), on two reference points (R14 and R28) and on three reference points (R14, R28 and R27). Figure 5.3 is the result of the three test results and the original result. Compared with the original result, the three test results are almost the same as the original in X, Y and Z. With this type of test, it can be proved that the distance has little influence on the result for a 1mm change. Similarly, coordinates X, Y and Z are relatively insensitive to an increase in the number of reference points with a 1mm change for distance.

5 Matching the Model with real world results

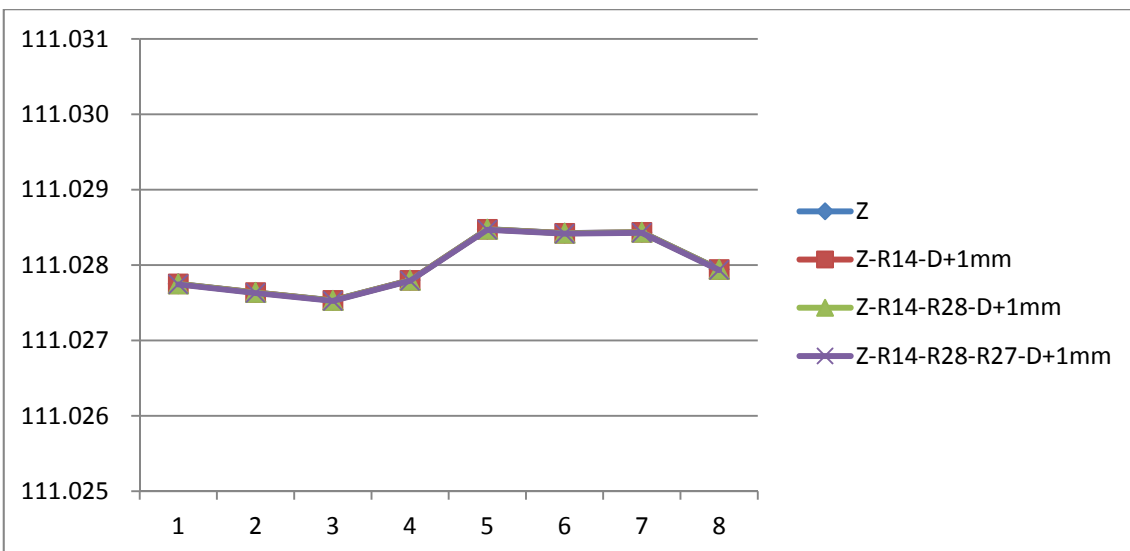
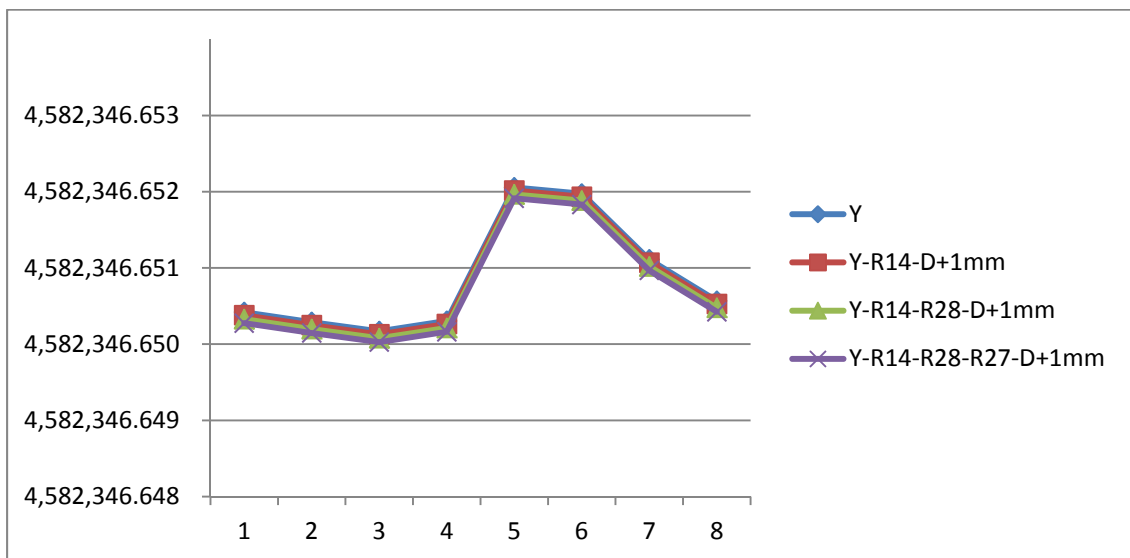
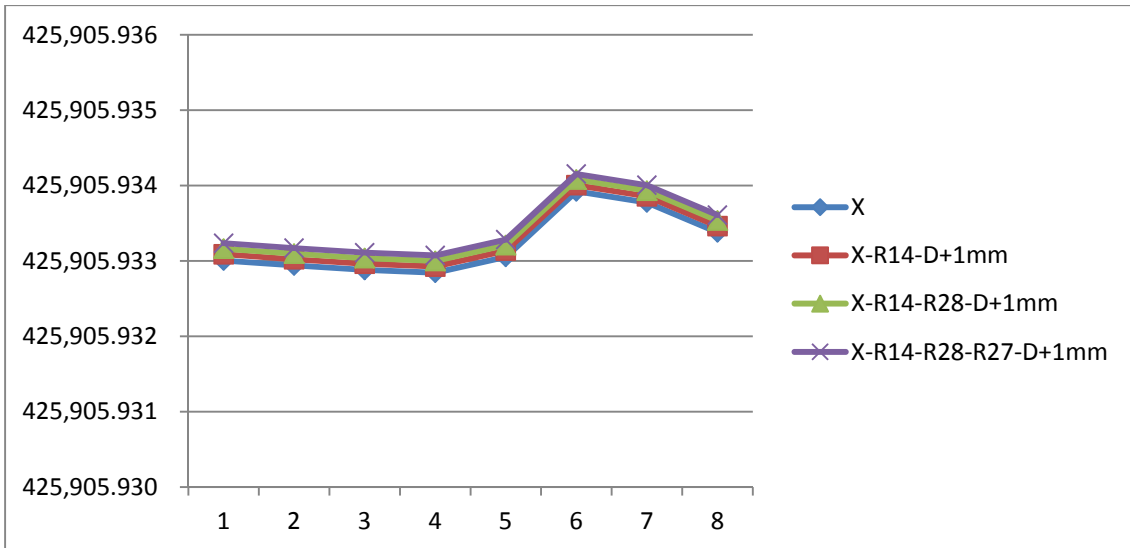


Figure 5.3 Sensitivity to distance: Evolution of the X, Y Z coordinate of the RTS when a 1mm change is introduced in one, two or three zenith angle measurements along the 8 epochs of a given day. Then coordinates (vertical axe) are expressed in m.

5.1.4 Conclusions about the sensitivity analysis

The above test results confirm the expectations that errors in the horizontal angle affect mostly the X and Y coordinates, errors in the zenith angle affect mostly the Z coordinate, and the change in distance affects coordinates X and Y. As expected, the differences are similar along the 8 epochs of the day.

In one configuration similar to the one that we have in the Campus Nord test area, the “normal” error in the measurements (small random errors) has a smaller effect on the results. Based on Figures 5.1, 5.2 and 5.3, we can particularize: an error of 10cc in a given horizontal angle (roughly the expected error) will modify the X and Y coordinates of the Total Station by about 0.1 mm; an error of 20cc in a given zenith angle will modify the Z coordinate of the Total Station by about 0.2 mm; and an error of 1 mm in a given distance measurement will modify the X and Y coordinates of the Total Station by about 0.2 mm.

This is favorable to the monitoring practice, because a single error has a small or moderate effect on the results. For instance: we may fail 1 mm in a given distance, but the RTS-computed coordinates only suffer a 0.2 mm misplacement. This “smoothing” of the importance of one error is a consequence of the redundancy of the setup (several extra reference prisms have been deployed in the scene).

This sensitivity analysis has been carried out on the coordinates XYZ of the RTS. Similar sensitivity may be found for the final coordinates of the control prisms. This analysis, however, has not been carried out here for time reasons; it must be done in the future.

5.2 Real monitoring results obtained with the standard system in the Campus Nord test area

In chapter 4, the test area around the Omega building in the Campus Nord, UPC, has been presented. In section 4.4 the acquisition system has been described. In relation to the RTS, we have 3 Robotic Total Stations, named A3-RTS, A6-RTS and N2-RTS, which acquire angles and distances (to the reference and control prisms spread around the area) following the standard procedure established by Soldata Group (Beth et al,

2005(Beth and Obre 2005)). . In particular, the acquisition is controlled by the Geoscope SW; after being checked and filtered, the values are published on an online database known as Geoscope-Web.

In the present section, these “standard” monitoring results have been drawn in graphs. They resemble results that are available in a normal monitoring project. The results are given in 4 subsections.

In section 5.2.1, we include the graphs showing the evolution of the X, Y and Z coordinates of the 9 control prisms located on the NW façade of the K2M building. These graphs can be qualified as the apparent movement of these 9 points over time. The information in this section is the information available on GW to the actors in a normal monitoring project (the constructor, the project director and the authorities).

In section 5.2.2, the evolution of the X, Y and Z coordinates of the RTS located in the A6 roof is presented. In a normal monitoring project, these values are not directly available from GW, because the results are intermediate or “in-house” results, and thus not directly useful to the main actors.

The people responsible for the monitoring (the engineers managing the monitoring system) can reach the RTS coordinates, epoch by epoch, but they are not available to the other actors. In this PhD work, for research reasons, this information has been made available to the R&D project, and is presented here.

In section 5.2.3, the information that is only available to this particular R&D project is shown. In a standard monitoring project, only the open-air temperature, which is acquired from a nearby meteorological station, is usually available; sometimes the humidity as well. In the aforementioned R&D project, we have installed a number of sensors (as shown in section 4.3) along the Omega building, which include temperature sensors, insolation sensors (also known as pyranometers), clinometers, and levelling sensors. This “extra” information has been of paramount importance to understand how the buildings and the monitoring system behave, and has been summarized in this section.

In section 5.2.4, we study the relationship between temperature evolution and the movement of the control prisms on the K2M building based on the results in section 5.2.1, section 5.2.2 and section 5.2.3.

Although the RTS have been working since July 2013, for the remaining of the analysis carried out in this PhD work, we have concentrated on a 45-day period: from 1st September, 2013 to 15th October, 2013. This period has the advantage of being representative of the main features that we wish to model in this work: We have high temperature (summer); a significant night/day variation in temperature; and at the end of the period, a sudden breakdown due to the transition to the fall season.

5.2.1 K2M control points movement

In a normal monitoring project, the final goal is to see the control points' movement: how many millimeters the movement value of the control points in one time unit is and which direction they move toward. From the GW, the data about the evolution of the X, Y and Z coordinates of the control points located on the NW façade of the K2M building are available to the actors (the constructor, the project director, the authorities).

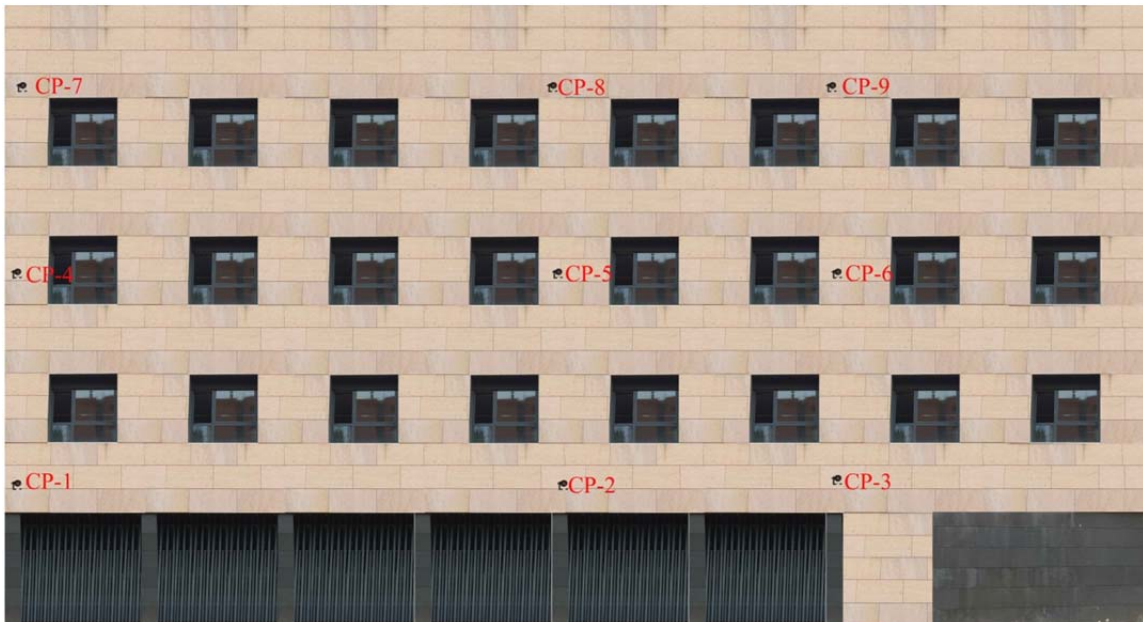


Figure 5.4 Distribution of control points on Façade-NW, K2M building.

In total, there are nine control points on the North West Façade of the K2M building which are monitored by the RTS on A6 building. The prisms CP1, CP2 and CP3 have

been installed between the ground floor and the first floor; CP4, CP5 and CP6 on the second floor; and CP7, CP8 and CP9 between the third floor and the roof level (Figure 5.4).

These are nine curve graphs which describe the movement trend of the control points on the K2M building over the period from 1st September 2013 to 15th October 2013: Figures 5.5 to 5.7 contain the movements of the control points in X-direction, Figures 5.8 to 5.10 contain the movements of the control points in Y-direction, and Figures 5.11 to 5.13 contain the movements of the control points in Z-direction. From the results of control points, it can be seen that in X-direction, the movement ranges are about 1mm for CP3, CP4, CP5, CP7 and CP8, 1.5mm for CP2 and CP9, 2mm for CP6; in Y-direction, the movement ranges are about 1mm for CP3, CP5, CP8 and CP9, 1.5mm for CP2, CP4, CP6 and CP7; in Z-direction, the movement ranges are about 1.5mm for CP2, CP3, CP4, CP5, CP7 and CP8, 2mm for CP9 and 2.5mm for CP6. Because of the influence of leaves in front of K2M building, the movement ranges of CP1 are very big, which are 3.1mm in X-direction, 5mm in Y-direction and 9.7mm in Z-direction.

The nine control points on the façade NW of the K2M building have been divided into three groups in order to analyze their behavior: group-1 contains CP-1, CP-4 and CP-7 on the left part of the façade; group-2 contains CP-2, and CP-5 and CP-8 in the middle part of the façade; and group-3 contains CP-3, CP-6 and CP-9 on the right part of the façade. As can be appreciated in Figure 5.4, the control points in each group belong to the same vertical column on the façade NW of the K2M building.

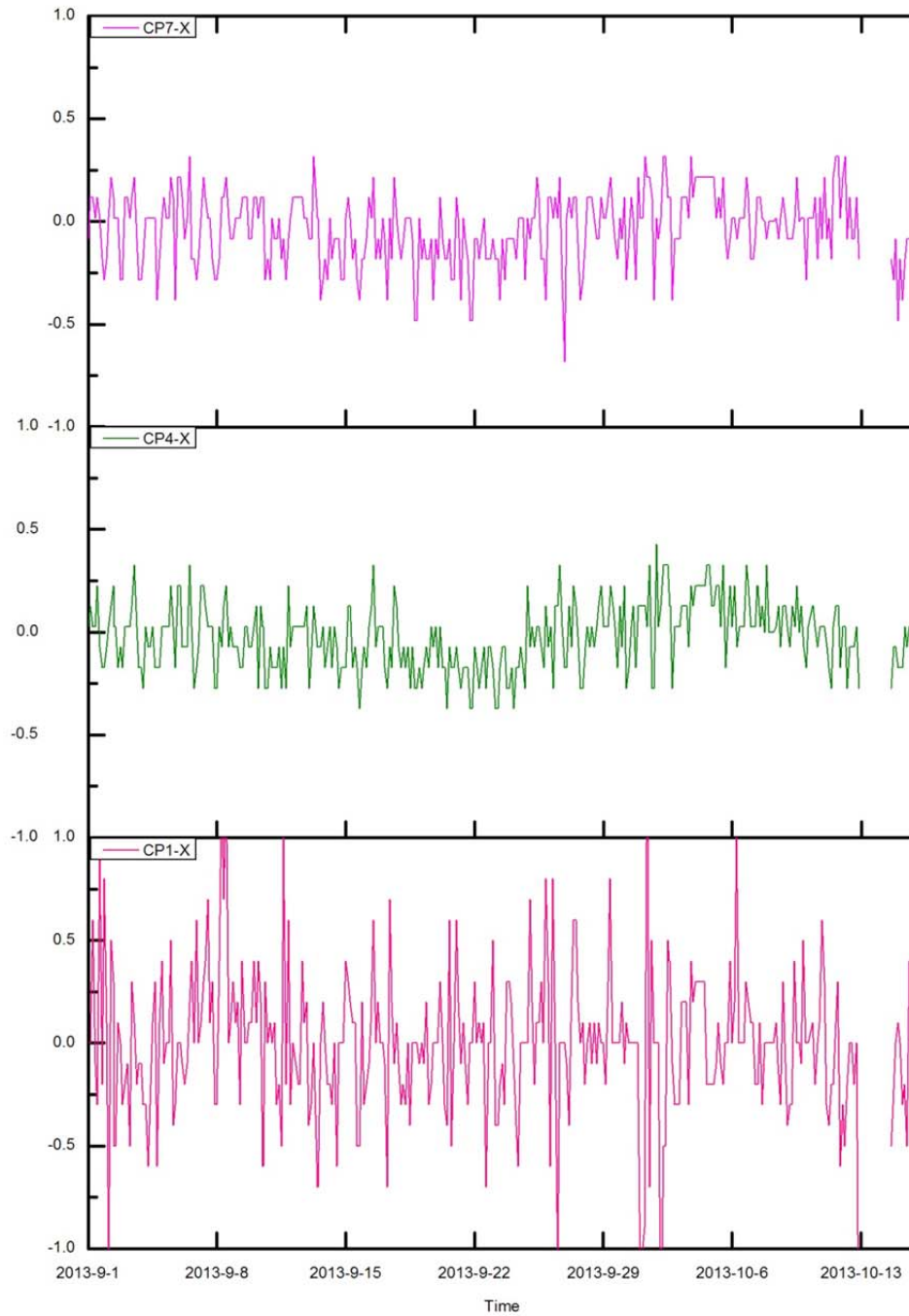


Figure 5.5 K2M, NW façade, left side, the movement of control points CP1, CP4 and CP7 in X-direction (mm).

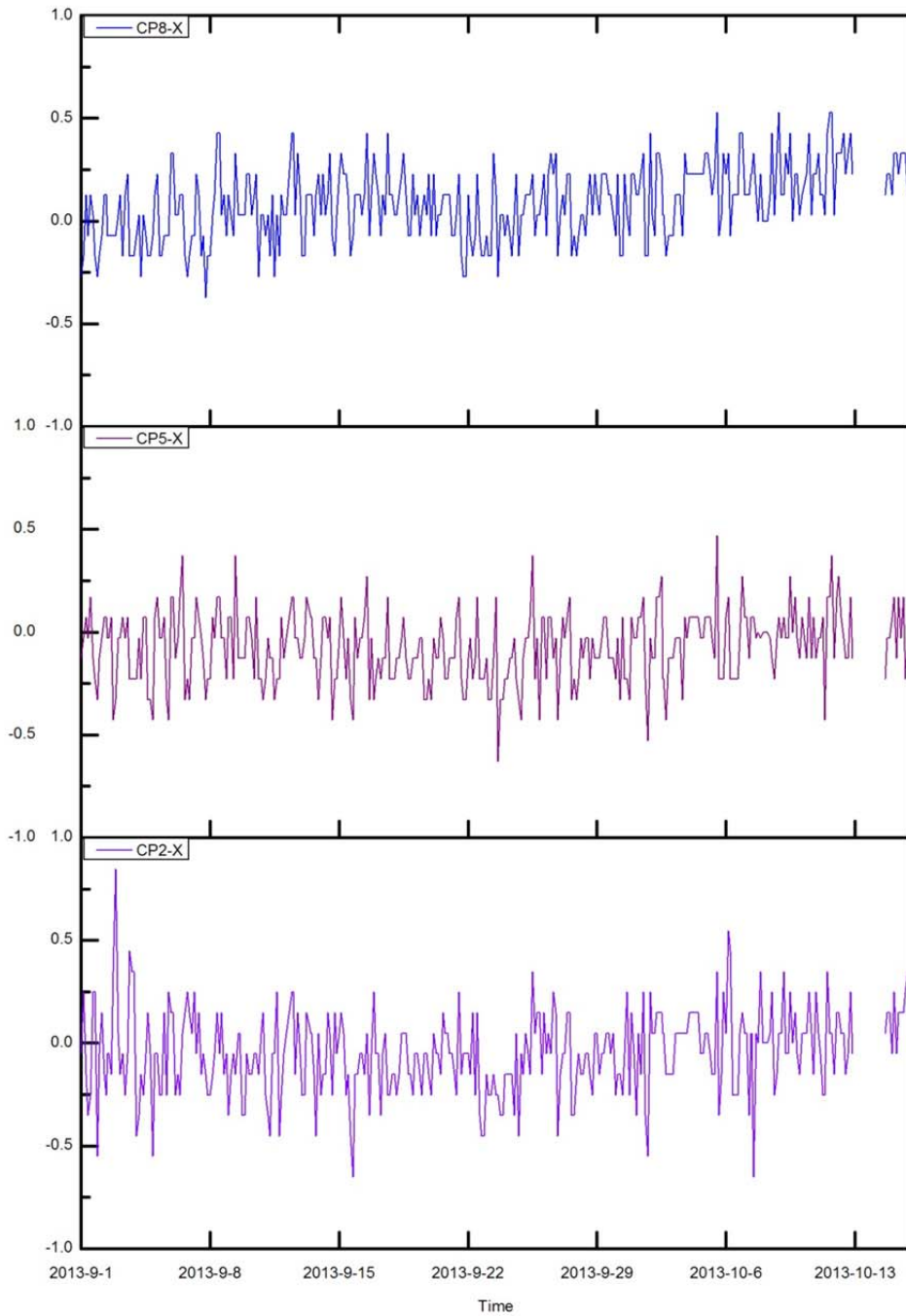


Figure 5.6 K2M, NW façade, center, the movement of control points CP2, CP5 and CP8 in X-direction (mm).

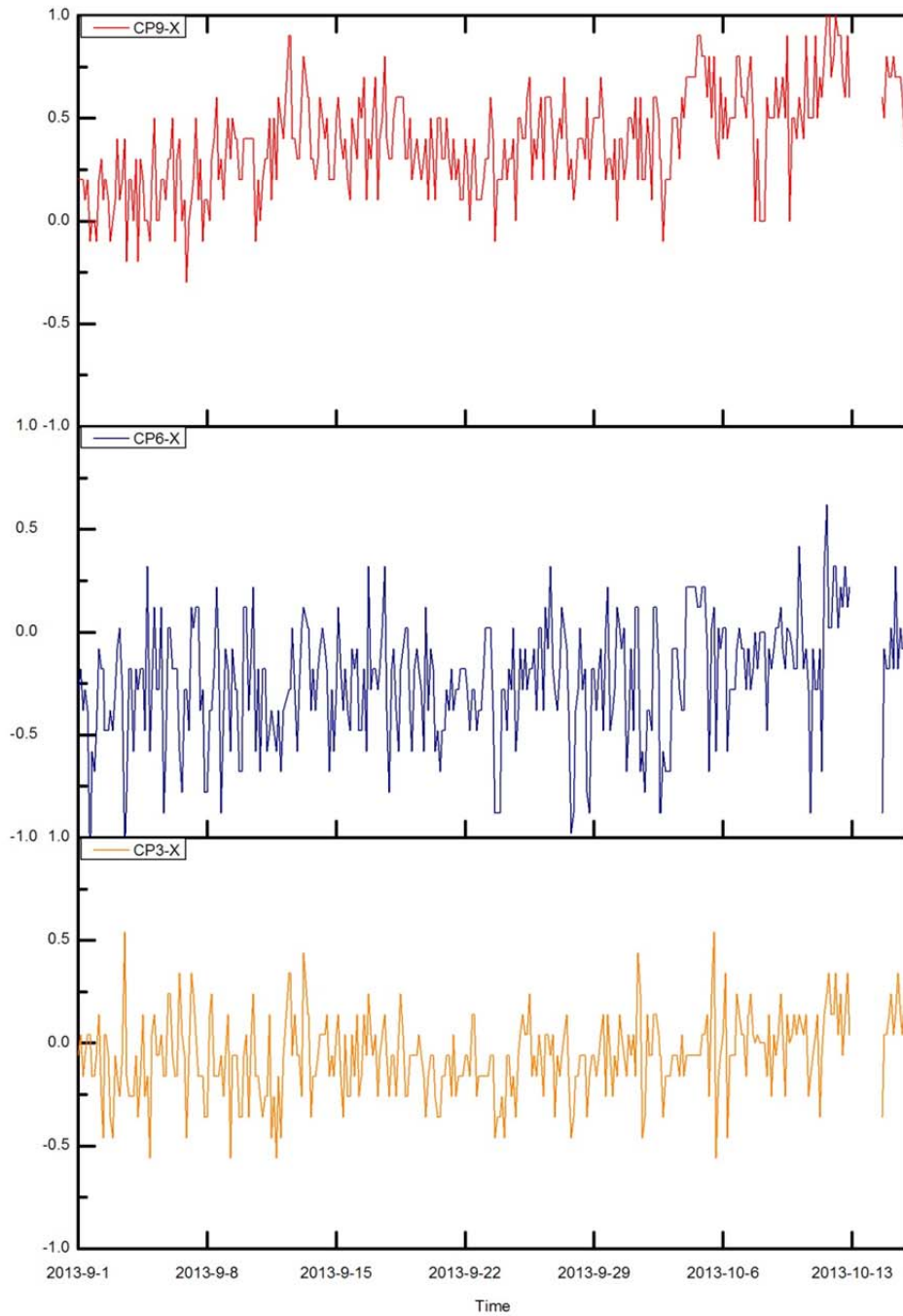


Figure 5.7 K2M, NW façade, right side, the movement of control points CP3, CP6 and CP9 in X-direction (mm).

In Figures 5.5 to 5.7, the curve graphs depict the movement of the control points in X-direction over the period from 1st September 2013 to 15th October 2013. For group 1, the control points 4 and 7 show a small daily movement within the range of ± 0.5 mm. The whole period looks somehow similar to the general aspect of the evolution of the RTS (presented later in Figure 5.14). This similarity will be more evident when analyzing the Y axis.

However, there are some jumps in the curve of control point 1 which are obviously well over the normal range of the displacement. The reason for this phenomenon is that there is a tree in front of control point 1, and the line of sight between control point 1 and the RTS is partially obstructed by the foliage, especially when the branches are swinging in the wind. Regarding the results in group 2 (Figure 5.6) and group 3 (Figure 5.7), the control points that are located at the bottom and in the middle (CP-2, CP-5, CP-3 and CP-6) display a fairly normal daily fluctuation during the period. Nevertheless, the two control points on the upper level (CP8 and CP9) exhibit a slight upward trend during the study period.

Figures 5.8 to 5.10 show the movement of the control points in Y-direction. The results for CP1 can be excluded for the same reason as before (the tree disturbance). The rest of the control points follow a common general trend. This means that there is a gradual reduction in the Y-coordinate starting in September which reaches the lowest point around 19th September. From then on, the curves go up until 5th October. After that, the curves fall noticeably. The inverse trend in the last part cannot be seen clearly, because there is a lack of two days' data on 13th October and 14th October. But it can be estimated that there is a turning point on 14th October followed by the upward trend on 15th October. Apart from that, the daily fluctuation is also present in all the graphs from Figures 5.8 to 5.10.

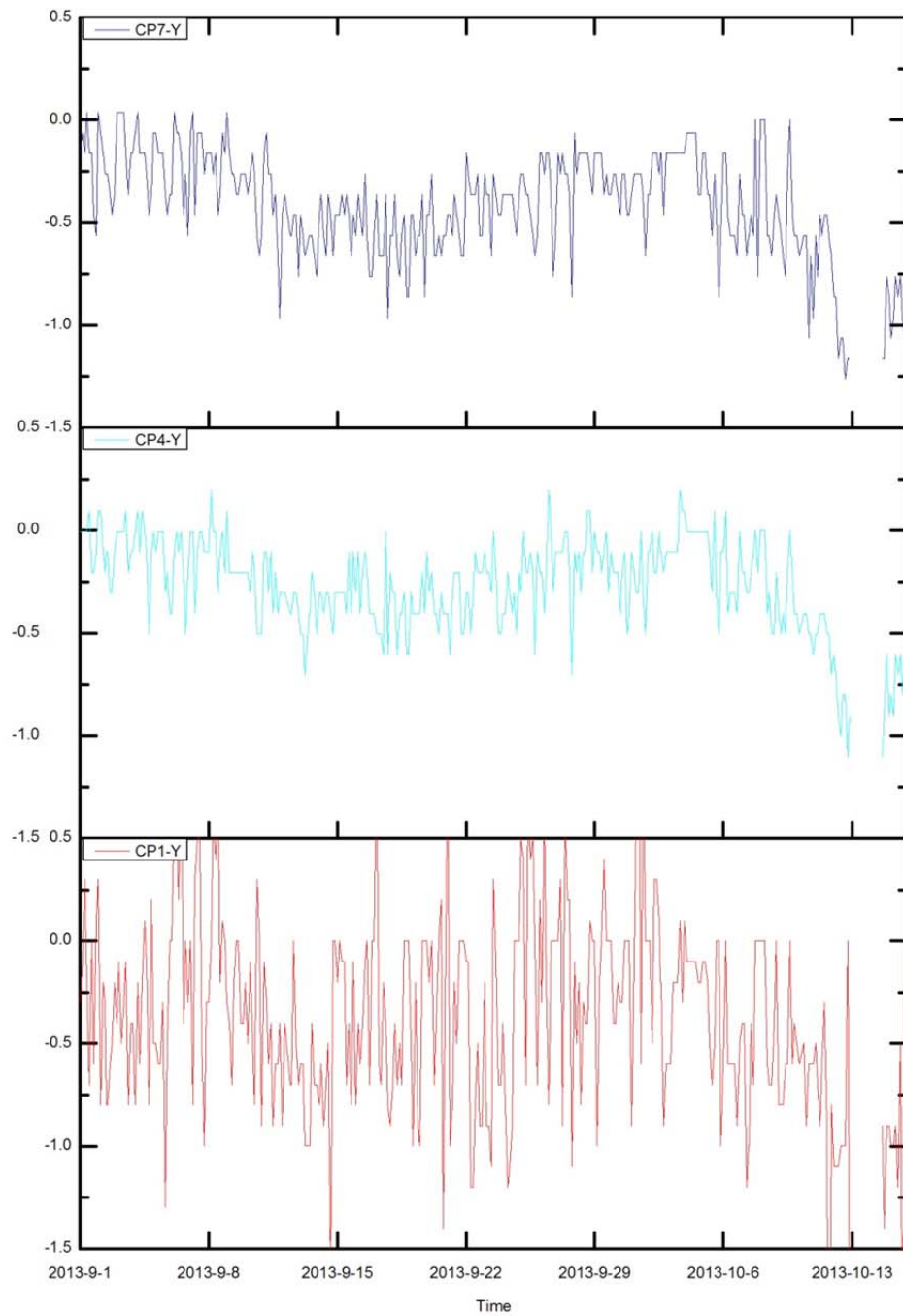


Figure 5.8 K2M, NW façade, left side, the movement of control points CP1, CP4 and CP7 in Y-direction (mm).

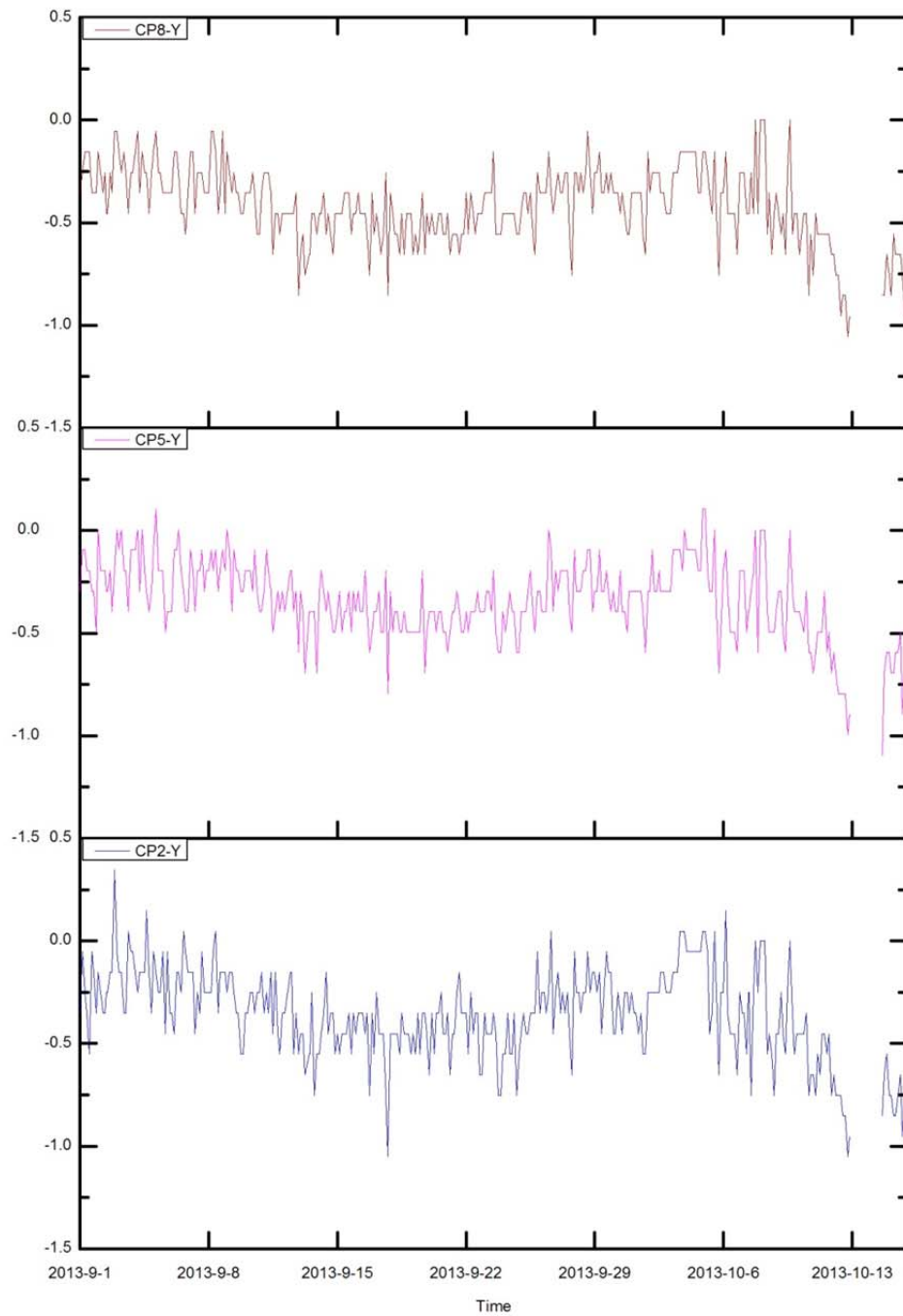


Figure 5.9 K2M, NW façade, center, the movement of control points CP2, CP5 and CP8 in Y-direction (mm).

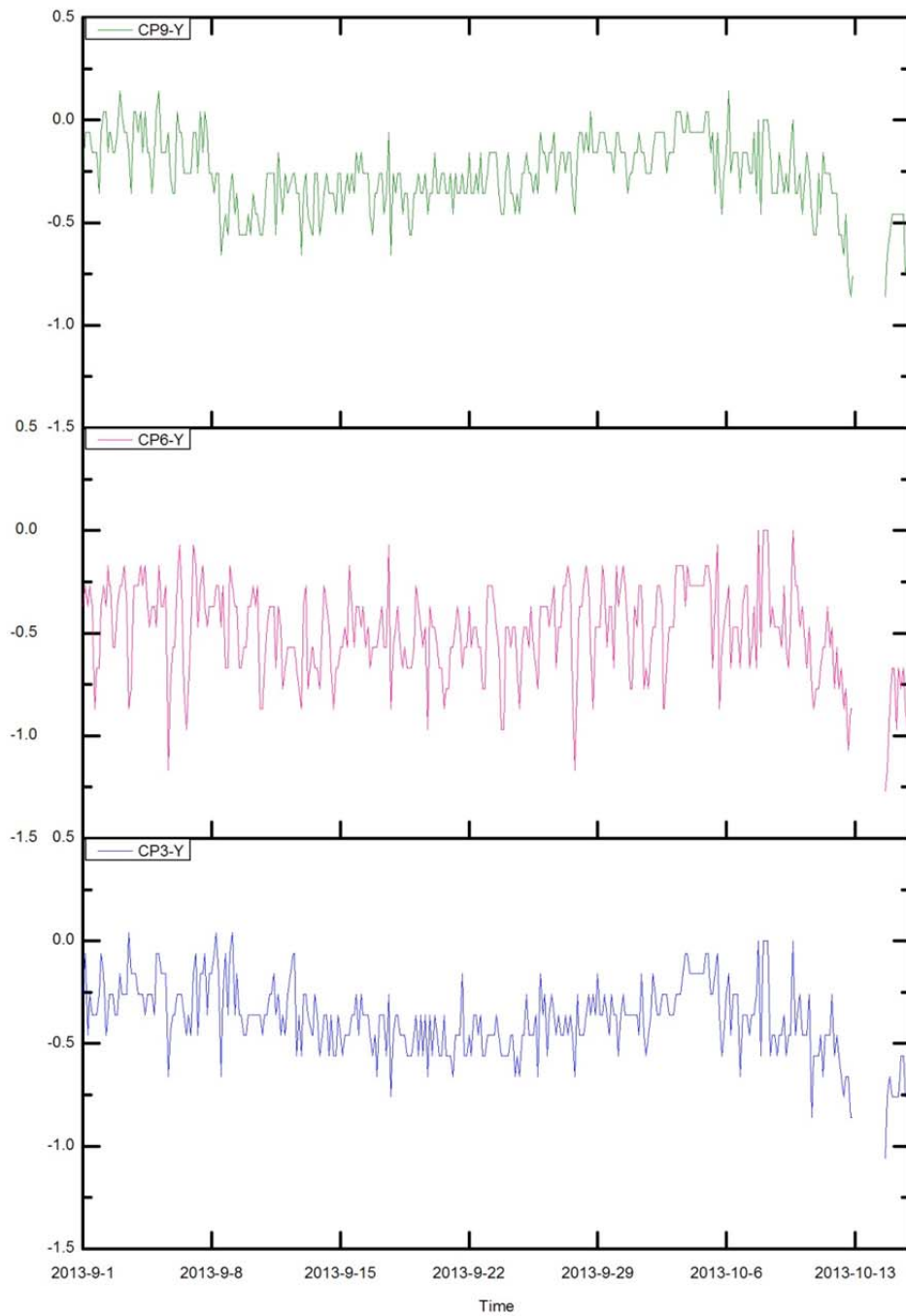


Figure 5.10 K2M, NW façade, right side, the movement of control points CP3, CP6 and CP9 in Y-direction (mm).

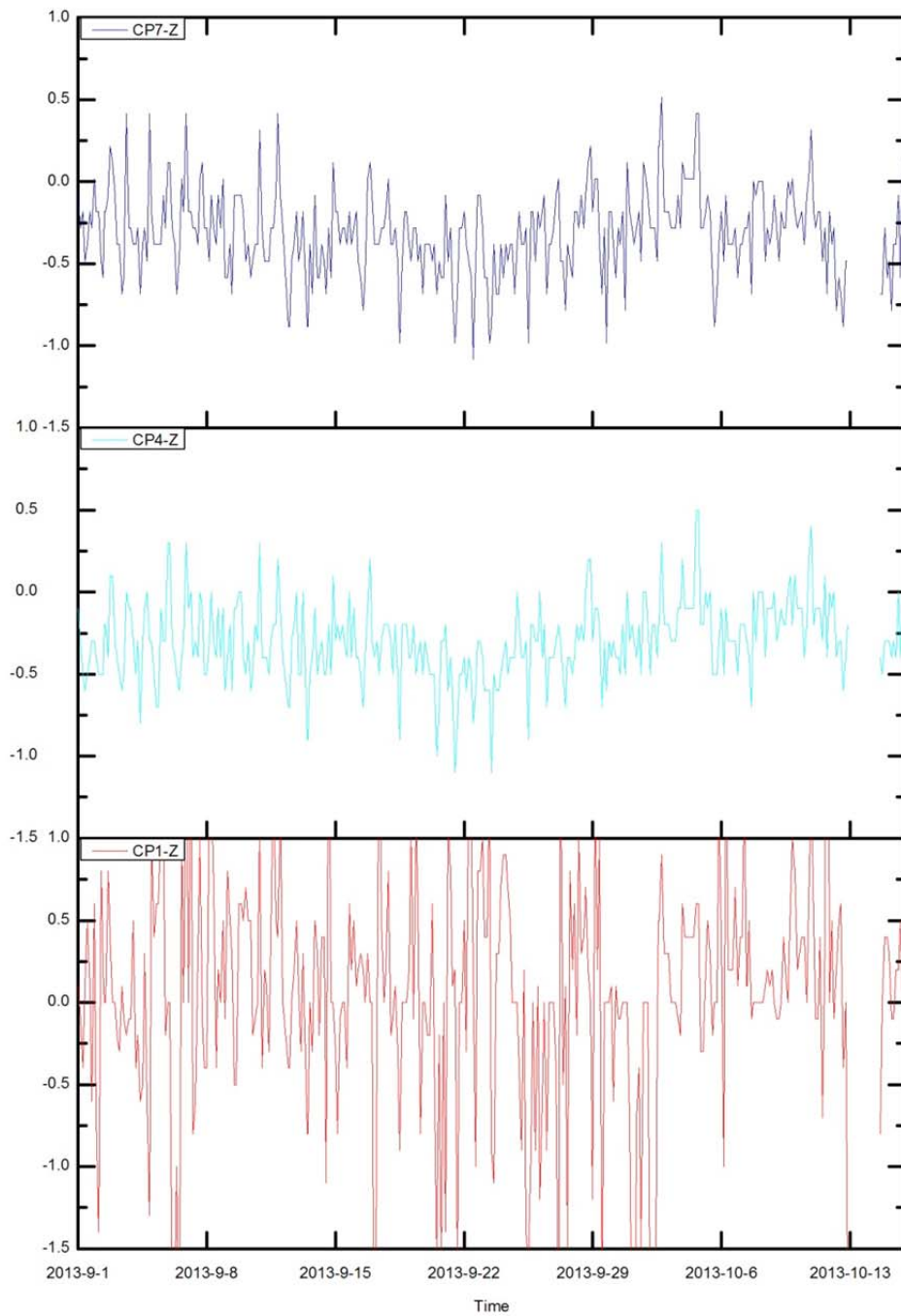


Figure 5.11 K2M, NW façade, left side, the movement of control points CP1, CP4 and CP7 in Z-direction (mm).

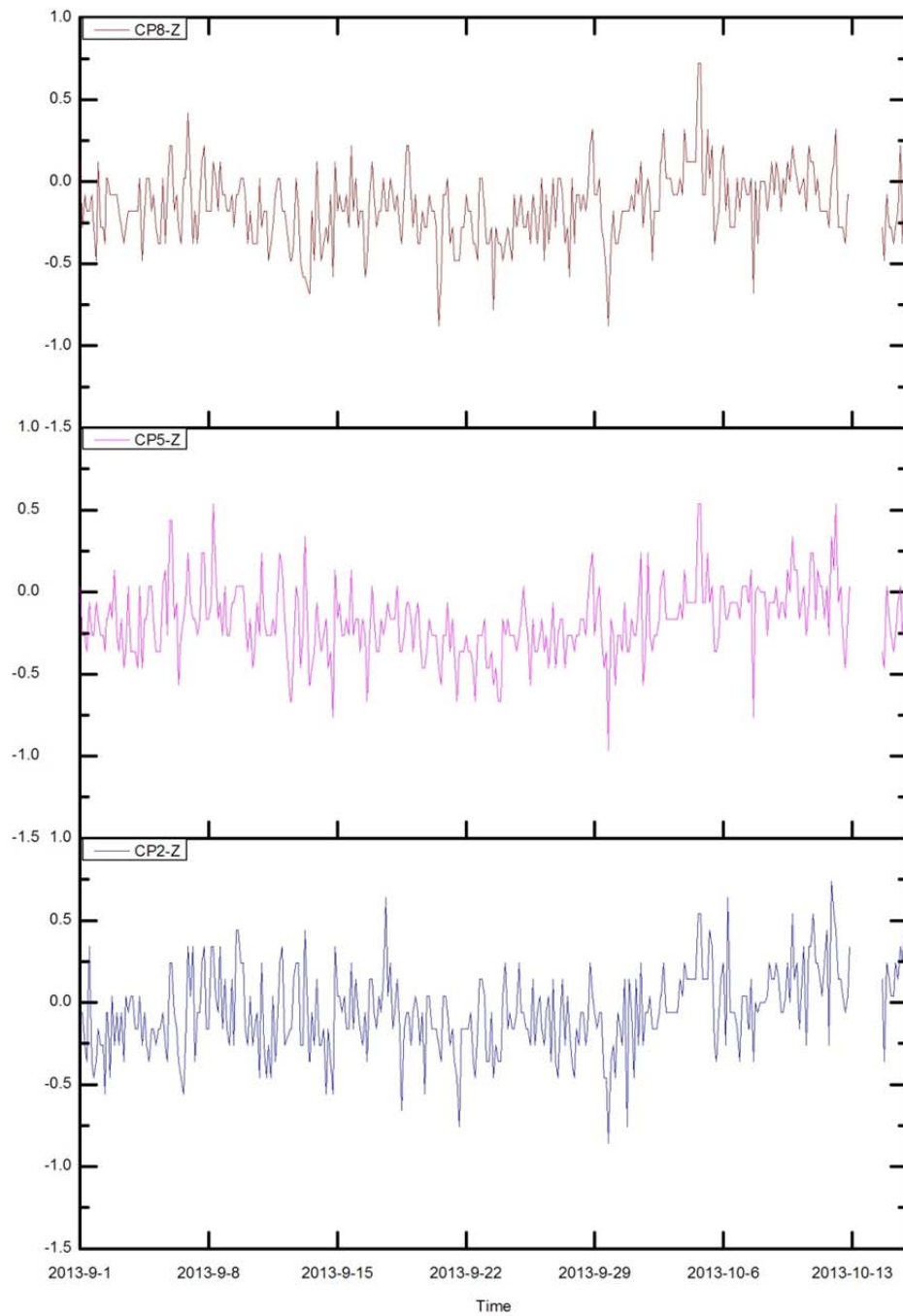


Figure 5.12 K2M, NW façade, center, the movement of control points CP2, CP5 and CP8 in Z-direction (mm).

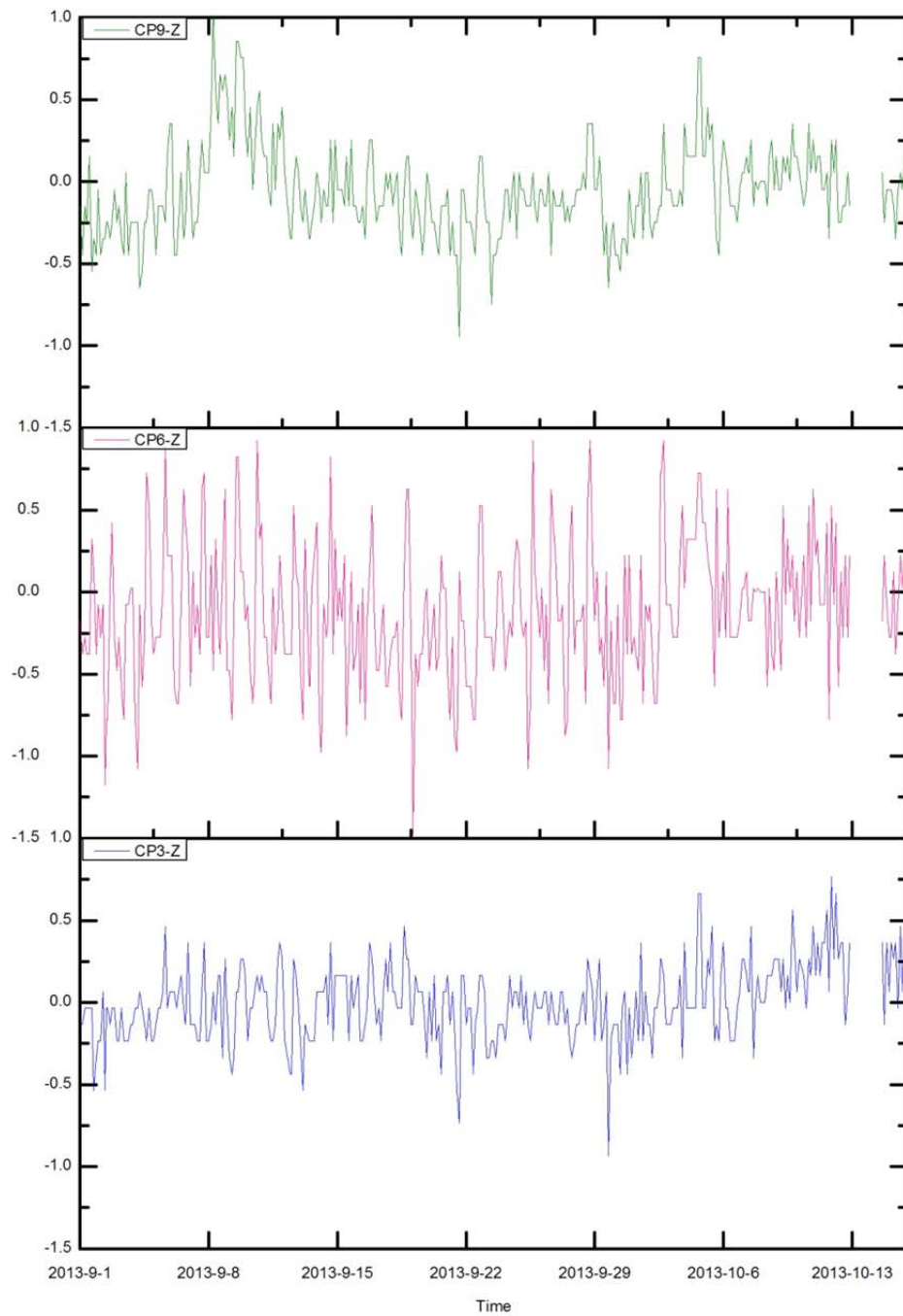


Figure 5.13 K2M, NW façade, right side, the movement of control points CP3, CP6 and CP9 in Z-direction (mm).

Finally, Figures 5.11 to 5.13 present the displacement of the control points in Z-direction. From the three graphs, it can be observed that the movements of the curves in Z-direction are similar, generally speaking, to the results in the X and Y axes. The total span of the movement is in the same order, and the daily fluctuations are also clear. It is reasonable to relate these fluctuations with changes in temperature. This issue will be addressed in section 5.2.4. Control point CP1 exhibits again different behavior in Z because of the tree (Figure 5.11). There is a marked increase around 10th September for control point CP9 (Figure 5.13). On the other hand, CP6 presents a wider daily Z-fluctuation. Checking back to the corresponding graphs for X (Figure 5.7) and Y (Figure 5.10), we realize that this wider fluctuation is present in the 3 axes for CP6. It may be concluded that some local factor is influencing (amplifying) the movement of the prism. Reviewing the installation of the prisms on the façade (Figure 4.4 in Chapter 4), one possibility is that the stones of the façade move the bar that supports the prism. It is advisable to disregard this CP6 in further detailed analysis.

5.2.2 A6-RTS movement

After the presentation about the evolution of the X, Y and Z coordinates of the 9 control prisms on the NW façade of K2M building, this section mainly focuses on the evolution of the X, Y and Z coordinates of the center of the Robotic Total Station A6, which is located on the roof of the A6 building.

Generally, the evolution of the X, Y and Z coordinates of the RTS is not available to everyone except the engineers of the project, but based on the aim of the research we have access to the data of the coordinates of the RTS, epoch by epoch, during the period between 1st September 2013 and 15th October 2013.

In the GeoscopeWeb system that manages the Campus Nord experimental data there are three RTS (working as a group) monitoring the K2M building (as shown in Figure 4.1 in Chapter 4). There are a total of 15 reference points related to the A6-RTS (13 reference points on the building and 2 reference points on the ground). Figures 5.14 to 5.16 show the movement of the A6-RTS in X, Y and Z directions. The movement ranges of RTS are 2.57mm (between -1.6mm and 0.97mm) in X-direction, 2.67mm (between -1.4mm and 1.27mm) in Y-direction, and 2.19mm (between -1.3mm and 0.89mm) in Z-direction.

From Figure 5.14 and 5.15, it can be seen that the A6-RTS follows the same movement trend in X-direction and Y-direction, where curves fall during the time from 1st September 2013 to 13th September 2013, after which they change direction and increase steadily in the time spanning from 13th September 2013 through to 2nd October 2013. Then the curves decrease again in the last study period. Figure 5.16 shows the A6-RTS movement in Z-direction. Unlike X and Y, the curve of Z follows a different trend, rising and falling in the time between 1st September 2013 and 4th October 2013, and dropping suddenly after that.

In the 3 graphs, there is a visible 24h repetition pattern, which can preliminarily be associated to the daily influence of the temperature. This preliminary relationship will be worked out in section 5.2.4.

5 Matching the Model with real world results

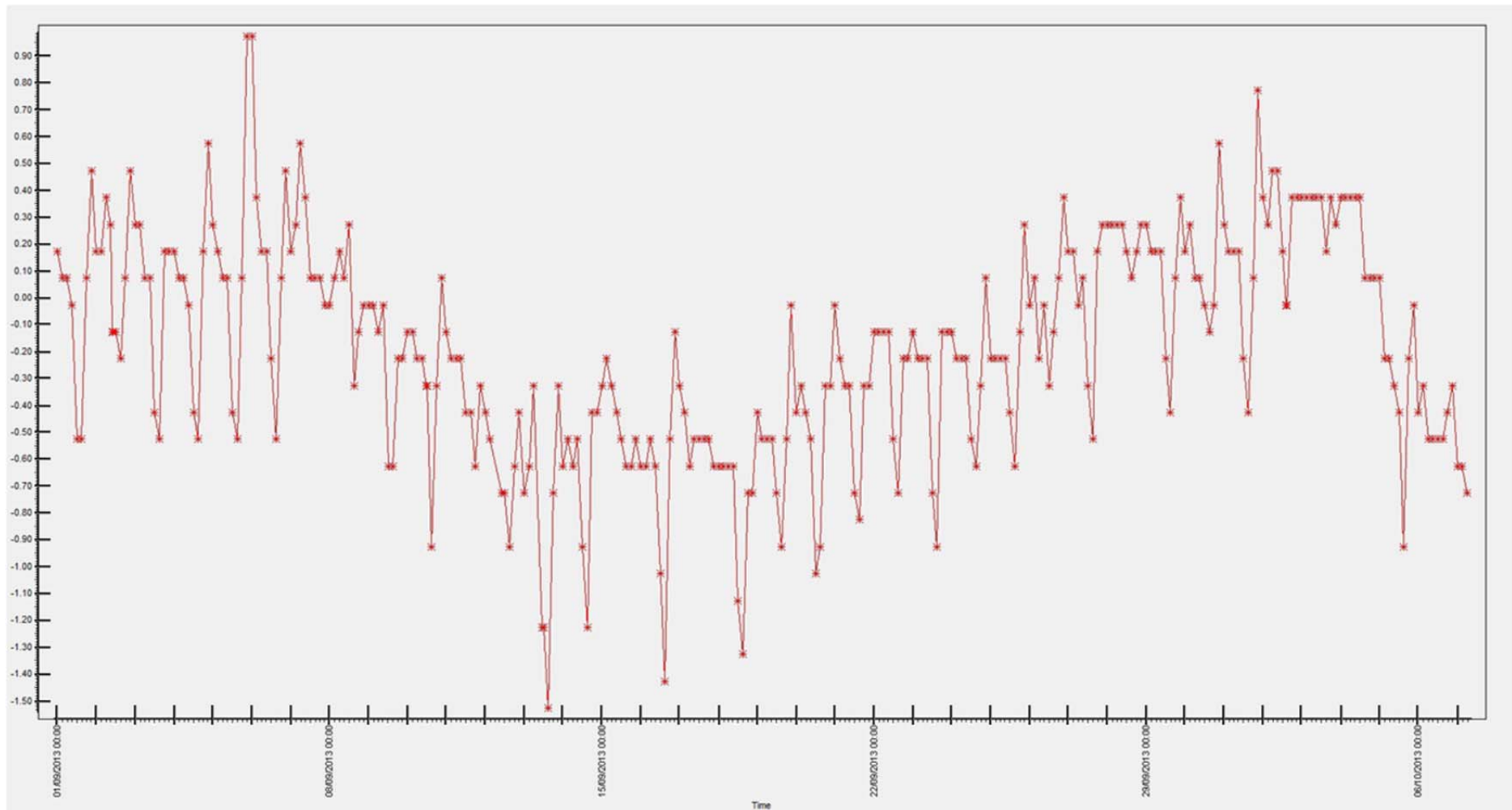


Figure 5.14 A6-RTS movement in X-direction during the study period. The vertical axis shows the change of the X coordinate in mm.

5 Matching the Model with real world results

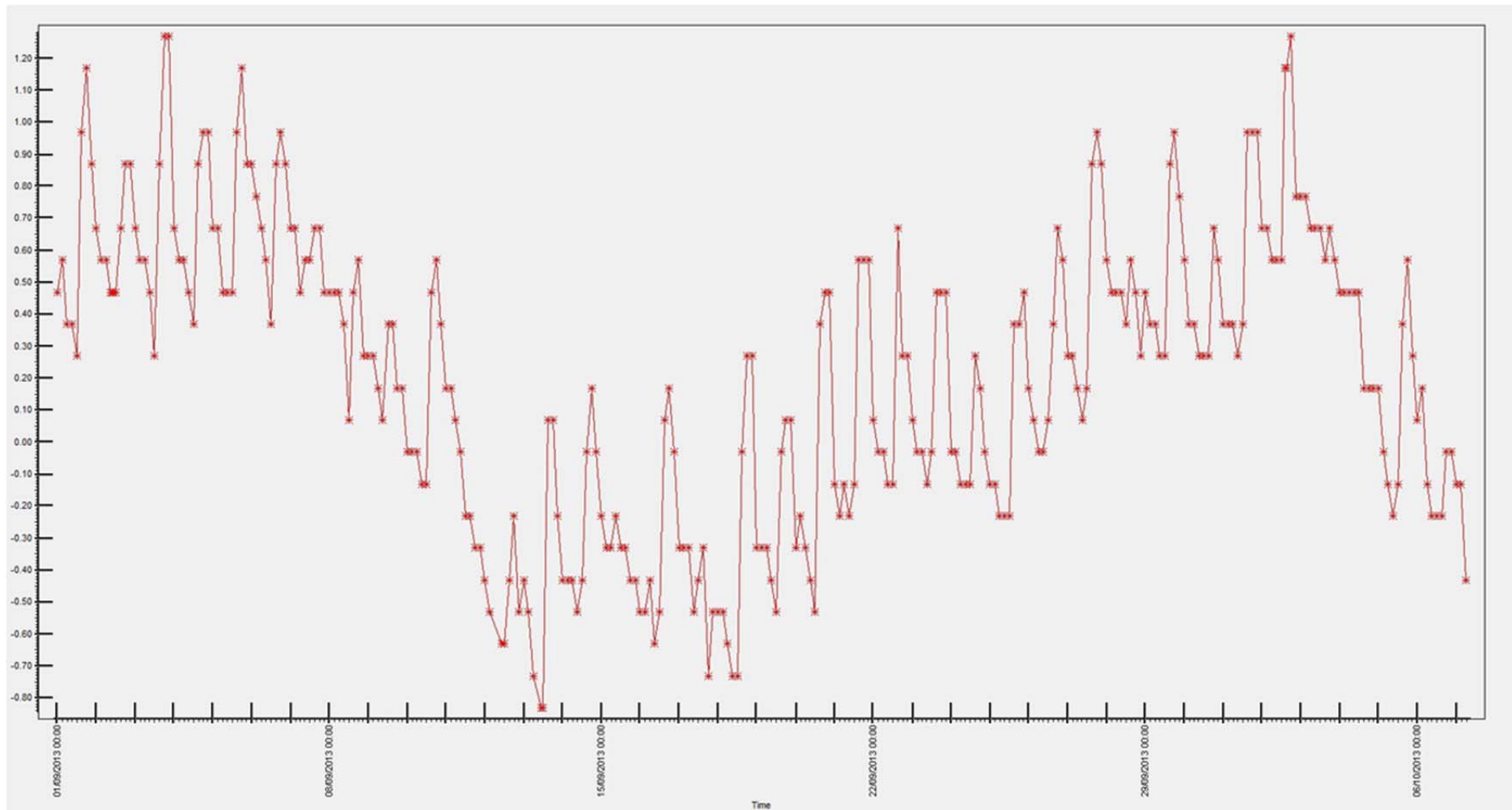


Figure 5.15 A6-RTS movement in Y-direction during the study period. The vertical axis shows the change of the Y coordinate in mm.

5 Matching the Model with real world results

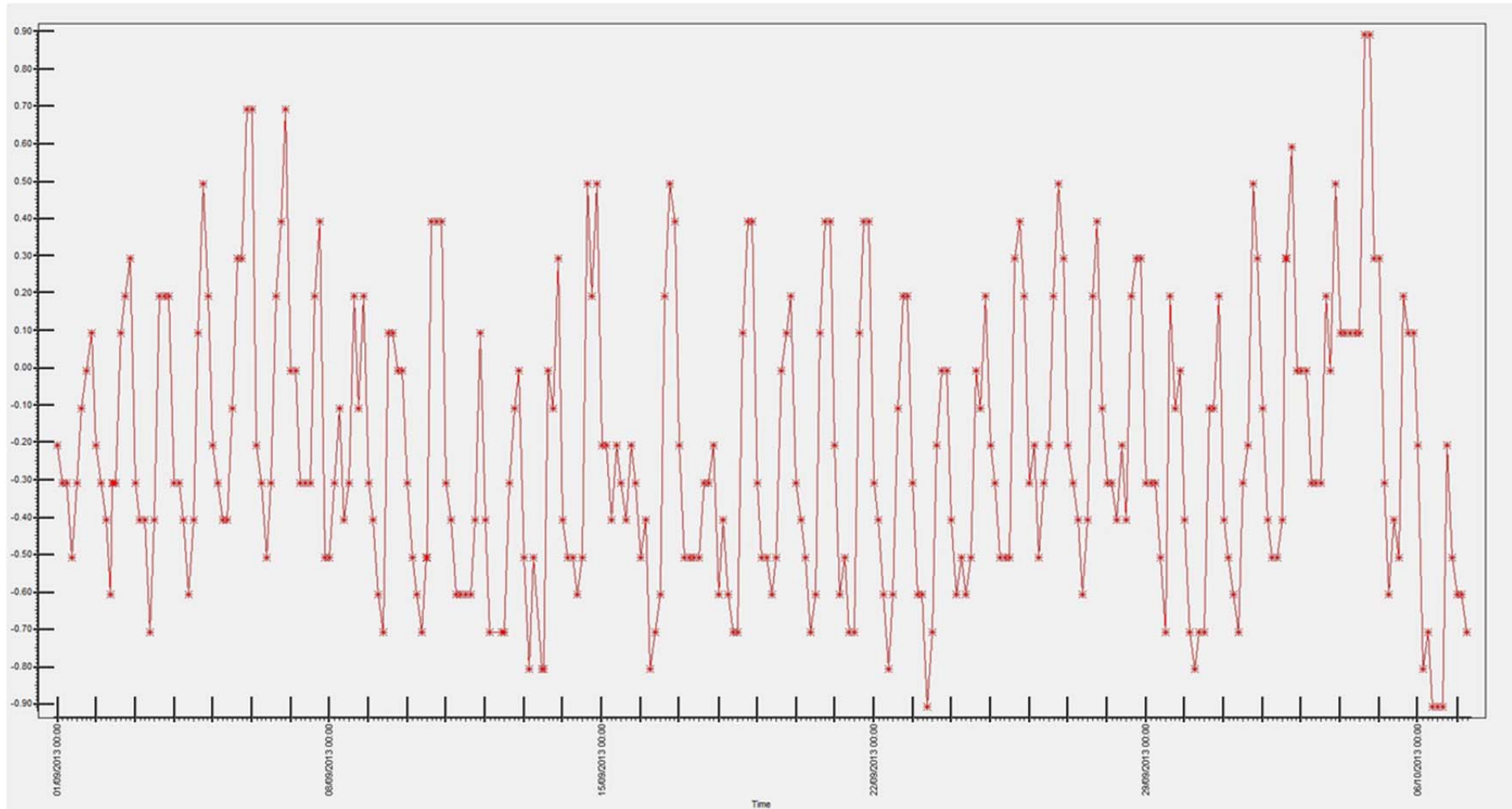


Figure 5.16 A6-RTS movement in Z-direction during the study period. The vertical axis shows the change of the Z coordinate in mm.

5.2.3 Temperature and Insolation evolution

Temperature is an important factor for structural deformation monitoring. For this particular R&D project, one meteorological station and a number of sensors (temperature sensors, insolation sensors, clinometers, and levelling sensors) have been installed to collect the maximum amount of data in order to understand how the buildings and the monitoring system behave.

The temperature and insolation data have been selected from the GeoscopeWeb software for analysis and study over the time period between 1st September, 2013 and 15th October, 2013.

Figures 5.17 and 5.18 show the changes in the outside and inside temperatures over the period from 1st September, 2013 to 15th October, 2013. For comparison, the Open Air Temperature evolution is also shown at the top of both figures. When we say “outside” temperature, we refer to the values measured by a thermometer inserted in the concrete column of the structure on the outer side (shown in Figure 4.5 in Chapter 4). On the other hand, the term “inside” in Figure 5.18 graph refers to the thermometer inserted in the same column on the inner side (shown in Figure 4.5 in Chapter 4). The term “average” that appears also in Figures 5.17 and 5.18 means that the values are an average of the temperatures registered by the 2 or 3 thermometers installed at different levels on this façade.

As can be seen from Figure 5.17, the open air temperature ranges between 10.6 °C and 31.4 °C during the period of time. The difference is about 21 degrees, which is a significant change in the 45 days. As for the three façades of the K2M building, their ranges are smaller. For Façade-NE, the fluctuation is from 16.07 °C to 26.68 °C; for Façade-NW, the fluctuation is between 15.63 °C and 26.62 °C, and for Façade-SE, the fluctuation spans from 17.60 °C through to 28.25 °C. What is more, great changes took place in October for the outside temperature curves. The open air temperature curve reaches the low point of 10.6°C at 15:00 pm on 6th October. At 9:00 am on 12th October, the curves of the three façades of the K2M building reach their low points: 16.07 °C on NE façade, 15.63 °C on the NW façade and 17.6 °C on the SE façade.

From Figure 5.18, it can be seen that there is not a great deal of difference among the three curves for the inside temperature on the three façades. Compared with the open air

temperature, the fluctuations of the three inside temperature curves are small in the period between 1st September and 15th October.

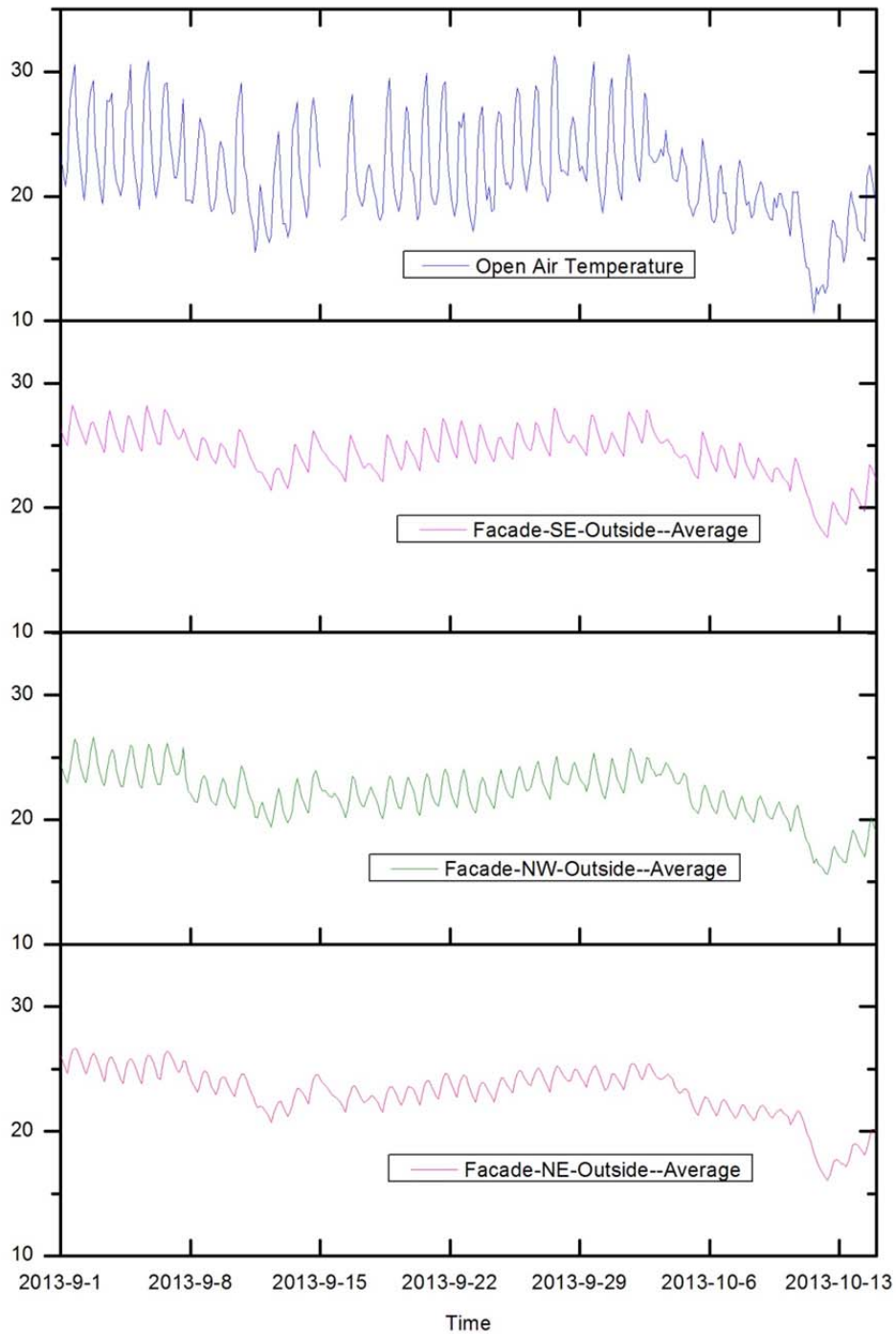


Figure 5.17 Outside temperature evolution (°C) of each facade of the K2M building from 1st September 2013 to 15th October 2013.

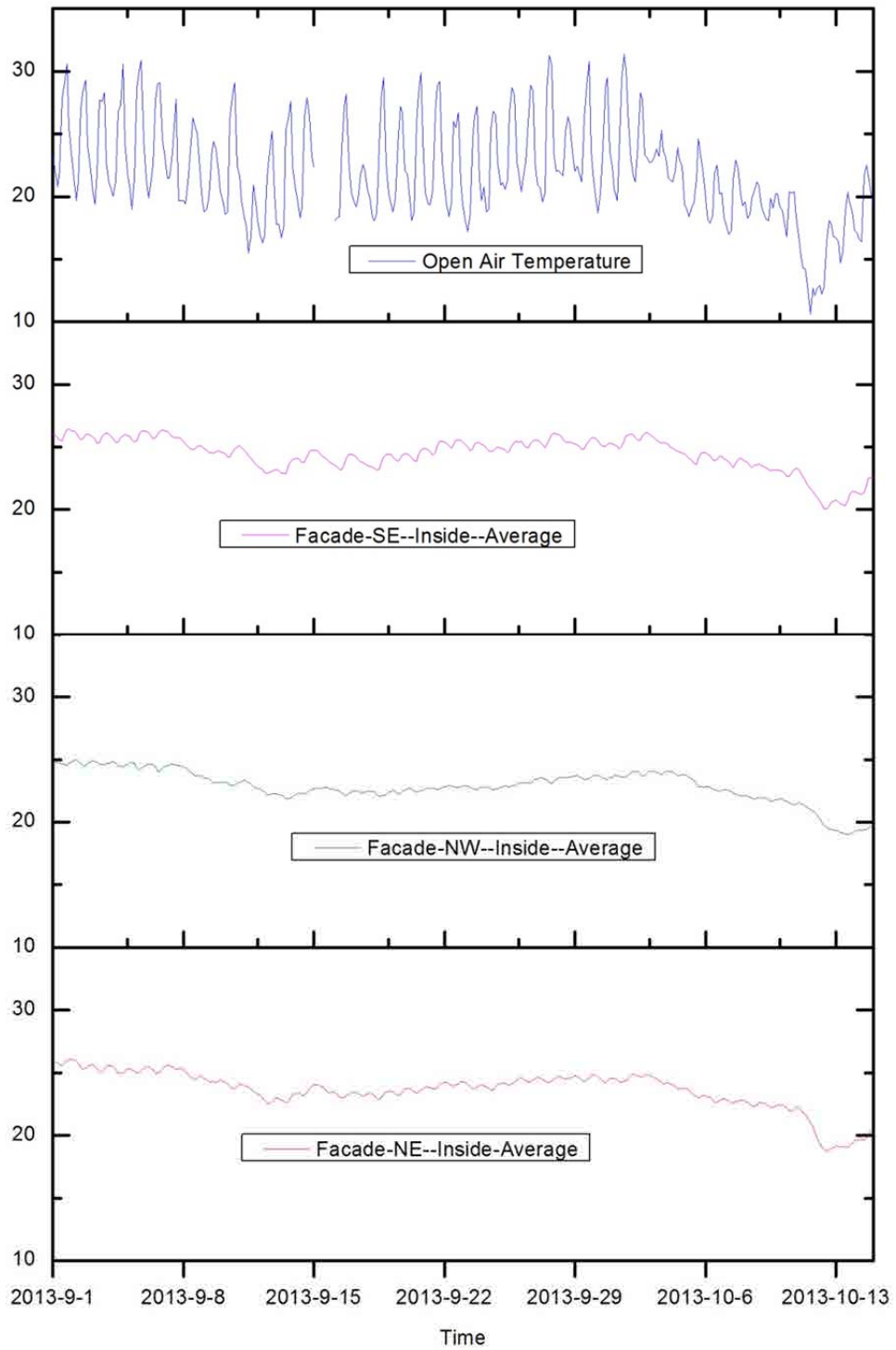


Figure 5.18 Inside temperature evolution ($^{\circ}\text{C}$) of each facade of K2M building from 1st September 2013 to 15th October 2013.

Insolation is the total amount of solar radiation energy received on a given surface area per unit of time, i.e. energy power per unit of surface. Sometimes it is also called solar irradiation. The amount of insolation that an area receives varies over the course of a day or a year. On a sunny day, the highest point of the sun's path in the sky is the time when the maximum amount (intensity) of insolation for the day reaches a location. By knowing the insolation levels of a particular region, we can determine the size of the solar collector that is required and how much of the sun's energy reaches the surface of the building. This enables us to understand the influence of the weather and climate patterns on a building. It is also useful for us in order to convert energy from the sun into temperature to obtain the structure's deformation over time. Solar insolation levels are generally expressed in W/m^2 , which is the amount of solar energy per second received by one square meter of the earth's surface.

In order to measure the influence of insolation on the surface temperature of the K2M building, three insolation sensors were installed on the three façades of the K2M building to collect the insolation intensity on each façade, which are façade-NE, façade-NW and façade-SE. Apart from that, we also received the insolation data from a 360-degree insolation sensor from Barcelona Meteorological Agency (X8 automatic station, near the C. Nord site).

Figure 5.19 describes the change in the insolation levels around the K2M building over our study period. It shows how much sunlight fell on the area (full angle insolation, 360°) and the building's surface (Façade-NE, Façade-NW, Façade-SE) that we studied during the time period indicated.

The insolation values plotted on those three graphs decreased during this period. From 1st September, 2013, to 31st September, 2013, the maximum value of the full angle insolation was received at 15:00 on 2nd September and it was 838 W/m^2 ; for Façade-NE, the highest point was 641 W/m^2 at 12:00 on 1st September; for Façade-NW, the biggest value was 412 W/m^2 at 18:00 on 3rd September; and for Façade-SE, the peak value was 720 W/m^2 at 15:00 on 4th September. In October, the maximum value for the full angle insolation was 754 W/m^2 at 12:00 on 8th October; for Façade-NE, the highest point was 169 W/m^2 at 9:00 on 1st October; for Façade-NW, the biggest value was 214 W/m^2 at 18:00 on 1st October; and for Façade-SE, the peak value was 673 W/m^2 at 15:00 on 6th October.

From the curves, it can be distinguished whether the day was sunny or cloudy by the insolation values. On a sunny day, the highest insolation values are higher than on cloudy days. Comparing the three façades' insolation with the full angle insolation, the intensity of the former is lower than that of the latter. The insolation intensity is lowest on façade-NW, which indicates that it only receives a small amount of insolation. Through this graph, it is proved that the orientation of the façade is an important factor for the insolation intensity.

Figure 5.20 below describes the evolution of the insolation over four selected days. Four curves appear for each day: Façade-NE, Façade-NW, Façade-SE and the full angle. The values plotted on this graph contain sunny days and partially cloudy days.

3rd September 2013 and 13th October 2013 were sunny, thus the insolation intensity changed relatively slowly. 3rd September 2013 was a typical sunny day, without clouds during the whole day. The full angle insolation increased step by step from 0 W/m² at 6:00 in the morning until the peak 860 W/m² at 14:00. After that, it dropped to zero at 21:00. However, the other three curves below the full angle curve show a different trend. Façade-NE curve rises from 0 W/m² to 547 W/m² over the period from 6:00am to 11:00am and later it drops sharply to 28 W/m² at 13:00, because the sun moves up over the façade, which only receives a little insolation. Façade-SE follows the same trend as the full angle insolation from 6:00am to 15:00pm. However, from then on it decreases dramatically from 696 W/m² at 15:00 to 24 W/m² at 17:00. For Façade-NW, the value of insolation remains steady from 8:00am to 16:00. After that, the curve suddenly climbs up to the highest point at 17:00; from then on it follows the same path as the full angle insolation. The curves on 13th October 2013 are similar to 3rd September 2013.

On 15th September 2013 and 4th October 2013, the weather was partially cloudy. The insolation values changed quickly during the day, resulting in some insolation peaks as shown in the graph. With rapid insolation changes in the range of 0 W/m² to 300 W/m² on 15th September 2013 and 0 W/m² to 180 W/m² on 4th October 2013, the four lines maintain a similar trend, in contrast with the pattern of the sunny day.

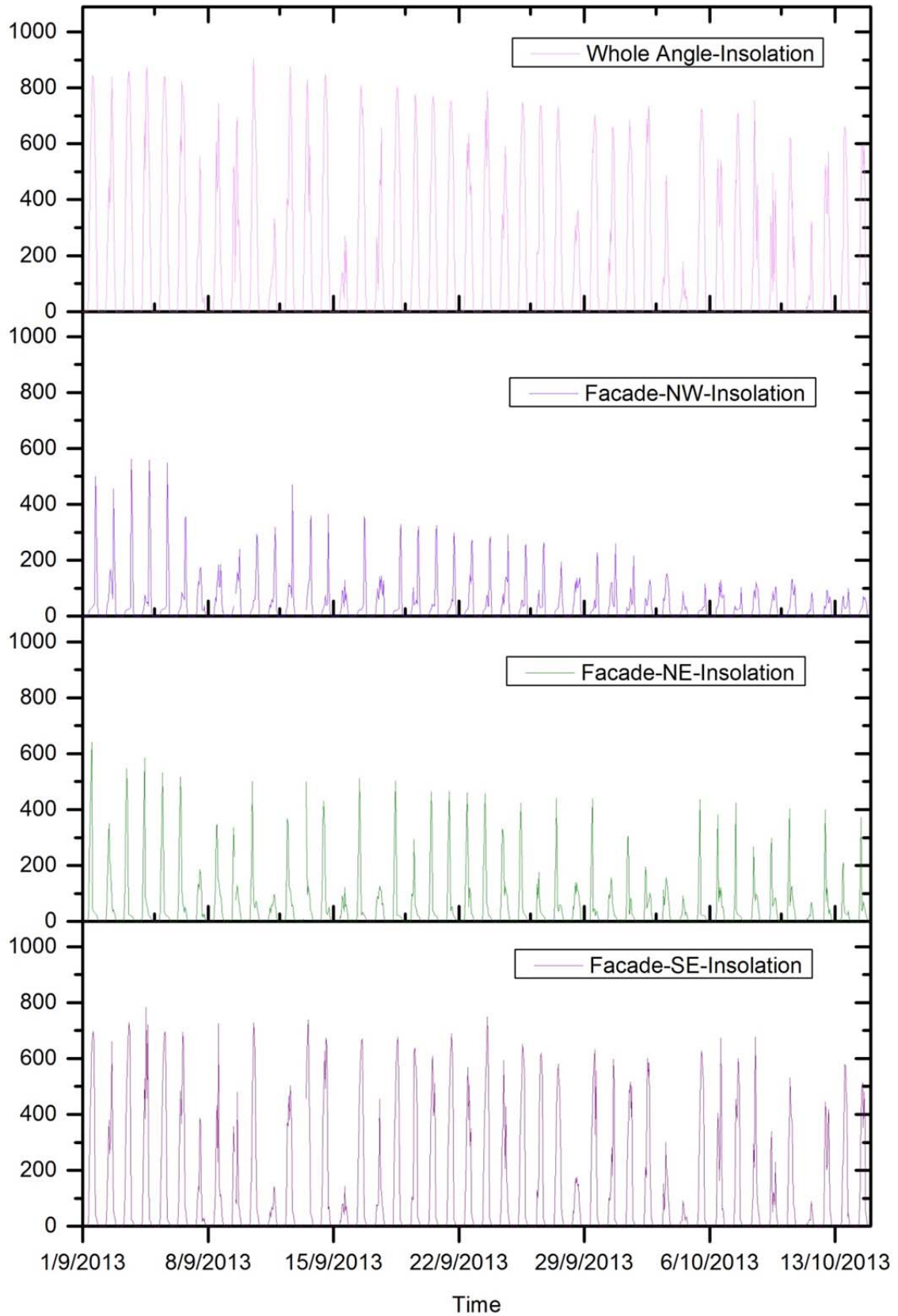


Figure 5.19 Insolation evolution (W/m^2) from 1st September 2013 to 15th October 2013, the K2M building.

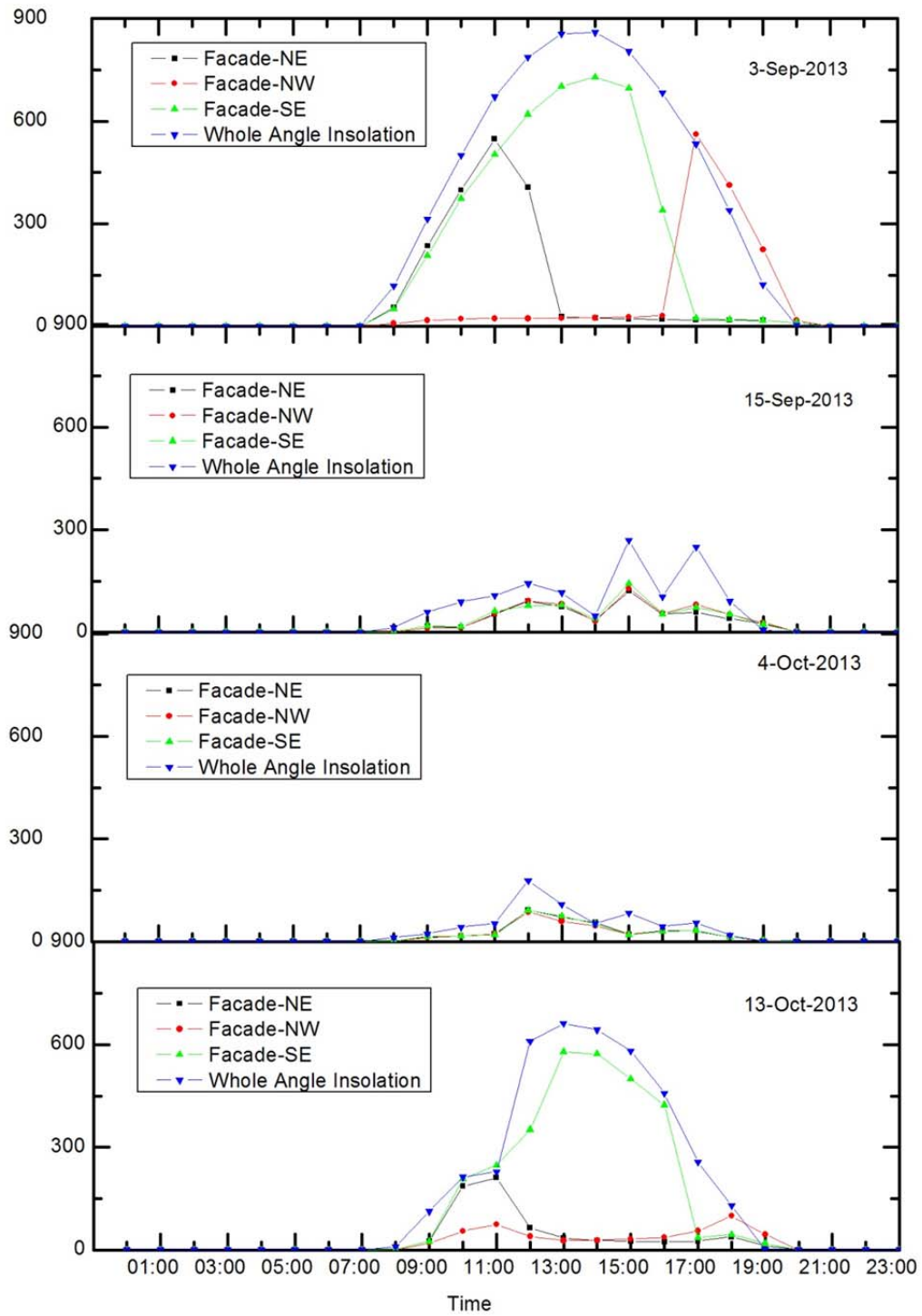


Figure 5.20 Insolation evolution (W/m^2) during four selected days, the K2M building.

5.2.4 Relationship between temperature and movements

In the present section 5.2, we have presented the movements of the control prisms on the K2M building and the Robotic Total Station on the A6 building over 45 days between 1st September 2013 and 15th October 2013 (section 5.2.1 and 5.2.2 respectively). On the other hand, the temperature evolution over the same period has been presented in section 5.2.3.

The Campus Nord was crossed by the L9 (Barcelona underground new Line “9”) tunnel in December 2009, but during the study period (September-October 2013) no public work was under development. As there are no major geotechnical problems in the foundation of the Campus Nord, the apparent movement of the points (Figures 5.5 to 5.13) does not correspond to any real settlement; the changes in the X, Y and Z coordinates must be attributed to the spurious influence of the so-called “Thermal effect” in the buildings over the study area.

What is actually happening is: each day, depending on the average temperature and on the power of the insolation, the buildings in the area deform following a certain pattern during the day. Consequently, the reference prisms (Reference points shown in Figure 4.1), the Robotic Total Stations (A3-RTS, A6-RTS, N2-RTS in Figure 4.3), and also the control prisms (CP in Figure 5.4) move. These movements are not fully considered in the computations normally undertaken by the monitoring software; only the RTS is allowed to change its precise position from one epoch to another. In particular, the coordinates of the Reference Prisms are always the same (constant values). This fact introduces an error into the computation process that is responsible for most of the coordinate oscillation visible in the aforementioned figures; only a small part of the oscillation could be attributed to the real movement of the K2M (due to the direct thermal action over the monitored building).

In Figures 5.5 to 5.13, a daily oscillation can be seen. Additionally, a phenomenon of decay in October can be appreciated. These two features of the evolution of the graphs can be clearly appreciated in the Open Air and façade temperature evolution in the same period (Figures 5.17 and 5.18). Comparing visually the two sets of figures (movements vs. temperature), it is clear that a great similarity exists. This “visual correlation” supports the cause-effect reasoning that has been outlined in the previous paragraph. In

the next section 5.3, we will try to establish the relationship between temperature evolution and the movement of the points through a physically-based simulation approach.

5.3 Numerical simulation of the standard monitoring system--- approach D

In Chapter 3 we have introduced the two main features to be used when modelling the behaviour of monitored buildings: the structural computation and the Least Squares Adjustment. Now, in this section we will combine the two features together and make a synthetic model (or numerical simulation) to analyze the temperature's influence on the K2M building monitoring.

This numerical simulation tries to reproduce the theoretical behaviour of the monitoring setup when subjected to a series of thermal changes, reproducing the principles of computation followed by a standard monitoring system like the one used by SOLDATA. This numerical simulation has been named “approach D” and is described in this section 5.3. Afterwards, in the section 5.4, we will compare the real world results with the simulated ones (approach D) in order to assess to what degree we have been able to capture the phenomenon. If the comparison is favorable, we will be ready to propose a new strategy to consider the thermal effect correctly (Chapter 6).

In abstract, what the so-called “standard practice” does (and our approach D tries to model) is overlook the influence of the thermal changes: everything in the scene is subjected to small movements due to the sun insolation and temperature changes; but, when computing the coordinates of the center of the RTS, we use in fact a set of constant coordinates for the reference prisms. This practice (constant coordinates instead of perturbed ones) introduces an error in the RTS coordinates that we obtain from the LSA. This error is later propagated to the coordinates of the control prisms. The final effect is that the results for the control points present a daily and seasonal variation that can be identified with the thermal action.

Our approach D needs the field of temperatures that is acting over each element of the structure at a given time (building by building). Then, it computes the displacements of

every node. This movement can be used to obtain the part of the monitoring that is due to the “thermal effect”. This overview of approach D justifies the input data needed and the basic assumptions that are presented in section 5.3.1 .

5.3.1 Input data

The approach D model uses the available raw data to compute the positions of the Control Prisms. The data used as input for the model are the temperature records (5.3.1.1), the coordinates of the Reference Prisms (5.3.1.2), the characteristics of the structure of the building (5.3.1.3) and the geometry of the buildings in the scene (5.3.1.4).

In the approach D modelling we work with 13 reference points (RP) located on the buildings B6, C5 and H0. The RTS is on the roof of the A6 building. The monitored object is the K2M building, with 9 control points (CP) on it. The period of study is from 1st September, 2013 to 15th October, 2013.

5.3.1.1 Thermal changes

The basic information about the thermal changes around the buildings in the scene is: the Open Air Temperature and the Sun Insolation.

The Open Air Temperature data (Figure 5.21) comes from an outside weather station. During this period, the day of 15th September, 2013 has no-data. So in the graph of Figure 5.21 there is a small gap on this day.

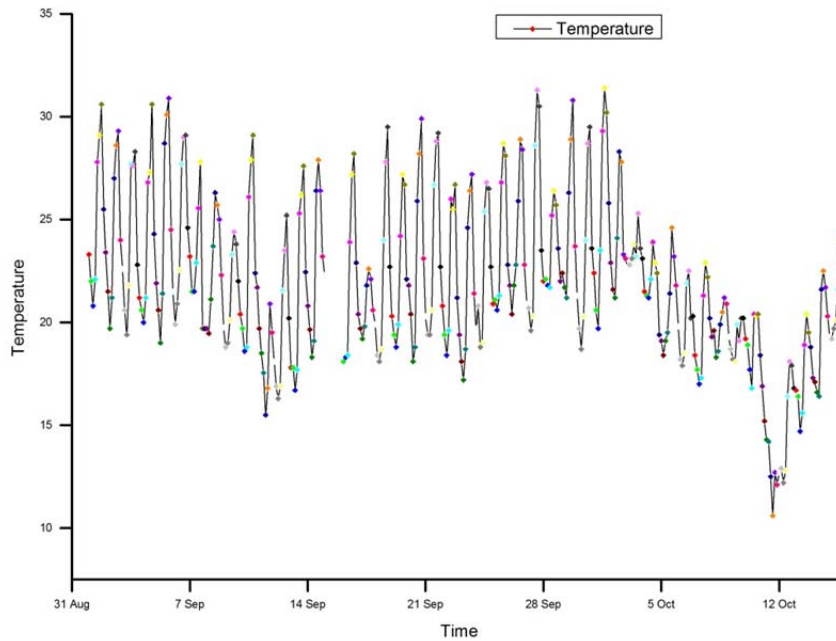


Figure 5.21 Open Air Temperature from 1st September, 2013 to 15th October, 2013.

Regarding the indoor temperature, we assume that the temperature inside the building is on average 21°C, as the indoor space is fully conditioned both in summer and in winter.

The Sun Insolation has been measured by several insolation cells, described in Chapter 4. There are 6 of these cells in the area, one attached to each of the main façades of the Omega building (3 in the K2M, 3 in the South-West block). But in a future scenario, the most probable setup will include a 360° insolation cell. For this reason, the equation 1, which will be introduced immediately, relies on the values of the 360° insolation cell.

Although we have up to 18 thermometers at several levels in the K2M pillars, this information is not enough to build the intended ΔT field. We need a ΔT value at every pillar and beam at the K2M building, but also in the other buildings in the scene (A6, HO, B6 etc). We cannot envisage having a lot of thermometers in a real future case. Finally, we decided to build the ΔT field based on the Open Air Temperature (OAT) and in the Insolation, values that are being measured during each day. The increment of temperature (ΔT) that we may consider a given façade is experimenting at a given time is formulated with this relationship:

$$\Delta T = CTT * (OAT - 21) + CI * Insolation * OF \quad 5.1$$

where

CTT—Coefficient of Temperature Transfer (dimensionless)

OAT—Open Air Temperature (°C)

CI—Coefficient of Insolation (°C·m²/W)

Insolation—Value of Insolation (W/m²)

OF—Orientation factor (dimensionless)

Equation 5.1 requires an explanation, which follows. The equation has two terms; the first one incorporates the variation related with the changes in the *OAT*. Even on a cloudy day, if the *OAT* increases, the façades of the building warm. On a given day, the change in the temperature of the structure elements (ΔT) is a fraction of the Open Air Temperature (*OAT*) fluctuation; in other words, the isolation of the façade prevents a wider temperature fluctuation in the structure. According to measures in the pillars of the K2M building (Figure 5.22), the total variation of the concrete temperature is about 1/5 the total variation of the open air temperature; so an initial value that can be considered is $CTT = 0.2$. In fact the conditions of a given building is very complex, so, later, when adjusting the real data to the simulations (Chapter 6), other values should be adopted in order to get better adjusts.

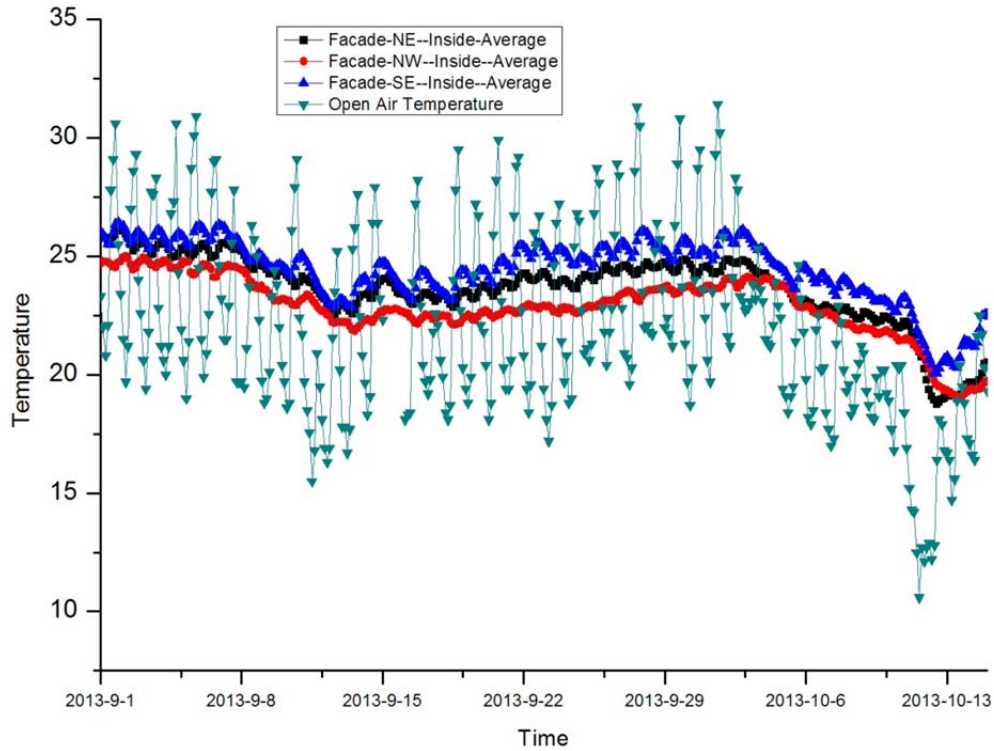


Figure 5.22 Open air temperature and inside temperature of K2M building(°C).

On the other hand, the second term takes into account the variation of the façade's temperature due to the energy that comes to them from the Sun. The exact time when the highest temperature is achieved depends on the orientation of the façade (OF). Furthermore, if the day is cloudy, the temperature is lower than the maximum, and this is considered through the *Insolation* variable. As we know, the different façades of one building receive a different amount of insolation at a given time. The position of the sun in the sky changes according to the hour of the day, the day of year and the site's latitude (as shown in Figure 5.23).

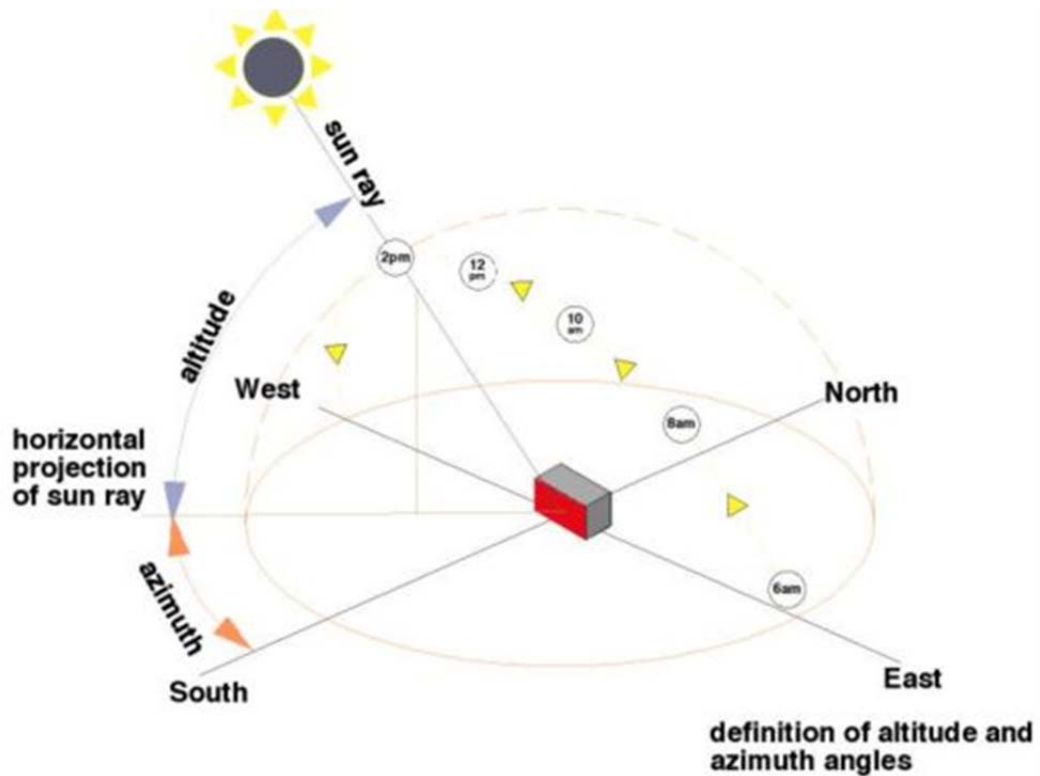


Figure 5.23 Schematic diagram about the building orientation and sun's passage(RIBA 2015).

It is possible to set up a general relationship between the orientation of the façade and insolation. Based on our limited data and experience, a simplified relationship for the study period (September and October 2013) has been adopted (Figure 5.24). The range of the orientation of the façade has been divided into 8 cases (as shown in the figure). Additionally, the first subfigure corresponds to the *OF* for the roof level, which receives the insolation all day long.

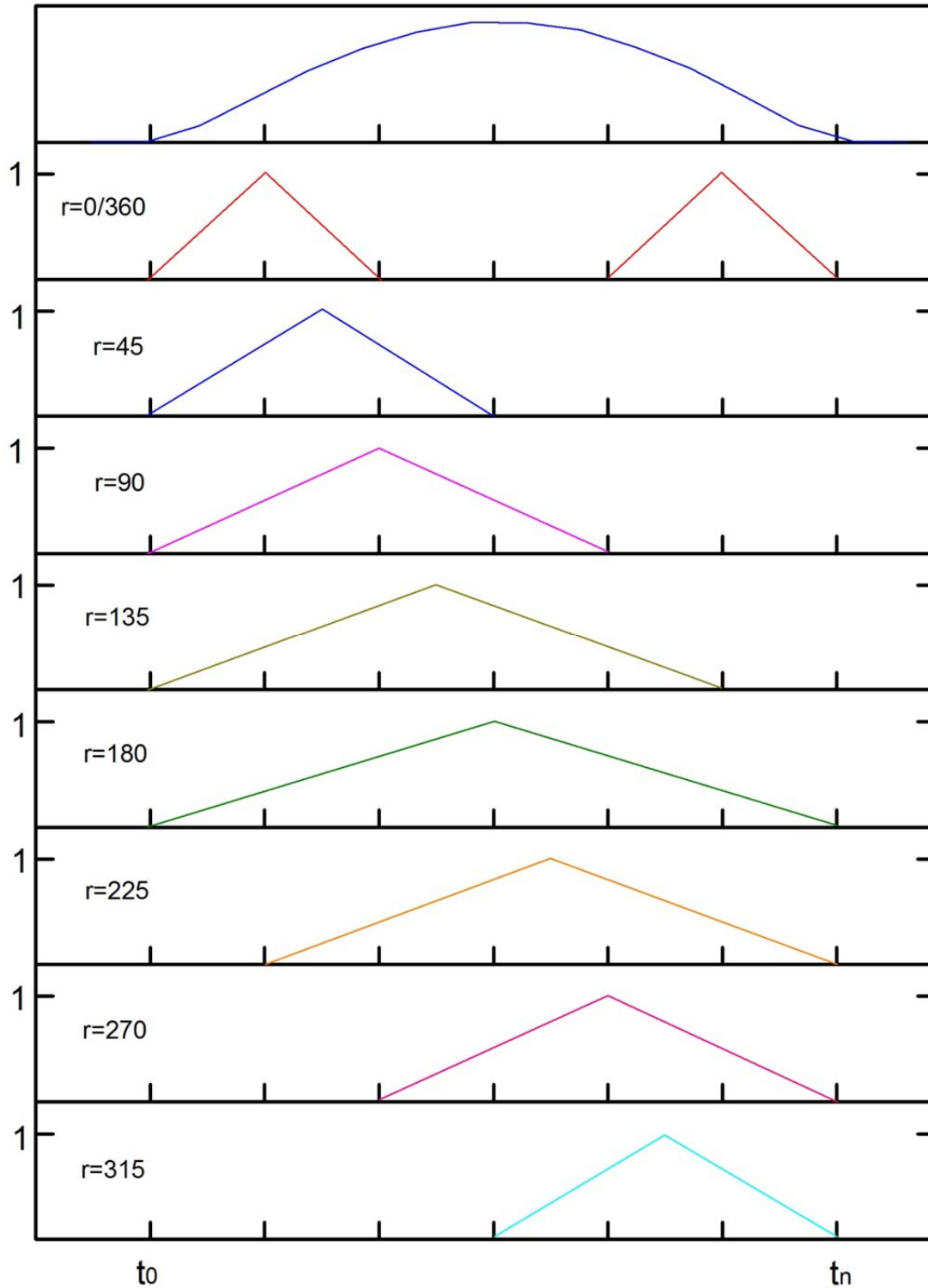


Figure 5.24 Orientation factor, OF , according to the azimuth of the façade (r). The full round (0° - 360°) has been divided into 8 cases, with 45° steps. Additionally, the first subfigure corresponds to the OF for the roof level, which receives the insolation all day long. t_0 and t_n are the times of the sunrise and the sunset, respectively.

When the azimuth of a given façade (r_3) is between the angles (r_1 and r_2) in the Figure 5.24, the OF can be calculated by interpolation:

When $r_1 < r_3 < r_2$,

$$OF(r_3) = \frac{OF(r_1)*\omega_1 + OF(r_2)*\omega_2}{\omega_1 + \omega_2} \quad 5.2$$

where

$$\omega_1 + \omega_2 = 1 \quad 5.3$$

$$\omega_2 = \frac{r_3 - r_1}{r_2 - r_1} \quad 5.4$$

5.3.1.2 Coordinates of the monitoring points

In the computation, it is necessary to know the coordinates of the reference points, RTS and control points (shown in Table 5.1, Table 5.2 and Table 5.3 respectively). The coordinates X and Y are UTM ones, reference system ED50, with a local adjustment. The Z coordinate is the orthometric elevation. All the values are relative to the positions of the Robotic Total Stations in A6 and A3, measured with GPS-RTK with Reference Base Point UPC1 (GPS Continuous Operating Reference point located in the D2 building, Campus Nord, UPC). Obviously, these coordinates are initial values that will be updated epoch by epoch according to the movements of the building.

Table 5.1 Reference point coordinates (m)

Reference Point	X	Y	Z
R14	425873.1522	4582364.047	111.27366
R28	425877.797	4582368.441	111.20751
R27	425872.5696	4582372.598	113.2609
R12	425812.7059	4582345.273	114.02529
R13	425821.7798	4582353.869	114.09328
R19	425908.5303	4582414.016	117.09156
R22	425934.5864	4582412.332	117.34891
R18	425892.1393	4582403.792	115.50347
R21	425917.4071	4582399.093	115.52763
R23	425937.3368	4582395.443	115.37324
R24	425948.5993	4582393.343	115.55571
R17	425890.3162	4582404.281	97.94174
R20	425916.0481	4582399.497	97.98848

Table 5.2 Control point coordinates (m)

Control Point	X	Y	Z
CP1	425938.4922	4582314.517	94.28218
CP2	425929.1955	4582306.76	94.29631
CP3	425924.5451	4582302.875	94.21496
CP4	425938.4756	4582314.501	99.58036
CP5	425929.2463	4582306.801	99.59326
CP6	425924.5489	4582302.888	99.57814
CP7	425938.4496	4582314.482	104.245
CP8	425929.2569	4582306.809	104.82161
CP9	425924.5573	4582302.894	104.82412

Table 5.3 RTS coordinates (m)

RTS	X	Y	Z
A6-RTS	425905.9329	4582346.65	111.02755

5.3.1.3 Structure model parameters

Three kinds of parameter files are needed as input for our program: the node coordinates file (Figure 5.25), the element node file (Figure 5.26) and the parameter file (Figure 5.27).

5 Matching the Model with real world results

```
nodeCoordinates - Notepad
File Edit Format View Help
0      0      0      ;
0.000  1.500  0.000  ;
0.000  9.500  0.000  ;
0.000  17.500 0.000  ;
4.000  0.000  0.000  ;
4.000  1.500  0.000  ;
4.000  9.500  0.000  ;
4.000  17.500 0.000  ;
8.000  0.000  0.000  ;
8.000  1.500  0.000  ;
8.000  9.500  0.000  ;
8.000  17.500 0.000  ;
12.000 0.000  0.000  ;
12.000 1.500  0.000  ;
12.000 9.500  0.000  ;
12.000 17.500 0.000  ;
16.000 0.000  0.000  ;
16.000 1.500  0.000  ;
      ;
```

Figure 5.25 Node Coordinates file, partial view. Local X, Y, Z (m) coordinates for the nodes of the structural model.

```
elementNodes - Notepad
File Edit Format View Help
1      65      ;
2      66      ;
3      67      ;
4      68      ;
5      69      ;
6      70      ;
7      71      ;
8      72      ;
9      73      ;
10     74      ;
11     75      ;
12     76      ;
14     78      ;
15     79      ;
16     80      ;
20     84      ;
24     88      ;
28     92      ;
      ;
```

Figure 5.26 Element Node file, partial view. Node connectivity that define the beams and pillars of the structural model.

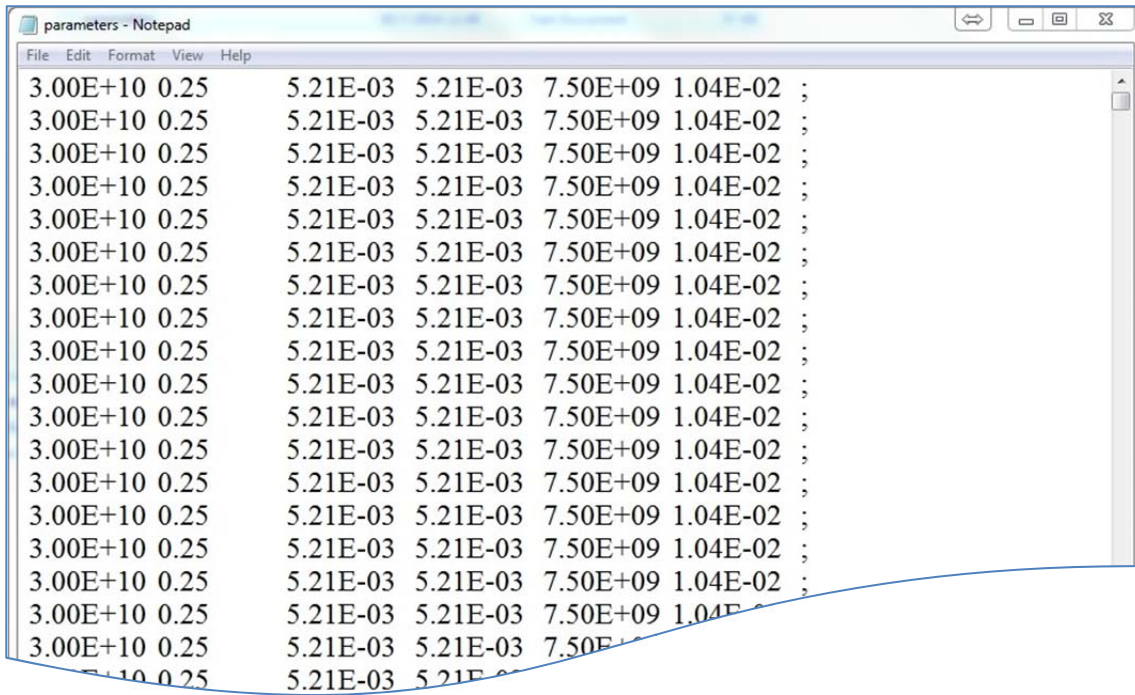


Figure 5.27 Parameters file, partial view. The columns stand for the Young modulus (E, N/m²), beam section area (m²), y-Inertia moment (m⁴), z-Inertia moment (m⁴), shear modulus (G, N/m²) and the Torsional Moment (J, m⁴).

5.3.1.4 Relationship between structure nodes and monitoring point location

From Figure 5.28 to Figure 5.32, we present the wire models of the structures corresponding to the buildings A6, B6, C5, H0 and K2M.

Nine control points have been installed on the K2M structure model, which are CP1 related to Node-100, CP2 related to Node-92, CP3 related to Node-88, CP4 related to Node-140, CP5 related to Node-132, CP6 related to Node-128, CP7 related to Node-160, CP8 related to Node-152 and CP9 related to Node-148.

On the A6 structure model, the RTS has been settled on node-196.

In total, we installed 13 reference points on B6, C5 and H0. On the B6 structure model, there are three reference points, which are R14 on node-115, R28 on node-116 and R27 on node-124. On the C5 structure model, there are two reference points, which are R12 on node-219 and R13 on node-221. On the H0 structure model, there are eight reference

5 Matching the Model with real world results

points, which are R19 on node-453, R22 on node-455, R18 on node-459, R21 on node-466, R23 on node-471, R24 on node-473, R17 on node-65 and R20 on node-93.

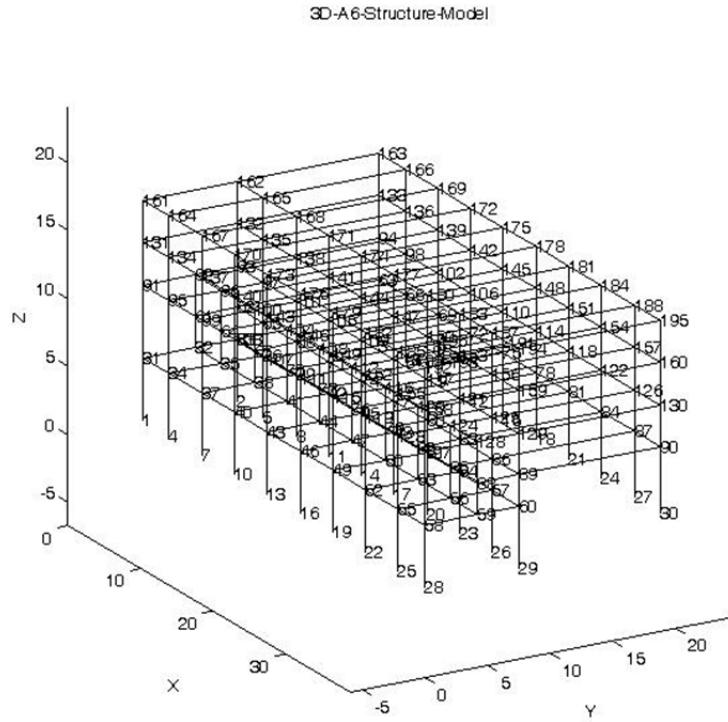


Figure 5.28 Wire model of A6 building. X, Y, Z (m) are local nodal coordinates.

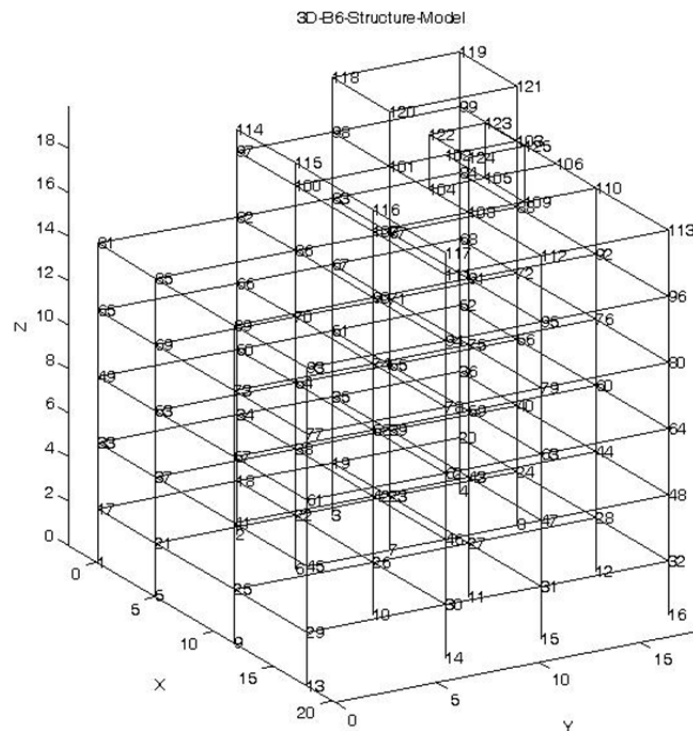


Figure 5.29 Wire model of B6 building. X, Y, Z (m) are local nodal coordinates.

5 Matching the Model with real world results

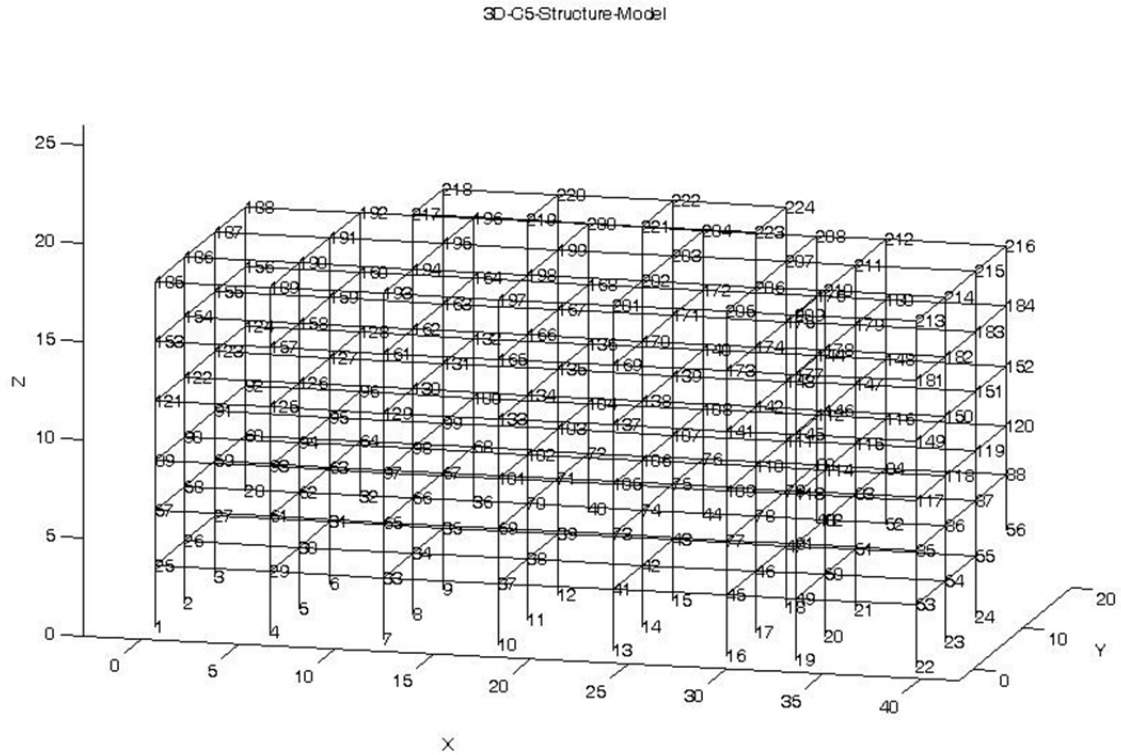


Figure 5.30 Wire model of C5 building. X, Y, Z (m) are local nodal coordinates.

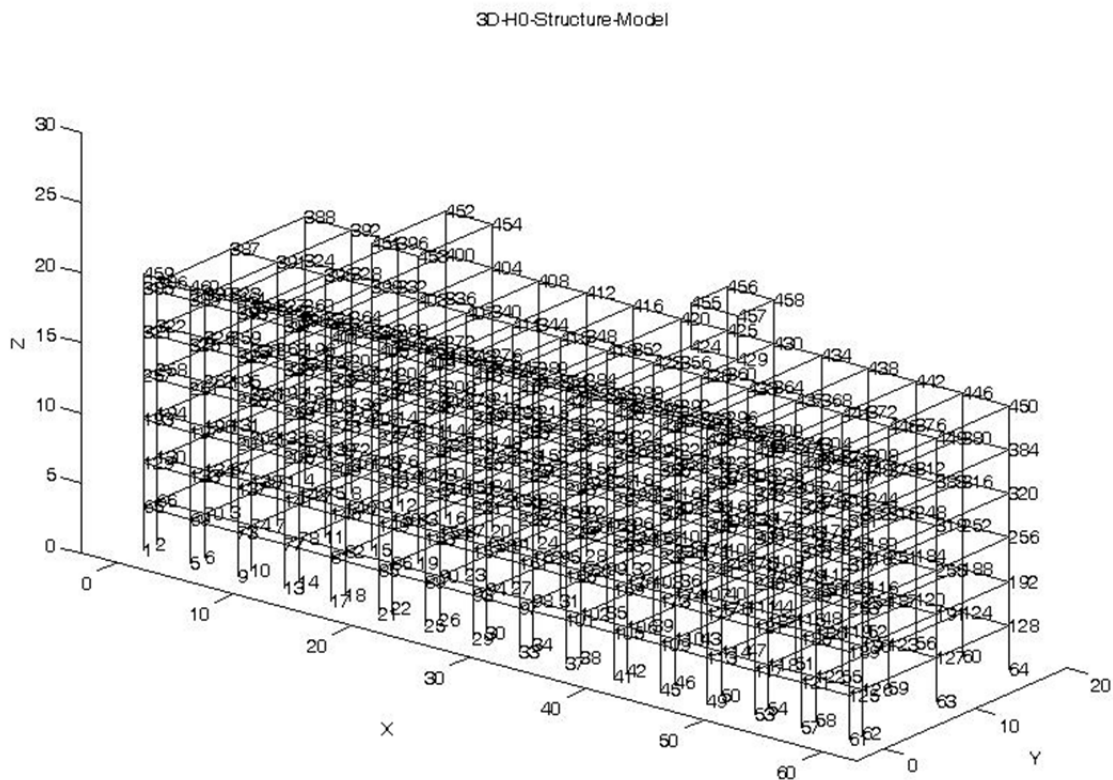


Figure 5.31 Wire model of H0 building. X, Y, Z (m) are local nodal coordinates.

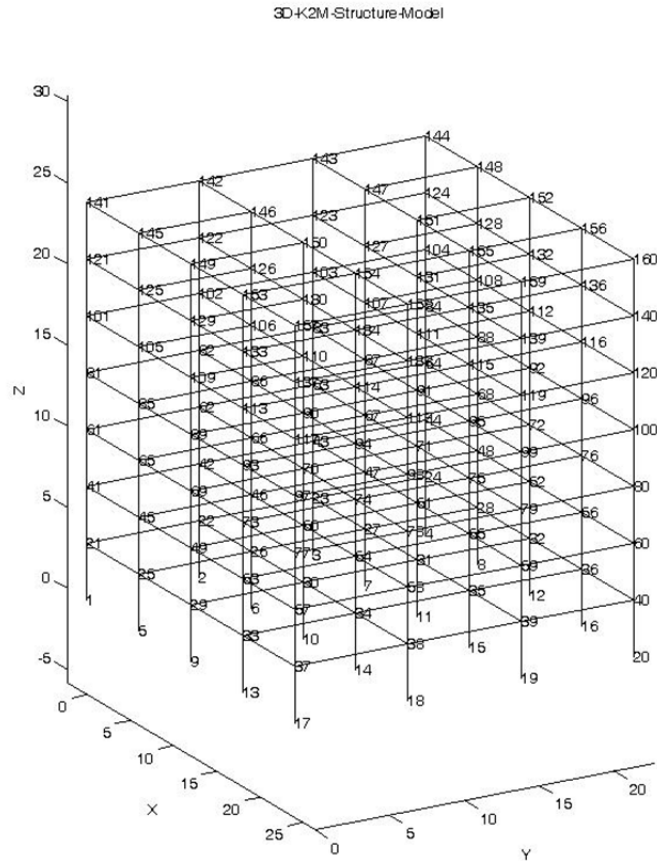


Figure 5.32 Wire model of K2M building. X, Y, Z (m) are local nodal coordinates.

5.3.2 Main steps of approach D

In approach D we follow the flowchart enclosed in Figure 5.33. We repeat the same process for each epoch of measurement (approximately, every 3h). After establishing the ΔT (equation 5.1), we introduce the temperature values in the structural model of each building, obtaining the thermal movement of control points, DX_{CP} , DY_{CP} , DZ_{CP} , the thermal movement of RTS, DX_{RTS} , DY_{RTS} , DZ_{RTS} , and the thermal movement of the reference points, DX_{RP} , DY_{RP} and DZ_{RP} (here 'D' stands for 'increment'). If we add these movements to the initial coordinates, we obtain the simulated ('s') coordinates occupied by the Control prisms, the Robotic Total Station and the Reference prisms in the present 'epoch', respectively:

$$\begin{aligned}
 X_{SCP} &= X_{CP} + DX_{CP} \\
 Y_{SCP} &= Y_{CP} + DY_{CP} \\
 Z_{SCP} &= Z_{CP} + DZ_{CP}
 \end{aligned}
 \tag{5.5}$$

$$\begin{aligned} X_{SRTS} &= X_{RTS} + DX_{RTS} \\ Y_{SRTS} &= Y_{RTS} + DY_{RTS} \\ Z_{SRTS} &= Z_{RTS} + DZ_{RTS} \end{aligned} \quad 5.6$$

$$\begin{aligned} X_{SRP} &= X_{RP} + DX_{RP} \\ Y_{SRP} &= Y_{RP} + DY_{RP} \\ Z_{SRP} &= Z_{RP} + DZ_{RP} \end{aligned} \quad 5.7$$

Now, we can compute the simulated raw data for the control points (H_{CP} , V_{CP} , d_{CP} ; i.e, the Horizontal Angle, the Vertical Angle and the distance) based on the simulated coordinates of the control points (equation 5.5) and the simulated coordinates of the RTS (equation 5.6). The simulated raw data of the Reference points (H_{RP} , V_{RP} , d_{RP}) also can also be computed based on the simulated coordinates of the RTS (equation 5.6) and the simulated coordinates of the reference points (equation 5.7).

Then, the coordinates of the RTS can be obtained as if we were working with a standard monitoring approach, that is, by least squares adjustment (LSA) based on the ‘official’ coordinates of the Reference Points (X_{RP} , Y_{RP} , Z_{RP}) and the simulated observational data (H_{RP} , V_{RP} , d_{RP}).

Lastly, the final coordinates of the control points can be calculated using the simulated raw data of the control points and RTS. The entire process is illustrated as flowchart in Figure 5.33.

5 Matching the Model with real world results

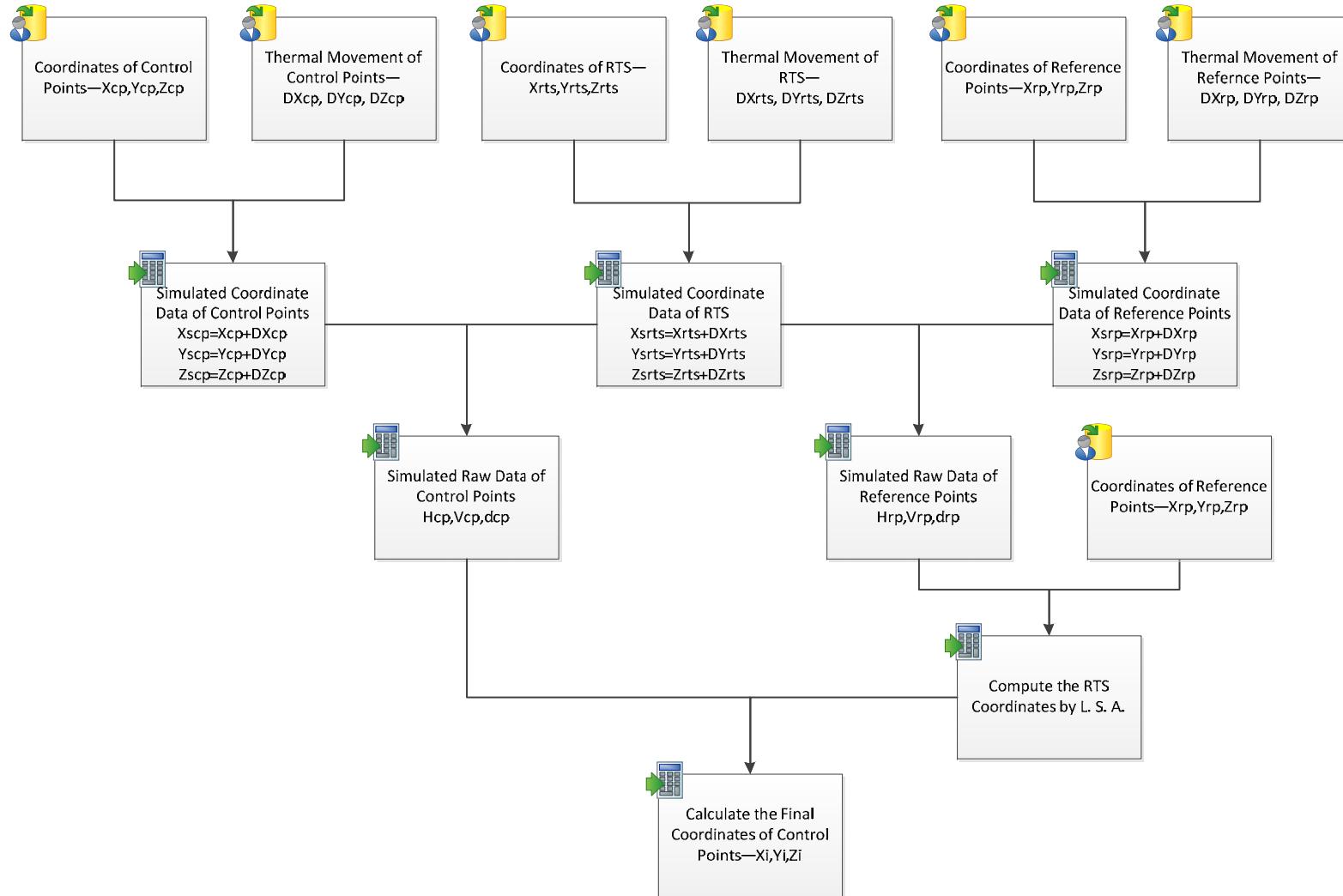


Figure 5.33 Flowchart of Approach-D.

In order to appreciate the computational effort necessary to run the program, the running times for one case similar to the Campus Nord site have been presented in Table 5.4. The computation has been carried out on a typical desktop personal computer with mean resources for CPU, RAM, etc.

Table 5.4 Approach-D computation time in seconds.

Task:	Structure Model	Calculate the Simulated Raw Data	Least Squares Adjustment	Total
Time	388.07	2.18	2.58	392.83

It can be seen that, the main effort has been devoted to the Structural model solving. This part is not the core of this PhD and might be optimized in the future if necessary.

5.3.3 Approach D results and analysis

A set of computations within the Approach-D strategy are presented and analyzed here in order to demonstrate its behaviour. First of all, the movement of the A6 building during one typical day is presented (section 5.3.3.1). The RTS is on the top of this building; its movement is presented later (section 5.3.3.2). Finally, the simulated movements for the Control Points are summarized in section 5.3.3.3.

5.3.3.1 Simulating the A6 movement induced by the ‘thermal effect’

In order to explore the impact of thermal changes on structure health monitoring, it is necessary to simulate the deformation of all the buildings in the scene. Thus, the structures of A6, B6, C5, H0 and K2M buildings have been simulated in the experiment.

In this section, the results for the A6 building will be presented in order to show in detail the extent and the pattern of the movements of one structure under thermal changes during one single day (1st September, 2013). The amount of data to visualize makes the use of graphs convenient (‘wire models’ of the structure). In the figures that follow, the scale of the movement on each node has been magnified 1000 times in order to make it appreciable.

Figure 5.34 shows the simulated displacement of the whole structure of A6 at eight different epochs on 1st September, 2013. It also shows that the structure expanded as the temperature increased and contracted as the temperature decreased.

The figures from 5.35 to 5.38 show more details about the structure's movement on four different façades, which are façade-SE, façade-SW, façade-NE and façade-NW. From the structure's movement, we can draw the following conclusions.

First of all, the results proved that the structure has been influenced by the temperature change; it means that the structure expands when the temperature increases and shrinks when the temperature decreases. In this way, it has been proved that thermal change is a very important factor for the structural health monitoring, and it is necessary to consider the thermal impact when monitoring the movements of the structures.

5 Matching the Model with real world results

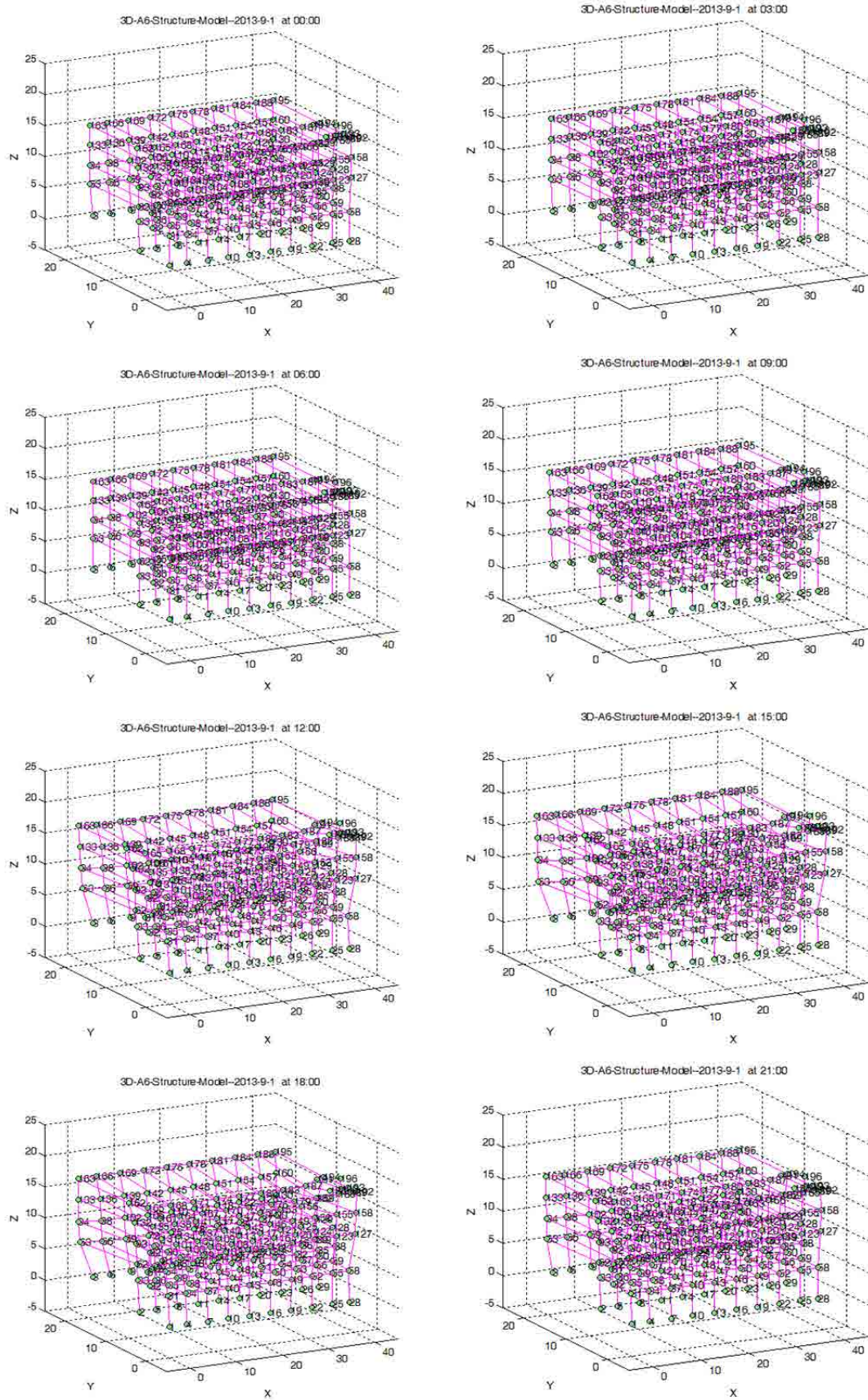


Figure 5.34 Movement of A6 building on 1st September 2013. Perspective view.

5 Matching the Model with real world results

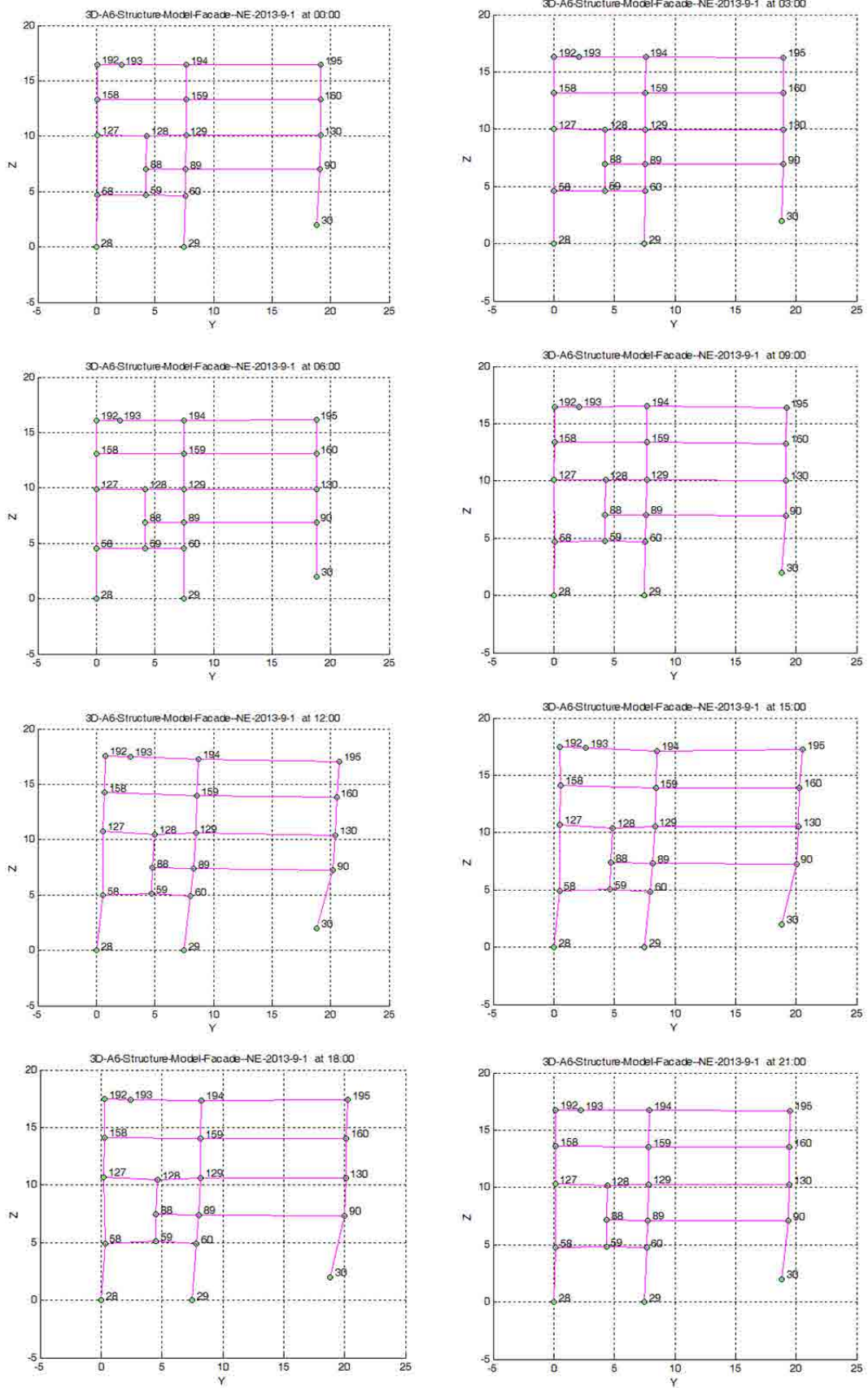


Figure 5.35 Movement of A6 building on 1st September 2013. Front view, Façade NE.

5 Matching the Model with real world results

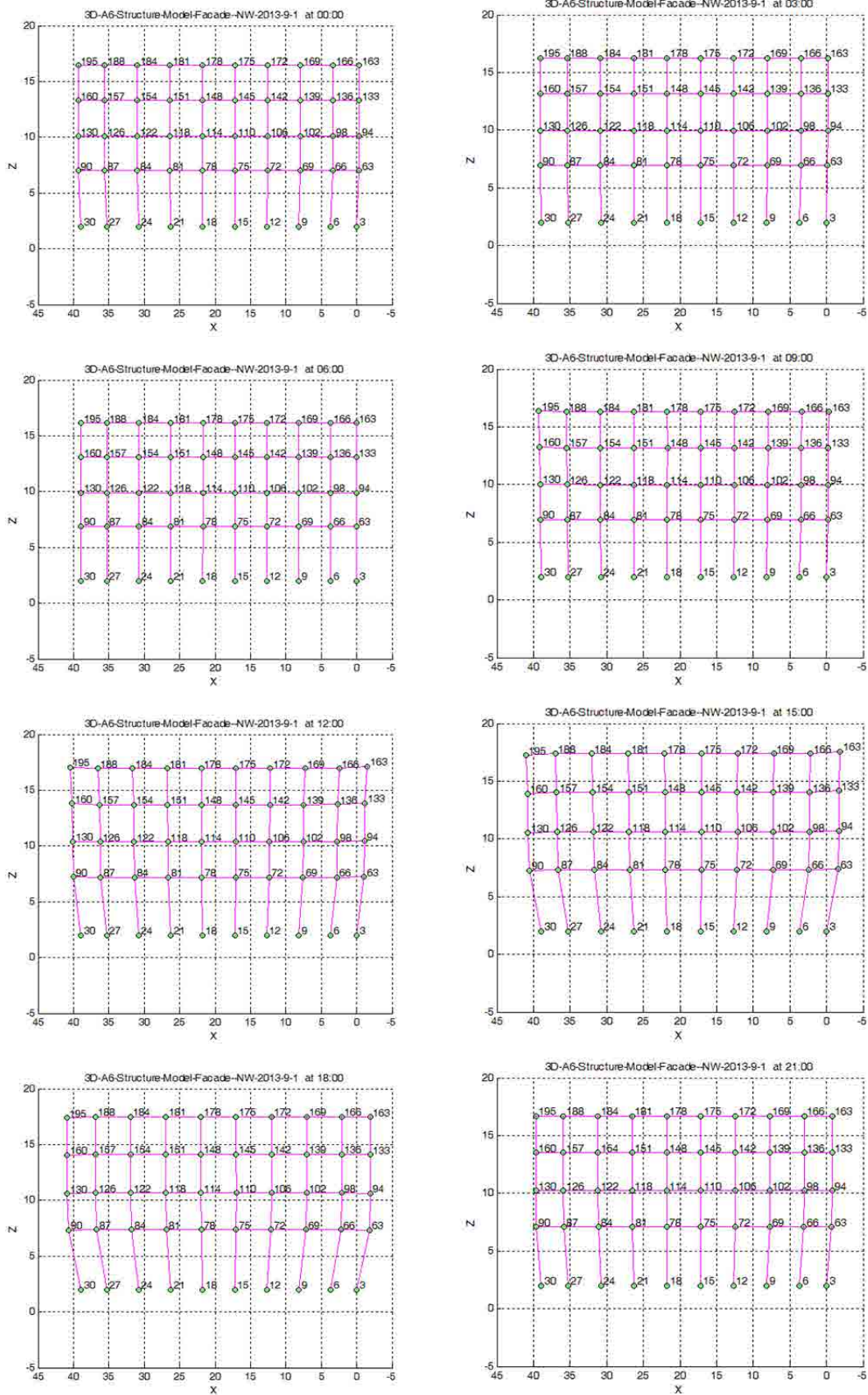


Figure 5.36 Movement of A6 building on 1st September 2013. Front view, Façade NW.

5 Matching the Model with real world results

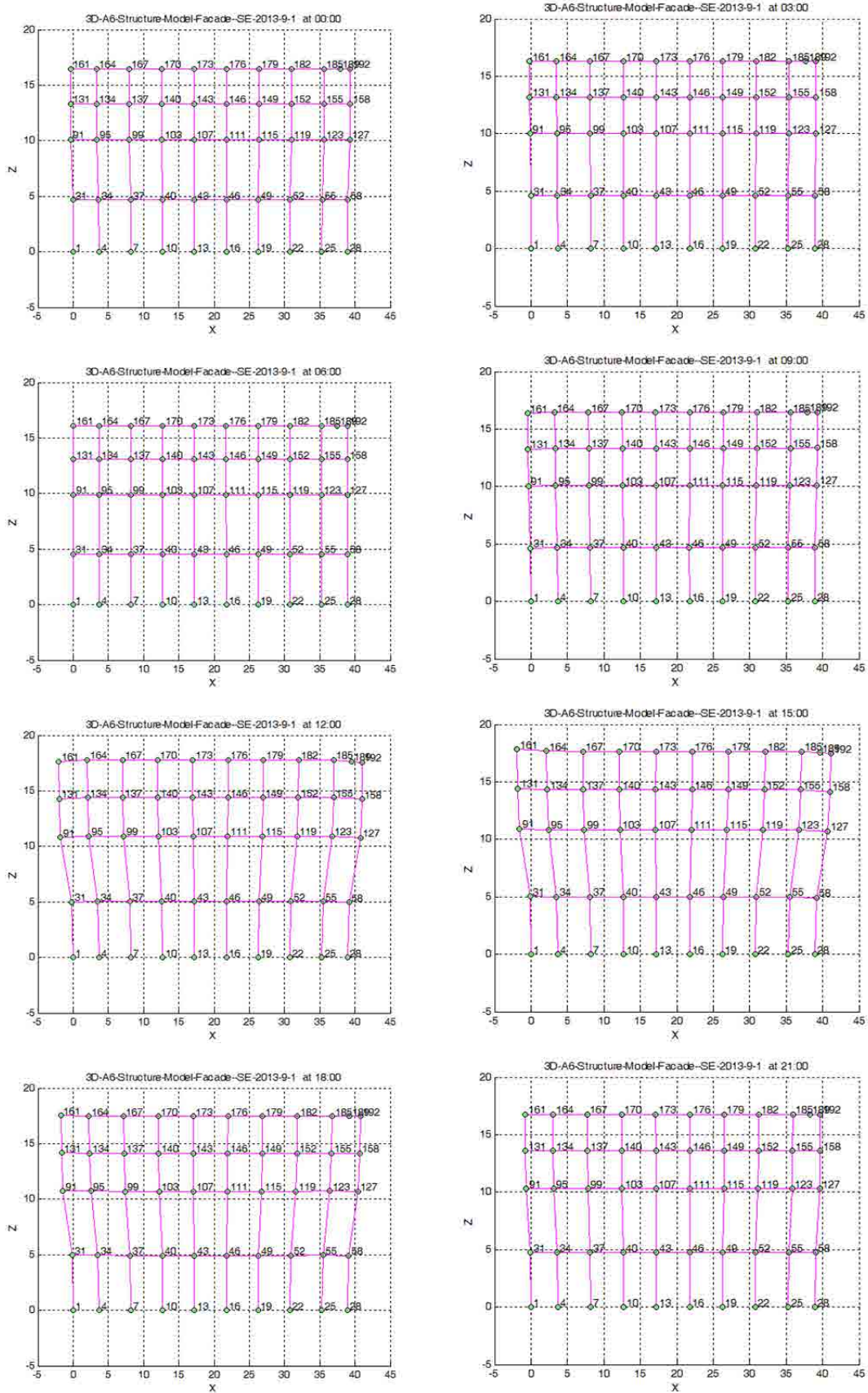


Figure 5.37 Movement of A6 building on 1st September 2013. Front view, Façade SE.

5 Matching the Model with real world results

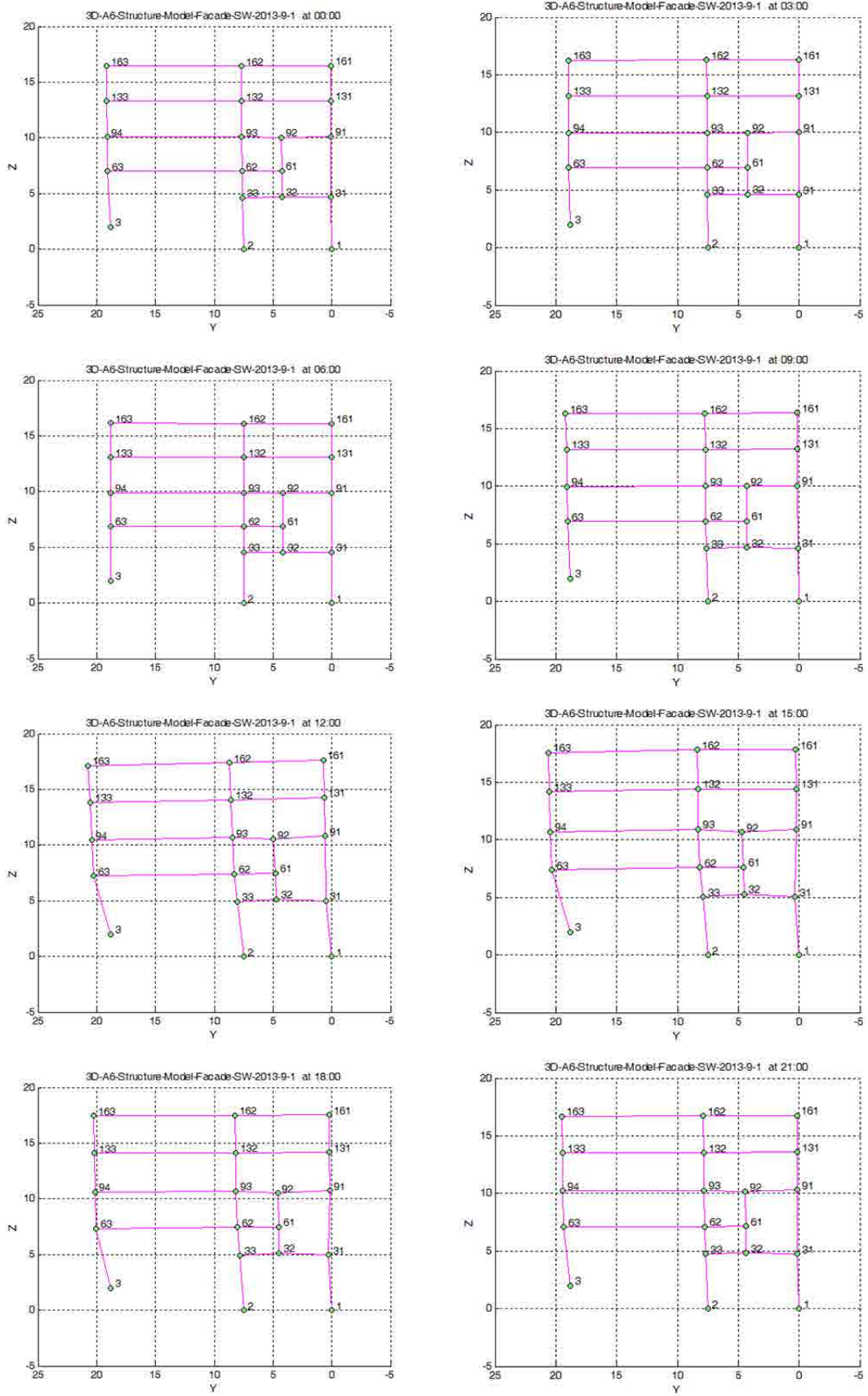


Figure 5.38 Movement of A6 building on 1st September 2013. Front view, Façade SW.

5.3.3.2 RTS on the top of the A6 building: Analysis of movement and its accuracy

After the modelling of the movement of the A6 building, we can now compute the coordinates of the center of the Total Station that has been working on the top of a pillar on the roof of the A6. Following the Approach-D, we will simulate the network of the Reference points and we will adjust the RTS coordinates by Least Squares (section 5.3.3.2.1). Afterwards, we will characterize the precision of the results by studying the theoretical errors of the results by means of the Root Mean Square Error and the Ellipse of error (section 5.3.3.2.2)

5.3.3.2.1 Movement of the RTS on top of the A6

In our simulation, one task of the least squares adjustment is to compute the total station's three coordinates, X, Y and Z. Knowing the coordinates of the RTS, we can compute the control points' coordinates using the observation data (H, V and D). Figures 5.39 to 5.41 show the result of the RTS' three coordinates based on the simulation data (H, V and D) during the time between 1st September and 15th October. From those three graphs, it can be seen that X, Y and Z have the same movement trend during the study period. The three figures show that the displacement range of X is from 425905.9324m to 425905.934m, the displacement range of Y is from 4582346.6492m to 4582346.6521m, and the displacement range of Z is from 111.0267m to 111.0286m. With the change in temperature, there is a significant drop in October when the curve falls and recovers following the temperature trend (in Figure 5). The results reflect the fact that the total station is influenced by the thermal changes, even if we use the least squares adjustment method to reduce its impact.

5 Matching the Model with real world results

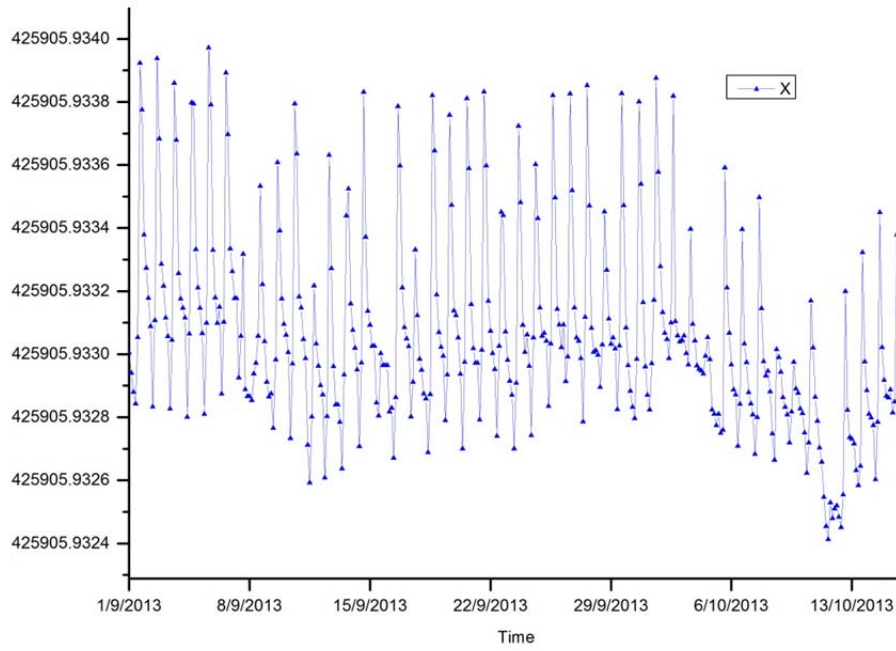


Figure 5.39 X movement (m) of A6 RTS in the study period, Approach-D.

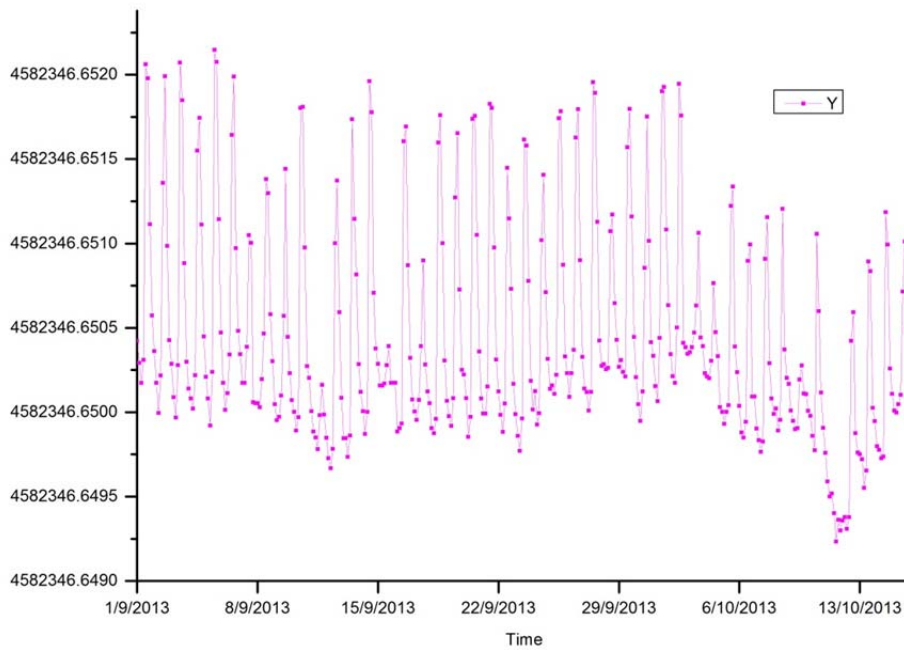


Figure 5.40 Y movement (m) of A6 RTS in the study period, Approach-D.

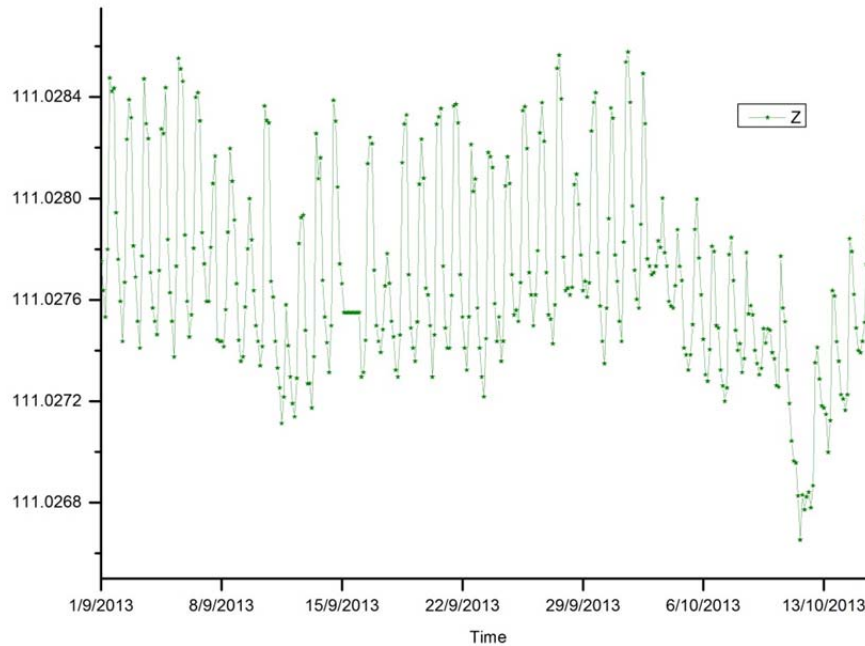


Figure 5.41 Z movement (m) of A6 RTS in the study period, Approach-D.

5.3.3.2.2 Precision assessment of the RTS computed movements

So far we have obtained the movement for the center of the RTS simulated with the Approach-D. Now it is time to assess the accuracy of these results, i.e. the degree of confidence we can attribute to our results. This assessment will be undertaken with two approximations: the Root Mean Square Error (RMS) and the Ellipse of error. The first one will deliver an estimation of the RMS on the X and Y movement of the center of the RTS during the study period (i.e. the error of Figure 5.39 and 5.40 X and Y graphs). The Ellipse of error will show us the confidence region around the mathematically computed solution.

a. Root Mean Square Error (RMS)

As presented previously in Chapter 3, after completing a least squares adjustment, the standard deviation in the coordinates of an adjusted station can be estimated from the covariance matrix. The computation of the RMS for the X and Y coordinates follows the classical formulation (Ghilani and Paul 2010) that we summarize in the following paragraphs.

The variance factor of the unit weight ($\hat{\sigma}_0^2$) can be computed from

$$\hat{\sigma}_0^2 = \frac{V^T P V}{r} \quad 5.8$$

For the indirect adjustment, letting

$$Z = \begin{pmatrix} l \\ \hat{x} \\ V \\ \hat{L} \end{pmatrix} = \begin{pmatrix} E \\ N_{bb}^{-1} B^T P \\ B N_{bb}^{-1} B^T P - E \\ B N_{bb}^{-1} B^T P \end{pmatrix} L - \begin{pmatrix} E \\ N_{bb}^{-1} B^T P \\ B N_{bb}^{-1} B^T P - E \\ B N_{bb}^{-1} B^T P \end{pmatrix} L_0 \quad 5.9$$

where: L is the observation vector
 \hat{x} is the parameter vector,
V is the correction vector
 \hat{L} is the vector of the observation value adjustment
E is unit vector,
 N_{bb} is coefficient matrix of the set of normal equations
B is coefficient matrix
P is weight matrix
 L_0 is vector of constants
l is the vector of numeric terms

Applying the law of propagation of variances to equation 5.9, it gives the following covariance matrices

$$Q_{ZZ} = \begin{pmatrix} Q_{LL} & Q_{L\hat{x}} & Q_{LV} & Q_{L\hat{L}} \\ Q_{L\hat{x}} & Q_{\hat{x}\hat{x}} & Q_{\hat{x}V} & Q_{\hat{x}\hat{L}} \\ Q_{LV} & Q_{\hat{x}V} & Q_{VV} & Q_{V\hat{L}} \\ Q_{L\hat{L}} & Q_{\hat{x}\hat{L}} & Q_{V\hat{L}} & Q_{\hat{L}\hat{L}} \end{pmatrix} = \begin{pmatrix} E \\ N_{bb}^{-1} B^T P \\ B N_{bb}^{-1} B^T P - E \\ B N_{bb}^{-1} B^T P \end{pmatrix} Q_{LL} \begin{pmatrix} E \\ P B N_{bb}^{-1} \\ P B N_{bb}^{-1} B^T - E \\ P B N_{bb}^{-1} B^T \end{pmatrix} \quad 5.10$$

Expanding the Equation 5.10, we obtain

$$Q_{ZZ} = \begin{pmatrix} Q_{LL} & B N_{bb}^{-1} & B N_{bb}^{-1} B^T - Q_{LL} & B N_{bb}^{-1} B^T \\ N_{bb}^{-1} B^T & N_{bb}^{-1} & 0 & N_{bb}^{-1} B^T \\ B N_{bb}^{-1} B^T - Q_{LL} & 0 & Q_{LL} - B N_{bb}^{-1} B^T & 0 \\ B N_{bb}^{-1} B^T & B N_{bb}^{-1} & 0 & B N_{bb}^{-1} B^T \end{pmatrix} \quad 5.11$$

The covariance matrix can be gotten from the equation 5.11,

$$Q_{\hat{x}\hat{x}} = N_{bb}^{-1} = \begin{pmatrix} Q_{\hat{x}_1 \hat{x}_1} & Q_{\hat{x}_1 \hat{x}_2} & \dots & Q_{\hat{x}_1 \hat{x}_t} \\ Q_{\hat{x}_2 \hat{x}_1} & Q_{\hat{x}_2 \hat{x}_2} & \dots & Q_{\hat{x}_2 \hat{x}_t} \\ \vdots & \vdots & \ddots & \vdots \\ Q_{\hat{x}_t \hat{x}_1} & Q_{\hat{x}_t \hat{x}_2} & \dots & Q_{\hat{x}_t \hat{x}_t} \end{pmatrix} \quad 5.12$$

If the X_{RTS} is in the i^{th} position of the unknown vector, the Root Mean Square Error (in terms of standard deviation) of the coordinate X, $\hat{\sigma}_{\hat{X}_i}$, is

$$\hat{\sigma}_{\hat{X}_i} = \hat{\sigma}_0 \sqrt{Q_{\hat{X}_{2i-1}\hat{X}_{2i-1}}} \quad 5.13$$

Similarly, for the Y_{RTS} ,

$$\hat{\sigma}_{\hat{Y}_i} = \hat{\sigma}_0 \sqrt{Q_{\hat{X}_{2i}\hat{X}_{2i}}} \quad 5.14$$

If we want, we can summarize the X and Y RMS in a single comprehensive value that is the Root Mean Square Error of the point, \hat{M}_i , i.e. the quadratic composition of the two previous ones:

$$\hat{M}_i = \hat{\sigma}_0 \sqrt{Q_{\hat{X}_{2i-1}\hat{X}_{2i-1}} + Q_{\hat{X}_{2i}\hat{X}_{2i}}} \quad 5.15$$

Figures 5.42, 5.43 and 5.44 show the evolution of $\hat{\sigma}_{\hat{X}_i}$, $\hat{\sigma}_{\hat{Y}_i}$, and \hat{M}_i , respectively, during the study period (1st September – 15th October , 2013). The RMSE in X ranges +-0.18 mm, whereas in Y it ranges +- 0.17mm. Accordingly, the RMSE of the RTS center is within +-0.24mm.

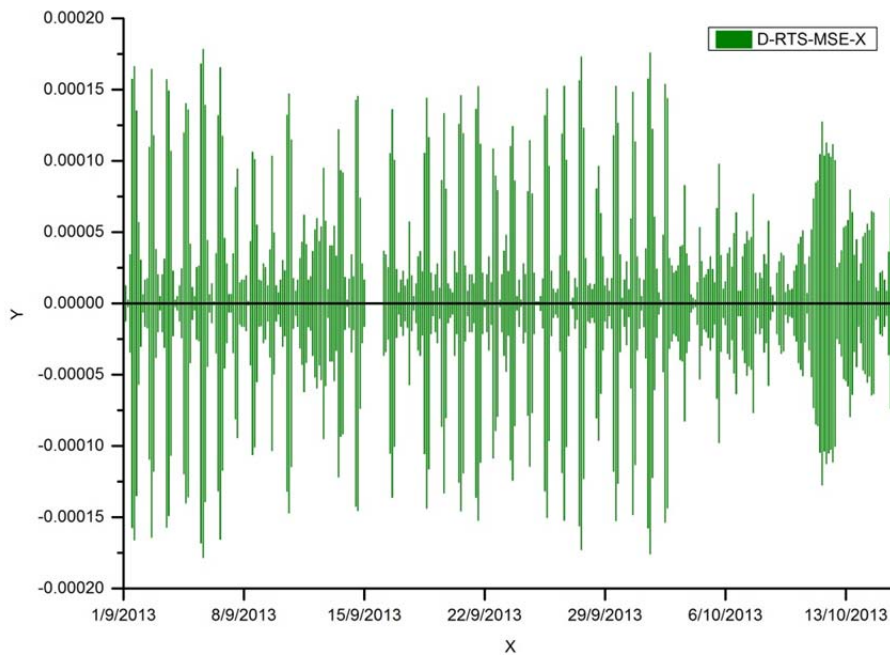


Figure 5.42 Root Mean Square Error of X_{RTS} (m) during the study period.

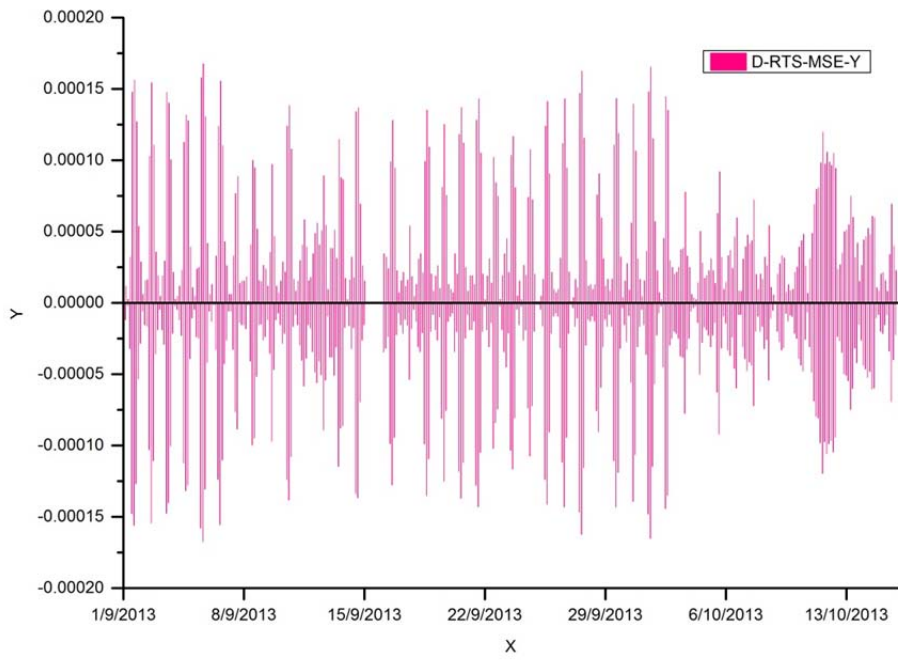


Figure 5.43 Root Mean Square Error of Y_{RTS} (m) during the study period.

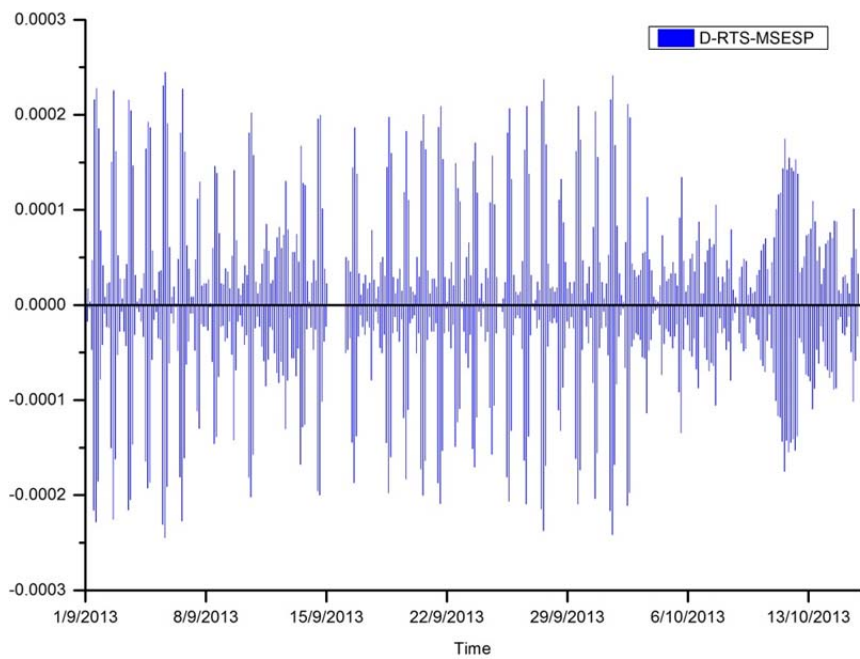


Figure 5.44 Root Mean Square Error of the RTS center point (m) during the study period.

b. Ellipse of Error

The Ellipse of Error is a classical tool to visualize the confidence region around the mathematically computed solution. After completing the LS adjustment, the covariance matrix will help us to draw the Ellipse of Error.

In the Annex VIII the formulation to construct the ellipse of error in order to visualize the confidence region around the mathematically computed solution is fully developed. The equations of this Annex obtain the orientation of the ellipse and the size (semi-axes). The computation has been applied for each epoch within the study period (1st September 2013 to 15th October 2013), and the resulting ellipses plotted in Figure 5.45.

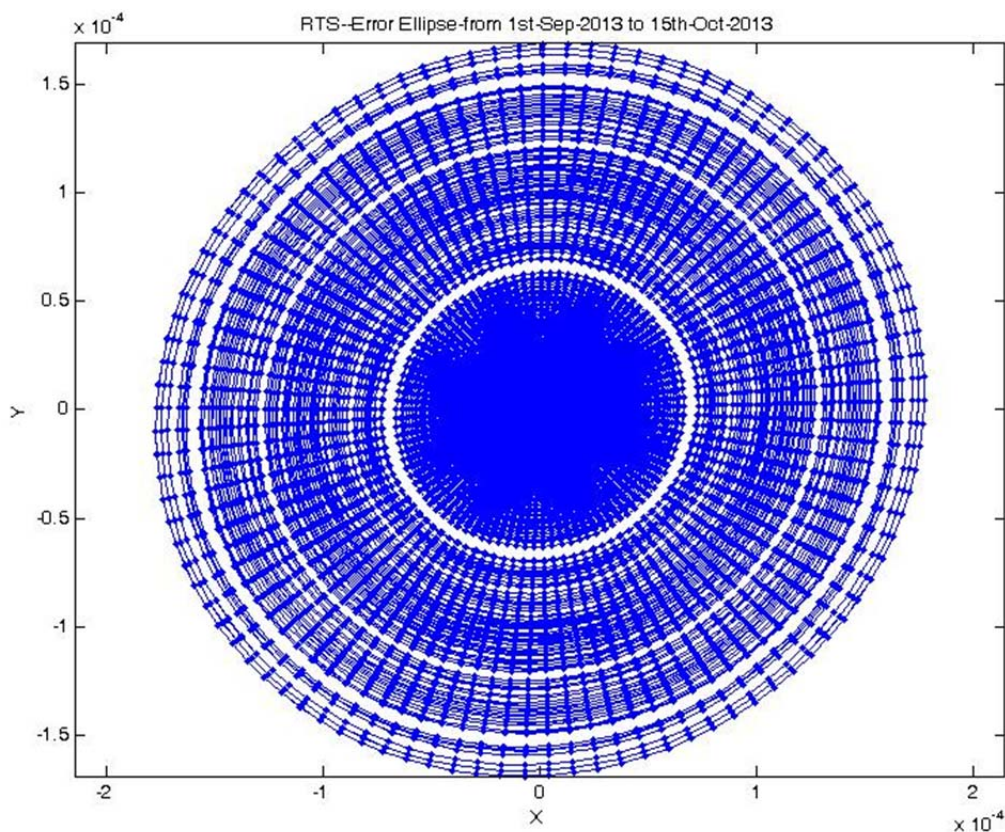


Figure 5.45 Error ellipses of the RTS. Axes unit is mm.

The position of all the ellipses has been fixed in the (0, 0). The figure shows the spread of sizes, the ellipses being almost circular. On the other hand, the orientation is quite constant. From the figure, it can be seen that the error ellipses range from about -0.2mm to 0.2mm in X-direction, and from about -0.18mm to 0.18mm in Y-direction. A good proportion of the ellipses fall in the range between -0.1mm and 0.1mm in X-direction

and Y-direction; this indicates that the error in the positioning of the RTS is quite convenient.

5.3.3.3 Simulated movement for the K2M Control Points.

After the computation, the results of the nine control points have been obtained. These Control Prisms were installed on the NW façade of the K2M building. In order to analyze the results, the nine control points have been divided into three groups according to their place and the control points in each group located in the same vertical: CP-1, CP-4 and CP-7 are in group 1; CP-2, CP-5 and CP-8 are in group 2; CP-3, CP-6 and CP-9 are in the group 3.

The figures from 5.46 to 5.48 show the displacement of the control points in X-direction during the study period. From those figures, it can be seen that the movement of the control points became increasingly bigger from the control point on the street level to the control point on the top floor in each group. This trend shows that the control points on the top of the building are more influenced by thermal change than the control points on the ground floor. Apart from that, there is another phenomenon the movement range of group 1 is smaller than group 3, and the nine control points' movement trends are similar. The movement ranges of control points in X-direction are about 0.5mm for CP1, CP2 and CP7, 1mm for CP4, 1.5mm for CP3 and CP5, 2.0mm for CP6 and CP8, 3.0mm for CP9.

The figures from 5.49 to 5.51 present the movement of control points in Y-direction. Looking at those three figures, it can be noticed that the movement trend in group-2 and group-3 are converse with the results in group-1. For the results in group-1, the three curves move in a similar step and direction; for the results in group-2 and group-3, the range of CP-8 is very small compared with the others, but they also have a parallel movement direction. From the figures from 5.49 to 5.51 it seems that the height of the building does not influence the result in Y-direction. The movement ranges of control points in Y-direction are about 0.5mm for CP8, 1.0mm for CP7, 1.5mm for CP1, CP2, CP4, CP5 and CP9, 2mm for CP3 and CP6.

The figures 5.52 to 5.54 display the movement of the control points in Z-direction. From those figures, it can be seen that the movement of the control points on the ground floor is very small compared with the changes on the upper floor. Similarly to the

movement in X-direction, all of the control points' curves have the same movement trend in the study time. The movement ranges of control points in Z-direction are about 0.5mm for CP1, CP2 and CP3, 1mm for CP7, 1.5mm for CP6, 2.0mm for CP4, CP5 and CP9, 2.5mm for CP8.

Figures 5.46 to 5.54 confirm that thermal change influences the structure deformation monitoring practice a great deal, and the structures move with thermal change. Moreover, it is also proved that the thermal influence on structure deformation monitoring can be simulated, which is very important in order to forecast the influence of thermal change on structure deformation monitoring. The apparent movement of the Control Prisms can be explained with two causes: the first one is that the RTS coordinates are not perfect, since they contain a certain amount of error that is inherited by the Control Prisms; the second one is that the K2M building moves, slightly, due to the thermal deformation.

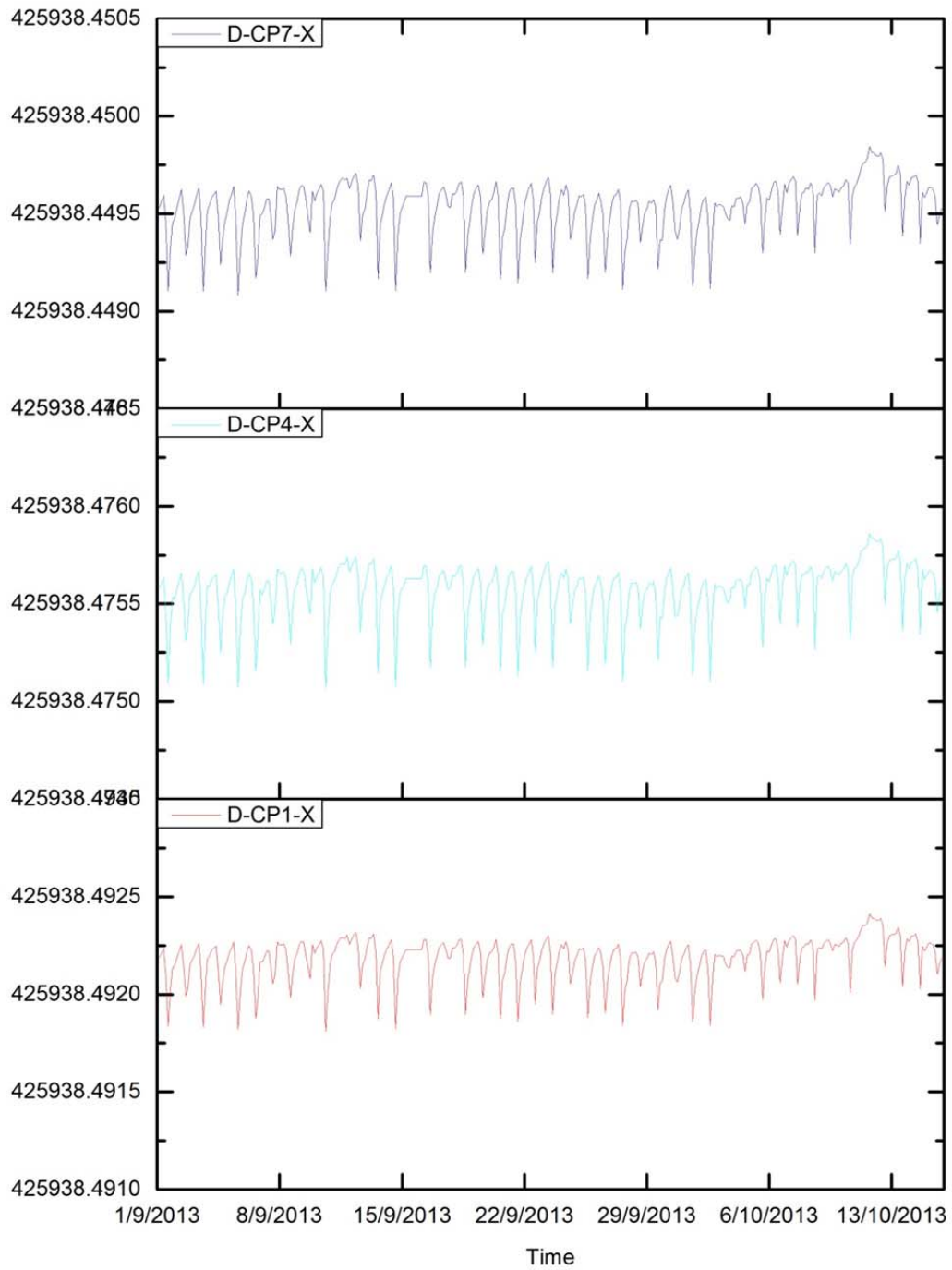


Figure 5.46 Control points 1, 4 and 7 movement (m) in X-direction.

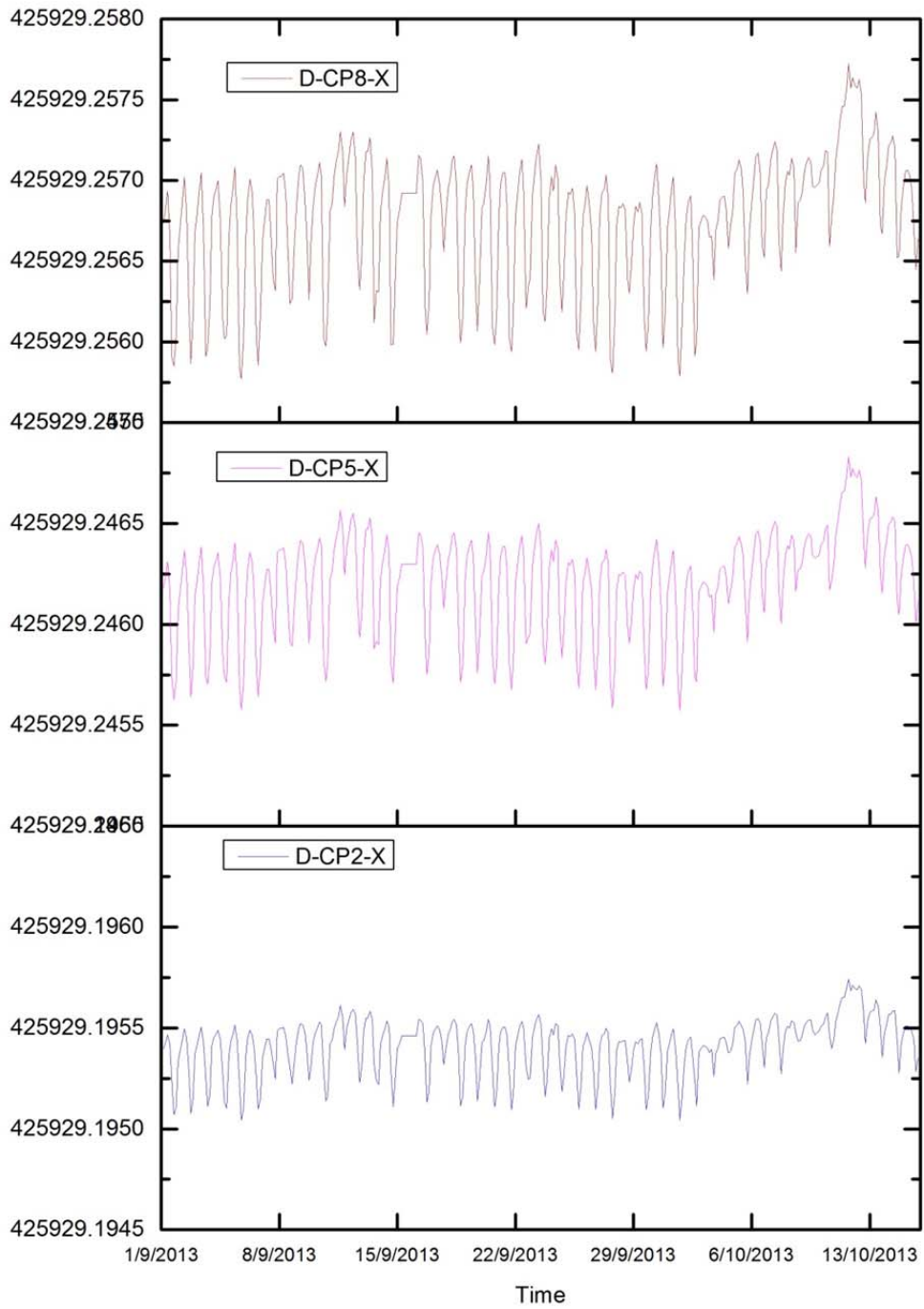


Figure 5.47 Control points 2, 5 and 8 movement (m) in X-direction.

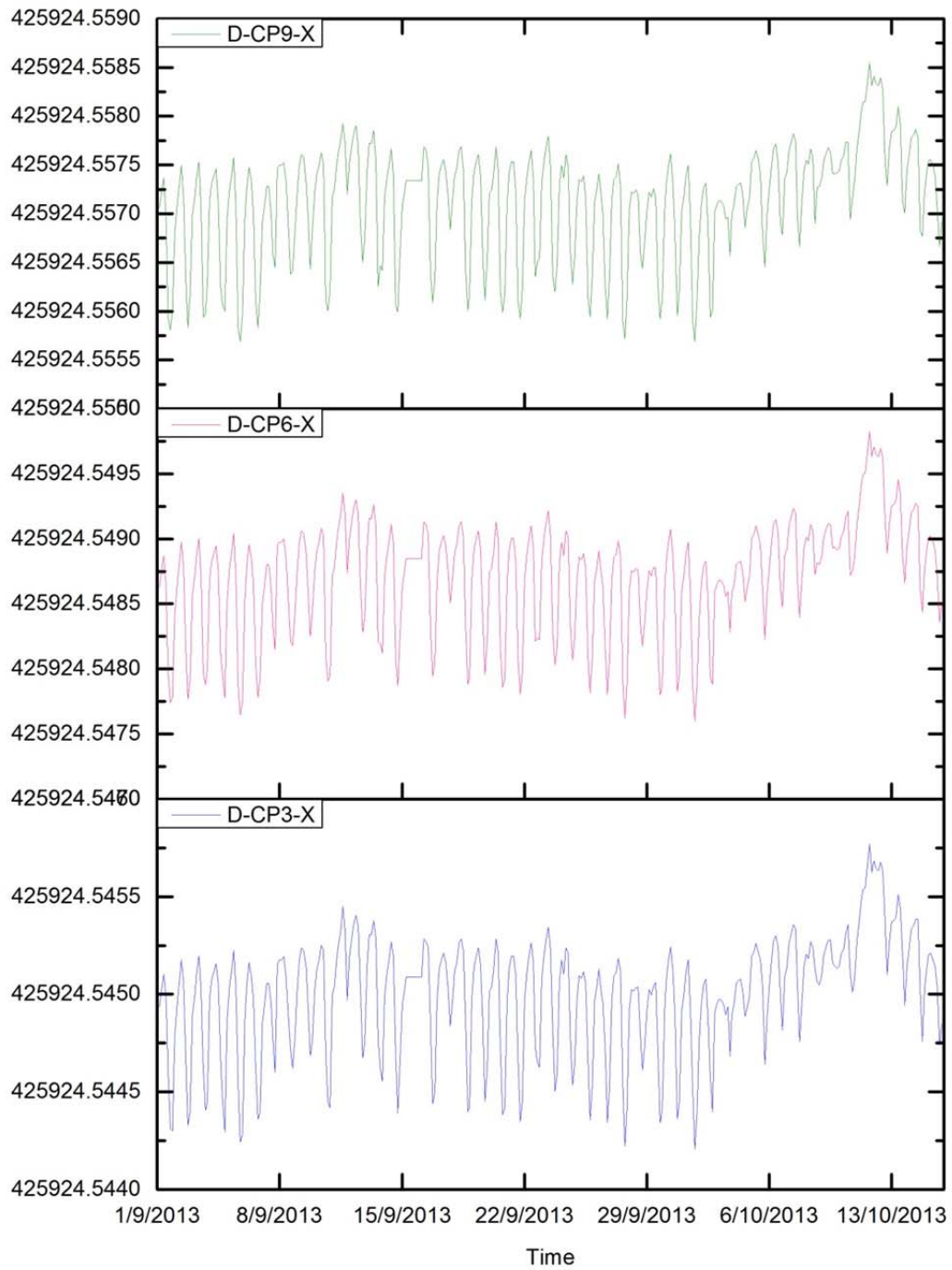


Figure 5.48 Control points 3, 6 and 9 movement (m) in X-direction.

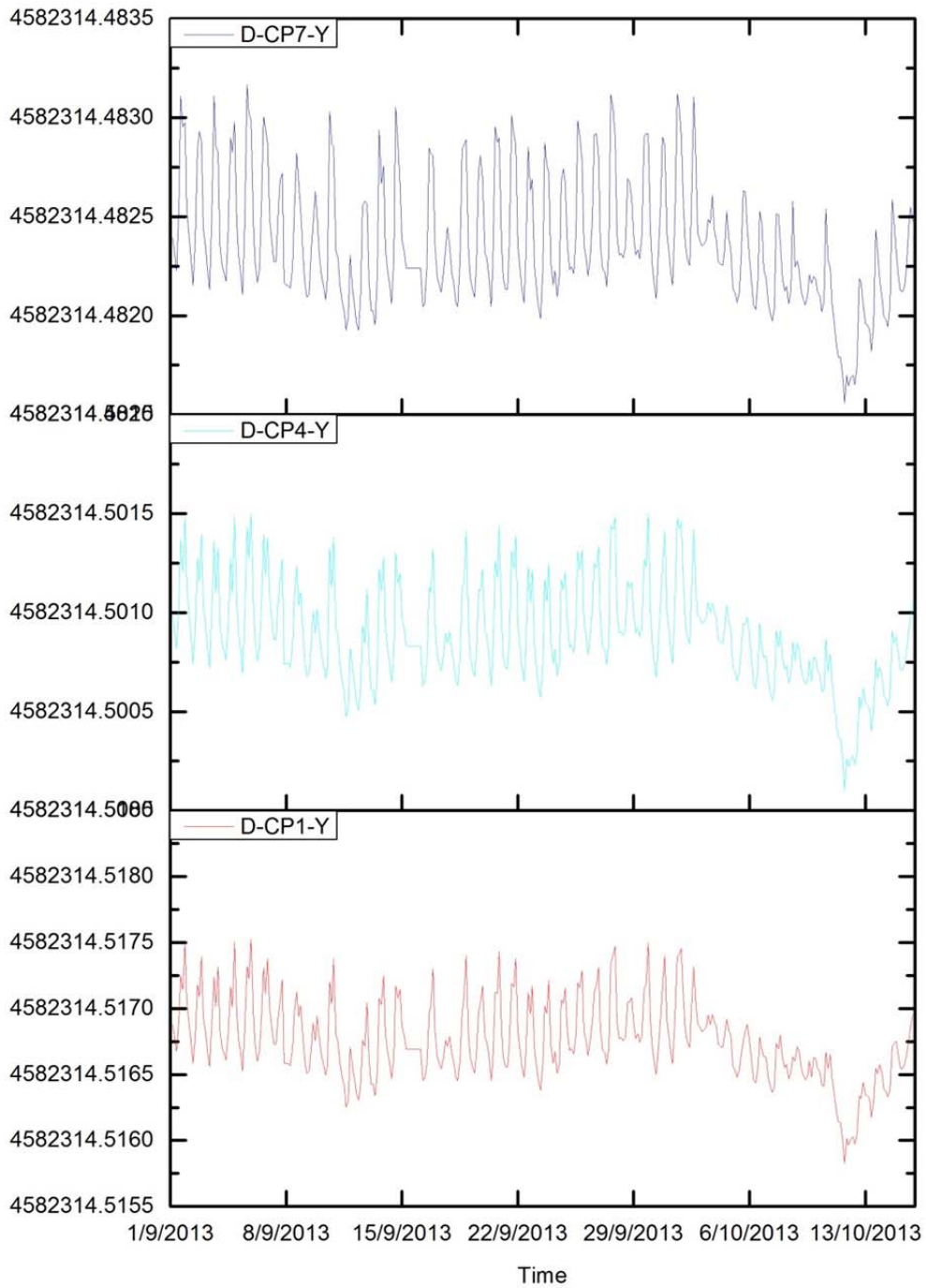


Figure 5.49 Control points 1, 4 and 7 movement (m) in Y-direction.

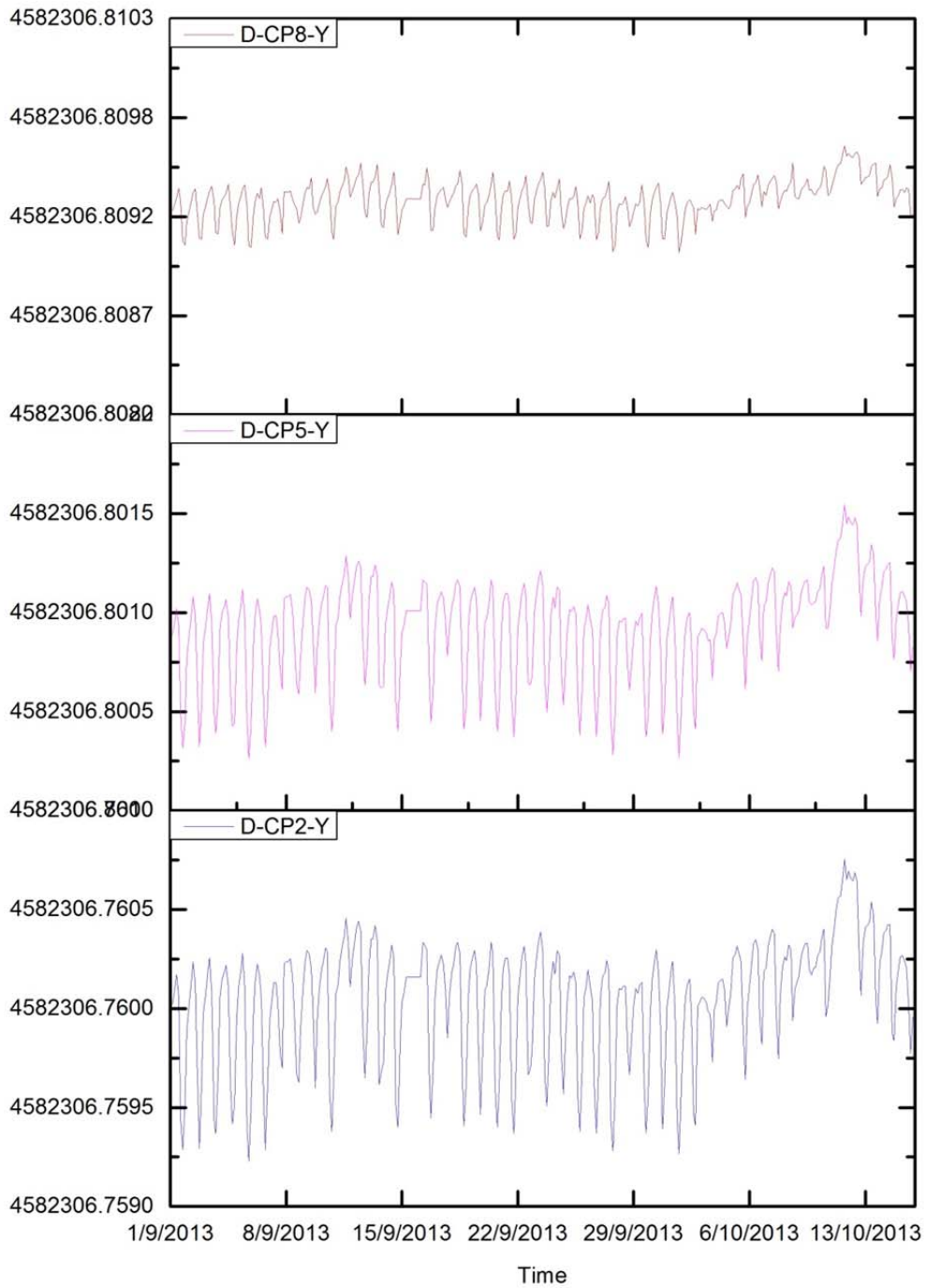


Figure 5.50 Control points 2, 5 and 8 movement (m) in Y-direction.

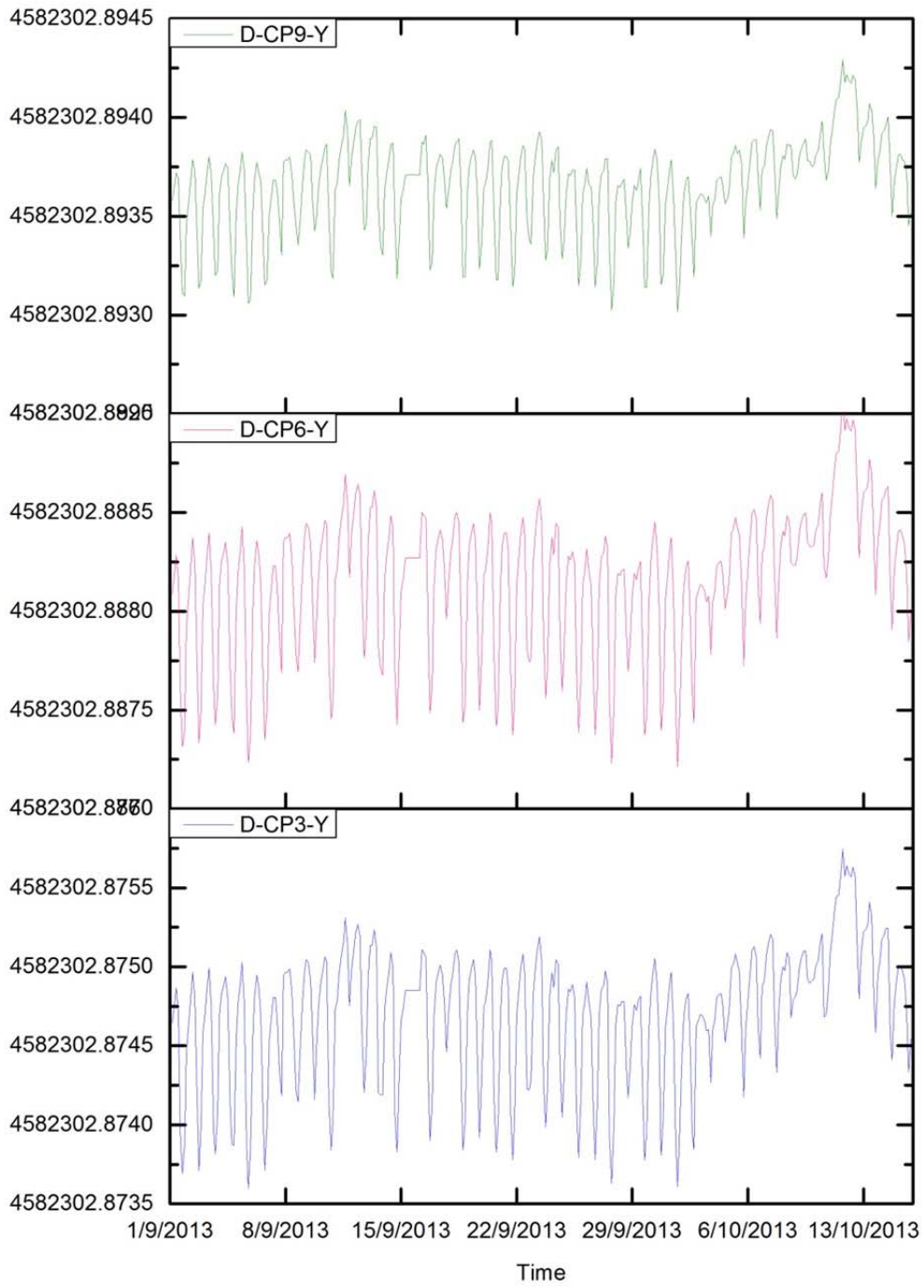


Figure 5.51 Control points 3, 6 and 9 movement (m) in Y-direction.

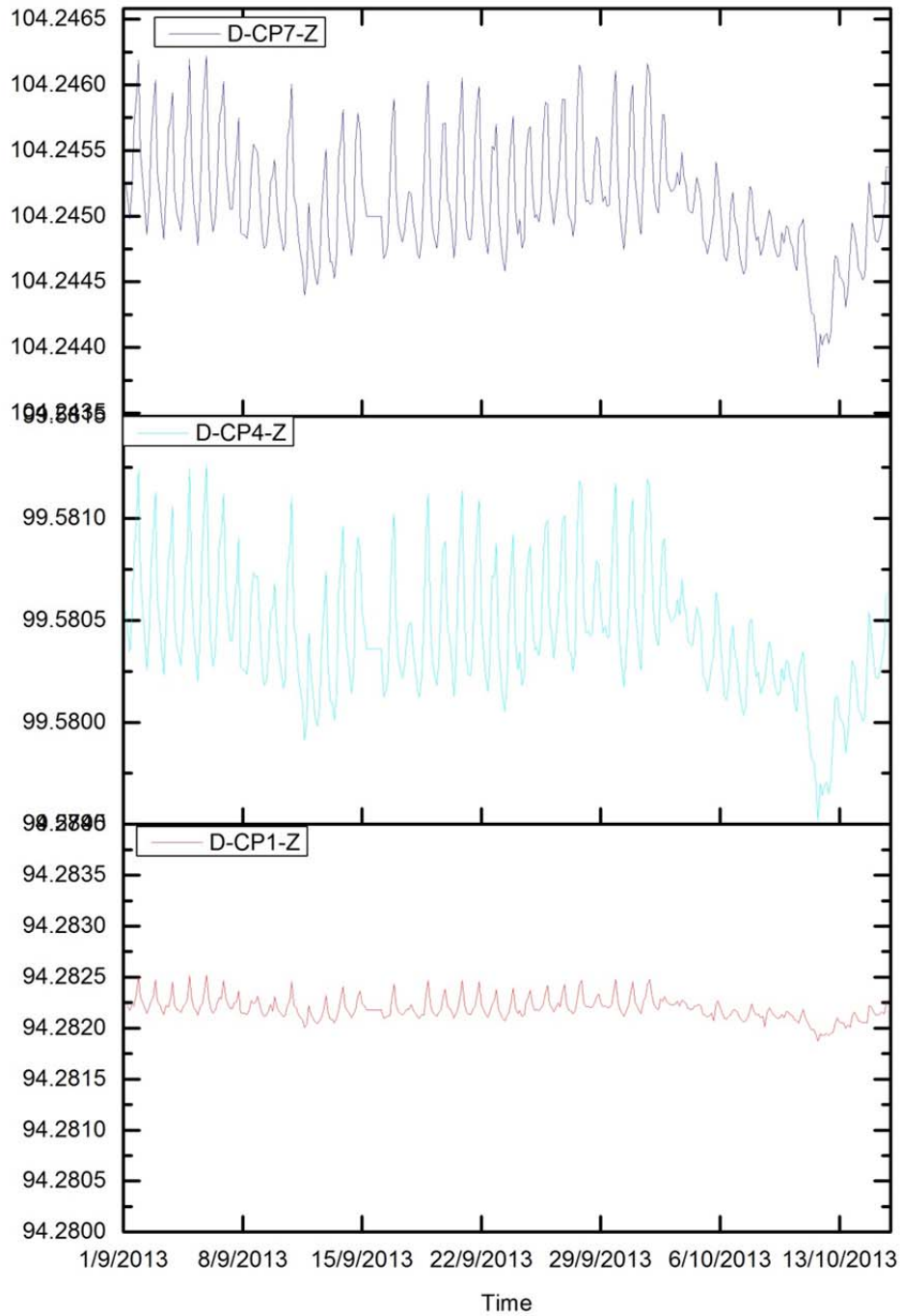


Figure 5.52 Control points 1, 4 and 7 movement (m) in Z-direction.

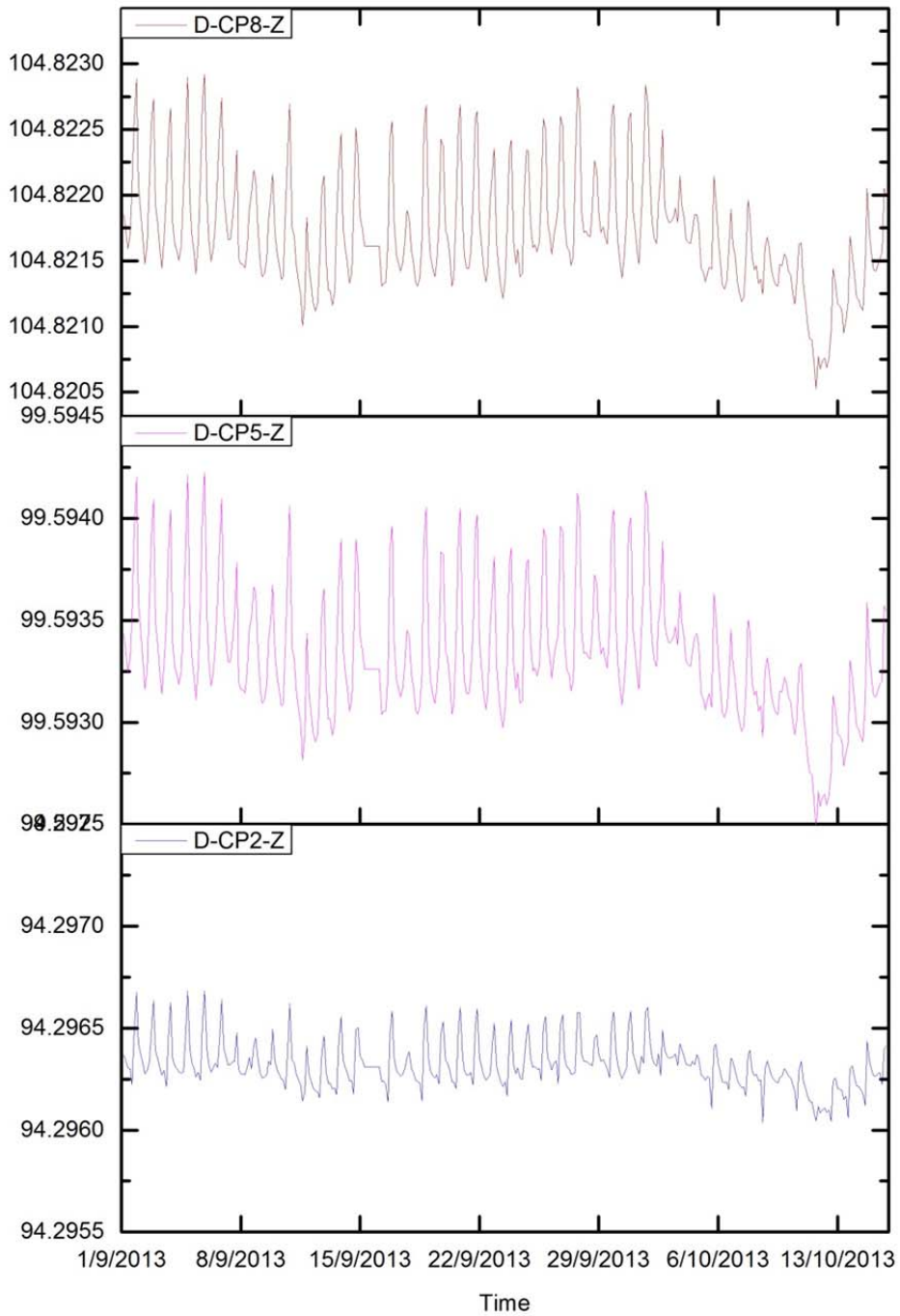


Figure 5.53 Control points 2, 5 and 8 movement (m) in Z-direction.

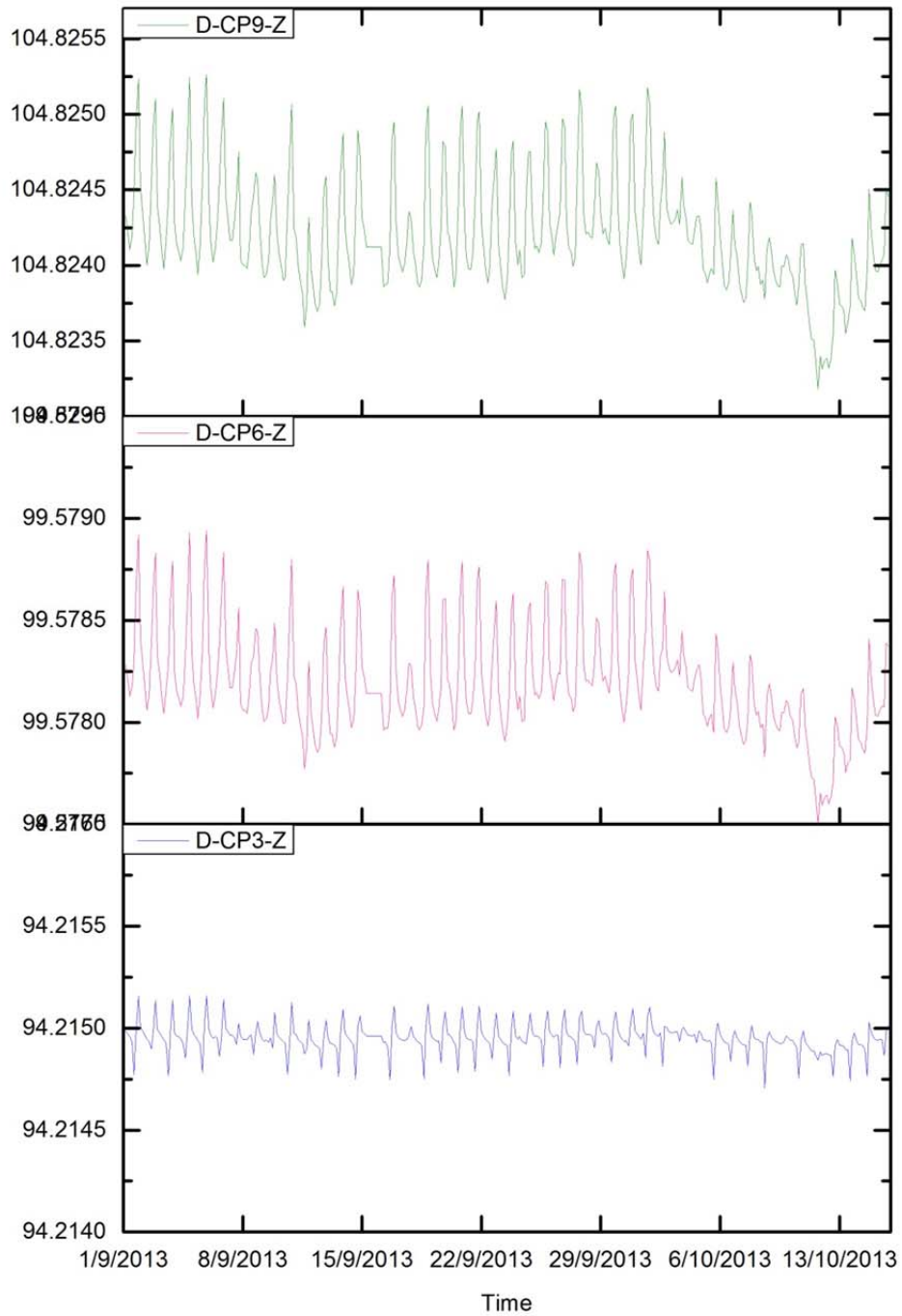


Figure 5.54 Control points 3, 6 and 9 movement (m) in Z-direction.

5.4 Comparing the real monitoring results with the simulated ones (approach D)

In this section we will compare the real world results (section 5.2) with the simulated ones (approach D, section 5.3) in order to assess to what degree we have been able to capture the phenomenon.

Firstly, the comparison is made at the RTS level (A6 building). Afterwards, the graphs of the Control Points in the façade of the K2M are analyzed.

5.4.1 Comparing the RTS real monitoring results with the simulated ones (approach-D)

The Figure 5.55 shows the two sources of the RTS movement: results from approach-D (labeled with 'D') and the real monitoring result obtained with the Soldata standard system (Geoscope-web system, labeled with 'G'). The study period is 1st September 2013 to 15th October 2013.

From this figure, it can be concluded that 1) for the RTS movement in X direction, the result of D can follow the movement trend of GW; 2) for the RTS movement in Y direction, the whole movement range of D is almost the same as GW, but the daily movement range of D is bigger than GW; 3) for the RTS movement in Z direction, the result of D has a perfect match with GW during the study time period.

From those three results about the RTS, it can be concluded that the thermal influence on the RTS can be simulated and computed, and that our simulated results are almost the same as the real monitoring results.

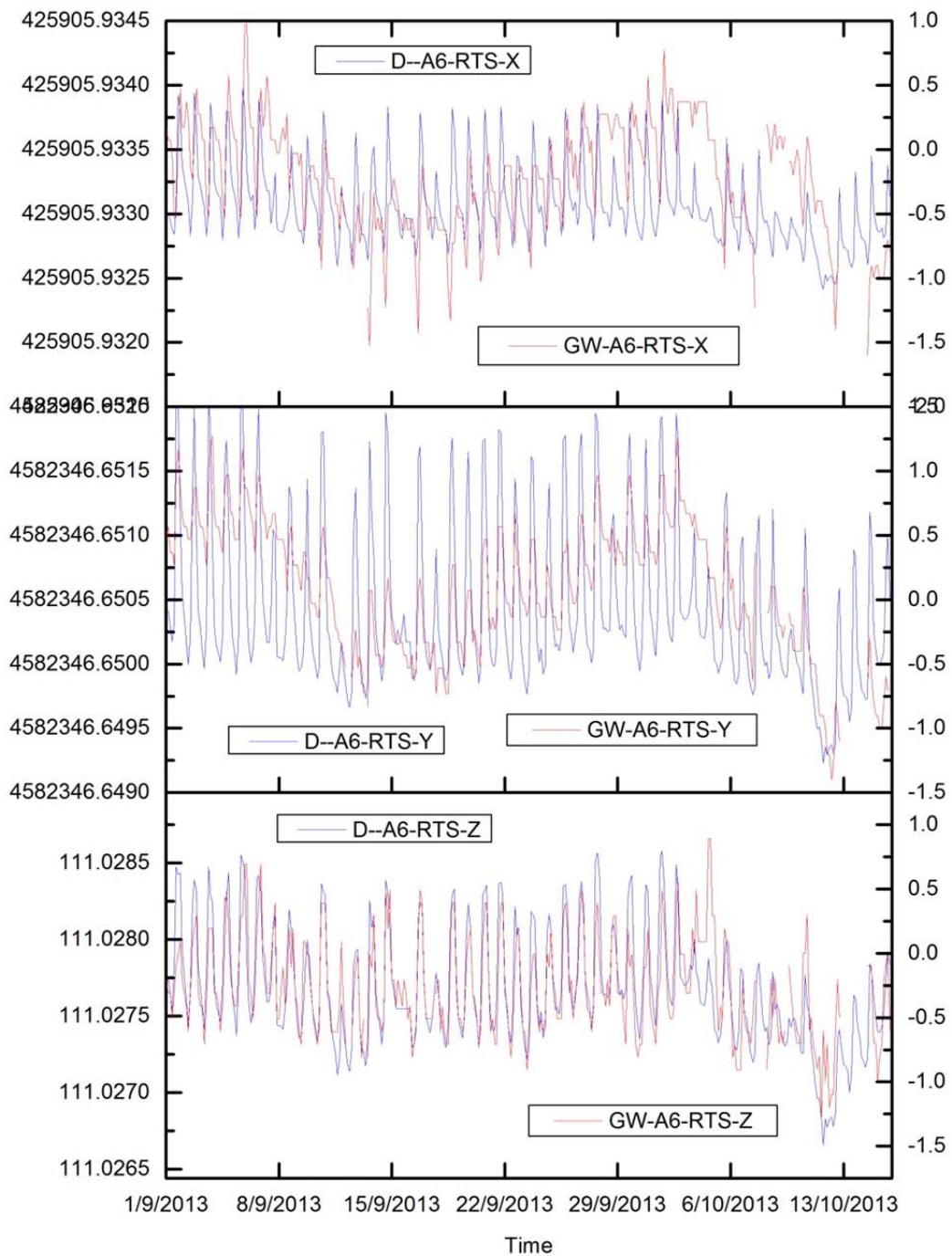


Figure 5.55 RTS movement: simulated result (D) and standard practice (GW). X (top); Y (middle), Z (bottom). Coordinates in meters.

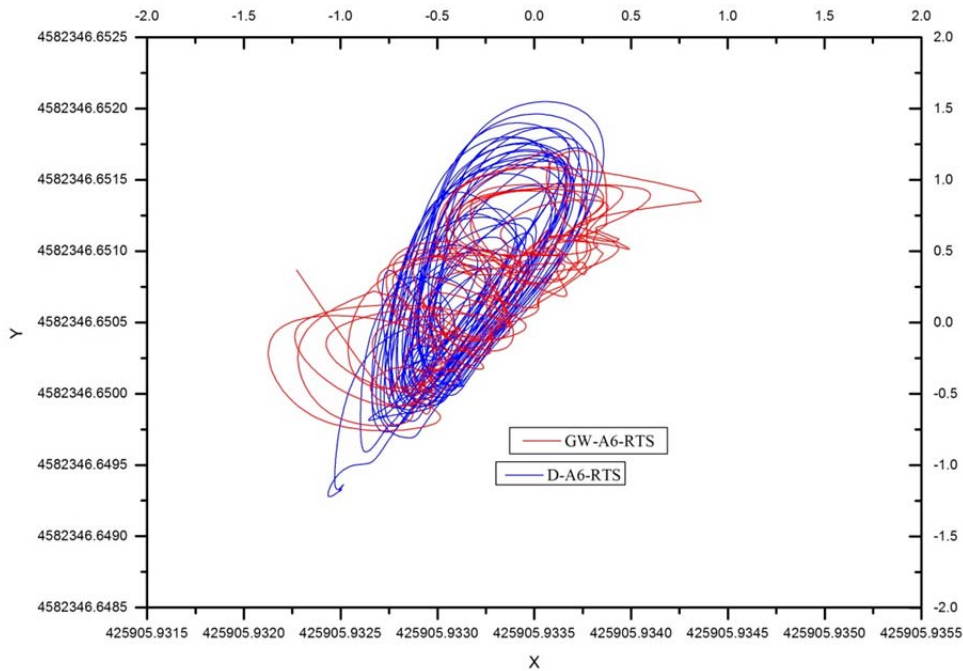


Figure 5.56 RTS movement in the XY plane during the study time period: simulated result (D) and standard practice (GW). Coordinates in meters.

In Figure 5.56 the RTS XY path of GW and simulated result (D) during the study period (1st September 2013 to 15th October 2013) is presented. In X-direction and Y-direction, the movement range of D is similar to the result of GW. It proves that the result of D can match the real movement of the RTS in practice, which is GW's result.

Let us have a closer look at what happens on one given day. Figure 5.57 illustrates the RTS movement (XY path) during one single day (1st September 2013). From this figure, it can be seen that, globally, the result of D followed the same movement trend as the result of GW. There is another interesting phenomenon: the movement range during the day light is bigger than the movement range at night. The reason is that the temperature changes more during the day than at night.

After this favorable comparison, in the next section we will see what happens with the control prisms at the K2M façade.

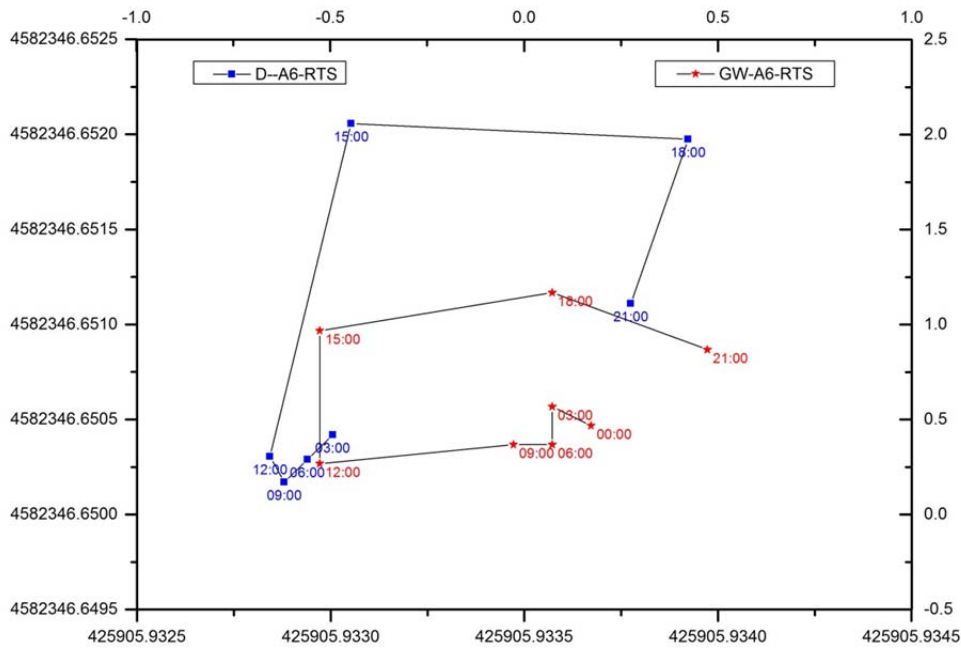


Figure 5.57 RTS movement in the XY plane during the 1st September 2013. Simulated result (D) and standard practice (GW). Coordinates in meters.

5.4.2 Comparing the Control Points real monitoring results with the simulated ones (approach-D)

Figures 5.58 to 5.66 show the comparison between the results of the real monitoring (GW) and the results of the simulation (Approach-D) during the study period (1st September 2013 to 15th October 2013). In general, the numerical model reproduces the real case observation curves quite well under thermal changes. The simulation results can match the real case results. But there are some parts of the curves that do not match the real case results. It is likely that, these differences can be attributed to the fact that the temperature distribution on the building of our simulation model is not completely equal to the real temperature distribution on the building; therefore, inaccuracies in the ΔT field applied to the buildings may be responsible for part of the differences found.

However, the comparison of the Approach-D results with the standard monitoring results (Geoscope web, GW) has been globally successful. We are ready to propose a new strategy to account for the Thermal Effect; this is the aim of the next Chapter.

5 Matching the Model with real world results

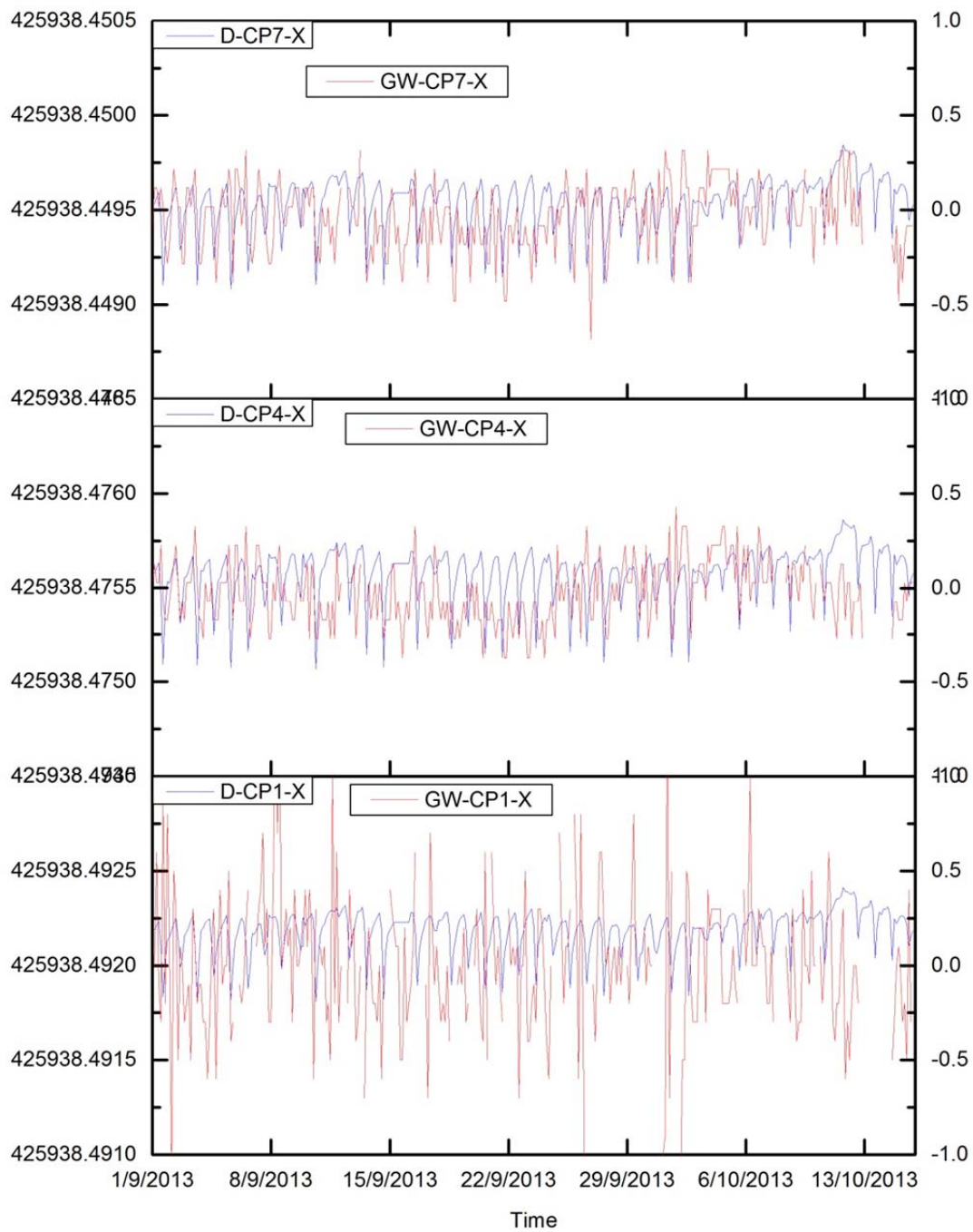


Figure 5.58 K2M, X-movement: CP1 (bottom), CP4 (middle) and CP7 (top). Simulated result (D) and standard practice (GW). Vertical Axes Unit: left is m, right is mm.

5 Matching the Model with real world results

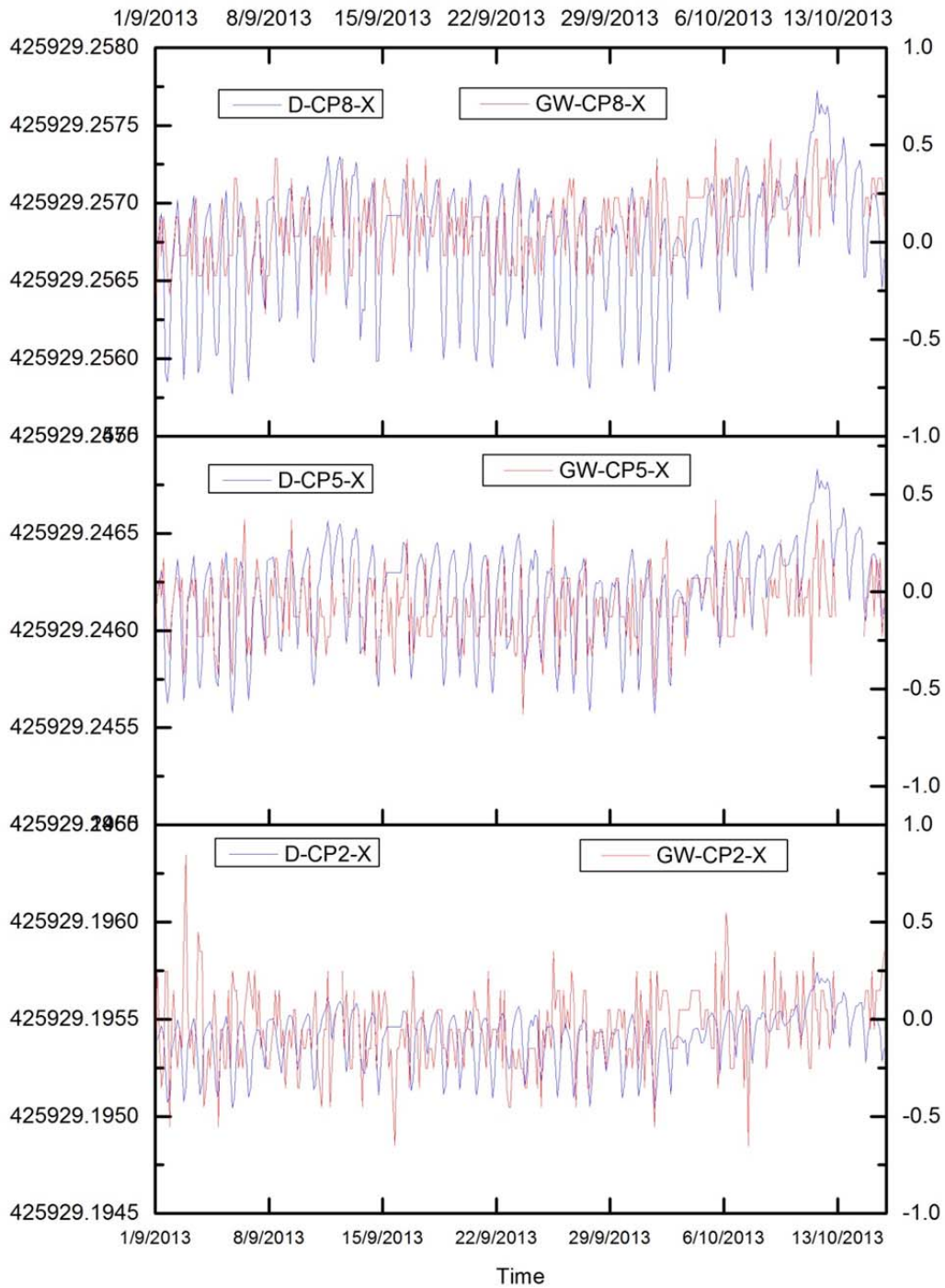


Figure 5.59 K2M, X-movement: CP2 (bottom), CP5 (middle) and CP8 (top). Simulated result (D) and standard practice (GW). Vertical Axes Unit: left is m, right is mm.

5 Matching the Model with real world results

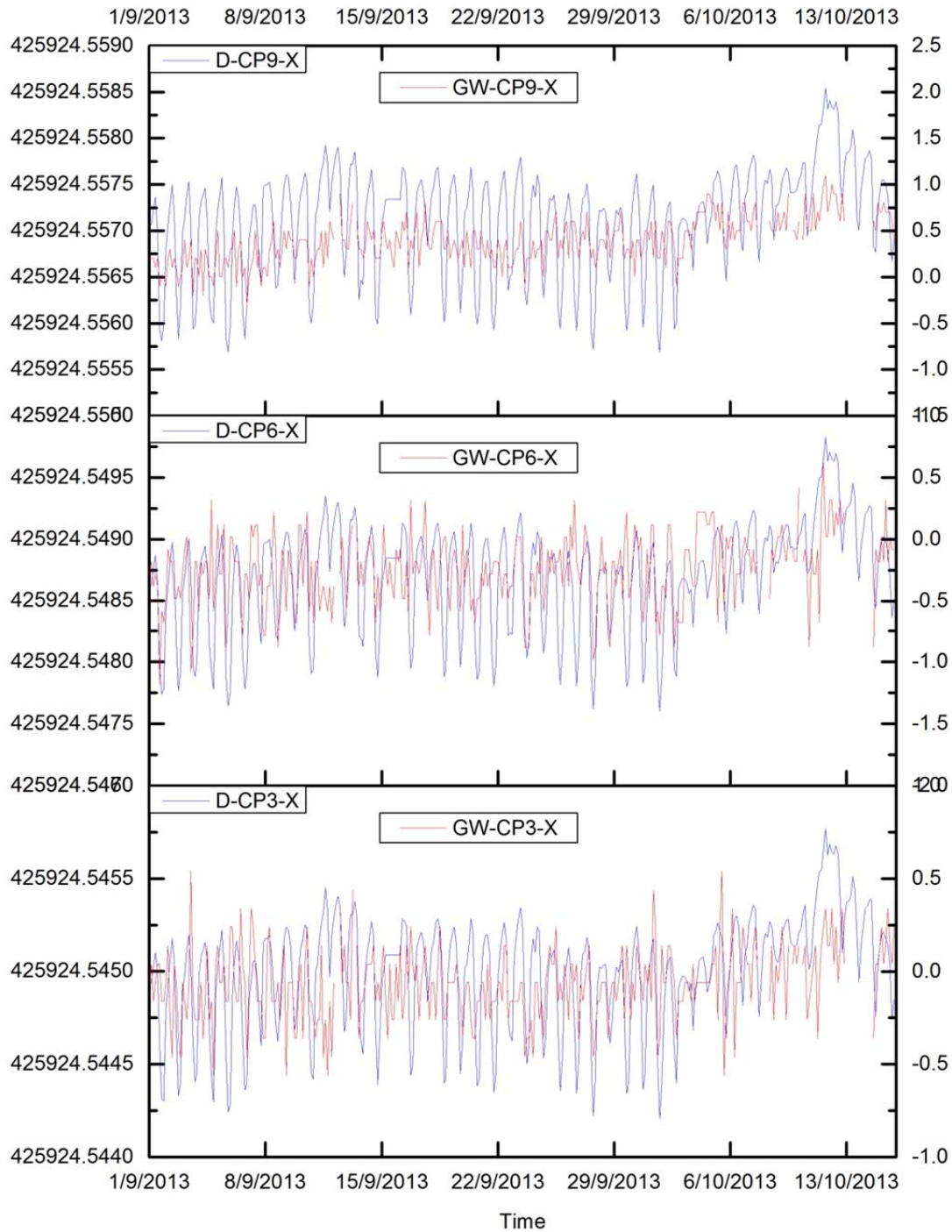


Figure 5.60 K2M, X-movement: CP3 (bottom), CP6 (middle) and CP9 (top). Simulated result (D) and standard practice (GW). Vertical Axes Unit: left is m, right is mm.

5 Matching the Model with real world results

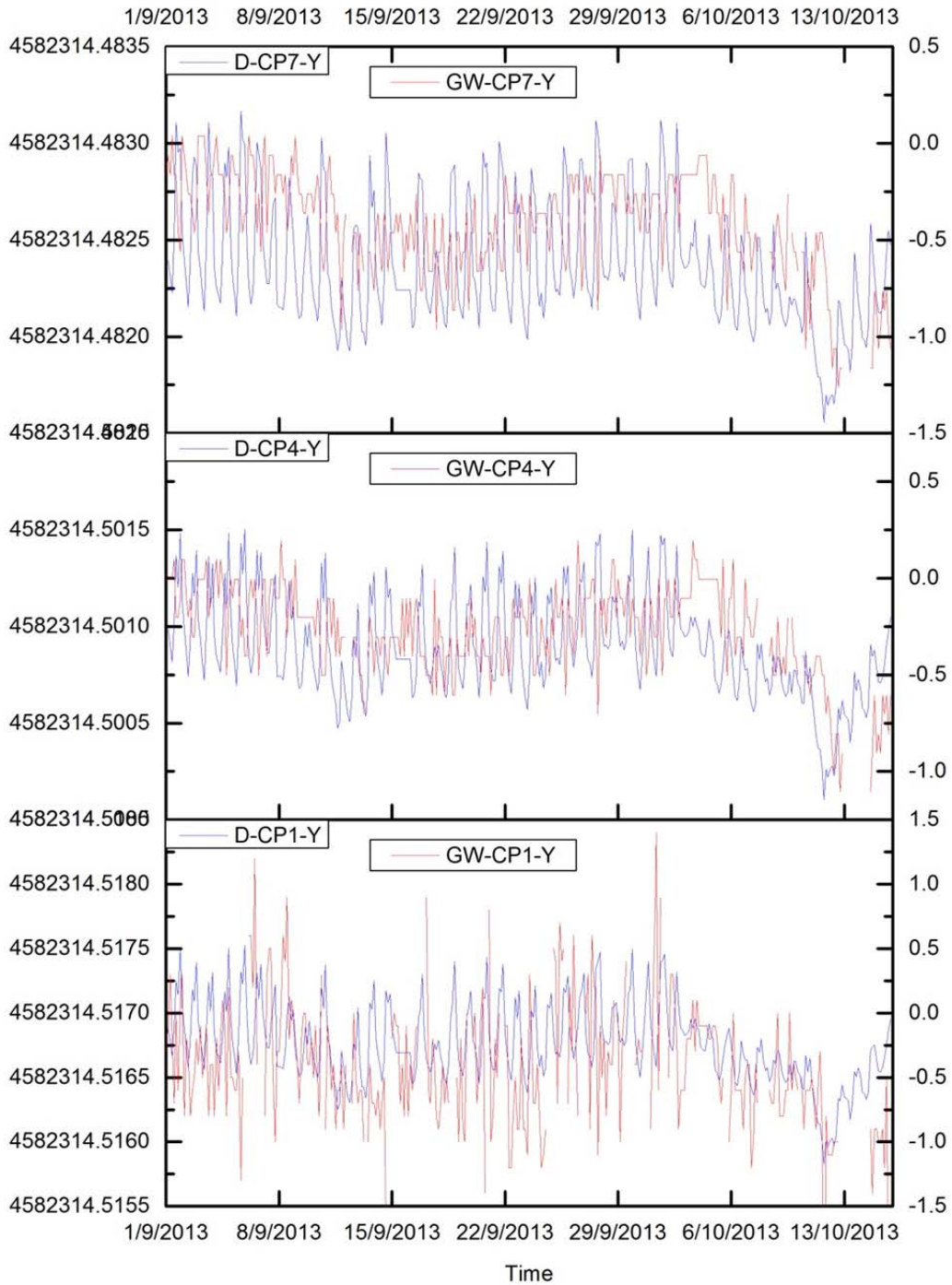


Figure 5.61 K2M, Y-movement: CP1 (bottom), CP4 (middle) and CP7 (top). Simulated result (D) and standard practice (GW). Vertical Axes Unit: left is m, right is mm.

5 Matching the Model with real world results

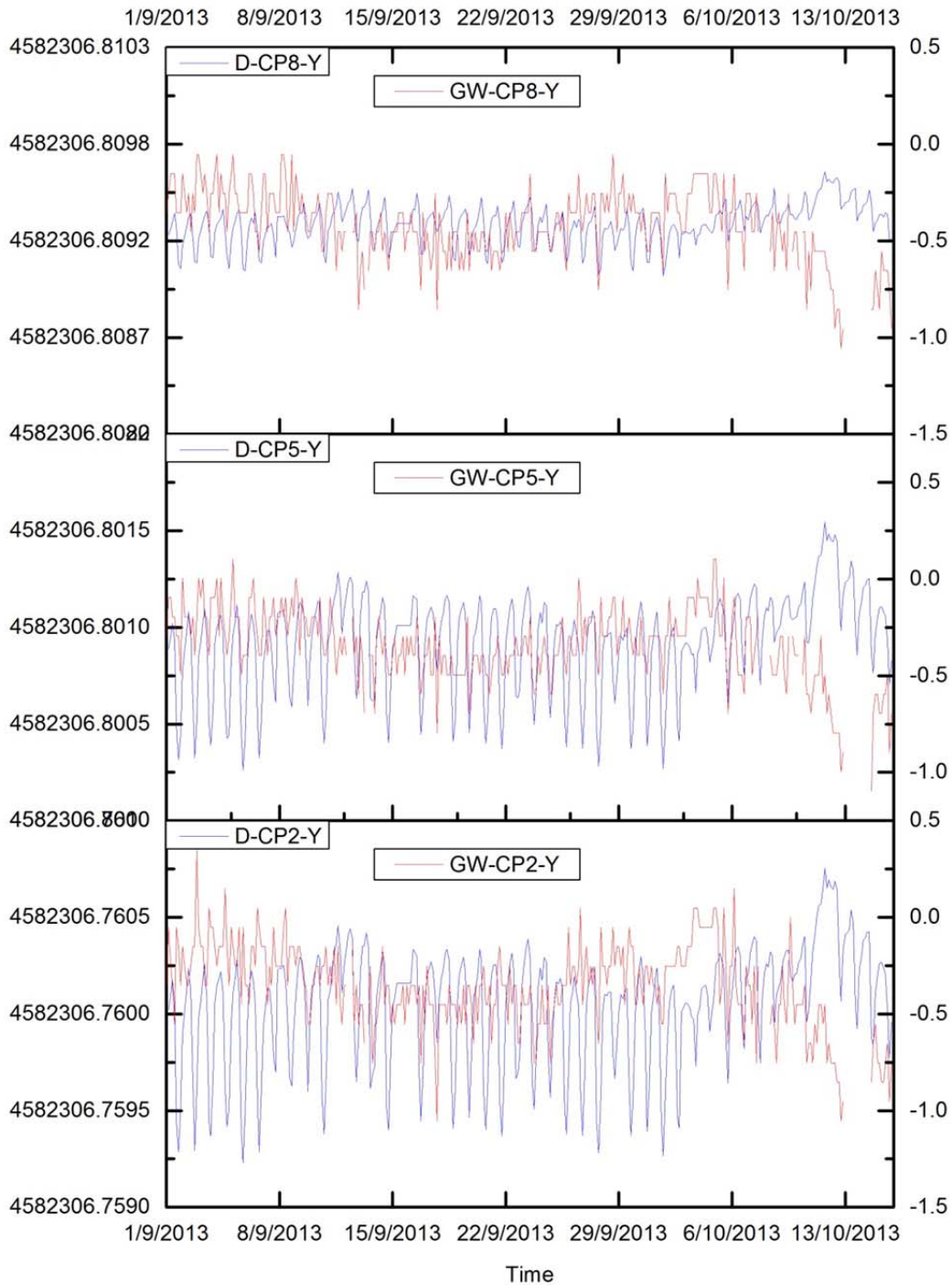


Figure 5.62 K2M, Y-movement: CP2 (bottom), CP5 (middle) and CP8 (top). Simulated result (D) and standard practice (GW). Vertical Axes Unit: left is m, right is mm.

5 Matching the Model with real world results

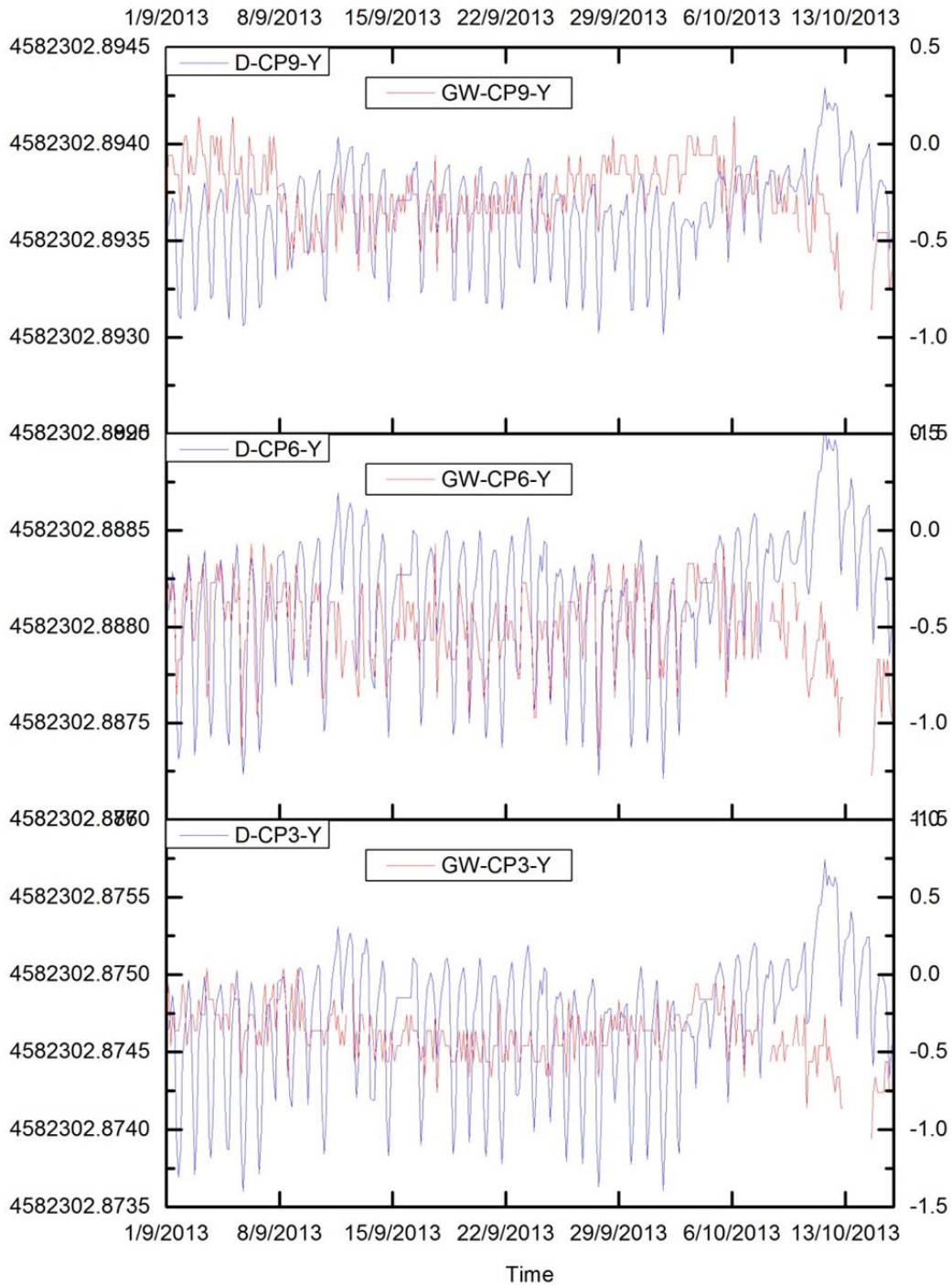


Figure 5.63 K2M, Y-movement: CP3 (bottom), CP6 (middle) and CP9 (top). Simulated result (D) and standard practice (GW). Vertical Axes Unit: left is m, right is mm.

5 Matching the Model with real world results

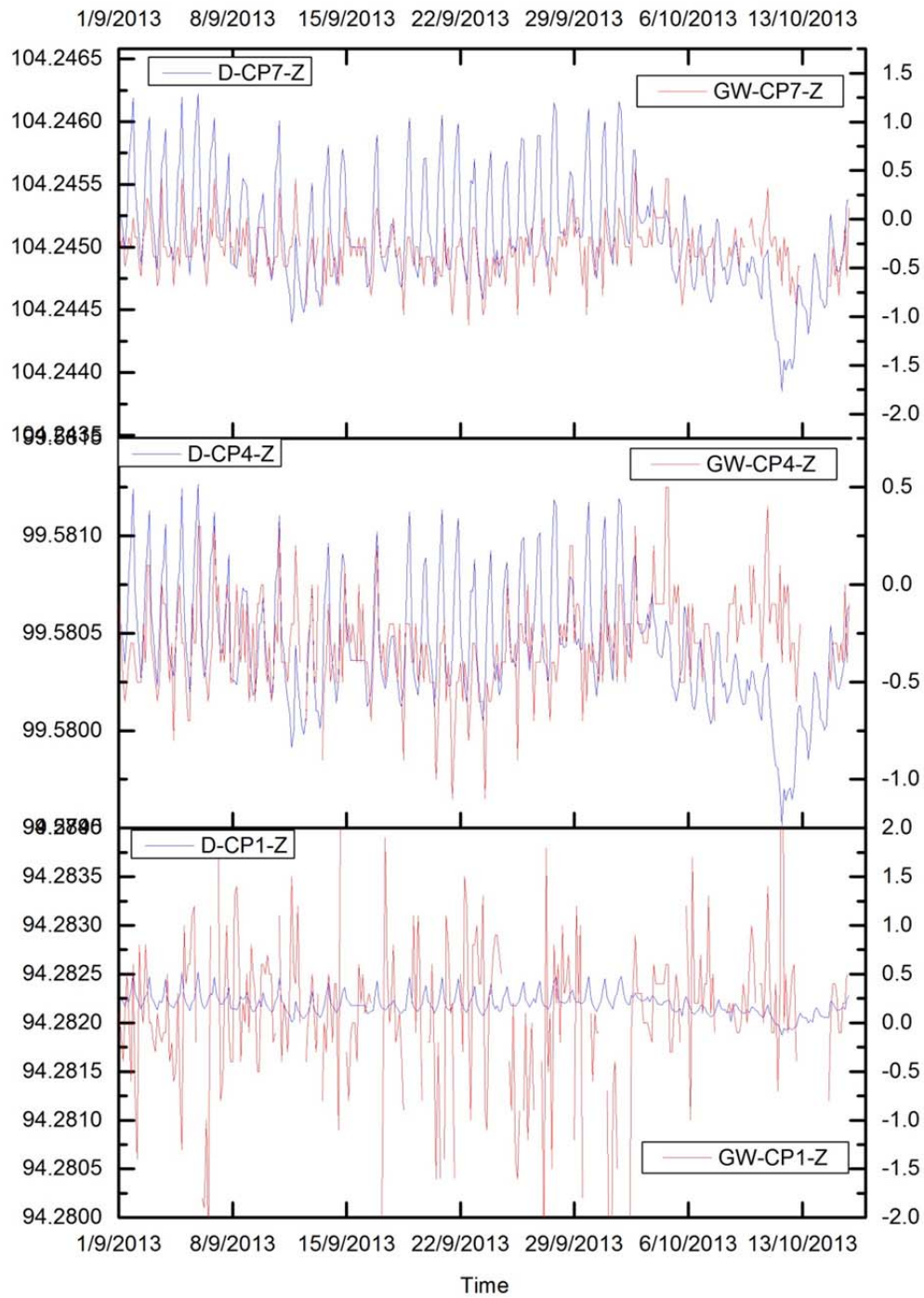


Figure 5.64 K2M, Z-movement: CP1 (bottom), CP4 (middle) and CP7 (top). Simulated result (D) and standard practice (GW). Vertical Axes Unit: left is m, right is mm.

5 Matching the Model with real world results

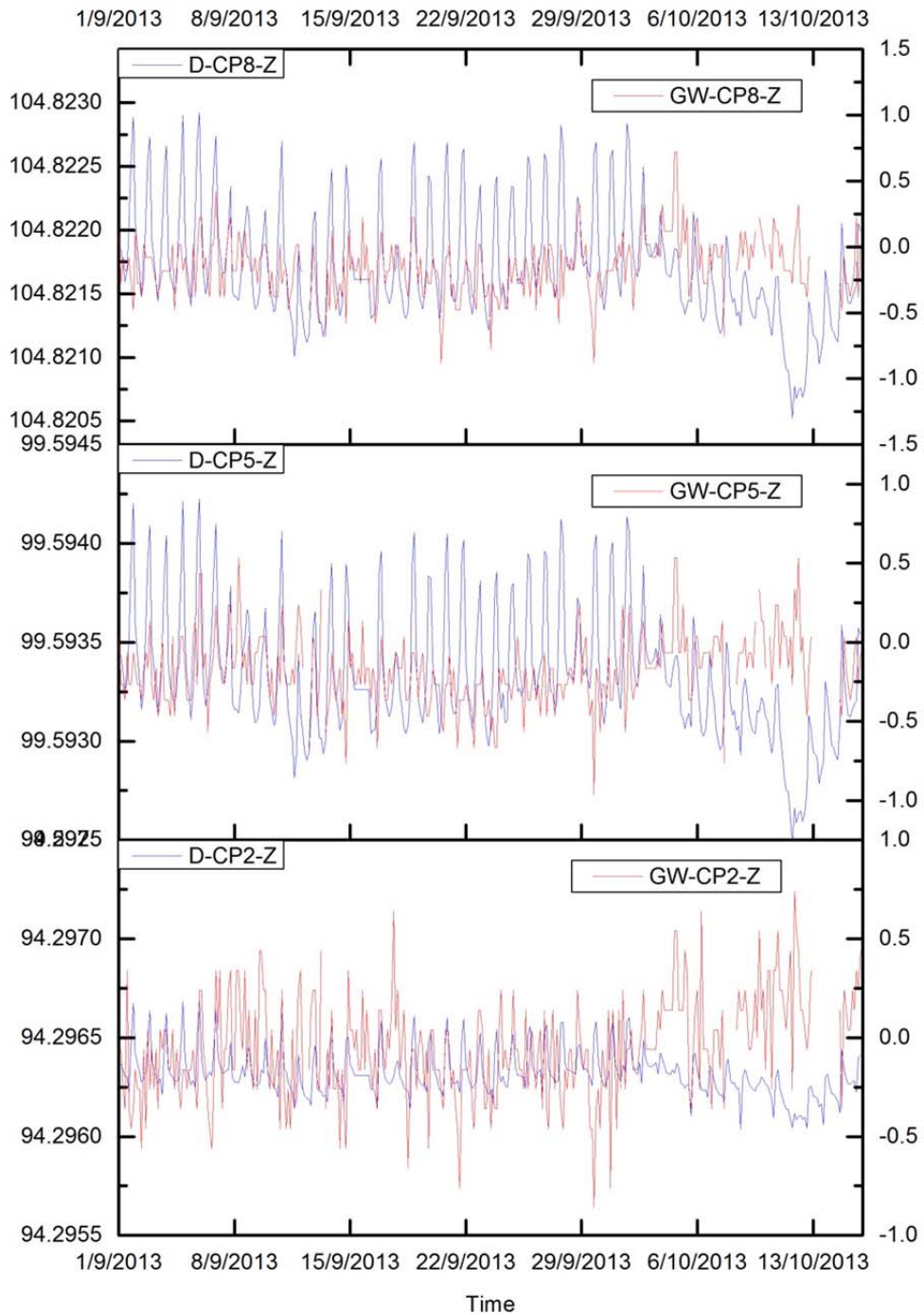


Figure 5.65 K2M, Z-movement: CP2 (bottom), CP5 (middle) and CP8 (top). Simulated result (D) and standard practice (GW). Vertical Axes Unit: left is m, right is mm.

5 Matching the Model with real world results

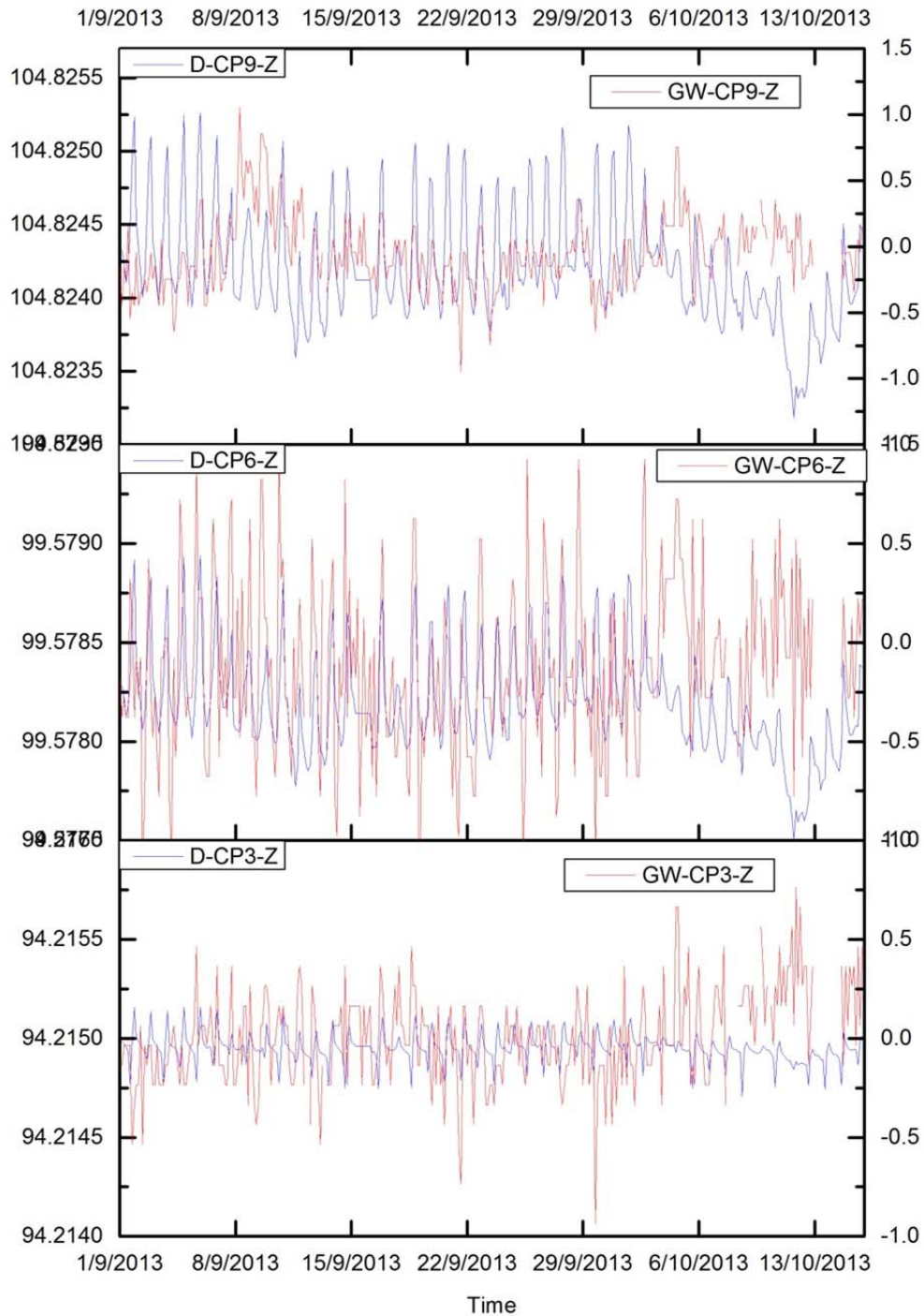


Figure 5.66 K2M, Z-movement: CP3 (bottom), CP6 (middle) and CP9 (top). Simulated result (D) and standard practice (GW). Vertical Axes Unit: left is m, right is mm.

6 Formulation of the strategy to consider thermal effects in building monitoring

6.1 Introduction

In chapter 5, after examining the monitoring results in the Campus Nord test area, we have implemented a model, Approach-D, which has permitted us to simulate the standard practice in building monitoring. After adjusting the model, starting from the evolution of the air temperature and sun insolation, we have been able to derive the variation of the coordinates of the control prisms located in the NW façade of the K2M building. The comparison of coordinate evolution according to Approach-D and the standard monitoring (Geoscope web, GW) has been globally successful. Now we are ready to define the procedure or strategy to take into account the deformation produced by the so-called Thermal Effect (variation of air temperature and sun insolation).

First of all, we have to remember the Equation 3.2

$$M_{corrected} = M_{observed} - M_{thermal} \quad 6.1$$

In this Equation, we can now identify that the $M_{observed}$ are the values measured by the standard monitoring system, such as the Geoscope Web used in the C.Nord test area. The best correction $M_{thermal}$ we have obtained so far comes from Approach-D, so we can write:

$$M_{corrected} = M_{GW} - M_{Approach_D} \quad 6.2$$

As an example of how to apply this equation, we may select a short period of time within the study period. Let us select the first week (1st September – 7th September 2013). Also, we will select one point to do the correction. Among the nine prisms in the

NW K2M façade, excluding the CP1 (affected by a tree), the most trusty set is the middle column: CP2, CP5, CP8. Among them, let us select the middle one, CP5, which is in center of the K2M façade.

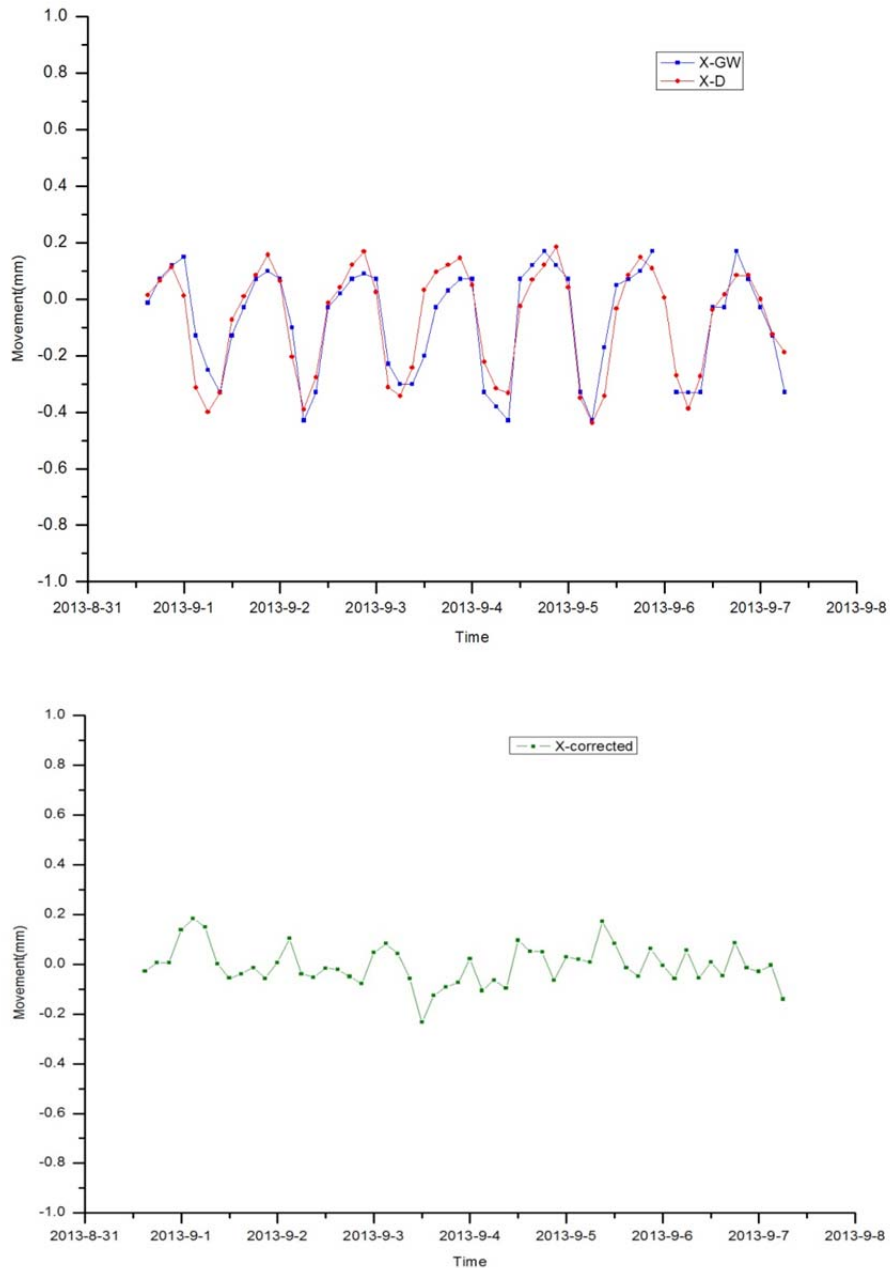


Figure 6.1 K2M, Control Prism CP5. Coordinate X corrected by subtracting the Simulated value (Approach-D) from the standard practice value (GW). See the first week in Figure 5.59.

In Figure 6.1, 6.2 and 6.3, the intended correction has been done for X, Y and Z respectively. First of all, the standard practice (GW) series has been filtered in order to

6 Formulation of two approaches to analysis Thermal Effects in standard monitoring

correct some extreme values that can be identified as out-of-the-trend. Then, the subtraction (eq. 6.2) has been done, obtaining the second graph that contains the movement corrected from the thermal effect. The improvement is evident, even in this low rise building.

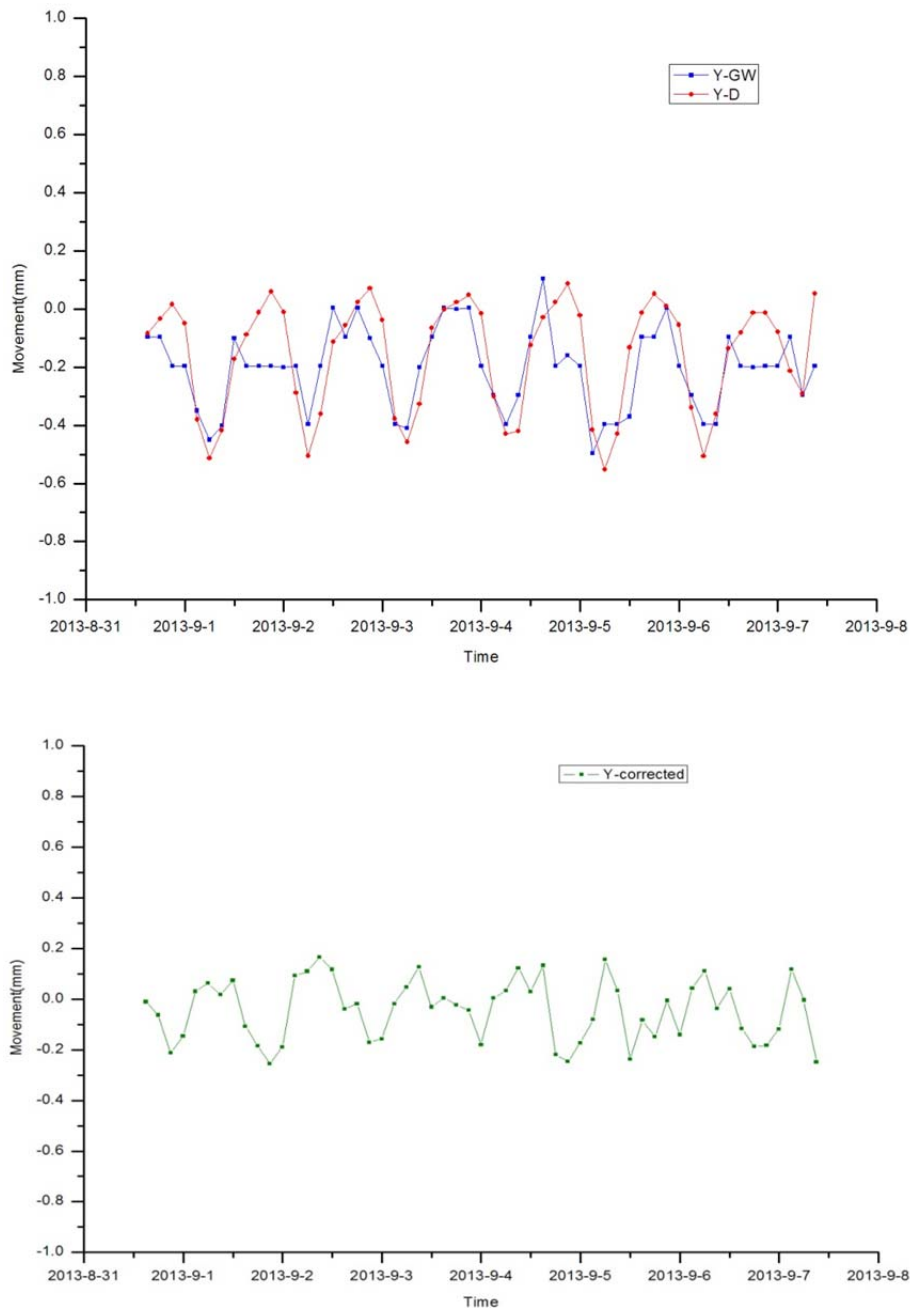


Figure 6.2 K2M, Control Prism CP5. Coordinate Y corrected by subtracting the Simulated value (Approach-D) from the standard practice value (GW) See the first week in Figure 5.62.

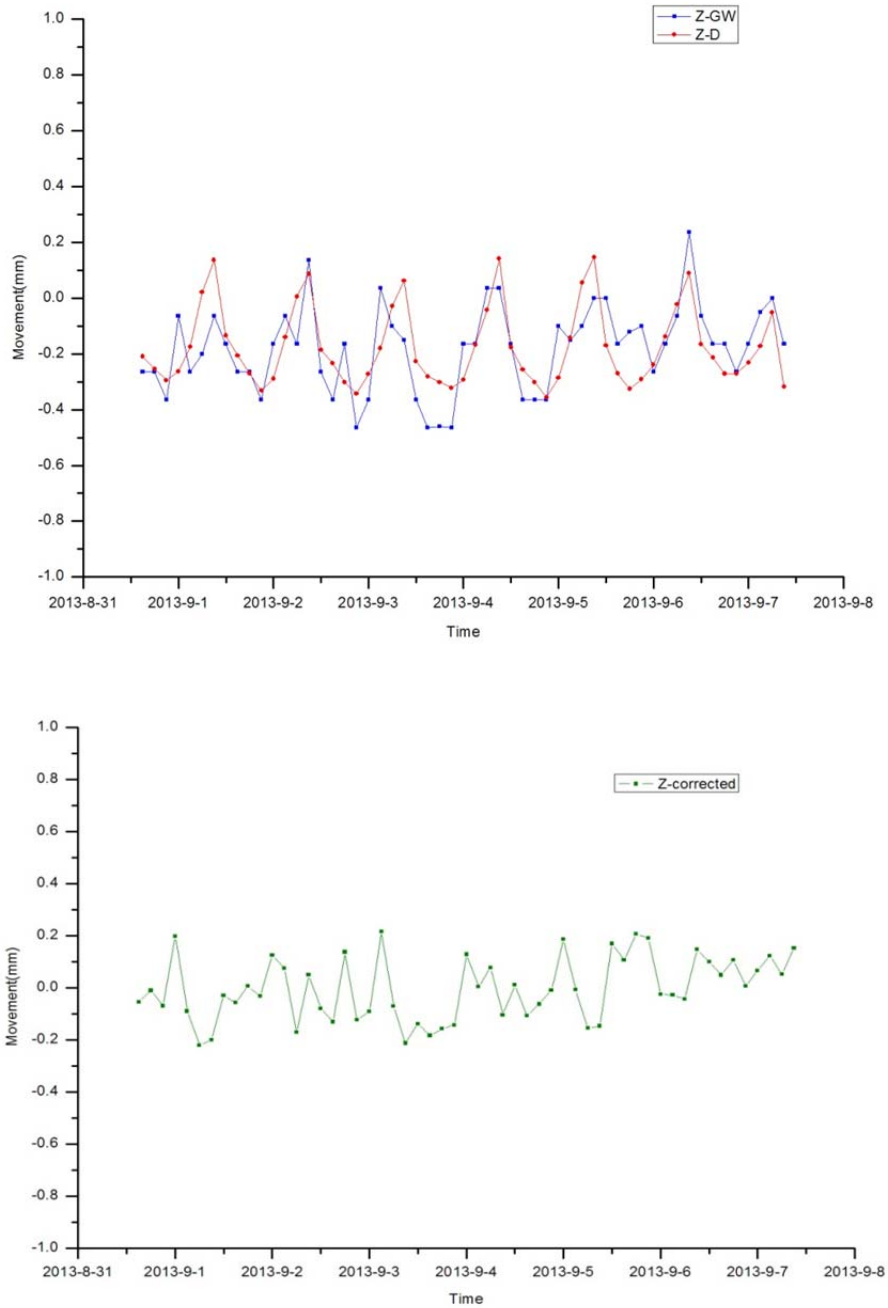


Figure 6.3 K2M, Control Prism CP5. Coordinate Z corrected by subtracting the Simulated value (Approach-D) from the standard practice value (GW) See the first week in Figure 5.65.

The expected values for the “Thermal-Effect-free” movements (evolution of the coordinates) are zero, as no underground (or any type of) public work was under construction in this area at the time. As can be observed from the previous figures, the results are promising but uneven. While the corrected X is quite small and stable, the

corrected Y and Z are bigger and more fluctuating. A residual daily fluctuation can be still identified, which corresponds to the limit in our modelling .

It must be recognized that on other days and with different Control Prisms, the results are not as good, but it has to be kept in mind that we are working with real data. The reasons for these nonzero values are diverse. First of all, there are the “non-modelled” effects, that is, the ϵ term in the Equation 3.2. This can include, for instance, the wind action or changes in humidity. Another cause is that the GW measurements are subject to accidental or random errors (angles and distance) that transmit pseudo-noise to the graphs; moreover, the results delivered by Geoscope Web were computed adjusting a “group” of three RTS, and some constraints in the other parts of the network (A3 or N2 Stations) may force the solution in some epochs. Thirdly, some points can have local constraints or obstacles, such as the tree in front of prism CP1. Fourthly, our modelling is based on very simplistic assumptions; for example, Equation 5.1 that obtains the temperature variation assumes 21°C as the inside temperature everywhere; additionally, this value is applied only to the façades. Finally, there is a general drawback that applies to all of the Campus Nord experimental area: the K2m+Omega building has only 3 levels, so the movements are relatively small, and it is easy to spoil this low ‘signal’ with whatever interference, such as those mentioned before.

However, with the correction carried out in Figure 6.1, 6.2 and 6.3, empirically the conceptual framework has been proved useful in correcting the effect of the temperature change. To fully demonstrate the capability of the model to correct the measurements affected by this effect, we have implemented a new “Approach-B” that is a modification of the Approach-D. We can conceive this new Approach-B as a “Numerical simulation of the target building NET movement after filtering all the thermal effects”. As this is a simulation (synthetic data, no real data), most of the drawbacks listed in the previous paragraph disappear, and the results must match the expected behavior perfectly. In this case, as we look for the “net movement after filtering all the thermal effects”, the expected value is zero.

The Approach-B algorithm is fully explained in section 6.2. It is also centered in the K2M building. We may anticipate here that Approach-B reproduces the expected behavior. Instead of fluctuations of Approach-D (or even the GW real data), the graphs

exhibit a constant value over time. The graphs have a horizontal line (Figures from 6.6 to 6.14); we have been successful in filtering the unwanted fluctuation.

However, it is possible that we have filtered too much. Each day (and each year) the K2M experiences small deformations because the building deforms due to temperature changes. In some cases, some users could be interested in maintaining the real movement of the building in the monitoring graphs. For this purpose, we have created a new “Approach-K”, that is a modification of the previous approaches D and B. We can conceive this new Approach-K as a “Numerical simulation of the REAL movement of the target building (preserving the small movement of the building due to the ΔT)”.

The Approach-K algorithm is fully explained in section 6.3. It is also centered in the K2M building. We may anticipate here that Approach-K reproduces the expected behavior. Instead of the noisy GW data fluctuations, the graphs exhibit a smooth waviness evolution over time (Figure from 6.28 to 6.36); we have been successful in filtering the unwanted Thermal Effect, but the real movement of the building is preserved.

From now on, the chapter describes Approach-B and K in sections 6.2 and 6.3, respectively. For each approach there are four subsections: the first illustrates the main steps of the approach; then running time is given; then the movements of the RTS and the Control Prisms are reported; and lastly, the results of each approach are compared with the GW results.

The chapter ends with an overview that summarizes the strategy to take into account the thermal effects in building monitoring.

6.2 Approach B

In order to explore the influence of the thermal movement of the reference points in the computation of the RTS coordinates, Approach-B incorporates the thermal movements of the reference points and A6-RTS into the computation to calculate the coordinates of the RTS by LSA. However, the K2M has been considered without self-deformation when calculating the raw data (H, V, d).

6.2.1 Main step steps of approach B

In approach B, we add thermal movement of RTS (DX_{RTS} , DY_{RTS} , DZ_{RTS}) to the original coordinates of RTS (X_{RTS} , Y_{RTS} , Z_{RTS}) to get the simulate coordinates data of RTS (X_{SRTS} , Y_{SRTS} , Z_{SRTS}).

$$\begin{aligned}X_{SRTS} &= X_{RTS} + DX_{RTS} \\ Y_{SRTS} &= Y_{RTS} + DY_{RTS} \\ Z_{SRTS} &= Z_{RTS} + DZ_{RTS}\end{aligned}\tag{6.3}$$

In the meantime, we add the thermal movement of reference points (DX_{RP} , DY_{RP} and DZ_{RP}) to the coordinates of reference points (X_{RP} , Y_{RP} , Z_{RP}) to get the simulated coordinates data of reference points (X_{SRP} , Y_{SRP} , Z_{SRP}).

$$\begin{aligned}X_{SRP} &= X_{RP} + DX_{RP} \\ Y_{SRP} &= Y_{RP} + DY_{RP} \\ Z_{SRP} &= Z_{RP} + DZ_{RP}\end{aligned}\tag{6.4}$$

6 Formulation of two approaches to analysis Thermal Effects in standard monitoring

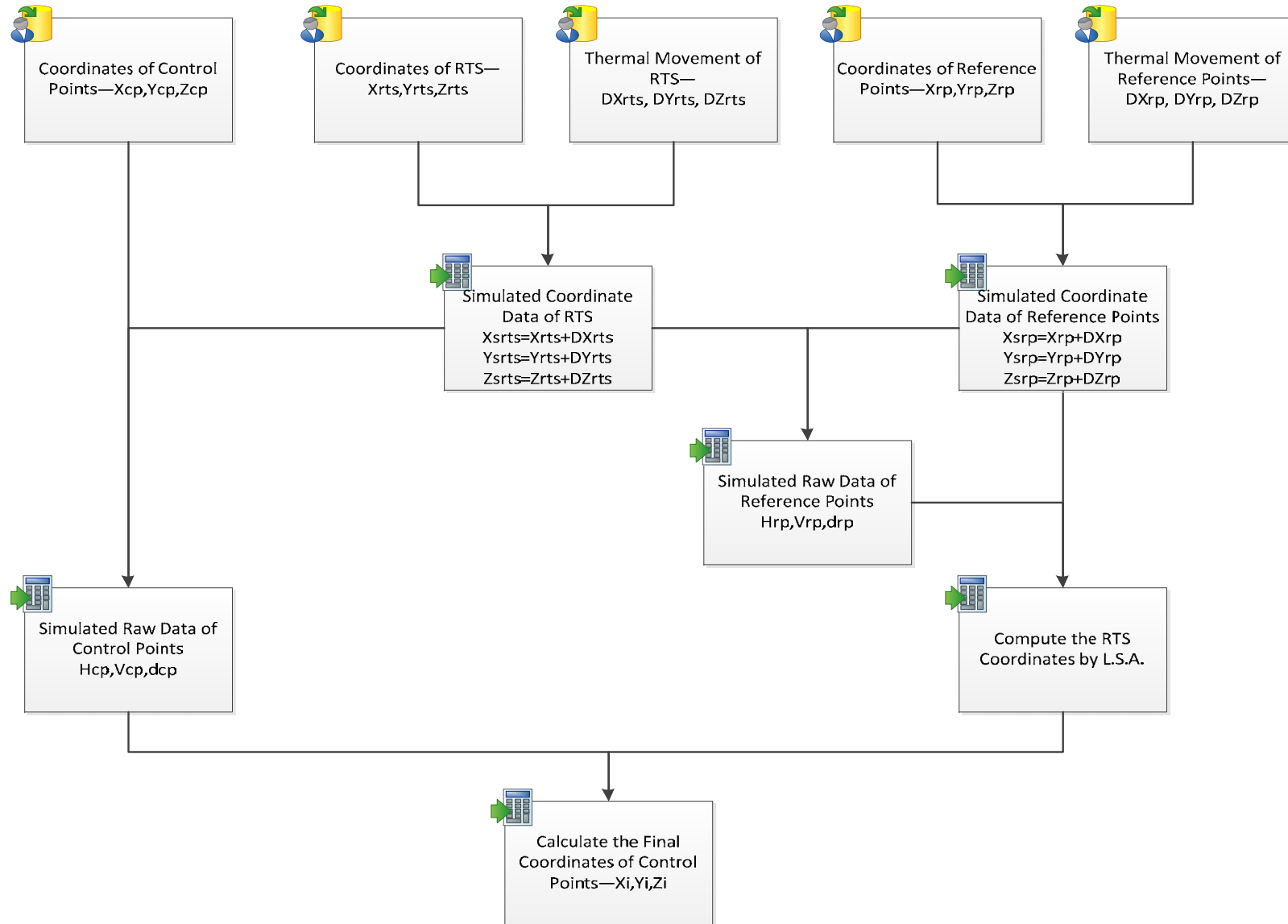


Figure 6.4 Flowchart of Approach B.

After that, the simulated raw data observations from the RTS to the control points (H_{CP} , V_{CP} , L_{CP}) and reference points (H_{RP} , V_{RP} , L_{RP}) can be computed with the coordinates of control points (X_{CP} , Y_{CP} , Z_{CP}) and the simulated coordinates of reference points (X_{SRP} , Y_{SRP} , Z_{SRP}) and RTS (X_{SRTS} , Y_{SRTS} , Z_{SRTS}).

In the program a new coordinates for the RTS will be computed by resection from the reference points with these simulated data. This process is illustrated in the Figure 6.4.

6.2.2 Running time

In the program, there three main time-costing parts which are structure model, calculate the simulated raw data and least square adjustment. For approach-B, the whole time cost is 394 seconds in total for the three parts which the part of structure model costs 388 seconds, this is the biggest time-costing part occupy by about 98 percent in the whole time-costing, other two parts are 3.3 seconds for the part of calculate the simulated raw data and 3.4 seconds for the part of least square adjustment (Table 6.1).

Table 6.1 Approach-B time cost.

Item	Structure Model(s)	Calculate the Simulated Raw Data(s)	Least Square Adjustment(s)	Total(s)
Time	388.07	3.35	3.45	394.88

6.2.3 Approach B's results

After the computation, all of the results have been presented in curve chart from Figure 6.5 to Figure 6.14. These graphs illustrate the movement trend of RTS and control points under the thermal change over the period from 1st September 2013 to 15th October 2013.

Figure 6.5 is a curve chart which describes the displacement trend of RTS in X-direction, Y-direction and Z-direction. It can be seen that there is a considerable change in October where the curves reached a bottom. The movement range in X-direction is between 425905.9323m and 425905.9342m; the movement range in Y-direction is between 4582346.6488m and 4582346.6528m; the movement range in Z-direction is between 111.0261m and 111.0292m. The RTS results in Figure 6.5 have a similar movement trend with the RTS results of standard model (D). In the process of

computing the RTS coordinates by LSA in approach-B, there is on different point with the standard model, which the thermal movements of reference points are not only used for simulating the raw data of reference points, but also used in the LSA computation to get the coordinates of RTS.

The results of the nine control points are plotted from Figure 6.6 to Figure 6.14. From these figures, it can be seen that all of the curves in the figures remained constant over the study period between 1st September 2013 and 15th October 2013. It is proved that if the data have zero or low noise, the result is stable and according to the expectations (zero movement). What is more, the figures lead us to the conclusion that the control points will not receive the thermal change influence from RTS and reference points if we introduce the thermal movement of reference points into the computation.

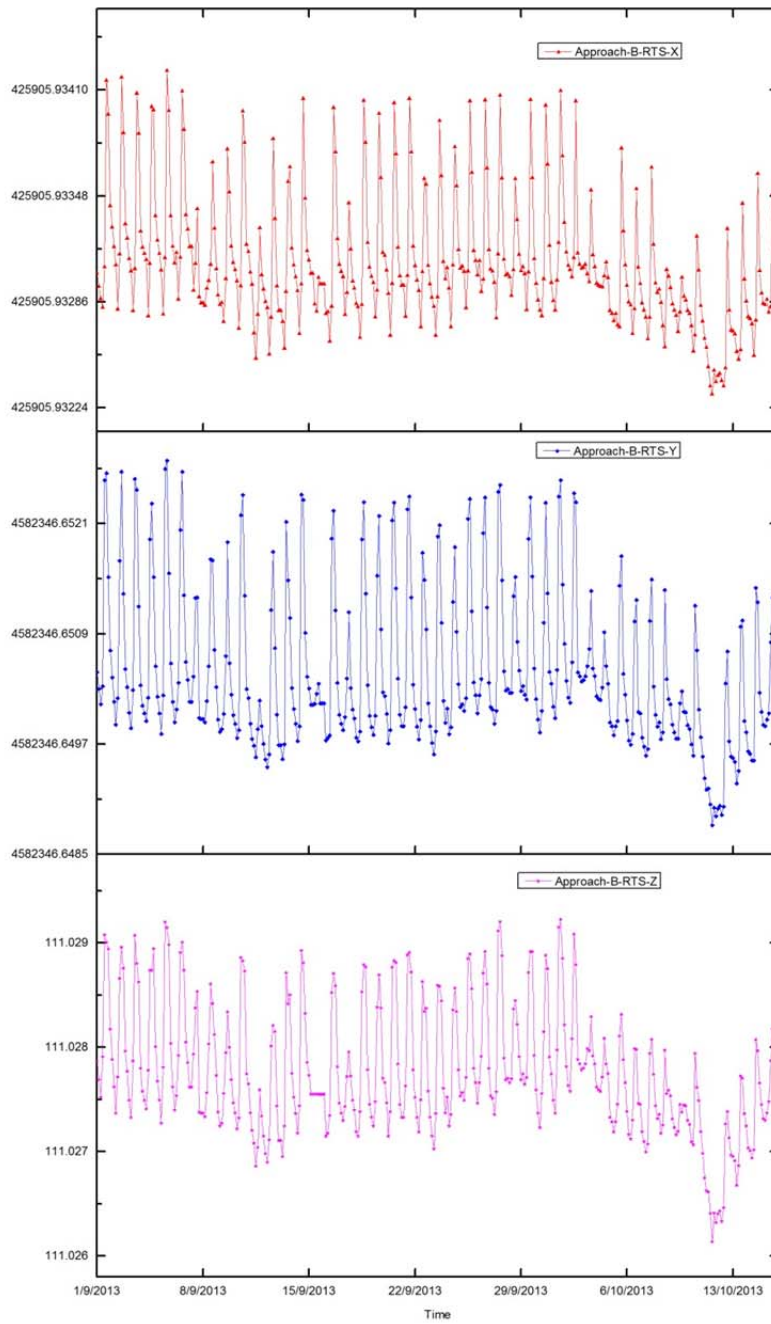


Figure 6.5 RTS movement (m) of approach-B.

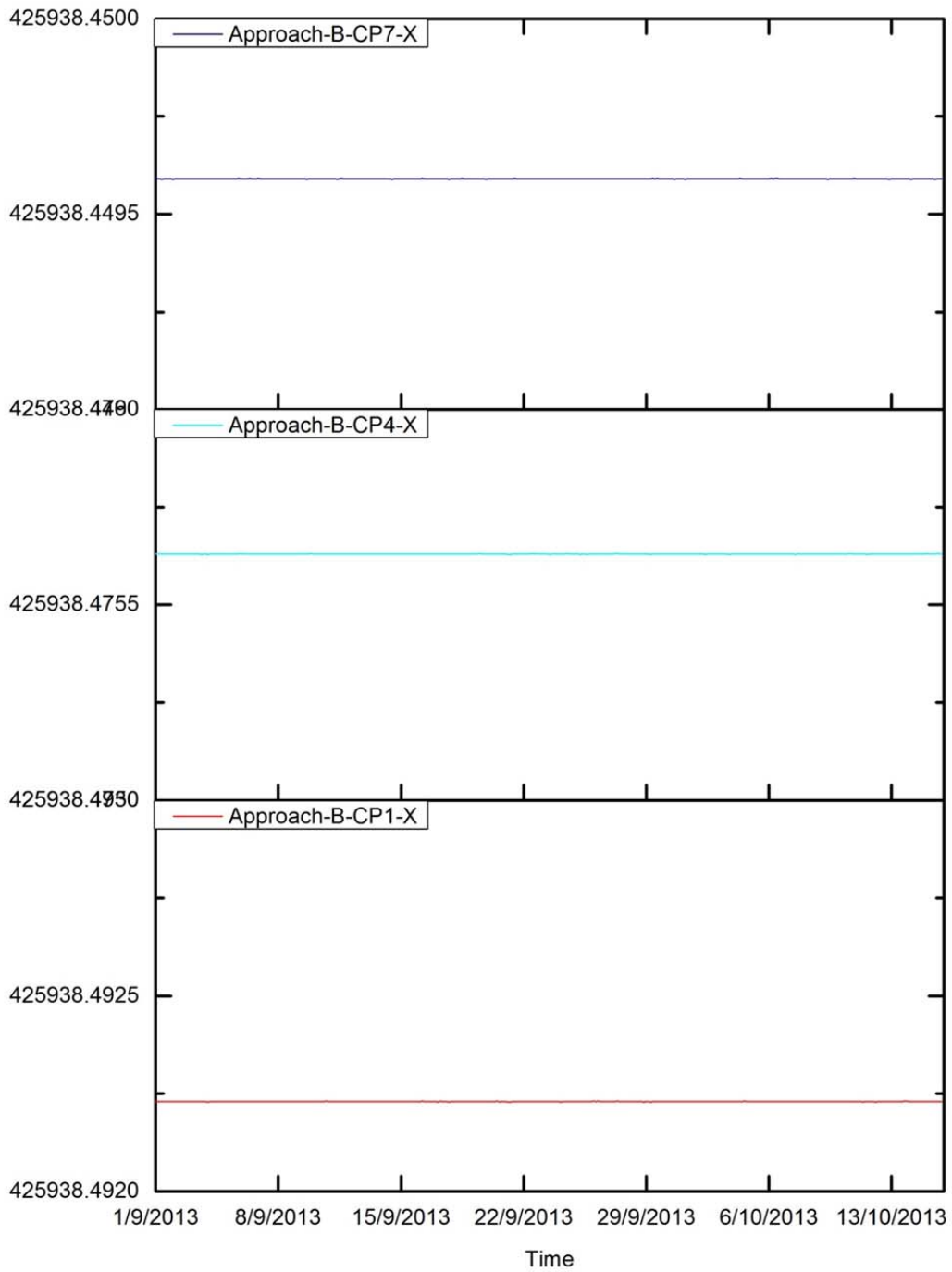


Figure 6.6 CP1, CP4 and CP7 movement (m) in X-direction.

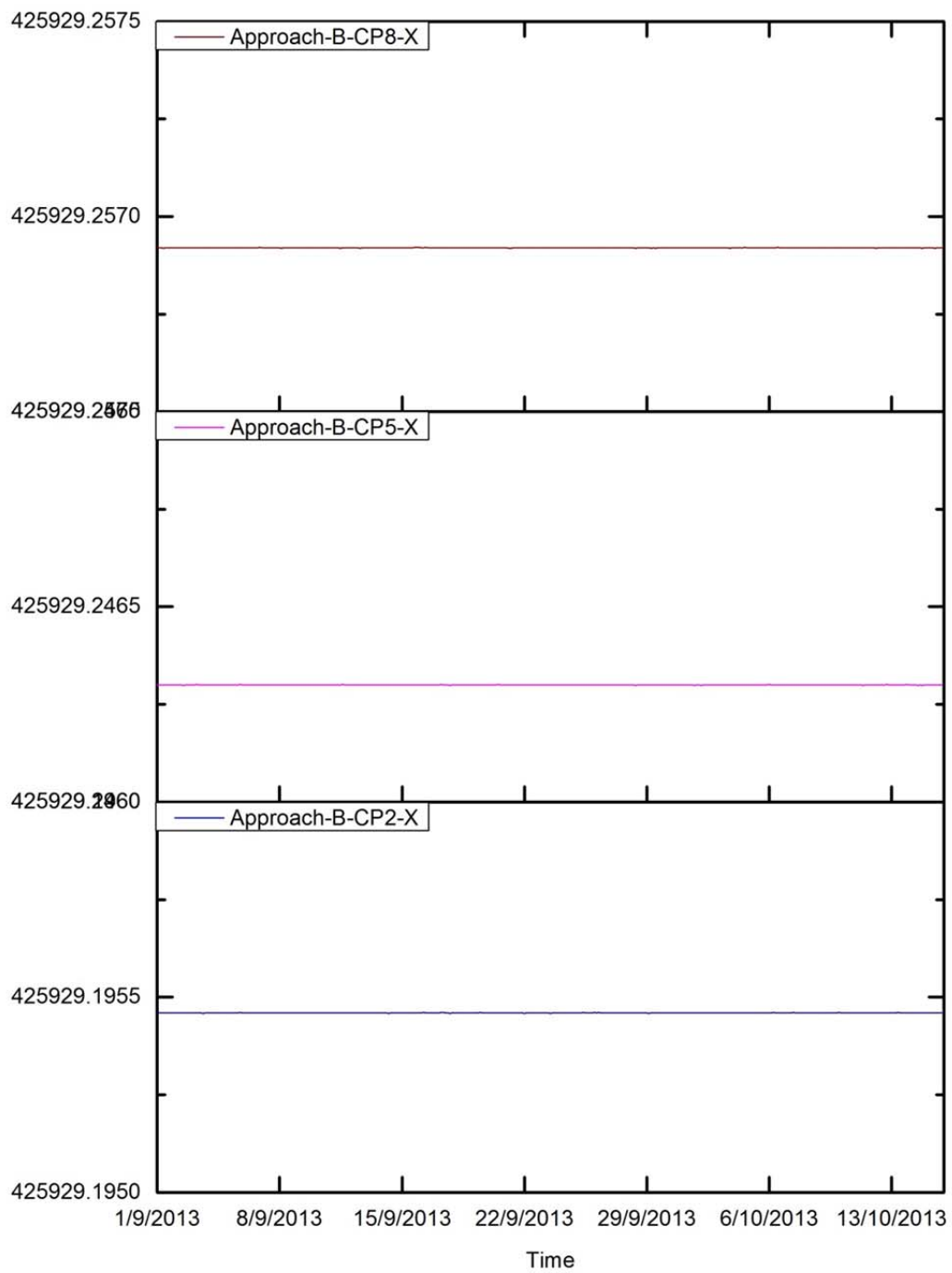


Figure 6.7 CP2, CP5 and CP8 movement (m) in X-direction.

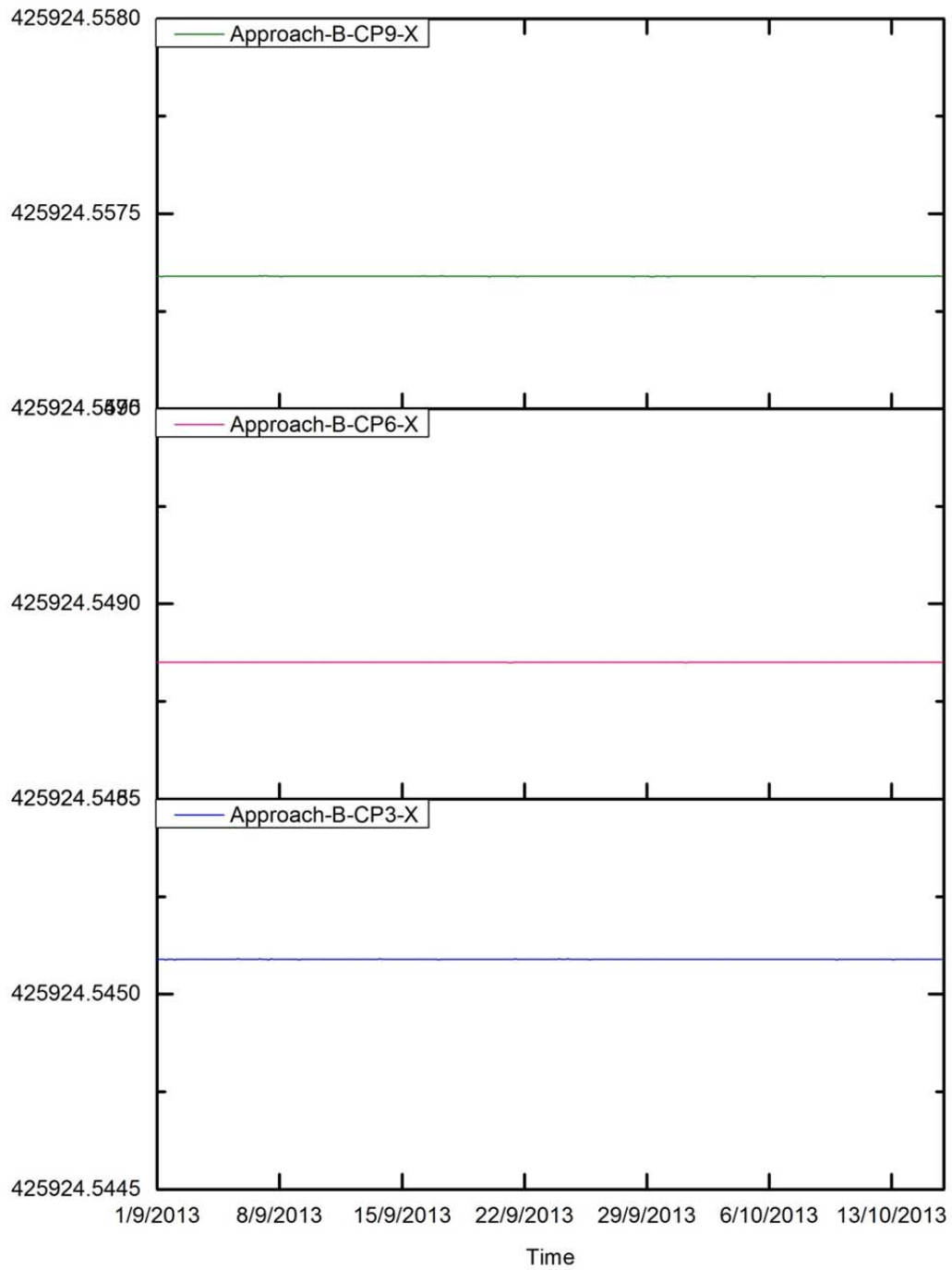


Figure 6.8 CP3, CP6 and CP9 movement (m) in X-direction.

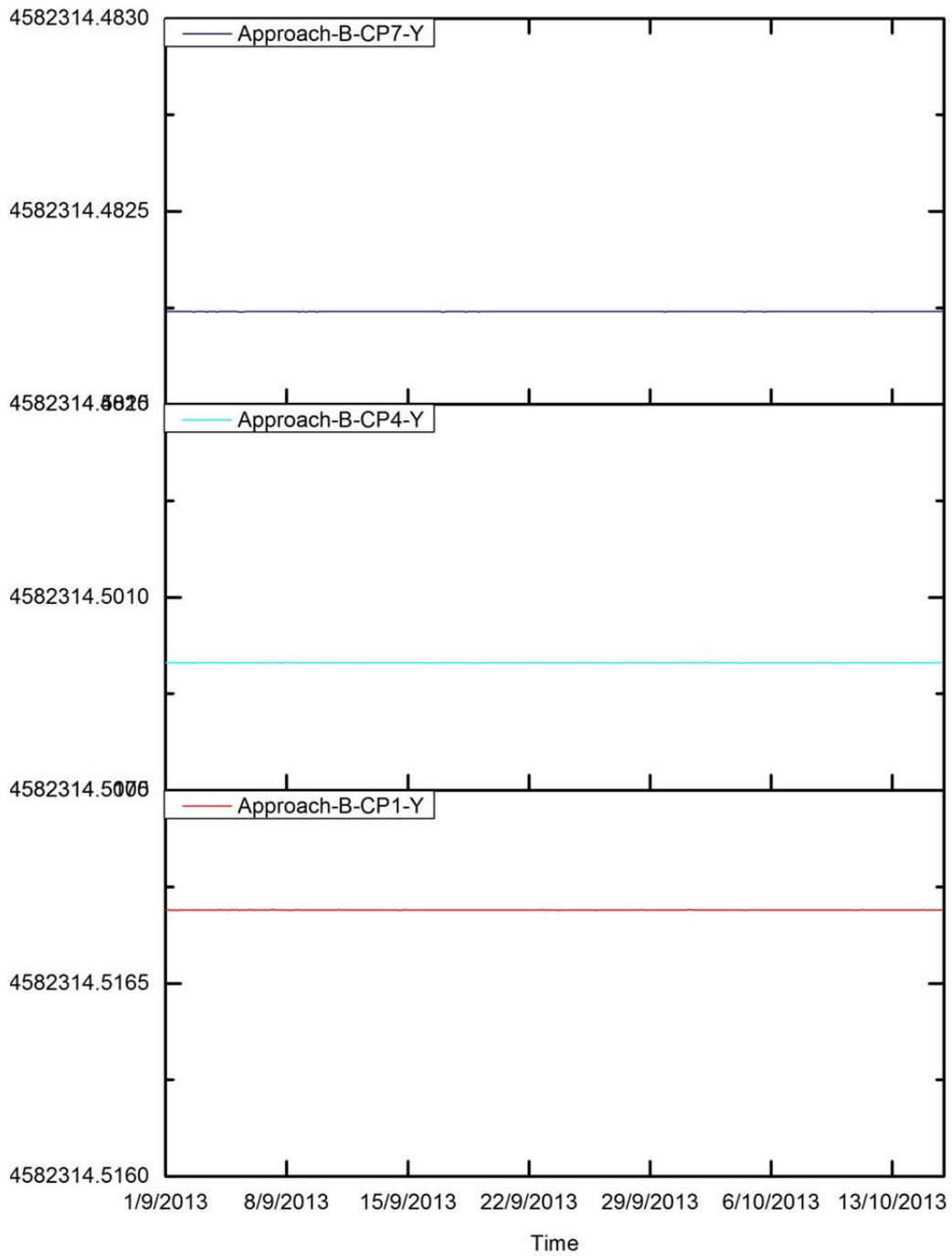


Figure 6.9 CP1, CP4 and CP7 movement (m) in Y-direction.

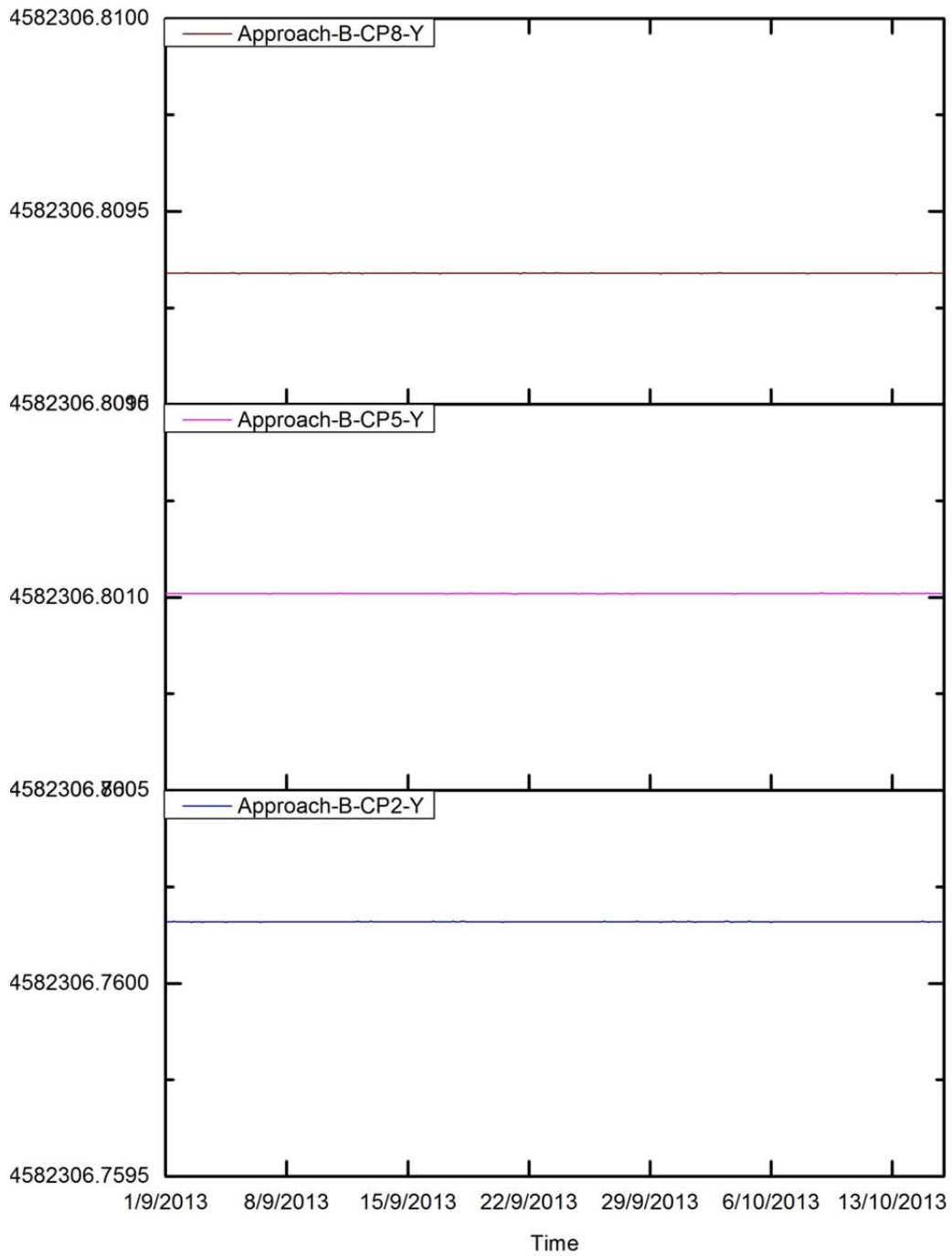


Figure 6.10 CP2, CP5 and CP8 movement (m) in Y-direction.

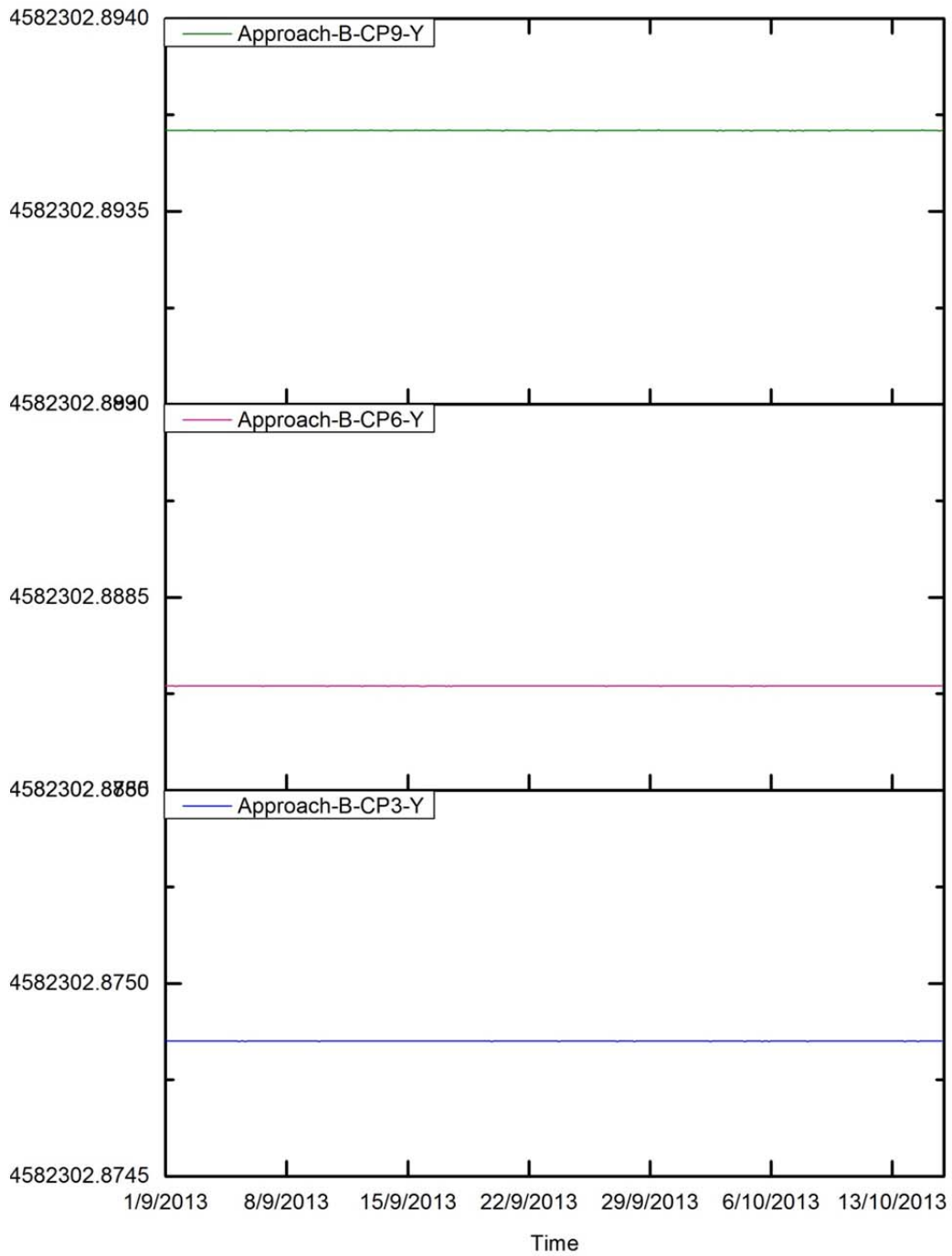


Figure 6.11 CP3, CP6 and CP9 movement (m) in Y-direction.

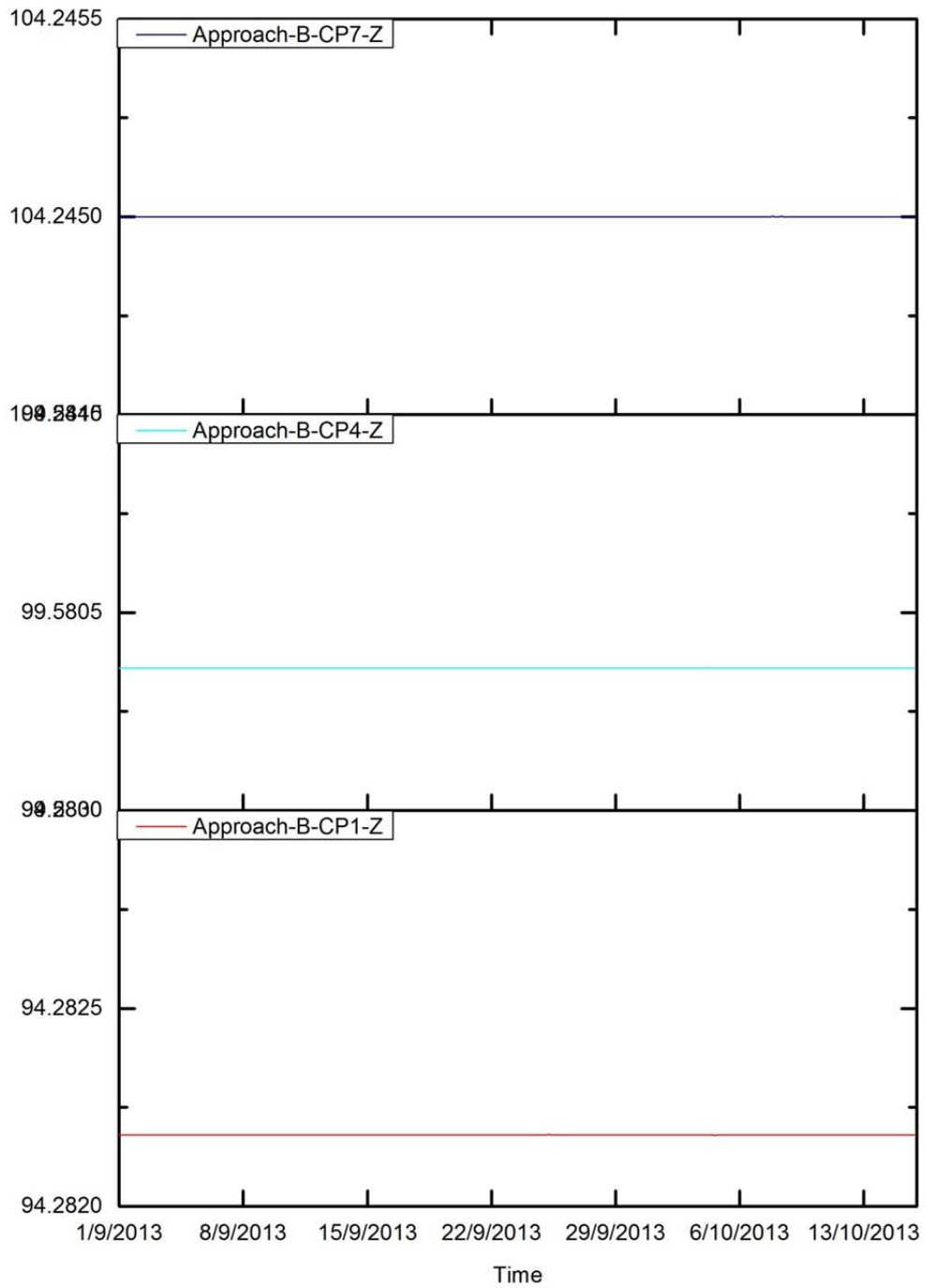


Figure 6.12 CP1, CP4 and CP7 movement (m) in Z-direction.

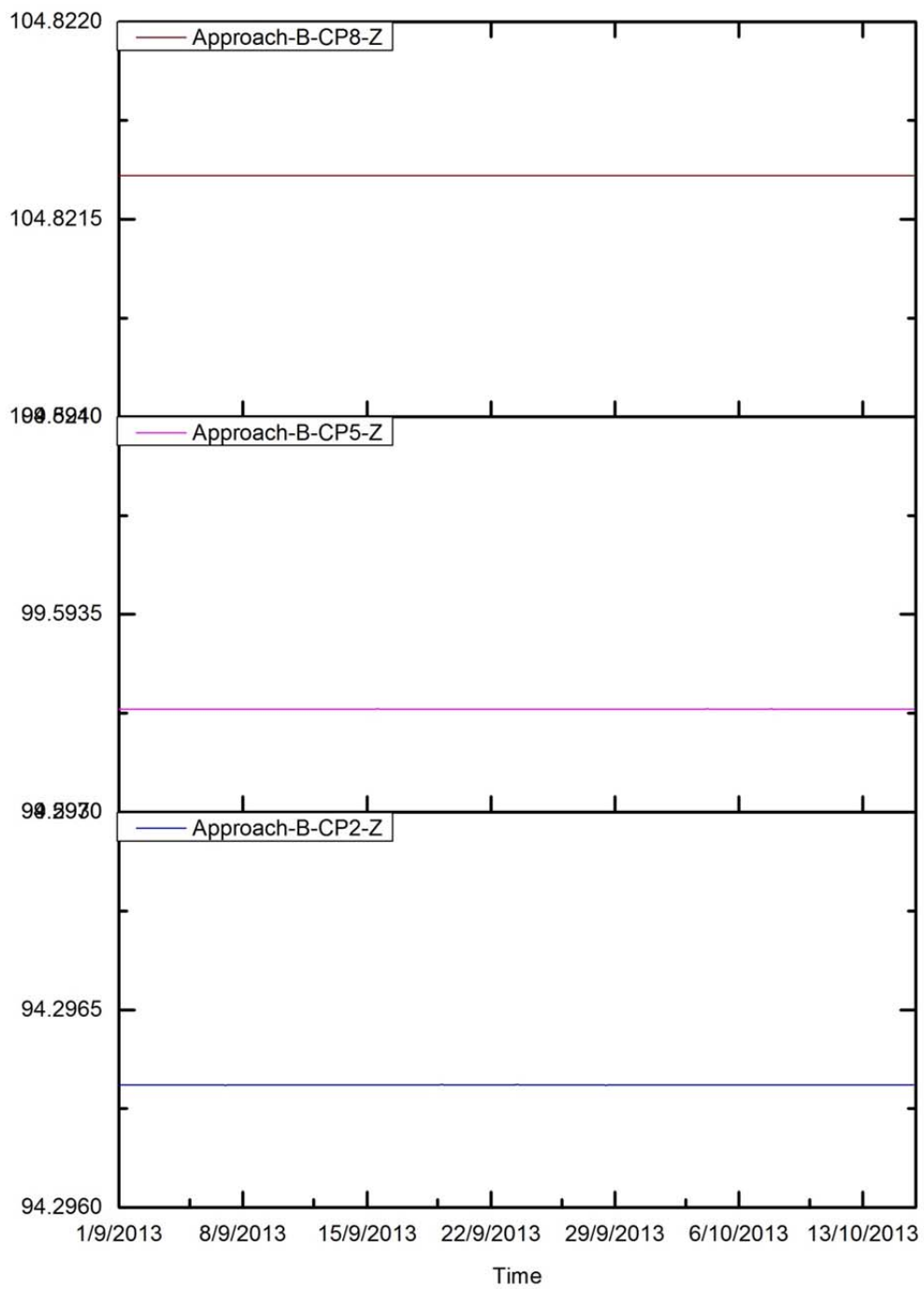


Figure 6.13 CP2, CP5 and CP8 movement (m) in Z-direction.

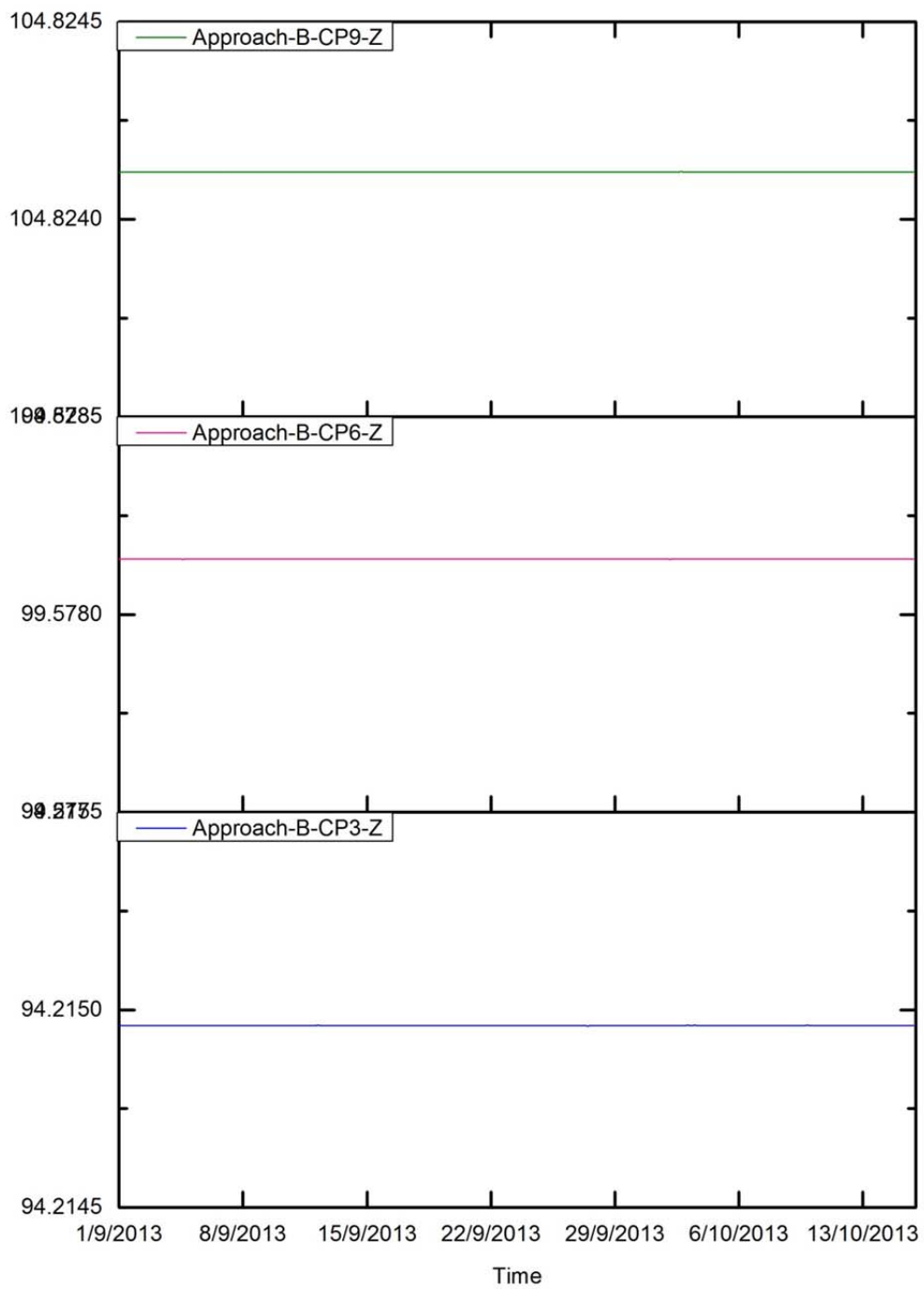


Figure 6.14 CP3, CP6 and CP9 movement (m) in Z-direction.

6.2.4 Compare approach B's results with GW

After the calculation of approach-B, in this section the comparisons between the results of approach-B and the results of GW have been done.

(a) RTS

Figure 6.15 shows the comparisons of RTS displacement tracks in X-Y plane between approach-B and GW over the period from 1st September 2013 to 15th October 2013. In this figure, it can be observed how much different of RTS displacement range between approach-B and GW. The displacement range in X-direction of GW is bigger than approach-B, which the displacement range in X-direction of GW is 2.57mm and the displacement range in X-direction of approach-B is 1.89mm. However, in Y-direction the displacement range of approach-B is bigger than GW, which the displacement range in Y-direction of approach-B is 3.96mm and the displacement range in Y-direction of GW is 2.67mm.

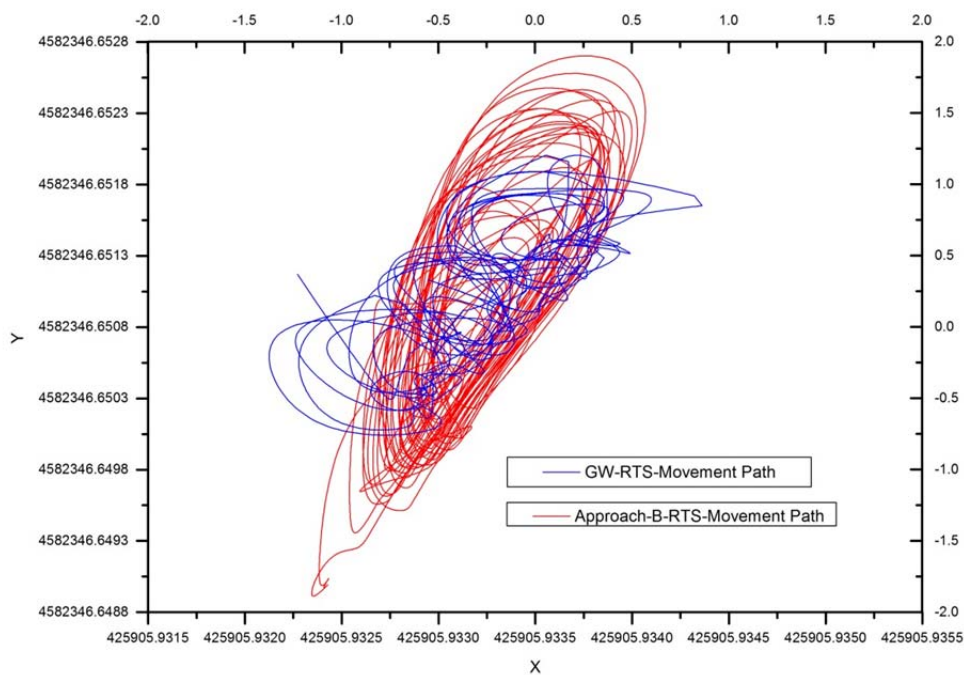


Figure 6.15 RTS movement path of approach-B and GW.

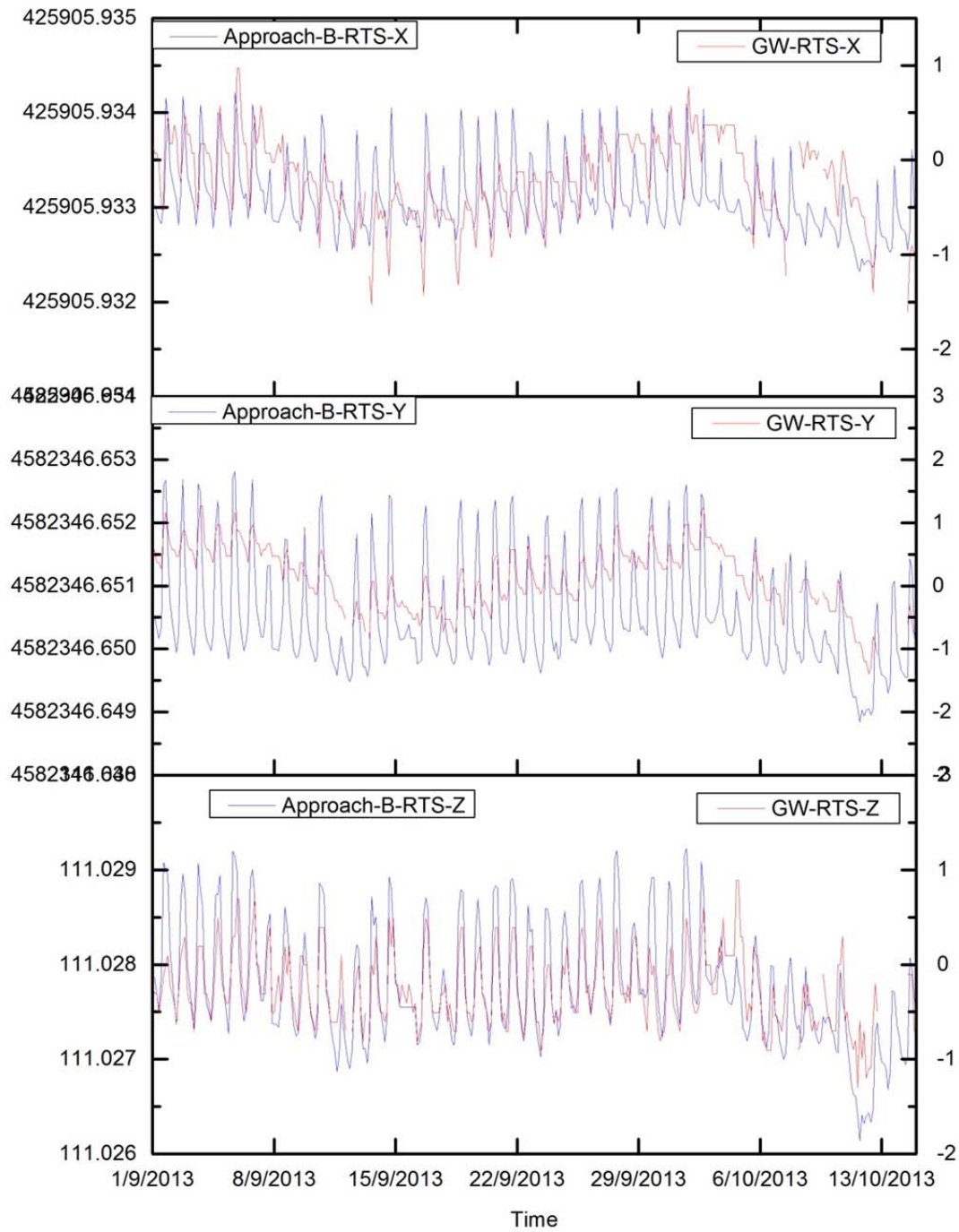


Figure 6.16 Comparison of the approach-B's RTS movement results and the GW RTS movement results. Vertical Axes Unit: left is m, right is mm.

Figure 6.13 shows the comparisons of the movement trend of approach-B and GW in X-direction, Y-direction and Z-direction respectively during the whole study time period. From the figure, it can be seen that the movement trend of approach-B and GW are similar and the daily movement of approach-B is clearer than GW. In X-direction, the fluctuation of approach-B is 1.89mm (between 425905.93232m and 425905.93421m), the fluctuation of GW is 2.573mm (between -1.6mm and 0.973mm); in Y-direction, the fluctuation of approach-B is 3.96mm (between 4582346.64885m and 4582346.65281m), the fluctuation of GW is 2.669mm (between -1.4mm and 1.269mm); in Z-direction, the fluctuation of approach-B is 3.09mm (between 111.02614m and 111.02923m), the fluctuation of GW is 2.19mm (between -1.3mm and 0.89mm).

In the above, the different between approach-B and GW have been illustrated. From the RTS results of comparisons between approach-B and GW as showed in Figure 12 and 13, it can be seen that the thermal variation is a very important influence factor for the RTS. The reasons for the different between approach-B and GW mainly come from other aspect's influence. One reason for that is the influence of environment except the thermal change. For example, wind, it can influence the building's movement in some degree. What is more, the thermal distribution on the building that introduced in the computation is different with the real condition of the building. This is another reason leads to the different results between approach-B and GW. Another possible reason is the computation method for the coordinates, especially for those redundant observation data, different method lead to different results.

(b) Control points

Figures from 14 to 22 show the comparisons of control points' movement in X-direction, Y-direction and Z-direction between the results of approach-B and the results of GW. Due to the fact that the thermal movements of reference points have been introduced into the computation and the control points have been fixed to simulate the raw observation data between RTS and control points, as expected, the results of approach-B always remain still during the study time period. However, as for the results of GW, the control points move up and down daily with the change of temperature. In X-direction, the fluctuation of GW is 3.1mm between -1.5mm and 1.6mm; in Y-direction, the fluctuation of GW is 5.0mm between -3.6mm and 1.4mm; in Z-direction, the fluctuation

of GW is 2.53mm between -3.6mm and 1.4mm (except CP-1, because there are some outliers due to the presence of a tree in the line of sight).

These comparisons of control points between approach-B and GW show the influence of thermal movements of reference points on the results of control points.

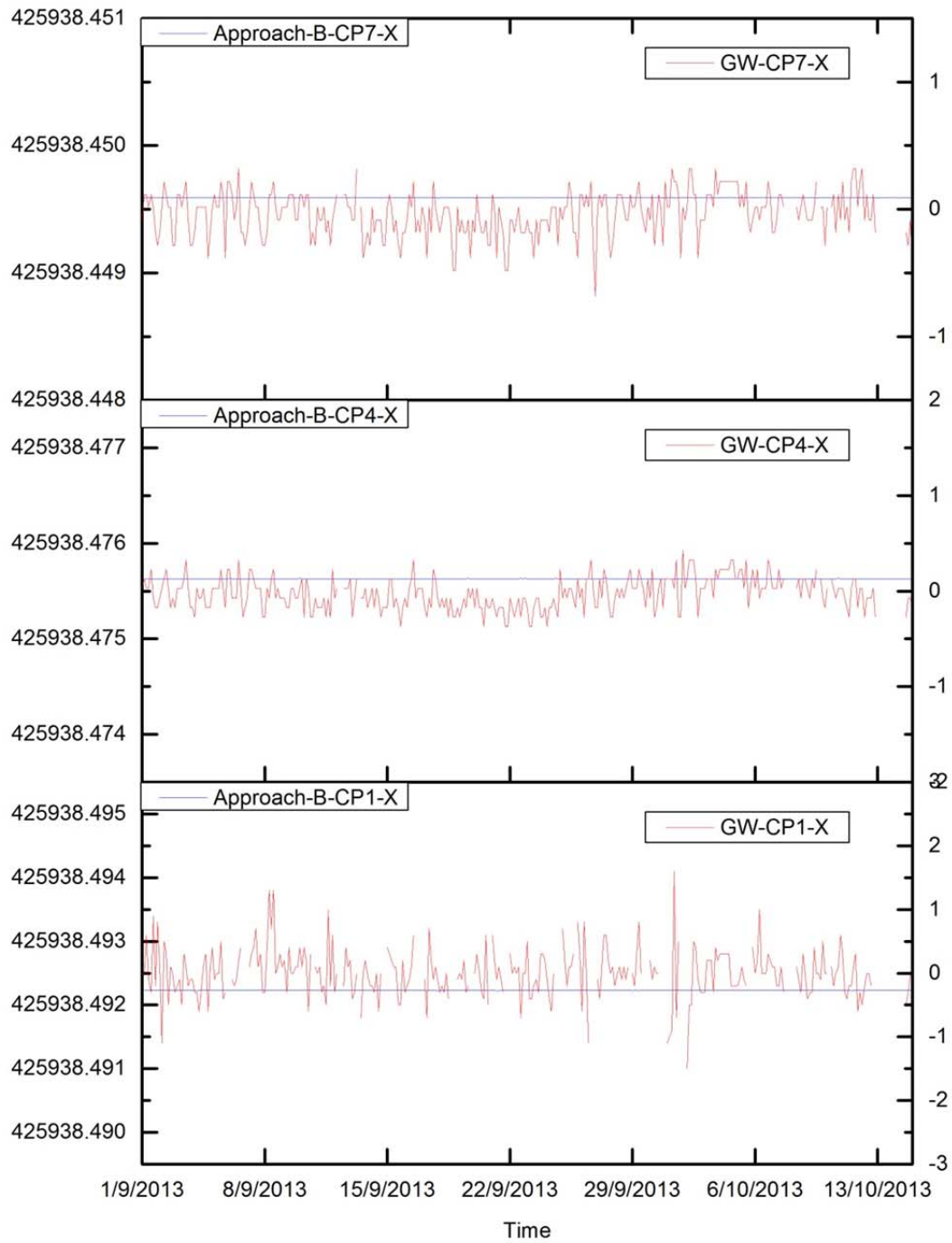


Figure 6.17 Comparison of approach-B and GW for CP1, CP4 and CP7 movement in X-direction. Vertical Axes Unit: left is m, right is mm.

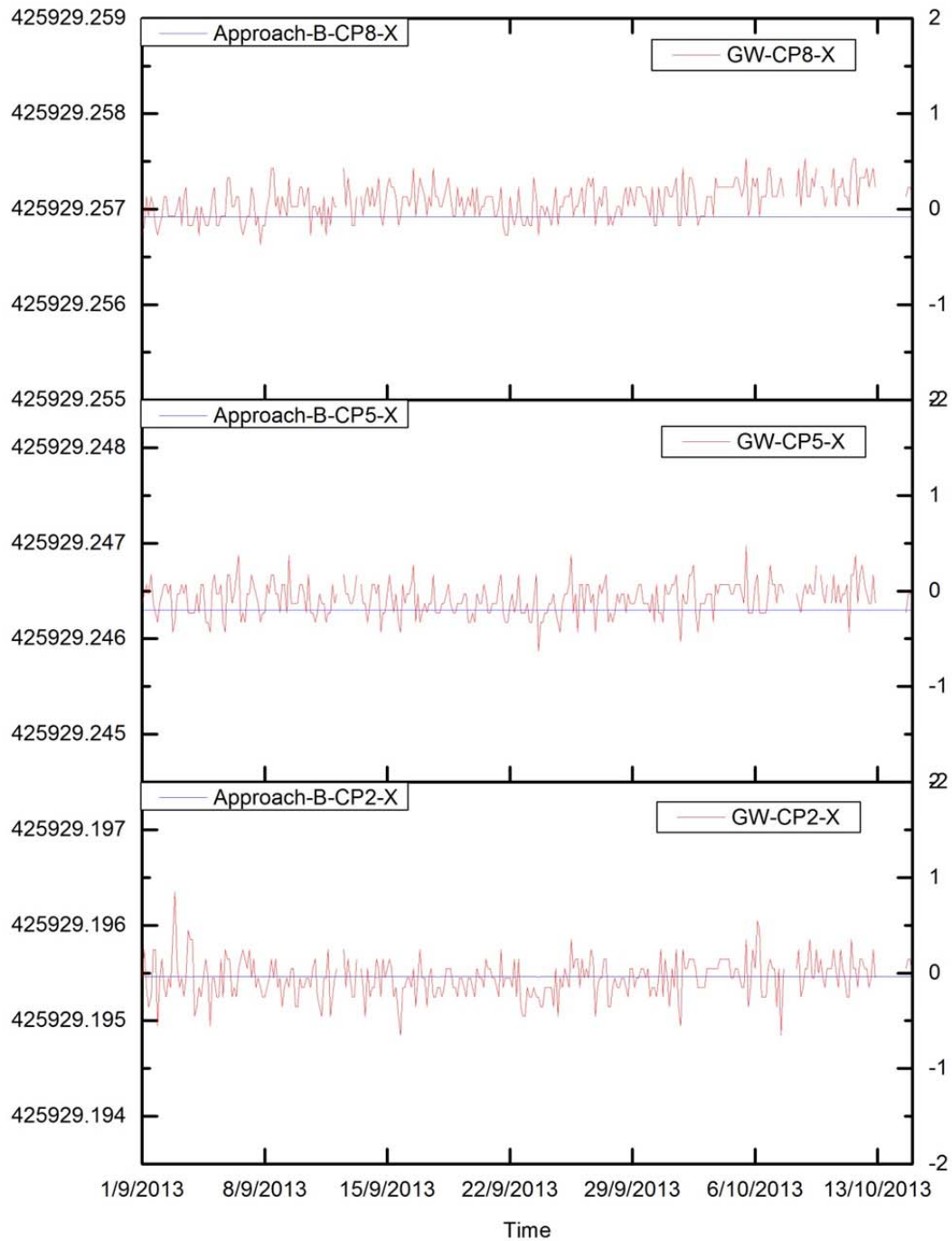


Figure 6.18 Comparison of approach-B and GW for CP2, CP5 and CP8 movement in X-direction. Vertical Axes Unit: left is m, right is mm.

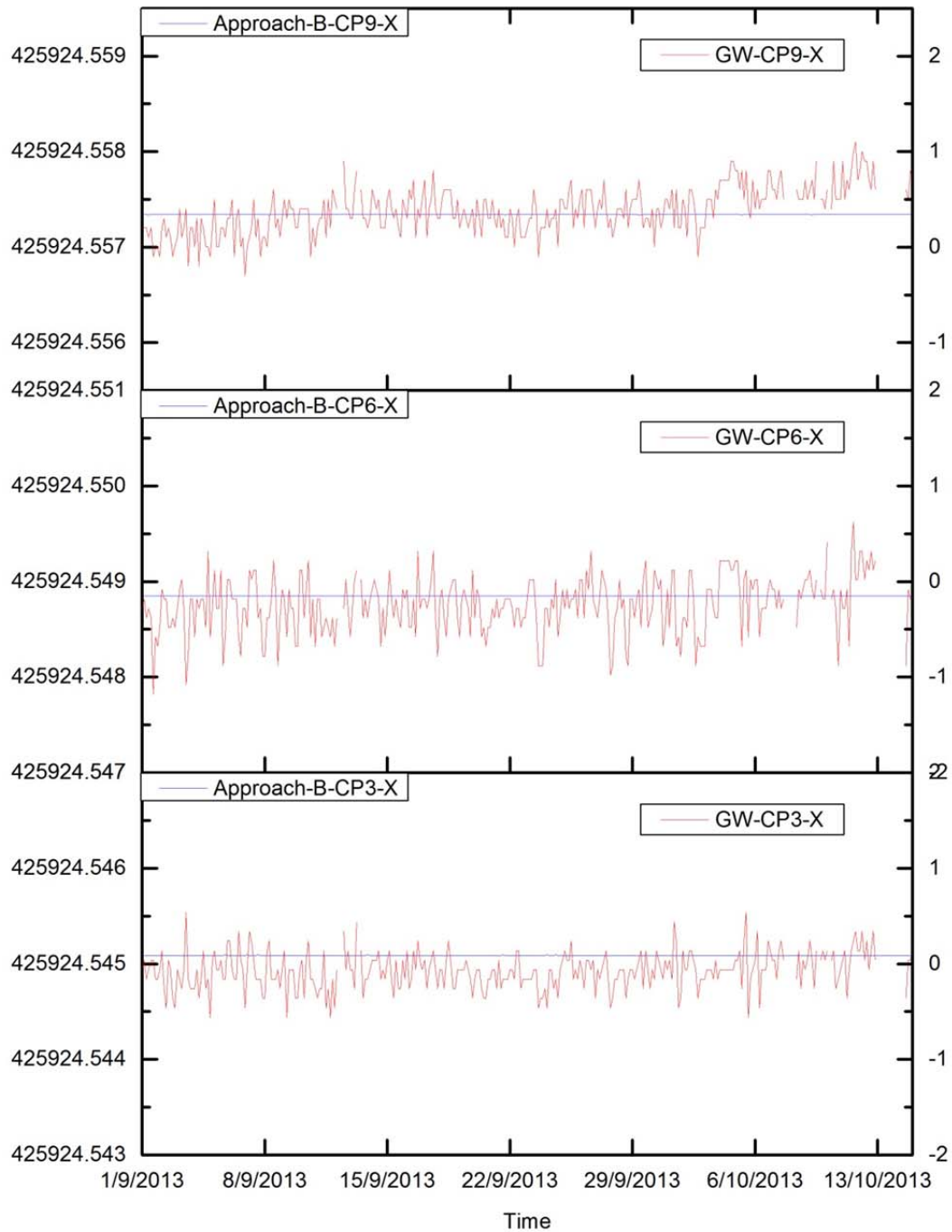


Figure 6.19 Comparison of approach-B and GW for CP3, CP6 and CP9 movement in X-direction. Vertical Axes Unit: left is m, right is mm.

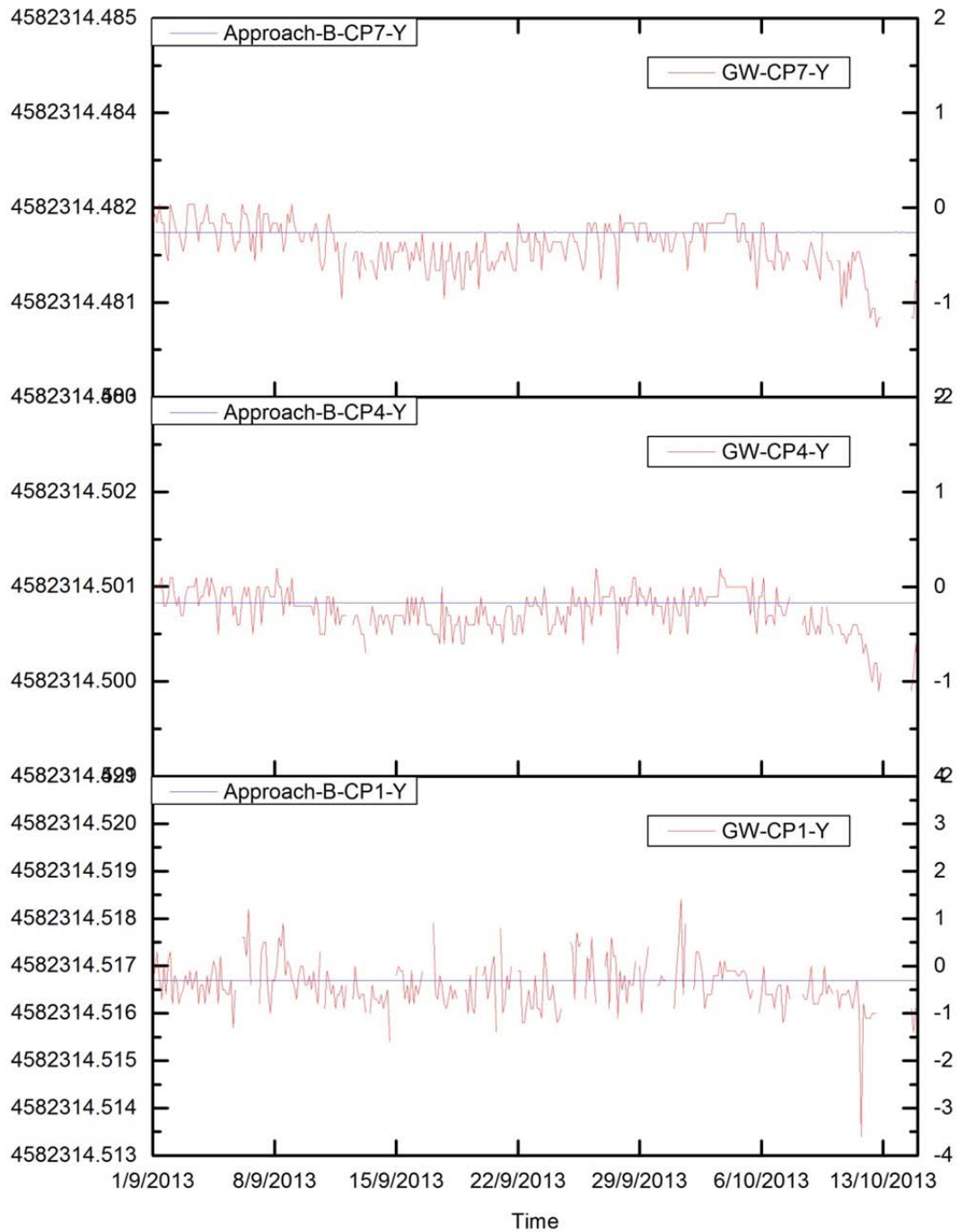


Figure 6.20 Comparison of approach-B and GW for CP1, CP4 and CP7 movement in Y-direction. Vertical Axes Unit: left is m, right is mm.

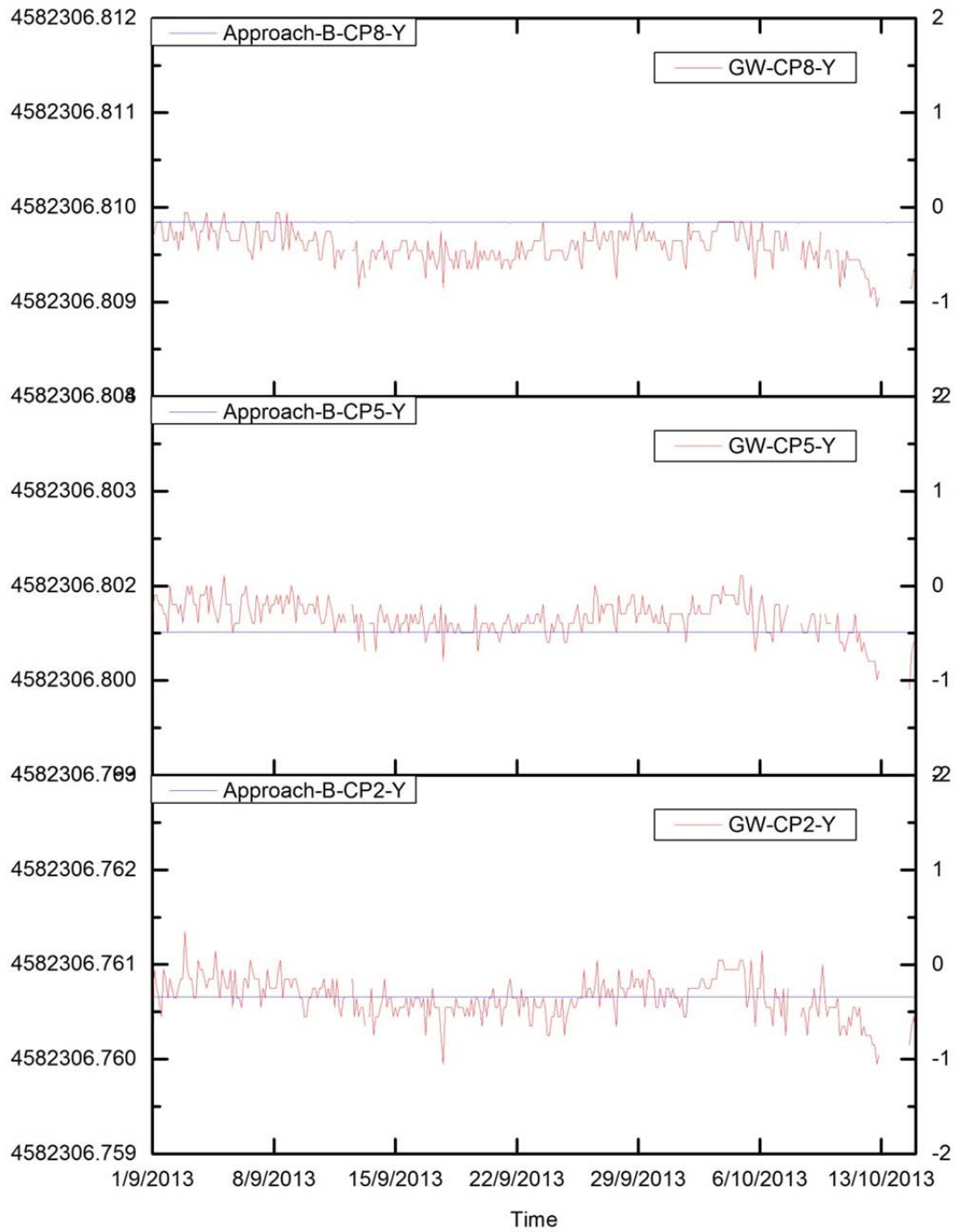


Figure 6.21 Comparison of approach-B and GW for CP2, CP5 and CP8 movement in Y-direction. Vertical Axes Unit: left is m, right is mm.

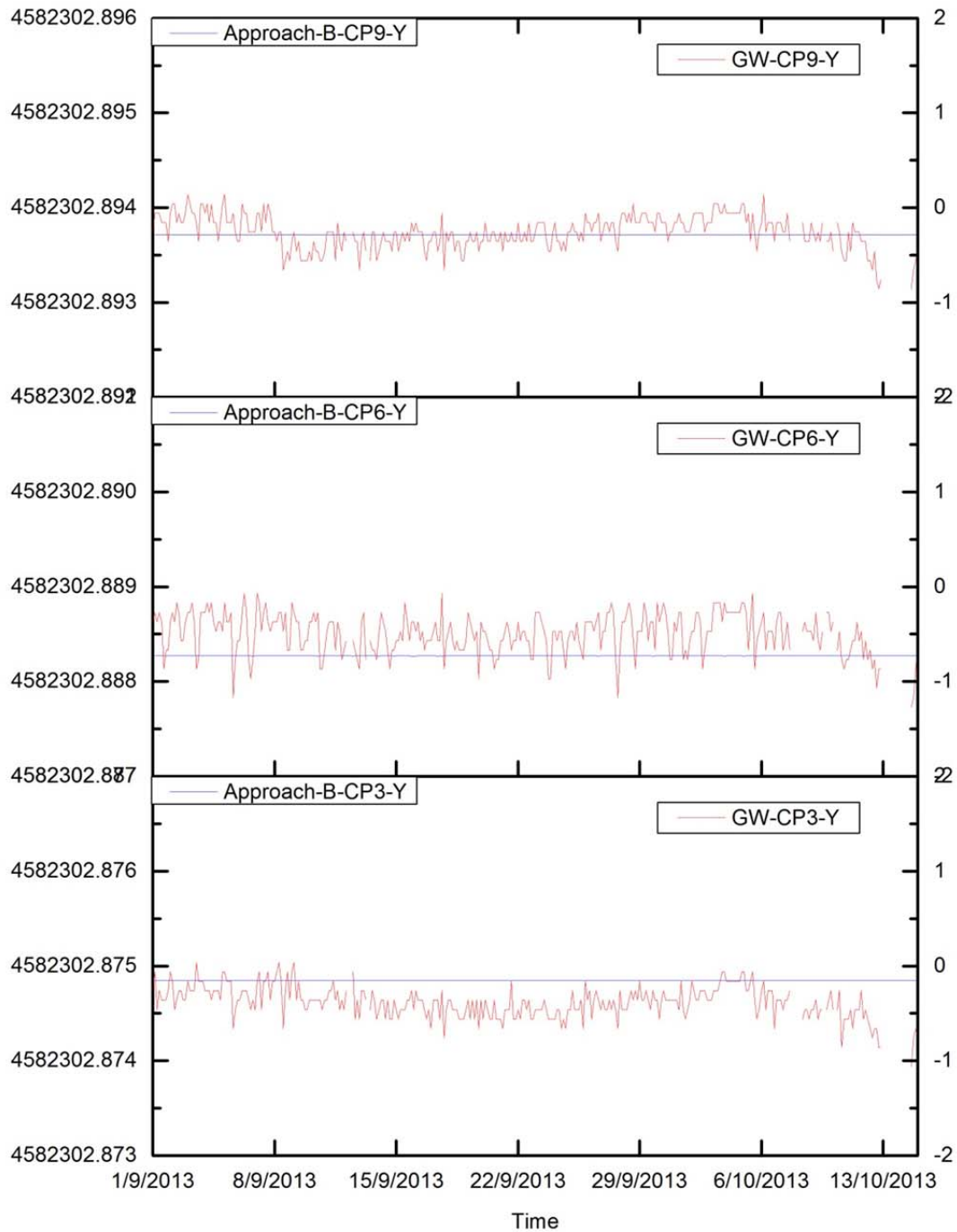


Figure 6.22 Comparison of approach-B and GW for CP3, CP6 and CP9 movement in Y-direction. Vertical Axes Unit: left is m, right is mm.

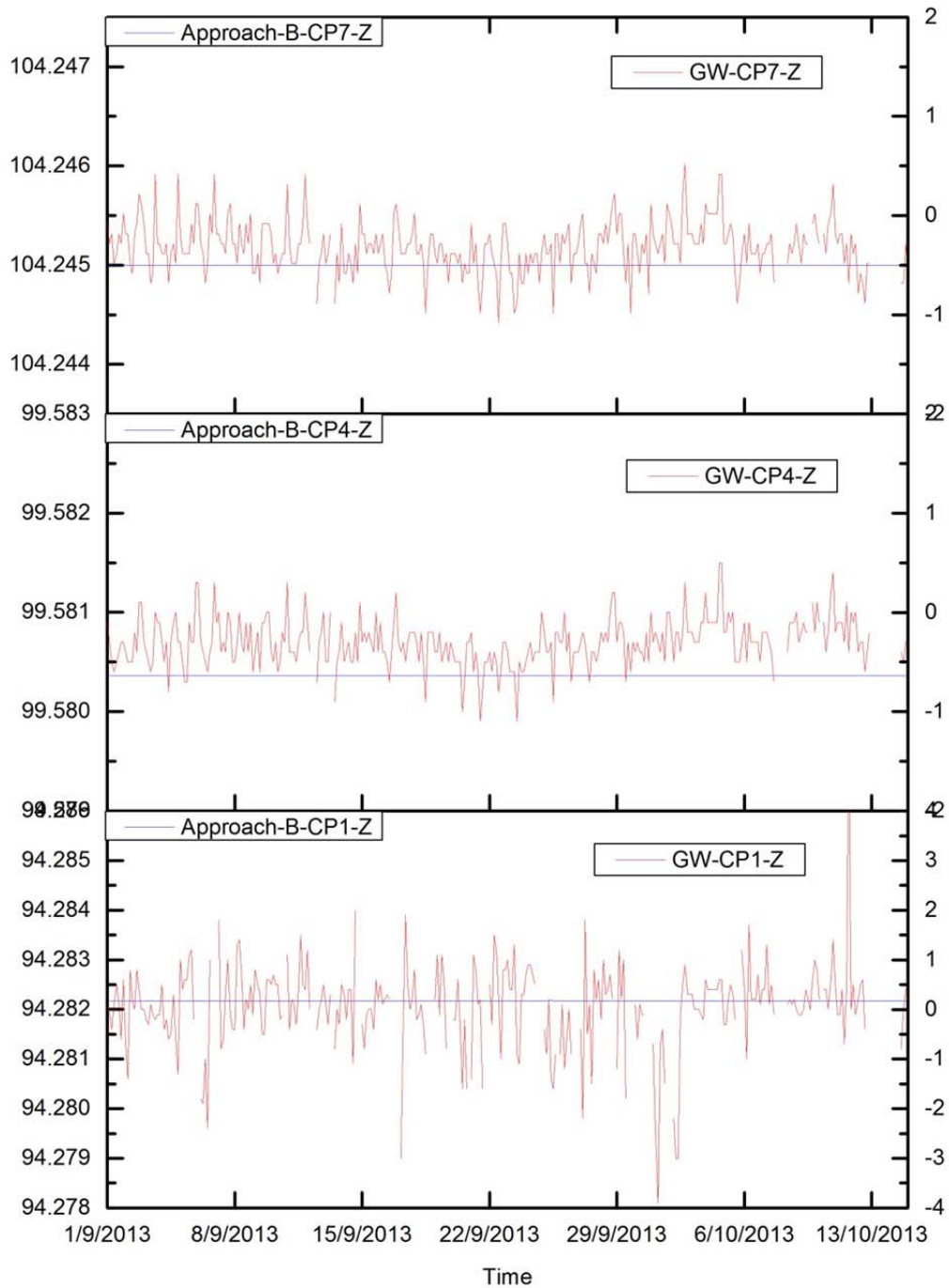


Figure 6.23 Comparison of approach-B and GW for CP1, CP4 and CP7 movement in Z-direction. Vertical Axes Unit: left is m, right is mm.

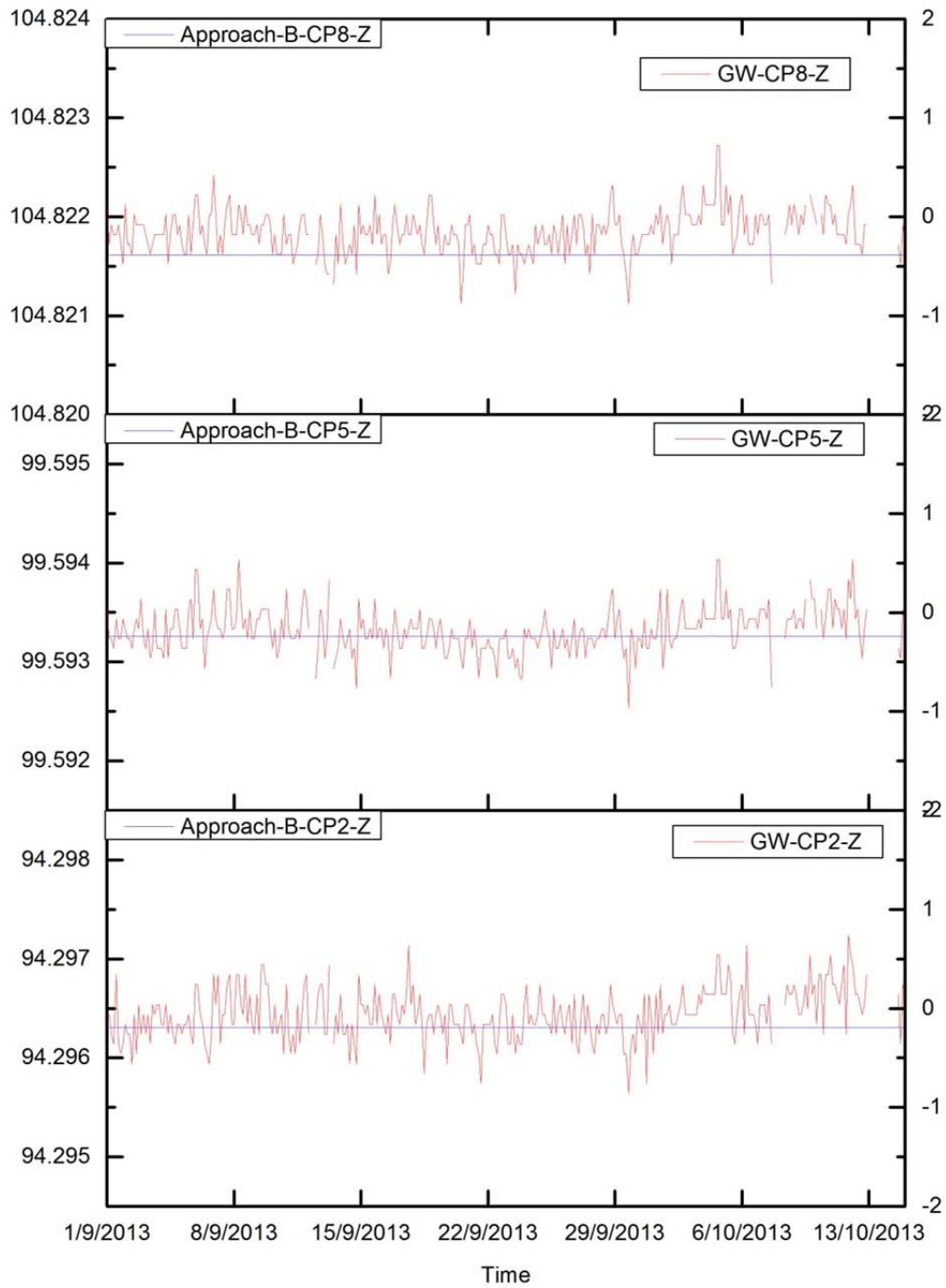


Figure 6.24 Comparison of approach-B and GW for CP2, CP5 and CP8 movement in Z-direction. Vertical Axes Unit: left is m, right is mm.

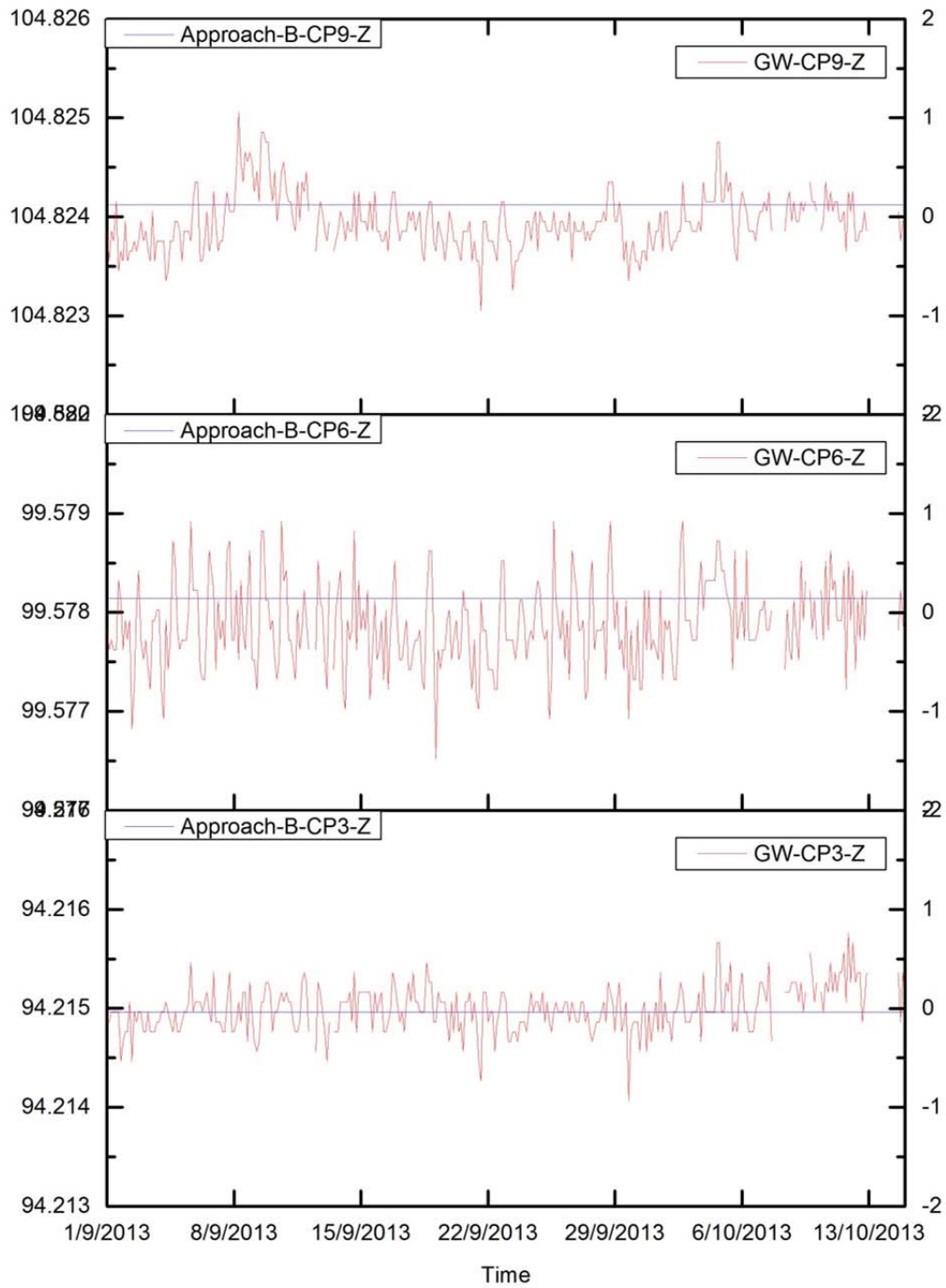


Figure 6.25 Comparison of approach-B and GW for CP3, CP6 and CP9 movement in Z-direction. Vertical Axes Unit: left is m, right is mm.

6.3 Approach K

In order to explore more the thermal influence on the structure deformation monitoring, approach-K was designed based on the approach-B. In approach-K, the thermal movement of control points had been introduced into the computation, which is the different point compared with approach-B.

6.3.1 Main steps of approach K

In approach B we used the settled coordinates of control points X_{CP} , Y_{CP} , Z_{CP} . Here, in Approach-K, the thermal movements of control points DX_{CP} , DY_{CP} , DZ_{CP} had been introduced to simulate the coordinates of control points

$$\begin{aligned} X_{SCP} &= X_{CP} + DX_{CP} \\ Y_{SCP} &= Y_{CP} + DY_{CP} \\ Z_{SCP} &= Z_{CP} + DZ_{CP} \end{aligned} \tag{6.5}$$

The simulated coordinates for RTS and RP are obtained in the same way than with the approach-B. After that, the raw data of control points (H_{CP} , V_{CP} , L_{CP}) have been simulated based on the simulated coordinates of control points (X_{SCP} , Y_{SCP} , Z_{SCP}) and on the simulated coordinates of RTS (X_{SRTS} , Y_{SRTS} , Z_{SRTS}). As well as, the simulated raw data of reference points (H_{RP} , V_{RP} , L_{RP}) also can be simulated by simulated coordinate's data of RTS (X_{SRTS} , Y_{SRTS} , Z_{SRTS}) and simulated coordinates of reference points (X_{SRP} , Y_{SRP} , Z_{SRP}).

Then, the approximate coordinates of RTS can be obtained by LSA based on the simulated coordinates of reference points (X_{SRP} , Y_{SRP} , Z_{SRP}) and (H_{RP} , V_{RP} , L_{RP})

The final coordinates of control points can be calculated use the simulated raw data of control points and RTS. All of that information is illustrated in the Flowchart of Approach K in the Figure 6.26.

6 Formulation of two approaches to analysis Thermal Effects in standard monitoring

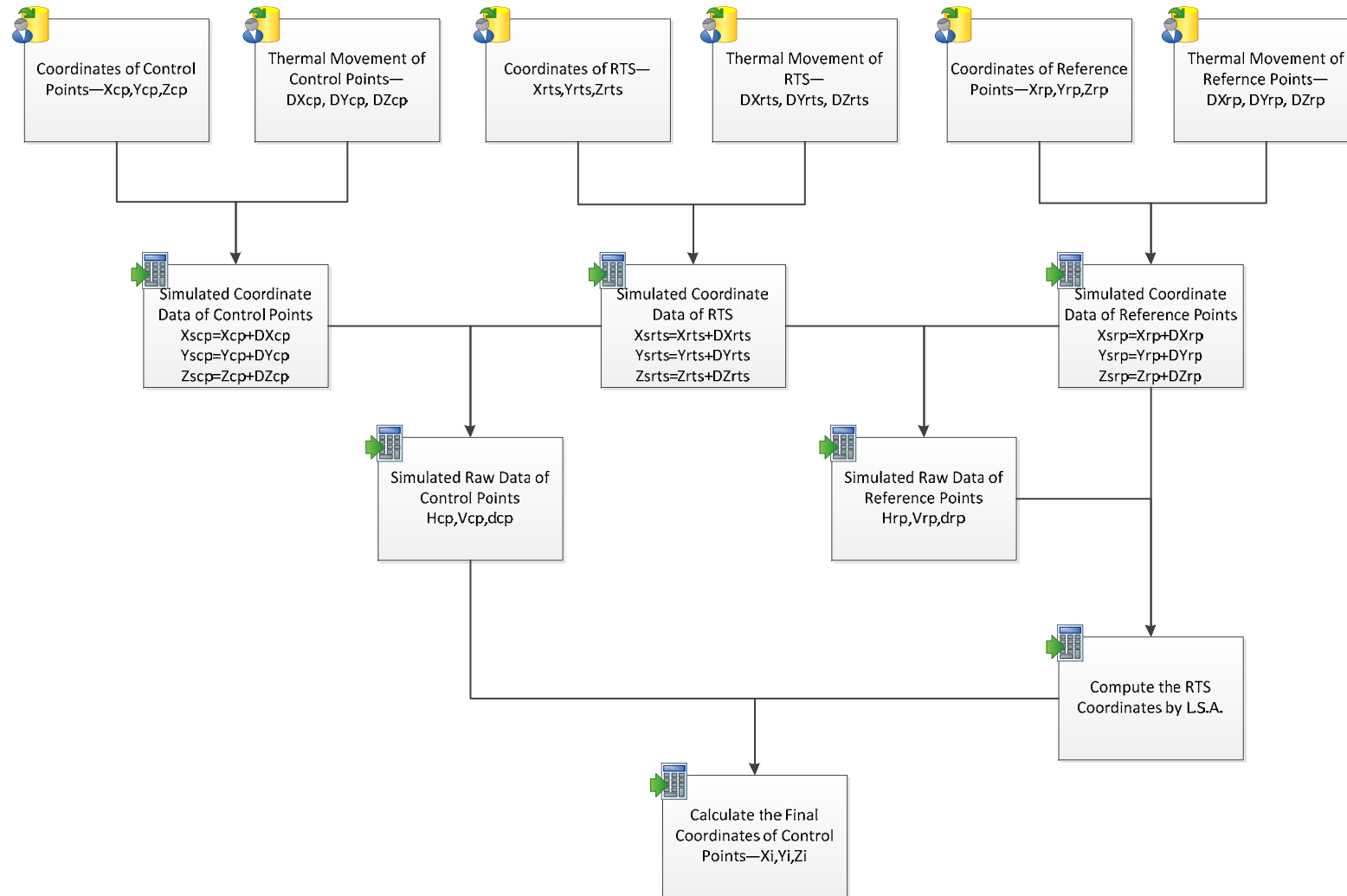


Figure 6.26 Flowchart of approach-K.

6.3.2 Running time

For approach-K, the running times can be appreciated in the Table 6.2.

Table 6.2 Approach-K time cost.

Item	Structure Model(s)	Calculate the Simulated Raw Data(s)	Least Square Adjustment(s)	Total(s)
Time	388.07	4.36	3.69	396.13

6.3.3 Approach K's results

After the computation, the results have been drawn in Figures from 6.27 to 6.36. Figure 6.27 shows the result of RTS in X-direction, Y-direction and Z-direction, it can be seen that the movement trend in the three directions is similar to the result of approach-D as shown in Figures from 5.39 to 5.41 in Chapter 5. The displacement range of X is 1.6mm (from 425905.9324m to 425905.934m), the displacement range of Y is 2.9mm (from 4582346.6492m to 4582346.6521m), and the displacement range of Z is 1.9mm (from 111.0267m to 111.0286m).

The figures from 6.28 to 6.36 illustrate the movement of control points under approach-K over the period from 1st September 2013 to 15th October 2013. The movement results of control points in X-direction under approach-K have been drawn in Figure 25, 26 and 27. From the three figures that presented in curve chart, it is can be seen that the displacement ranges of CP1, CP4, CP7, CP2 and CP5 fluctuates within 1mm and the curves change in periodical variation. The displacement rang of the rest of the control points are bigger than the ranges of CP1, CP4, CP7, CP2 and CP5, the movement range of CP8 and CP3 up to about 1.5mm, the movement range of CP6 and CP9 are approximate 2mm and 2.5mm respectively.

Figure 6.31, 6.32 and 6.33 are curve graphs which describes the trend of the movement of control points in Y-direction under approach-K. The movement range of the nine curve graphs are different, which the displacement range of CP2, CP5 and CP9 are less than 0.5mm, the displacement range of CP8, CP3 and CP6 are no more than 1mm, the displacement range of CP1, CP4 and CP7 are about 2.5mm, 2mm, 3mm respectively.

Figure 6.34, 6.35 and 6.36 display the movement results of the nine control points in Z-direction under approach-K. From the figures, it can be seen that the displacement range

of CP7, CP8 and CP9 are very big which up to 3.5mm, the displacement range of CP4 and CP5 are 3mm, the displacement range of CP1 and CP3 are 1.5mm, the displacement range of CP6 and CP2 are 2.5mm and 2mm. From these results, it can be concluded that the movement of control points in Z-direction increase from the control points located on the ground floor to the control points at top floor.

With the fact that the thermal movements of RTS and reference points have been considered in approach-K, it can be concluded that the results of control points are the real movement and without the thermal influence from reference points and RTS.

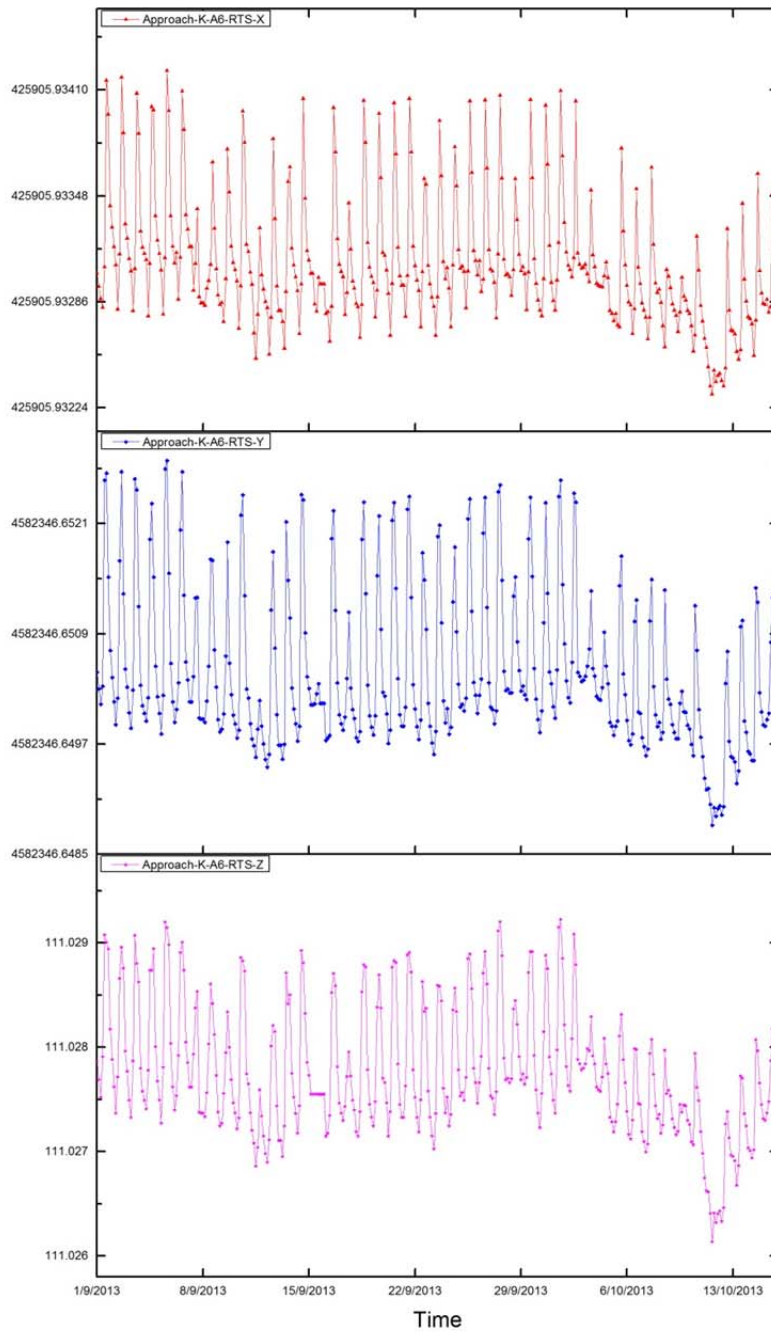


Figure 6.27 RTS movement (m) of approach-K.

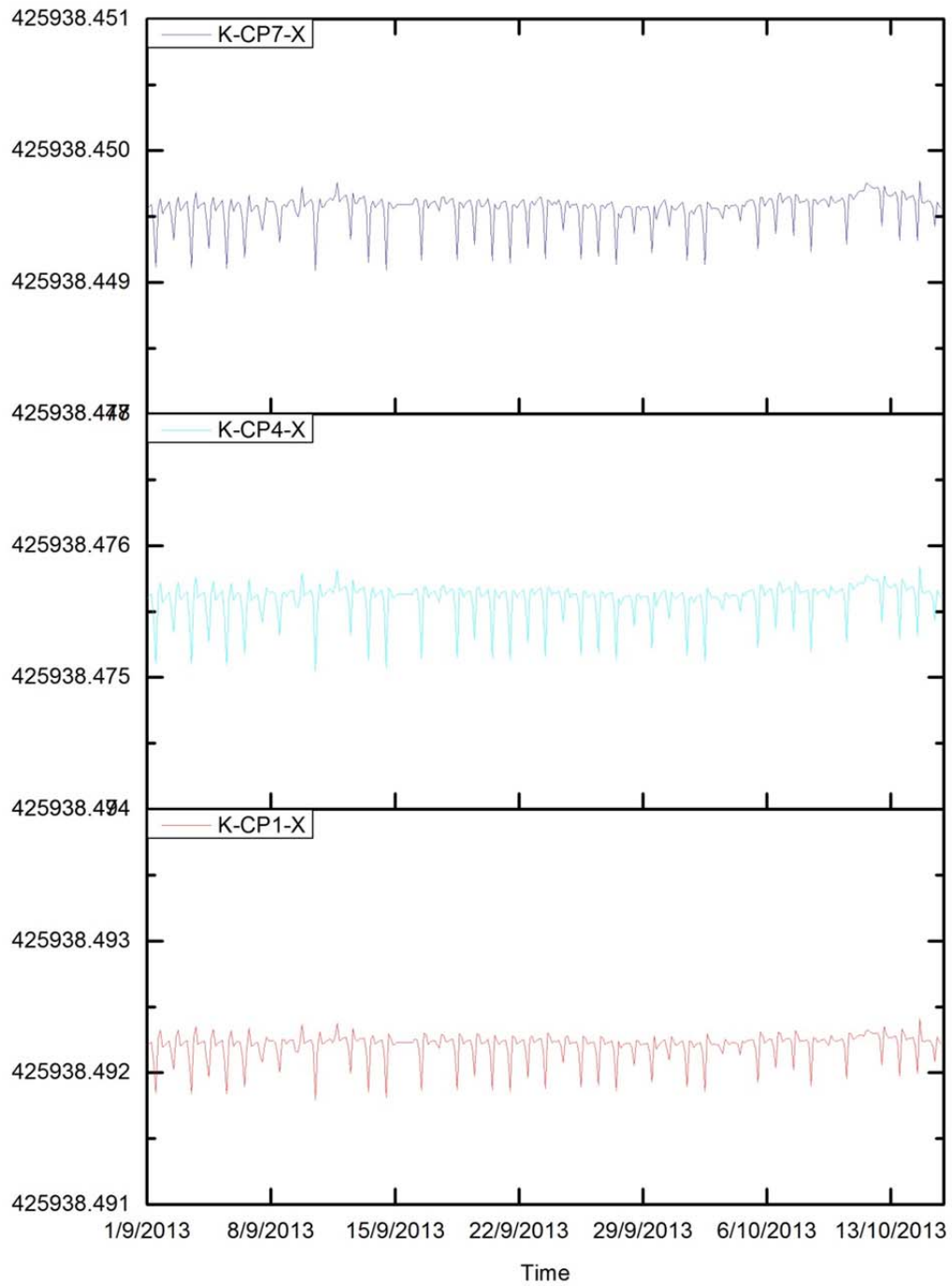


Figure 6.28 CP1, CP4 and CP7 movement (m) in X-direction.

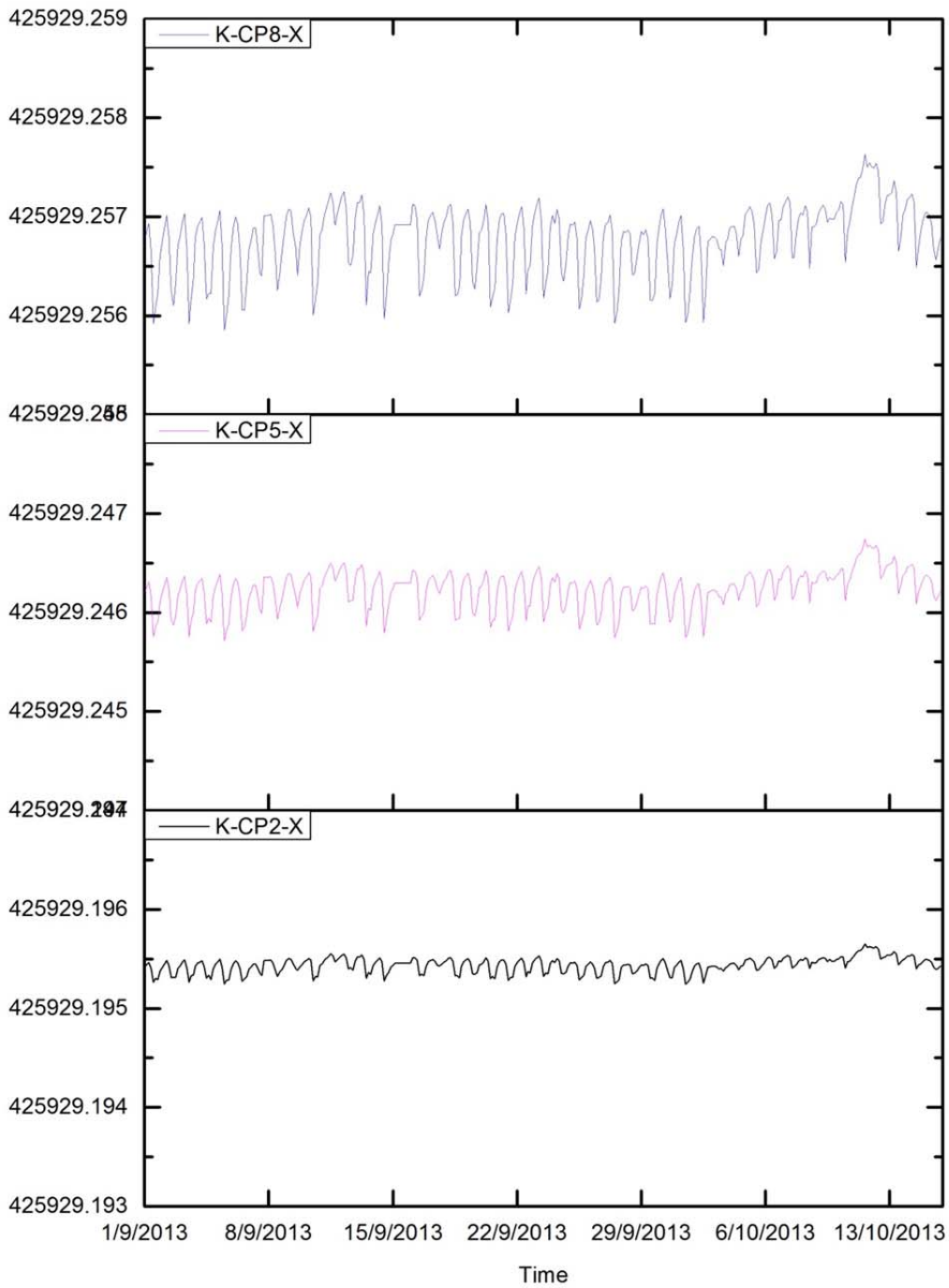


Figure 6.29 CP2, CP5 and CP8 movement (m) in X-direction.

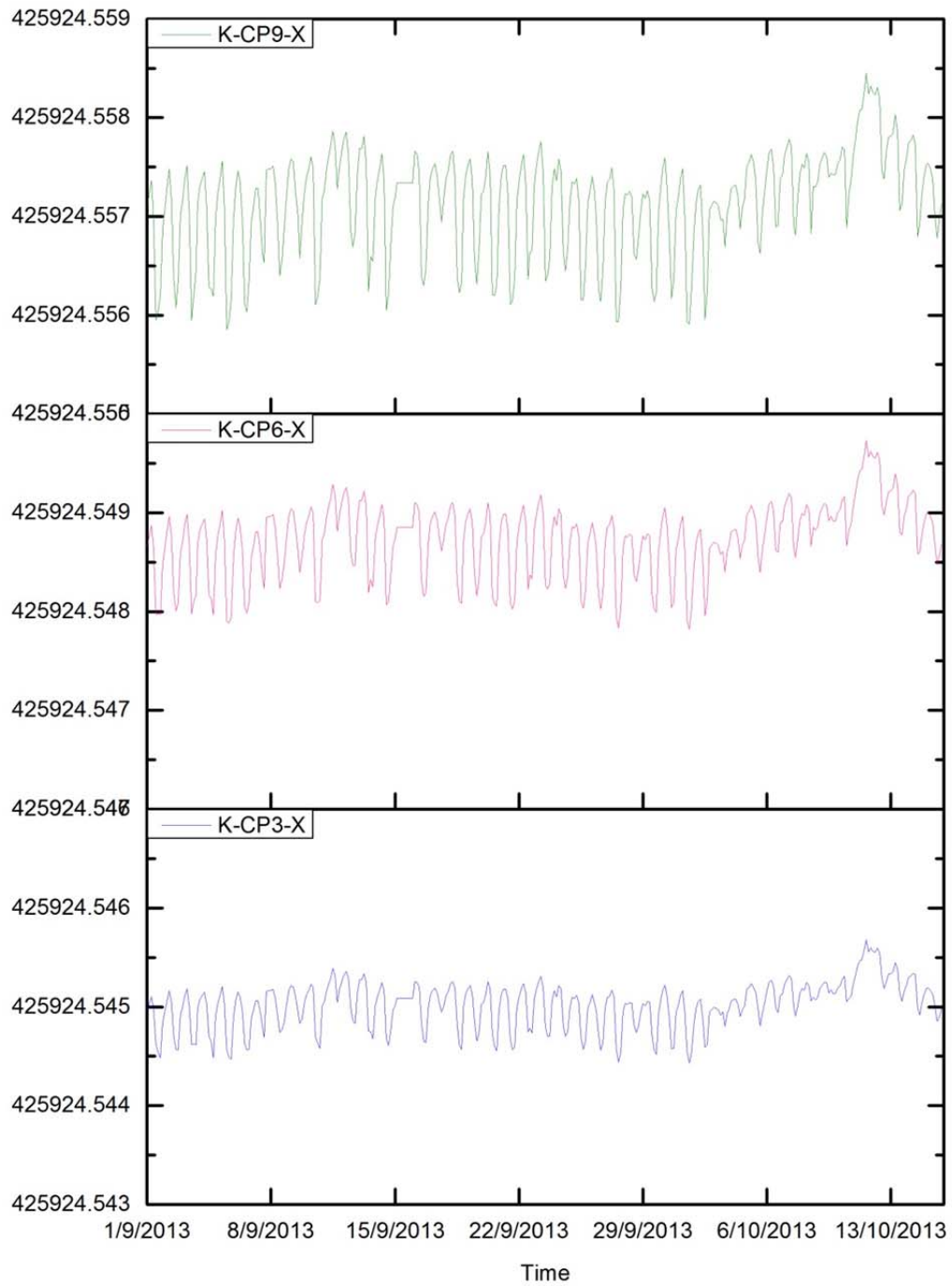


Figure 6.30 CP3, CP6 and CP9 movement (m) in X-direction.

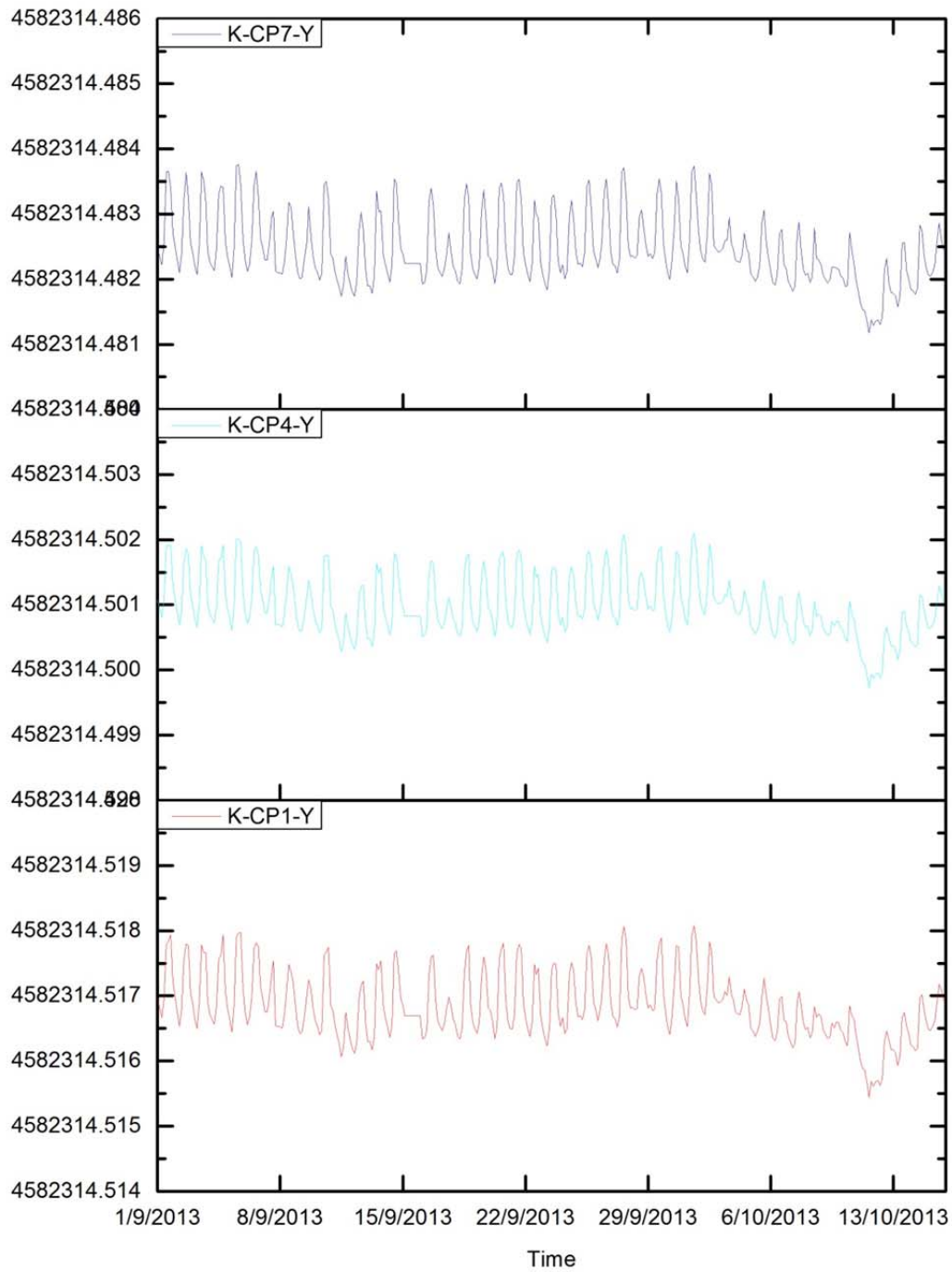


Figure 6.31 CP1, CP4 and CP7 movement (m) in Y-direction.

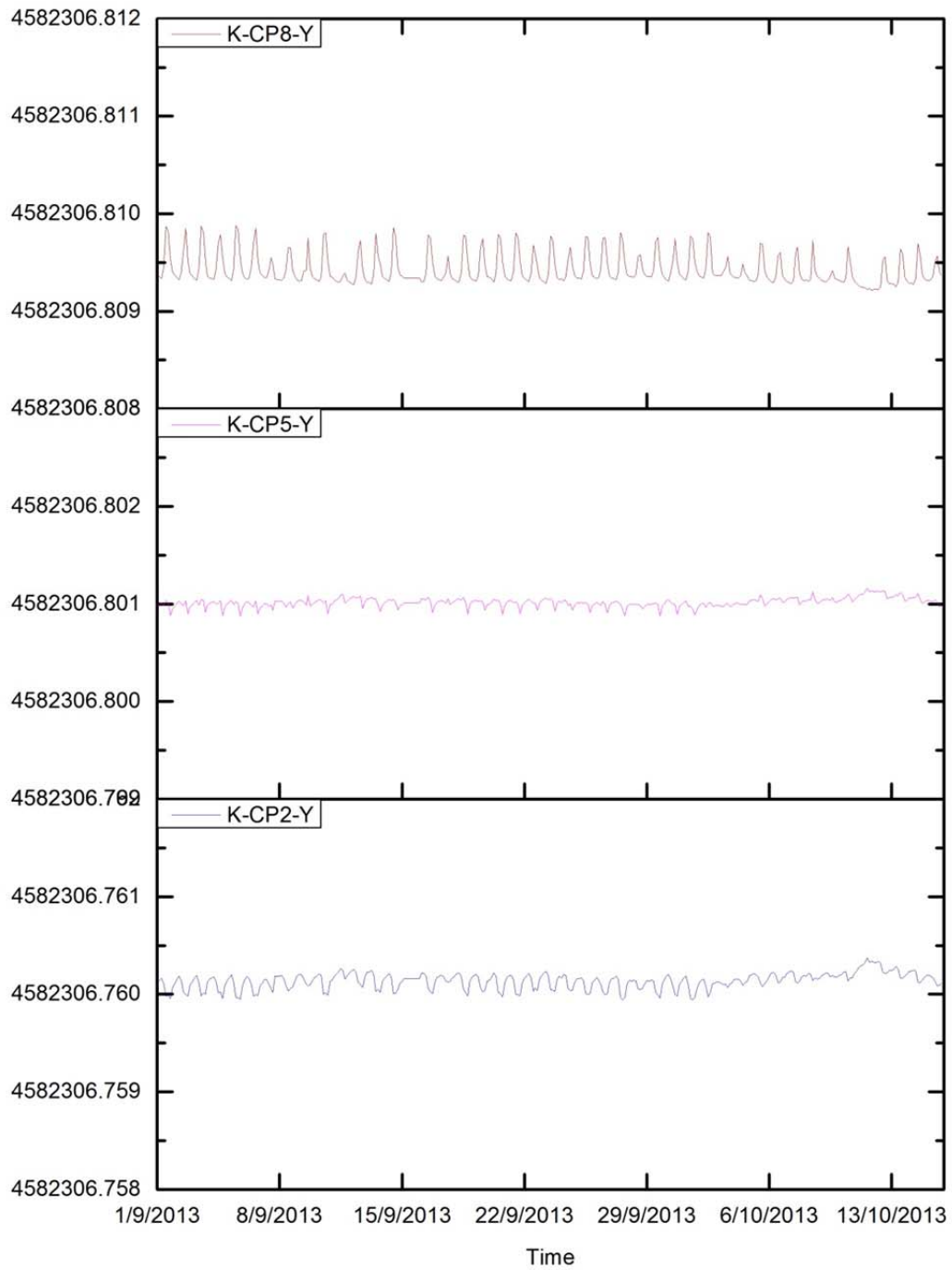


Figure 6.32 CP2, CP5 and CP8 movement (m) in Y-direction.

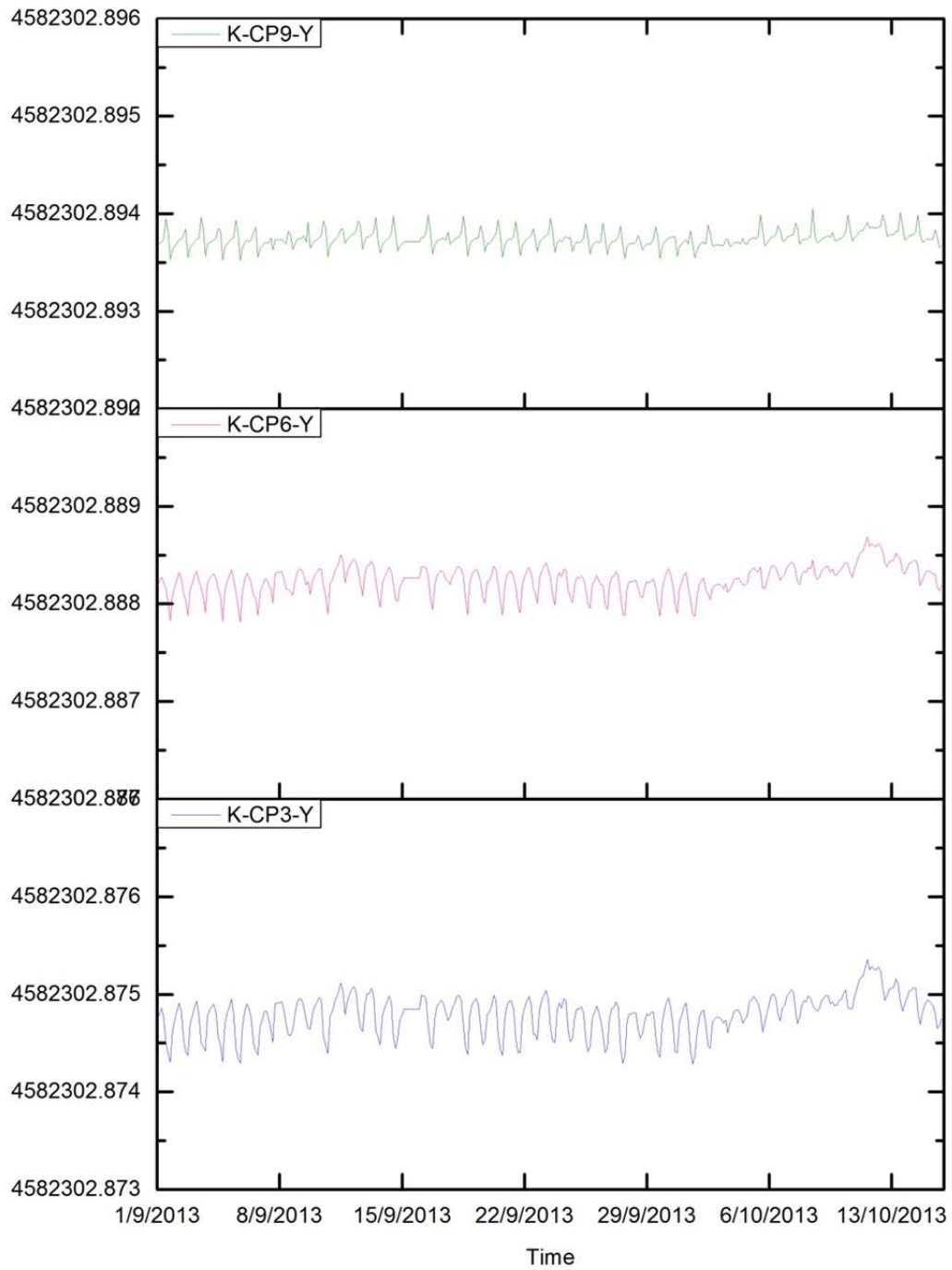


Figure 6.33 CP3, CP6 and CP9 movement (m) in Y-direction.

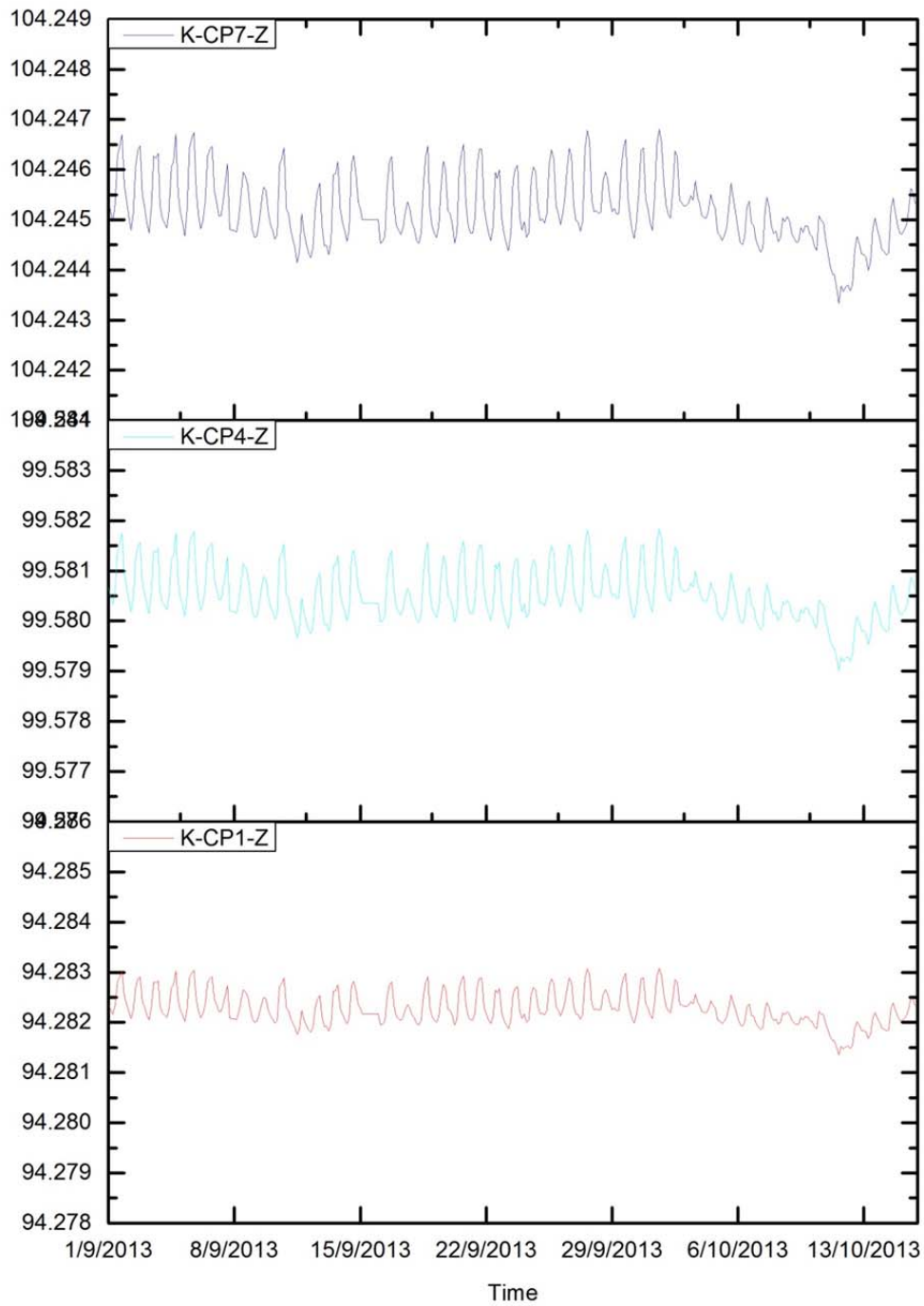


Figure 6.34 CP1, CP4 and CP7 movement (m) in Z-direction.

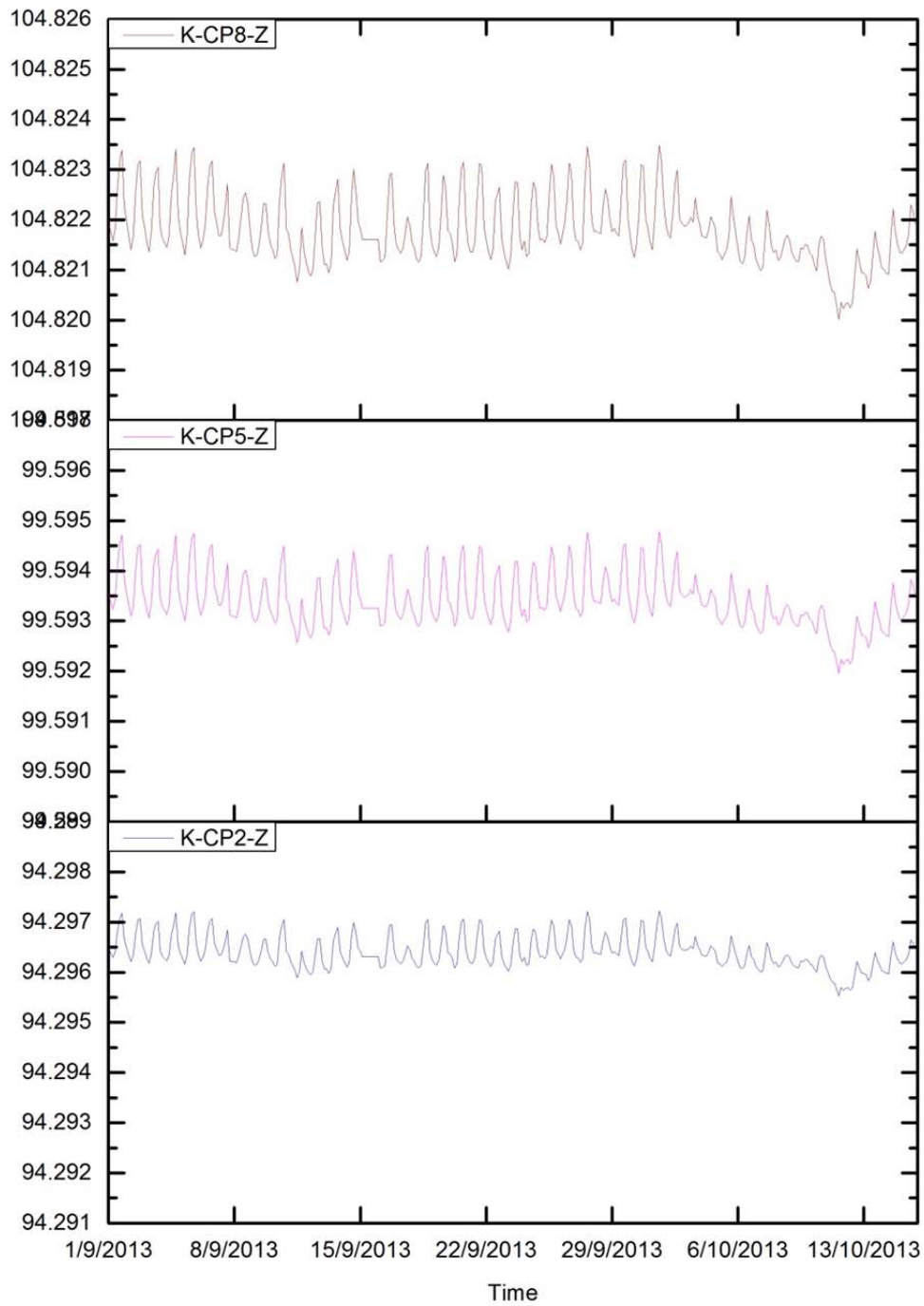


Figure 6.35 CP2, CP5 and CP8 movement (m) in Z-direction.

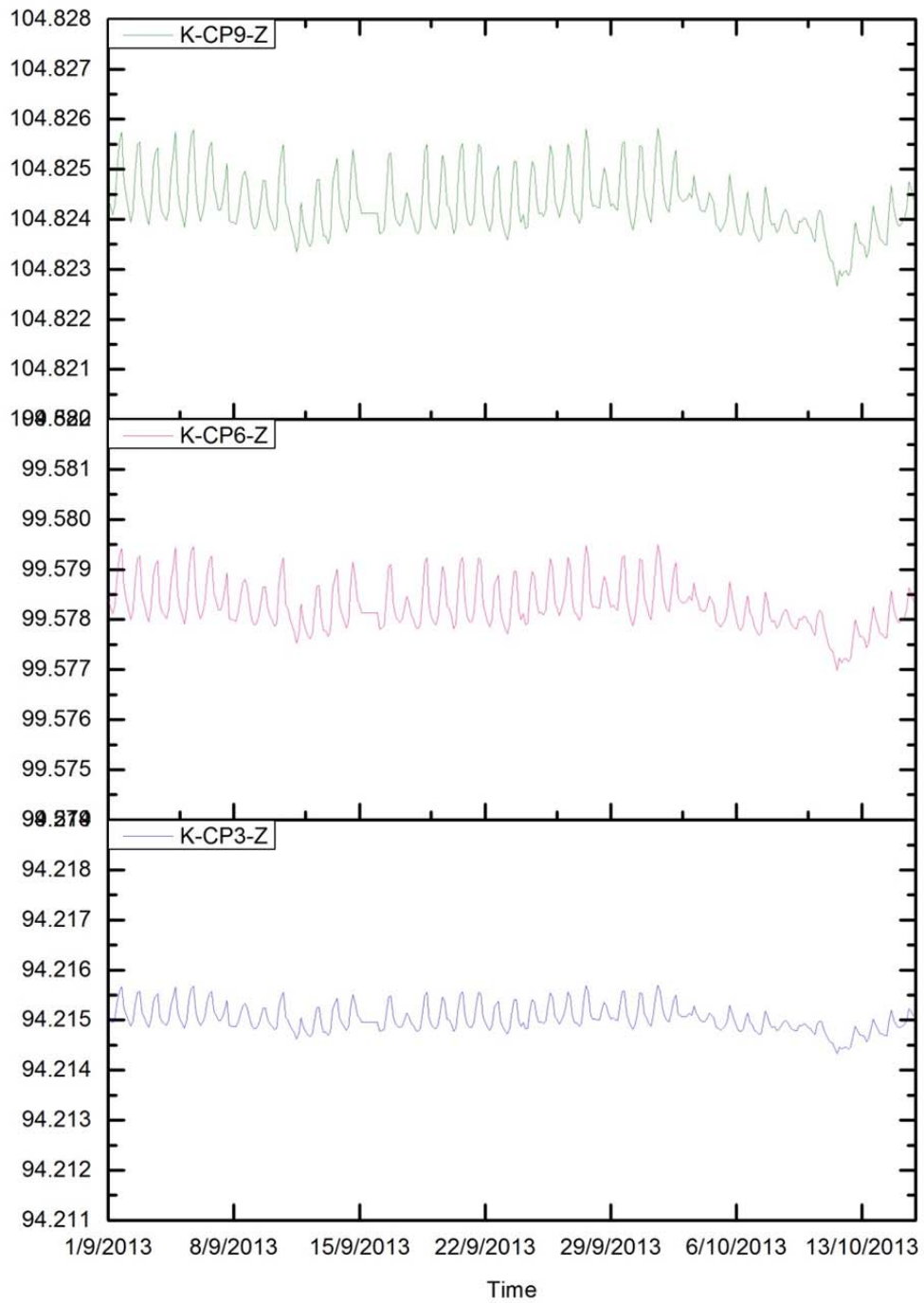


Figure 6.36 CP3, CP6 and CP9 movement (m) in Z-direction.

6.3.4 Comparison and analysis between approach-K and GW

In order to study how much the influence of the thermal movements of reference points and control points, the thermal movements of reference points and control points have been introduced into the computation in approach-K. After the calculation, the results of approach-K have been compared with the results of GW.

This comparison is focused only in the control points since for the approach-K, the results of RTS are the same as the results in approach-B, because approach-K and approach-B used the same data to compute its coordinates.

Figures from 6.39 to 6.47 show the comparisons of control points between approach-K and GW in X-direction, Y-direction and Z-direction during the time from 1st September 2015 to 15th October 2015.

In X-direction, the movement ranges of CP2, CP3, CP4, CP5 and CP7 are almost same between approach-K and GW, the fluctuations are about 1mm. The movement ranges of CP6 for approach-K and GW are also same, the fluctuations are 2mm. For the rest of the control points, their fluctuations are different. The movement range of CP8 in approach-K is bigger than in GW, which are 1.5mm in approach-K and 1mm in GW; as same as CP8, the movement range of CP9 in approach-K is bigger than in GW, which are 2.5mm in approach-K and 1.5mm in GW.

In Y-direction, the control points which are located on the middle part and right part of the K2M building move more stable in approach-K than the results of GW as shown in Figure 6.43 and 6.44, which the fluctuations of CP2, CP5, CP6 and CP9 are less than 0.5mm in approach-K and 1mm in GW. However, for control points CP1, CP4 and CP7 that located on the left part of K2M building, the movement ranges in approach-K are bigger than in GW, which are about 2.5mm in approach-K and 1.5mm in GW (except CP1).

In Z-direction, compared with the results in GW, the results of control prisms in approach-K are different. From the Figure from 6.45 to 6.47, it can be seen that the movement range of control prisms in approach-K increased from the ground floor to the top floor, which the movement range went up from about 1.5mm for CP1, CP2 and CP3 to about 3.5mm for CP7, CP8 and CP9. But the movement ranges of GW keep around 2mm for all of the control points (except CP1).

From the results of comparisons between approach-K and GW in X, Y and Z directions, it can be seen that there are some control points move very stable during the study time period and fill the expectation that the control points more stable if the thermal movements of both all the prisms and RTS have been introduced into the computation, such as, CP1, CP2, CP3, CP4, CP5 and CP7 in X-direction, CP2, CP3, CP5, CP6, CP8 and CP9 in Y-direction and CP1 in Z-direction.

However, compare with these stable results in approach-K, there are some control points' results in approach-K vary in a big extent, such as, CP6, CP8 and CP9 in X-direction, CP1, CP4 and CP7 in Y-direction, CP2, CP3, CP4, CP5, CP6, CP7, CP8 and CP9 in Z-direction. One reason for this phenomenon probably is that the simulated results in structure model in approach-K have been overestimated.

On the other hand, the movement range of CP1 in approach-K is full our expectations, but the results in GW contained several outliers, generated by the tree's leaves in front of the K2M building.

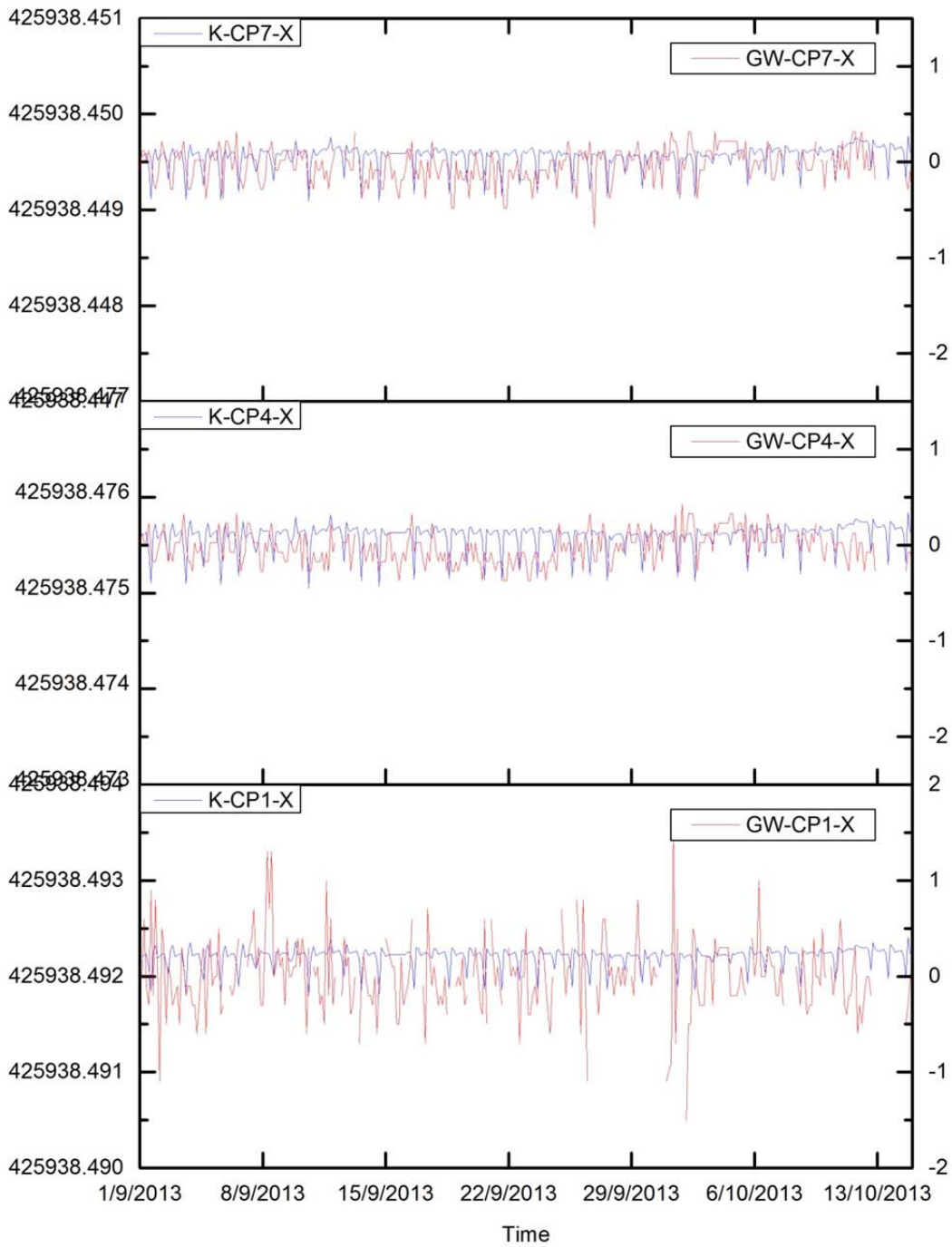


Figure 6.37 Comparison of approach-K and GW for CP1, CP4 and CP7 movement in X-direction. Vertical Axes Unit: left is m, right is mm.

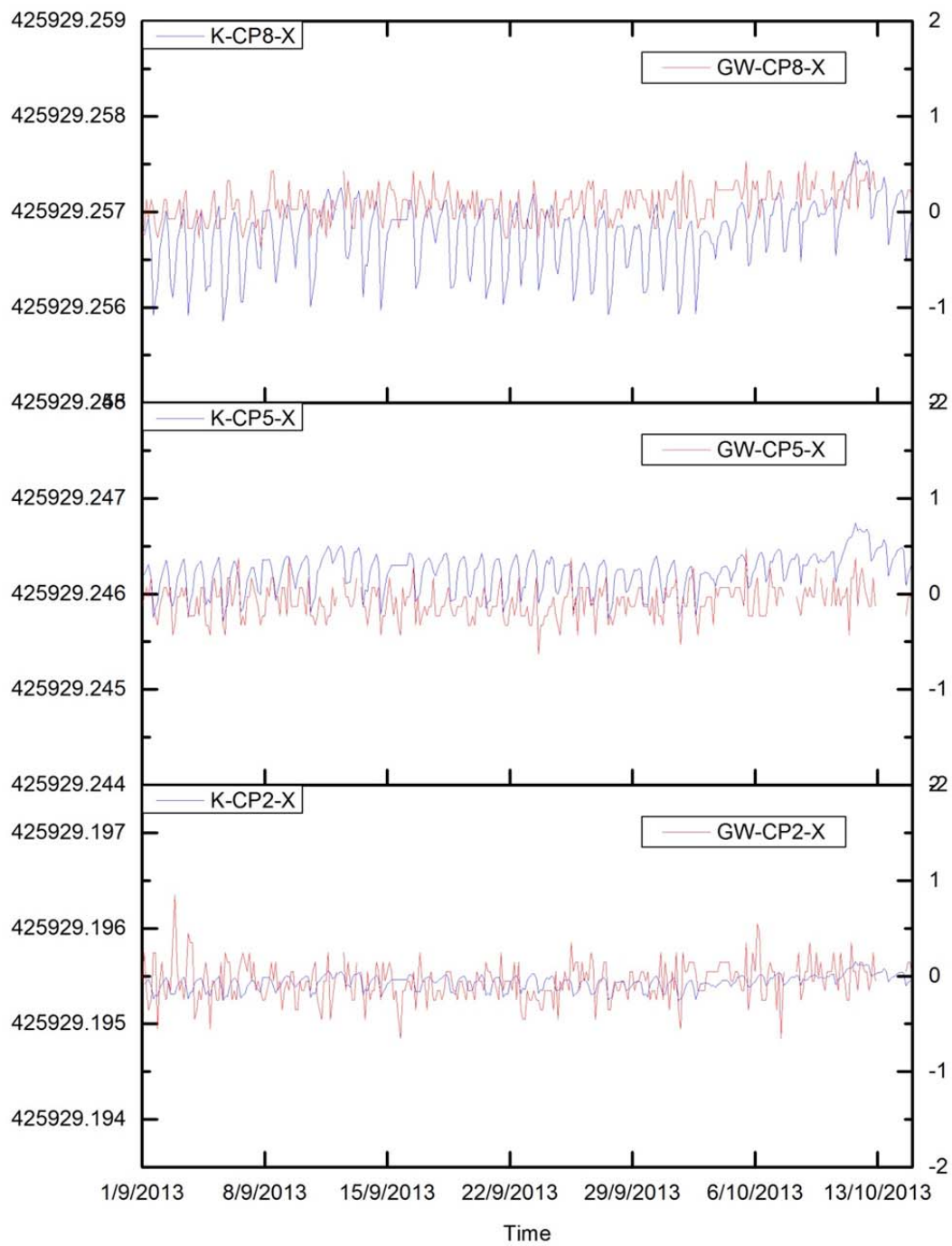


Figure 6.38 Comparison of approach-K and GW for CP2, CP5 and CP8 movement in X-direction. Vertical Axes Unit: left is m, right is mm.

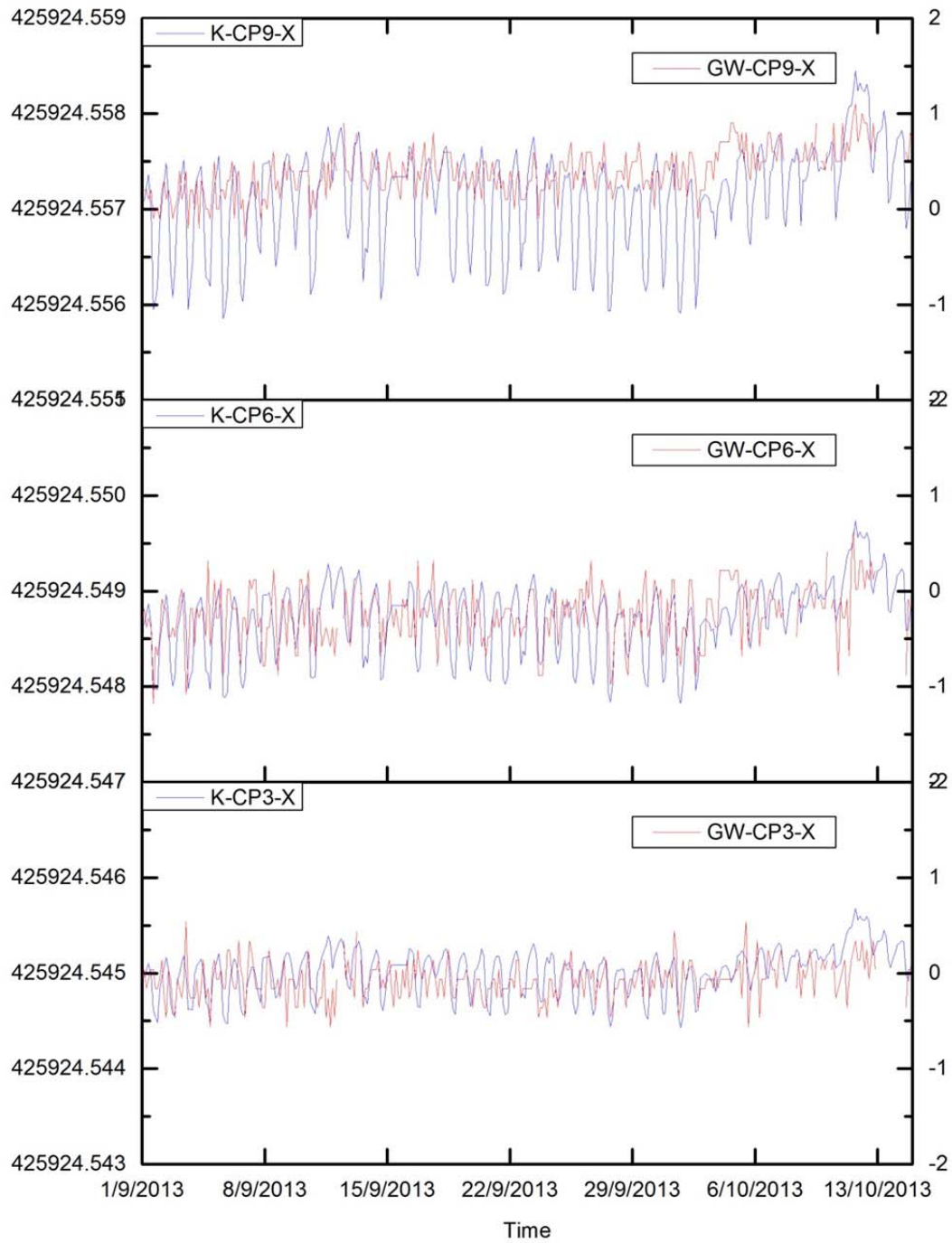


Figure 6.39 Comparison of approach-K and GW for CP3, CP6 and CP9 movement in X-direction. Vertical Axes Unit: left is m, right is mm.

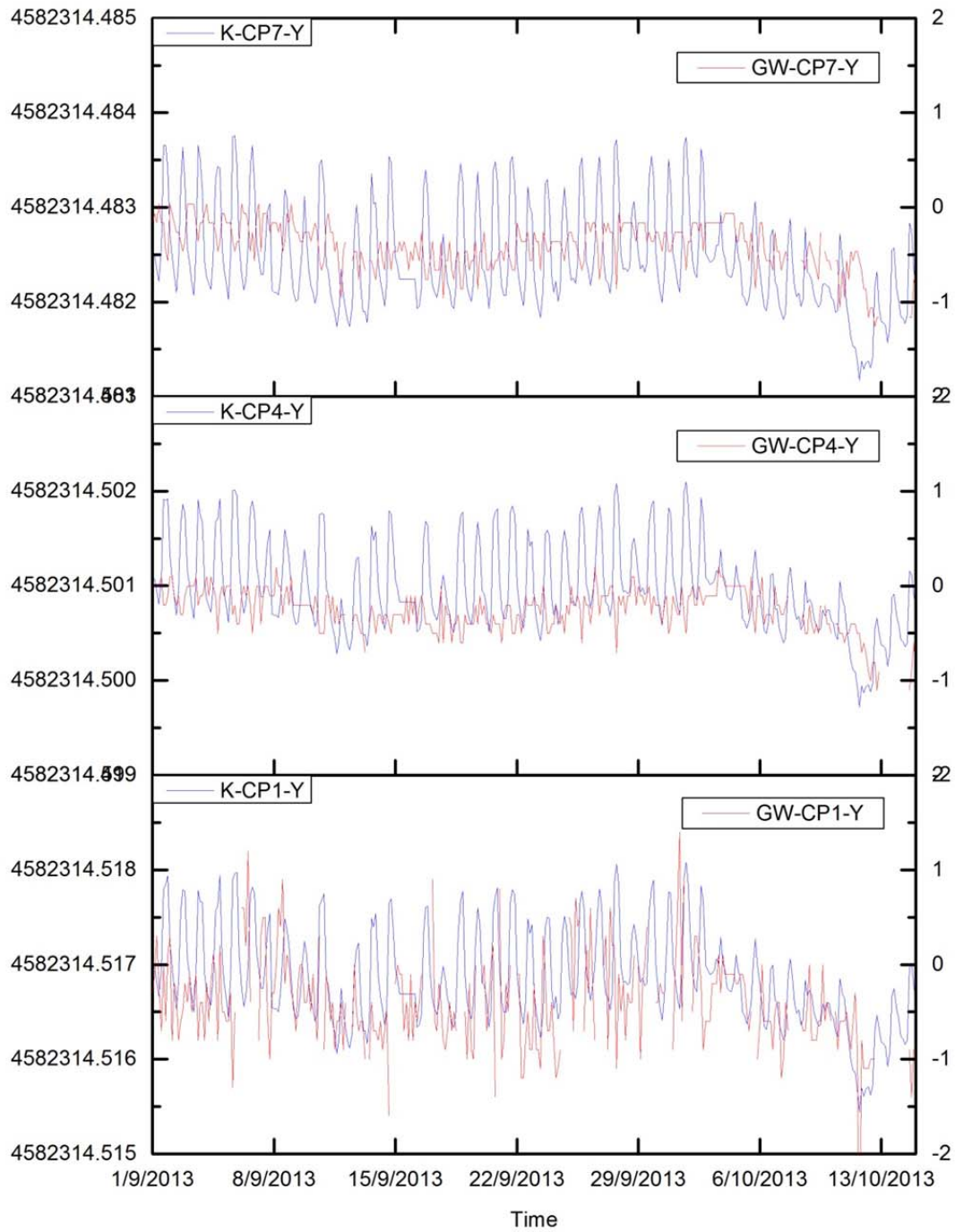


Figure 6.40 Comparison of approach-K and GW for CP1, CP4 and CP7 movement in Y-direction. Vertical Axes Unit: left is m, right is mm.

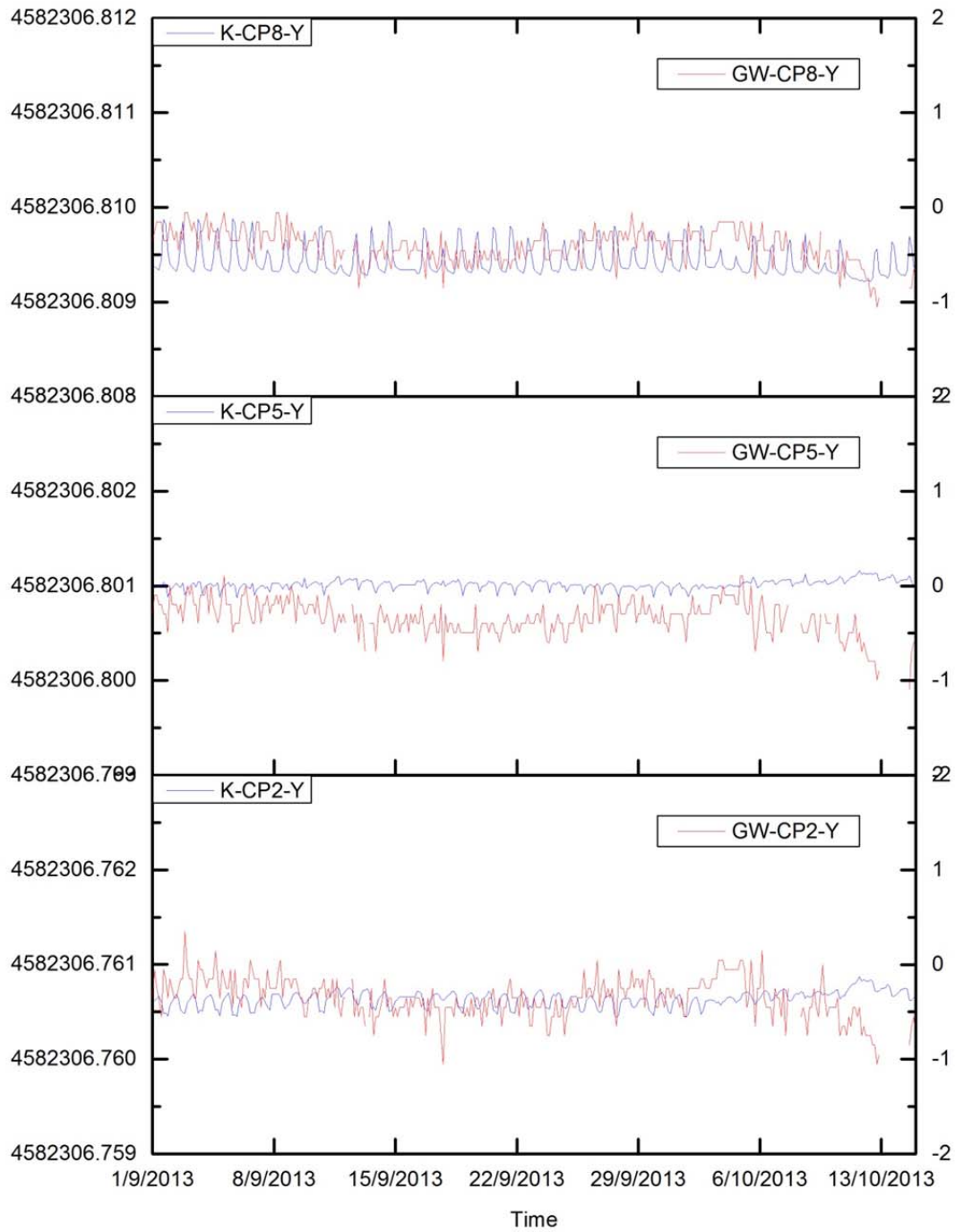


Figure 6.41 Comparison of approach-K and GW for CP2, CP5 and CP8 movement in Y-direction. Vertical Axes Unit: left is m, right is mm.

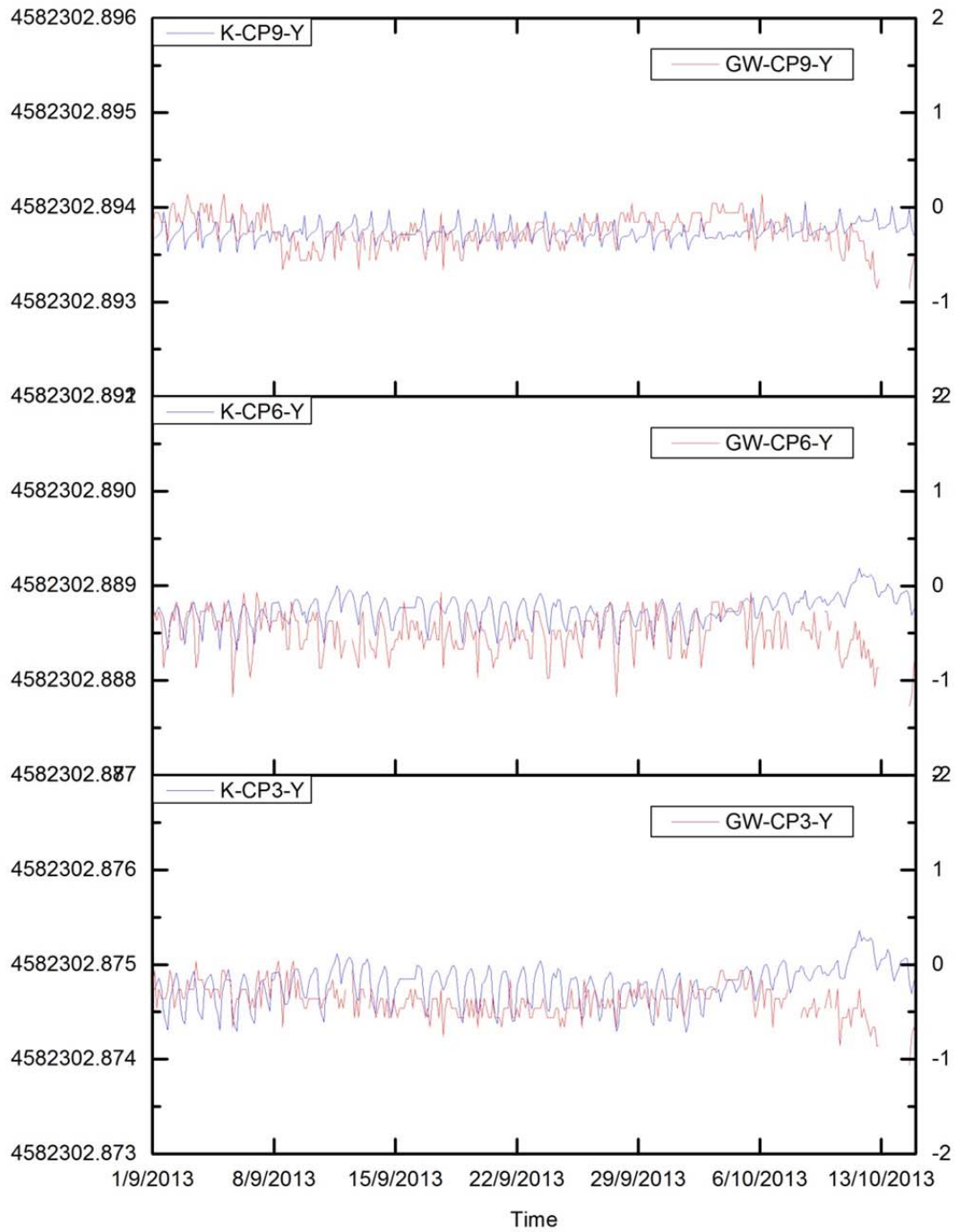


Figure 6.42 Comparison of approach-K and GW for CP3, CP6 and CP9 movement in Y-direction. Vertical Axes Unit: left is m, right is mm.

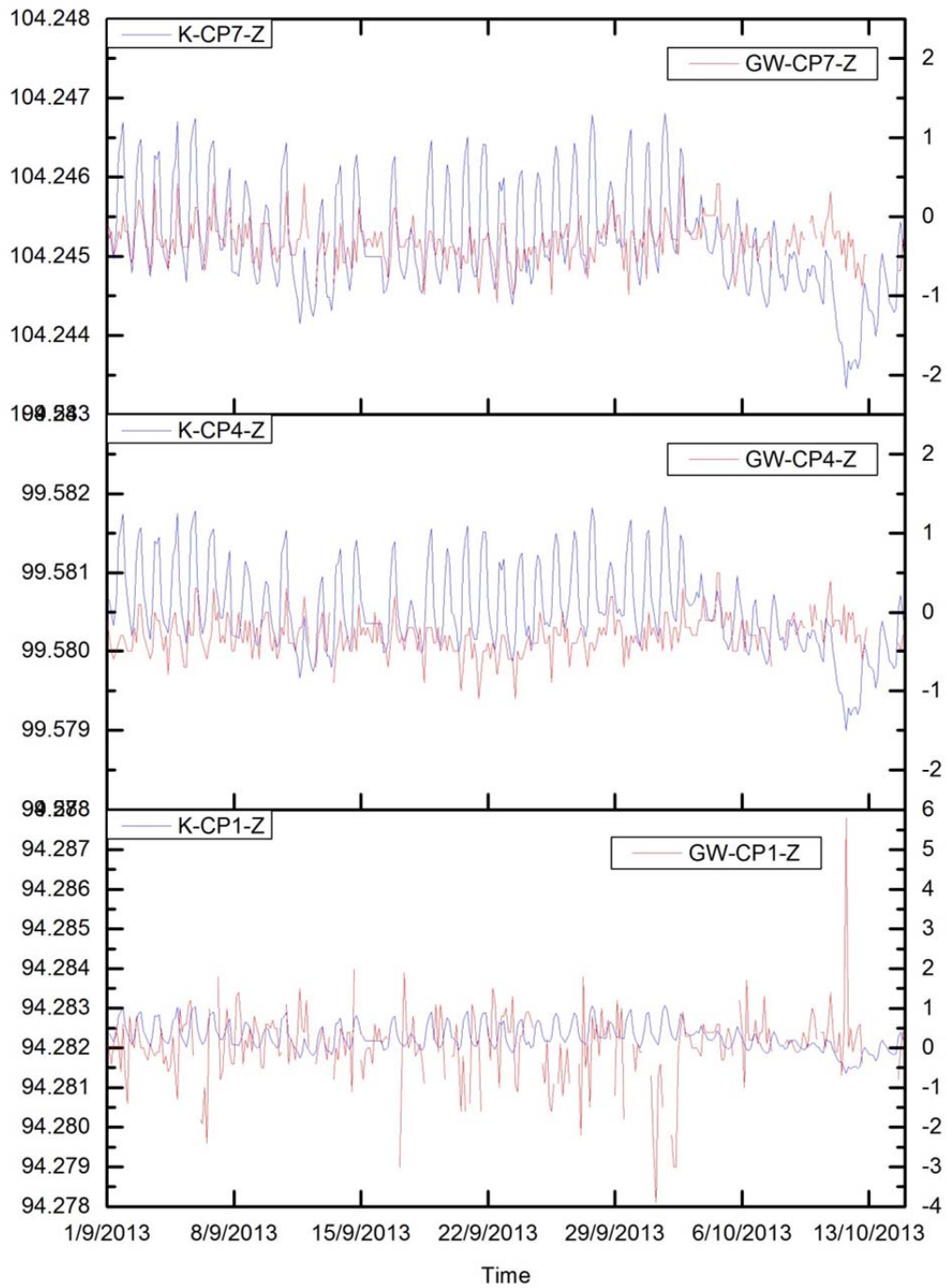


Figure 6.43 Comparison of approach-K and GW for CP1, CP4 and CP7 movement in Z-direction. Vertical Axes Unit: left is m, right is mm.

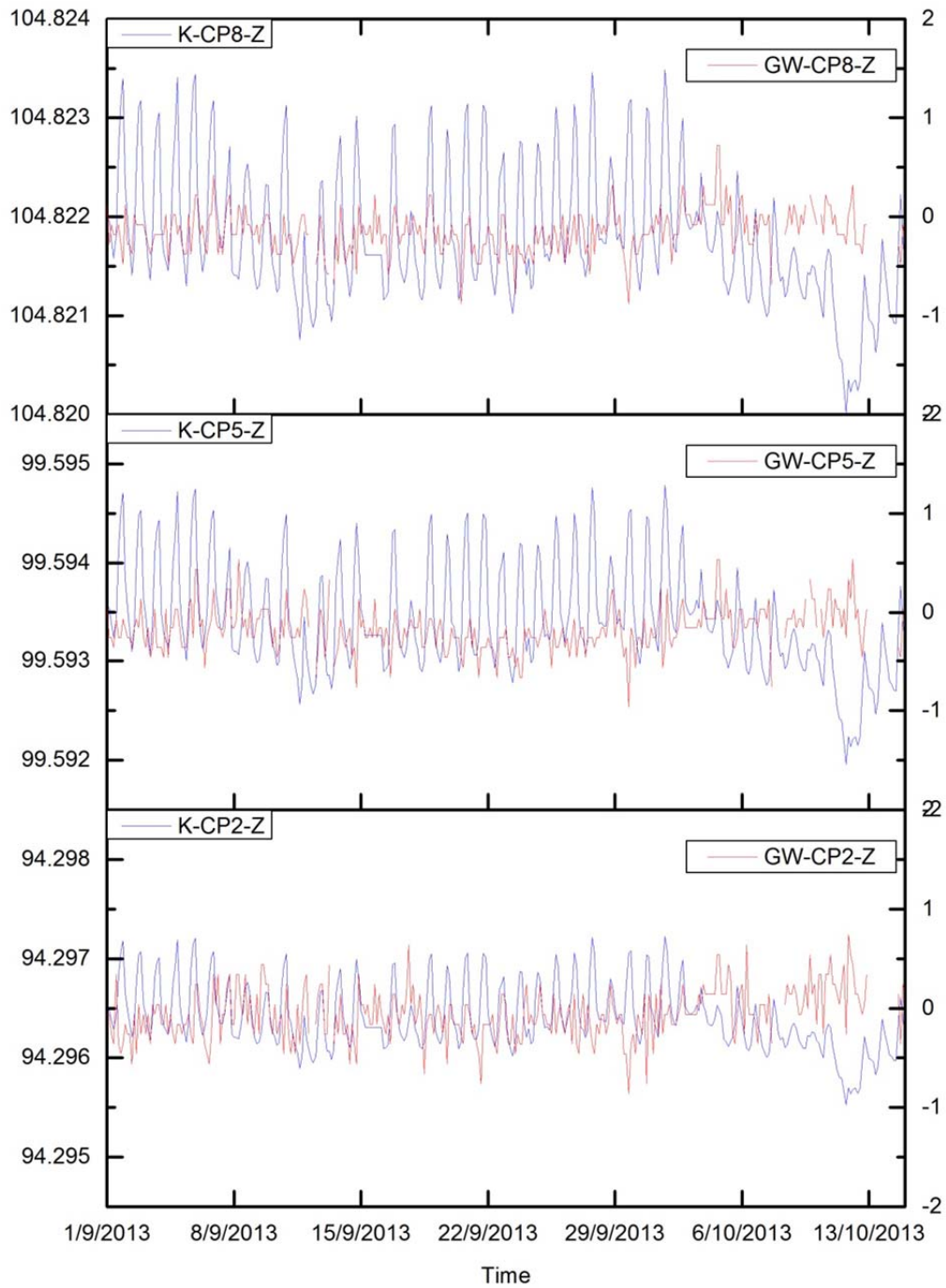


Figure 6.44 Comparison of approach-K and GW for CP2, CP5 and CP8 movement in Z-direction. Vertical Axes Unit: left is m, right is mm.

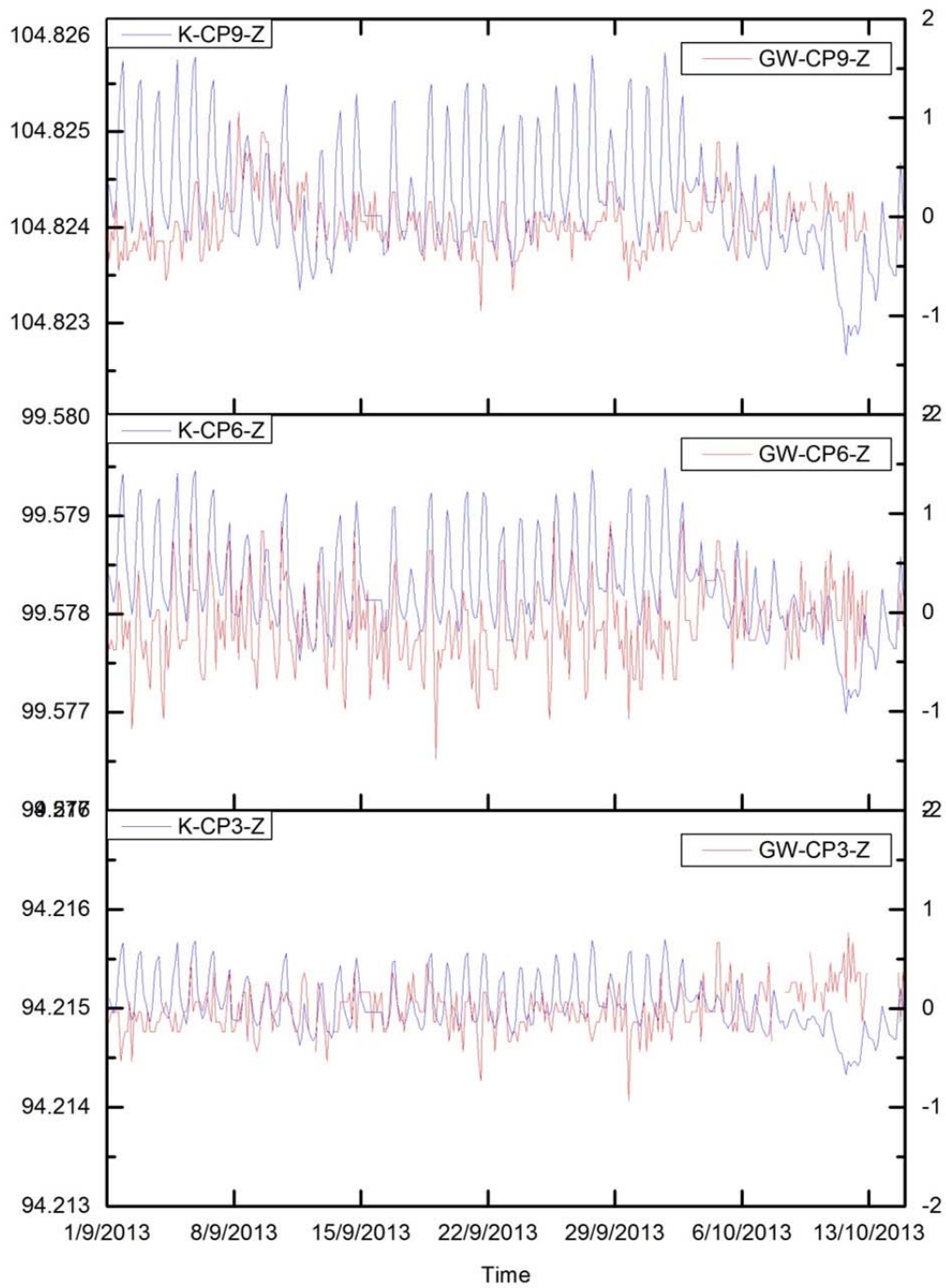


Figure 6.45 Comparison of approach-K and GW for CP3, CP6 and CP9 movement in Z-direction. Vertical Axes Unit: left is m, right is mm.

6.4 Overview

The chapter ends with an overview that summarizes the strategy to take into account the thermal effects in building monitoring, which is preconized by this Thesis.

To filter the Thermal Effect we must apply a correction $M_{Approach_D}$, which is the thermal deformation simulated by Approach-D (Section 5.3), to the values measured by the standard monitoring system, such as the Geoscope Web, M_{GW} :

$$M_{corrected} = M_{GW} - M_{Approach_D} \quad 6.6$$

The resulting graphs (XYZ evolution over time) are flat in average, because the thermal noise has been removed, except the REAL movements of the building related to the possible public works (tunneling, excavation) under development in the area. However, in a calm situation, the graphs tend to be horizontal lines.

If we want to appreciate the small movements that the building experiences in reality, daily or yearly, we may consider recovering the movement simulated with Approach-K:

$$M_{corrected}' = M_{GW} - M_{Approach_D} + M_{Approach_K} \quad 6.7$$

NOTE 1: this last term added to M can be obtained with Approach-K. Alternatively, we can use the displacement computed with the Structural program directly (that is, the DX_{CP} , DY_{CP} , DZ_{CP} values that appear in the flowchart of Approach-K, Figure 6.26)

NOTE 2: to make the correction operational, a unique Approach-DK is envisaged. This new approach would be a combination between the present approaches D and K, with a flag question at the beginning for the user to decide whether to preserve the small movements that affect the building. The correction equation would read as:

$$M_{corrected} = M_{GW} - M_{Approach_DK} \quad 6.8$$

This new Approach-DK can be named “Numerical simulation of the thermal effect correction with the option to preserve the small movement of the building due to the ΔT ”.

In this way, we are able to filter the deformation associated exclusively with the so-called “Thermal Effect”, a correction that is important to consider in order to carry out high precision monitoring practice.

7 Conclusions and future work

Finally, we proceed here to summarize the main conclusions and to outline the possible ways to follow up this work.

7.1 Conclusions

This thesis is dedicated to exploring the influence of thermal change on structure health monitoring in urban areas during underground works and to improving the basic knowledge. The work presented in this PhD thesis is a contribution to assessing the influence of thermal change on the current building health monitoring practice. In the following paragraphs, the main achievements of this research are summarized.

- 1) A model based on the theories, which are elastic deformation of structure, thermal effect law, stiffness matrix method, least square adjustment, distance correction and blunder detection through simulating the building's behavior under the thermal change, is established and formulated. This model is implemented into Matlab software. A series of numerical simulation tests have been implemented in order to prove that the model is reasonable and confirms the hypothesis. The model can simulate the real phenomenon (the building moves when the temperature changes) and proves that the thermal influence on structure deformation monitoring cannot be ignored in the practice.
- 2) A field experiment was set up to carry out a long-term building deformation monitoring in real time in UPC Campus Nord. The devices used in the experiment include Robotic Total Station (RTS), sensors (for collecting temperature data, insolation, levelling, etc.), prisms and a meteorological station (for collecting air temperature, air pressure, wind speed and direction, rainfall etc.). The results of this real scale study verify that the building moves with the temperature and insolation change. At the same time, the fieldwork and data processing have been used to improve the numerical simulation model.

- 3) RTS observation data sensitivity test provides the opportunity to validate how small errors in the measurements (Horizontal angle, Zenith angle and distances) will influence the results. The results demonstrate that the plane coordinates (X and Y) are very sensitive to changes in the horizontal angle, the vertical coordinate (Z) is sensitive to the zenith angle change and the change in distance affects all three of the coordinates.
- 4) Approach-D (the so-called “standard approach”) was carried out to investigate the environmental influence on the structure deformation monitoring by numerically simulating it, based on the changes in the real environmental conditions that were observed by GW. In the GW results, the movement ranges of RTS are 2.57mm in X -direction, 2.67mm in Y -direction, and 2.19mm in Z -direction; the movement ranges of control points are 1) in X -direction, about 1mm for CP3, CP4, CP5, CP7 and CP8, 1.5mm for CP2 and CP9, 2mm for CP6; 2) in Y -direction 1mm for CP3, CP5, CP8 and CP9, 1.5mm for CP2, CP4, CP6 and CP7; 3) in Z -direction, the movement ranges are about 1.5mm for CP2, CP3, CP4, CP5, CP7 and CP8, 2mm for CP9 and 2.5mm for CP6. For the results of approach-D, the movement ranges of RTS are 1.6mm in X -direction, 2.9mm in Y -direction, 1.9mm in Z -direction; the movement ranges of control points are 1) in X -direction, about 0.5mm for CP1, CP2 and CP7, 1mm for CP4, 1.5mm for CP3 and CP5, 2.0mm for CP6 and CP8, 3.0mm for CP9; 2) in Y -direction, about 0.5mm for CP8, 1.0mm for CP7, 1.5mm for CP1, CP2, CP4, CP5 and CP9, 2mm for CP3 and CP6; 3) in Z -direction; about 0.5mm for CP1, CP2 and CP3, 1mm for CP7, 1.5mm for CP6, 2.0mm for CP4, CP5 and CP9, 2.5mm for CP8; the RMSE in X ranges ± 0.18 mm, whereas in Y ranges ± 0.17 mm. Comparing the real movement of the building with the simulation results, the displacement of RTS and control points has been successfully simulated by the proposed approach. Based on these results, it can be concluded that the standard model has been matched with the real world results of GW.
- 5) In order to explore the influence of thermal movement of the reference points in the computation of coordinates of RTS, approach-B was established based on approach-D. In approach-B, both the thermal movements of reference points and RTS have been put into the computation to calculate the coordinates of RTS, and the control points have been fixed to compute the raw data. The movement range of RTS in approach-B is 1.9mm in X -direction; 4.0mm in Y -direction; 3.1mm in

Z-direction. The results show that the displacement of RTS correlates with the thermal changes and the control points stay constant during the study period. The results of approach-B further verify that thermal changes are an important factor in the structure health monitoring practice.

- 6) Approach-K was designed and carried out to further explore the thermal influence on the structure deformation monitoring. In approach-K, the thermal movements of control points have also been introduced into the computation under the conditions of approach-B. The movement range of RTS in approach-K are the same that the obtained in the approach-B. For the movement range of the control pints, in X-direction, the range is 1mm for CP2, CP5 and CP9, 1.5mm for CP3 and CP8, 2mm for CP6 and 2.5mm for CP9; in Y-direction, the range is 0.5mm for CP2, CP5 and CP9, 1mm for CP3, CP6 and CP8, 2mm for CP4, 2.5mm for CP1, and 3mm for CP7; in Z-direction, the range is 1.5mm for CP1 and CP3, 2mm for CP2, 2.5mm for CP6, 3mm for CP4 and CP5 and 3,5mm for CP7, CP8 and CP9. The results of approach-K preserve the real movement of the building but the spurious apparent movement related with the thermal influence has been removed.

7.2 Future work

This thesis has started the path towards discovering how to accommodate the thermal influence on the structure monitoring (SHM). Whilst it presents some initial findings, some future work is suggested for further investigation as follows.

- The present model is currently too complex to be applied in the general practice. Although the model can be applied to singular buildings, it is too complicated to obtain the basic data in a general urban case. Therefore, the model needs to be further simplified in order to make it easier to be applied.
- The Matlab code can be successfully used to compute the displacement of buildings and to adjust the observations, but it is not integrated. Future software development to integrate the codes is recommended.
- In the model, the inside temperature of the building is a constant value which is not the real condition of the building. Hence, further improvements are needed

in the actual structure deformation monitoring practice to introduce the dynamic inside temperature into the calculation.

- Insolation was recognized as an important influence factor for the thermal distribution of the building during the day. In this thesis, one equation between insolation and temperature on the surface of the building was established based on experience. It needs to be further validated in the practice. The relationships between the hour of the day and the percentage of the solar radiation on a given façade can be easily improved and generalized.

References

- RIBA,(2015). from <http://www.architecture.com/RIBA/Aboutus/SustainabilityHub/Designstrategies/Earth/1-1-3-2-Buildingorientation.aspx>.
- Abad, V. (2013). Anàlisi retrospectiu de dades de monitorització d'edificis a prop del túnel de la L9 a l'Hospitalet de Llobregat (Barcelona). Construction Engineering Degree, Technical University of Catalonia.
- Afeni, T. B. (2011). An approach to eradicate the effects of atmospheric variations on total station distance measurement in a surface mine environment, Faculty of Engineering and the Built Environment, University of the Witwatersrand.
- Afeni, T. B. (2012). An approach to eradicate the effects of atmospheric variations on total station distance measurement in a surface mine environment: The impact of taking measurement through a glass medium. Doctor, University of the Witwatersrand.
- Afeni, T. B. and F. T. Cawood (2013). "Slope Monitoring using Total Station: What are the Challenges and How Should These be Mitigated?" South African Journal of Geomatics **2**(1): 41-53.
- Alba, M., G. Bernardini, A. Giussani, P. P. Ricci, F. Roncoroni, M. Scaioni, P. Valgoi and K. Zhang (2008). "Measurement of dam deformations by terrestrial interferometric techniques." The International Archives of the Photogrammetry, Remote Sensing and Spatial Information Sciences **37**: 133-139.
- Alba, M., L. Fregonese, F. Prandi, M. Scaioni and P. Valgoi (2006). "Structural monitoring of a large dam by terrestrial laser scanning." International Archives of Photogrammetry, Remote Sensing and Spatial Information Sciences **36**(Part 5).
- Amer, F. (1979). Theoretical Reliability Studies for Some Elementary Photogrammetric Procedures. Proceedings of the Aerial Triangulation Symposium, Department of Surveying, University of Queensland, Brisbane, Australia.
- Antonello, G., N. Casagli, P. Farina, D. Leva, G. Nico, A. J. Sieber and D. Tarchi (2004). "Ground-based SAR interferometry for monitoring mass movements." Landslides **1**(1): 21-28.
- Aroca, J. V. (2005). "Tuneles:como se hacen." Retrieved February 08, from <http://hemeroteca.lavanguardia.com/preview/2005/02/08/pagina-6/33694467/pdf.html?search=Carmel%20metro%202005>.
- Baarda, W. (1968). "A testing procedure for use in geodetic networks." Delft, Kanaalweg 4, Rijkscommissie voor Geodesie, 1968. **1**.
- Bailey, S. and R. Bez (1994). A parametric study of traffic load effects in medium span bridges. in: Developments in Short and Medium Span Bridge Engineering94, The Canadian Society for Civil Engineering, Citeseer.
- Barrell, H. and J. Sears (1939). "The refraction and dispersion of air for the visible spectrum." Philosophical Transactions of the Royal Society of London. Series A, Mathematical and Physical Sciences **238**(786): 1-64.
- Bennett, P. J., K. Soga, I. Wassell, P. Fidler, K. Abe, Y. Kobayashi and M. Vanicek (2010). "Wireless sensor networks for underground railway applications: case studies in Prague and London." Smart Structures and Systems **6**(5-6): 619-639.
- Berkelaar, R., L. Huisman and C. Luijten (2007). Deformation Monitoring of the Underground Metro Station Rotterdam CS: A Case Study. 7th FMGM 2007, American Society of Civil Engineers: 1-12.

- Bernardini, G., P. Ricci and F. Coppi (2007). A ground based microwave interferometer with imaging capabilities for remote measurements of displacements.
- Beth, M. and X. Obre (2005). "Ground movement monitoring at King's Cross Station, London." Proceedings of the ICE-Geotechnical Engineering **158**(3): 125-133.
- Bhalla, S., Y. W. Yang, J. Zhao and C. K. Soh (2005). "Structural health monitoring of underground facilities – Technological issues and challenges." Tunnelling and Underground Space Technology **20**(5): 487-500.
- Boehler, W., M. Bordas Vicent and A. Marbs (2003). "Investigating laser scanner accuracy." The International Archives of Photogrammetry, Remote Sensing and Spatial Information Sciences **34**(Part 5): 696-701.
- Boscardin, M. D. and E. J. Cording (1989). "Building response to excavation-induced settlement." Journal of Geotechnical Engineering **115**(1): 1-21.
- Breuer, P., T. Chmielewski, P. Górski and E. Konopka (2002). "Application of GPS technology to measurements of displacements of high-rise structures due to weak winds." Journal of Wind Engineering and Industrial Aerodynamics **90**(3): 223-230.
- Breuer, P., T. Chmielewski, P. Górski, E. Konopka and L. Tarczyński (2008). "The Stuttgart TV Tower—displacement of the top caused by the effects of sun and wind." Engineering Structures **30**(10): 2771-2781.
- Brownjohn, J. (2007). "Structural health monitoring of civil infrastructure." Philosophical Transactions of the Royal Society A: Mathematical, Physical and Engineering Sciences **365**(1851): 589-622.
- Brownjohn, J. M. W., F. Magalhaes, E. Caetano and A. Cunha (2010). "Ambient vibration re-testing and operational modal analysis of the Humber Bridge." Engineering Structures **32**(8): 2003-2018.
- Brownjohn, J. M. W., K. Worden, E. Cross, D. List, R. Cole and T. Wood (2009). Thermal effects on performance on Tamar Bridge. The Fourth International Conference on Structural Health Monitoring of Intelligent Infrastructure Zurich, Switzerland.
- Casas, J. and P. Cruz (2003). "Fiber Optic Sensors for Bridge Monitoring." Journal of Bridge Engineering **8**(6): 362-373.
- Catbas, F. N., M. Susoy and D. M. Frangopol (2008). "Structural health monitoring and reliability estimation: Long span truss bridge application with environmental monitoring data." Engineering Structures **30**(9): 2347-2359.
- Celebi, M. and A. Sanli (2002). "GPS in pioneering dynamic monitoring of long-period structures." Earthquake Spectra **18**(1): 47-61.
- Centis, S. and G. Giacomini (2004). "EPB tunnelling in highly variable ground—the experience of Oporto Light Metro." Tunnelling and Underground Space Technology **19**(4): 358-358.
- Centre, B. F. S. (2005). "Carmel Tunnel Collapse in Barcelona." from <http://geographyfieldwork.com/CarmelTunnel.htm>.
- Chae, M., H. Yoo, J. Kim and M. Cho (2012). "Development of a wireless sensor network system for suspension bridge health monitoring." Automation in Construction **21**: 237-252.
- Chen, R. P., J. Zhu, W. Liu and X. W. Tang (2011). "Ground movement induced by parallel EPB tunnels in silty soils." Tunnelling and Underground Space Technology **26**(1): 163-171.
- Ciampalini, A., F. Bardi, S. Bianchini, W. Frodella, C. Del Ventisette, S. Moretti and N. Casagli (2014). "Analysis of building deformation in landslide area using multisensor PSInSAR™ technique." International Journal of Applied Earth Observation and Geoinformation **33**(0): 166-180.

- Cong, E. (2004). Study of ground surface settlement caused by shield tunneling in Beijing. Master Degree Dissertation, Tianjin University, China.
- Cook, D. (2006). "Robotic total stations and remote data capture: Challenges in construction." Geotechnical News-Vancouver **24**(4): 42.
- Cosser, E., G. W. Roberts, X. Meng and A. H. Dodson (2003). Measuring the dynamic deformation of bridges using a total station. Proceedings of the 11 th FIG symposium on deformation measurements, Santorini, May.
- Crosetto, M., O. Monserrat, M. Cuevas-González, N. Devanthery, G. Luzi and B. Crippa (2014). "Measuring thermal expansion using X-band persistent scatterer interferometry." ISPRS Journal of Photogrammetry and Remote Sensing(0).
- Cuevas, M., O. Monserrat, M. Crosetto and B. Crippa (2011). A new product from persistent scatterer interferometry: The thermal dilation maps. Urban Remote Sensing Event (JURSE), 2011 Joint, IEEE.
- de Rienzo, F., P. Oreste and S. Pelizza (2008). "Subsurface geological-geotechnical modelling to sustain underground civil planning." Engineering Geology **96**(3–4): 187-204.
- Dvořáček, F. (2012). Calibration of Electronic Distance Meters. Master Master, CZECH TECHNICAL UNIVERSITY IN PRAGUE.
- Eric Lichtblau and R. Simon. (1995). "Report Blames Contractors for Tunnel Collapse." Retrieved October 20, 1995, from http://articles.latimes.com/1995-10-20/news/mn-59073_1_tunnel-collapse.
- Farina, P., L. Leoni, F. Babboni, F. Coppi, L. Mayer and P. Ricci IBIS-M, an innovative radar for monitoring slopes in open-pit mines.
- Fornaro, G., D. Reale and S. Verde (2013). "Bridge thermal dilation monitoring with millimeter sensitivity via multidimensional SAR imaging." Geoscience and Remote Sensing Letters, IEEE **10**(4): 677-681.
- Fröhlich, C. and M. Mettenleiter (2004). "Terrestrial laser scanning—new perspectives in 3D surveying." International archives of photogrammetry, remote sensing and spatial information sciences **36**(Part 8): W2.
- Franzius, J. N. (2003). Behaviour of buildings due to tunnel induced subsidence, University of London.
- Fu, H. (2006). Study on ground subsidence due to construction of metro tunnel with un-pumping construction method. Doctor Degree Dissertation, Southwest Jiaotong University, China.
- Gernhardt, S. and R. Bamler (2012). "Deformation monitoring of single buildings using meter-resolution SAR data in PSI." ISPRS Journal of Photogrammetry and Remote Sensing **73**(0): 68-79.
- Getachew, A. (2003). "Traffic load effects on bridges, statistical analysis of collected and Monte Carlo simulated vehicle data."
- Ghilani, C. D. and W. R. Paul (2010). Adjustment computations: spatial data analysis, John Wiley & Sons.
- Ghorbani, M., M. Sharifzadeh, S. Yasrobi and M. Daiyan (2012). "Geotechnical, structural and geodetic measurements for conventional tunnelling hazards in urban areas—The case of Niayesh road tunnel project." Tunnelling and Underground Space Technology **31**: 1-8.
- Gili, J. A., J. Corominas and J. Rius (2000). "Using Global Positioning System techniques in landslide monitoring." Engineering Geology **55**(3): 167-192.
- Gili, J. A., M. d. L. N. Lantada, M. A. Núñez, Z. Lian, I. Zabaleta Zenarrutzabeitia, C. Puig i Polo, D. Tamagnan and L. Alonso (2013). Long term real scale experiment to assess the thermal effects on the deformation monitoring of buildings. A Joint

- International Symposium on Deformation Monitoring. "2nd Joint International Symposium on Deformation Monitoring (JISDM). Nottingham UK: 1-3.
- Gordon, S., D. Lichti, J. Franke and M. Stewart (2004). Measurement of structural deformation using terrestrial laser scanners. 1st FIG International Symposium on Engineering Surveys for Construction Works and Structural Engineering, Nottingham, United Kingdom.
- Gordon, S. J., D. Lichti, M. Stewart and J. Franke (2005). Structural deformation measurement using terrestrial laser scanners, Curtin University of Technology.
- Grinzato, E., P. G. Bison and S. Marinetti (2002). "Monitoring of ancient buildings by the thermal method." Journal of Cultural Heritage **3**(1): 21-29.
- Grosso, A. d. and F. Lanata (2013). "A long-term static monitoring experiment on RC beams: damage identification under environmental effect." Structure and Infrastructure Engineering(ahead-of-print): 1-10.
- Guo, J., L. Xu, L. Dai, M. McDonald, J. Wu and Y. Li (2005). "Application of the real-time kinematic Global Positioning System in bridge safety monitoring." Journal of Bridge Engineering **10**(2): 163-168.
- Hampshire, T. A. and H. Adeli (2000). "Monitoring the behavior of steel structures using distributed optical fiber sensors." Journal of Constructional Steel Research **53**(3): 267-281.
- Harvey, B. R. (1994). "Computer Based Learning and Least Squares Analysis." Australian Journal of Geodesy Photogrammetry and Surveying: 21-32.
- Herrera, G., J. A. Fernández-Merodo, J. Mulas, M. Pastor, G. Luzi and O. Monserrat (2009). "A landslide forecasting model using ground based SAR data: The Portalet case study." Engineering Geology **105**(3): 220-230.
- Hill, C. D. and K. D. Sippel (2002). Modern deformation monitoring: A multi sensor approach. FIG XXII International Congress. Washington, DC USA.
- Hisatake, M. (2011). "A proposed methodology for analysis of ground settlements caused by tunneling, with particular reference to the "buoyancy" effect." Tunnelling and Underground Space Technology **26**(1): 130-138.
- Iglesias, R., J. J. Mallorqui, D. Monells, C. López-Martínez, X. Fabregas, A. Aguasca, J. A. Gili and J. Corominas (2015). "PSI Deformation Map Retrieval by Means of Temporal Sublook Coherence on Reduced Sets of SAR Images." Remote Sensing **7**(1): 530-563.
- Intrieri, E., F. Di Traglia, C. Del Ventisette, G. Gigli, F. Mugnai, G. Luzi and N. Casagli (2013). "Flank instability of Stromboli volcano (Aeolian Islands, Southern Italy): integration of GB-InSAR and geomorphological observations." Geomorphology **201**: 60-69.
- James, G. (2003). Analysis of traffic load effects an railway bridges. Doctoral, Royal Institute of Technology.
- Junhuan, P. (2005). "The asymptotic variance–covariance matrix, Baarda test and the reliability of L1-norm estimates." Journal of Geodesy **78**(11-12): 668-682.
- Karoumi, R., J. Wiberg and A. Liljencrantz (2005). "Monitoring traffic loads and dynamic effects using an instrumented railway bridge." Engineering Structures **27**(12): 1813-1819.
- Kijewski-Correa, T. and M. Kochly (2007). "Monitoring the wind-induced response of tall buildings: GPS performance and the issue of multipath effects." Journal of Wind Engineering and Industrial Aerodynamics **95**(9–11): 1176-1198.
- Kontogianni, V. A. and S. C. Stiros (2005). "Induced deformation during tunnel excavation: evidence from geodetic monitoring." Engineering geology **79**(1): 115-126.

- Koo, K., J. Brownjohn, D. List and R. Cole (2012). "Structural health monitoring of the Tamar suspension bridge." Structural Control and Health Monitoring.
- Kowalczyk, K. and J. Rapinski (2014). "Investigating the Error Sources in Reflectorless EDM." Journal of Surveying Engineering **140**(4): 06014002.
- López, R. B., A. G. Tapia, J. A. Gili, F. L. Pros and J. J. B. Martínez (2012). Nivelación de la estación GPS de la torre de control y del mareógrafo de la Autoridad Portuaria de Barcelona. Congreso Iberoamericano de Geomática y Ciencias de la Tierra. Madrid, Ilustre Colegio Oficial de Ingenieros Técnicos en Topografía de España.
- Lantada, M. d. L. N., M. A. Núñez, J. A. Gili, F. Buill Pozuelo, C. Puig i Polo, I. Zabaleta Zenarrutzabeitia, J. Rodríguez Jordana and G. Luzi (2012). "Ensayo a escala real de varias técnicas geomáticas de monitorización de movimientos de edificios."
- Lantada, N., A. Núñez, J. A. Gili, F. Buill, C. Puig, I. Zabaleta and J. J. Rodríguez (2012). Ensayo a escala real de varias técnicas geomáticas de monitorización de movimientos de edificios. Congreso Iberoamericano de Geomática y Ciencias de la Tierra. Madrid, Ilustre Colegio Oficial de Ingenieros Técnicos en Topografía de España.
- Law, R. H.-c. (2001). Effect of existing building on tunneling-induced ground movements, Massachusetts Institute of Technology.
- Lehman, S. (2007). "Bodies Found in Sao Paulo Subway Crater." Retrieved January 15, 2007, from http://www.washingtonpost.com/wp-dyn/content/article/2007/01/15/AR2007011500678_pf.html.
- Leva, D., G. Nico, D. Tarchi, J. Fortuny-Guasch and A. J. Sieber (2003). "Temporal analysis of a landslide by means of a ground-based SAR interferometer." Geoscience and Remote Sensing, IEEE Transactions on **41**(4): 745-752.
- Leva, D., C. Rivolta, S. Kuzuoka and T. Mizuno (2005). Using a ground based interferometric synthetic aperture radar (GBinSAR) sensor to monitor a landslide in Japan, IEEE.
- Li, H.-N., D.-S. Li and G.-B. Song (2004). "Recent applications of fiber optic sensors to health monitoring in civil engineering." Engineering Structures **26**(11): 1647-1657.
- Li, H., S. Li, J. Ou and H. Li (2010). "Modal identification of bridges under varying environmental conditions: temperature and wind effects." Structural Control and Health Monitoring **17**(5): 495-512.
- Li, X., L. Ge, E. Ambikairajah, C. Rizos, Y. Tamura and A. Yoshida (2006). "Full-scale structural monitoring using an integrated GPS and accelerometer system." GPS Solutions **10**(4): 233-247.
- Lovse, J., W. Teskey, G. Lachapelle and M. Cannon (1995). "Dynamic Deformation Monitoring of Tall Structure Using GPS Technology." Journal of Surveying Engineering **121**(1): 35-40.
- Malet, J.-P., P. Ulrich, A. Déprez, F. Masson, C. Lissak and O. Maquaire (2011). Continuous monitoring and near-real time processing of GPS observations for landslide analysis: a methodological framework. Proceedings of the Second World Landslide Forum.
- Malet, J. P., O. Maquaire and E. Calais (2002). "The use of Global Positioning System techniques for the continuous monitoring of landslides: application to the Super-Sauze earthflow (Alpes-de-Haute-Provence, France)." Geomorphology **43**(1-2): 33-54.
- Mananjara, H.-P. (2011). Automatic monitoring in extreme heat conditions. 8th International Symposium on Field Measurements in GeoMechanics. Berlin, Germany.
- Matthias Bartsch, Andrea Brandt, Guido Kleinhubert and M. Schreiber. (2009). "Cologne Archive Catastrophe: Were Subway Builders Cautious Enough?" Retrieved March 09, 2009, from <http://www.spiegel.de/international/germany/cologne-archive-catastrophe-were-subway-builders-cautious-enough-a-612129.html>.

- Monserrat, O. and M. Crosetto (2008). "Deformation measurement using terrestrial laser scanning data and least squares 3D surface matching." ISPRS Journal of Photogrammetry and Remote Sensing **63**(1): 142-154.
- Monserrat, O., M. Crosetto and G. Luzi (2014). "A review of ground-based SAR interferometry for deformation measurement." ISPRS Journal of Photogrammetry and Remote Sensing **93**(0): 40-48.
- Morris, H., M. Wang and X. Zhu (2012). Deformations and loads in an LVL building with 3-storey post-tensioned shear walls. World Conference on Timber Engineering, 15 - 19 July 2012: 8.
- Mosalam, K. M., S. M. Takhirov and S. Park (2014). "Applications of laser scanning to structures in laboratory tests and field surveys." Structural Control and Health Monitoring **21**(1): 115-134.
- Mosavi, A., H. Sedarat and M. Guimaraes (2011). Review of fiber optic sensors for monitoring structures in the nuclear industry. 5th International Conference on Structural Health Monitoring of Intelligent Infrastructure (SHMII-5) 2011 11-15 December 2011, Cancún, México.
- Moschas, F. and S. Stiros (2011). "Measurement of the dynamic displacements and of the modal frequencies of a short-span pedestrian bridge using GPS and an accelerometer." Engineering Structures **33**(1): 10-17.
- O'Connor, A. and E. J. O'Brien (2005). "Traffic load modelling and factors influencing the accuracy of predicted extremes." Canadian Journal of Civil Engineering **32**(1): 270-278.
- Ogaja, C., J. Wang and C. Rizos (2003). "Detection of Wind-Induced Response by Wavelet Transformed GPS Solutions." Journal of Surveying Engineering **129**(3): 99-104.
- Park, H., Y. Shin, S. Choi and Y. Kim (2013). "An Integrative Structural Health Monitoring System for the Local/Global Responses of a Large-Scale Irregular Building under Construction." Sensors **13**(7): 9085-9103.
- Park, H. S., H. M. Lee, H. Adeli and I. Lee (2007). "A New Approach for Health Monitoring of Structures: Terrestrial Laser Scanning." Computer-Aided Civil and Infrastructure Engineering **22**(1): 19-30.
- Park, H. S., H. G. Sohn, I. S. Kim and J. H. Park (2008). "Application of GPS to monitoring of wind - induced responses of high - rise buildings." The Structural Design of Tall and Special Buildings **17**(1): 117-132.
- Peeters, B. and G. De Roeck (2001). "One-year monitoring of the Z 24-Bridge: environmental effects versus damage events." Earthquake engineering & structural dynamics **30**(2): 149-171.
- Pieraccini, M. (2013). "Monitoring of Civil Infrastructures by Interferometric Radar: A Review." The Scientific World Journal **2013**: 8.
- Pieraccini, M., G. Luzi, D. Mecatti, M. Fratini, L. Noferini, L. Carissimi, G. Franchioni and C. Atzeni (2004). "Remote sensing of building structural displacements using a microwave interferometer with imaging capability." NDT & E International **37**(7): 545-550.
- Psimoulis, P., S. Pytharouli, D. Karambalis and S. Stiros (2008). "Potential of Global Positioning System (GPS) to measure frequencies of oscillations of engineering structures." Journal of Sound and Vibration **318**(3): 606-623.
- Psimoulis, P. A. and S. C. Stiros (2007). "Measurement of deflections and of oscillation frequencies of engineering structures using Robotic Theodolites (RTS)." Engineering Structures **29**(12): 3312-3324.

- Psimoulis, P. A. and S. C. Stiros (2013). "Measuring Deflections of a Short-Span Railway Bridge Using a Robotic Total Station." Journal of Bridge Engineering **18**(2): 182-185.
- Reale, D., G. Fornaro, A. Pauciuolo, X. Zhu and R. Bamler (2011). "Tomographic imaging and monitoring of buildings with very high resolution SAR data." Geoscience and Remote Sensing Letters, IEEE **8**(4): 661-665.
- RIBA. (2015). "Last accessed September 2015." from <http://www.architecture.com/RIBA/Aboutus/SustainabilityHub/Designstrategies/Earth/1-1-3-2-Buildingorientation.aspx>.
- Roberts, G., X. Meng and A. Dodson (2004). "Integrating a Global Positioning System and Accelerometers to Monitor the Deflection of Bridges." Journal of Surveying Engineering **130**(2): 65-72.
- Salimi, A., M. Esmaili and B. Salehi (2013). "Analysis of a TBM Tunneling Effect on Surface Subsidence: A Case Study from Tehran, Iran." World Academy of Science, Engineering and Technology **8**: 11.
- Schneider, D. (2006). Terrestrial laser scanning for area based deformation analysis of towers and water dams. 3rd IAG / 12th FIG Symposium.
- Schwarz, C. R. and J. J. Kok (1993). "Blunder detection and data snooping in LS and robust adjustments." Journal of surveying engineering **119**(4): 127-136.
- Schwarz, H., F. Valdemarin and D. Tamagnan (2011). A network of robotic total stations to monitor the construction of Line 9 of Metro Barcelona the case of the double tunnel of Sagrera-Valdemarin. 8th International Symposium on Field Measurements in GeoMechanics, Berlin, Germany.
- Seco, A., F. Tirapu, F. Ramírez, B. García and J. Cabrejas (2007). "Assessing building displacement with GPS." Building and Environment **42**(1): 393-399.
- Slob, S. and R. Hack (2004). 3D terrestrial laser scanning as a new field measurement and monitoring technique. Engineering Geology for Infrastructure Planning in Europe, Springer: 179-189.
- Standing, J. and J. Burland (2008). "Impact of underground works on existing infrastructure." Post-Mining 2008.
- Stiros, S. C. and P. A. Psimoulis (2010). "Identification of nearshore wave characteristics using robotic total stations." Journal of Surveying Engineering **136**(4): 172-179.
- Stiros, S. C. and P. A. Psimoulis (2012). "Response of a historical short-span railway bridge to passing trains: 3-D deflections and dominant frequencies derived from Robotic Total Station (RTS) measurements." Engineering Structures **45**(0): 362-371.
- Talich, M., M. Glöckner, O. Böhm, F. Antoš, L. Soukup, J. Havrlant and J. Šolc (2014). The Application of the Ground-based InSAR Technique for the Deformation Monitoring of Concrete Hydropower Dam Orlík on Vltava River. 6th International Conference on Engineering Surveying.
- Tamura, Y., M. Matsui, L.-C. Pagnini, R. Ishibashi and A. Yoshida (2002). "Measurement of wind-induced response of buildings using RTK-GPS." Journal of Wind Engineering and Industrial Aerodynamics **90**(12-15): 1783-1793.
- Tapete, D., N. Casagli, G. Luzi, R. Fanti, G. Gigli and D. Leva (2013). "Integrating radar and laser-based remote sensing techniques for monitoring structural deformation of archaeological monuments." Journal of Archaeological Science **40**(1): 176-189.
- Tarchi, D., N. Casagli, R. Fanti, D. D. Leva, G. Luzi, A. Pasuto, M. Pieraccini and S. Silvano (2003). "Landslide monitoring by using ground-based SAR interferometry: an example of application to the Tessina landslide in Italy." Engineering Geology **68**(1): 15-30.

- Tarchi, D., H. Rudolf, G. Luzi, L. Chiarantini, P. Coppo and A. J. Sieber (1999). SAR interferometry for structural changes detection: a demonstration test on a dam, IEEE.
- Tarchi, D., H. Rudolf, M. Pieraccini and C. Atzeni (2000). "Remote monitoring of buildings using a ground-based SAR: application to cultural heritage survey." International Journal of Remote Sensing **21**(18): 3545-3551.
- Telegraph. (2013). "Sinkhole swallows whole building complex in China." Retrieved January 29, 2013, from <http://www.telegraph.co.uk/news/worldnews/asia/china/9833738/Sinkhole-swallows-whole-building-complex-in-China.html>.
- Tomás, R., M. Cano, J. García-Barba, F. Vicente, G. Herrera, J. M. Lopez-Sanchez and J. J. Mallorquí (2013). "Monitoring an earthfill dam using differential SAR interferometry: La Pedrera dam, Alicante, Spain." Engineering Geology **157**(0): 21-32.
- Tsakiri, M., D. Lichti and N. Pfeifer (2006). Terrestrial laser scanning for deformation monitoring. 3rd IAG / 12th FIG Symposium, Baden, Citeseer.
- Unzu, R., J. Nazabal, G. Vargas, R. Hernández, C. Fernández-Valdivielso, N. Urriza, M. Galarza and M. Lopez-Amo (2013). "Fiber optic and KNX sensors network for remote monitoring a new building cladding system." Automation in Construction **30**: 9-14.
- Urbain, T. S. e. S. (1997). UNDERGROUND WORKS IN URBAN ENVIRONMENT. XIVth International Conference on Soil Mechanics & Foundation Engineering, Germany, Hamburg.
- Van der Auweraer, H. and B. Peeters (2003). "Sensors and systems for structural health monitoring." Journal of structural control **10**(2): 117-125.
- van der Poel, J., E. Gastine and F. Kaalberg (2006). Monitoring for construction of the North/South metro line in Amsterdam, The Netherlands. Proc., 5th Int. Conf. on Geotechnical Aspects of Underground Construction in Soft Ground.
- Walker, G., A. Hitchcock, C. Rasmussen and D. Farnham (2006). "Monitoring the impact of tunnel construction on existing infrastructure and its successful implementation for the Airside Road Tunnel, Heathrow."
- Watson, C., T. Watson and R. Coleman (2007). "Structural Monitoring of Cable-Stayed Bridge: Analysis of GPS versus Modeled Deflections." Journal of Surveying Engineering **133**(1): 23-28.
- West, H. H. and L. F. Geshwindner (2002). Fundamentals of structural analysis(Second Edition), John Wiley & Sons, Incorporated.
- Wu, L., L. Wang, S. Su, X. Li, G. Wang, J. Wei, Q. Liu, L. Shen, Y. Dong and J. Qian (2004). Wireless sensor network based solution for nuclear radiation detection. Proceedings of the 5' World Congress on intelligent Control and Automation, Hangzhou, IEEE.
- Xia, Y., B. Chen, X. Zhou and Y. Xu (2012). "Field monitoring and numerical analysis of Tsing Ma Suspension Bridge temperature behavior." Structural Control and Health Monitoring.
- Xia, Y., H. Hao, G. Zanardo and A. Deeks (2006). "Long term vibration monitoring of an RC slab: Temperature and humidity effect." Engineering Structures **28**(3): 441-452.
- Xia, Y., P. Zhang, Y.-q. Ni and H.-p. Zhu (2014). "Deformation monitoring of a super-tall structure using real-time strain data." Engineering Structures **67**(0): 29-38.
- Xie, Z. and M. Gu (2009). "Across - wind dynamic response of high - rise building under wind action with interference effects from one and two tall buildings." The Structural Design of Tall and Special Buildings **18**(1): 37-57.
- Xu, C. and Q. Hu (2009). Dynamic structural monitoring using the kinematic positioning of a robotic total station. Electronic Measurement & Instruments, 2009. ICEMI'09. 9th International Conference on, IEEE.

- Xu, Y., B. Chen, C. Ng, K. Wong and W. Chan (2010). "Monitoring temperature effect on a long suspension bridge." Structural Control and Health Monitoring **17**(6): 632-653.
- Ye, X. W., Y. H. Su and J. P. Han (2014). "Structural Health Monitoring of Civil Infrastructure Using Optical Fiber Sensing Technology: A Comprehensive Review." The Scientific World Journal **2014**: 11.
- Yi, T. H., H. N. Li and M. Gu (2011). "Optimal sensor placement for structural health monitoring based on multiple optimization strategies." The Structural Design of Tall and Special Buildings **20**(7): 881-900.
- Yi, T. H., H. N. Li and M. Gu (2012). "Recent research and applications of GPS - based monitoring technology for high - rise structures." Structural Control and Health Monitoring.
- Yigit, C. O., C. Inal and M. Yetkin (2008). Monitoring of tall building's dynamic behaviour using precision inclination sensors. 13th FIG Symposium on Deformation Measurement and Analysis. 4th IAG Symposium on Geodesy for Geotechnical and Structural Engineering. Lisbon, Portugal.
- Yuen, K.-V. and S.-C. Kuok (2010). "Ambient interference in long-term monitoring of buildings." Engineering Structures **32**(8): 2379-2386.
- Zarikas, V., V. Gikas and C. P. Kitsos (2010). "Evaluation of the optimal design "cosinor model" for enhancing the potential of robotic theodolite kinematic observations." Measurement **43**(10): 1416-1424.
- ZC, M., C. Liao and R. Hwang (1994). "BUILDING PROTECTIDN FOR UNDERGROUND 'WORKS."
- Zhang, J.-F., J.-J. Chen, J.-H. Wang and Y.-F. Zhu (2013). "Prediction of tunnel displacement induced by adjacent excavation in soft soil." Tunnelling and Underground Space Technology **36**(0): 24-33.
- Zhang, L., X. Wu, Q. Chen and M. J. Skibniewski (2014). "Towards a safety management approach for adjacent buildings in tunneling environments: case study in China." Building and Environment(0).
- Zhang, P., Y. Xia and Y. Ni (2012). Prediction of Temperature Induced Deformation of a Supertall Structure Using Structural Health Monitoring Data. 6th European Workshop on Structural Health Monitoring and 1st european conference of the prognostics and health management society 2012: 7.
- Zhou, H., J. Hu, X. Liu and P. Ren (2012). Ground deformation monitoring of Shenzhen metro area with Interferometric Point Target Analysis. Geoinformatics (GEOINFORMATICS), 2012 20th International Conference on, IEEE.
- Zhu, H. (2010). Analysis and Interactive Processing of the Subway Surface Subsidence Monitoring Data. Master Degree Dissertation, Xi'an University of Architecture and Technology, China.
- Zogg, H. M. and H. Ingensand (2008). "Terrestrial Laser Scanning for Deformation Monitoring–Load Tests on the Felsenau Viaduct (CH)." International Archives of Photogrammetry and Remote Sensing **37**: 555-562.

Annexes

LIST OF ANNEXES

A.I	Raw data of the least square adjustment test example in chapter 3.4.4	281
A.II	Results of the least square adjustment test example in chapter 3.4.4	290
A.III	Distance correction steps	295
A.IV	Computing Approximation Coordinates in the Resection Problem	298
A.V	Least Square Adjustment Principle	301
A.VI	Error Equations Linearization Using Taylor's Theorem	304
A.VII	W. Baarda test method	308
A.VIII	Ellipse of Error	310
A.IX	Local Stiffness Matrix for 3D Beam Elements	315
A.X	Transformation from local to global coordinates (3D structures)	318
A.XI	Thermal Effect Modelling Program	320

Annexes-I

A.I Raw data of the least square adjustment test example in chapter 3.4.4

Table 1 Reference Point Raw Data-- 1/9/2013 0:00

Reference Point	H	V	L	X	Y	Z
R14	331.061428	99.577935	37.111575	425873.1522	4582364.047	111.27366
R28	341.952867	99.678198	35.587703	425877.797	4582368.441	111.20751
R27	342.082107	96.639269	42.3246	425872.5696	4582372.598	113.2609
R12	299.060052	97.953872	93.285042	425812.7059	4582345.273	114.02529
R13	305.448174	97.690283	84.517504	425821.7798	4582353.869	114.09328
R19	2.453858	94.28903	67.68776	425908.5303	4582414.016	117.09156
R22	26.188291	94.398728	71.938616	425934.5864	4582412.332	117.34891
R18	384.921225	95.161931	58.952827	425892.1393	4582403.792	115.50347
R21	13.713525	94.675975	53.871795	425917.4071	4582399.093	115.52763
R23	36.407385	95.241131	58.188105	425937.3368	4582395.443	115.37324
R24	47.133913	95.450243	63.412966	425948.5993	4582393.343	115.55571
R17	383.153968	113.734919	61.126823	425890.3162	4582404.281	97.94174
R20	12.040394	115.135712	55.363806	425916.0481	4582399.497	97.98848

Table 2 Reference Point Raw Data-- 1/9/2013 3:00

Reference Point	H	V	L	X	Y	Z
R14	331.060981	99.577867	37.111621	425873.1522	4582364.047	111.27366
R28	341.952404	99.678126	35.587722	425877.797	4582368.441	111.20751
R27	342.081731	96.639217	42.32461	425872.5696	4582372.598	113.2609
R12	299.059923	97.953864	93.285209	425812.7059	4582345.273	114.02529
R13	305.448029	97.690275	84.517665	425821.7798	4582353.869	114.09328
R19	2.453621	94.289003	67.68769	425908.5303	4582414.016	117.09156
R22	26.188026	94.398697	71.938444	425934.5864	4582412.332	117.34891

Annexes-II

R18	384.921018	95.161905	58.952813	425892.1393	4582403.792	115.50347
R21	13.713144	94.675934	53.871743	425917.4071	4582399.093	115.52763
R23	36.407065	95.241078	58.187883	425937.3368	4582395.443	115.37324
R24	47.133685	95.450189	63.412665	425948.5993	4582393.343	115.55571
R17	383.153759	113.734888	61.126734	425890.3162	4582404.281	97.94174
R20	12.039971	115.13566	55.363786	425916.0481	4582399.497	97.98848

Table 3 Reference Point Raw Data-- 1/9/2013 6:00

Reference Point	H	V	L	X	Y	Z
R14	331.060569	99.577805	37.111664	425873.1522	4582364.047	111.27366
R28	341.951977	99.678062	35.58774	425877.797	4582368.441	111.20751
R27	342.081384	96.639168	42.32462	425872.5696	4582372.598	113.2609
R12	299.059804	97.953859	93.285362	425812.7059	4582345.273	114.02529
R13	305.447896	97.690269	84.517813	425821.7798	4582353.869	114.09328
R19	2.453403	94.288981	67.687625	425908.5303	4582414.016	117.09156
R22	26.187782	94.398669	71.938284	425934.5864	4582412.332	117.34891
R18	384.920828	95.161881	58.9528	425892.1393	4582403.792	115.50347
R21	13.712794	94.675896	53.871697	425917.4071	4582399.093	115.52763
R23	36.40677	95.241031	58.187677	425937.3368	4582395.443	115.37324
R24	47.133474	95.45014	63.412387	425948.5993	4582393.343	115.55571
R17	383.153566	113.734862	61.126652	425890.3162	4582404.281	97.94174
R20	12.039583	115.135612	55.363766	425916.0481	4582399.497	97.98848

Table 4 Reference Point Raw Data-- 1/9/2013 9:00

Reference Point	H	V	L	X	Y	Z
R14	331.061016	99.577872	37.111618	425873.1522	4582364.047	111.27366
R28	341.95244	99.678132	35.587721	425877.797	4582368.441	111.20751

Annexes-II

R27	342.081761	96.63922	42.324609	425872.5696	4582372.598	113.2609
R12	299.059932	97.953865	93.285196	425812.7059	4582345.273	114.02529
R13	305.44804	97.690276	84.517652	425821.7798	4582353.869	114.09328
R19	2.453639	94.289005	67.687696	425908.5303	4582414.016	117.09156
R22	26.188047	94.398699	71.938457	425934.5864	4582412.332	117.34891
R18	384.921034	95.161907	58.952813	425892.1393	4582403.792	115.50347
R21	13.713175	94.675936	53.871748	425917.4071	4582399.093	115.52763
R23	36.40709	95.241082	58.187899	425937.3368	4582395.443	115.37324
R24	47.133703	95.450193	63.412688	425948.5993	4582393.343	115.55571
R17	383.153775	113.734891	61.126741	425890.3162	4582404.281	97.94174
R20	12.040005	115.135664	55.363787	425916.0481	4582399.497	97.98848

Table 5 Reference Point Raw Data-- 1/9/2013 12:00

Reference Point	H	V	L	X	Y	Z
R14	331.062977	99.578168	37.111417	425873.1522	4582364.047	111.27366
R28	341.95447	99.678442	35.587638	425877.797	4582368.441	111.20751
R27	342.083407	96.63945	42.324567	425872.5696	4582372.598	113.2609
R12	299.060497	97.953895	93.284464	425812.7059	4582345.273	114.02529
R13	305.448676	97.690307	84.516947	425821.7798	4582353.869	114.09328
R19	2.454678	94.289117	67.688004	425908.5303	4582414.016	117.09156
R22	26.189208	94.398835	71.939214	425934.5864	4582412.332	117.34891
R18	384.92194	95.162018	58.952874	425892.1393	4582403.792	115.50347
R21	13.714842	94.676116	53.871971	425917.4071	4582399.093	115.52763
R23	36.408491	95.241309	58.188877	425937.3368	4582395.443	115.37324
R24	47.134704	95.450427	63.41401	425948.5993	4582393.343	115.55571
R17	383.154691	113.73502	61.127131	425890.3162	4582404.281	97.94174
R20	12.041854	115.13589	55.363879	425916.0481	4582399.497	97.98848

Annexes-II

Table 6 Reference Point Raw Data-- 1/9/2013 15:00

Reference Point	H	V	L	X	Y	Z
R14	331.063424	99.578234	37.111371	425873.1522	4582364.047	111.27366
R28	341.954934	99.678514	35.587618	425877.797	4582368.441	111.20751
R27	342.083783	96.639502	42.324557	425872.5696	4582372.598	113.2609
R12	299.060626	97.953902	93.284298	425812.7059	4582345.273	114.02529
R13	305.448821	97.690314	84.516786	425821.7798	4582353.869	114.09328
R19	2.454914	94.289142	67.688074	425908.5303	4582414.016	117.09156
R22	26.189473	94.398867	71.939387	425934.5864	4582412.332	117.34891
R18	384.922146	95.162043	58.952888	425892.1393	4582403.792	115.50347
R21	13.715223	94.676156	53.872021	425917.4071	4582399.093	115.52763
R23	36.408811	95.24136	58.189101	425937.3368	4582395.443	115.37324
R24	47.134932	95.450481	63.414312	425948.5993	4582393.343	115.55571
R17	383.1549	113.735049	61.127221	425890.3162	4582404.281	97.94174
R20	12.042276	115.13594	55.3639	425916.0481	4582399.497	97.98848

Table 7 Reference Point Raw Data-- 1/9/2013 18:00

Reference Point	H	V	L	X	Y	Z
R14	331.063939	99.578311	37.111317	425873.1522	4582364.047	111.27366
R28	341.955465	99.678594	35.587595	425877.797	4582368.441	111.20751
R27	342.084216	96.639562	42.324545	425872.5696	4582372.598	113.2609
R12	299.060774	97.95391	93.284106	425812.7059	4582345.273	114.02529
R13	305.448987	97.690323	84.5166	425821.7798	4582353.869	114.09328
R19	2.455188	94.289172	67.688155	425908.5303	4582414.016	117.09156
R22	26.189779	94.398903	71.939585	425934.5864	4582412.332	117.34891
R18	384.922385	95.162073	58.952903	425892.1393	4582403.792	115.50347

Annexes-II

R21	13.715663	94.676203	53.87208	425917.4071	4582399.093	115.52763
R23	36.40918	95.24142	58.189358	425937.3368	4582395.443	115.37324
R24	47.135196	95.450542	63.414659	425948.5993	4582393.343	115.55571
R17	383.155141	113.735083	61.127322	425890.3162	4582404.281	97.94174
R20	12.042763	115.135999	55.363924	425916.0481	4582399.497	97.98848

Table 8 Reference Point Raw Data-- 1/9/2013 21:00

Reference Point	H	V	L	X	Y	Z
R14	331.062184	99.578047	37.111498	425873.1522	4582364.047	111.27366
R28	341.95365	99.678317	35.58767	425877.797	4582368.441	111.20751
R27	342.082743	96.639357	42.324584	425872.5696	4582372.598	113.2609
R12	299.060269	97.953883	93.284759	425812.7059	4582345.273	114.02529
R13	305.448419	97.690295	84.517231	425821.7798	4582353.869	114.09328
R19	2.454259	94.289072	67.687879	425908.5303	4582414.016	117.09156
R22	26.18874	94.39878	71.938908	425934.5864	4582412.332	117.34891
R18	384.921575	95.161973	58.95285	425892.1393	4582403.792	115.50347
R21	13.714169	94.676043	53.87188	425917.4071	4582399.093	115.52763
R23	36.407926	95.241217	58.188482	425937.3368	4582395.443	115.37324
R24	47.134301	95.450332	63.413477	425948.5993	4582393.343	115.55571
R17	383.154321	113.734968	61.126973	425890.3162	4582404.281	97.94174
R20	12.041109	115.135798	55.363842	425916.0481	4582399.497	97.98848

Annexes-II

Table 9 Control Point Raw Data-- 1/9/2013 0:00

Control Point	H	V	L
CP1	149.58028	122.339268	48.714308
CP2	166.389053	122.129772	49.115008
CP3	174.406149	121.628693	50.451336
CP4	149.612223	115.610129	47.155618
CP5	166.300098	115.456062	47.562607
CP6	174.394468	115.040585	48.915501
CP7	149.656101	109.371867	46.239795
CP8	166.281621	108.506872	46.581145
CP9	174.381113	108.257902	47.957887

Table 10 Control Point Raw Data-- 1/9/2013 3:00

Control Point	H	V	L
CP1	149.580661	122.339247	48.714285
CP2	166.389369	122.129707	49.115077
CP3	174.406438	121.62861	50.451449
CP4	149.6126	115.610131	47.1556
CP5	166.300427	115.456029	47.562688
CP6	174.394768	115.040539	48.91563
CP7	149.656478	109.37188	46.239777
CP8	166.28197	108.506865	46.581232
CP9	174.381447	108.257886	47.958024

Annexes-II

Table 11 Control Point Raw Data-- 1/9/2013 6:00

Control Point	H	V	L
CP1	149.581011	122.339231	48.714264
CP2	166.389663	122.129648	49.115141
CP3	174.406704	121.628535	50.451554
CP4	149.612947	115.610132	47.155585
CP5	166.300728	115.455999	47.562763
CP6	174.395045	115.040496	48.91575
CP7	149.656826	109.371895	46.239761
CP8	166.28229	108.50686	46.581312
CP9	174.381738	108.257873	47.958151

Table 12 Control Point Raw Data-- 1/9/2013 9:00

Control Point	H	V	L
CP1	149.580631	122.339249	48.714287
CP2	166.389345	122.129712	49.115072
CP3	174.406416	121.628617	50.45144
CP4	149.61257	115.61013	47.155602
CP5	166.300401	115.456031	47.562682
CP6	174.394745	115.040542	48.91562
CP7	149.656448	109.37188	46.239778
CP8	166.281942	108.506866	46.581225
CP9	174.381422	108.257888	47.958014

Annexes-II

Table 13 Control Point Raw Data-- 1/9/2013 12:00

Control Point	H	V	L
CP1	149.578964	122.339334	48.714389
CP2	166.387955	122.129993	49.114766
CP3	174.405149	121.628973	50.45094
CP4	149.610918	115.61012	47.155677
CP5	166.298965	115.456175	47.562325
CP6	174.393428	115.040744	48.915053
CP7	149.654795	109.371813	46.239854
CP8	166.280419	108.506895	46.580842
CP9	174.380036	108.257952	47.957413

Table 14 Control Point Raw Data-- 1/9/2013 15:00

Control Point	H	V	L
CP1	149.578583	122.339352	48.714412
CP2	166.387637	122.130058	49.114697
CP3	174.40486	121.629054	50.450826
CP4	149.610542	115.610119	47.155693
CP5	166.298636	115.456207	47.562244
CP6	174.393128	115.040789	48.914924
CP7	149.654418	109.371799	46.23987
CP8	166.280071	108.506901	46.580756
CP9	174.379721	108.257966	47.957276

Annexes-II

Table 15 Control Point Raw Data-- 1/9/2013 18:00

Control Point	H	V	L
CP1	149.578145	122.339373	48.714441
CP2	166.387272	122.130131	49.114617
CP3	174.404527	121.629148	50.450696
CP4	149.610108	115.610114	47.155714
CP5	166.298259	115.456243	47.562151
CP6	174.392782	115.040842	48.914775
CP7	149.653983	109.37178	46.239891
CP8	166.279671	108.506908	46.580656
CP9	174.379356	108.257981	47.957118

Table 16 Control Point Raw Data-- 1/9/2013 21:00

Control Point	H	V	L
CP1	149.579637	122.339299	48.714349
CP2	166.388516	122.12988	49.11489
CP3	174.40566	121.628828	50.451142
CP4	149.611585	115.610123	47.155646
CP5	166.299543	115.456117	47.56247
CP6	174.393959	115.040662	48.915282
CP7	149.655463	109.37184	46.239823
CP8	166.281033	108.506883	46.580998
CP9	174.380595	108.257926	47.957656

A.II Results of the least square adjustment test example in chapter 3.4.4

Table 1 Result—RTS

Time	RTS-X	RTS-Y	RTS-Z
1/9/2013 0:00	425905.9326	4582346.65	111.02761
1/9/2013 3:00	425905.9328	4582346.65	111.027576
1/9/2013 6:00	425905.9329	4582346.65	111.027545
1/9/2013 9:00	425905.9327	4582346.65	111.027578
1/9/2013 12:00	425905.9319	4582346.649	111.027727
1/9/2013 15:00	425905.9318	4582346.649	111.027761
1/9/2013 18:00	425905.9315	4582346.649	111.0278
1/9/2013 21:00	425905.9323	4582346.65	111.027667

Table 2 Result—Control Point 1

Time	CP-1-X	CP-1-Y	CP-1-Z
1/9/2013 0:00	425938.4924	4582314.517	94.282201
1/9/2013 3:00	425938.4923	4582314.517	94.28219
1/9/2013 6:00	425938.4922	4582314.517	94.282178
1/9/2013 9:00	425938.4923	4582314.517	94.28219
1/9/2013 12:00	425938.4926	4582314.517	94.282243
1/9/2013 15:00	425938.4927	4582314.517	94.282256
1/9/2013 18:00	425938.4928	4582314.517	94.28227
1/9/2013 21:00	425938.4925	4582314.517	94.282222

Table 3 Result—Control Point 2

Time	CP-2-X	CP-2-Y	CP-2-Z
1/9/2013 0:00	425929.1955	4582306.76	94.296329
1/9/2013 3:00	425929.1955	4582306.76	94.296319
1/9/2013 6:00	425929.1955	4582306.76	94.296309
1/9/2013 9:00	425929.1955	4582306.76	94.296319
1/9/2013 12:00	425929.1957	4582306.761	94.296369
1/9/2013 15:00	425929.1957	4582306.761	94.296379
1/9/2013 18:00	425929.1958	4582306.761	94.296392
1/9/2013 21:00	425929.1956	4582306.76	94.296348

Table 4 Result—Control Point 3

Time	CP-3-X	CP-3-Y	CP-3-Z
1/9/2013 0:00	425924.5452	4582302.875	94.214979
1/9/2013 3:00	425924.5451	4582302.875	94.214969
1/9/2013 6:00	425924.5451	4582302.875	94.214959
1/9/2013 9:00	425924.5451	4582302.875	94.214969
1/9/2013 12:00	425924.5453	4582302.875	94.215019
1/9/2013 15:00	425924.5453	4582302.875	94.21503
1/9/2013 18:00	425924.5454	4582302.876	94.215042
1/9/2013 21:00	425924.5452	4582302.875	94.214999

Table 5 Result—Control Point 4

Time	CP-4-X	CP-4-Y	CP-4-Z
1/9/2013 0:00	425938.4758	4582314.501	99.580415
1/9/2013 3:00	425938.4757	4582314.501	99.580384
1/9/2013 6:00	425938.4756	4582314.501	99.580355
1/9/2013 9:00	425938.4757	4582314.501	99.580386
1/9/2013 12:00	425938.476	4582314.501	99.580524
1/9/2013 15:00	425938.4761	4582314.501	99.580555
1/9/2013 18:00	425938.4762	4582314.502	99.580593
1/9/2013 21:00	425938.4759	4582314.501	99.580469

Table 6 Result—Control Point 5

Time	CP-5-X	CP-5-Y	CP-5-Z
1/9/2013 0:00	425929.2464	4582306.801	99.593313
1/9/2013 3:00	425929.2463	4582306.801	99.593283
1/9/2013 6:00	425929.2463	4582306.801	99.593256
1/9/2013 9:00	425929.2463	4582306.801	99.593285
1/9/2013 12:00	425929.2465	4582306.802	99.593416
1/9/2013 15:00	425929.2466	4582306.802	99.593446
1/9/2013 18:00	425929.2467	4582306.802	99.593481
1/9/2013 21:00	425929.2465	4582306.801	99.593363

Table 7 Result—Control Point 6

Time	CP-6-X	CP-6-Y	CP-6-Z
1/9/2013 0:00	425924.5489	4582302.888	99.578193
1/9/2013 3:00	425924.5489	4582302.888	99.578163
1/9/2013 6:00	425924.5489	4582302.888	99.578136
1/9/2013 9:00	425924.5489	4582302.888	99.578166
1/9/2013 12:00	425924.5491	4582302.889	99.578296
1/9/2013 15:00	425924.5491	4582302.889	99.578327
1/9/2013 18:00	425924.5492	4582302.889	99.578361
1/9/2013 21:00	425924.549	4582302.889	99.578244

Table 8 Result—Control Point 7

Time	CP-7-X	CP-7-Y	CP-7-Z
1/9/2013 0:00	425938.4497	4582314.482	104.245074
1/9/2013 3:00	425938.4496	4582314.482	104.245033
1/9/2013 6:00	425938.4496	4582314.482	104.244993
1/9/2013 9:00	425938.4497	4582314.482	104.245035
1/9/2013 12:00	425938.45	4582314.483	104.245221
1/9/2013 15:00	425938.4501	4582314.483	104.245263
1/9/2013 18:00	425938.4502	4582314.483	104.245313
1/9/2013 21:00	425938.4499	4582314.483	104.245146

Table 9 Result—Control Point 8

Time	CP-8-X	CP-8-Y	CP-8-Z
1/9/2013 0:00	425929.257	4582306.81	104.821682
1/9/2013 3:00	425929.257	4582306.809	104.821641
1/9/2013 6:00	425929.2569	4582306.809	104.821603
1/9/2013 9:00	425929.257	4582306.809	104.821644
1/9/2013 12:00	425929.2572	4582306.81	104.821823
1/9/2013 15:00	425929.2573	4582306.81	104.821864
1/9/2013 18:00	425929.2574	4582306.81	104.821911
1/9/2013 21:00	425929.2571	4582306.81	104.821751

Table 10 Result—Control Point 9

Time	CP-9-X	CP-9-Y	CP-9-Z
1/9/2013 0:00	425924.5574	4582302.894	104.824192
1/9/2013 3:00	425924.5574	4582302.894	104.824152
1/9/2013 6:00	425924.5574	4582302.894	104.824114
1/9/2013 9:00	425924.5574	4582302.894	104.824154
1/9/2013 12:00	425924.5576	4582302.894	104.824333
1/9/2013 15:00	425924.5577	4582302.894	104.824374
1/9/2013 18:00	425924.5578	4582302.895	104.824422
1/9/2013 21:00	425924.5575	4582302.894	104.824261

A.III Distance correction steps

a) Calculate the Wet-bulb Temperature

The values that should be used to calculate the Wet-bulb temperature are

- Dry temperature (°C)
- Pressure (mbar)
- Relative humidity (%)

It shall be calculated using the following steps:

Saturation Vapor Pressure

$$SVP = 6.112 \times 10^{\left(\frac{7.5 \times T_{dry}^{\circ C}}{237.7 + T_{dry}^{\circ C}}\right)} \quad 1$$

Actual Vapor Pressure:

$$AVP = Hum_{rel\%} \times SVP \quad 2$$

Dewpoint Temperature:

$$Dewpt_{\circ C} = \frac{237.7 \times \ln\left(\frac{AVP}{6.112}\right)}{7.5 - \ln\left(\frac{AVP}{6.112}\right)} \quad 3$$

Gamma:

$$\chi = 0.00066 \times Patm_{mbar} \quad 4$$

Delta:

$$\delta = \frac{4098 \times AVP}{(Dewpt_{\circ C} + 237.7)^2} \quad 5$$

Wet-bulb temperature

$$Thum_{\circ C} = \frac{(\chi \times T_{sec_{\circ C}}) + (\delta \times Dewpt_{\circ C})}{\chi + \delta} \quad 6$$

b) Estimating parameter (No) for the distance meter

The standard conditions used to calculate the parameters for distance meter are:

- Dry temperature (°C)=12 °C
- Pressure (mbar)=1013.25
- Relative humidity (60%)
- Wavelength distance meter (Leica TCA2003/TCA 1800): $\lambda = .0850\mu\text{m}$

$$N_0=281.7$$

7

c) Calculate the distance correction

The data that used to measure the distance correction or gross distance D at each ETMA are:

- Dry temperature (°K)
- Pressure (mmHg)
- Wet-bulb temperature (°K)
- Wavelength distance meter (Leica TCA2003/TCA 1800): $\lambda = .0850\mu\text{m}$

Calculation of correction

The group refractive index N_{go} is determined rather experimentally than mathematically. Following equation 96 according to Barrell and Sears (Barrell and Sears 1939) was derived from experiments at wavelengths (λ) between 436 and 644nm and it was adopted by IUGG in Berkley in 1963(Dvořáček 2012).

$$N_{go} = 287.604 + \frac{4.8864}{\lambda^2} + \frac{0.0680}{\lambda^4}$$

8

It is valid for visible light in standard conditions (dry air, temperature 0 °C, pressure 1013.25hPa, 0.03 % CO₂). λ is the “effective” wavelength in vacuum in micrometers. Equation ** describes the group refractive index with an accuracy of 0.1 ppm or better. The formula can be used to calculate the group refractive index for wavelength to 900 nm (infra-red radiation) with the similar accuracy. The error of 5 nm in the wavelength causes an error of 0.3 ppm in the group refractive index.

If the temperature T_{sec} , barometric pressure P, and humidity of the air differ from the standard conditions, then the group refractive index N is calculated from

$$N = N_{go} \times \frac{273.15 \times P_{mmHg}}{760 \times T_{sec \circ K}} - CoefCorrHum$$

9

where $CoefCorrHum$ is the coefficient of correction of humidity.

If there is no sensor for humidity, we approximate:

$$CoefCorrhum \approx 0.6 \quad 10$$

If there is a sensor for humidity, we calculate:

$$CoefCorrhum = \frac{15.026 \times P_{vap}}{T_{sec^{\circ}K}} \quad 11$$

With

$$P_{vap} = P_s - 0.00067 \times P_{mmHg} \times (T_{sec^{\circ}K} - Thum^{\circ}K) \quad 12$$

And

$$P_s = e^{(1.53 + 0.07 \times Thum^{\circ}C - 0.000222 \times Thum^{\circ}C^2)} \quad 13$$

Final corrected distance

$$D_{corrected} = D_{initial} + D_{initial} \times (N_0 - N) \times 0.000001 \quad 14$$

A.IV Computing Approximation Coordinates in the Resection Problem

Consider the resection position computation for the occupied station A in Figure 1 having observed the three horizontal reading shown between station A and stations P₁, P₂ and P₃ whose positions are known. In order to determine the coordinates of station A, two angles 1 & 2 could be obtained. This is the method about known as “Potherot problem”. Using stations P₁, P₂ and P₃, a procedure to calculate the station A’s approximate coordinate values is as follows.

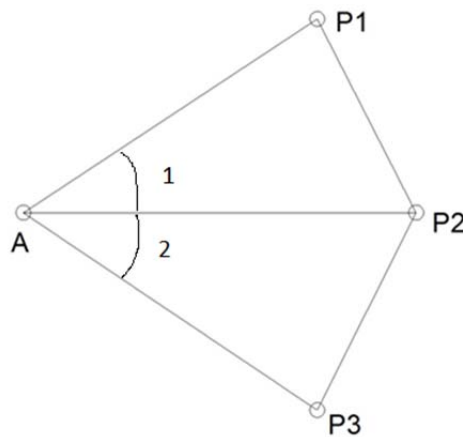


Figure 1 Indirect observation example

Let

$$\angle P_2 P_1 A + \angle A P_3 P_2 = G = 360^\circ - (\angle 1 + \angle 2 + \angle P_1 P_2 P_3) \quad 1$$

Using the sine law with triangle P₁ P₂ P₃,

$$\frac{P_2 A}{\sin \angle P_2 P_1 A} = \frac{P_1 P_2}{\sin \angle 1} \quad 2$$

And with triangle P₂ P₃ A,

$$\frac{P_2 A}{\sin \angle P_2 P_3 A} = \frac{P_3 P_2}{\sin \angle 2} \quad 3$$

Solving Equations 2 and 3 for P₂A and setting the resulting equations equal to each other yields

$$\frac{P_1 P_2 \sin \angle P_2 P_1 A}{\sin \angle 1} = \frac{P_3 P_2 \sin \angle P_2 P_3 A}{\sin \angle 2} \quad 4$$

From Equation 4, let H be defined as

$$H = \frac{\sin \angle P_2 P_1 A}{\sin \angle AP_3 P_2} = \frac{P_2 P_3 \sin \angle 1}{P_1 P_2 \sin \angle 2} \quad 5$$

From Equation 1,

$$\angle P_2 P_1 A = G - \angle AP_3 P_2 \quad 6$$

Solving Equation 5 for $\sin \angle P_2 P_1 A$ and substituting Equation 6 into the result yields

$$\sin(G - \angle AP_3 P_2) = H \sin \angle AP_3 P_2 \quad 7$$

From trigonometry,

$$\sin(\alpha - \beta) = \sin \alpha \cos \beta - \cos \alpha \sin \beta \quad 8$$

Applying this relationship to Equation 7 gives us

$$\sin(G - \angle AP_3 P_2) = \sin G \cos \angle AP_3 P_2 - \cos G \sin \angle AP_3 P_2 \quad 9$$

$$\sin(G - \angle AP_3 P_2) = H \sin \angle AP_3 P_2 \quad 10$$

Dividing Equation 10 by $\cos \angle AP_3 P_2$ and rearranging yields

$$\sin G = \tan \angle AP_3 P_2 (H + \cos G) \quad 11$$

Solving Equation 11 for $\angle AP_3 P_2$ yields

$$\angle AP_3 P_2 = \tan^{-1} \frac{\sin G}{H + \cos G} \quad 12$$

From Figure 1,

$$\angle P_3 P_2 A = 180^\circ - (\angle 2 + \angle AP_3 P_2) \quad 13$$

Again applying the law yields

$$AP_3 = \frac{P_3 P_2 \sin \angle P_3 P_2 A}{\sin \angle 2} \quad 14$$

Finally, the initial coordinates for station A are

$$x_A = x_{P_3} + AP_3 \sin(A_{Z_{P_3 P_2}} - \angle AP_3 P_2) \quad 15$$

$$y_A = y_{P_3} + AP_3 \cos(A_{Z_{P_3 P_2}} - \angle AP_3 P_2) \quad 16$$

A.V Least Square Adjustment Principle

Suppose that there are n observations, and its cofactor matrix Q equals P^{-1} , the number of necessary observation is t . For t independent factor \hat{X} , its approximate value is $\hat{X} = X^0 + \hat{x}$. And it is adjustment value of the observation that sum up the observation L and correction V , namely $\hat{L} = L + V$. Based on the adjustment problem, we can write the equations as follow,

$$L_i + v_i = a_i \hat{X}_1 + b_i \hat{X}_2 + \cdots + t_i \hat{X}_t + d_i \quad (i = 1, 2, 3, \dots, n) \quad 1$$

Let

$$L_{n,1} = [L_1 \quad L_2 \quad \cdots \quad L_n]^T \quad 2$$

$$V_{n,1} = [V_1 \quad V_2 \quad \cdots \quad V_n]^T \quad 3$$

$$\hat{X}_{n,1} = [\hat{X}_1 \quad \hat{X}_2 \quad \cdots \quad \hat{X}_n]^T \quad 4$$

$$d_{n,1} = [d_1 \quad d_2 \quad \cdots \quad d_n]^T \quad 5$$

$$B_{n,t} = \begin{bmatrix} a_1 & b_1 & \cdots & t_1 \\ a_2 & b_2 & \cdots & t_2 \\ \vdots & \vdots & \ddots & \vdots \\ a_n & b_n & \cdots & t_n \end{bmatrix} \quad 6$$

The equation 1 can be re-arranged into a matrix form

$$L + V = B\hat{X} + d \quad 7$$

Let

$$\hat{X} = X^0 + \hat{x} \quad 8$$

$$l = L - (BX^0 + d) \quad 9$$

The value of X^0 is the approximate value of the factor, so the error equation is

$$V = B\hat{x} - l \quad 10$$

Using the least squares theory with the error equation 10

$$\frac{\partial V^T P V}{\partial \hat{x}} = 2V^T P \frac{\partial V}{\partial \hat{x}} = V^T P B = 0 \quad 11$$

Transposition the equation 11,

$$B^T P V = 0 \quad 12$$

Solving Equation 10 for V and substituting Equation 10 onto Equation 12,

$$B^T P B \hat{x} - B^T P l = 0 \quad 13$$

Let

$$N_{bb} = B^T P B \quad 14$$

$$W = B^T P l \quad 15$$

The Equation 13 can be write as follows,

$$N_{bb} \hat{x} - W = 0 \quad 16$$

Equation 16 is normal equation of the indirect adjustment. In the equation the matrix N_{bb} is full rank matrix, it means $R(N_{bb}) = t$, and \hat{x} has only one solution,

$$\hat{x} = N_{bb}^{-1} W \quad 17$$

or

$$\hat{x} = (B^T P B)^{-1} W \quad 18$$

Substituting the solution of \hat{x} into Equation 10, the matrix V can be obtained. So the results of the indirect adjustment are

$$\hat{L} = L + V, \quad \hat{X} = X^0 + \hat{x} \quad 19$$

Specially, when matrix P is diagonal matrix, namely the relationship is independent between the observation values. Hence, the normal equation can be write in other form as follow,

$$\left. \begin{array}{l} [paa]\hat{x}_1 + [pab]\hat{x}_2 + \cdots + [pat]\hat{x}_t = [pal] \\ [pab]\hat{x}_1 + [pbb]\hat{x}_2 + \cdots + [pbt]\hat{x}_t = [pbl] \\ \vdots \\ [pat]\hat{x}_1 + [pbt]\hat{x}_2 + \cdots + [ptt]\hat{x}_t = [ptl] \end{array} \right\} 20$$

A.VI Error Equations Linearization Using Taylor's Theorem

When the error equation is not linearization, it needs to be linearized using the Taylor's theorem.

$$\widehat{L}_i = L_i + V_i = f_i(\widehat{X}_1, \widehat{X}_2, \dots, \widehat{X}_t) = f_i(X_1^0 + \widehat{x}_1, X_2^0 + \widehat{x}_2, \dots, X_t^0 + \widehat{x}_t) \quad 1$$

Equation 1 can be expanded using Taylor's theorem, and the higher order terms can be neglected because the correction \widehat{x}_t is small, giving the following linear approximation

$$v_i = \left(\frac{\partial f_i}{\partial \widehat{X}_1}\right)_0 \widehat{x}_1 + \left(\frac{\partial f_i}{\partial \widehat{X}_2}\right)_0 \widehat{x}_2 + \dots + \left(\frac{\partial f_i}{\partial \widehat{X}_t}\right)_0 \widehat{x}_t - (L_i - f_i(X_1^0, X_2^0, \dots, X_t^0)) \quad 2$$

Let,

$$a_i = \left(\frac{\partial f_i}{\partial \widehat{X}_1}\right)_0, b_i = \left(\frac{\partial f_i}{\partial \widehat{X}_2}\right)_0, \dots, t_i = \left(\frac{\partial f_i}{\partial \widehat{X}_t}\right)_0 \quad 3$$

$$l_i = L_i - f_i(X_1^0, X_2^0, \dots, X_t^0) = L_i - L_i^0 \quad 4$$

Where L_i^0 is the approximate value, the free term l_i is the observation value L_i minus its approximate value L_i^0 . So, the equation 2 can be written in the following form

$$v_i = a_i \widehat{x}_1 + b_i \widehat{x}_2 + \dots + t_i \widehat{x}_t - l_i \quad 5$$

where,

$$V = \begin{bmatrix} v_1 \\ v_2 \\ \vdots \\ v_t \end{bmatrix} \quad B = \begin{bmatrix} a_1 & b_1 \\ a_2 & b_2 \\ \vdots & \vdots \\ a_t & b_t \end{bmatrix} \quad \widehat{x} = \begin{bmatrix} \widehat{x}_1 \\ \widehat{x}_2 \\ \vdots \\ \widehat{x}_t \end{bmatrix} \quad l = \begin{bmatrix} l_1 \\ l_2 \\ \vdots \\ l_t \end{bmatrix} \quad 6$$

Equation 5 also can be expressed in matrix notation as

$$V = B\widehat{x} - l \quad 7$$

(a) Linear Observation Equation for Measured Angle

For the angle observation L_i (As shown in Figure 1), its observation equation is

$$L_i + v_i = \widehat{\alpha}_{jk} - \widehat{\alpha}_{jh} \quad 8$$

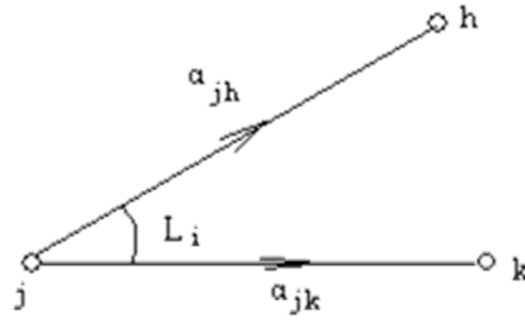


Figure 1 Angle observation example

Substituting

$$l_i = L_i - (\alpha_{jk}^0 - \alpha_{jh}^0) = L_i - L_i^0 \quad 9$$

Into the equation 8, the result is

$$v_i = \delta\alpha_{jk} - \delta\alpha_{jh} - l_i \quad 10$$

If all of the points h, j and k are unknown, equation 10 can be expressed in form as

$$v_i = \frac{\rho'' \Delta Y_{jk}^0}{(S_{jk}^0)^2} \hat{x}_j - \frac{\rho'' \Delta X_{jk}^0}{(S_{jk}^0)^2} \hat{y}_j - \frac{\rho'' \Delta Y_{jk}^0}{(S_{jk}^0)^2} \hat{x}_k + \frac{\rho'' \Delta X_{jk}^0}{(S_{jk}^0)^2} \hat{y}_k - \left\{ \frac{\rho'' \Delta Y_{jh}^0}{(S_{jh}^0)^2} \hat{x}_j - \frac{\rho'' \Delta X_{jh}^0}{(S_{jh}^0)^2} \hat{y}_j - \frac{\rho'' \Delta Y_{jh}^0}{(S_{jh}^0)^2} \hat{x}_h + \frac{\rho'' \Delta X_{jh}^0}{(S_{jh}^0)^2} \hat{y}_h \right\} - l_i \quad 11$$

Combining the similar items of the equation 11, the results is

$$v_i = \rho'' \left\{ \frac{\Delta Y_{jk}^0}{(S_{jk}^0)^2} - \frac{\Delta Y_{jh}^0}{(S_{jh}^0)^2} \right\} \hat{x}_j - \rho'' \left\{ \frac{\Delta X_{jk}^0}{(S_{jk}^0)^2} - \frac{X_{jh}^0}{(S_{jh}^0)^2} \right\} \hat{y}_j - \rho'' \frac{\Delta Y_{jk}^0}{(S_{jk}^0)^2} \hat{x}_k + \rho'' \frac{\Delta X_{jk}^0}{(S_{jk}^0)^2} \hat{y}_k + \rho'' \frac{\Delta Y_{jh}^0}{(S_{jh}^0)^2} \hat{x}_h - \rho'' \frac{\Delta X_{jh}^0}{(S_{jh}^0)^2} \hat{y}_h - l_i \quad 12$$

(b) Linear Observation Equation for Measured Distance

In the Figure 2, supposed that, the distance is L_i , and the factors of the coordinates adjustment value of the unknown points is \hat{X}_j , \hat{Y}_j , \hat{X}_k and \hat{Y}_k .

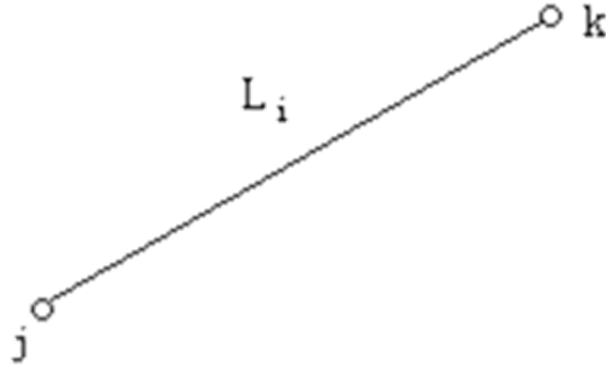


Figure 2 Distance observation example

Let

$$\hat{X}_j = X_j^0 + \hat{x}_j \quad 13$$

$$\hat{Y}_j = Y_j^0 + \hat{y}_j \quad 14$$

$$\hat{X}_k = X_k^0 + \hat{x}_k \quad 15$$

$$\hat{Y}_k = Y_k^0 + \hat{y}_k \quad 16$$

From the Figure 2, the adjustment equation of the distance L_i can be obtained

$$L_i = L_i + v_i = \sqrt{(\hat{X}_k - \hat{X}_j)^2 + (\hat{Y}_k - \hat{Y}_j)^2} \quad 17$$

Expand the equation 17 using the Taylor's equation,

$$L_i + v_i = S_{jk}^0 + \frac{\Delta X_{jk}^0}{S_{jk}^0} (\hat{x}_k - \hat{x}_j) + \frac{\Delta Y_{jk}^0}{S_{jk}^0} (\hat{y}_k - \hat{y}_j) \quad 18$$

Where

$$\Delta X_{jk}^0 = X_k^0 - X_j^0, \Delta Y_{jk}^0 = Y_k^0 - Y_j^0 \quad 19$$

$$S_{jk}^0 = \sqrt{(X_k^0 - X_j^0)^2 + (Y_k^0 - Y_j^0)^2} \quad 20$$

Let

$$l_i = L_i - S_{jk}^0 \quad 21$$

From the equation 18, the error equation of the distance is

$$v_i = -\frac{\Delta X_{jk}^0}{S_{jk}^0} \hat{x}_j - \frac{\Delta Y_{jk}^0}{S_{jk}^0} \hat{y}_j + \frac{\Delta X_{jk}^0}{S_{jk}^0} \hat{x}_k + \frac{\Delta Y_{jk}^0}{S_{jk}^0} \hat{y}_k - l_i \quad 22$$

A.VII W. Baarda test method

In practice surveying works, it is impossible that the data sets are free of blunders(Kowalczyk and Rapinski 2014). It means that blunders are those errors that occur rarely and have identifiable causes (Schwarz and Kok 1993, Junhuan 2005). The aim of blunder detection is looking for blunders in a set of observations and remove them from the data set. The method of W. Baarda(Baarda 1968) test has been introduced into the program to detect the outlier in observations.

The cofactor matrix

$$Q_{vv} = P^{-1} - BN^{-1}B^T \quad 1$$

where

$$N = B^T P B \quad 2$$

The variance factor of the unit weight can be computed from

$$\sigma_0^2 = \frac{V^T P V}{r} \quad 3$$

Or

$$\sigma_0 = \sqrt{\frac{V^T P V}{r}} \quad 4$$

Baarda first constructed the corresponding test statistic as follows,

$$\frac{v_i}{\sigma_0 \sqrt{q_{ii}}} \sim N(0,1) \quad 5$$

Here q_{ii} is the i -th diagonal element of the cofactor matrix Q_{vv} of the residuals.

If

$$\frac{|v_i|}{\sigma_0 \sqrt{q_{ii}}} > \text{rejection level} \quad 6$$

, the i -th observation is referred to as an outlier, and it will be removed from the data set. Here, we use the same criterion for rejection of blunders with Amer F.(Amer 1979) and Harvey B. R. (Harvey 1994), which is 3.29 as the rejection level in the program.

A.VIII Ellipse of Error

This annex develops the formulation to construct the ellipse of error in order to visualize the confidence region around the mathematically computed solution. This ellipse can be constructed just after the completion of a Least Square Adjustment, and use the covariance matrix as starting point.

Figure 1 shows the position error (Δ_φ) of point P at any direction in relation with the error PP' expressed in its X and Y components. Δ_φ can be calculated by the equation 1.

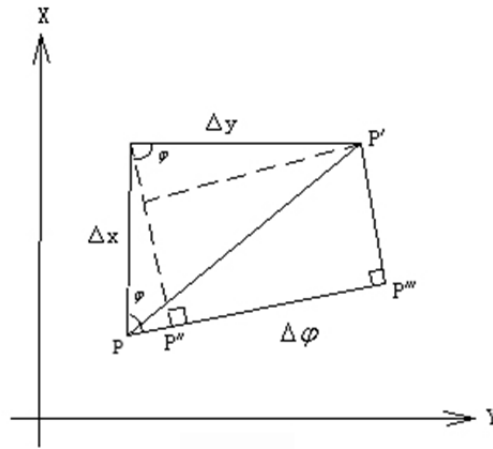


Figure 1 Relation between the error at point P (PP') and the projection of the error to any other direction defined by the angle φ (Δ_φ).

$$\Delta_\varphi = \overline{PP''} + \overline{P''P'''} = \Delta_x \cos \varphi + \Delta_y \sin \varphi \quad 1$$

According to the law of propagation of variances,

$$\begin{aligned} Q_{\varphi\varphi} &= Q_{xx} \cos^2 \varphi + Q_{yy} \sin^2 \varphi + 2Q_{xy} \sin \varphi \cos \varphi \\ &= Q_{xx} \cos^2 \varphi + Q_{yy} \sin^2 \varphi + Q_{xy} \sin 2\varphi \end{aligned} \quad 2$$

where $Q_{\varphi\varphi}$ is the covariance in the direction φ . We can express the same relationship in terms of variances, obtaining the variance in the direction φ is

$$\sigma_\varphi^2 = \sigma_0^2 Q_{\varphi\varphi} = \sigma_0^2 (Q_{xx} \cos^2 \varphi + Q_{yy} \sin^2 \varphi + Q_{xy} \sin 2\varphi) \quad 3$$

Simplifying the equation 3, we get

$$\hat{\sigma}_\varphi^2 = \hat{\sigma}_0^2 (Q_{xx} \cos^2 \varphi + Q_{yy} \sin^2 \varphi + Q_{xy} \sin 2\varphi) \quad 4$$

After finishing the adjustment all the values in the previous equation ($\hat{\sigma}_0^2, Q_{xx}, Q_{xy}, Q_{yy}$) are known and constant. So the value of $\hat{\sigma}_\varphi^2$ depends mainly on the direction of φ . In the following points (a) to (c) the steps to solve the basic data for the Ellipse (size and orientation) are given.

(a) Calculate the angle of φ_0

In order to find the angle that produces the extreme values of $Q_{\varphi\varphi}$, the partial derivatives of $Q_{\varphi\varphi}$ with respect to φ are equaled to zero, i.e.:

$$\frac{dQ_{\varphi\varphi}}{d\varphi} = 0 \quad 5$$

Substituting the equation 2 into 5,

$$\frac{d}{d\varphi} (Q_{xx} \cos^2 \varphi_E + Q_{yy} \sin^2 \varphi_E + Q_{xy} \sin 2\varphi_E) = 0 \quad 6$$

Expanding the equation 6,

$$\begin{aligned} -2Q_{xx} \cos \varphi_0 \sin \varphi_0 \\ + 2Q_{yy} \cos \varphi_0 \sin \varphi_0 + 2Q_{xy} \cos 2\varphi_0 = 0 \end{aligned} \quad 7$$

Reducing the equation 7 yields,

$$-(Q_{xx} - Q_{yy}) \sin 2\varphi_0 + 2Q_{xy} \cos 2\varphi_0 = 0 \quad 8$$

Finally, rearranging equation 8 yields

$$\tan 2\varphi_0 = \frac{2Q_{xy}}{(Q_{xx} - Q_{yy})} \quad 9$$

This equation delivers us the angle φ_0 that identifies the major axes of the ellipse. However, there is another solution which is

$$\tan 2\varphi_0 = \tan(2\varphi_0 + 180^\circ) \quad 10$$

Consequently, the equation 9 has two solutions, $\varphi = \varphi_0$, and $\varphi = \varphi_0 + 90^\circ$. The first solution produces, for instance, the maximum value for $Q_{\varphi\varphi}$, whereas the other produces the minimum.

(b) Confirm the direction of the angle φ_E and φ_F

This step is used to find the directions of the maximum and the minimum (φ_E for the maximum, φ_F for the minimum value).

Introducing some trigonometric identities ($\cos^2 \varphi_0 = \frac{1+\cos 2\varphi_0}{2}$, $\sin^2 \varphi_0 = \frac{1-\cos 2\varphi_0}{2}$, $\sin^2 2\varphi_0 = \frac{1}{1+\cot^2 2\varphi_0}$, $\cos^2 2\varphi_0 = \frac{1}{1+\tan^2 2\varphi_0}$) in Equation 2, we get:

$$\begin{aligned}
 Q_{\varphi\varphi} &= \left(Q_{xx} \frac{1 + \cos 2\varphi_0}{2} + Q_{yy} \frac{1 - \cos 2\varphi_0}{2} + Q_{xy} \sin 2\varphi_0 \right) \\
 &= \frac{1}{2} [(Q_{xx} + Q_{yy}) + (Q_{xx} - Q_{yy}) \cos 2\varphi_0 + 2 Q_{xy} \sin 2\varphi_0] \\
 &= \frac{1}{2} \left(Q_{xx} + Q_{yy} + \frac{2Q_{xy}}{\tan 2\varphi_0} \cos 2\varphi_0 + 2 Q_{xy} \sin 2\varphi_0 \right) \\
 &= \frac{1}{2} \{ (Q_{xx} + Q_{yy}) + 2(\cot^2 2\varphi_0 + 1) Q_{xy} \sin 2\varphi_0 \}
 \end{aligned} \tag{11}$$

In the equation 11, the first term ($Q_{xx} + Q_{yy}$) is always greater than zero, the second term being positive or negative,. When the second term is positive, $Q_{\varphi\varphi}$ produces the maximum value; conversely, $Q_{\varphi\varphi}$ produces the minimum value.

(1) Confirming the quadrant of the angle φ_E

When the second part of the equation 11 $2(\cot^2 2\varphi_0 + 1) Q_{xy} \sin 2\varphi_0 > 0$, $Q_{\varphi\varphi}$ produces the maximum value, and then $\varphi_0 = \varphi_E$. $(\cot^2 2\varphi_0 + 1)$ is always positive. The signs of Q_{xy} and $\sin 2\varphi_0$ are equal. It means that $Q_{xy} > 0$, $\sin 2\varphi_0 > 0$ or $Q_{xy} < 0$, $\sin 2\varphi_0 < 0$.

When $Q_{xy} > 0$, $\sin 2\varphi_0 > 0$, $0^\circ < 2\varphi_0 < 180^\circ$ or $0^\circ < \varphi_0 < 90^\circ$. Because $\sin 2\varphi_0 = \sin(2\varphi_0 + 360^\circ) = \sin 2(\varphi_0 + 180^\circ)$, for φ_0 and $\varphi_0 + 180^\circ$, theirs sin values are greater than zero. We can obtain φ_E located in the first and third quadrants.

When $Q_{xy} < 0$, $\sin 2\varphi_0 < 0$, $180^\circ < 2\varphi_0 < 360^\circ$ or $90^\circ < \varphi_0 < 180^\circ$. Similarly, we can obtain φ_E located in the second and fourth quadrants.

(2) Confirming the quadrant of the angle φ_F

When the second part of the equation 11 $2(\cot^2 2\varphi_0 + 1) Q_{xy} \sin 2\varphi_0 < 0$, $Q_{\varphi\varphi}$ gets the minimum value, and then $\varphi_0 = \varphi_F$.

The condition that the second part is negative is that if $Q_{xy}\sin 2\varphi_0$ is less than zero, namely, the signs of Q_{xy} and $\sin 2\varphi_0$ are different. It means that $Q_{xy} > 0, \sin 2\varphi_0 < 0$ or $Q_{xy} < 0, \sin 2\varphi_0 > 0$.

When $Q_{xy} > 0$ and $\sin 2\varphi_0 < 0$, it is $180^\circ < 2\varphi_0 < 360^\circ$ or $90^\circ < \varphi_0 < 180^\circ$. Theirs sin values are less than zero. We can obtain φ_F located in the second and fourth quadrants.

When $Q_{xy} < 0$ and $\sin 2\varphi_0 > 0$, it is $0^\circ < 2\varphi_0 < 180^\circ$ or $0^\circ < \varphi_0 < 90^\circ$. Similarly, we can obtain φ_F located in the first and third quadrants.

In summary, the method for confirming the quadrants of φ_E and φ_F is repeated here, in order, for convenience.

When $Q_{xy} > 0$, φ_E locates in the first and third quadrants, and φ_F locates in the second and fourth quadrants;

When $Q_{xy} < 0$, φ_E locates in the second and fourth quadrants, and φ_F locates in the first and third quadrants.

(c) Calculation of the maximum value, E, and the minimum value, F

The maximum value E and the minimum F correspond to the major and minor semi-axes. The values can be calculated by introducing the angles φ_E, φ_F into the equation 4.

$$\frac{|v_i|}{\sigma_0\sqrt{q_{ii}}} > rejection\ level \tag{12}$$

$$\frac{|v_i|}{\sigma_0\sqrt{q_{ii}}} > rejection\ level \tag{13}$$

There is another way to obtain the values of E and F:

From the trigonometric identity,

$$\sin 2\varphi_0 = \mp \frac{1}{\sqrt{1 + \cot^2 2\varphi_0}} \tag{14}$$

From equation 5, we can obtain

$$\cot^2 2\varphi_0 = \frac{(Q_{xx} - Q_{yy})^2}{4Q_{xy}^2} \quad 15$$

$$1 + \cot^2 2\varphi_0 = \frac{(Q_{xx} - Q_{yy})^2 + 4Q_{xy}^2}{4Q_{xy}^2} \quad 16$$

$$\sin 2\varphi_0 = \mp \frac{2Q_{xy}}{\sqrt{(Q_{xx} - Q_{yy})^2 + 4Q_{xy}^2}} \quad 17$$

Equation 16 also can be written into another form,

$$1 + \cot^2 2\varphi_0 = \frac{1}{\sin^2 2\varphi_0} \quad 18$$

Combing the equation 18, and substituting the equation 17 into equation 11, arranging the equations yields

$$Q_{\varphi\varphi} = \frac{1}{2} \left\{ (Q_{xx} + Q_{yy}) \mp \sqrt{(Q_{xx} - Q_{yy})^2 + 4Q_{xy}^2} \right\} \quad 19$$

Letting

$$H = \sqrt{(Q_{xx} - Q_{yy})^2 + 4Q_{xy}^2} \quad 20$$

The equation 19 has the general form

$$Q_{\varphi\varphi} = \frac{1}{2} \{ (Q_{xx} + Q_{yy}) \mp H \} \quad 21$$

where H is always greater than zero. So when the sign of H is positive, $Q_{\varphi\varphi}$ will produce the maximum value, otherwise, it will get the minimum value.

$$E^2 = \frac{1}{2} \hat{\sigma}_0^2 (Q_{xx} + Q_{yy} + H) \quad 22$$

$$F^2 = \frac{1}{2} \hat{\sigma}_0^2 (Q_{xx} + Q_{yy} - H) \quad 23$$

relates the forces at the i end (first subscript) to the displacement at the j end (second subscript). Similarly, $[k]_{ji}$ is a cross stiffness matrix relating the forces at the j end to the displacements at the i end.

The equation 1 can be further simplified as

$$\{F\} = [k]\{\delta\} \quad 6$$

where $\{F\}$ is the vector of the external forces on the member extremes, and $\{\delta\}$ is displacement vectors, and $[k]$ is the stiffness matrix of the beam. The matrix $[k]$ contains different coefficients depending on the type of structure as seen in this section. All the vectors are expressed in local reference system. They will be transformed to global in next section.

A.X Transformation from local to global coordinates (3D structures)

Before we can apply the equations of equilibrium we first have to convert all variables of the structure, so that they refer to a common, global system of coordinates.

The coefficients of the transformation matrix are formed by the cosines of the angles between the individual global and local systems (shown in Figure 1).

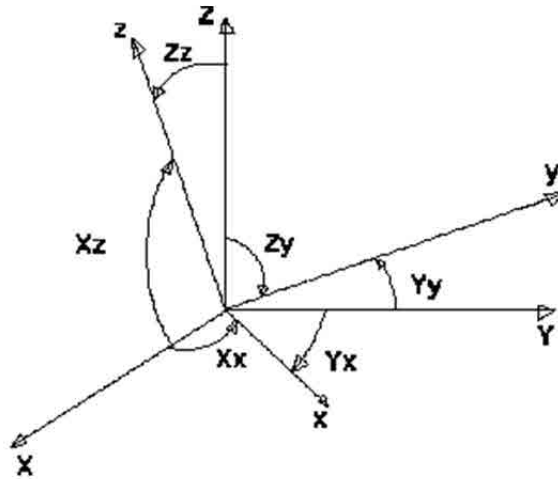


Figure 1 Angles between individual global and local systems

The transformation from local to global coordinates is made by two times multiplying the sub-matrices with the transformation matrix.

$$K = T^T k T \quad 1$$

where T is the transformation matrix between the global axis system (K) and local axis system (k). T is defined as

$$T = \begin{bmatrix} t & \mathbf{0} \\ \mathbf{0} & t \end{bmatrix} \quad 2$$

being

$$t = \begin{bmatrix} C_{Xx} & C_{Xy} & C_{Xz} \\ C_{Yx} & C_{Yy} & C_{Yz} \\ C_{Zx} & C_{Zy} & C_{Zz} \end{bmatrix} \quad 3$$

In this notation, the term (one example)

$$C_{Xx} = \cos\theta_{Xx} \quad 4$$

where angles θ_{Xx} , θ_{Yx} and θ_{Zx} etc. are measured from global axes X, Y and Z, with respect to the local axis x, y, and z respectively.

A.XI Thermal Effect Modelling Program

XI.1 Implementation Language and computer

(1) The Language of Technical Computing

MATLAB® is a high-level language and interactive environment for numerical computation, visualization, and programming. Using MATLAB, you can analyze data, develop algorithms, and create models and applications. The language, tools, and built-in math functions enable you to explore multiple approaches and reach a solution faster than with spreadsheets or traditional programming languages, such as C/C++ or Java®. You can use MATLAB for a range of applications, including signal processing and communications, image and video processing, control systems, test and measurement, computational finance, and computational biology. More than a million engineers and scientists in industry and academia use MATLAB, the language of technical computing.

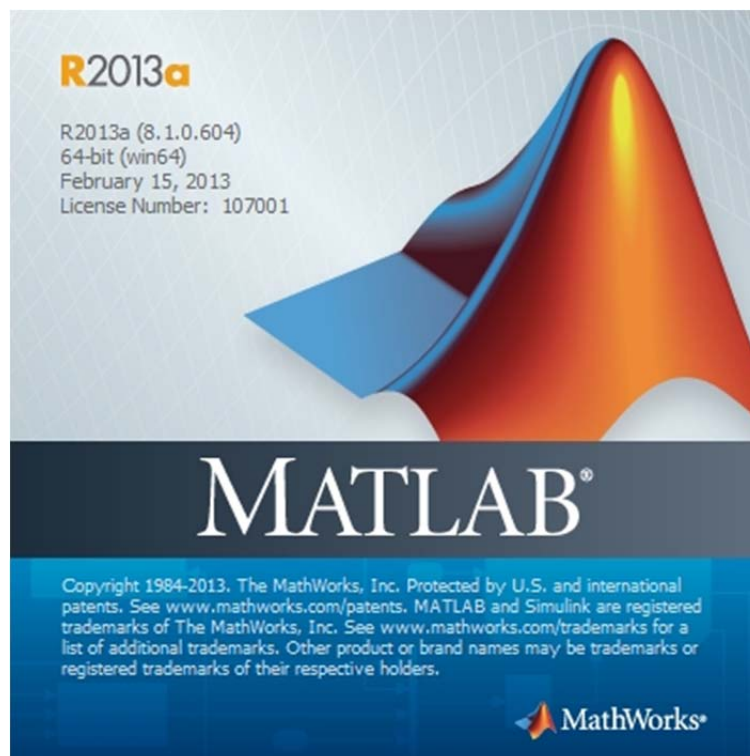


Figure 1 Matlab software

(2) Key Features of Matlab

- (a) High-level language for numerical computation, visualization, and application development

- (b) Interactive environment for iterative exploration, design, and problem solving
- (c) Mathematical functions for linear algebra, statistics, Fourier analysis, filtering, optimization, numerical integration, and solving ordinary differential equations
- (d) Built-in graphics for visualizing data and tools for creating custom plots
- (e) Development tools for improving code quality and maintainability and maximizing performance
- (f) Tools for building applications with custom graphical interfaces
- (g) Functions for integrating MATLAB based algorithms with external applications and languages such as C, Java, .NET, and Microsoft® Excel®

(3) System Requirements

Table 1 Matlab R2013a system requirements

Operating Systems	Processors	Disk Space	RAM
Windows 8.1 Windows 8 Windows 7 Service Pack 1 Windows Vista Service Pack 2 Windows XP Service Pack 3 Windows XP x64 Edition Service Pack 2 Windows Server 2012 Windows Server 2008 R2 Service Pack 1 Windows Server 2008 Service Pack 2	Any Intel or AMD x86 processor supporting SSE2 instruction set	1 GB for MATLAB only, 3–4 GB for a typical installation	1024 MB (At least 2048 MB recommended)

Operating Systems	Processors	Disk Space	RAM
Windows Server 2003 R2 Service Pack 2			

(4) Our computer

Windows Edition:

Windows 7 Enterprise

Product ID: 00392-918-5000002-85219

System:

Processor: Intel® Core™ i5-3470 CPU @ 3.20GHz 3.20GHz

Installed memory (RAM): 8.00GB

System type: 64-bit Operating System

Disk Space: 1T

XI.2 Structure model program code

XI.2.1 A6 structure model program code

```

% MATLAB codes for A6 model
tic

% clear memory
clear all

mon=10;
SetsNum=15;
insolationX8=load('c:\Model-Data\Insolation-X8-Oct.txt');

Diameter=0.3;
alfa=1.2e-5;
CI=0.02;
hc=1.45;
Mx=0;
My=0;

%Rotation angle between local system and global system

```

```

rotationA=315;

%read parameters of the structure
parameters=load('c:\Model-Data\A6\parameters.txt');

%read coordinates of each node of the structure
nodeCoordinates=load('c:\Model-Data\A6\nodeCoordinates.txt');

xx=nodeCoordinates(:,1);
yy=nodeCoordinates(:,2);
zz=nodeCoordinates(:,3);

% read the nodes of each element's start and end
elementNodes=load('c:\Model-Data\A6\elementNodes.txt');

numberNodes=size(nodeCoordinates,1);
numberElements=size(elementNodes,1);

% GDof: global number of degrees of freedom
GDof=6*numberNodes;

RowN=0;

for t=1:SetsNum

    a=(t-1)*24+1;
    b=t*24;
    Insolation=insolationX8(a:b,:);

    for tt=1:8

        Insolation360=Insolation((1+(tt-1)*3),4);

        % read force vector
        so=strcat('c:\Model-Data\A6-Force\F-',int2str(mon),'-
',int2str(t),'-',int2str(tt),'.txt');
        force=load(so);

        % calculation of the system stiffness matrix
        [stiffness]=...
            formStiffness3DframeRectangle01(GDof,numberElements,...
            elementNodes,numberNodes,nodeCoordinates,parameters);

        % boundary conditions and solution
        prescribedDof=[1,2,3,7,8,9,13,14,15,...
19,20,21,25,26,27,31,32,33,37,38,39,43,44,45,49,50,51,55,56,57,61,62,6
3,...
67,68,69,73,74,75,79,80,81,85,86,87,91,92,93,97,98,99,103,104,105,...
109,110,111,115,116,117,121,122,123,127,128,129,133,134,135,139,140,14
1,...
145,146,147,151,152,153,157,158,159,163,164,165,169,170,171,175,176,17
7,...];

        % solution
        displacements=solution(GDof,prescribedDof,stiffness,force);

        a=length(displacements);
        b=a/6;

```

```

dis=[b,6];
k=1;

for i=1:b
    for j=1:6
        dis(i,j)=displacements(k,1);
        k=k+1;
    end
end

DT=CI*Insolation360;
M=Diameter*(1-cos(alfa*hc*DT/Diameter))/(alfa*DT);

switch tt
    case 4
        Mx=-sin(60*pi()/180)*M;
        My=-cos(60*pi()/180)*M;
    case 5
        Mx=-sin(135*pi()/180)*M;
        My=-cos(135*pi()/180)*M;
    case 6
        Mx=-sin(210*pi()/180)*M;
        My=-cos(210*pi()/180)*M;
    case 7
        Mx=-sin(285*pi()/180)*M;
        My=-cos(285*pi()/180)*M;
end

RowN=RowN+1;

NodeMovement196(RowN,1)=mon;
NodeMovement196(RowN,2)=t;
NodeMovement196(RowN,3)=tt;

NodeMovement196(RowN,4)=dis(196,1)*cos(rotationA*pi/180)+dis(196,2)*sin(rotationA*pi/180)+Mx;
NodeMovement196(RowN,5)=-dis(196,1)*sin(rotationA*pi/180)+dis(196,2)*cos(rotationA*pi/180)+My;
NodeMovement196(RowN,6)=dis(196,3);

n1=size(dis,1);
s1=strcat('c:\Model-Data\A6-result','\dis-',int2str(mon),'-',int2str(t),'-',int2str(tt),'.txt');
fid1=fopen(s1,'w');
for ii=1:n1
    for jj=1:6
        fprintf(fid1,'%6f\t',dis(ii,jj));
        if rem(jj,6)==0
            fprintf(fid1,'\r\n');
        end
    end
end
end

fclose(fid1);

jj=1:GDof; format long
f=[jj; displacements'];

%drawing mesh and deformed shape

```

```

U=displacements;
clf

%%%%%%%%%%%%%%%%%%%%%%%%%%%%%%%%%%%%%%%%%%%%%%%%%%%%%%%%%%%%%%%%%%%%%%%%%%%%%%----draw A6--building

figure(1);

DrawStructure(nodeCoordinates+1000*[U(1:6:6*numberNodes)...
    U(2:6:6*numberNodes) U(3:6:6*numberNodes)],elementNodes);

hold on
% setting axis label and the title of the picture
xlabel('X');
ylabel('Y');
zlabel('Z');

switch tt

    case 1
        title(['3D-A6-Structure-Model--2013-',num2str(mon),'-
',num2str(t),' at 00:00']);
    case 2
        title(['3D-A6-Structure-Model--2013-',num2str(mon),'-
',num2str(t),' at 03:00']);
    case 3
        title(['3D-A6-Structure-Model--2013-',num2str(mon),'-
',num2str(t),' at 06:00']);
    case 4
        title(['3D-A6-Structure-Model--2013-',num2str(mon),'-
',num2str(t),' at 09:00']);
    case 5
        title(['3D-A6-Structure-Model--2013-',num2str(mon),'-
',num2str(t),' at 12:00']);
    case 6
        title(['3D-A6-Structure-Model--2013-',num2str(mon),'-
',num2str(t),' at 15:00']);
    case 7
        title(['3D-A6-Structure-Model--2013-',num2str(mon),'-
',num2str(t),' at 18:00']);
    case 8
        title(['3D-A6-Structure-Model--2013-',num2str(mon),'-
',num2str(t),' at 21:00']);
    end

%adding the numbers of every nodes
numbernoders=length(nodeCoordinates);
for i=1:numbernoders
    a=(i-1)*6;
    x1=nodeCoordinates(i,1)+1000*U((1+a),1);
    y1=nodeCoordinates(i,2)+1000*U((2+a),1);
    z1=nodeCoordinates(i,3)+1000*U((3+a),1);
    number=num2str(i);
    text(x1,y1,z1,number);
end

% setting the view point

axis([-5 45 -5 25 -5 25]);

```

```

hold off

view(-28,20);

saveas(gcf,['c:\Model-Data\A6-result-picture','\A6-movement-
',int2str(mon),'-',...
      int2str(t),'-',int2str(tt),'.bmp']);

%%%%%%%%%%-----draw Facade-SW

figure(2);
Nodedisplacement=nodeCoordinates+1000*[U(1:6:6*numberNodes)...
      U(2:6:6*numberNodes) U(3:6:6*numberNodes)];

DrawFacade(nodeCoordinates,elementNodes,Nodedisplacement,0,1);

hold on
% setting axis label and the title of the picture
xlabel('X');
ylabel('Y');
zlabel('Z');

switch tt

    case 1
        title(['3D-A6-Structure-Model-Facade-SW-2013-
',num2str(mon),'-',num2str(t),' at 00:00']);
    case 2
        title(['3D-A6-Structure-Model-Facade-SW-2013-
',num2str(mon),'-',num2str(t),' at 03:00']);
    case 3
        title(['3D-A6-Structure-Model-Facade-SW-2013-
',num2str(mon),'-',num2str(t),' at 06:00']);
    case 4
        title(['3D-A6-Structure-Model-Facade-SW-2013-
',num2str(mon),'-',num2str(t),' at 09:00']);
    case 5
        title(['3D-A6-Structure-Model-Facade-SW-2013-
',num2str(mon),'-',num2str(t),' at 12:00']);
    case 6
        title(['3D-A6-Structure-Model-Facade-SW-2013-
',num2str(mon),'-',num2str(t),' at 15:00']);
    case 7
        title(['3D-A6-Structure-Model-Facade-SW-2013-
',num2str(mon),'-',num2str(t),' at 18:00']);
    case 8
        title(['3D-A6-Structure-Model-Facade-SW-2013-
',num2str(mon),'-',num2str(t),' at 21:00']);
    end

%adding the numbers of every nodes
SWPlaneCoordinates=PlaneNodeCoordinates(nodeCoordinates,0,1);
SWnodenumber=size(SWPlaneCoordinates,1);
for i=1:SWnodenumber
    aa=SWPlaneCoordinates(i,1);
    a=(aa-1)*6;
    x1=SWPlaneCoordinates(i,2)+1000*U((1+a),1);

```

```

        y1=SWPlaneCoordinates(i,3)+1000*U((2+a),1)-0.4;
        z1=SWPlaneCoordinates(i,4)+1000*U((3+a),1)+0.4;
        number=num2str(aa);
        text(x1,y1,z1,number);
    end

    grid on
    axis([-5 45 -5 25 -5 20]);

    hold off

% setting the view point
    view(-90,0);

    saveas(gcf,['c:\Model-Data\A6-result-picture','\A6-movement-SW-
',int2str(mon),'-',...
        int2str(t),'-',int2str(tt),'.bmp']);

    %%%%%%%%%%-----draw Facade--NE

    figure(3);

    Nodedisplacement=nodeCoordinates+1000*[U(1:6:6*numberNodes)...
        U(2:6:6*numberNodes) U(3:6:6*numberNodes)];

    DrawFacade(nodeCoordinates,elementNodes,Nodedisplacement,38.94,1);

    hold on
    % setting axis label and the title of the picture
    xlabel('X');
    ylabel('Y');
    zlabel('Z');

    switch tt

        case 1
            title(['3D-A6-Structure-Model-Facade--NE-2013-
',num2str(mon),'-',num2str(t),' at 00:00']);
        case 2
            title(['3D-A6-Structure-Model-Facade--NE-2013-
',num2str(mon),'-',num2str(t),' at 03:00']);
        case 3
            title(['3D-A6-Structure-Model-Facade--NE-2013-
',num2str(mon),'-',num2str(t),' at 06:00']);
        case 4
            title(['3D-A6-Structure-Model-Facade--NE-2013-
',num2str(mon),'-',num2str(t),' at 09:00']);
        case 5
            title(['3D-A6-Structure-Model-Facade--NE-2013-
',num2str(mon),'-',num2str(t),' at 12:00']);
        case 6
            title(['3D-A6-Structure-Model-Facade--NE-2013-
',num2str(mon),'-',num2str(t),' at 15:00']);
    end

```

```

    case 7
        title(['3D-A6-Structure-Model-Facade--NE-2013-
',num2str(mon),'-',num2str(t),' at 18:00']);
    case 8
        title(['3D-A6-Structure-Model-Facade--NE-2013-
',num2str(mon),'-',num2str(t),' at 21:00']);
    end

    %adding the numbers of every nodes
    NEPlaneCoordinates=PlaneNodeCoordinates(nodeCoordinates,38.94,1);
    NEnodenummer=size(NEPlaneCoordinates,1);
    for i=1:NEnodenummer
        aa=NEPlaneCoordinates(i,1);
        a=(aa-1)*6;
        x1=NEPlaneCoordinates(i,2)+1000*U((1+a),1);
        y1=NEPlaneCoordinates(i,3)+1000*U((2+a),1)+0.4;
        z1=NEPlaneCoordinates(i,4)+1000*U((3+a),1)+0.4;
        number=num2str(aa);
        text(x1,y1,z1,number);
    end

    % setting the view point
    grid on
    axis([-5 45 -5 25 -5 20]);

    hold off

    view(90,0);
    saveas(gcf,['c:\Model-Data\A6-result-picture','\A6-movement-NE-
',int2str(mon),'-',...
        int2str(t),'-',int2str(tt),'.bmp']);

    %%%%%%%%%%%%%%%%%%%%%%%%%%%-----draw Facade--SE
    figure(4);

    Nodedisplacement=nodeCoordinates+1000*[U(1:6:6*numberNodes)...
        U(2:6:6*numberNodes) U(3:6:6*numberNodes)];

    DrawFacade(nodeCoordinates,elementNodes,Nodedisplacement,0,2);

    hold on
    % setting axis label and the title of the picture
    xlabel('X');
    ylabel('Y');
    zlabel('Z');

    switch tt

        case 1
            title(['3D-A6-Structure-Model-Facade--SE-2013-
',num2str(mon),'-',num2str(t),' at 00:00']);
        case 2
            title(['3D-A6-Structure-Model-Facade--SE-2013-
',num2str(mon),'-',num2str(t),' at 03:00']);
        case 3

```

```

        title(['3D-A6-Structure-Model-Facade--SE-2013-
',num2str(mon),'-',num2str(t),' at 06:00']);
        case 4
            title(['3D-A6-Structure-Model-Facade--SE-2013-
',num2str(mon),'-',num2str(t),' at 09:00']);
        case 5
            title(['3D-A6-Structure-Model-Facade--SE-2013-
',num2str(mon),'-',num2str(t),' at 12:00']);
        case 6
            title(['3D-A6-Structure-Model-Facade--SE-2013-
',num2str(mon),'-',num2str(t),' at 15:00']);
        case 7
            title(['3D-A6-Structure-Model-Facade--SE-2013-
',num2str(mon),'-',num2str(t),' at 18:00']);
        case 8
            title(['3D-A6-Structure-Model-Facade--SE-2013-
',num2str(mon),'-',num2str(t),' at 21:00']);
        end

    %adding the numbers of every nodes
    SEPlaneCoordinates=PlaneNodeCoordinates(nodeCoordinates,0,2);
    SEnodenumber=size(SEPlaneCoordinates,1);
    for i=1:SEnodenumber
        aa=SEPlaneCoordinates(i,1);
        a=(aa-1)*6;
        x1=SEPlaneCoordinates(i,2)+1000*U((1+a),1)+0.4;
        y1=SEPlaneCoordinates(i,3)+1000*U((2+a),1);
        z1=SEPlaneCoordinates(i,4)+1000*U((3+a),1)+0.4;
        number=num2str(aa);
        text(x1,y1,z1,number);
    end

    % setting the view point
    grid on
    axis([-5 45 -5 25 -5 20]);

    hold off

    view(0,0);
    saveas(gcf,['c:\Model-Data\A6-result-picture','\A6-movement-SE-
',int2str(mon),'-',...
        int2str(t),'-',int2str(tt),'.bmp']);

    %%%%%%%%%%%-----draw Facade--NW

    figure(5);

    Nodedisplacement=nodeCoordinates+1000*[U(1:6:6*numberNodes)...
        U(2:6:6*numberNodes) U(3:6:6*numberNodes)];

    DrawFacade(nodeCoordinates,elementNodes,Nodedisplacement,18.81,2);

    hold on
    % setting axis label and the title of the picture
    xlabel('X');
    ylabel('Y');
    zlabel('Z');

```

```

switch tt

    case 1
        title(['3D-A6-Structure-Model-Facade--NW-2013-
',num2str(mon),'-',num2str(t),' at 00:00']);
    case 2
        title(['3D-A6-Structure-Model-Facade--NW-2013-
',num2str(mon),'-',num2str(t),' at 03:00']);
    case 3
        title(['3D-A6-Structure-Model-Facade--NW-2013-
',num2str(mon),'-',num2str(t),' at 06:00']);
    case 4
        title(['3D-A6-Structure-Model-Facade--NW-2013-
',num2str(mon),'-',num2str(t),' at 09:00']);
    case 5
        title(['3D-A6-Structure-Model-Facade--NW-2013-
',num2str(mon),'-',num2str(t),' at 12:00']);
    case 6
        title(['3D-A6-Structure-Model-Facade--NW-2013-
',num2str(mon),'-',num2str(t),' at 15:00']);
    case 7
        title(['3D-A6-Structure-Model-Facade--NW-2013-
',num2str(mon),'-',num2str(t),' at 18:00']);
    case 8
        title(['3D-A6-Structure-Model-Facade--NW-2013-
',num2str(mon),'-',num2str(t),' at 21:00']);
    end

%adding the numbers of every nodes
NWPlaneCoordinates=PlaneNodeCoordinates(nodeCoordinates,18.81,2);
NWnodenumber=size(NWPlaneCoordinates,1);
for i=1:NWnodenumber
    aa=NWPlaneCoordinates(i,1);
    a=(aa-1)*6;
    x1=NWPlaneCoordinates(i,2)+1000*U((1+a),1)-0.4;
    y1=NWPlaneCoordinates(i,3)+1000*U((2+a),1);
    z1=NWPlaneCoordinates(i,4)+1000*U((3+a),1)+0.4;
    number=num2str(aa);
    text(x1,y1,z1,number);
end

% setting the view point
grid on
axis([-5 45 -5 25 -5 20]);

hold off

view(180,0);
saveas(gcf,['c:\Model-Data\A6-result-picture','\A6-movement-NW-
',int2str(mon),'-',...
    int2str(t),'-',int2str(tt),'.bmp']);

%%%%%%%%%%-----draw Facade--Top

figure(6);

Nodedisplacement=nodeCoordinates+1000*[U(1:6:6*numberNodes)...
    U(2:6:6*numberNodes) U(3:6:6*numberNodes)];

```

```

DrawFacade(nodeCoordinates,elementNodes,Nodedisplacement,16.15,3);

hold on
% setting axis label and the title of the picture
xlabel('X');
ylabel('Y');
zlabel('Z');

switch tt

    case 1
        title(['3D-A6-Structure-Model-Facade--Top-2013-'
,num2str(mon),'-',num2str(t),' at 00:00']);
    case 2
        title(['3D-A6-Structure-Model-Facade--Top-2013-'
,num2str(mon),'-',num2str(t),' at 03:00']);
    case 3
        title(['3D-A6-Structure-Model-Facade--Top-2013-'
,num2str(mon),'-',num2str(t),' at 06:00']);
    case 4
        title(['3D-A6-Structure-Model-Facade--Top-2013-'
,num2str(mon),'-',num2str(t),' at 09:00']);
    case 5
        title(['3D-A6-Structure-Model-Facade--Top-2013-'
,num2str(mon),'-',num2str(t),' at 12:00']);
    case 6
        title(['3D-A6-Structure-Model-Facade--Top-2013-'
,num2str(mon),'-',num2str(t),' at 15:00']);
    case 7
        title(['3D-A6-Structure-Model-Facade--Top-2013-'
,num2str(mon),'-',num2str(t),' at 18:00']);
    case 8
        title(['3D-A6-Structure-Model-Facade--Top-2013-'
,num2str(mon),'-',num2str(t),' at 21:00']);
    end

%adding the numbers of every nodes
TopPlaneCoordinates=PlaneNodeCoordinates(nodeCoordinates,16.15,3);
Topnodenumber=size(TopPlaneCoordinates,1);
for i=1:Topnodenumber
    aa=TopPlaneCoordinates(i,1);
    a=(aa-1)*6;
    x1=TopPlaneCoordinates(i,2)+1000*U((1+a),1);
    y1=TopPlaneCoordinates(i,3)+1000*U((2+a),1)+0.5;
    z1=TopPlaneCoordinates(i,4)+1000*U((3+a),1);
    number=num2str(aa);
    text(x1,y1,z1,number);
end

% setting the view point
grid on
axis([-5 45 -5 25 -5 25]);

hold off

view(0,90);

saveas(gcf,['c:\Model-Data\A6-result-picture','\A6-movement-Top-'
,int2str(mon),'-',...
,int2str(t),'-',int2str(tt),'.bmp']);

```

```

        end
    end

    %%%%%%%%%%Output the displacement of the RTS

    %%%%%%%%%%Node-196-RTS

        NM=NodeMovement196;
        nn=size(NM,1);
        s1=strcat('c:\Model-Data\A6-result','\NodeMovement-
',int2str(mon),'-Node-196-A6.txt');
        fid1=fopen(s1,'w');
        for ii=1:nn
            for jj=1:6
                fprintf(fid1,'%6f\t',NM(ii,jj));
                if rem(jj,6)==0
                    fprintf(fid1,'\r\n');
                end
            end
        end
        fclose(fid1);

Ta6model=toc    %%%record the running time

```

XI.2.2 B6 structure model program code

```

% MATLAB codes for B6 model
tic

% clear memory
clear all

mon=10;
SetsNum=15;

%Rotation angle between local system and global system
rotationA=315;

%read parameters of the structure
parameters=load('c:\Model-Data\B6\parameters.txt');

%read coordinates of each node of the structure
nodeCoordinates=load('c:\Model-Data\B6\nodeCoordinates.txt');

xx=nodeCoordinates(:,1);
yy=nodeCoordinates(:,2);
zz=nodeCoordinates(:,3);

% read the nodes of each element's start and end
elementNodes=load('c:\Model-Data\B6\elementNodes.txt');

numberNodes=size(nodeCoordinates,1);
numberElements=size(elementNodes,1);

```

```

% GDof: global number of degrees of freedom
GDof=6*numberNodes;

RowN=0;

for t=1:SetsNum

    for tt=1:8

        % read force vector
        so=strcat('c:\Model-Data\B6-Force\F-',int2str(mon),'-
',int2str(t),'-',int2str(tt),'.txt');
        force=load(so);

        % calculation of the system stiffness matrix
        [stiffness]=...
            formStiffness3DframeRectangle01(GDof,numberElements,...
            elementNodes,numberNodes,nodeCoordinates,parameters);

        % boundary conditions and solution
        prescribedDof=[1,2,3,7,8,9,13,14,15,19,20,21,25,26,27,31,32,33,...
            37,38,39,43,44,45,49,50,51,55,56,57,61,62,63,...
            67,68,69,73,74,75,79,80,81,85,86,87,91,92,93];

        % solution -- displacements: displacement vector
        displacements=solution(GDof,prescribedDof,stiffness,force);

        a=length(displacements);
        b=a/6;
        dis=[b,6];
        k=1;

        for i=1:b
            for j=1:6
                dis(i,j)=displacements(k,1);
                k=k+1;
            end
        end

        RowN=RowN+1;

        NodeMovement115(RowN,1)=mon;
        NodeMovement115(RowN,2)=t;
        NodeMovement115(RowN,3)=tt;

        NodeMovement115(RowN,4)=dis(115,1)*cos(rotationA*pi/180)+dis(115,2)*si
n(rotationA*pi/180);
        NodeMovement115(RowN,5)=-
dis(115,1)*sin(rotationA*pi/180)+dis(115,2)*cos(rotationA*pi/180);
        NodeMovement115(RowN,6)=dis(115,3);

        NodeMovement116(RowN,1)=mon;
        NodeMovement116(RowN,2)=t;
        NodeMovement116(RowN,3)=tt;

        NodeMovement116(RowN,4)=dis(116,1)*cos(rotationA*pi/180)+dis(116,2)*si
n(rotationA*pi/180);

```

```

NodeMovement116(RowN,5)=-
dis(116,1)*sin(rotationA*pi/180)+dis(116,2)*cos(rotationA*pi/180);
NodeMovement116(RowN,6)=dis(116,3);

NodeMovement124(RowN,1)=mon;
NodeMovement124(RowN,2)=t;
NodeMovement124(RowN,3)=tt;

NodeMovement124(RowN,4)=dis(124,1)*cos(rotationA*pi/180)+dis(124,2)*sin(rotationA*pi/180);
NodeMovement124(RowN,5)=-
dis(124,1)*sin(rotationA*pi/180)+dis(124,2)*cos(rotationA*pi/180);
NodeMovement124(RowN,6)=dis(124,3);

n1=size(dis,1);
s1=strcat('c:\Model-Data\B6-result','\dis-',int2str(mon),'-',int2str(t),'-',int2str(tt),'.txt');
fid1=fopen(s1,'w');
for ii=1:n1
    for jj=1:6
        fprintf(fid1,'%0.6f\t',dis(ii,jj));
        if rem(jj,6)==0
            fprintf(fid1,'\r\n');
        end
    end
end
fclose(fid1);

jj=1:GDof; format long
f=[jj; displacements'];

%drawing mesh and deformed shape
U=displacements;
clf

%%%%%%%%%%%%%%%%%%%%%%%%%%%%%%%%%%%%%%%%%%%%%%%%%%%%%%%%%%%%%%%%%%%%%%%%%%%%-----draw B6-building

figure(1);

DrawStructure(nodeCoordinates+1000*[U(1:6:6*numberNodes)...
    U(2:6:6*numberNodes) U(3:6:6*numberNodes)],elementNodes);

hold on
% setting axis label and the title of the picture
xlabel('X');
ylabel('Y');
zlabel('Z');

switch tt

    case 1
        title(['3D-B6-Structure-Model--2013-',num2str(mon),'-',num2str(t),' at 00:00']);
    case 2
        title(['3D-B6-Structure-Model--2013-',num2str(mon),'-',num2str(t),' at 03:00']);
    case 3
        title(['3D-B6-Structure-Model--2013-',num2str(mon),'-',num2str(t),' at 06:00']);

```

```

        case 4
            title(['3D-B6-Structure-Model--2013-', num2str(mon), '-
', num2str(t), ' at 09:00']);
        case 5
            title(['3D-B6-Structure-Model--2013-', num2str(mon), '-
', num2str(t), ' at 12:00']);
        case 6
            title(['3D-B6-Structure-Model--2013-', num2str(mon), '-
', num2str(t), ' at 15:00']);
        case 7
            title(['3D-B6-Structure-Model--2013-', num2str(mon), '-
', num2str(t), ' at 18:00']);
        case 8
            title(['3D-B6-Structure-Model--2013-', num2str(mon), '-
', num2str(t), ' at 21:00']);
    end

    %adding the numbers of every nodes
    numbernodes=length(nodeCoordinates);
    for i=1:numbernodes
        a=(i-1)*6;
        x1=nodeCoordinates(i,1)+1000*U((1+a),1)+0.2;
        y1=nodeCoordinates(i,2)+1000*U((2+a),1);
        z1=nodeCoordinates(i,3)+1000*U((3+a),1);
        number=num2str(i);
        text(x1,y1,z1,number);
    end

    % setting the view point
    axis([-5 20 -5 25 -5 25]);

    hold off

    % setting the view point
    view(11,17);

    %save the graph
    saveas(gcf,['c:\Model-Data\B6-result-picture', '\B6-movement-
', int2str(mon), '-', ...
        int2str(t), '-', int2str(tt), '.bmp']);

    end
end

%%%%%%%%%%Output the displacement of the reference points

%%%%%%%%%%Node-115---A6R14

    NM=NodeMovement115;
    nn=size(NM,1);
    s1=strcat('c:\Model-Data\B6-result', '\NodeMovement-
', int2str(mon), '-Node-115-A6R14.txt');
    fid1=fopen(s1,'w');
    for ii=1:nn
        for jj=1:6
            fprintf(fid1, '%.6f\t', NM(ii, jj));
            if rem(jj,6)==0
                fprintf(fid1, '\r\n');
            end
        end
    end

```

```

        end
    end
    fclose(fid1);

%%%%%%Node-116---A6R28

    NM=NodeMovement116;
    nn=size(NM,1);
    s1=strcat('c:\Model-Data\B6-result','\NodeMovement-
',int2str(mon),'-Node-116-A6R28.txt');
    fid1=fopen(s1,'w');
    for ii=1:nn
        for jj=1:6
            fprintf(fid1,'% .6f\t',NM(ii,jj));
            if rem(jj,6)==0
                fprintf(fid1,'\r\n');
            end
        end
    end
    fclose(fid1);

%%%%%%Node-124---A6R27

    NM=NodeMovement124;
    nn=size(NM,1);
    s1=strcat('c:\Model-Data\B6-result','\NodeMovement-
',int2str(mon),'-Node-124-A6R27.txt');
    fid1=fopen(s1,'w');
    for ii=1:nn
        for jj=1:6
            fprintf(fid1,'% .6f\t',NM(ii,jj));
            if rem(jj,6)==0
                fprintf(fid1,'\r\n');
            end
        end
    end
    fclose(fid1);

Tb6model=toc    %%%record the running time

```

XI.2.3 structure model program code

```

% MATLAB codes for C5 model

tic

% clear memory
clear all

mon=10;
SetsNum=15;

%Rotation angle between local system and global system
rotationA=315;

```

```

%read parameters of the structure
parameters=load('c:\Model-Data\C5\parameters.txt');

%read coordinates of each node of the structure
nodeCoordinates=load('c:\Model-Data\C5\nodeCoordinates.txt');

xx=nodeCoordinates(:,1);
yy=nodeCoordinates(:,2);
zz=nodeCoordinates(:,3);

% read the nodes of each element's start and end
elementNodes=load('c:\Model-Data\C5\elementNodes.txt');

numberNodes=size(nodeCoordinates,1);
numberElements=size(elementNodes,1);

% GDof: global number of degrees of freedom
GDof=6*numberNodes;

RowN=0;

for t=1:SetsNum

    for tt=1:8

        % read force vector
        so=strcat('c:\Model-Data\C5-Force\F-',int2str(mon),'-',
'int2str(t),'-',int2str(tt),'.txt');
        force=load(so);

        % calculation of the system stiffness matrix
        [stiffness]=...
            formStiffness3DframeRectangle01(GDof,numberElements,...
            elementNodes,numberNodes,nodeCoordinates,parameters);

        % boundary conditions and solution
        prescribedDof=[1,2,3,7,8,9,13,14,15,19,20,21,...
25,26,27,31,32,33,37,38,39,43,44,45,49,50,51,55,56,57,61,62,63,...
67,68,69,73,74,75,79,80,81,85,86,87,...
91,92,93,97,98,99,103,104,105,109,110,111,115,116,117,121,122,123,...
127,128,129,133,134,135,139,140,141,163,164,165,187,188,189,211,212,21
3,...
235,236,237,259,260,261,283,284,285,307,308,309,331,332,333];

        % solution -- displacements: displacement vector
        displacements=solution(GDof,prescribedDof,stiffness,force);

        a=length(displacements);
        b=a/6;
        dis=[b,6];
        k=1;

        for i=1:b
            for j=1:6
                dis(i,j)=displacements(k,1);
            end
        end
    end
end

```

```

        k=k+1;
    end
end

RowN=RowN+1;

NodeMovement219(RowN,1)=mon;
NodeMovement219(RowN,2)=t;
NodeMovement219(RowN,3)=tt;

NodeMovement219(RowN,4)=dis(219,1)*cos(rotationA*pi/180)+dis(219,2)*sin(rotationA*pi/180);
NodeMovement219(RowN,5)=-
dis(219,1)*sin(rotationA*pi/180)+dis(219,2)*cos(rotationA*pi/180);
NodeMovement219(RowN,6)=dis(219,3);

NodeMovement221(RowN,1)=mon;
NodeMovement221(RowN,2)=t;
NodeMovement221(RowN,3)=tt;

NodeMovement221(RowN,4)=dis(221,1)*cos(rotationA*pi/180)+dis(221,2)*sin(rotationA*pi/180);
NodeMovement221(RowN,5)=-
dis(221,1)*sin(rotationA*pi/180)+dis(221,2)*cos(rotationA*pi/180);
NodeMovement221(RowN,6)=dis(221,3);

n1=size(dis,1);
s1=strcat('c:\Model-Data\C5-result','\dis-',int2str(mon),'-',int2str(t),'-',int2str(tt),'.txt');
fid1=fopen(s1,'w');
for ii=1:n1
    for jj=1:6
        fprintf(fid1,'%6f\t',dis(ii,jj));
        if rem(jj,6)==0
            fprintf(fid1,'\r\n');
        end
    end
end
fclose(fid1);

jj=1:GDof; format long
f=[jj; displacements'];

%drawing mesh and deformed shape
U=displacements;
clf

%%%%%%%%%%%%%%%%%%%%%%%%%%%%%%%%%%%%%%%%%%%%%%%%%%%%%%%%%%%%%%%%%%%%%%%%%%%%-----draw C5--building

figure(1);

DrawStructure(nodeCoordinates+1000*[U(1:6:6*numberNodes)...
    U(2:6:6*numberNodes) U(3:6:6*numberNodes)],elementNodes);

hold on

% setting axis label and the title of the picture
xlabel('X');
ylabel('Y');

```

```

zlabel('Z');

switch tt

    case 1
        title(['3D-C5-Structure-Model--2013-', num2str(mon), '-
', num2str(t), ' at 00:00']);
    case 2
        title(['3D-C5-Structure-Model--2013-', num2str(mon), '-
', num2str(t), ' at 03:00']);
    case 3
        title(['3D-C5-Structure-Model--2013-', num2str(mon), '-
', num2str(t), ' at 06:00']);
    case 4
        title(['3D-C5-Structure-Model--2013-', num2str(mon), '-
', num2str(t), ' at 09:00']);
    case 5
        title(['3D-C5-Structure-Model--2013-', num2str(mon), '-
', num2str(t), ' at 12:00']);
    case 6
        title(['3D-C5-Structure-Model--2013-', num2str(mon), '-
', num2str(t), ' at 15:00']);
    case 7
        title(['3D-C5-Structure-Model--2013-', num2str(mon), '-
', num2str(t), ' at 18:00']);
    case 8
        title(['3D-C5-Structure-Model--2013-', num2str(mon), '-
', num2str(t), ' at 21:00']);
    end

%adding the numbers of every nodes
numbernoders=length(nodeCoordinates);
for i=1:numbernoders
    a=(i-1)*6;
    x1=nodeCoordinates(i,1)+1000*U((1+a),1);
    y1=nodeCoordinates(i,2)+1000*U((2+a),1);
    z1=nodeCoordinates(i,3)+1000*U((3+a),1);
    number=num2str(i);
    text(x1,y1,z1,number);
end

% setting the view point
axis([-5 45 -5 25 -5 25]);

hold off

% setting the view point
view(11,17);

%save the graph
saveas(gcf,['c:\Model-Data\C5-result-picture', '\C5-movement-
',int2str(mon), '- ', ...
    int2str(t), '- ',int2str(tt), '.bmp']);

end
end

%%%%%%%%%%%%%%%%%%%%%%%%%%%%%%%%%%%%%%%%%%%%%%%%%%%%%%%%%%%%%%%%%%%%%%%%Output the displacement of the reference points

```

```

%%%%%%%%%%%%%%%%%%%%%%%%%%%%%%%%%%%%%%%%%%%%%%%%%%%%%%%%%%%%%%%%%%%%%%%%Node-219--A6R12

    NM=NodeMovement219;
    nn=size(NM,1);
    s1=strcat('c:\Model-Data\C5-result','\NodeMovement-
',int2str(mon),'-Node-219-A6R12.txt');
    fid1=fopen(s1,'w');
    for ii=1:nn
        for jj=1:6
            fprintf(fid1,'%6f\t',NM(ii,jj));
            if rem(jj,6)==0
                fprintf(fid1,'\r\n');
            end
        end
    end
    fclose(fid1);

%%%%%%%%%%%%%%%%%%%%%%%%%%%%%%%%%%%%%%%%%%%%%%%%%%%%%%%%%%%%%%%%%%%%%%%%Node-221--A6R13

    NM=NodeMovement221;
    nn=size(NM,1);
    s1=strcat('c:\Model-Data\C5-result','\NodeMovement-
',int2str(mon),'-Node-221-A6R13.txt');
    fid1=fopen(s1,'w');
    for ii=1:nn
        for jj=1:6
            fprintf(fid1,'%6f\t',NM(ii,jj));
            if rem(jj,6)==0
                fprintf(fid1,'\r\n');
            end
        end
    end
    fclose(fid1);

Tc5model=toc    %%%record the running time

```

XI.2.4 H0 structure model program code

```

% MATLAB codes for H0 model

tic

% clear memory
clear all

mon=10;
SetsNum=15;

%Rotation angle between local system and global system
rotationA=11;

%read parameters of the structure
parameters=load('c:\Model-Data\H0\parameters.txt');

%read coordinates of each node of the structure

```

```

nodeCoordinates=load('c:\Model-Data\H0\nodeCoordinates.txt');

xx=nodeCoordinates(:,1);
yy=nodeCoordinates(:,2);
zz=nodeCoordinates(:,3);

% read the nodes of each element's start and end
elementNodes=load('c:\Model-Data\H0\elementNodes.txt');

numberNodes=size(nodeCoordinates,1);
numberElements=size(elementNodes,1);

% GDof: global number of degrees of freedom
GDof=6*numberNodes;

RowN=0;

for t=1:SetsNum

    for tt=1:8

        % read force vector
        so=strcat('c:\Model-Data\H0-Force\F-',int2str(mon),'-
',int2str(t),'-',int2str(tt),'.txt');
        force=load(so);

        % calculation of the system stiffness matrix

        [stiffness]=...
            formStiffness3DframeRectangle01(GDof,numberElements,...
            elementNodes,numberNodes,nodeCoordinates,parameters);

        % boundary conditions and solution

prescribedDof=[1,2,3,7,8,9,13,14,15,19,20,21,25,26,27,31,32,33,37,38,3
9,...
    43,44,45,49,50,51,55,56,57,61,62,63,67,68,69,...

73,74,75,79,80,81,85,86,87,91,92,93,97,98,99,103,104,105,109,110,111,..
..

115,116,117,121,122,123,127,128,129,133,134,135,139,140,141,145,146,14
7,...
    151,152,153,157,158,159,163,164,165,...

169,170,171,175,176,177,181,182,183,187,188,189,193,194,195,199,200,20
1,...

205,206,207,211,212,213,217,218,219,223,224,225,229,230,231,235,236,23
7,...
    241,242,243,247,248,249,253,254,255,...

259,260,261,265,266,267,271,272,273,277,278,279,283,284,285,289,290,29
1,...

295,296,297,301,302,303,307,308,309,313,314,315,319,320,321,325,326,32
7,...
    331,332,333,337,338,339,343,344,345,...

```

349, 350, 351, 355, 356, 357, 361, 362, 363, 367, 368, 369, 373, 374, 375, 379, 380, 381];

```

% solution -- displacements: displacement vector
displacements=solution(GDof,prescribedDof,stiffness,force);

a=length(displacements);
b=a/6;
dis=[b,6];
k=1;

for i=1:b
    for j=1:6
        dis(i,j)=displacements(k,1);
        k=k+1;
    end
end

RowN=RowN+1;

NodeMovement447(RowN,1)=mon;
NodeMovement447(RowN,2)=t;
NodeMovement447(RowN,3)=tt;

NodeMovement447(RowN,4)=dis(447,1)*cos(rotationA*pi/180)+dis(447,2)*sin(rotationA*pi/180);
NodeMovement447(RowN,5)=-
dis(447,1)*sin(rotationA*pi/180)+dis(447,2)*cos(rotationA*pi/180);
NodeMovement447(RowN,6)=dis(447,3);

NodeMovement455(RowN,1)=mon;
NodeMovement455(RowN,2)=t;
NodeMovement455(RowN,3)=tt;

NodeMovement455(RowN,4)=dis(455,1)*cos(rotationA*pi/180)+dis(455,2)*sin(rotationA*pi/180);
NodeMovement455(RowN,5)=-
dis(455,1)*sin(rotationA*pi/180)+dis(455,2)*cos(rotationA*pi/180);
NodeMovement455(RowN,6)=dis(455,3);

NodeMovement453(RowN,1)=mon;
NodeMovement453(RowN,2)=t;
NodeMovement453(RowN,3)=tt;

NodeMovement453(RowN,4)=dis(453,1)*cos(rotationA*pi/180)+dis(453,2)*sin(rotationA*pi/180);
NodeMovement453(RowN,5)=-
dis(453,1)*sin(rotationA*pi/180)+dis(453,2)*cos(rotationA*pi/180);
NodeMovement453(RowN,6)=dis(453,3);

NodeMovement65(RowN,1)=mon;
NodeMovement65(RowN,2)=t;
NodeMovement65(RowN,3)=tt;

NodeMovement65(RowN,4)=dis(65,1)*cos(rotationA*pi/180)+dis(65,2)*sin(rotationA*pi/180);
NodeMovement65(RowN,5)=-
dis(65,1)*sin(rotationA*pi/180)+dis(65,2)*cos(rotationA*pi/180);
NodeMovement65(RowN,6)=dis(65,3);

```

```

NodeMovement93(RowN,1)=mon;
NodeMovement93(RowN,2)=t;
NodeMovement93(RowN,3)=tt;

NodeMovement93(RowN,4)=dis(93,1)*cos(rotationA*pi/180)+dis(93,2)*sin(r
otationA*pi/180);
NodeMovement93(RowN,5)=-
dis(93,1)*sin(rotationA*pi/180)+dis(93,2)*cos(rotationA*pi/180);
NodeMovement93(RowN,6)=dis(93,3);

NodeMovement459(RowN,1)=mon;
NodeMovement459(RowN,2)=t;
NodeMovement459(RowN,3)=tt;

NodeMovement459(RowN,4)=dis(459,1)*cos(rotationA*pi/180)+dis(459,2)*si
n(rotationA*pi/180);
NodeMovement459(RowN,5)=-
dis(459,1)*sin(rotationA*pi/180)+dis(459,2)*cos(rotationA*pi/180);
NodeMovement459(RowN,6)=dis(459,3);

NodeMovement466(RowN,1)=mon;
NodeMovement466(RowN,2)=t;
NodeMovement466(RowN,3)=tt;

NodeMovement466(RowN,4)=dis(466,1)*cos(rotationA*pi/180)+dis(466,2)*si
n(rotationA*pi/180);
NodeMovement466(RowN,5)=-
dis(466,1)*sin(rotationA*pi/180)+dis(466,2)*cos(rotationA*pi/180);
NodeMovement466(RowN,6)=dis(466,3);

NodeMovement471(RowN,1)=mon;
NodeMovement471(RowN,2)=t;
NodeMovement471(RowN,3)=tt;

NodeMovement471(RowN,4)=dis(471,1)*cos(rotationA*pi/180)+dis(471,2)*si
n(rotationA*pi/180);
NodeMovement471(RowN,5)=-
dis(471,1)*sin(rotationA*pi/180)+dis(471,2)*cos(rotationA*pi/180);
NodeMovement471(RowN,6)=dis(471,3);

NodeMovement473(RowN,1)=mon;
NodeMovement473(RowN,2)=t;
NodeMovement473(RowN,3)=tt;

NodeMovement473(RowN,4)=dis(473,1)*cos(rotationA*pi/180)+dis(473,2)*si
n(rotationA*pi/180);
NodeMovement473(RowN,5)=-
dis(473,1)*sin(rotationA*pi/180)+dis(473,2)*cos(rotationA*pi/180);
NodeMovement473(RowN,6)=dis(473,3);

n1=size(dis,1);
s1=strcat('c:\Model-Data\H0-result','\dis-',int2str(mon),'-
',int2str(t),'-',int2str(tt),'.txt');
fidl=fopen(s1,'w');
for ii=1:n1
    for jj=1:6
        fprintf(fidl,'%6f\t',dis(ii,jj));
        if rem(jj,6)==0
            fprintf(fidl,'\r\n');

```

```

        end
    end
end
fclose(fid1);

jj=1:GDof; format long
f=[jj; displacements'];

%drawing mesh and deformed shape
U=displacements;
clf

%%%%%%%%%%%%%%%%%%%%%%%%%%%%%%%%%%%%%%%%%%%%%%%%%%%%%%%%%%%%%%%%%%%%%%%%%%%%----- draw H0--building

figure(1);

DrawStructure(nodeCoordinates+1000*[U(1:6:6*numberNodes)...
    U(2:6:6*numberNodes) U(3:6:6*numberNodes)],elementNodes);

hold on
% setting axis label and the title of the picture
xlabel('X');
ylabel('Y');
zlabel('Z');

switch tt

    case 1
        title(['3D-H0-Structure-Model--2013-',num2str(mon),'-
',num2str(t),' at 00:00']);
    case 2
        title(['3D-H0-Structure-Model--2013-',num2str(mon),'-
',num2str(t),' at 03:00']);
    case 3
        title(['3D-H0-Structure-Model--2013-',num2str(mon),'-
',num2str(t),' at 06:00']);
    case 4
        title(['3D-H0-Structure-Model--2013-',num2str(mon),'-
',num2str(t),' at 09:00']);
    case 5
        title(['3D-H0-Structure-Model--2013-',num2str(mon),'-
',num2str(t),' at 12:00']);
    case 6
        title(['3D-H0-Structure-Model--2013-',num2str(mon),'-
',num2str(t),' at 15:00']);
    case 7
        title(['3D-H0-Structure-Model--2013-',num2str(mon),'-
',num2str(t),' at 18:00']);
    case 8
        title(['3D-H0-Structure-Model--2013-',num2str(mon),'-
',num2str(t),' at 21:00']);
    end

%adding the numbers of every nodes
numbernoders=length(nodeCoordinates);
for i=1:numbernoders
    a=(i-1)*6;
    x1=nodeCoordinates(i,1)+1000*U((1+a),1)+0.4;
    y1=nodeCoordinates(i,2)+1000*U((2+a),1);

```

```

        z1=nodeCoordinates(i,3)+1000*U((3+a),1);
        number=num2str(i);
        text(x1,y1,z1,number);
    end

    % setting the view point

    axis([-5 65 -5 25 -5 25]);

    hold off

    % setting the view point
    view(11,17);

    %save the graph
    saveas(gcf,['c:\Model-Data\H0-result-picture','\H0-movement-
',int2str(mon),'-',...
        int2str(t),'-',int2str(tt),'.bmp']);

    end
end

%%%%%%%%%%Output the displacement of the reference points

%%%%%%%%%%Node-447

    NM=NodeMovement447;
    nn=size(NM,1);
    s1=strcat('c:\Model-Data\H0-result','\NodeMovement-
',int2str(mon),'-Node-447.txt');
    fid1=fopen(s1,'w');
    for ii=1:nn
        for jj=1:6
            fprintf(fid1,'%6f\t',NM(ii,jj));
            if rem(jj,6)==0
                fprintf(fid1,'\r\n');
            end
        end
    end
    fclose(fid1);

%%%%%%%%%%Node-455---A6R22

    NM=NodeMovement455;
    nn=size(NM,1);
    s1=strcat('c:\Model-Data\H0-result','\NodeMovement-
',int2str(mon),'-Node-455-A6R22.txt');
    fid1=fopen(s1,'w');
    for ii=1:nn
        for jj=1:6
            fprintf(fid1,'%6f\t',NM(ii,jj));
            if rem(jj,6)==0
                fprintf(fid1,'\r\n');
            end
        end
    end
    fclose(fid1);

%%%%%%%%%%Node-453---A6R19

```

```
NM=NodeMovement453;
nn=size(NM,1);
s1=strcat('c:\Model-Data\H0-result','\NodeMovement-
',int2str(mon),'-Node-453-A6R19.txt');
fidl=fopen(s1,'w');
for ii=1:nn
    for jj=1:6
        fprintf(fidl,'% .6f\t',NM(ii,jj));
        if rem(jj,6)==0
            fprintf(fidl,'\r\n');
        end
    end
end
fclose(fidl);

%%%%%%%%Node-65---A6R17

NM=NodeMovement65;
nn=size(NM,1);
s1=strcat('c:\Model-Data\H0-result','\NodeMovement-
',int2str(mon),'-Node-65-A6R17.txt');
fidl=fopen(s1,'w');
for ii=1:nn
    for jj=1:6
        fprintf(fidl,'% .6f\t',NM(ii,jj));
        if rem(jj,6)==0
            fprintf(fidl,'\r\n');
        end
    end
end
fclose(fidl);

%%%%%%%%Node-93---A6R20

NM=NodeMovement93;
nn=size(NM,1);
s1=strcat('c:\Model-Data\H0-result','\NodeMovement-
',int2str(mon),'-Node-93-A6R20.txt');
fidl=fopen(s1,'w');
for ii=1:nn
    for jj=1:6
        fprintf(fidl,'% .6f\t',NM(ii,jj));
        if rem(jj,6)==0
            fprintf(fidl,'\r\n');
        end
    end
end
fclose(fidl);

%%%%%%%%Node-459---A6R18

NM=NodeMovement459;
nn=size(NM,1);
s1=strcat('c:\Model-Data\H0-result','\NodeMovement-
',int2str(mon),'-Node-459-A6R18.txt');
fidl=fopen(s1,'w');
for ii=1:nn
    for jj=1:6
        fprintf(fidl,'% .6f\t',NM(ii,jj));
```

```

        if rem(jj,6)==0
            fprintf(fid1, '\r\n');
        end
    end
end
fclose(fid1);

%%%%%%%%Node-466---A6R21

NM=NodeMovement466;
nn=size(NM,1);
s1=strcat('c:\Model-Data\H0-result', '\NodeMovement-
',int2str(mon), '-Node-466-A6R21.txt');
fid1=fopen(s1, 'w');
for ii=1:nn
    for jj=1:6
        fprintf(fid1, '%.6f\t', NM(ii, jj));
        if rem(jj,6)==0
            fprintf(fid1, '\r\n');
        end
    end
end
fclose(fid1);

%%%%%%%%Node-471---A6R23

NM=NodeMovement471;
nn=size(NM,1);
s1=strcat('c:\Model-Data\H0-result', '\NodeMovement-
',int2str(mon), '-Node-471-A6R23.txt');
fid1=fopen(s1, 'w');
for ii=1:nn
    for jj=1:6
        fprintf(fid1, '%.6f\t', NM(ii, jj));
        if rem(jj,6)==0
            fprintf(fid1, '\r\n');
        end
    end
end
fclose(fid1);

%%%%%%%%Node-473---A6R24

NM=NodeMovement473;
nn=size(NM,1);
s1=strcat('c:\Model-Data\H0-result', '\NodeMovement-
',int2str(mon), '-Node-473-A6R24.txt');
fid1=fopen(s1, 'w');
for ii=1:nn
    for jj=1:6
        fprintf(fid1, '%.6f\t', NM(ii, jj));
        if rem(jj,6)==0
            fprintf(fid1, '\r\n');
        end
    end
end
fclose(fid1);

Th0model=toc    %%%record the running time

```

XI.2.5 K2M structure model program code

```

% MATLAB codes for K2M
tic
% clear memory
clear all

%read parameters of the structure
parameters=load('c:\Model-Data\K2M\parameters.txt');

mon=10;
SetsNum=15;

%Rotation angle between local system and global system
rotationA=321;

%read coordinates of each node of the structure
nodeCoordinates=load('c:\Model-Data\K2M\nodeCoordinates.txt');

xx=nodeCoordinates(:,1);
yy=nodeCoordinates(:,2);
zz=nodeCoordinates(:,3);

% read the nodes of each element's start and end
elementNodes=load('c:\Model-Data\K2M\elementNodes.txt');

numberNodes=size(nodeCoordinates,1);
numberElements=size(elementNodes,1);

% GDof: global number of degrees of freedom
GDof=6*numberNodes;

RowN=0;

for t=1:SetsNum

    for tt=1:8

        % %reand force vector
        so=strcat('c:\Model-Data\K2M-Force\F-',int2str(mon),'-',
'int2str(t),'-',int2str(tt),'.txt');
        force=load(so);

        % calculation of the system stiffness matrix
        [stiffness]=...
        formStiffness3DframeRectangle01(GDof,numberElements,...
        elementNodes,numberNodes,nodeCoordinates,parameters);

        % boundary conditions and solution
        prescribedDof=[1,2,3,7,8,9,13,14,15,...
19,20,21,25,26,27,31,32,33,37,38,39,43,44,45,49,50,51,55,56,57,61,62,6
3,...
67,68,69,73,74,75,79,80,81,85,86,87,91,92,93,97,98,99,103,104,105,...

```

```

109,110,111,115,116,117,121,122,123,127,128,129,133,134,135,139,140,14
1,...

145,146,147,151,152,153,157,158,159,163,164,165,169,170,171,175,176,17
7,...
];

% solution--displacements: displacement vector
displacements=solution(GDof,prescribedDof,stiffness,force);

a=length(displacements);
b=a/6;
dis=[b,6];
k=1;

for i=1:b
    for j=1:6
        dis(i,j)=displacements(k,1);
        k=k+1;
    end
end

RowN=RowN+1;

%%-----A6
NodeMovement100(RowN,1)=mon;
NodeMovement100(RowN,2)=t;
NodeMovement100(RowN,3)=tt;

NodeMovement100(RowN,4)=dis(100,1)*cos(rotationA*pi/180)+dis(100,2)*si
n(rotationA*pi/180);
NodeMovement100(RowN,5)=-
dis(100,1)*sin(rotationA*pi/180)+dis(100,2)*cos(rotationA*pi/180);
NodeMovement100(RowN,6)=dis(100,3);

NodeMovement92(RowN,1)=mon;
NodeMovement92(RowN,2)=t;
NodeMovement92(RowN,3)=tt;

NodeMovement92(RowN,4)=dis(92,1)*cos(rotationA*pi/180)+dis(92,2)*sin(r
otationA*pi/180);
NodeMovement92(RowN,5)=-
dis(92,1)*sin(rotationA*pi/180)+dis(92,2)*cos(rotationA*pi/180);
NodeMovement92(RowN,6)=dis(92,3);

NodeMovement88(RowN,1)=mon;
NodeMovement88(RowN,2)=t;
NodeMovement88(RowN,3)=tt;

NodeMovement88(RowN,4)=dis(88,1)*cos(rotationA*pi/180)+dis(88,2)*sin(r
otationA*pi/180);
NodeMovement88(RowN,5)=-
dis(88,1)*sin(rotationA*pi/180)+dis(88,2)*cos(rotationA*pi/180);
NodeMovement88(RowN,6)=dis(88,3);

```

```

NodeMovement140(RowN,1)=mon;
NodeMovement140(RowN,2)=t;
NodeMovement140(RowN,3)=tt;

NodeMovement140(RowN,4)=dis(140,1)*cos(rotationA*pi/180)+dis(140,2)*sin(rotationA*pi/180);
NodeMovement140(RowN,5)=-
dis(140,1)*sin(rotationA*pi/180)+dis(140,2)*cos(rotationA*pi/180);
NodeMovement140(RowN,6)=dis(140,3);

NodeMovement132(RowN,1)=mon;
NodeMovement132(RowN,2)=t;
NodeMovement132(RowN,3)=tt;

NodeMovement132(RowN,4)=dis(132,1)*cos(rotationA*pi/180)+dis(132,2)*sin(rotationA*pi/180);
NodeMovement132(RowN,5)=-
dis(132,1)*sin(rotationA*pi/180)+dis(132,2)*cos(rotationA*pi/180);
NodeMovement132(RowN,6)=dis(132,3);

NodeMovement128(RowN,1)=mon;
NodeMovement128(RowN,2)=t;
NodeMovement128(RowN,3)=tt;

NodeMovement128(RowN,4)=dis(128,1)*cos(rotationA*pi/180)+dis(128,2)*sin(rotationA*pi/180);
NodeMovement128(RowN,5)=-
dis(128,1)*sin(rotationA*pi/180)+dis(128,2)*cos(rotationA*pi/180);
NodeMovement128(RowN,6)=dis(128,3);

NodeMovement160(RowN,1)=mon;
NodeMovement160(RowN,2)=t;
NodeMovement160(RowN,3)=tt;

NodeMovement160(RowN,4)=dis(160,1)*cos(rotationA*pi/180)+dis(160,2)*sin(rotationA*pi/180);
NodeMovement160(RowN,5)=-
dis(160,1)*sin(rotationA*pi/180)+dis(160,2)*cos(rotationA*pi/180);
NodeMovement160(RowN,6)=dis(160,3);

NodeMovement152(RowN,1)=mon;
NodeMovement152(RowN,2)=t;
NodeMovement152(RowN,3)=tt;

NodeMovement152(RowN,4)=dis(152,1)*cos(rotationA*pi/180)+dis(152,2)*sin(rotationA*pi/180);
NodeMovement152(RowN,5)=-
dis(152,1)*sin(rotationA*pi/180)+dis(152,2)*cos(rotationA*pi/180);
NodeMovement152(RowN,6)=dis(152,3);

NodeMovement148(RowN,1)=mon;
NodeMovement148(RowN,2)=t;
NodeMovement148(RowN,3)=tt;

NodeMovement148(RowN,4)=dis(148,1)*cos(rotationA*pi/180)+dis(148,2)*sin(rotationA*pi/180);
NodeMovement148(RowN,5)=-
dis(148,1)*sin(rotationA*pi/180)+dis(148,2)*cos(rotationA*pi/180);
NodeMovement148(RowN,6)=dis(148,3);

```

```

n1=size(dis,1);
s1=strcat('c:\Model-Data\K2M-result','\dis-',int2str(mon),'-
',int2str(t),'-',int2str(tt),'.txt');
fid1=fopen(s1,'w');
for ii=1:n1
    for jj=1:6
        fprintf(fid1,'% .6f\t',dis(ii,jj));
        if rem(jj,6)==0
            fprintf(fid1,'\r\n');
        end
    end
end
fclose(fid1);

% displacements

jj=1:GDof; format long
f=[jj; displacements'];

%drawing mesh and deformed shape
U=displacements;
clf

DrawStructure(nodeCoordinates+1000*[U(1:6:6*numberNodes)...
    U(2:6:6*numberNodes) U(3:6:6*numberNodes)],elementNodes);

hold on
% setting axis label and the title of the picture
xlabel('X');
ylabel('Y');
zlabel('Z');

switch tt

    case 1
        title(['3D-K2M-Structure-Model--2013-',num2str(mon),'-
',num2str(t),' at 00:00']);
    case 2
        title(['3D-K2M-Structure-Model--2013-',num2str(mon),'-
',num2str(t),' at 03:00']);
    case 3
        title(['3D-K2M-Structure-Model--2013-',num2str(mon),'-
',num2str(t),' at 06:00']);
    case 4
        title(['3D-K2M-Structure-Model--2013-',num2str(mon),'-
',num2str(t),' at 09:00']);
    case 5
        title(['3D-K2M-Structure-Model--2013-',num2str(mon),'-
',num2str(t),' at 12:00']);
    case 6
        title(['3D-K2M-Structure-Model--2013-',num2str(mon),'-
',num2str(t),' at 15:00']);
    case 7
        title(['3D-K2M-Structure-Model--2013-',num2str(mon),'-
',num2str(t),' at 18:00']);
    case 8
        title(['3D-K2M-Structure-Model--2013-',num2str(mon),'-
',num2str(t),' at 21:00']);
end

```

```

%adding the numbers of every nodes
nummernoders=length(nodeCoordinates);
for i=1:nummernoders
    x1=nodeCoordinates(i,1);
    y1=nodeCoordinates(i,2);
    z1=nodeCoordinates(i,3);
    number=num2str(i);
    text(x1,y1,z1,number);
end

% setting the view point
grid on

axis([-5 25 -5 25 -5 30]);

view(60,20);

saveas(gcf,['c:\Model-Data\K2M-result-picture','\K2M-movement-
',int2str(mon),'-',...
        int2str(t),'-',int2str(tt),'.bmp']);

%%%%%%%%%%%%%%%%%%%%%%%%%%%%%%%%%%%%%%%%%%%%%%%%%%%%%%%%%%%%%%%%%%%%%%%%

end
end

%%%%%%%%%%%%%%%%%%%%%%%%%%%%%%%%%%%%%%%%%%%%%%%%%%%%%%%%%%%%%%%%%%%%%%%%Output the node movement

%%%%%%%%%%%%%%%%%%%%%%%%%%%%%%%%%%%%%%%%%%%%%%%%%%%%%%%%%%%%%%%%%%%%%%%%Facade--C-----A6
NM=NodeMovement100;
nn=size(NM,1);
s1=strcat('c:\Model-Data\K2M-result','\NodeMovement-
',int2str(mon),'-Node-100-A6P01.txt');
fid1=fopen(s1,'w');
for ii=1:nn
    for jj=1:6
        fprintf(fid1,'%6f\t',NM(ii,jj));
        if rem(jj,6)==0
            fprintf(fid1,'\r\n');
        end
    end
end
end
fclose(fid1);

NM=NodeMovement92;
nn=size(NM,1);
s1=strcat('c:\Model-Data\K2M-result','\NodeMovement-
',int2str(mon),'-Node-92-A6P02.txt');
fid1=fopen(s1,'w');
for ii=1:nn
    for jj=1:6
        fprintf(fid1,'%6f\t',NM(ii,jj));
        if rem(jj,6)==0
            fprintf(fid1,'\r\n');
        end
    end
end
end
fclose(fid1);

```



```
NM=NodeMovement88;
nn=size(NM,1);
s1=strcat('c:\Model-Data\K2M-result','\NodeMovement-
',int2str(mon),'-Node-88-A6P03.txt');
fidl=fopen(s1,'w');
for ii=1:nn
    for jj=1:6
        fprintf(fidl,'% .6f\t',NM(ii,jj));
        if rem(jj,6)==0
            fprintf(fidl,'\r\n');
        end
    end
end
fclose(fidl);

NM=NodeMovement140;
nn=size(NM,1);
s1=strcat('c:\Model-Data\K2M-result','\NodeMovement-
',int2str(mon),'-Node-140-A6P04.txt');
fidl=fopen(s1,'w');
for ii=1:nn
    for jj=1:6
        fprintf(fidl,'% .6f\t',NM(ii,jj));
        if rem(jj,6)==0
            fprintf(fidl,'\r\n');
        end
    end
end
fclose(fidl);

NM=NodeMovement132;
nn=size(NM,1);
s1=strcat('c:\Model-Data\K2M-result','\NodeMovement-
',int2str(mon),'-Node-132-A6P05.txt');
fidl=fopen(s1,'w');
for ii=1:nn
    for jj=1:6
        fprintf(fidl,'% .6f\t',NM(ii,jj));
        if rem(jj,6)==0
            fprintf(fidl,'\r\n');
        end
    end
end
fclose(fidl);

NM=NodeMovement128;
nn=size(NM,1);
s1=strcat('c:\Model-Data\K2M-result','\NodeMovement-
',int2str(mon),'-Node-128-A6P06.txt');
fidl=fopen(s1,'w');
for ii=1:nn
    for jj=1:6
        fprintf(fidl,'% .6f\t',NM(ii,jj));
        if rem(jj,6)==0
            fprintf(fidl,'\r\n');
        end
    end
end
fclose(fidl);
```

```

    NM=NodeMovement160;
    nn=size(NM,1);
    s1=strcat('c:\Model-Data\K2M-result','\NodeMovement-
',int2str(mon),'-Node-160-A6P07.txt');
    fid1=fopen(s1,'w');
    for ii=1:nn
        for jj=1:6
            fprintf(fid1,'% .6f\t',NM(ii,jj));
            if rem(jj,6)==0
                fprintf(fid1,'\r\n');
            end
        end
    end
    fclose(fid1);

    NM=NodeMovement152;
    nn=size(NM,1);
    s1=strcat('c:\Model-Data\K2M-result','\NodeMovement-
',int2str(mon),'-Node-152-A6P08.txt');
    fid1=fopen(s1,'w');
    for ii=1:nn
        for jj=1:6
            fprintf(fid1,'% .6f\t',NM(ii,jj));
            if rem(jj,6)==0
                fprintf(fid1,'\r\n');
            end
        end
    end
    fclose(fid1);

    NM=NodeMovement148;
    nn=size(NM,1);
    s1=strcat('c:\Model-Data\K2M-result','\NodeMovement-
',int2str(mon),'-Node-148-A6P09.txt');
    fid1=fopen(s1,'w');
    for ii=1:nn
        for jj=1:6
            fprintf(fid1,'% .6f\t',NM(ii,jj));
            if rem(jj,6)==0
                fprintf(fid1,'\r\n');
            end
        end
    end
    fclose(fid1);

    %%%%%%%%%%%%%%%%%%%%%%%%%%%%%%%%%%%%%%%%%%%%%%%%%%%%%%%%%%%%%%%%%%%%%%%%%

Tk2mmodel=toc    %%%record the running time

```

XI.3 Calculate the forces on each node of the structure program code

XI.3.1 Calculate the forces on A6 structure

%Matlab code for calculate the foreces on A6building

```

tic
clear all
%the month and days need to be calculated
Month=10;
Day=15;
%read the air temperature
airtemperature=load('c:\Model-Data\T-0-Oct-3h.txt');
%read the insolation
insolationX8=load('c:\Model-Data\Insolation-X8-Oct.txt');

%node amount
Node=196;

E=3e10;
alfa=1.2e-5;
%coefficient of temperature transfer
CTT=0.7;
% coefficient insolation and isolation
CI=0.005;

m=size(airtemperature,1);

sizeI=size(insolationX8,1);

for t=1:Day

    a=(t-1)*24+1;
    b=t*24;
    Insolation=insolationX8(a:b,:);

    for tt=1:8

        F=zeros(Node*6,1);
        Insolation360=Insolation((1+(tt-1)*3),4);

        for i=1:m

            if airtemperature(i,2)==t && airtemperature(i,3)==tt

                Tse=airtemperature(i,4);
                Tsw=airtemperature(i,4);
                Tnw=airtemperature(i,4);
                Tne=airtemperature(i,4);
                Ttop=airtemperature(i,4);
                %inside temperature
                IT=21;

                DTse=Tse-IT;
                DTsw=Tsw-IT;
                DTnw=Tnw-IT;
                DTne=Tne-IT;

                DTtop=Ttop-IT;

                Time=(tt-1)*3;

                %%%%%%%%%%%%%%%%%%%%%%%%%%%%%%%%%%%%%%%%%%%%%%%%%%%%%%%%%%%%%%%%%%%%%%%%%
                %% Calculate Oreintation Factor

```

Annexes-XI

```
OFse=calculateOF(Insolation,135,Time);  
OFsw=calculateOF(Insolation,225,Time);  
OFnw=calculateOF(Insolation,315,Time);  
OFne=calculateOF(Insolation,45,Time);  
OFtop=calculateOF(Insolation,-10,Time);
```

%%%

```
F(361)=-1*0.1225*E*alfa*(CTT*DTse+CI*Insolation360*OFse);  
F(362)=-1*0.1225*E*alfa*(CTT*DTsw+CI*Insolation360*OFsw);  
F(373)=-1*0.1225*E*alfa*(CTT*DTnw+CI*Insolation360*OFnw);  
F(374)=1*0.1225*E*alfa*(CTT*DTsw+CI*Insolation360*OFsw);  
F(523)=1*0.1225*E*alfa*(CTT*DTse+CI*Insolation360*OFse);  
F(524)=-1*0.1225*E*alfa*(CTT*DTne+CI*Insolation360*OFne);  
F(535)=1*0.1225*E*alfa*(CTT*DTnw+CI*Insolation360*OFnw);  
F(536)=1*0.1225*E*alfa*(CTT*DTne+CI*Insolation360*OFne);  
F(541)=-1*0.1225*E*alfa*(CTT*DTse+CI*Insolation360*OFse);  
F(542)=-1*0.1225*E*alfa*(CTT*DTsw+CI*Insolation360*OFsw);  
F(559)=-1*0.1225*E*alfa*(CTT*DTnw+CI*Insolation360*OFnw);  
F(560)=1*0.1225*E*alfa*(CTT*DTsw+CI*Insolation360*OFsw);  
F(577)=1*0.1225*E*alfa*(CTT*DTse+CI*Insolation360*OFse);  
F(758)=-1*0.1225*E*alfa*(CTT*DTne+CI*Insolation360*OFne);  
F(775)=1*0.1225*E*alfa*(CTT*DTnw+CI*Insolation360*OFnw);  
F(776)=1*0.1225*E*alfa*(CTT*DTne+CI*Insolation360*OFne);  
F(781)=-1*0.1225*E*alfa*(CTT*DTse+CI*Insolation360*OFse);  
F(782)=-1*0.1225*E*alfa*(CTT*DTsw+CI*Insolation360*OFsw);  
F(793)=-1*0.1225*E*alfa*(CTT*DTnw+CI*Insolation360*OFnw);  
F(794)=1*0.1225*E*alfa*(CTT*DTsw+CI*Insolation360*OFsw);  
F(943)=1*0.1225*E*alfa*(CTT*DTse+CI*Insolation360*OFse);  
F(944)=-1*0.1225*E*alfa*(CTT*DTne+CI*Insolation360*OFne);  
F(955)=1*0.1225*E*alfa*(CTT*DTnw+CI*Insolation360*OFnw);  
F(956)=1*0.1225*E*alfa*(CTT*DTne+CI*Insolation360*OFne);  
F(961)=-  
1*0.1225*E*alfa*(CTT*(DTse+DTtop)*0.5+CI*Insolation360*(OFse+OFtop)*0.  
5);  
F(962)=-  
1*0.1225*E*alfa*(CTT*(DTsw+DTtop)*0.5+CI*Insolation360*(OFsw+OFtop)*0.  
5);  
F(963)=1*0.2475*E*alfa*(CTT*(DTse+DTsw)*0.5+CI*Insolation360*(OFse+OFs  
w)*0.5);  
F(967)=-1*0.1225*E*alfa*(CTT*DTtop+CI*Insolation360*OFtop);  
F(969)=1*0.1925*E*alfa*(CTT*DTsw+CI*Insolation360*OFsw);  
F(973)=-  
1*0.1225*E*alfa*(CTT*(DTnw+DTtop)*0.5+CI*Insolation360*(OFnw+OFtop)*0.  
5);  
F(974)=1*0.1225*E*alfa*(CTT*(DTsw+DTtop)*0.5+CI*Insolation360*(OFsw+OF  
top)*0.5);  
F(975)=1*0.2100*E*alfa*(CTT*(DTnw+DTsw)*0.5+CI*Insolation360*(OFnw+OFs  
w)*0.5);  
F(980)=-1*0.1225*E*alfa*(CTT*DTtop+CI*Insolation360*OFtop);  
F(981)=1*0.2475*E*alfa*(CTT*DTse+CI*Insolation360*OFse);  
F(992)=1*0.1225*E*alfa*(CTT*DTtop+CI*Insolation360*OFtop);  
F(993)=1*0.2100*E*alfa*(CTT*DTnw+CI*Insolation360*OFnw);  
F(998)=-1*0.1225*E*alfa*(CTT*DTtop+CI*Insolation360*OFtop);  
F(999)=1*0.2475*E*alfa*(CTT*DTse+CI*Insolation360*OFse);  
F(1010)=1*0.1225*E*alfa*(CTT*DTtop+CI*Insolation360*OFtop);  
F(1011)=1*0.2100*E*alfa*(CTT*DTnw+CI*Insolation360*OFnw);
```

```

F(1016)=-1*0.1225*E*alfa*(CTT*DTtop+CI*Insolation360*OFtop);
F(1017)=1*0.2475*E*alfa*(CTT*DTse+CI*Insolation360*OFse);
F(1028)=1*0.1225*E*alfa*(CTT*DTtop+CI*Insolation360*OFtop);
F(1029)=1*0.2100*E*alfa*(CTT*DTnw+CI*Insolation360*OFnw);
F(1034)=-1*0.1225*E*alfa*(CTT*DTtop+CI*Insolation360*OFtop);
F(1035)=1*0.2475*E*alfa*(CTT*DTse+CI*Insolation360*OFse);
F(1046)=1*0.1225*E*alfa*(CTT*DTtop+CI*Insolation360*OFtop);
F(1047)=1*0.2100*E*alfa*(CTT*DTnw+CI*Insolation360*OFnw);
F(1052)=-1*0.1225*E*alfa*(CTT*DTtop+CI*Insolation360*OFtop);
F(1053)=1*0.2475*E*alfa*(CTT*DTse+CI*Insolation360*OFse);
F(1064)=1*0.1225*E*alfa*(CTT*DTtop+CI*Insolation360*OFtop);
F(1065)=1*0.2100*E*alfa*(CTT*DTnw+CI*Insolation360*OFnw);
F(1070)=-1*0.1225*E*alfa*(CTT*DTtop+CI*Insolation360*OFtop);
F(1071)=1*0.2475*E*alfa*(CTT*DTse+CI*Insolation360*OFse);
F(1082)=1*0.1225*E*alfa*(CTT*DTtop+CI*Insolation360*OFtop);
F(1083)=1*0.2100*E*alfa*(CTT*DTnw+CI*Insolation360*OFnw);
F(1088)=-1*0.1225*E*alfa*(CTT*DTtop+CI*Insolation360*OFtop);
F(1089)=1*0.2475*E*alfa*(CTT*DTse+CI*Insolation360*OFse);
F(1100)=1*0.1225*E*alfa*(CTT*DTtop+CI*Insolation360*OFtop);
F(1101)=1*0.2100*E*alfa*(CTT*DTnw+CI*Insolation360*OFnw);
F(1106)=-1*0.1225*E*alfa*(CTT*DTtop+CI*Insolation360*OFtop);
F(1107)=1*0.2475*E*alfa*(CTT*DTse+CI*Insolation360*OFse);
F(1124)=1*0.1225*E*alfa*(CTT*DTtop+CI*Insolation360*OFtop);
F(1125)=1*0.2100*E*alfa*(CTT*DTnw+CI*Insolation360*OFnw);

F(1147)=1*0.1225*E*alfa*(CTT*(DTtop+DTse)*0.5+CI*Insolation360*(OFtop+
OFse)*0.5);
F(1148)=-
1*0.1225*E*alfa*(CTT*(DTne+DTtop)*0.5+CI*Insolation360*(OFne+OFtop)*0.
5);

F(1149)=1*0.2475*E*alfa*(CTT*(DTne+DTse)*0.5+CI*Insolation360*(OFne+OF
se)*0.5);
F(1159)=1*0.1225*E*alfa*(CTT*DTtop+CI*Insolation360*OFtop);
F(1161)=1*0.1925*E*alfa*(CTT*DTne+CI*Insolation360*OFne);

F(1165)=1*0.1225*E*alfa*(CTT*(DTtop+DTnw)*0.5+CI*Insolation360*(OFtop+
OFnw)*0.5);

F(1166)=1*0.1225*E*alfa*(CTT*(DTne+DTtop)*0.5+CI*Insolation360*(OFne+O
Ftop)*0.5);

F(1167)=1*0.2100*E*alfa*(CTT*(DTne+DTnw)*0.5+CI*Insolation360*(OFne+OF
nw)*0.5);
F(1173)=1*0.0900*E*alfa*(CTT*DTtop+CI*Insolation360*OFtop);
F(1137)=-1*0.0900*E*alfa*(CTT*DTtop+CI*Insolation360*OFtop);
F(1130)=-1*0.1225*E*alfa*(CTT*DTtop+CI*Insolation360*OFtop);
F(1142)=1*0.1225*E*alfa*(CTT*DTtop+CI*Insolation360*OFtop);
F(1111)=-1*0.1225*E*alfa*(CTT*DTtop+CI*Insolation360*OFtop);
F(1153)=1*0.1225*E*alfa*(CTT*DTtop+CI*Insolation360*OFtop);

end
end

%%output the force vector
n1=size(F,1);
s1=strcat('c:\Model-Data\A6-Force','\F-',int2str(Month),'-
',int2str(t),'-',int2str(tt),'.txt');
fidl=fopen(s1,'w');
for ii=1:n1
for jj=1:1

```

```

        fprintf(fid1, '%.6f\t', F(ii, jj));
        if rem(jj, 1) == 0
            fprintf(fid1, '\r\n');
        end
    end
end
end
fclose(fid1);

end
end

```

```
Ta6force=toc    %%%record the running time
```

XI.3.2 Calculate the forces on B6 structure

```

%Matlab code for calculate the forces on B6 building
tic
clear all

%the month and days need to be calculated
Month=10;
Day=15;
%read the air temperature
airtemperature=load('c:\Model-Data\T-0-Oct-3h.txt');
%read the insolation
insolationX8=load('c:\Model-Data\Insolation-X8-Oct.txt');

%node amount
Node=125;

E=3e10;
alfa=1.2e-5;
%coefficient of temperature transfer
CTT=0.5;
% coefficient insolation and isolation
CI=0.005;

m=size(airtemperature,1);

for t=1:Day

    a=(t-1)*24+1;
    b=t*24;
    Insolation=insolationX8(a:b,:);

    for tt=1:8
        F=zeros(Node*6,1);
        Insolation360=Insolation((1+(tt-1)*3),4);

        for i=1:m

            if airtemperature(i,2)==t && airtemperature(i,3)==tt

                Tse=airtemperature(i,4);
            end
        end
    end
end

```

```

Tsw=airtemperature(i,4);
Tnw=airtemperature(i,4);
Tne=airtemperature(i,4);
Ttop=airtemperature(i,4);

%      inside temperature
IT=21;

DTse=Tse-IT;
DTsw=Tsw-IT;
DTnw=Tnw-IT;
DTne=Tne-IT;

DTtop=Ttop-IT;

Time=(tt-1)*3;

%%%%%%%%%%%%-----OF
OFse=calculateOF(Insolation,135,Time);
OFsw=calculateOF(Insolation,225,Time);
OFnw=calculateOF(Insolation,315,Time);
OFne=calculateOF(Insolation,45,Time);
OFtop=calculateOF(Insolation,-10,Time);

%%%%%%%%%%%%
%%%%%%%%%%%%

%Forces
F(289)=-1*0.0900*E*alfa*(CTT*DTse+CI*Insolation360*OFse);
F(290)=-1*0.0900*E*alfa*(CTT*DTsw+CI*Insolation360*OFsw);
F(307)=-1*0.0900*E*alfa*(CTT*DTnw+CI*Insolation360*OFnw);
F(308)=1*0.0900*E*alfa*(CTT*DTsw+CI*Insolation360*OFsw);
F(362)=-1*0.0900*E*alfa*(CTT*DTne+CI*Insolation360*OFne);
F(380)=1*0.0900*E*alfa*(CTT*DTne+CI*Insolation360*OFne);
F(385)=-1*0.0900*E*alfa*(CTT*DTse+CI*Insolation360*OFse);
F(386)=-1*0.0900*E*alfa*(CTT*DTsw+CI*Insolation360*OFsw);
F(403)=-1*0.0900*E*alfa*(CTT*DTnw+CI*Insolation360*OFnw);
F(404)=1*0.0900*E*alfa*(CTT*DTsw+CI*Insolation360*OFsw);
F(458)=-1*0.0900*E*alfa*(CTT*DTne+CI*Insolation360*OFne);
F(476)=1*0.0900*E*alfa*(CTT*DTne+CI*Insolation360*OFne);
F(481)=-
1*0.0900*E*alfa*(CTT*(DTse+DTtop)*0.5+CI*Insolation360*(OFse+OFtop)*0.
5);
F(482)=-
1*0.0900*E*alfa*(CTT*(DTsw+DTtop)*0.5+CI*Insolation360*(OFsw+OFtop)*0.
5);
F(487)=-1*0.0900*E*alfa*(CTT*DTse+CI*Insolation360*OFse);
F(499)=-1*0.0900*E*alfa*(CTT*DTnw+CI*Insolation360*OFnw);
F(500)=1*0.0900*E*alfa*(CTT*DTsw+CI*Insolation360*OFsw);
F(554)=-
1*0.0900*E*alfa*(CTT*(DTne+DTtop)*0.5+CI*Insolation360*(OFne+OFtop)*0.
5);
F(572)=1*0.0900*E*alfa*(CTT*DTne+CI*Insolation360*OFne);
F(577)=-1*0.0900*E*alfa*(CTT*DTse+CI*Insolation360*OFse);
F(578)=-
1*0.0900*E*alfa*(CTT*(DTsw+DTtop)*0.5+CI*Insolation360*(OFsw+OFtop)*0.
5);
F(583)=-
1*0.0900*E*alfa*(CTT*(DTse+DTtop)*0.5+CI*Insolation360*(OFse+OFtop)*0.
5);

```

Annexes-XI

$F(589) = -1 * 0.0900 * E * \alpha * (CTT * DTnw + CI * Insolation360 * OFnw);$
 $F(607) = -1 * 0.0900 * E * \alpha * (CTT * DTtop + CI * Insolation360 * OFtop);$
 $F(621) = -$
 $1 * 0.0225 * E * \alpha * (CTT * (DTse + DTsw) * 0.5 + CI * Insolation360 * (OFse + OFsw) * 0.5);$
 $F(627) = -$
 $1 * 0.0225 * E * \alpha * (CTT * (DTnw + DTsw) * 0.5 + CI * Insolation360 * (OFnw + OFsw) * 0.5);$
 $F(651) = -$
 $1 * 0.0225 * E * \alpha * (CTT * (DTnw + DTne) * 0.5 + CI * Insolation360 * (OFnw + OFne) * 0.5);$
 $F(679) = -1 * 0.0225 * E * \alpha * (CTT * DTse + CI * Insolation360 * OFse);$
 $F(703) = -$
 $1 * 0.0225 * E * \alpha * (CTT * (DTse + DTtop) * 0.5 + CI * Insolation360 * (OFse + OFtop) * 0.5);$
 $F(709) = -$
 $1 * 0.0225 * E * \alpha * (CTT * (DTnw + DTtop) * 0.5 + CI * Insolation360 * (OFnw + OFtop) * 0.5);$
 $F(727) = -$
 $1 * 0.0225 * E * \alpha * (CTT * (DTse + DTtop) * 0.5 + CI * Insolation360 * (OFse + OFtop) * 0.5);$
 $F(733) = -$
 $1 * 0.0225 * E * \alpha * (CTT * (DTnw + DTtop) * 0.5 + CI * Insolation360 * (OFnw + OFtop) * 0.5);$
 $F(361) = 1 * 0.0900 * E * \alpha * (CTT * DTse + CI * Insolation360 * OFse);$
 $F(379) = 1 * 0.0900 * E * \alpha * (CTT * DTnw + CI * Insolation360 * OFnw);$
 $F(457) = 1 * 0.0900 * E * \alpha * (CTT * DTse + CI * Insolation360 * OFse);$
 $F(475) = 1 * 0.0900 * E * \alpha * (CTT * DTnw + CI * Insolation360 * OFnw);$
 $F(483) = 1 * 0.0900 * E * \alpha * (CTT * (DTse + DTsw) * 0.5 + CI * Insolation360 * (OFse + OFsw) * 0.5);$
 $F(507) = 1 * 0.0900 * E * \alpha * (CTT * DTse + CI * Insolation360 * OFse);$
 $F(531) = 1 * 0.0900 * E * \alpha * (CTT * DTse + CI * Insolation360 * OFse);$
 $F(553) = 1 * 0.0900 * E * \alpha * (CTT * (DTse + DTtop) * 0.5 + CI * Insolation360 * (OFse + OFtop) * 0.5);$
 $F(555) = 1 * 0.0900 * E * \alpha * (CTT * (DTne + DTse) * 0.5 + CI * Insolation360 * (OFne + OFse) * 0.5);$
 $F(559) = 1 * 0.0900 * E * \alpha * (CTT * DTse + CI * Insolation360 * OFse);$
 $F(571) = 1 * 0.0900 * E * \alpha * (CTT * DTnw + CI * Insolation360 * OFnw);$
 $F(590) = 1 * 0.0900 * E * \alpha * (CTT * DTsw + CI * Insolation360 * OFsw);$
 $F(596) = -1 * 0.0900 * E * \alpha * (CTT * DTtop + CI * Insolation360 * OFtop);$
 $F(614) = 1 * 0.0900 * E * \alpha * (CTT * (DTne + DTtop) * 0.5 + CI * Insolation360 * (OFne + OFtop) * 0.5);$
 $F(620) = -$
 $1 * 0.0900 * E * \alpha * (CTT * (DTtop + DTsw) * 0.5 + CI * Insolation360 * (OFtop + OFsw) * 0.5);$
 $F(632) = 1 * 0.0900 * E * \alpha * (CTT * DTtop + CI * Insolation360 * OFtop);$
 $F(638) = -1 * 0.0900 * E * \alpha * (CTT * DTtop + CI * Insolation360 * OFtop);$
 $F(649) = 1 * 0.0900 * E * \alpha * (CTT * (DTnw + DTtop) * 0.5 + CI * Insolation360 * (OFnw + OFtop) * 0.5);$
 $F(656) = 1 * 0.0900 * E * \alpha * (CTT * DTtop + CI * Insolation360 * OFtop);$
 $F(657) = 1 * 0.0900 * E * \alpha * (CTT * DTnw + CI * Insolation360 * OFnw);$
 $F(661) = 1 * 0.0900 * E * \alpha * (CTT * DTse + CI * Insolation360 * OFse);$
 $F(662) = -$
 $1 * 0.0900 * E * \alpha * (CTT * (DTne + DTtop) * 0.5 + CI * Insolation360 * (OFne + OFtop) * 0.5);$
 $F(667) = 1 * 0.0900 * E * \alpha * (CTT * DTtop + CI * Insolation360 * OFtop);$
 $F(669) = 1 * 0.0900 * E * \alpha * (CTT * DTne + CI * Insolation360 * OFne);$

Annexes-XI

$$F(673)=1*0.0900*E*alfa*(CTT*(DTnw+DTtop)*0.5+CI*Insolation360*(OFnw+OFtop)*0.5);$$

$$F(674)=1*0.0900*E*alfa*(CTT*(DTne+DTtop)*0.5+CI*Insolation360*(OFne+OFtop)*0.5);$$

$$F(675)=1*0.0900*E*alfa*(CTT*(DTne+DTnw)*0.5+CI*Insolation360*(OFne+OFnw)*0.5);$$

$$F(681)=1*0.0225*E*alfa*(CTT*(DTse+DTtop)*0.5+CI*Insolation360*(OFse+OFtop)*0.5);$$

$$F(687)=1*0.0225*E*alfa*(CTT*DTse+CI*Insolation360*OFse);$$

$$F(693)=1*0.0225*E*alfa*(CTT*DTse+CI*Insolation360*OFse);$$

$$F(697)=1*0.0225*E*alfa*(CTT*DTse+CI*Insolation360*OFse);$$

$$F(699)=1*0.0225*E*alfa*(CTT*(DTne+DTse)*0.5+CI*Insolation360*(OFne+OFse)*0.5);$$

$$F(704)=-$$

$$1*0.0225*E*alfa*(CTT*(DTsw+DTtop)*0.5+CI*Insolation360*(OFsw+OFtop)*0.5);$$

$$F(705)=1*0.0225*E*alfa*(CTT*(DTse+DTsw)*0.5+CI*Insolation360*(OFse+OFsw)*0.5);$$

$$F(711)=1*0.0225*E*alfa*(CTT*(DTnw+DTsw)*0.5+CI*Insolation360*(OFnw+OFsw)*0.5);$$

$$F(715)=1*0.0225*E*alfa*(CTT*(DTse+DTtop)*0.5+CI*Insolation360*(OFse+OFtop)*0.5);$$

$$F(717)=1*0.0225*E*alfa*(CTT*(DTse+DTne)*0.5+CI*Insolation360*(OFse+OFne)*0.5);$$

$$F(721)=1*0.0225*E*alfa*(CTT*(DTnw+DTtop)*0.5+CI*Insolation360*(OFnw+OFtop)*0.5);$$

$$F(723)=1*0.0225*E*alfa*(CTT*(DTne+DTnw)*0.5+CI*Insolation360*(OFne+OFnw)*0.5);$$

$$F(729)=1*0.0225*E*alfa*(CTT*(DTse+DTsw)*0.5+CI*Insolation360*(OFse+OFsw)*0.5);$$

$$F(735)=1*0.0225*E*alfa*(CTT*(DTnw+DTsw)*0.5+CI*Insolation360*(OFnw+OFsw)*0.5);$$

$$F(739)=1*0.0225*E*alfa*(CTT*(DTse+DTtop)*0.5+CI*Insolation360*(OFse+OFtop)*0.5);$$

$$F(741)=1*0.0225*E*alfa*(CTT*(DTse+DTne)*0.5+CI*Insolation360*(OFse+OFne)*0.5);$$

$$F(745)=1*0.0225*E*alfa*(CTT*(DTnw+DTtop)*0.5+CI*Insolation360*(OFnw+OFtop)*0.5);$$

$$F(747)=1*0.0225*E*alfa*(CTT*(DTnw+DTne)*0.5+CI*Insolation360*(OFnw+OFne)*0.5);$$

$$F(619)=-$$

$$0.09*E*alfa*(CTT*(DTse+DTtop)*0.5+CI*Insolation360*(OFse+OFtop)*0.5)+1*0.0900*E*alfa*(CTT*DTtop+CI*Insolation360*OFtop);$$

$F(501)=0.16 * E * \alpha * (CTT * (DTsw+DTnw) * 0.5 + CI * Insolation360 * (OFsw+OFnw) * 0.5) -$
 $1 * 0.0900 * E * \alpha * (CTT * (DTsw+DTnw) * 0.5 + CI * Insolation360 * (OFsw+OFnw) * 0.5) ;$
 $F(561)=0.16 * E * \alpha * (CTT * DTne + CI * Insolation360 * OFne) -$
 $1 * 0.0900 * E * \alpha * (CTT * (DTse+DTne) * 0.5 + CI * Insolation360 * (OFse+OFne) * 0.5) ;$
 $F(525)=0.16 * E * \alpha * (CTT * DTnw + CI * Insolation360 * OFnw) -$
 $1 * 0.0900 * E * \alpha * (CTT * DTnw + CI * Insolation360 * OFnw) ;$
 $F(489)=0.16 * E * \alpha * (CTT * DTsw + CI * Insolation360 * OFsw) -$
 $1 * 0.0900 * E * \alpha * (CTT * (DTsw+DTse) * 0.5 + CI * Insolation360 * (OFsw+OFse) * 0.5) ;$
 $F(495)=0.16 * E * \alpha * (CTT * DTsw + CI * Insolation360 * OFsw) -$
 $1 * 0.0900 * E * \alpha * (CTT * DTsw + CI * Insolation360 * OFsw) ;$

$F(710)=1 * 0.0225 * E * \alpha * (CTT * (DTsw+DTtop) * 0.5 + CI * Insolation360 * (OFsw+OFtop) * 0.5) ;$
 $F(716)=-$
 $1 * 0.0225 * E * \alpha * (CTT * (DTne+DTtop) * 0.5 + CI * Insolation360 * (OFne+OFtop) * 0.5) ;$

$F(722)=1 * 0.0225 * E * \alpha * (CTT * (DTne+DTtop) * 0.5 + CI * Insolation360 * (OFne+OFtop) * 0.5) ;$
 $F(728)=-$
 $1 * 0.0225 * E * \alpha * (CTT * (DTsw+DTtop) * 0.5 + CI * Insolation360 * (OFsw+OFtop) * 0.5) ;$

$F(734)=1 * 0.0225 * E * \alpha * (CTT * (DTsw+DTtop) * 0.5 + CI * Insolation360 * (OFsw+OFtop) * 0.5) ;$
 $F(740)=-$
 $1 * 0.0225 * E * \alpha * (CTT * (DTne+DTtop) * 0.5 + CI * Insolation360 * (OFne+OFtop) * 0.5) ;$

$F(746)=1 * 0.0225 * E * \alpha * (CTT * (DTne+DTtop) * 0.5 + CI * Insolation360 * (OFne+OFtop) * 0.5) ;$
 $F(506)=-1 * 0.0900 * E * \alpha * (CTT * DTtop + CI * Insolation360 * OFtop) ;$
 $F(512)=1 * 0.0900 * E * \alpha * (CTT * DTtop + CI * Insolation360 * OFtop) ;$
 $F(530)=-1 * 0.0900 * E * \alpha * (CTT * DTtop + CI * Insolation360 * OFtop) ;$
 $F(536)=1 * 0.0900 * E * \alpha * (CTT * DTtop + CI * Insolation360 * OFtop) ;$
 $F(549)=-$

$F(657)+1 * 0.0900 * E * \alpha * (CTT * DTnw + CI * Insolation360 * OFnw) ;$
 $F(643)=-$

$F(667)+1 * 0.0900 * E * \alpha * (CTT * (DTse+DTtop) * 0.5 + CI * Insolation360 * (OFse+OFtop) * 0.5) ;$
 $F(567)=-$

$F(669)+1 * 0.0900 * E * \alpha * (CTT * DTne + CI * Insolation360 * OFne) ;$
 $F(573)=-$

$F(675)+1 * 0.0900 * E * \alpha * (CTT * (DTsw+DTnw) * 0.5 + CI * Insolation360 * (OFsw+OFnw) * 0.5) ;$
 $F(579)=-$

$F(681)+1 * 0.0900 * E * \alpha * (CTT * (DTsw+DTse) * 0.5 + CI * Insolation360 * (OFsw+OFse) * 0.5) ;$
 $F(597)=-$

$F(687)+1 * 0.0900 * E * \alpha * (CTT * DTse + CI * Insolation360 * OFse) ;$
 $F(639)=-$

$F(693)+1 * 0.0900 * E * \alpha * (CTT * DTse + CI * Insolation360 * OFse) ;$
 $F(663)=-$

$F(699)+1 * 0.0900 * E * \alpha * (CTT * (DTse+DTne) * 0.5 + CI * Insolation360 * (OFse+OFne) * 0.5) ;$
 $F(585)=-$

$F(705)+1 * 0.0900 * E * \alpha * (CTT * DTsw + CI * Insolation360 * OFsw) ;$

```

    F(591)=-
F(711)+1*0.0900*E*alfa*(CTT*(DTsw+DTnw)*0.5+CI*Insolation360*(OFsw+OFn
w)*0.5);
    F(615)=-
F(723)+1*0.0900*E*alfa*(CTT*DTnw+CI*Insolation360*OFnw);
    F(387)=-
F(483)+1*0.1600*E*alfa*(CTT*(DTsw+DTse)*0.5+CI*Insolation360*(OFsw+OFs
e)*0.5);
    F(411)=-
F(507)+1*0.1600*E*alfa*(CTT*DTse+CI*Insolation360*OFse);
    F(435)=-
F(531)+1*0.1600*E*alfa*(CTT*DTse+CI*Insolation360*OFse);
    F(459)=-
F(555)+1*0.1600*E*alfa*(CTT*(DTse+DTne)*0.5+CI*Insolation360*(OFse+OFn
e)*0.5);
    F(488)=-F(500)-F(482);
    F(560)=-F(572)-F(554);
    F(584)=-F(578)-F(590);
    F(602)=-F(596)-F(614);
    F(626)=-F(620)-F(632);
    F(625)=-F(649)-F(607);
    F(613)=-F(673)-F(589);
    F(644)=-F(638)-
1*0.0900*E*alfa*(CTT*(DTne+DTtop)*0.5+CI*Insolation360*(OFne+OFtop)*0.
5);
    F(650)=-
F(656)+1*0.0900*E*alfa*(CTT*(DTne+DTtop)*0.5+CI*Insolation360*(OFne+OF
top)*0.5);
    F(601)=-F(583)-
1*0.0900*E*alfa*(CTT*DTtop+CI*Insolation360*OFtop);

    end

    end

    %%output the data
    n1=size(F,1);
    s1=strcat('c:\Model-Data\B6-Force','\F-',int2str(Month),'-
',int2str(t),'-',int2str(tt),'.txt');
    fid1=fopen(s1,'w');
    for ii=1:n1
        for jj=1:1
            fprintf(fid1,'%6f\t',F(ii,jj));
            if rem(jj,1)==0
                fprintf(fid1,'\r\n');
            end
        end
    end
    end
    end
    fclose(fid1);

    end
end

Tb6force=toc    %%record the running time

```

XI.3.3 Calculate the forces on C5 structure

```
%Matlab code for calculate the forces on C5 building
tic
clear all

%the month and days need to be calculated
Month=10;
Day=15;
%read the air temperature
airtemperature=load('c:\Model-Data\T-O-Oct-3h.txt');
%read the insolation
insolationX8=load('c:\Model-Data\Insolation-X8-Oct.txt');

%node amount
Node=224;

F=zeros(Node*6,1);
E=3e10;
alfa=1.2e-5;
%coefficient of temperature transfer
CTT=0.5;
% coefficient insolation and isolation
CI=0.005;

m=size(airtemperature,1);

for t=1:Day

    a=(t-1)*24+1;
    b=t*24;
    Insolation=insolationX8(a:b,:);

    for tt=1:8

        F=zeros(Node*6,1);
        Insolation360=Insolation((1+(tt-1)*3),4);

        for i=1:m

            if airtemperature(i,2)==t && airtemperature(i,3)==tt

                Tse=airtemperature(i,4);
                Tsw=airtemperature(i,4);
                Tnw=airtemperature(i,4);
                Tne=airtemperature(i,4);
                Ttop=airtemperature(i,4);

                %inside temperature
                IT=21;

                DTse=Tse-IT;
                DTsw=Tsw-IT;
                DTnw=Tnw-IT;
                DTne=Tne-IT;

                DTtop=Ttop-IT;
```

Annexes-XI

```

Time=(tt-1)*3;

%-----OF
OFse=calculateOF(Insolation,135,Time);
OFsw=calculateOF(Insolation,225,Time);
OFnw=calculateOF(Insolation,315,Time);
OFne=calculateOF(Insolation,45,Time);
OFtop=calculateOF(Insolation,-10,Time);

%%%%%%%%%%%%%%%%%%%%%%%%%%%%%%%%%%%%%%%%%%%%%%%%%%%%%%%%%%%%%%%%%%%%%%%%%%
%%%%%%%%%%%%%%%%%%%%%%%%%%%%%%%%%%%%%%%%%%%%%%%%%%%%%%%%%%%%%%%%%%%%%%%%%%

%-----Forces

F(721)=-1*0.0900*E*alfa*(CTT*DTse+CI*Insolation360*OFse);
F(722)=-1*0.0900*E*alfa*(CTT*DTsw+CI*Insolation360*OFsw);
F(739)=-1*0.0900*E*alfa*(CTT*DTnw+CI*Insolation360*OFnw);
F(740)=1*0.0900*E*alfa*(CTT*DTsw+CI*Insolation360*OFsw);
F(889)=1*0.0900*E*alfa*(CTT*DTse+CI*Insolation360*OFse);
F(890)=-1*0.0900*E*alfa*(CTT*DTne+CI*Insolation360*OFne);
F(907)=1*0.0900*E*alfa*(CTT*DTnw+CI*Insolation360*OFnw);
F(908)=1*0.0900*E*alfa*(CTT*DTne+CI*Insolation360*OFne);
F(913)=-1*0.0900*E*alfa*(CTT*DTse+CI*Insolation360*OFse);
F(914)=-1*0.0900*E*alfa*(CTT*DTsw+CI*Insolation360*OFsw);
F(931)=-1*0.0900*E*alfa*(CTT*DTnw+CI*Insolation360*OFnw);
F(932)=1*0.0900*E*alfa*(CTT*DTsw+CI*Insolation360*OFsw);
F(1081)=1*0.0900*E*alfa*(CTT*DTse+CI*Insolation360*OFse);
F(1082)=-1*0.0900*E*alfa*(CTT*DTne+CI*Insolation360*OFne);
F(1099)=1*0.0900*E*alfa*(CTT*DTnw+CI*Insolation360*OFnw);
F(1100)=1*0.0900*E*alfa*(CTT*DTne+CI*Insolation360*OFne);
F(1105)=-
1*0.0900*E*alfa*(CTT*(DTse+DTtop)*0.5+CI*Insolation360*(OFse+OFtop)*0.
5);
F(1106)=-
1*0.0900*E*alfa*(CTT*(DTsw+DTtop)*0.5+CI*Insolation360*(OFsw+OFtop)*0.
5);

F(1107)=1*0.0900*E*alfa*(CTT*(DTsw+DTse)*0.5+CI*Insolation360*(OFsw+OF
se)*0.5);
F(1111)=-1*0.0900*E*alfa*(CTT*DTtop+CI*Insolation360*OFtop);
F(1113)=1*0.0900*E*alfa*(CTT*DTsw+CI*Insolation360*OFsw);
F(1117)=-1*0.0900*E*alfa*(CTT*DTtop+CI*Insolation360*OFtop);
F(1119)=1*0.0900*E*alfa*(CTT*DTsw+CI*Insolation360*OFsw);
F(1123)=-
1*0.0900*E*alfa*(CTT*(DTnw+DTtop)*0.5+CI*Insolation360*(OFnw+OFtop)*0.
5);

F(1124)=1*0.0900*E*alfa*(CTT*(DTsw+DTtop)*0.5+CI*Insolation360*(OFsw+O
Ftop)*0.5);

F(1125)=1*0.0900*E*alfa*(CTT*(DTsw+DTnw)*0.5+CI*Insolation360*(OFsw+OF
nw)*0.5);
F(1130)=-1*0.0900*E*alfa*(CTT*DTtop+CI*Insolation360*OFtop);
F(1131)=1*0.0900*E*alfa*(CTT*DTse+CI*Insolation360*OFse);
F(1148)=1*0.0900*E*alfa*(CTT*DTtop+CI*Insolation360*OFtop);
F(1149)=1*0.0900*E*alfa*(CTT*DTnw+CI*Insolation360*OFnw);
F(1154)=-1*0.0900*E*alfa*(CTT*DTtop+CI*Insolation360*OFtop);
F(1155)=1*0.0900*E*alfa*(CTT*DTse+CI*Insolation360*OFse);
F(1172)=1*0.0900*E*alfa*(CTT*DTtop+CI*Insolation360*OFtop);
F(1173)=1*0.0900*E*alfa*(CTT*DTnw+CI*Insolation360*OFnw);

```

Annexes-XI

$F(1178) = -1 * 0.0900 * E * \alpha * (CTT * DT_{top} + CI * Insolation_{360} * OF_{top});$
 $F(1179) = 1 * 0.0900 * E * \alpha * (CTT * DT_{se} + CI * Insolation_{360} * OF_{se});$
 $F(1196) = 1 * 0.0900 * E * \alpha * (CTT * DT_{top} + CI * Insolation_{360} * OF_{top});$
 $F(1197) = 1 * 0.0900 * E * \alpha * (CTT * DT_{nw} + CI * Insolation_{360} * OF_{nw});$
 $F(1202) = -1 * 0.0900 * E * \alpha * (CTT * DT_{top} + CI * Insolation_{360} * OF_{top});$
 $F(1203) = 1 * 0.0900 * E * \alpha * (CTT * DT_{se} + CI * Insolation_{360} * OF_{se});$
 $F(1220) = 1 * 0.0900 * E * \alpha * (CTT * DT_{top} + CI * Insolation_{360} * OF_{top});$
 $F(1221) = 1 * 0.0900 * E * \alpha * (CTT * DT_{nw} + CI * Insolation_{360} * OF_{nw});$
 $F(1226) = -1 * 0.0900 * E * \alpha * (CTT * DT_{top} + CI * Insolation_{360} * OF_{top});$
 $F(1227) = 1 * 0.0900 * E * \alpha * (CTT * DT_{se} + CI * Insolation_{360} * OF_{se});$
 $F(1244) = 1 * 0.0900 * E * \alpha * (CTT * DT_{top} + CI * Insolation_{360} * OF_{top});$
 $F(1245) = 1 * 0.0900 * E * \alpha * (CTT * DT_{nw} + CI * Insolation_{360} * OF_{nw});$
 $F(1250) = -1 * 0.0900 * E * \alpha * (CTT * DT_{top} + CI * Insolation_{360} * OF_{top});$
 $F(1251) = 1 * 0.0900 * E * \alpha * (CTT * DT_{se} + CI * Insolation_{360} * OF_{se});$
 $F(1268) = 1 * 0.0900 * E * \alpha * (CTT * DT_{top} + CI * Insolation_{360} * OF_{top});$
 $F(1269) = 1 * 0.0900 * E * \alpha * (CTT * DT_{nw} + CI * Insolation_{360} * OF_{nw});$

$F(1273) = 1 * 0.0900 * E * \alpha * (CTT * (DT_{se} + DT_{top}) * 0.5 + CI * Insolation_{360} * (OF_{se} + OF_{top}) * 0.5);$
 $F(1274) = -$
 $1 * 0.0900 * E * \alpha * (CTT * (DT_{ne} + DT_{top}) * 0.5 + CI * Insolation_{360} * (OF_{ne} + OF_{top}) * 0.5);$

$F(1275) = 1 * 0.0900 * E * \alpha * (CTT * (DT_{ne} + DT_{se}) * 0.5 + CI * Insolation_{360} * (OF_{ne} + OF_{se}) * 0.5);$
 $F(1279) = 1 * 0.0900 * E * \alpha * (CTT * DT_{top} + CI * Insolation_{360} * OF_{top});$
 $F(1281) = 1 * 0.0900 * E * \alpha * (CTT * DT_{ne} + CI * Insolation_{360} * OF_{ne});$
 $F(1285) = 1 * 0.0900 * E * \alpha * (CTT * DT_{top} + CI * Insolation_{360} * OF_{top});$
 $F(1287) = 1 * 0.0900 * E * \alpha * (CTT * DT_{ne} + CI * Insolation_{360} * OF_{ne});$

$F(1291) = 1 * 0.0900 * E * \alpha * (CTT * (DT_{nw} + DT_{top}) * 0.5 + CI * Insolation_{360} * (OF_{nw} + OF_{top}) * 0.5);$

$F(1292) = 1 * 0.0900 * E * \alpha * (CTT * (DT_{ne} + DT_{top}) * 0.5 + CI * Insolation_{360} * (OF_{ne} + OF_{top}) * 0.5);$

$F(1293) = 1 * 0.0900 * E * \alpha * (CTT * (DT_{ne} + DT_{nw}) * 0.5 + CI * Insolation_{360} * (OF_{ne} + OF_{nw}) * 0.5);$
 $F(1297) = -$
 $1 * 0.09 * E * \alpha * (CTT * (DT_{se} + DT_{top}) * 0.5 + CI * Insolation_{360} * (OF_{se} + OF_{top}) * 0.5);$
 $F(1298) = -$
 $1 * 0.09 * E * \alpha * (CTT * (DT_{sw} + DT_{top}) * 0.5 + CI * Insolation_{360} * (OF_{sw} + OF_{top}) * 0.5);$

$F(1299) = 1 * 0.09 * E * \alpha * (CTT * (DT_{sw} + DT_{se}) * 0.5 + CI * Insolation_{360} * (OF_{sw} + OF_{se}) * 0.5);$
 $F(1303) = -$
 $1 * 0.09 * E * \alpha * (CTT * (DT_{nw} + DT_{top}) * 0.5 + CI * Insolation_{360} * (OF_{nw} + OF_{top}) * 0.5);$

$F(1304) = 1 * 0.09 * E * \alpha * (CTT * (DT_{sw} + DT_{top}) * 0.5 + CI * Insolation_{360} * (OF_{sw} + OF_{top}) * 0.5);$

$F(1305) = 1 * 0.09 * E * \alpha * (CTT * (DT_{sw} + DT_{nw}) * 0.5 + CI * Insolation_{360} * (OF_{sw} + OF_{nw}) * 0.5);$
 $F(1310) = -1 * 0.09 * E * \alpha * (CTT * DT_{top} + CI * Insolation_{360} * OF_{top});$
 $F(1311) = 1 * 0.09 * E * \alpha * (CTT * DT_{se} + CI * Insolation_{360} * OF_{se});$
 $F(1316) = 1 * 0.09 * E * \alpha * (CTT * DT_{top} + CI * Insolation_{360} * OF_{top});$
 $F(1317) = 1 * 0.09 * E * \alpha * (CTT * DT_{nw} + CI * Insolation_{360} * OF_{nw});$
 $F(1322) = -1 * 0.09 * E * \alpha * (CTT * DT_{top} + CI * Insolation_{360} * OF_{top});$
 $F(1323) = 1 * 0.09 * E * \alpha * (CTT * DT_{se} + CI * Insolation_{360} * OF_{se});$
 $F(1328) = 1 * 0.09 * E * \alpha * (CTT * DT_{top} + CI * Insolation_{360} * OF_{top});$
 $F(1329) = 1 * 0.09 * E * \alpha * (CTT * DT_{nw} + CI * Insolation_{360} * OF_{nw});$

```

F(1333)=1*0.09*E*alfa*(CTT*(DTse+DTtop)*0.5+CI*Insolation360*(OFse+OFtop)*0.5);
    F(1334)=-
1*0.09*E*alfa*(CTT*(DTne+DTtop)*0.5+CI*Insolation360*(OFne+OFtop)*0.5);

F(1335)=1*0.09*E*alfa*(CTT*(DTse+DTne)*0.5+CI*Insolation360*(OFse+OFne)*0.5);

F(1339)=1*0.09*E*alfa*(CTT*(DTnw+DTtop)*0.5+CI*Insolation360*(OFnw+OFtop)*0.5);

F(1340)=1*0.09*E*alfa*(CTT*(DTne+DTtop)*0.5+CI*Insolation360*(OFne+OFtop)*0.5);

F(1341)=1*0.09*E*alfa*(CTT*(DTne+DTnw)*0.5+CI*Insolation360*(OFne+OFnw)*0.5);
    F(1160)=-F(1154)-
1*0.09*E*alfa*(CTT*(DTsw+DTtop)*0.5+CI*Insolation360*(OFsw+OFtop)*0.5);
    F(1166)=-
F(1172)+1*0.09*E*alfa*(CTT*(DTsw+DTtop)*0.5+CI*Insolation360*(OFsw+OFtop)*0.5);
    F(1184)=1*0.09*E*alfa*(CTT*DTtop+CI*Insolation360*OFtop);
    F(1190)=-1*0.09*E*alfa*(CTT*DTtop+CI*Insolation360*OFtop);
    F(1208)=1*0.09*E*alfa*(CTT*DTtop+CI*Insolation360*OFtop);
    F(1214)=-1*0.09*E*alfa*(CTT*DTtop+CI*Insolation360*OFtop);
    F(1232)=-F(1226)-
1*0.09*E*alfa*(CTT*(DTne+DTtop)*0.5+CI*Insolation360*(OFne+OFtop)*0.5);
    F(1238)=-
F(1244)+1*0.09*E*alfa*(CTT*(DTne+DTtop)*0.5+CI*Insolation360*(OFne+OFtop)*0.5);
    F(1159)=-F(1111)-
1*0.09*E*alfa*(CTT*(DTse+DTtop)*0.5+CI*Insolation360*(OFse+OFtop)*0.5);
    F(1231)=-
F(1279)+1*0.09*E*alfa*(CTT*(DTse+DTtop)*0.5+CI*Insolation360*(OFse+OFtop)*0.5);
    F(1165)=-F(1117)-
1*0.09*E*alfa*(CTT*(DTnw+DTtop)*0.5+CI*Insolation360*(OFnw+OFtop)*0.5);
    F(1237)=-
F(1285)+1*0.09*E*alfa*(CTT*(DTnw+DTtop)*0.5+CI*Insolation360*(OFnw+OFtop)*0.5);

    end

    end

    %%output the data
    n1=size(F,1);
    s1=strcat('c:\Model-Data\C5-Force','\F-',int2str(Month),'-',int2str(t),'-',int2str(tt),'.txt');
    fid1=fopen(s1,'w');
    for ii=1:n1
        for jj=1:1
            fprintf(fid1,'%0.6f\t',F(ii,jj));
            if rem(jj,1)==0
                fprintf(fid1,'\r\n');
            end
        end
    end
end
end

```

```

        fclose(fid1);

    end
end

Tc5force=toc    %%%record the running time

```

XI.3.4 Calculate the forces on H0 structure

```

%Matlab code for calculate the forces on H0 building
tic

clear all

%the month and days need to be calculated
Month=10;
Day=15;
%read the air temperature
airtemperature=load('c:\Model-Data\T-O-Oct-3h.txt');
%read the insolation
insolationX8=load('c:\Model-Data\Insolation-X8-Oct.txt');
%node amount
Node=474;

F=zeros(Node*6,1);
E=3e10;
alfa=1.2e-5;
%coefficient of temperature transfer
CTT=0.1;
% coefficient insolation
CI=0.001;

m=size(airtemperature,1);

for t=1:Day

    a=(t-1)*24+1;
    b=t*24;
    Insolation=insolationX8(a:b,:);

    for tt=1:8

        F=zeros(Node*6,1);
        Insolation360=Insolation((1+(tt-1)*3),4);

        for i=1:m

            if airtemperature(i,2)==t && airtemperature(i,3)==tt

                Tse=airtemperature(i,4);
                Tsw=airtemperature(i,4);
                Tnw=airtemperature(i,4);
                Tne=airtemperature(i,4);
                Ttop=airtemperature(i,4);
            end
        end
    end
end

```



```
%inside temperature
IT=21;
```

```
DTse=(Tse-IT);
DTsw=Tsw-IT;
DTnw=(Tnw-IT);
DTne=Tne-IT;
```

```
DTtop=(Ttop-IT);
```

```
Time=(tt-1)*3;
```

```
%%%%%%%%%%%%%%%%%%%%%%%%%%%%%%%%%%%%%%%%%%%%%%%%%%%%%%%%%%%%%%%%%%%%%%%%%
```

```
%OF
```

```
OFse=calculateOF(Insolation,101,Time);
OFsw=calculateOF(Insolation,191,Time);
OFnw=calculateOF(Insolation,281,Time);
OFne=calculateOF(Insolation,11,Time);
OFtop=calculateOF(Insolation,-10,Time);
```

```
%%%%%%%%%%%%%%%%%%%%%%%%%%%%%%%%%%%%%%%%%%%%%%%%%%%%%%%%%%%%%%%%%%%%%%%%%
```

```
%Forces
```

```
F(385)=-1*0.0900*E*alfa*(CTT*DTsw+CI*Insolation360*OFsw);
F(403)=-1*0.0900*E*alfa*(CTT*DTne+CI*Insolation360*OFne);
F(745)=1*0.0900*E*alfa*(CTT*DTsw+CI*Insolation360*OFsw);
F(746)=-1*0.0900*E*alfa*(CTT*DTse+CI*Insolation360*OFse);
F(763)=1*0.0900*E*alfa*(CTT*DTne+CI*Insolation360*OFne);
F(764)=1*0.0900*E*alfa*(CTT*DTse+CI*Insolation360*OFse);
F(769)=-1*0.0900*E*alfa*(CTT*DTsw+CI*Insolation360*OFsw);
F(787)=-1*0.0900*E*alfa*(CTT*DTne+CI*Insolation360*OFne);
F(1129)=1*0.0900*E*alfa*(CTT*DTsw+CI*Insolation360*OFsw);
F(1130)=-1*0.0900*E*alfa*(CTT*DTse+CI*Insolation360*OFse);
F(1147)=1*0.0900*E*alfa*(CTT*DTne+CI*Insolation360*OFne);
F(1148)=1*0.0900*E*alfa*(CTT*DTse+CI*Insolation360*OFse);
F(1153)=-1*0.0900*E*alfa*(CTT*DTsw+CI*Insolation360*OFsw);
F(1171)=-1*0.0900*E*alfa*(CTT*DTne+CI*Insolation360*OFne);
F(1513)=1*0.0900*E*alfa*(CTT*DTsw+CI*Insolation360*OFsw);
F(1514)=-1*0.0900*E*alfa*(CTT*DTse+CI*Insolation360*OFse);
F(1531)=1*0.0900*E*alfa*(CTT*DTne+CI*Insolation360*OFne);
F(1532)=1*0.0900*E*alfa*(CTT*DTse+CI*Insolation360*OFse);
F(1537)=-1*0.0900*E*alfa*(CTT*DTsw+CI*Insolation360*OFsw);
F(1555)=-1*0.0900*E*alfa*(CTT*DTne+CI*Insolation360*OFne);
F(1897)=1*0.0900*E*alfa*(CTT*DTsw+CI*Insolation360*OFsw);
F(1898)=-1*0.0900*E*alfa*(CTT*DTse+CI*Insolation360*OFse);
F(1915)=1*0.0900*E*alfa*(CTT*DTne+CI*Insolation360*OFne);
F(1916)=1*0.0900*E*alfa*(CTT*DTse+CI*Insolation360*OFse);
F(1921)=-1*0.0900*E*alfa*(CTT*DTsw+CI*Insolation360*OFsw);
F(1922)=-1*0.0900*E*alfa*(CTT*DTnw+CI*Insolation360*OFnw);
F(1939)=-1*0.0900*E*alfa*(CTT*DTne+CI*Insolation360*OFne);
F(1940)=1*0.0900*E*alfa*(CTT*DTnw+CI*Insolation360*OFnw);
F(2281)=1*0.0900*E*alfa*(CTT*DTsw+CI*Insolation360*OFsw);
F(2282)=-1*0.0900*E*alfa*(CTT*DTse+CI*Insolation360*OFse);
F(2299)=1*0.0900*E*alfa*(CTT*DTne+CI*Insolation360*OFne);
F(2300)=1*0.0900*E*alfa*(CTT*DTse+CI*Insolation360*OFse);
F(2305)=-1*0.0900*E*alfa*(CTT*DTsw+CI*Insolation360*OFsw);
```

Annexes-XI

$F(2306) = -1 * 0.0900 * E * \alpha * (CTT * (DTnw + DTtop) * 0.5 + CI * Insolation360 * (OFnw + OFtop) * 0.5);$
 $F(2311) = -1 * 0.0900 * E * \alpha * (CTT * DTtop + CI * Insolation360 * OFtop);$
 $F(2313) = 1 * 0.2500 * E * \alpha * (CTT * DTnw + CI * Insolation360 * OFnw);$
 $F(2317) = -1 * 0.0900 * E * \alpha * (CTT * DTtop + CI * Insolation360 * OFtop);$
 $F(2319) = 1 * 0.2500 * E * \alpha * (CTT * DTnw + CI * Insolation360 * OFnw);$
 $F(2323) = -1 * 0.0900 * E * \alpha * (CTT * DTne + CI * Insolation360 * OFne);$
 $F(2324) = 1 * 0.0900 * E * \alpha * (CTT * (DTnw + DTtop) * 0.5 + CI * Insolation360 * (OFnw + OFtop) * 0.5);$
 $F(2325) = 1 * 0.2500 * E * \alpha * (CTT * (DTne + DTnw) * 0.5 + CI * Insolation360 * (OFne + OFnw) * 0.5);$
 $F(2330) = -1 * 0.0900 * E * \alpha * (CTT * DTtop + CI * Insolation360 * OFtop);$
 $F(2348) = 1 * 0.0900 * E * \alpha * (CTT * DTtop + CI * Insolation360 * OFtop);$
 $F(2349) = 1 * 0.2500 * E * \alpha * (CTT * DTne + CI * Insolation360 * OFne);$
 $F(2354) = -1 * 0.0900 * E * \alpha * (CTT * DTtop + CI * Insolation360 * OFtop);$
 $F(2372) = 1 * 0.0900 * E * \alpha * (CTT * DTtop + CI * Insolation360 * OFtop);$
 $F(2373) = 1 * 0.2500 * E * \alpha * (CTT * DTne + CI * Insolation360 * OFne);$
 $F(2378) = -1 * 0.0900 * E * \alpha * (CTT * DTtop + CI * Insolation360 * OFtop);$
 $F(2396) = 1 * 0.0900 * E * \alpha * (CTT * (DTnw + DTtop) * 0.5 + CI * Insolation360 * (OFnw + OFtop) * 0.5);$
 $F(2402) = -1 * 0.0900 * E * \alpha * (CTT * DTtop + CI * Insolation360 * OFtop);$
 $F(2420) = 1 * 0.0900 * E * \alpha * (CTT * (DTse + DTtop) * 0.5 + CI * Insolation360 * (OFse + OFtop) * 0.5);$
 $F(2426) = -1 * 0.0900 * E * \alpha * (CTT * DTtop + CI * Insolation360 * OFtop);$
 $F(2444) = 1 * 0.0900 * E * \alpha * (CTT * DTtop + CI * Insolation360 * OFtop);$
 $F(2445) = 1 * 0.2500 * E * \alpha * (CTT * DTne + CI * Insolation360 * OFne);$
 $F(2450) = -1 * 0.0900 * E * \alpha * (CTT * DTtop + CI * Insolation360 * OFtop);$
 $F(2468) = 1 * 0.0900 * E * \alpha * (CTT * DTtop + CI * Insolation360 * OFtop);$
 $F(2469) = 1 * 0.2500 * E * \alpha * (CTT * DTne + CI * Insolation360 * OFne);$
 $F(2474) = -1 * 0.0900 * E * \alpha * (CTT * DTtop + CI * Insolation360 * OFtop);$
 $F(2492) = 1 * 0.0900 * E * \alpha * (CTT * DTtop + CI * Insolation360 * OFtop);$
 $F(2493) = 1 * 0.2500 * E * \alpha * (CTT * DTne + CI * Insolation360 * OFne);$
 $F(2498) = -1 * 0.0900 * E * \alpha * (CTT * DTtop + CI * Insolation360 * OFtop);$
 $F(2516) = 1 * 0.0900 * E * \alpha * (CTT * DTtop + CI * Insolation360 * OFtop);$
 $F(2517) = 1 * 0.2500 * E * \alpha * (CTT * DTne + CI * Insolation360 * OFne);$
 $F(2522) = -1 * 0.0900 * E * \alpha * (CTT * DTtop + CI * Insolation360 * OFtop);$
 $F(2539) = -$
 $1 * 0.0900 * E * \alpha * (CTT * (DTsw + DTtop) * 0.5 + CI * Insolation360 * (OFsw + OFtop) * 0.5);$
 $F(2541) = -$
 $1 * 0.0900 * E * \alpha * (CTT * (DTsw + DTnw) * 0.5 + CI * Insolation360 * (OFsw + OFnw) * 0.5);$
 $F(2546) = 1 * 0.09 * E * \alpha * (CTT * (DTnw + DTtop) * 0.5 + CI * Insolation360 * (OFnw + OFtop) * 0.5);$
 $F(2552) = -1 * 0.0900 * E * \alpha * (CTT * DTtop + CI * Insolation360 * OFtop);$
 $F(2569) = 1 * 0.0900 * E * \alpha * (CTT * (DTtop + DTsw) * 0.5 + CI * Insolation360 * (OFtop + OFsw) * 0.5);$
 $F(2571) = -$
 $1 * 0.0900 * E * \alpha * (CTT * (DTse + DTsw) * 0.5 + CI * Insolation360 * (OFse + OFsw) * 0.5);$
 $F(2576) = 1 * 0.0900 * E * \alpha * (CTT * (DTse + DTtop) * 0.5 + CI * Insolation360 * (OFse + OFtop) * 0.5);$
 $F(2582) = -1 * 0.0900 * E * \alpha * (CTT * DTtop + CI * Insolation360 * OFtop);$
 $F(2600) = 1 * 0.0900 * E * \alpha * (CTT * DTtop + CI * Insolation360 * OFtop);$
 $F(2601) = 1 * 0.2500 * E * \alpha * (CTT * DTne + CI * Insolation360 * OFne);$

Annexes-XI

$F(2606) = -1 * 0.0900 * E * \alpha * (CTT * DT_{top} + CI * Insolation_{360} * OF_{top});$
 $F(2624) = 1 * 0.0900 * E * \alpha * (CTT * DT_{top} + CI * Insolation_{360} * OF_{top});$
 $F(2625) = 1 * 0.2500 * E * \alpha * (CTT * DT_{ne} + CI * Insolation_{360} * OF_{ne});$
 $F(2630) = -1 * 0.0900 * E * \alpha * (CTT * DT_{top} + CI * Insolation_{360} * OF_{top});$
 $F(2648) = 1 * 0.0900 * E * \alpha * (CTT * DT_{top} + CI * Insolation_{360} * OF_{top});$
 $F(2649) = 1 * 0.2500 * E * \alpha * (CTT * DT_{ne} + CI * Insolation_{360} * OF_{ne});$
 $F(2654) = -1 * 0.0900 * E * \alpha * (CTT * DT_{top} + CI * Insolation_{360} * OF_{top});$
 $F(2672) = 1 * 0.0900 * E * \alpha * (CTT * DT_{top} + CI * Insolation_{360} * OF_{top});$
 $F(2673) = 1 * 0.2500 * E * \alpha * (CTT * DT_{ne} + CI * Insolation_{360} * OF_{ne});$
 $F(2677) = 1 * 0.0900 * E * \alpha * (CTT * DT_{sw} + CI * Insolation_{360} * OF_{sw});$
 $F(2678) = -$
 $1 * 0.0900 * E * \alpha * (CTT * (DT_{se} + DT_{top}) * 0.5 + CI * Insolation_{360} * (OF_{se} + OF_{top}) * 0.5);$
 $F(2683) = 1 * 0.0900 * E * \alpha * (CTT * DT_{top} + CI * Insolation_{360} * OF_{top});$
 $F(2685) = 1 * 0.2500 * E * \alpha * (CTT * DT_{se} + CI * Insolation_{360} * OF_{se});$
 $F(2689) = 1 * 0.0900 * E * \alpha * (CTT * DT_{top} + CI * Insolation_{360} * OF_{top});$
 $F(2691) = 1 * 0.2500 * E * \alpha * (CTT * DT_{se} + CI * Insolation_{360} * OF_{se});$
 $F(2695) = 1 * 0.0900 * E * \alpha * (CTT * DT_{ne} + CI * Insolation_{360} * OF_{ne});$

 $F(2696) = 1 * 0.0900 * E * \alpha * (CTT * (DT_{se} + DT_{top}) * 0.5 + CI * Insolation_{360} * (OF_{se} + OF_{top}) * 0.5);$

 $F(2697) = 1 * 0.2500 * E * \alpha * (CTT * (DT_{ne} + DT_{se}) * 0.5 + CI * Insolation_{360} * (OF_{ne} + OF_{se}) * 0.5);$
 $F(2701) = -$
 $1 * 0.0900 * E * \alpha * (CTT * (DT_{sw} + DT_{top}) * 0.5 + CI * Insolation_{360} * (OF_{sw} + OF_{top}) * 0.5);$
 $F(2702) = -$
 $1 * 0.0900 * E * \alpha * (CTT * (DT_{nw} + DT_{top}) * 0.5 + CI * Insolation_{360} * (OF_{nw} + OF_{top}) * 0.5);$

 $F(2703) = 1 * 0.0900 * E * \alpha * (CTT * (DT_{nw} + DT_{sw}) * 0.5 + CI * Insolation_{360} * (OF_{nw} + OF_{sw}) * 0.5);$
 $F(2707) = -$
 $1 * 0.0900 * E * \alpha * (CTT * (DT_{ne} + DT_{top}) * 0.5 + CI * Insolation_{360} * (OF_{ne} + OF_{top}) * 0.5);$

 $F(2708) = 1 * 0.0900 * E * \alpha * (CTT * (DT_{nw} + DT_{top}) * 0.5 + CI * Insolation_{360} * (OF_{nw} + OF_{top}) * 0.5);$

 $F(2709) = 1 * 0.0900 * E * \alpha * (CTT * (DT_{ne} + DT_{nw}) * 0.5 + CI * Insolation_{360} * (OF_{ne} + OF_{nw}) * 0.5);$

 $F(2713) = 1 * 0.0900 * E * \alpha * (CTT * (DT_{sw} + DT_{top}) * 0.5 + CI * Insolation_{360} * (OF_{sw} + OF_{top}) * 0.5);$
 $F(2714) = -$
 $1 * 0.0900 * E * \alpha * (CTT * (DT_{se} + DT_{top}) * 0.5 + CI * Insolation_{360} * (OF_{se} + OF_{top}) * 0.5);$

 $F(2715) = 1 * 0.0900 * E * \alpha * (CTT * (DT_{sw} + DT_{se}) * 0.5 + CI * Insolation_{360} * (OF_{sw} + OF_{se}) * 0.5);$

 $F(2719) = 1 * 0.0900 * E * \alpha * (CTT * (DT_{ne} + DT_{top}) * 0.5 + CI * Insolation_{360} * (OF_{ne} + OF_{top}) * 0.5);$

 $F(2720) = 1 * 0.0900 * E * \alpha * (CTT * (DT_{se} + DT_{top}) * 0.5 + CI * Insolation_{360} * (OF_{se} + OF_{top}) * 0.5);$

 $F(2721) = 1 * 0.0900 * E * \alpha * (CTT * (DT_{ne} + DT_{se}) * 0.5 + CI * Insolation_{360} * (OF_{ne} + OF_{se}) * 0.5);$

Annexes-XI

$F(2725) = -1 * 0.0900 * E * \alpha * (CTT * (DTsw + DTtop) * 0.5 + CI * \text{Insolation360} * (OFsw + OFtop) * 0.5);$

$F(2726) = -1 * 0.0900 * E * \alpha * (CTT * (DTnw + DTtop) * 0.5 + CI * \text{Insolation360} * (OFnw + OFtop) * 0.5);$

$F(2727) = 1 * 0.0900 * E * \alpha * (CTT * (DTsw + DTnw) * 0.5 + CI * \text{Insolation360} * (OFsw + OFnw) * 0.5);$

$F(2731) = -1 * 0.0900 * E * \alpha * (CTT * (DTne + DTtop) * 0.5 + CI * \text{Insolation360} * (OFne + OFtop) * 0.5);$

$F(2732) = 1 * 0.0900 * E * \alpha * (CTT * (DTnw + DTtop) * 0.5 + CI * \text{Insolation360} * (OFnw + OFtop) * 0.5);$

$F(2733) = 1 * 0.0900 * E * \alpha * (CTT * (DTne + DTnw) * 0.5 + CI * \text{Insolation360} * (OFne + OFnw) * 0.5);$

$F(2737) = 1 * 0.0900 * E * \alpha * (CTT * (DTsw + DTtop) * 0.5 + CI * \text{Insolation360} * (OFsw + OFtop) * 0.5);$

$F(2738) = -1 * 0.0900 * E * \alpha * (CTT * (DTse + DTtop) * 0.5 + CI * \text{Insolation360} * (OFse + OFtop) * 0.5);$

$F(2739) = 1 * 0.0900 * E * \alpha * (CTT * (DTse + DTsw) * 0.5 + CI * \text{Insolation360} * (OFse + OFsw) * 0.5);$

$F(2743) = 1 * 0.0900 * E * \alpha * (CTT * (DTne + DTtop) * 0.5 + CI * \text{Insolation360} * (OFne + OFtop) * 0.5);$

$F(2744) = 1 * 0.0900 * E * \alpha * (CTT * (DTse + DTtop) * 0.5 + CI * \text{Insolation360} * (OFse + OFtop) * 0.5);$

$F(2745) = 1 * 0.0900 * E * \alpha * (CTT * (DTne + DTse) * 0.5 + CI * \text{Insolation360} * (OFne + OFse) * 0.5);$

$F(2749) = -1 * 0.0900 * E * \alpha * (CTT * (DTsw + DTtop) * 0.5 + CI * \text{Insolation360} * (OFsw + OFtop) * 0.5);$

$F(2751) = 1 * 0.0900 * E * \alpha * (CTT * (DTsw + DTnw) * 0.5 + CI * \text{Insolation360} * (OFsw + OFnw) * 0.5);$

$F(2757) = 1 * 0.0900 * E * \alpha * (CTT * DTsw + CI * \text{Insolation360} * OFsw);$

$F(2763) = 1 * 0.0900 * E * \alpha * (CTT * DTsw + CI * \text{Insolation360} * OFsw);$

$F(2769) = 1 * 0.0900 * E * \alpha * (CTT * DTsw + CI * \text{Insolation360} * OFsw);$

$F(2775) = 1 * 0.0900 * E * \alpha * (CTT * DTsw + CI * \text{Insolation360} * OFsw);$

$F(2781) = 1 * 0.0900 * E * \alpha * (CTT * DTsw + CI * \text{Insolation360} * OFsw);$

$F(2787) = 1 * 0.0900 * E * \alpha * (CTT * DTsw + CI * \text{Insolation360} * OFsw);$

$F(2793) = 1 * 0.0900 * E * \alpha * (CTT * DTsw + CI * \text{Insolation360} * OFsw);$

$F(2799) = 1 * 0.0900 * E * \alpha * (CTT * DTsw + CI * \text{Insolation360} * OFsw);$

$F(2805) = 1 * 0.0900 * E * \alpha * (CTT * DTsw + CI * \text{Insolation360} * OFsw);$

$F(2811) = 1 * 0.0900 * E * \alpha * (CTT * DTsw + CI * \text{Insolation360} * OFsw);$

$F(2817) = 1 * 0.0900 * E * \alpha * (CTT * DTsw + CI * \text{Insolation360} * OFsw);$

$F(2823) = 1 * 0.0900 * E * \alpha * (CTT * DTsw + CI * \text{Insolation360} * OFsw);$

$F(2829) = 1 * 0.0900 * E * \alpha * (CTT * DTsw + CI * \text{Insolation360} * OFsw);$

$F(2835) = 1 * 0.0900 * E * \alpha * (CTT * DTsw + CI * \text{Insolation360} * OFsw);$

$F(2839) = 1 * 0.0900 * E * \alpha * (CTT * (DTsw + DTtop) * 0.5 + CI * \text{Insolation360} * (OFsw + OFtop) * 0.5);$

Annexes-XI

$$F(2841) = 1 * 0.0900 * E * \alpha * (CTT * (DTsw + DTse) * 0.5 + CI * Insolation360 * (OFsw + OFse) * 0.5);$$

$$F(2389) = -F(2317) - 1 * 0.09 * E * \alpha * (CTT * (DTsw + DTtop) * 0.5 + CI * Insolation360 * (OFsw + OFtop) * 0.5);$$

$$F(2390) = -F(2378) - F(2396);$$

$$F(2413) = -$$

$$F(2689) + 1 * 0.09 * E * \alpha * (CTT * (DTsw + DTtop) * 0.5 + CI * Insolation360 * (OFsw + OFtop) * 0.5);$$

$$F(2414) = -F(2420) - F(2402);$$

$$F(2397) = -$$

$$F(2709) + 1 * 0.25 * E * \alpha * (CTT * DTne + CI * Insolation360 * OFne);$$

$$F(2421) = -$$

$$F(2721) + 1 * 0.25 * E * \alpha * (CTT * DTne + CI * Insolation360 * OFne);$$

$$F(2540) = -F(2546) - F(2522);$$

$$F(2570) = -F(2576) - F(2552);$$

$$F(2547) = -$$

$$F(2733) + 1 * 0.25 * E * \alpha * (CTT * DTne + CI * Insolation360 * OFne);$$

$$F(2577) = -$$

$$F(2745) + 1 * 0.25 * E * \alpha * (CTT * DTne + CI * Insolation360 * OFne);$$

$$F(2307) = -$$

$$F(2751) + 1 * 0.25 * E * \alpha * (CTT * (DTsw + DTnw) * 0.5 + CI * Insolation360 * (OFsw + OFnw) * 0.5);$$

$$F(2331) = -$$

$$F(2757) + 1 * 0.25 * E * \alpha * (CTT * DTsw + CI * Insolation360 * OFsw);$$

$$F(2355) = -$$

$$F(2763) + 1 * 0.25 * E * \alpha * (CTT * DTsw + CI * Insolation360 * OFsw);$$

$$F(2379) = -$$

$$F(2769) + 1 * 0.25 * E * \alpha * (CTT * DTsw + CI * Insolation360 * OFsw);$$

$$F(2403) = -$$

$$F(2775) + 1 * 0.25 * E * \alpha * (CTT * DTsw + CI * Insolation360 * OFsw);$$

$$F(2427) = -$$

$$F(2781) + 1 * 0.25 * E * \alpha * (CTT * DTsw + CI * Insolation360 * OFsw);$$

$$F(2451) = -$$

$$F(2787) + 1 * 0.25 * E * \alpha * (CTT * DTsw + CI * Insolation360 * OFsw);$$

$$F(2475) = -$$

$$F(2793) + 1 * 0.25 * E * \alpha * (CTT * DTsw + CI * Insolation360 * OFsw);$$

$$F(2499) = -$$

$$F(2799) + 1 * 0.25 * E * \alpha * (CTT * DTsw + CI * Insolation360 * OFsw);$$

$$F(2523) = -$$

$$F(2805) + 1 * 0.25 * E * \alpha * (CTT * DTsw + CI * Insolation360 * OFsw);$$

$$F(2553) = -$$

$$F(2811) + 1 * 0.25 * E * \alpha * (CTT * DTsw + CI * Insolation360 * OFsw);$$

$$F(2583) = -$$

$$F(2817) + 1 * 0.25 * E * \alpha * (CTT * DTsw + CI * Insolation360 * OFsw);$$

$$F(2607) = -$$

$$F(2823) + 1 * 0.25 * E * \alpha * (CTT * DTsw + CI * Insolation360 * OFsw);$$

$$F(2631) = -$$

$$F(2829) + 1 * 0.25 * E * \alpha * (CTT * DTsw + CI * Insolation360 * OFsw);$$

$$F(2655) = -$$

$$F(2835) + 1 * 0.25 * E * \alpha * (CTT * DTsw + CI * Insolation360 * OFsw);$$

$$F(2679) = -$$

$$F(2841) + 1 * 0.25 * E * \alpha * (CTT * (DTsw + DTse) * 0.5 + CI * Insolation360 * (OFsw + OFse) * 0.5);$$

```

end

end

%%%output the data
n1=size(F,1);
s1=strcat('c:\Model-Data\H0-Force','\F-',int2str(Month),'-
',int2str(t),'-',int2str(tt),'.txt');
fid1=fopen(s1,'w');
for ii=1:n1
    for jj=1:1
        fprintf(fid1,'% .6f\t',F(ii,jj));
        if rem(jj,1)==0
            fprintf(fid1,'\r\n');
        end
    end
end
end
fclose(fid1);

end
end

Th0force=toc    %%%record the running time

```

XI.3.5 Calculate the forces on K2M structure

```

%Matlab code for calculate the forces on K2M building
tic

clear all
%the month and days need to be calculated
Month=10;
Day=15;
%read the air temperature
airtemperature=load('c:\Model-Data\T-O-Oct-3h.txt');
%read the insolation
insolationX8=load('c:\Model-Data\Insolation-X8-Oct.txt');
%node amount
Node=160;

F=zeros(Node*6,1);
E=3e10;
alfa=1.2e-5;
%coefficient of temperature transfer
CTT=0.7;
% coefficient insolation
CI=0.005;

m=size(airtemperature,1);

for t=1:Day

    a=(t-1)*24+1;
    b=t*24;
    Insolation=insolationX8(a:b,:);

```

```

for tt=1:8

    F=zeros(Node*6,1);
    Insolation360=Insolation((1+(tt-1)*3),4);

    for i=1:m

        if airtemperature(i,2)==t && airtemperature(i,3)==tt &&
airtemperature(i,4)>0

            %%%Outside Temperature
            OTne=outsidetemperatureNE(i,4);
            OTse=outsidetemperatureSE(i,4);
            OTnw=outsidetemperatureNW(i,4);
            Ttop=airtemperature(i,4);

            %%%Inside Temperature
            IT=21;

            %%%Temperature different
            DTse=(OTse-IT);
            DTsw=OTsw-IT;
            DTnw=(OTnw-IT);
            DTne=OTne-IT;
            DTtop=(Ttop-IT);

            Time=(tt-1)*3;

            %%%
            %OF
            OFse=calculateOF(Insolation,141,Time);
            OFnw=calculateOF(Insolation,321,Time);
            OFne=calculateOF(Insolation,51,Time);
            OFtop=calculateOF(Insolation,-10,Time);

            %%%

            % %%forces on the nodes

            F(241)=-1*0.245*E*alfa*(CTT*DTse+CI*Insolation360*OFse);
            F(337)=1*0.245*E*alfa*(CTT*DTse+CI*Insolation360*OFse);
            F(338)=-1*0.245*E*alfa*(CTT*DTne+CI*Insolation360*OFne);
            F(356)=1*0.245*E*alfa*(CTT*DTne+CI*Insolation360*OFne);
            F(361)=-1*0.245*E*alfa*(CTT*DTse+CI*Insolation360*OFse);
            F(457)=1*0.245*E*alfa*(CTT*DTse+CI*Insolation360*OFse);
            F(458)=-1*0.245*E*alfa*(CTT*DTne+CI*Insolation360*OFne);
            F(476)=1*0.245*E*alfa*(CTT*DTne+CI*Insolation360*OFne);
            F(481)=-1*0.245*E*alfa*(CTT*DTse+CI*Insolation360*OFse);
            F(499)=-1*0.245*E*alfa*(CTT*DTnw+CI*Insolation360*OFnw);
            F(577)=1*0.245*E*alfa*(CTT*DTse+CI*Insolation360*OFse);
            F(578)=-1*0.245*E*alfa*(CTT*DTne+CI*Insolation360*OFne);
            F(595)=1*0.245*E*alfa*(CTT*DTnw+CI*Insolation360*OFnw);
            F(596)=1*0.245*E*alfa*(CTT*DTne+CI*Insolation360*OFne);
            F(601)=-1*0.245*E*alfa*(CTT*DTse+CI*Insolation360*OFse);
            F(619)=-1*0.245*E*alfa*(CTT*DTnw+CI*Insolation360*OFnw);
            F(697)=1*0.245*E*alfa*(CTT*DTse+CI*Insolation360*OFse);
            F(698)=-1*0.245*E*alfa*(CTT*DTne+CI*Insolation360*OFne);
            F(715)=1*0.245*E*alfa*(CTT*DTnw+CI*Insolation360*OFnw);

```

Annexes-XI

```

F(716)=1*0.245*E*alfa*(CTT*DTne+CI*Insolation360*OFne);
F(721)=-1*0.245*E*alfa*(CTT*DTse+CI*Insolation360*OFse);
F(739)=-1*0.245*E*alfa*(CTT*DTnw+CI*Insolation360*OFnw);
F(817)=1*0.245*E*alfa*(CTT*DTse+CI*Insolation360*OFse);
F(818)=-1*0.245*E*alfa*(CTT*DTne+CI*Insolation360*OFne);
F(835)=1*0.245*E*alfa*(CTT*DTnw+CI*Insolation360*OFnw);
F(836)=1*0.245*E*alfa*(CTT*DTne+CI*Insolation360*OFne);
F(841)=-
1*0.245*E*alfa*(CTT*(DTse+DTtop)*0.5+CI*Insolation360*(OFse+OFtop)*0.5
);
F(842)=-1*0.245*E*alfa*(CTT*DTtop+CI*Insolation360*OFtop);
F(843)=1*0.1225*E*alfa*(CTT*DTse+CI*Insolation360*OFse);
F(847)=-1*0.245*E*alfa*(CTT*DTtop+CI*Insolation360*OFtop);
F(853)=-1*0.245*E*alfa*(CTT*DTtop+CI*Insolation360*OFtop);
F(859)=-
1*0.245*E*alfa*(CTT*(DTnw+DTtop)*0.5+CI*Insolation360*(OFnw+OFtop)*0.5
);
F(860)=1*0.245*E*alfa*(CTT*DTtop+CI*Insolation360*OFtop);
F(861)=1*0.1225*E*alfa*(CTT*DTnw+CI*Insolation360*OFnw);
F(866)=-1*0.245*E*alfa*(CTT*DTtop+CI*Insolation360*OFtop);
F(867)=1*0.14*E*alfa*(CTT*DTse+CI*Insolation360*OFse);
F(872)=1*0.245*E*alfa*(CTT*DTtop+CI*Insolation360*OFtop);
F(878)=-1*0.245*E*alfa*(CTT*DTtop+CI*Insolation360*OFtop);
F(884)=1*0.245*E*alfa*(CTT*DTtop+CI*Insolation360*OFtop);
F(885)=1*0.14*E*alfa*(CTT*DTnw+CI*Insolation360*OFnw);
F(890)=-1*0.245*E*alfa*(CTT*DTtop+CI*Insolation360*OFtop);
F(891)=1*0.14*E*alfa*(CTT*DTse+CI*Insolation360*OFse);
F(896)=1*0.245*E*alfa*(CTT*DTtop+CI*Insolation360*OFtop);
F(902)=-1*0.245*E*alfa*(CTT*DTtop+CI*Insolation360*OFtop);
F(908)=1*0.245*E*alfa*(CTT*DTtop+CI*Insolation360*OFtop);
F(909)=1*0.14*E*alfa*(CTT*DTnw+CI*Insolation360*OFnw);
F(914)=-1*0.245*E*alfa*(CTT*DTtop+CI*Insolation360*OFtop);
F(915)=1*0.14*E*alfa*(CTT*DTse+CI*Insolation360*OFse);
F(932)=1*0.245*E*alfa*(CTT*DTtop+CI*Insolation360*OFtop);
F(933)=1*0.14*E*alfa*(CTT*DTnw+CI*Insolation360*OFnw);

F(937)=1*0.245*E*alfa*(CTT*(DTse+DTtop)*0.5+CI*Insolation360*(OFse+OFt
op)*0.5);
F(938)=-
1*0.245*E*alfa*(CTT*(DTne+DTtop)*0.5+CI*Insolation360*(OFne+OFtop)*0.5
);

F(939)=1*0.1225*E*alfa*(CTT*(DTse+DTne)*0.5+CI*Insolation360*(OFse+OFn
e)*0.5);
F(943)=1*0.245*E*alfa*(CTT*DTtop+CI*Insolation360*OFtop);
F(945)=1*0.14*E*alfa*(CTT*DTne+CI*Insolation360*OFne);
F(949)=1*0.245*E*alfa*(CTT*DTtop+CI*Insolation360*OFtop);
F(951)=1*0.14*E*alfa*(CTT*DTne+CI*Insolation360*OFne);

F(955)=1*0.245*E*alfa*(CTT*(DTnw+DTtop)*0.5+CI*Insolation360*(OFnw+OFt
op)*0.5);

F(956)=1*0.245*E*alfa*(CTT*(DTne+DTtop)*0.5+CI*Insolation360*(OFne+OFt
op)*0.5);

F(957)=1*0.1225*E*alfa*(CTT*(DTne+DTnw)*0.5+CI*Insolation360*(OFne+OFn
w)*0.5);

end
end
%outp the data

```



```

        n1=size(F,1);
        s1=strcat('c:\Model-Data\K2M-Force','\F-',int2str(Month),'-
',int2str(t),'-',int2str(tt),'.txt');
        fid1=fopen(s1,'w');
        for ii=1:n1
            for jj=1:1
                fprintf(fid1,'%0.6f\t',F(ii,jj));
                if rem(jj,1)==0
                    fprintf(fid1,'\r\n');
                end
            end
        end
    end
    fclose(fid1);

end
end

Tk2mforce=toc    %%%record the running time

```

XI.4 Least square adjustment program code

```

tic

clear all

%%%%%%%%%%%%%%%%%%%%%%%%%%%%%%%%%%%%%%%%%%%%%%%%%%%%%%%%%%%%%%%%%%%%%%%%%setting the initial values%%%%%%%%%%%%%%%%%%%%%%%%%%%%%%%%%%%%%%%%%%%%%%%%%%%%%%%%%%%%%%%%%%%%%%%%%

mon=9;                %the month
SetsNum=30;           %the number of the data files

Xminus=425000;
Yminus=4582000;

DR=[];
SC=[];                % record the coordinates of the RTS

RIT=0;

AngleDifferent=[];   % angle different between two systems

errorellipse=[];    % record the parameters of error ellipse
equationdiscard=[]; % record the discard equations
ED=1;
RTSC=[];             % record the coordinates of RTS

CPN=1;
ControlPoint1=[];
ControlPoint2=[];
ControlPoint3=[];
ControlPoint4=[];
ControlPoint5=[];
ControlPoint6=[];
ControlPoint7=[];
ControlPoint8=[];

```

```

ControlPoint9=[];

%%%%%read the Soldata data of the RTS movement for drawing the
picture
Soldata=load('c:\Inputdata\A6-RTS-Soldata-Sep.txt');

%%%%%%%%%%%%%%%%%%%%%%%%%%%%%%%%%%%%%%%%%%%%%%%%%%%%%%%%%%%%%%%%%%%%%%%%

%%%%%%%%% Calculate the Coordinates of RTS %%%%%%%%%

%%%%%%%%%%%%%%%%%%%%%%%%%%%%%%%%%%%%%%%%%%%%%%%%%%%%%%%%%%%%%%%%%%%%%%%%

for t=1:SetsNum

    for tt=1:8

        %%%%%%%%%read the observation values and coordinates
file%%%%%%%%%
        so=strcat('c:\Inputdata\RTS-Data\RTS-',int2str(mon),'-
',int2str(t),'-',int2str(tt),'.txt');
        Tem1=load(so);
        eval(['RData',num2str(tt),'=Tem1',';']) %%RData- Reference Data
        eval(['ReferenceValues=RData',num2str(tt),';'])

        %the number of reference points
        numberreference=size(ReferenceValues,1);

        if numberreference<2
            Xa=0;
            Ya=0;
            XY(1,1)=0;
            XY(2,1)=0;
            SC(tt,1)=XY(1,1);
            SC(tt,2)=XY(2,1);
            SC(tt,3)=0;
            continue;
        end

        ReferenceValues=sortrows(ReferenceValues,4);

        NamePoints=ReferenceValues(:,3);

        ObservationValues=ReferenceValues(:,4:6);

        Rcoordinates=ReferenceValues(:,7:9);

        for i=1:numberreference
            Rcoordinates(i,1)=Rcoordinates(i,1)-Xminus;
            Rcoordinates(i,2)=Rcoordinates(i,2)-Yminus;
        end

        NOC=[ObservationValues,Rcoordinates];

        n=size(ObservationValues,1);

        %%%%%%%%%Input the approximate coordinate of RTS
X0Y0=[905.9328900;346.6501900];    %%A6

```

```

Xa=X0Y0(1,1);
Ya=X0Y0(2,1);

%%%%%%%%%%%%%%%%%%%%%%%%%%%%%%%%%%%%%%%%%%%%%%%%%%%%%%%%%%%%%%%%%%%%%%%%

%%%%%%%%%%%%%%%%%%%%%%%%%%%%%%%%%%%%%%%%%%%%%%%%%%%%%%%%%%%%%%%%%%%%%%%% the measuring accuracy of distance and angle %%%%%%%%%

%Distance measuring accuracy:1mm+2ppm
DMA1=1;
DMA2=2;
%Angle measuring accuracy:7cc
AMA=7;

%%%%%%%%%%%%%%%%%%%%%%%%%%%%%%%%%%%%%%%%%%%%%%%%%%%%%%%%%%%%%%%%%%%%%%%%
iterationtime=0;

while(1)
    RIT=RIT+1;

    iterationtime=iterationtime+1;
    if iterationtime>10
        break;
    end
    %%Angle matrix---B
    B=calculatematrixB(Rcoordinates,ObservationValues,Xa,Ya);

    %%Distance matrix----L
    L=calculatematrixL(Rcoordinates,ObservationValues,Xa,Ya);

    %%Distance D
    D=calculatematrixD(Rcoordinates,ObservationValues,Xa,Ya);

    %%Weight matrix----P

P=calculatematrixP(Rcoordinates,ObservationValues,Xa,Ya,DMA1,DMA2,AMA);

xy=((B')*P*B)\((B')*P*L);

%calculate the matrix of V
V=B*xy-L;

%%%%%%%%%%%%%%%%%%%%%%%%%%%%%%%%%%%%%%%%%%%%%%%%%%%%%%%%%%%%%%%%%%%%%%%%---Test W-Baarda--%%%%%%%%%%%%%%%%%%%%%%%%%%%%%%%%%%%%%%%%%%%%%%%%%%%%%%%%%%%%%%%%%%%%%%%%

Baarda=calculateBaarda(B,P,V);
Mbaarda=size(Baarda,1);
for i=1:Mbaarda
    BAD(i,ED)=Baarda(i,1);
end

%%%%%%%%%%%%%%%%%%%%%%%%%%%%%%%%%%%%%%%%%%%%%%%%%%%%%%%%%%%%%%%%%%%%%%%%
%%%%%%%%%%%%%%%%%%%%%%%%%%%%%%%%%%%%%%%%%%%%%%%%%%%%%%%%%%%%%%%%%%%%%%%%Identify the gross error

ma=size(B,1);

DR(RIT,1)=t;
DR(RIT,2)=tt;
DR(RIT,3)=iterationtime;

```

```

DC=[];    %%delete the equations-----DC
jj=1;

for i=1:ma
    errorvalue=abs(Baarda(i,1));
    if errorvalue>3.29

        DC(jj)=i;
        jj=jj+1;

        if i<((ma+1)/2)
            na=NamePoints(i,1)*2-1+3;
            DR(RIT,na)=1;

        else
            ni=i-(ma-1)/2;
            nd=NamePoints(ni,1)*2+3;
            DR(RIT,nd)=1;

        end

    end

end

if size(DC,1)>0
    L(DC,:)=[];
    B(DC,:)=[];
    P(DC,:)=[];
    P(:,DC)=[];

end

xy=((B')*P*B)\((B')*P*L);

%%calculate the matrix of V
V=B*xy-L;

%%%%%%%%%%%%%%%%%%%%%%%%%%%%%%%%%%%%%%%%%%%%%%%%%%%%%%%%%%%%%%%%%%%%%%%%

%%calculate the coordinates of station point(RTS)
XY(1,1)=Xa+xy(1,1);
XY(2,1)=Ya+xy(2,1);

Xa=XY(1,1);
Ya=XY(2,1);

if xy(1,1)<0.00001 && xy(2,1)<0.00001
    break;
end

end

SC(tt,1)=XY(1,1)+Xminus;
SC(tt,2)=XY(2,1)+Yminus;

RTSC(ED,1)=mon;
RTSC(ED,2)=t;
RTSC(ED,3)=tt;
RTSC(ED,4)=XY(1,1)+Xminus;

```

```

RTSC(ED,5)=XY(2,1)+Yminus;

%%%%%%%%%%%%%%%%%%%%%%%%%%%%%%%%%%%%%%%%%%%%%%%%%%%%%%%%%%%%%%%%%%%%%%%%calculate the angle between the two systems

AngleDifferent(tt,1)=calculateAngleDifferent(Rcoordinates,ObservationV
alues,XY);

%%%%%%%%%%%%%%%%%%%%%%%%%%%%%%%%%%%%%%%%%%%%%%%%%%%%%%%%%%%%%%%%%%%%%%%%

%%%%%%%%%%%%%%%%%%%%%%%%%%%%%%%%%%%%%%%%%%%%%%%%%%%%%%%%%%%%%%%%%%%%%%%%Height Net
Adjustment%%%%%%%%%%%%%%%%%%%%%%%%%%%%%%%%%%%%%%%%%%%%%%%%%%%%%%%%%%%%%%%%%%%%%%%%

%%%%%%%%%%%%%%%%%%%%%%%%%%%%%%%%%%%%%%%%%%%%%%%%%%%%%%%%%%%%%%%%%%%%%%%%

%%%%%%%%%%%%%%%%%%%%%%%%%%%%%%%%%%%%%%%%%%%%%%%%%%%%%%%%%%%%%%%%%%%%%%%%caculate the matrix of Lz
Lz=zeros(n,1);

for i=1:n
    Lz(i,1)=-
ObservationValues(i,3)*cos(ObservationValues(i,2)*pi/200)...
    +Rcoordinates(i,3);
end

%%%%%%%%%%%%%%%%%%%%%%%%%%%%%%%%%%%%%%%%%%%%%%%%%%%%%%%%%%%%%%%%%%%%%%%%caculate the weight matrix---Pz
Pz=eye(n);

for i=1:n
    ed=(DMA1+DMA2*ObservationValues(i,3)/1000)/1000;    %unit:m
    ev=(AMA/10000)*pi/200;                               %unit:rad
    Zerror=sqrt(((ObservationValues(i,3)+ed)...
        *cos(ObservationValues(i,2)*pi/200)-
ObservationValues(i,3)*...

cos(ObservationValues(i,2)*pi/200)).^2+(ObservationValues(i,3)*...
    cos(ObservationValues(i,2)*pi/200+ev)-...

ObservationValues(i,3)*cos(ObservationValues(i,2)*pi/200)).^2);
    Pz(i,i)=1/(Zerror.^2);
end

Bz=zeros(n,1);

for i=1:n
    Bz(i,1)=1;
end

Nbbz=Bz'*Pz*Bz;
Wz=Bz'*Pz*Lz;

z=Nbbz\Wz;    %%%unit:m

%calculate the matrix of Vz
Vz=Bz-Lz;

%calculate the height of point
ZZ=z;

SC(tt,3)=ZZ;

```

```

RTSC(ED,6)=ZZ;

ED=ED+1;

%%%%%%%%%read the prism's data file%%%%%%%%%
PrismData=[];

sp=strcat('c:\Inputdata\ControlPoints-Data\CPO-',int2str(mon),'-
',int2str(t),'-',int2str(tt),'.txt');
Tem3=load(sp);
PrismData=Tem3; %RCDATA-Reference Coordinates Data

m=size(PrismData,1);
%%compute the prism's coordinates%%%%%%%%%
for i=1:m
    bb=PrismData(i,1);

    switch bb
        case 1
            a1=PrismData(i,2)*pi/200-AngleDifferent(tt,1)*pi/200;
            b1=PrismData(i,3)*pi/200;
            ControlPoint1(CPN,1)=mon;
            ControlPoint1(CPN,2)=t;
            ControlPoint1(CPN,3)=tt;

ControlPoint1(CPN,4)=SC(tt,1)+PrismData(i,4)*sin(b1)*sin(a1);

ControlPoint1(CPN,5)=SC(tt,2)+PrismData(i,4)*sin(b1)*cos(a1);
            ControlPoint1(CPN,6)=SC(tt,3)+PrismData(i,4)*cos(b1);
        case 2

            a2=PrismData(i,2)*pi/200-AngleDifferent(tt,1)*pi/200;
            b2=PrismData(i,3)*pi/200;
            ControlPoint2(CPN,1)=mon;
            ControlPoint2(CPN,2)=t;
            ControlPoint2(CPN,3)=tt;

ControlPoint2(CPN,4)=SC(tt,1)+PrismData(i,4)*sin(b2)*sin(a2);

ControlPoint2(CPN,5)=SC(tt,2)+PrismData(i,4)*sin(b2)*cos(a2);
            ControlPoint2(CPN,6)=SC(tt,3)+PrismData(i,4)*cos(b2);
        case 3

            a3=PrismData(i,2)*pi/200-AngleDifferent(tt,1)*pi/200;
            b3=PrismData(i,3)*pi/200;
            ControlPoint3(CPN,1)=mon;
            ControlPoint3(CPN,2)=t;
            ControlPoint3(CPN,3)=tt;

ControlPoint3(CPN,4)=SC(tt,1)+PrismData(i,4)*sin(b3)*sin(a3);

ControlPoint3(CPN,5)=SC(tt,2)+PrismData(i,4)*sin(b3)*cos(a3);
            ControlPoint3(CPN,6)=SC(tt,3)+PrismData(i,4)*cos(b3);
        case 4
            a4=PrismData(i,2)*pi/200-AngleDifferent(tt,1)*pi/200;
            b4=PrismData(i,3)*pi/200;
            ControlPoint4(CPN,1)=mon;

```

```

ControlPoint4(CPN,2)=t;
ControlPoint4(CPN,3)=tt;

ControlPoint4(CPN,4)=SC(tt,1)+PrismData(i,4)*sin(b4)*sin(a4);

ControlPoint4(CPN,5)=SC(tt,2)+PrismData(i,4)*sin(b4)*cos(a4);
ControlPoint4(CPN,6)=SC(tt,3)+PrismData(i,4)*cos(b4);

case 5
a5=PrismData(i,2)*pi/200-AngleDifferent(tt,1)*pi/200;
b5=PrismData(i,3)*pi/200;
ControlPoint5(CPN,1)=mon;
ControlPoint5(CPN,2)=t;
ControlPoint5(CPN,3)=tt;

ControlPoint5(CPN,4)=SC(tt,1)+PrismData(i,4)*sin(b5)*sin(a5);

ControlPoint5(CPN,5)=SC(tt,2)+PrismData(i,4)*sin(b5)*cos(a5);
ControlPoint5(CPN,6)=SC(tt,3)+PrismData(i,4)*cos(b5);

case 6
a6=PrismData(i,2)*pi/200-AngleDifferent(tt,1)*pi/200;
b6=PrismData(i,3)*pi/200;
ControlPoint6(CPN,1)=mon;
ControlPoint6(CPN,2)=t;
ControlPoint6(CPN,3)=tt;

ControlPoint6(CPN,4)=SC(tt,1)+PrismData(i,4)*sin(b6)*sin(a6);

ControlPoint6(CPN,5)=SC(tt,2)+PrismData(i,4)*sin(b6)*cos(a6);
ControlPoint6(CPN,6)=SC(tt,3)+PrismData(i,4)*cos(b6);

case 7
a7=PrismData(i,2)*pi/200-AngleDifferent(tt,1)*pi/200;
b7=PrismData(i,3)*pi/200;
ControlPoint7(CPN,1)=mon;
ControlPoint7(CPN,2)=t;
ControlPoint7(CPN,3)=tt;

ControlPoint7(CPN,4)=SC(tt,1)+PrismData(i,4)*sin(b7)*sin(a7);

ControlPoint7(CPN,5)=SC(tt,2)+PrismData(i,4)*sin(b7)*cos(a7);
ControlPoint7(CPN,6)=SC(tt,3)+PrismData(i,4)*cos(b7);

case 8
a8=PrismData(i,2)*pi/200-AngleDifferent(tt,1)*pi/200;
b8=PrismData(i,3)*pi/200;
ControlPoint8(CPN,1)=mon;
ControlPoint8(CPN,2)=t;
ControlPoint8(CPN,3)=tt;

ControlPoint8(CPN,4)=SC(tt,1)+PrismData(i,4)*sin(b8)*sin(a8);

ControlPoint8(CPN,5)=SC(tt,2)+PrismData(i,4)*sin(b8)*cos(a8);
ControlPoint8(CPN,6)=SC(tt,3)+PrismData(i,4)*cos(b8);

case 9
a9=PrismData(i,2)*pi/200-AngleDifferent(tt,1)*pi/200;
b9=PrismData(i,3)*pi/200;
ControlPoint9(CPN,1)=mon;

```

```

        ControlPoint9(CPN,2)=t;
        ControlPoint9(CPN,3)=tt;

ControlPoint9(CPN,4)=SC(tt,1)+PrismData(i,4)*sin(b9)*sin(a9);

ControlPoint9(CPN,5)=SC(tt,2)+PrismData(i,4)*sin(b9)*cos(a9);
        ControlPoint9(CPN,6)=SC(tt,3)+PrismData(i,4)*cos(b9);

        end

        end

        CPN=CPN+1;

        end

end

%%%%%%%%%%%%%%%%%%%%%%%%%%%%%%%%%%%%%%%%%%%%%%%%%%%%%%%%%%%%%%%%%%%%%%%%%%%%%%Output the Prisms' Data%%%%%%%%%%%%%%%%%%%%%%%%%%%%%%%%%%%%%%%%%%%%%%%%%%%%%%%%%%%%%%%%%%%%%%%%%%%%%%

%%Output the First Prisms' Data%%
s1=strcat('c:\Outputdata\LSB-P1-C-2013-',int2str(mon),'.txt');
fid1=fopen(s1,'w');

fprintf(fid1,'%s\t','Month','Day','Time','X',' ','Y',' ','Z');
fprintf(fid1,'\r\n');
m1=size(ControlPoint1,1);
for ii=1:m1
    for jj=1:6
        fprintf(fid1,'%f\t',ControlPoint1(ii,jj));
        if rem(jj,6)==0
            fprintf(fid1,'\r\n');
        end
    end
end
end

fclose(fid1);

%%Output the Second Prisms' Data%%
s2=strcat('c:\Outputdata\LSB-P2-C-2013-',int2str(mon),'.txt');
fid2=fopen(s2,'w');

fprintf(fid2,'%s\t','Month','Day','Time','X',' ','Y',' ','Z');
fprintf(fid2,'\r\n');
m2=size(ControlPoint2,1);
for ii=1:m2
    for jj=1:6
        fprintf(fid2,'%f\t',ControlPoint2(ii,jj));
        if rem(jj,6)==0
            fprintf(fid2,'\r\n');
        end
    end
end
end

fclose(fid2);

```



```
%%Output the Third Prisms' Data%%%
s3=strcat('c:\Outputdata\LSB-P3-C-2013-',int2str(mon),'.txt');
fid3=fopen(s3,'w');

fprintf(fid3,'%s\t','Month','Day','Time','X',' ','Y',' ','Z');
fprintf(fid3,'\r\n');
m3=size(ControlPoint3,1);
for ii=1:m3
    for jj=1:6
        fprintf(fid3,'%f\t',ControlPoint3(ii,jj));
        if rem(jj,6)==0
            fprintf(fid3,'\r\n');
        end
    end
end
end

fclose(fid3);

%%Output the Fourth Prisms' Data%%%
s4=strcat('c:\Outputdata\LSB-P4-C-2013-',int2str(mon),'.txt');
fid4=fopen(s4,'w');

fprintf(fid4,'%s\t','Month','Day','Time','X',' ','Y',' ','Z');
fprintf(fid4,'\r\n');
m4=size(ControlPoint4,1);
for ii=1:m4
    for jj=1:6
        fprintf(fid4,'%f\t',ControlPoint4(ii,jj));
        if rem(jj,6)==0
            fprintf(fid4,'\r\n');
        end
    end
end
end

fclose(fid4);

%%Output the Fifth Prisms' Data%%%
s5=strcat('c:\Outputdata\LSB-P5-C-2013-',int2str(mon),'.txt');
fid5=fopen(s5,'w');

fprintf(fid5,'%s\t','Month','Day','Time','X',' ','Y',' ','Z');
fprintf(fid5,'\r\n');
m5=size(ControlPoint5,1);
for ii=1:m5
    for jj=1:6
        fprintf(fid5,'%f\t',ControlPoint5(ii,jj));
        if rem(jj,6)==0
            fprintf(fid5,'\r\n');
        end
    end
end
end

fclose(fid5);

%%Output the Sixth Prisms' Data%%%
s6=strcat('c:\Outputdata\LSB-P6-C-2013-',int2str(mon),'.txt');
fid6=fopen(s6,'w');
```

```
fprintf(fid6, '%s\t', 'Month', 'Day', 'Time', 'X', ' ', 'Y', ' ', 'Z');
fprintf(fid6, '\r\n');
m6=size(ControlPoint6,1);
for ii=1:m6
    for jj=1:6
        fprintf(fid6, '%f\t', ControlPoint6(ii, jj));
        if rem(jj,6)==0
            fprintf(fid6, '\r\n');
        end
    end
end
end

fclose(fid6);

%%Output the Seventh Prisms' Data%%%
s7=strcat('c:\Outputdata\LSB-P7-C-2013-', int2str(mon), '.txt');
fid7=fopen(s7, 'w');

fprintf(fid7, '%s\t', 'Month', 'Day', 'Time', 'X', ' ', 'Y', ' ', 'Z');
fprintf(fid7, '\r\n');
m7=size(ControlPoint7,1);
for ii=1:m7
    for jj=1:6
        fprintf(fid7, '%f\t', ControlPoint7(ii, jj));
        if rem(jj,6)==0
            fprintf(fid7, '\r\n');
        end
    end
end
end

fclose(fid7);

%%Output the Eighth Prisms' Data%%%
s8=strcat('c:\Outputdata\LSB-P8-C-2013-', int2str(mon), '.txt');
fid8=fopen(s8, 'w');

fprintf(fid8, '%s\t', 'Month', 'Day', 'Time', 'X', ' ', 'Y', ' ', 'Z');
fprintf(fid8, '\r\n');
m8=size(ControlPoint8,1);
for ii=1:m8
    for jj=1:6
        fprintf(fid8, '%f\t', ControlPoint8(ii, jj));
        if rem(jj,6)==0
            fprintf(fid8, '\r\n');
        end
    end
end
end

fclose(fid8);

%%Output the Ninth Prisms' Data%%%
s9=strcat('c:\Outputdata\LSB-P9-C-2013-', int2str(mon), '.txt');
fid9=fopen(s9, 'w');

fprintf(fid9, '%s\t', 'Month', 'Day', 'Time', 'X', ' ', 'Y', ' ', 'Z');
fprintf(fid9, '\r\n');
m9=size(ControlPoint9,1);
for ii=1:m9
```

```

    for jj=1:6
        fprintf(fid9, '%f\t', ControlPoint9(ii, jj));
        if rem(jj,6)==0
            fprintf(fid9, '\r\n');
        end
    end
end
end

fclose(fid9);

%%%%%%%%%%%%%%%%%%%%%%%%%%%%%%%%%%%%%%%%%%%%%%%%%%%%%%%%%%%%%%%%%%%%%%%%

%%%%%%%%Output the Robotic Total Station' Coordinates%%%%%%%%

s10=strcat('c:\Outputdata\LSB-RTSC-2013-', int2str(mon), '.txt');

fid10=fopen(s10, 'w');

fprintf(fid10, '%s\t', 'Month', 'Day', 'Time', 'X', ' ', 'Y', ' ', 'Z');
fprintf(fid10, '\r\n');
m11=size(RTSC,1);

for ii=1:m11
    for jj=1:6
        fprintf(fid10, '%f\t', RTSC(ii, jj));
        if rem(jj,6)==0
            fprintf(fid10, '\r\n');
        end
    end
end
end

fclose(fid10);

%%%%%%%%%%%%%%%%%%%%%%%%%%%%%%%%%%%%%%%%%%%%%%%%%%%%%%%%%%%%%%%%%%%%%%%%

%%%%%%%%Draw the picture to show the RTS results%%%%%%%%

%%%%%%%%%%%%%%%%%%%%%%%%%%%%%%%%%%%%%%%%%%%%%%%%%%%%%%%%%%%%%%%%%%%%%%%%

n=size(RTSC,1);
PT=1:1:n;

%%%%%%%%%%%%draw the the displacement of X---
RTS%%%%%%%%
figure

PX=RTSC(:,4);
DX=PX-PX(1,1);

% Soldata RTS movement-X
XS=Soldata(:,1);
DXS=XS-Soldata(1,1);

plot(PT,DX, 'color', 'red', 'linestyle', '- ', 'marker', 'o')

hold on
plot(PT,DXS, 'color', 'blue', 'linestyle', '- ', 'marker', '*')

```

```

legend('LSB-I-F', 'Soldata');

title('X-Displacement')
xlabel('Time'),ylabel('Displacement')

hold on
%%%%%%%%%%%%%%%%%%%%%%%%%%%%%%%%%%%%%%%%%%%%%%%%%%%%%%%%%%%%%%%%%%%%%%%%---draw the the displacement of Y---
RTS%%%%%%%%%%%%%%%%%%%%%%%%%%%%%%%%%%%%%%%%%%%%%%%%%%%%%%%%%%%%%%%%%%%%%%%%
figure

PY=RTSC(:,5);
DY=PY-PY(1,1);

% Soldata RTS movement-Y
YS=Soldata(:,2);
DYS=YS-Soldata(1,2);

plot(PT,DY,'color','red','linestyle','-','marker','o')
hold on

plot(PT,DYS,'color','blue','linestyle','-','marker','*')
legend('LSB-I-F', 'Soldata');

title('Y-Displacement')
xlabel('Time'),ylabel('Displacement')

hold on
%%%%%%%%%%%%%%%%%%%%%%%%%%%%%%%%%%%%%%%%%%%%%%%%%%%%%%%%%%%%%%%%%%%%%%%%---draw the displacement of Z---RTS%%%%%%%%%%%%%%%%%%%%%%%%%%%%%%%%%%%%%%%%%%%%%%%%%%%%%%%%%%%%%%%%%%%%%%%%
figure

PZ=RTSC(:,6);
DZ=PZ-PZ(1,1);

% Soldata RTS movement-Z
ZS=Soldata(:,3);
DZS=ZS-Soldata(1,3);

plot(PT,DZ,'color','red','linestyle','-','marker','o')
hold on

plot(PT,DZS,'color','blue','linestyle','-','marker','*')
legend('LSB-I-F', 'Soldata');

title('Z-Displacement')
xlabel('Time'),ylabel('Displacement')
%%%%%%%%%%%%%%%%%%%%%%%%%%%%%%%%%%%%%%%%%%%%%%%%%%%%%%%%%%%%%%%%%%%%%%%%

Tlsa=toc    %%%record the running time

```

XI.5 Functions

XI.5.1 Calculate the weight matrix----P

```

function
matrixP=calculatematrixP(Rcoordinates,ObservationValues,Xa,Ya,DMA1,DMA
2,AMA)

%%calculate the weight matrix----P

%Input
% Rcoordinates----coordinates of the reference points
% ObservationValues----observation data
% Xa----RTS coordinates of X
% Ya----RTS coordinates of Y
% DMA1----Instrument distance measuring fixed error--1
% DMA2----Instrument distance measuring ratio error--2
% AMA---- Instrument angle measuring accuracy

n=size(ObservationValues,1);

    for i=1:n

        D(i,1)=sqrt((Rcoordinates(i,1)-Xa).^2+(Rcoordinates(i,2)-
Ya).^2);

    end

    for i=1:n
        m=sqrt(DMA1.^2+(DMA2*D(i,1)/1000).^2);
        m=m/1000;                                %unit:m
        P(i+n-1,i+n-1)=1/(m*m);

    end

    for i=1:n-1
        P(i,i)=1/(AMA*AMA);
    end

matrixP=P;

```

XI.5.2 Calculate the matrix----L

```

function matrixL=calculatematrixL(Rcoordinates,ObservationValues,Xa,Ya)

% function to calculate the matrix L

%Input
% Rcoordinates----coordinates of the reference points
% ObservationValues----observation data
% Xa----RTS coordinates of X
% Ya----RTS coordinates of Y

n=size(ObservationValues,1);

```

```

%%%%Angle matrix----first part--L
for i=1:n-1

    DX1=Rcoordinates(i,1)-Xa;
    DY1=Rcoordinates(i,2)-Ya;

    DX2=Rcoordinates(i+1,1)-Xa;
    DY2=Rcoordinates(i+1,2)-Ya;

    Li=ObservationValues(i+1,1)-ObservationValues(i,1);

    if Li<0
        Li=Li+400;
    end

    if Li>200
        Li=400-Li;
    end

    Arctan2=atan(DX2/DY2);

    if DX2>0 && DY2>0
        Arctan2=Arctan2*200/pi;
    end

    if DX2>0 && DY2<0
        Arctan2=Arctan2*200/pi+200;
    end

    if DX2<0 && DY2<0
        Arctan2=Arctan2*200/pi+200;
    end

    if DX2<0 && DY2>0
        Arctan2=Arctan2*200/pi+400;
    end

    az=Rcoordinates(i,1)-Xa;
    bz=Rcoordinates(i,2)-Ya;

    Arctan1=atan(az/bz);

    if DX1>0 && DY1>0
        Arctan1=Arctan1*200/pi;
    end

    if DX1>0 && DY1<0
        Arctan1=Arctan1*200/pi+200;
    end

    if DX1<0 && DY1<0
        Arctan1=Arctan1*200/pi+200;
    end

    if DX1<0 && DY1>0
        Arctan1=Arctan1*200/pi+400;
    end
end

```

```

AA=Arctan2-Arctan1;

if AA<0
    AA=AA+400;
end

if AA>200
    AA=400-AA;
end

l1=(Li-AA)*10000;

L(i,1)=l1;

end

%%Distance matrix----second part--L
for i=1:n

    DX1=Rcoordinates(i,1)-Xa;
    DY1=Rcoordinates(i,2)-Ya;

    S=sqrt(DX1.^2+DY1.^2);

    l11=ObservationValues(i,3);
    l12=sin(ObservationValues(i,2)*pi/200);
    l=l11*l12-S;

    L(i+n-1,1)=l;    %unit:m

end

matrixL=L;

```

XI.5.3 Calculate the matrix----B

```

function matrixB=calculatematrixB(Rcoordinates,ObservationValues,Xa,Ya)
% function to calculate the matrix B

%Input
% Rcoordinates----coordinates of the reference points
% ObservationValues----observation data
% Xa----RTS coordinates of X
% Ya----RTS coordinates of Y

n=size(ObservationValues,1);

%%Angle matrix----first part--B
for i=1:n-1

    DX1=Xa-Rcoordinates(i,1);
    DY1=Rcoordinates(i,2)-Ya;

```

```

DX2=Xa-Rcoordinates(i+1,1);
DY2=Rcoordinates(i+1,2)-Ya;

S1=sqrt(DX1*DX1+DY1*DY1);

S2=sqrt(DX2*DX2+DY2*DY2);

b1=(DY1/(S1*S1)-DY2/(S2*S2))*636620;
b2=(DX1/(S1*S1)-DX2/(S2*S2))*636620;

B(i,1)=b1;
B(i,2)=b2;

end

%%Distance matrix----second part--B
for i=1:n

    DX1=Xa-Rcoordinates(i,1);
    DY1=Ya-Rcoordinates(i,2);

    S=sqrt(DX1.^2+DY1.^2);

    b1=DX1/S;
    b2=DY1/S;

    B(i+n-1,1)=b1;    %unit:m
    B(i+n-1,2)=b2;    %unit:m

end

matrixB=B;

```

XI.5.4 Calculate the matrix of distance----D

```

function matrixD=calculatematrixD(Rcoordinates,ObservationValues,Xa,Ya)
% function to calculate the matrix of distance

%Input
% Rcoordinates----coordinates of the reference points
% ObservationValues----observation data
% Xa----RTS coordinates of X
% Ya----RTS coordinates of Y

n=size(ObservationValues,1);

for i=1:n

    D(i,1)=sqrt((Rcoordinates(i,1)-Xa).^2+(Rcoordinates(i,2)-
Ya).^2);

```



```
end

matrixD=D;
```

XI.5.5 Calculate the Baarda value

```
function Baarda=calculateBaarda(B,P,V)
    %%% calculate the values of W-Baarda

    %Input
    % the matrix of B
    % the matrix of P
    % the matrix of V

    ma=size(B,1);

    Qbb=inv(P)-B*inv(B'*P*B)*B';

    Sbb2=(V'*P*V)/(ma-2);

    Sbb=Sbb2*Qbb;

    for i=1:ma

        Baarda(i,1)=V(i,1)/sqrt(Sbb(i,i));

    end;

    Baarda;
```

XI.5.6 Calculate the angle between the two systems

```
function
AngleD=calculateAngleDifferent(Rcoordinates,ObservationValues,XY)

    %calculate the angle between the two systems

    %input
    % Rcoordinates----coordinates of the reference points
    % ObservationValues----observation data
    % XY----RTS coordinates of X and Y

    SumAngle=0;
    DAngle=[];
    n=size(Rcoordinates,1);

    for i=1:n
```

```

DX1=Rcoordinates(i,1)-XY(1,1);
DY1=Rcoordinates(i,2)-XY(2,1);

Angle=atan(DX1/DY1);

if DX1>0 && DY1>0
    Angle=Angle*200/pi;
end
if DX1>0 && DY1<0
    Angle=Angle*200/pi+200;
end
if DX1<0 && DY1<0
    Angle=Angle*200/pi+200;
end
if DX1<0 && DY1>0
    Angle=Angle*200/pi+400;
end

DAngle(i,1)=ObservationValues(i,1)-Angle;

if DAngle(i,1)<0
    DAngle(i,1)=DAngle(i,1)+400;
end
if DAngle(i,1)>200
    DAngle(i,1)=400-DAngle(i,1);
end

SumAngle=SumAngle+DAngle(i,1);
end

AngleD=SumAngle/n;

```

XI.5.7 Calculate the stiffness matrix

```

function [stiffness]=...
    formStiffness3DframeRectangle01(GDof,numberElements,...
    elementNodes,numberNodes,nodeCoordinates,parameters)

stiffness=zeros(GDof);

% computation of the system stiffness matrix
for e=1:numberElements;
    % elementDof: element degrees of freedom (Dof)
    indice=elementNodes(e,:);
    elementDof=[6*indice(1)-5 6*indice(1)-4 6*indice(1)-3 ...
                6*indice(1)-2 6*indice(1)-1 6*indice(1)...
                6*indice(2)-5 6*indice(2)-4 6*indice(2)-3 ...
                6*indice(2)-2 6*indice(2)-1 6*indice(2)] ;
    x1=nodeCoordinates(indice(1),1);
    y1=nodeCoordinates(indice(1),2);
    z1=nodeCoordinates(indice(1),3);
    x2=nodeCoordinates(indice(2),1);
    y2=nodeCoordinates(indice(2),2);
    z2=nodeCoordinates(indice(2),3);

```

```

L = sqrt((x2-x1)*(x2-x1) + (y2-y1)*(y2-y1) + ...
        (z2-z1)*(z2-z1));
k1 = parameters(e,1)*parameters(e,2)/L;
k2 = 12*parameters(e,1)*parameters(e,3)/(L*L*L);
k3 = 6*parameters(e,1)*parameters(e,3)/(L*L);
k4 = 4*parameters(e,1)*parameters(e,3)/L;
k5 = 2*parameters(e,1)*parameters(e,3)/L;
k6 = 12*parameters(e,1)*parameters(e,4)/(L*L*L);
k7 = 6*parameters(e,1)*parameters(e,4)/(L*L);
k8 = 4*parameters(e,1)*parameters(e,4)/L;
k9 = 2*parameters(e,1)*parameters(e,4)/L;
k10 = parameters(e,5)*parameters(e,6)/L;

a=[k1 0 0; 0 k2 0; 0 0 k6];
b=[ 0 0 0;0 0 k3; 0 -k7 0];
c=[k10 0 0;0 k8 0; 0 0 k4];
d=[-k10 0 0;0 k9 0;0 0 k5];

k = [a b -a b;b' c -b' d; (-a)' -b a -b;b' d' (-b)' c];

if x1 == x2 && y1 == y2
    if z2 > z1
        Lambda = [0 0 -1 ; 0 1 0 ; 1 0 0];
    else
        Lambda = [0 0 1 ; 0 1 0 ; -1 0 0];
    end
else
    if z1==z2 && y1 == y2
        if x2 > x1
            Lambda=[1 0 0;0 1 0;0 0 1];
        else
            Lambda=[-1 0 0;0 -1 0;0 0 1];
        end
    elseif z1==z2 && x1 == x2
        if y2 > y1
            Lambda=[0 -1 0;1 0 0;0 0 1];
        else
            Lambda=[0 1 0;-1 0 0;0 0 1];
        end
    end
end
end

R = [Lambda zeros(3,9); zeros(3) Lambda zeros(3,6);
     zeros(3,6) Lambda zeros(3);zeros(3,9) Lambda];

stiffness(elementDof,elementDof)=...
    stiffness(elementDof,elementDof)+R*k'*R';

end

```

XI.5.8 Calculate the solution

```
function displacements=solution(GDof,prescribedDof,stiffness,force)
```

```

% function to find solution in terms of global displacements
activeDof=setdiff([1:GDof]',...
    [prescribedDof]);
U=stiffness(activeDof,activeDof)\force(activeDof);
displacements=zeros(GDof,1);
displacements(activeDof)=U;

```

XI.5.9 Draw structure

```

function DrawStructure=DrawStructure(nodeCoordinates,elementNodes)

n=size(elementNodes,1);

for i=1:n
    a=elementNodes(i,1);
    b=elementNodes(i,2);

    x1=nodeCoordinates(a,1);
    y1=nodeCoordinates(a,2);
    z1=nodeCoordinates(a,3);

    x2=nodeCoordinates(b,1);
    y2=nodeCoordinates(b,2);
    z2=nodeCoordinates(b,3);

    X=[x1,x2];
    Y=[y1,y2];
    Z=[z1,z2];

    plot3(X,Y,Z,'-mo','LineWidth',1,...
        'MarkerEdgeColor','k','MarkerFaceColor',[.49 1 .63],...
        'markerSize',5);

    grid on

    hold on

end

```

XI.5.10 Draw facade

```

function
DrawFacade=DrawFacade(nodeCoordinates,elementNodes,Nodedisplacement,P,
D)

Nnc=size(nodeCoordinates,1);

Ncn=size(elementNodes,1);

PlaneCoordinates=[];

```

```

PlaneElement=[];

N=1;

for i=1:Nnc
    if nodeCoordinates(i,D)==P
        PlaneCoordinates(N,1)=i;
        PlaneCoordinates(N,2)=nodeCoordinates(i,1);
        PlaneCoordinates(N,3)=nodeCoordinates(i,2);
        PlaneCoordinates(N,4)=nodeCoordinates(i,3);
        N=N+1;
    end
end

PlaneNode=PlaneCoordinates(:,1)';

M=1;
for i=1:Ncn
    a=elementNodes(i,1);
    b=elementNodes(i,2);
    if ismember(a,PlaneNode)==1 && ismember(b,PlaneNode)==1
        PlaneElement(M,1)=a;
        PlaneElement(M,2)=b;
        M=M+1;
    end
end

DrawStructure(Nodedisplacement,PlaneElement);

```

XI.5.11 Plane node coordinates

```

function PlaneNodeCoordinates=PlaneNodeCoordinates(nodeCoordinates,P,D)

Nnc=size(nodeCoordinates,1);

PlaneNodeCoordinates=[];

N=1;

for i=1:Nnc
    if nodeCoordinates(i,D)==P
        PlaneNodeCoordinates(N,1)=i;
        PlaneNodeCoordinates(N,2)=nodeCoordinates(i,1);
        PlaneNodeCoordinates(N,3)=nodeCoordinates(i,2);
        PlaneNodeCoordinates(N,4)=nodeCoordinates(i,3);
        N=N+1;
    end
end

```

XI.6 Simulate reference points' observation data

XI.6.1 With the influence of thermal movement of A6

```

tic

clear all

%%input the month and days
mon=9;
n=30;

%%load the coordinates
RTSA6C=load('c:\Model-Data\A6-RTS-Coordinates.txt'); %RTS-A6-
Coordinates

RPC=load('c:\Model-Data\A6-ReferencePointCoordinates.txt'); %A6-
ReferencePointCoordinates

%%load the simulate movement of the control points and the RTS which
are
%%relates to A6

%%%%%%%%-----A6--RTS
sa6=strcat('c:\Inputdata\A6-SRP\NodeMovement-',int2str(mon),'-Node-
196-A6.txt');
SA6RTSM=load(sa6);

%%%%%%%%-----Reference Points

%%%%%%%%%%%%%%-----B6
sp1=strcat('c:\Inputdata\A6-SRP\NodeMovement-',int2str(mon),'-Node-
115-A6R14.txt');
SA6R14M=load(sp1);

sp2=strcat('c:\Inputdata\A6-SRP\NodeMovement-',int2str(mon),'-Node-
116-A6R28.txt');
SA6R28M=load(sp2);

sp3=strcat('c:\Inputdata\A6-SRP\NodeMovement-',int2str(mon),'-Node-
124-A6R27.txt');
SA6R27M=load(sp3);

%%%%%%%%%%%%%%-----C5
sp4=strcat('c:\Inputdata\A6-SRP\NodeMovement-',int2str(mon),'-Node-
219-A6R12.txt');
SA6R12M=load(sp4);

sp5=strcat('c:\Inputdata\A6-SRP\NodeMovement-',int2str(mon),'-Node-
221-A6R13.txt');
SA6R13M=load(sp5);

%%%%%%%%%%%%%%-----H0

sp6=strcat('c:\Inputdata\A6-SRP\NodeMovement-',int2str(mon),'-Node-
453-A6R19.txt');
SA6R19M=load(sp6);

```

```

sp7=strcat('c:\Inputdata\A6-SRP\NodeMovement-',int2str(mon),'-Node-
455-A6R22.txt');
SA6R22M=load(sp7);

sp8=strcat('c:\Inputdata\A6-SRP\NodeMovement-',int2str(mon),'-Node-
459-A6R18.txt');
SA6R18M=load(sp8);

sp9=strcat('c:\Inputdata\A6-SRP\NodeMovement-',int2str(mon),'-Node-
466-A6R21.txt');
SA6R21M=load(sp9);

sp10=strcat('c:\Inputdata\A6-SRP\NodeMovement-',int2str(mon),'-Node-
471-A6R23.txt');
SA6R23M=load(sp10);

sp11=strcat('c:\Inputdata\A6-SRP\NodeMovement-',int2str(mon),'-Node-
473-A6R24.txt');
SA6R24M=load(sp11);

sp12=strcat('c:\Inputdata\A6-SRP\NodeMovement-',int2str(mon),'-Node-
65-A6R17.txt');
SA6R17M=load(sp12);

sp13=strcat('c:\Inputdata\A6-SRP\NodeMovement-',int2str(mon),'-Node-
93-A6R20.txt');
SA6R20M=load(sp13);

%%simulate observation data
SOD=[];

lengthRTS=size(SA6RTSM,1);

SA6RTSC=SA6RTSM;

SA6R14C=SA6R14M;
SA6R28C=SA6R28M;
SA6R27C=SA6R27M;

SA6R12C=SA6R12M;
SA6R13C=SA6R13M;

SA6R19C=SA6R19M;
SA6R22C=SA6R22M;
SA6R18C=SA6R18M;
SA6R21C=SA6R21M;
SA6R23C=SA6R23M;
SA6R24C=SA6R24M;
SA6R17C=SA6R17M;
SA6R20C=SA6R20M;

for i=1:lengthRTS

    SA6RTSC(i,4)=SA6RTSC(i,4)+RTSA6C(1,1);
    SA6RTSC(i,5)=SA6RTSC(i,5)+RTSA6C(1,2);
    SA6RTSC(i,6)=SA6RTSC(i,6)+RTSA6C(1,3);

```

```
SA6R14C(i,4)=SA6R14C(i,4)+RPC(1,2);
SA6R14C(i,5)=SA6R14C(i,5)+RPC(1,3);
SA6R14C(i,6)=SA6R14C(i,6)+RPC(1,4);

SA6R28C(i,4)=SA6R28C(i,4)+RPC(2,2);
SA6R28C(i,5)=SA6R28C(i,5)+RPC(2,3);
SA6R28C(i,6)=SA6R28C(i,6)+RPC(2,4);

SA6R27C(i,4)=SA6R27C(i,4)+RPC(3,2);
SA6R27C(i,5)=SA6R27C(i,5)+RPC(3,3);
SA6R27C(i,6)=SA6R27C(i,6)+RPC(3,4);

SA6R12C(i,4)=SA6R12C(i,4)+RPC(4,2);
SA6R12C(i,5)=SA6R12C(i,5)+RPC(4,3);
SA6R12C(i,6)=SA6R12C(i,6)+RPC(4,4);

SA6R13C(i,4)=SA6R13C(i,4)+RPC(5,2);
SA6R13C(i,5)=SA6R13C(i,5)+RPC(5,3);
SA6R13C(i,6)=SA6R13C(i,6)+RPC(5,4);

SA6R19C(i,4)=SA6R19C(i,4)+RPC(6,2);
SA6R19C(i,5)=SA6R19C(i,5)+RPC(6,3);
SA6R19C(i,6)=SA6R19C(i,6)+RPC(6,4);

SA6R22C(i,4)=SA6R22C(i,4)+RPC(7,2);
SA6R22C(i,5)=SA6R22C(i,5)+RPC(7,3);
SA6R22C(i,6)=SA6R22C(i,6)+RPC(7,4);

SA6R18C(i,4)=SA6R18C(i,4)+RPC(8,2);
SA6R18C(i,5)=SA6R18C(i,5)+RPC(8,3);
SA6R18C(i,6)=SA6R18C(i,6)+RPC(8,4);

SA6R21C(i,4)=SA6R21C(i,4)+RPC(9,2);
SA6R21C(i,5)=SA6R21C(i,5)+RPC(9,3);
SA6R21C(i,6)=SA6R21C(i,6)+RPC(9,4);

SA6R23C(i,4)=SA6R23C(i,4)+RPC(10,2);
SA6R23C(i,5)=SA6R23C(i,5)+RPC(10,3);
SA6R23C(i,6)=SA6R23C(i,6)+RPC(10,4);

SA6R24C(i,4)=SA6R24C(i,4)+RPC(11,2);
SA6R24C(i,5)=SA6R24C(i,5)+RPC(11,3);
SA6R24C(i,6)=SA6R24C(i,6)+RPC(11,4);

SA6R17C(i,4)=SA6R17C(i,4)+RPC(12,2);
SA6R17C(i,5)=SA6R17C(i,5)+RPC(12,3);
SA6R17C(i,6)=SA6R17C(i,6)+RPC(12,4);

SA6R20C(i,4)=SA6R20C(i,4)+RPC(13,2);
SA6R20C(i,5)=SA6R20C(i,5)+RPC(13,3);
SA6R20C(i,6)=SA6R20C(i,6)+RPC(13,4);
```

```
end
```

```
N=0;
```

```
for i=1:n
    for j=1:8
```



```

N=N+1;

%%%%%%%%%%%%%%%%%%%%%%%%%%%%%%%%%%%%%%%%%%%%%%%%%%%%%%%%%%%%%%%%%%%%%%%% Refernce point---No. 14
DX1=SA6R14C(N,4)-SA6RTSC(N,4);
DY1=SA6R14C(N,5)-SA6RTSC(N,5);
DZ1=SA6R14C(N,6)-SA6RTSC(N,6);

L1=sqrt(DX1.^2+DY1.^2+DZ1.^2);

H1=atan(DX1/DY1);

if DX1>0 && DY1>0
    H1=H1;
end
if DX1>0 && DY1<0
    H1=H1+pi;
end
if DX1<0 && DY1<0
    H1=H1+pi;
end
if DX1<0 && DY1>0
    H1=H1+2*pi;
end

V1=acos(DZ1/L1);

%%%simulate observation data

SOD(1,1)=i;
SOD(1,2)=j;
SOD(1,3)=14;
SOD(1,4)=H1*200/pi;
SOD(1,5)=V1*200/pi;
SOD(1,6)=L1;
SOD(1,7)=SA6R14C(N,4);
SOD(1,8)=SA6R14C(N,5);
SOD(1,9)=SA6R14C(N,6);

%%%%%%%%%%%%%%%%%%%%%%%%%%%%%%%%%%%%%%%%%%%%%%%%%%%%%%%%%%%%%%%%%%%%%%%% Refernce point---No. 28
DX2=SA6R28C(N,4)-SA6RTSC(N,4);
DY2=SA6R28C(N,5)-SA6RTSC(N,5);
DZ2=SA6R28C(N,6)-SA6RTSC(N,6);

L2=sqrt(DX2*DX2+DY2*DY2+DZ2.^2);

H2=atan(DX2/DY2);

if DX2>0 && DY2>0
    H2=H2;
end
if DX2>0 && DY2<0
    H2=H2+pi;
end
if DX2<0 && DY2<0
    H2=H2+pi;
end
if DX2<0 && DY2>0
    H2=H2+2*pi;
end

```

```

end

V2=acos(DZ2/L2);

%%simulate observation data
SOD(2,1)=i;
SOD(2,2)=j;
SOD(2,3)=28;
SOD(2,4)=H2*200/pi;
SOD(2,5)=V2*200/pi;
SOD(2,6)=L2;
SOD(2,7)=SA6R28C(N,4);
SOD(2,8)=SA6R28C(N,5);
SOD(2,9)=SA6R28C(N,6);

%%%%%%%%%%%%% Refernce point---No. 27
DX3=SA6R27C(N,4)-SA6RTSC(N,4);
DY3=SA6R27C(N,5)-SA6RTSC(N,5);
DZ3=SA6R27C(N,6)-SA6RTSC(N,6);

L3=sqrt(DX3*DX3+DY3*DY3+DZ3.^2);

H3=atan(DX3/DY3);

if DX3>0 && DY3>0
    H3=H3;
end
if DX3>0 && DY3<0
    H3=H3+pi;
end
if DX3<0 && DY3<0
    H3=H3+pi;
end
if DX3<0 && DY3>0
    H3=H3+2*pi;
end

V3=acos(DZ3/L3);

%%simulate observation data
SOD(3,1)=i;
SOD(3,2)=j;
SOD(3,3)=27;
SOD(3,4)=H3*200/pi;
SOD(3,5)=V3*200/pi;
SOD(3,6)=L3;
SOD(3,7)=SA6R27C(N,4);
SOD(3,8)=SA6R27C(N,5);
SOD(3,9)=SA6R27C(N,6);

%%%%%%%%%%%%% Refernce point---No. 12
DX4=SA6R12C(N,4)-SA6RTSC(N,4);
DY4=SA6R12C(N,5)-SA6RTSC(N,5);
DZ4=SA6R12C(N,6)-SA6RTSC(N,6);

L4=sqrt(DX4*DX4+DY4*DY4+DZ4.^2);

H4=atan(DX4/DY4);

```

```

if DX4>0 && DY4>0
    H4=H4;
end
if DX4>0 && DY4<0
    H4=H4+pi;
end
if DX4<0 && DY4<0
    H4=H4+pi;
end
if DX4<0 && DY4>0
    H4=H4+2*pi;
end

V4=acos(DZ4/L4);

%%simulate observation data
SOD(4,1)=i;
SOD(4,2)=j;
SOD(4,3)=12;
SOD(4,4)=H4*200/pi;
SOD(4,5)=V4*200/pi;
SOD(4,6)=L4;
SOD(4,7)=SA6R12C(N,4);
SOD(4,8)=SA6R12C(N,5);
SOD(4,9)=SA6R12C(N,6);

%%%%%%%%%%%%% Refernce point---No. 13
DX5=SA6R13C(N,4)-SA6RTSC(N,4);
DY5=SA6R13C(N,5)-SA6RTSC(N,5);
DZ5=SA6R13C(N,6)-SA6RTSC(N,6);

L5=sqrt(DX5*DX5+DY5*DY5+DZ5.^2);

H5=atan(DX5/DY5);

if DX5>0 && DY5>0
    H5=H5;
end
if DX5>0 && DY5<0
    H5=H5+pi;
end
if DX5<0 && DY5<0
    H5=H5+pi;
end
if DX5<0 && DY5>0
    H5=H5+2*pi;
end

V5=acos(DZ5/L5);

%%simulate observation data
SOD(5,1)=i;
SOD(5,2)=j;
SOD(5,3)=13;
SOD(5,4)=H5*200/pi;
SOD(5,5)=V5*200/pi;
SOD(5,6)=L5;
SOD(5,7)=SA6R13C(N,4);
SOD(5,8)=SA6R13C(N,5);
SOD(5,9)=SA6R13C(N,6);

```

```

%%%%%%%%%%%%% Refernce point---No. 19
DX6=SA6R19C(N,4)-SA6RTSC(N,4);
DY6=SA6R19C(N,5)-SA6RTSC(N,5);
DZ6=SA6R19C(N,6)-SA6RTSC(N,6);

L6=sqrt(DX6*DX6+DY6*DY6+DZ6.^2);

H6=atan(DX6/DY6);

if DX6>0 && DY6>0
    H6=H6;
end
if DX6>0 && DY6<0
    H6=H6+pi;
end
if DX6<0 && DY6<0
    H6=H6+pi;
end
if DX6<0 && DY6>0
    H6=H6+2*pi;
end

V6=acos(DZ6/L6);

%%simulate observation data
SOD(6,1)=i;
SOD(6,2)=j;
SOD(6,3)=19;
SOD(6,4)=H6*200/pi;
SOD(6,5)=V6*200/pi;
SOD(6,6)=L6;
SOD(6,7)=SA6R19C(N,4);
SOD(6,8)=SA6R19C(N,5);
SOD(6,9)=SA6R19C(N,6);

%%%%%%%%%%%%% Refernce point---No. 22
DX7=SA6R22C(N,4)-SA6RTSC(N,4);
DY7=SA6R22C(N,5)-SA6RTSC(N,5);
DZ7=SA6R22C(N,6)-SA6RTSC(N,6);

L7=sqrt(DX7*DX7+DY7*DY7+DZ7.^2);

H7=atan(DX7/DY7);

if DX7>0 && DY7>0
    H7=H7;
end
if DX7>0 && DY7<0
    H7=H7+pi;
end
if DX7<0 && DY7<0
    H7=H7+pi;
end
if DX7<0 && DY7>0
    H7=H7+2*pi;
end

V7=acos(DZ7/L7);

```

```

%%%simulate observation data
SOD(7,1)=i;
SOD(7,2)=j;
SOD(7,3)=22;
SOD(7,4)=H7*200/pi;
SOD(7,5)=V7*200/pi;
SOD(7,6)=L7;
SOD(7,7)=SA6R22C(N,4);
SOD(7,8)=SA6R22C(N,5);
SOD(7,9)=SA6R22C(N,6);

%%%%%%%%%%%%% Refernce point---No. 18
DX8=SA6R18C(N,4)-SA6RTSC(N,4);
DY8=SA6R18C(N,5)-SA6RTSC(N,5);
DZ8=SA6R18C(N,6)-SA6RTSC(N,6);

L8=sqrt(DX8*DX8+DY8*DY8+DZ8.^2);

H8=atan(DX8/DY8);

if DX8>0 && DY8>0
    H8=H8;
end
if DX8>0 && DY8<0
    H8=H8+pi;
end
if DX8<0 && DY8<0
    H8=H8+pi;
end
if DX8<0 && DY8>0
    H8=H8+2*pi;
end

V8=acos(DZ8/L8);

%%%simulate observation data
SOD(8,1)=i;
SOD(8,2)=j;
SOD(8,3)=18;
SOD(8,4)=H8*200/pi;
SOD(8,5)=V8*200/pi;
SOD(8,6)=L8;
SOD(8,7)=SA6R18C(N,4);
SOD(8,8)=SA6R18C(N,5);
SOD(8,9)=SA6R18C(N,6);

%%%%%%%%%%%%% Refernce point---No. 21
DX9=SA6R21C(N,4)-SA6RTSC(N,4);
DY9=SA6R21C(N,5)-SA6RTSC(N,5);
DZ9=SA6R21C(N,6)-SA6RTSC(N,6);

L9=sqrt(DX9*DX9+DY9*DY9+DZ9.^2);

H9=atan(DX9/DY9);

if DX9>0 && DY9>0
    H9=H9;
end

```

```

if DX9>0 && DY9<0
    H9=H9+pi;
end
if DX9<0 && DY9<0
    H9=H9+pi;
end
if DX9<0 && DY9>0
    H9=H9+2*pi;
end

V9=acos(DZ9/L9);

%%%simulate observation data
SOD(9,1)=i;
SOD(9,2)=j;
SOD(9,3)=21;
SOD(9,4)=H9*200/pi;
SOD(9,5)=V9*200/pi;
SOD(9,6)=L9;
SOD(9,7)=SA6R21C(N,4);
SOD(9,8)=SA6R21C(N,5);
SOD(9,9)=SA6R21C(N,6);

%%%%%%%%%%%%% Refernce point---No. 23

DX10=SA6R23C(N,4)-SA6RTSC(N,4);
DY10=SA6R23C(N,5)-SA6RTSC(N,5);
DZ10=SA6R23C(N,6)-SA6RTSC(N,6);

L10=sqrt(DX10*DX10+DY10*DY10+DZ10.^2);

H10=atan(DX10/DY10);

if DX10>0 && DY10>0
    H10=H10;
end
if DX10>0 && DY10<0
    H10=H10+pi;
end
if DX10<0 && DY10<0
    H10=H10+pi;
end
if DX10<0 && DY10>0
    H10=H10+2*pi;
end

V10=acos(DZ10/L10);

%%%simulate observation data
SOD(10,1)=i;
SOD(10,2)=j;
SOD(10,3)=23;
SOD(10,4)=H10*200/pi;
SOD(10,5)=V10*200/pi;
SOD(10,6)=L10;
SOD(10,7)=SA6R23C(N,4);
SOD(10,8)=SA6R23C(N,5);
SOD(10,9)=SA6R23C(N,6);

```

```
%%%%%%%%%%%%% Refernce point---No. 24
```

```
DX11=SA6R24C(N,4)-SA6RTSC(N,4);
DY11=SA6R24C(N,5)-SA6RTSC(N,5);
DZ11=SA6R24C(N,6)-SA6RTSC(N,6);

L11=sqrt(DX11*DX11+DY11*DY11+DZ11.^2);

H11=atan(DX11/DY11);

if DX11>0 && DY11>0
    H11=H11;
end
if DX11>0 && DY11<0
    H11=H11+pi;
end
if DX11<0 && DY11<0
    H11=H11+pi;
end
if DX11<0 && DY11>0
    H11=H11+2*pi;
end

V11=acos(DZ11/L11);

%%simulate observation data
SOD(11,1)=i;
SOD(11,2)=j;
SOD(11,3)=24;
SOD(11,4)=H11*200/pi;
SOD(11,5)=V11*200/pi;
SOD(11,6)=L11;
SOD(11,7)=SA6R24C(N,4);
SOD(11,8)=SA6R24C(N,5);
SOD(11,9)=SA6R24C(N,6);
```

```
%%%%%%%%%%%%% Refernce point---No. 17
```

```
DX12=SA6R17C(N,4)-SA6RTSC(N,4);
DY12=SA6R17C(N,5)-SA6RTSC(N,5);
DZ12=SA6R17C(N,6)-SA6RTSC(N,6);

L12=sqrt(DX12*DX12+DY12*DY12+DZ12.^2);

H12=atan(DX12/DY12);

if DX12>0 && DY12>0
    H12=H12;
end
if DX12>0 && DY12<0
    H12=H12+pi;
end
if DX12<0 && DY12<0
    H12=H12+pi;
end
if DX12<0 && DY12>0
    H12=H12+2*pi;
end
```

```

V12=acos(DZ12/L12);

%%%simulate observation data
SOD(12,1)=i;
SOD(12,2)=j;
SOD(12,3)=17;
SOD(12,4)=H12*200/pi;
SOD(12,5)=V12*200/pi;
SOD(12,6)=L12;
SOD(12,7)=SA6R17C(N,4);
SOD(12,8)=SA6R17C(N,5);
SOD(12,9)=SA6R17C(N,6);

%%%%%%%%%%%%% Refernce point---No. 20

DX13=SA6R20C(N,4)-SA6RTSC(N,4);
DY13=SA6R20C(N,5)-SA6RTSC(N,5);
DZ13=SA6R20C(N,6)-SA6RTSC(N,6);

L13=sqrt(DX13*DX13+DY13*DY13+DZ13.^2);

H13=atan(DX13/DY13);

if DX13>0 && DY13>0
    H13=H13;
end
if DX13>0 && DY13<0
    H13=H13+pi;
end
if DX13<0 && DY13<0
    H13=H13+pi;
end
if DX13<0 && DY13>0
    H13=H13+2*pi;
end

V13=acos(DZ13/L13);

%%%simulate observation data
SOD(13,1)=i;
SOD(13,2)=j;
SOD(13,3)=20;
SOD(13,4)=H13*200/pi;
SOD(13,5)=V13*200/pi;
SOD(13,6)=L13;
SOD(13,7)=SA6R20C(N,4);
SOD(13,8)=SA6R20C(N,5);
SOD(13,9)=SA6R20C(N,6);

%%%%%%%%%%%%% Refernce point---No. 6
DX6=425862.508940-SA6RTSC(N,4);
DY6=4582252.560500-SA6RTSC(N,5);
DZ6=91.055200-SA6RTSC(N,6);

L6=sqrt(DX6.^2+DY6.^2+DZ6.^2);

H1=atan(DX6/DY6);

if DX6>0 && DY6>0

```

```

        H6=H6;
    end
    if DX6>0 && DY6<0
        H6=H6+pi;
    end
    if DX6<0 && DY6<0
        H6=H6+pi;
    end
    if DX6<0 && DY6>0
        H6=H6+2*pi;
    end

    V6=acos(DZ6/L6);

    %%simulate observation data
    SOD(14,1)=i;
    SOD(14,2)=j;
    SOD(14,3)=6;
    SOD(14,4)=H6*200/pi;
    SOD(14,5)=V6*200/pi;
    SOD(14,6)=L6;
    SOD(14,7)=RPC(14,2);
    SOD(14,8)=RPC(14,3);
    SOD(14,9)=RPC(14,4);

    %%%%%%%%%%% Refernce point---No. 3
    DX3=425965.947610-SA6RTSC(N,4);
    DY3=4582289.268300-SA6RTSC(N,5);
    DZ3=89.997940-SA6RTSC(N,6);

    L3=sqrt(DX3.^2+DY3.^2+DZ3.^2);

    H3=atan(DX3/DY3);

    if DX3>0 && DY3>0
        H3=H3;
    end
    if DX3>0 && DY3<0
        H3=H3+pi;
    end
    if DX3<0 && DY3<0
        H3=H3+pi;
    end
    if DX3<0 && DY3>0
        H3=H3+2*pi;
    end

    V3=acos(DZ3/L3);

    %%simulate observation data
    SOD(15,1)=i;
    SOD(15,2)=j;
    SOD(15,3)=3;
    SOD(15,4)=H3*200/pi;
    SOD(15,5)=V3*200/pi;
    SOD(15,6)=L3;
    SOD(15,7)=425965.947610;
    SOD(15,8)=4582289.268300;
    SOD(15,9)=89.997940;

```

```

    %%%output the data
    s1=strcat('c:\Model-
Data\SimulateReferencePointsObservationData-B-with ground reference
points\RTS-',int2str(mon),'-',int2str(i),'-',int2str(j),'.txt');
    fid1=fopen(s1,'w');
    for ii=1:21
        for jj=1:9
            fprintf(fid1,'% .6f\t',SOD(ii,jj));
            if rem(jj,9)==0
                fprintf(fid1,'\r\n');
            end
        end
    end
end
fclose(fid1);

end
end

Tappb=toc    %%%record the running time

```

XI.6.2 Without the influence of thermal movement of A6

```

tic

clear all

%%input the month and days
mon=10;
n=15;

%%load the coordinates
RTSA6C=load('c:\Model-Data\A6-RTS-Coordinates.txt'); %RTS-A6-
Coordinates

RPC=load('c:\Model-Data\A6-ReferencePointCoordinates.txt'); %A6-
ReferencePointCoordinates

%%load the simulate movement of the control points and the RTS which
are
%%relates to A6

%%%%%%%%%-----A6--RTS
sa6=strcat('c:\Inputdata\A6-SRP\NodeMovement-',int2str(mon),'-Node-
196-A6.txt');
SA6RTSM=load(sa6);

%%%%%%%%%-----Reference Points

%%%%%%%%%-----B6
sp1=strcat('c:\Inputdata\A6-SRP\NodeMovement-',int2str(mon),'-Node-
115-A6R14.txt');
SA6R14M=load(sp1);

```

```

sp2=strcat('c:\Inputdata\A6-SRP\NodeMovement-',int2str(mon),'-Node-
116-A6R28.txt');
SA6R28M=load(sp2);

sp3=strcat('c:\Inputdata\A6-SRP\NodeMovement-',int2str(mon),'-Node-
124-A6R27.txt');
SA6R27M=load(sp3);

%%%%%%%%%%%%-----C5
sp4=strcat('c:\Inputdata\A6-SRP\NodeMovement-',int2str(mon),'-Node-
219-A6R12.txt');
SA6R12M=load(sp4);

sp5=strcat('c:\Inputdata\A6-SRP\NodeMovement-',int2str(mon),'-Node-
221-A6R13.txt');
SA6R13M=load(sp5);

%%%%%%%%%%%%-----H0

sp6=strcat('c:\Inputdata\A6-SRP\NodeMovement-',int2str(mon),'-Node-
453-A6R19.txt');
SA6R19M=load(sp6);

sp7=strcat('c:\Inputdata\A6-SRP\NodeMovement-',int2str(mon),'-Node-
455-A6R22.txt');
SA6R22M=load(sp7);

sp8=strcat('c:\Inputdata\A6-SRP\NodeMovement-',int2str(mon),'-Node-
459-A6R18.txt');
SA6R18M=load(sp8);

sp9=strcat('c:\Inputdata\A6-SRP\NodeMovement-',int2str(mon),'-Node-
466-A6R21.txt');
SA6R21M=load(sp9);

sp10=strcat('c:\Inputdata\A6-SRP\NodeMovement-',int2str(mon),'-Node-
471-A6R23.txt');
SA6R23M=load(sp10);

sp11=strcat('c:\Inputdata\A6-SRP\NodeMovement-',int2str(mon),'-Node-
473-A6R24.txt');
SA6R24M=load(sp11);

sp12=strcat('c:\Inputdata\A6-SRP\NodeMovement-',int2str(mon),'-Node-
65-A6R17.txt');
SA6R17M=load(sp12);

sp13=strcat('c:\Inputdata\A6-SRP\NodeMovement-',int2str(mon),'-Node-
93-A6R20.txt');
SA6R20M=load(sp13);

%%%simulate observation data
SOD=[];

lengthRTS=size(SA6RTSM,1);

SA6RTSC=SA6RTSM;

```

```
SA6R14C=SA6R14M;  
SA6R28C=SA6R28M;  
SA6R27C=SA6R27M;
```

```
SA6R12C=SA6R12M;  
SA6R13C=SA6R13M;
```

```
SA6R19C=SA6R19M;  
SA6R22C=SA6R22M;  
SA6R18C=SA6R18M;  
SA6R21C=SA6R21M;  
SA6R23C=SA6R23M;  
SA6R24C=SA6R24M;  
SA6R17C=SA6R17M;  
SA6R20C=SA6R20M;
```

```
for i=1:lengthRTS
```

```
    SA6RTSC(i,4)=SA6RTSC(i,4)+RTSA6C(1,1);  
    SA6RTSC(i,5)=SA6RTSC(i,5)+RTSA6C(1,2);  
    SA6RTSC(i,6)=SA6RTSC(i,6)+RTSA6C(1,3);
```

```
    SA6R14C(i,4)=SA6R14C(i,4)+RPC(1,2);  
    SA6R14C(i,5)=SA6R14C(i,5)+RPC(1,3);  
    SA6R14C(i,6)=SA6R14C(i,6)+RPC(1,4);
```

```
    SA6R28C(i,4)=SA6R28C(i,4)+RPC(2,2);  
    SA6R28C(i,5)=SA6R28C(i,5)+RPC(2,3);  
    SA6R28C(i,6)=SA6R28C(i,6)+RPC(2,4);
```

```
    SA6R27C(i,4)=SA6R27C(i,4)+RPC(3,2);  
    SA6R27C(i,5)=SA6R27C(i,5)+RPC(3,3);  
    SA6R27C(i,6)=SA6R27C(i,6)+RPC(3,4);
```

```
    SA6R12C(i,4)=SA6R12C(i,4)+RPC(4,2);  
    SA6R12C(i,5)=SA6R12C(i,5)+RPC(4,3);  
    SA6R12C(i,6)=SA6R12C(i,6)+RPC(4,4);
```

```
    SA6R13C(i,4)=SA6R13C(i,4)+RPC(5,2);  
    SA6R13C(i,5)=SA6R13C(i,5)+RPC(5,3);  
    SA6R13C(i,6)=SA6R13C(i,6)+RPC(5,4);
```

```
    SA6R19C(i,4)=SA6R19C(i,4)+RPC(6,2);  
    SA6R19C(i,5)=SA6R19C(i,5)+RPC(6,3);  
    SA6R19C(i,6)=SA6R19C(i,6)+RPC(6,4);
```

```
    SA6R22C(i,4)=SA6R22C(i,4)+RPC(7,2);  
    SA6R22C(i,5)=SA6R22C(i,5)+RPC(7,3);  
    SA6R22C(i,6)=SA6R22C(i,6)+RPC(7,4);
```

```
    SA6R18C(i,4)=SA6R18C(i,4)+RPC(8,2);  
    SA6R18C(i,5)=SA6R18C(i,5)+RPC(8,3);  
    SA6R18C(i,6)=SA6R18C(i,6)+RPC(8,4);
```

```
    SA6R21C(i,4)=SA6R21C(i,4)+RPC(9,2);  
    SA6R21C(i,5)=SA6R21C(i,5)+RPC(9,3);  
    SA6R21C(i,6)=SA6R21C(i,6)+RPC(9,4);
```

```

SA6R23C(i,4)=SA6R23C(i,4)+RPC(10,2);
SA6R23C(i,5)=SA6R23C(i,5)+RPC(10,3);
SA6R23C(i,6)=SA6R23C(i,6)+RPC(10,4);

SA6R24C(i,4)=SA6R24C(i,4)+RPC(11,2);
SA6R24C(i,5)=SA6R24C(i,5)+RPC(11,3);
SA6R24C(i,6)=SA6R24C(i,6)+RPC(11,4);

SA6R17C(i,4)=SA6R17C(i,4)+RPC(12,2);
SA6R17C(i,5)=SA6R17C(i,5)+RPC(12,3);
SA6R17C(i,6)=SA6R17C(i,6)+RPC(12,4);

SA6R20C(i,4)=SA6R20C(i,4)+RPC(13,2);
SA6R20C(i,5)=SA6R20C(i,5)+RPC(13,3);
SA6R20C(i,6)=SA6R20C(i,6)+RPC(13,4);

end

N=0;

for i=1:n
    for j=1:8

        N=N+1;

        %%%%%%%%%%%%%%%%%%%%%%%%%%%%%%%%%%%%%%%%%

        %%%%%%%%%%%%%%% Refernce point---No. 14
        DX1=SA6R14C(N,4)-SA6RTSC(N,4);
        DY1=SA6R14C(N,5)-SA6RTSC(N,5);
        DZ1=SA6R14C(N,6)-SA6RTSC(N,6);

        L1=sqrt(DX1.^2+DY1.^2+DZ1.^2);

        H1=atan(DX1/DY1);

        if DX1>0 && DY1>0
            H1=H1;
        end
        if DX1>0 && DY1<0
            H1=H1+pi;
        end
        if DX1<0 && DY1<0
            H1=H1+pi;
        end
        if DX1<0 && DY1>0
            H1=H1+2*pi;
        end

        V1=acos(DZ1/L1);

        %%%simulate observation data

        SOD(1,1)=i;
        SOD(1,2)=j;
        SOD(1,3)=14;
        SOD(1,4)=H1*200/pi;
        SOD(1,5)=V1*200/pi;

```

```

SOD(1,6)=L1;
SOD(1,7)=RPC(1,2);
SOD(1,8)=RPC(1,3);
SOD(1,9)=RPC(1,4);

%%%%%%%%%%%%%%%%%%%%%%%%%%%%%%%%%%%%%%%%%%%%%%%%%%%%%%%%%%%%%%%%%%%%%%%% Refernce point---No. 28
DX2=SA6R28C(N,4)-SA6RTSC(N,4);
DY2=SA6R28C(N,5)-SA6RTSC(N,5);
DZ2=SA6R28C(N,6)-SA6RTSC(N,6);

L2=sqrt(DX2*DX2+DY2*DY2+DZ2.^2);

H2=atan(DX2/DY2);

if DX2>0 && DY2>0
    H2=H2;
end
if DX2>0 && DY2<0
    H2=H2+pi;
end
if DX2<0 && DY2<0
    H2=H2+pi;
end
if DX2<0 && DY2>0
    H2=H2+2*pi;
end

V2=acos(DZ2/L2);

%%%simulate observation data
SOD(2,1)=i;
SOD(2,2)=j;
SOD(2,3)=28;
SOD(2,4)=H2*200/pi;
SOD(2,5)=V2*200/pi;
SOD(2,6)=L2;
SOD(2,7)=RPC(2,2);
SOD(2,8)=RPC(2,3);
SOD(2,9)=RPC(2,4);

%%%%%%%%%%%%%%%%%%%%%%%%%%%%%%%%%%%%%%%%%%%%%%%%%%%%%%%%%%%%%%%%%%%%%%%% Refernce point---No. 27
DX3=SA6R27C(N,4)-SA6RTSC(N,4);
DY3=SA6R27C(N,5)-SA6RTSC(N,5);
DZ3=SA6R27C(N,6)-SA6RTSC(N,6);

L3=sqrt(DX3*DX3+DY3*DY3+DZ3.^2);

H3=atan(DX3/DY3);

if DX3>0 && DY3>0
    H3=H3;
end
if DX3>0 && DY3<0
    H3=H3+pi;
end
if DX3<0 && DY3<0
    H3=H3+pi;
end
if DX3<0 && DY3>0

```

```

        H3=H3+2*pi;
    end

    V3=acos(DZ3/L3);

    %%simulate observation data
    SOD(3,1)=i;
    SOD(3,2)=j;
    SOD(3,3)=27;
    SOD(3,4)=H3*200/pi;
    SOD(3,5)=V3*200/pi;
    SOD(3,6)=L3;
    SOD(3,7)=RPC(3,2);
    SOD(3,8)=RPC(3,3);
    SOD(3,9)=RPC(3,4);

    %%%%%%%%%%%%%%%%%%%%%%%%%%%%%%%%%%%%%%%%%%%%%%%%%%%%%%%%%%%%%%%%%%%%%%%%%

    %%%%%%%%%%%%%% Refernce point---No. 12
    DX4=SA6R12C(N,4)-SA6RTSC(N,4);
    DY4=SA6R12C(N,5)-SA6RTSC(N,5);
    DZ4=SA6R12C(N,6)-SA6RTSC(N,6);

    L4=sqrt(DX4*DX4+DY4*DY4+DZ4.^2);

    H4=atan(DX4/DY4);

    if DX4>0 && DY4>0
        H4=H4;
    end
    if DX4>0 && DY4<0
        H4=H4+pi;
    end
    if DX4<0 && DY4<0
        H4=H4+pi;
    end
    if DX4<0 && DY4>0
        H4=H4+2*pi;
    end

    V4=acos(DZ4/L4);

    %%simulate observation data
    SOD(4,1)=i;
    SOD(4,2)=j;
    SOD(4,3)=12;
    SOD(4,4)=H4*200/pi;
    SOD(4,5)=V4*200/pi;
    SOD(4,6)=L4;
    SOD(4,7)=RPC(4,2);
    SOD(4,8)=RPC(4,3);
    SOD(4,9)=RPC(4,4);

    %%%%%%%%%%%%%% Refernce point---No. 13
    DX5=SA6R13C(N,4)-SA6RTSC(N,4);
    DY5=SA6R13C(N,5)-SA6RTSC(N,5);
    DZ5=SA6R13C(N,6)-SA6RTSC(N,6);

    L5=sqrt(DX5*DX5+DY5*DY5+DZ5.^2);

```

```

H5=atan(DX5/DY5);

if DX5>0 && DY5>0
    H5=H5;
end
if DX5>0 && DY5<0
    H5=H5+pi;
end
if DX5<0 && DY5<0
    H5=H5+pi;
end
if DX5<0 && DY5>0
    H5=H5+2*pi;
end

V5=acos(DZ5/L5);

%%simulate observation data
SOD(5,1)=i;
SOD(5,2)=j;
SOD(5,3)=13;
SOD(5,4)=H5*200/pi;
SOD(5,5)=V5*200/pi;
SOD(5,6)=L5;
SOD(5,7)=RPC(5,2);
SOD(5,8)=RPC(5,3);
SOD(5,9)=RPC(5,4);

%%%%%%%%%%%%%%%%%%%%%%%%%%%%%%%%%%%%%%%%%%%%%%%%%%%%%%%%%%%%%%%%%%%%%%%%

%%%%%%%%%%%%%%%%%%%%%%%%%%%%%%%%%%%%%%%%%%%%%%%%%%%%%%%%%%%%%%%%%%%%%%%% Refernce point---No. 19
DX6=SA6R19C(N,4)-SA6RTSC(N,4);
DY6=SA6R19C(N,5)-SA6RTSC(N,5);
DZ6=SA6R19C(N,6)-SA6RTSC(N,6);

L6=sqrt(DX6*DX6+DY6*DY6+DZ6.^2);

H6=atan(DX6/DY6);

if DX6>0 && DY6>0
    H6=H6;
end
if DX6>0 && DY6<0
    H6=H6+pi;
end
if DX6<0 && DY6<0
    H6=H6+pi;
end
if DX6<0 && DY6>0
    H6=H6+2*pi;
end

V6=acos(DZ6/L6);

%%simulate observation data
SOD(6,1)=i;
SOD(6,2)=j;
SOD(6,3)=19;

```

```

SOD(6,4)=H6*200/pi;
SOD(6,5)=V6*200/pi;
SOD(6,6)=L6;
SOD(6,7)=RPC(6,2);
SOD(6,8)=RPC(6,3);
SOD(6,9)=RPC(6,4);

%%%%%%%%%%%%% Refernce point---No. 22
DX7=SA6R22C(N,4)-SA6RTSC(N,4);
DY7=SA6R22C(N,5)-SA6RTSC(N,5);
DZ7=SA6R22C(N,6)-SA6RTSC(N,6);

L7=sqrt(DX7*DX7+DY7*DY7+DZ7.^2);

H7=atan(DX7/DY7);

if DX7>0 && DY7>0
    H7=H7;
end
if DX7>0 && DY7<0
    H7=H7+pi;
end
if DX7<0 && DY7<0
    H7=H7+pi;
end
if DX7<0 && DY7>0
    H7=H7+2*pi;
end

V7=acos(DZ7/L7);

%%%simulate observation data
SOD(7,1)=i;
SOD(7,2)=j;
SOD(7,3)=22;
SOD(7,4)=H7*200/pi;
SOD(7,5)=V7*200/pi;
SOD(7,6)=L7;
SOD(7,7)=RPC(7,2);
SOD(7,8)=RPC(7,3);
SOD(7,9)=RPC(7,4);

%%%%%%%%%%%%% Refernce point---No. 18
DX8=SA6R18C(N,4)-SA6RTSC(N,4);
DY8=SA6R18C(N,5)-SA6RTSC(N,5);
DZ8=SA6R18C(N,6)-SA6RTSC(N,6);

L8=sqrt(DX8*DX8+DY8*DY8+DZ8.^2);

H8=atan(DX8/DY8);

if DX8>0 && DY8>0
    H8=H8;
end
if DX8>0 && DY8<0
    H8=H8+pi;
end
if DX8<0 && DY8<0
    H8=H8+pi;
end

```

```

end
if DX8<0 && DY8>0
    H8=H8+2*pi;
end

V8=acos(DZ8/L8);

%%simulate observation data
SOD(8,1)=i;
SOD(8,2)=j;
SOD(8,3)=18;
SOD(8,4)=H8*200/pi;
SOD(8,5)=V8*200/pi;
SOD(8,6)=L8;
SOD(8,7)=RPC(8,2);
SOD(8,8)=RPC(8,3);
SOD(8,9)=RPC(8,4);

%%%%%%%%%%%%% Refernce point---No. 21
DX9=SA6R21C(N,4)-SA6RTSC(N,4);
DY9=SA6R21C(N,5)-SA6RTSC(N,5);
DZ9=SA6R21C(N,6)-SA6RTSC(N,6);

L9=sqrt(DX9*DX9+DY9*DY9+DZ9.^2);

H9=atan(DX9/DY9);

if DX9>0 && DY9>0
    H9=H9;
end
if DX9>0 && DY9<0
    H9=H9+pi;
end
if DX9<0 && DY9<0
    H9=H9+pi;
end
if DX9<0 && DY9>0
    H9=H9+2*pi;
end

V9=acos(DZ9/L9);

%%simulate observation data
SOD(9,1)=i;
SOD(9,2)=j;
SOD(9,3)=21;
SOD(9,4)=H9*200/pi;
SOD(9,5)=V9*200/pi;
SOD(9,6)=L9;
SOD(9,7)=RPC(9,2);
SOD(9,8)=RPC(9,3);
SOD(9,9)=RPC(9,4);

%%%%%%%%%%%%% Refernce point---No. 23
DX10=SA6R23C(N,4)-SA6RTSC(N,4);
DY10=SA6R23C(N,5)-SA6RTSC(N,5);
DZ10=SA6R23C(N,6)-SA6RTSC(N,6);

```

```

L10=sqrt(DX10*DX10+DY10*DY10+DZ10.^2);

H10=atan(DX10/DY10);

if DX10>0 && DY10>0
    H10=H10;
end
if DX10>0 && DY10<0
    H10=H10+pi;
end
if DX10<0 && DY10<0
    H10=H10+pi;
end
if DX10<0 && DY10>0
    H10=H10+2*pi;
end

V10=acos(DZ10/L10);

%%simulate observation data
SOD(10,1)=i;
SOD(10,2)=j;
SOD(10,3)=23;
SOD(10,4)=H10*200/pi;
SOD(10,5)=V10*200/pi;
SOD(10,6)=L10;
SOD(10,7)=RPC(10,2);
SOD(10,8)=RPC(10,3);
SOD(10,9)=RPC(10,4);

%%%%%%%%%%%%% Refernce point---No. 24

DX11=SA6R24C(N,4)-SA6RTSC(N,4);
DY11=SA6R24C(N,5)-SA6RTSC(N,5);
DZ11=SA6R24C(N,6)-SA6RTSC(N,6);

L11=sqrt(DX11*DX11+DY11*DY11+DZ11.^2);

H11=atan(DX11/DY11);

if DX11>0 && DY11>0
    H11=H11;
end
if DX11>0 && DY11<0
    H11=H11+pi;
end
if DX11<0 && DY11<0
    H11=H11+pi;
end
if DX11<0 && DY11>0
    H11=H11+2*pi;
end

V11=acos(DZ11/L11);

%%simulate observation data
SOD(11,1)=i;
SOD(11,2)=j;
SOD(11,3)=24;

```

```

SOD(11,4)=H11*200/pi;
SOD(11,5)=V11*200/pi;
SOD(11,6)=L11;
SOD(11,7)=RPC(11,2);
SOD(11,8)=RPC(11,3);
SOD(11,9)=RPC(11,4);

##### Refernce point---No. 17

DX12=SA6R17C(N,4)-SA6RTSC(N,4);
DY12=SA6R17C(N,5)-SA6RTSC(N,5);
DZ12=SA6R17C(N,6)-SA6RTSC(N,6);

L12=sqrt(DX12*DX12+DY12*DY12+DZ12.^2);

H12=atan(DX12/DY12);

if DX12>0 && DY12>0
    H12=H12;
end
if DX12>0 && DY12<0
    H12=H12+pi;
end
if DX12<0 && DY12<0
    H12=H12+pi;
end
if DX12<0 && DY12>0
    H12=H12+2*pi;
end

V12=acos(DZ12/L12);

###simulate observation data
SOD(12,1)=i;
SOD(12,2)=j;
SOD(12,3)=17;
SOD(12,4)=H12*200/pi;
SOD(12,5)=V12*200/pi;
SOD(12,6)=L12;
SOD(12,7)=RPC(12,2);
SOD(12,8)=RPC(12,3);
SOD(12,9)=RPC(12,4);

##### Refernce point---No. 20

DX13=SA6R20C(N,4)-SA6RTSC(N,4);
DY13=SA6R20C(N,5)-SA6RTSC(N,5);
DZ13=SA6R20C(N,6)-SA6RTSC(N,6);

L13=sqrt(DX13*DX13+DY13*DY13+DZ13.^2);

H13=atan(DX13/DY13);

if DX13>0 && DY13>0
    H13=H13;
end
if DX13>0 && DY13<0
    H13=H13+pi;
end

```

```

if DX13<0 && DY13<0
    H13=H13+pi;
end
if DX13<0 && DY13>0
    H13=H13+2*pi;
end

V13=acos(DZ13/L13);

%%simulate observation data
SOD(13,1)=i;
SOD(13,2)=j;
SOD(13,3)=20;
SOD(13,4)=H13*200/pi;
SOD(13,5)=V13*200/pi;
SOD(13,6)=L13;
SOD(13,7)=RPC(13,2);
SOD(13,8)=RPC(13,3);
SOD(13,9)=RPC(13,4);

%%%%%%%%%%%%% Refernce point---No. 6
DX6=425862.508940-SA6RTSC(N,4);
DY6=4582252.560500-SA6RTSC(N,5);
DZ6=91.055200-SA6RTSC(N,6);

L6=sqrt(DX6.^2+DY6.^2+DZ6.^2);

H1=atan(DX6/DY6);

if DX6>0 && DY6>0
    H6=H6;
end
if DX6>0 && DY6<0
    H6=H6+pi;
end
if DX6<0 && DY6<0
    H6=H6+pi;
end
if DX6<0 && DY6>0
    H6=H6+2*pi;
end

V6=acos(DZ6/L6);

%%simulate observation data
SOD(14,1)=i;
SOD(14,2)=j;
SOD(14,3)=6;
SOD(14,4)=H6*200/pi;
SOD(14,5)=V6*200/pi;
SOD(14,6)=L6;
SOD(14,7)=RPC(14,2);
SOD(14,8)=RPC(14,3);
SOD(14,9)=RPC(14,4);

%%%%%%%%%%%%% Refernce point---No. 3
DX3=425965.947610-SA6RTSC(N,4);
DY3=4582289.268300-SA6RTSC(N,5);
DZ3=89.997940-SA6RTSC(N,6);

```

```

L3=sqrt(DX3.^2+DY3.^2+DZ3.^2);

H3=atan(DX3/DY3);

    if DX3>0 && DY3>0
        H3=H3;
    end
    if DX3>0 && DY3<0
        H3=H3+pi;
    end
    if DX3<0 && DY3<0
        H3=H3+pi;
    end
    if DX3<0 && DY3>0
        H3=H3+2*pi;
    end

V3=acos(DZ3/L3);

%%%simulate observation data
SOD(15,1)=i;
SOD(15,2)=j;
SOD(15,3)=3;
SOD(15,4)=H3*200/pi;
SOD(15,5)=V3*200/pi;
SOD(15,6)=L3;
SOD(15,7)=425965.947610;
SOD(15,8)=4582289.268300;
SOD(15,9)=89.997940;

%%%output the data
s1=strcat('c:\Model-
Data\SimulateReferencePointsObservationData-C-with ground reference
points\RTS-',int2str(mon),'-',int2str(i),'-',int2str(j),'.txt');
fidl=fopen(s1,'w');
for ii=1:15    %13
    for jj=1:9
        fprintf(fidl,'%6f\t',SOD(ii,jj));
        if rem(jj,9)==0
            fprintf(fidl,'\r\n');
        end
    end
end
end
fclose(fidl);

end
end

Tappc=toc    %%%record the running time

```

XI.7 Simulate control points' observation data

XI.7.1 With the influence of thermal movement of K2M

```
tic

clear all

%%input the month and days
mon=9;
n=30;

%%load the coordinates
RTSA6C=load('c:\Model-Data\A6-RTS-Coordinates.txt'); %RTS-A6-
Coordinates

K2MCPC=load('c:\Model-Data\K2M-A6-CPC.txt'); %K2M-A6-Control Points
Coordinates

%%load the simulate movement of the control points and the RTS which
are
%%relates to A6

%%%%%%%%-----A6--RTS
sa6=strcat('c:\Inputdata\A6-SRP\NodeMovement-',int2str(mon),'-Node-
196-A6.txt');
SA6RTSM=load(sa6);

%%%%%%%%-----K2M
sp1=strcat('c:\Inputdata\A6-SRP\NodeMovement-',int2str(mon),'-Node-
100-A6P01.txt');
SA6P1M=load(sp1);

sp2=strcat('c:\Inputdata\A6-SRP\NodeMovement-',int2str(mon),'-Node-92-
A6P02.txt');
SA6P2M=load(sp2);

sp3=strcat('c:\Inputdata\A6-SRP\NodeMovement-',int2str(mon),'-Node-88-
A6P03.txt');
SA6P3M=load(sp3);

sp4=strcat('c:\Inputdata\A6-SRP\NodeMovement-',int2str(mon),'-Node-
140-A6P04.txt');
SA6P4M=load(sp4);

sp5=strcat('c:\Inputdata\A6-SRP\NodeMovement-',int2str(mon),'-Node-
132-A6P05.txt');
SA6P5M=load(sp5);

sp6=strcat('c:\Inputdata\A6-SRP\NodeMovement-',int2str(mon),'-Node-
128-A6P06.txt');
SA6P6M=load(sp6);

sp7=strcat('c:\Inputdata\A6-SRP\NodeMovement-',int2str(mon),'-Node-
160-A6P07.txt');
SA6P7M=load(sp7);

sp8=strcat('c:\Inputdata\A6-SRP\NodeMovement-',int2str(mon),'-Node-
152-A6P08.txt');
SA6P8M=load(sp8);
```

```

sp9=strcat('c:\Inputdata\A6-SRP\NodeMovement-',int2str(mon),'-Node-
148-A6P09.txt');
SA6P9M=load(sp9);

%%simulate observation data
SOD=[];

lengthRTS=size(SA6RTSM,1);

SA6RTSC=SA6RTSM;

SA6P1C=SA6P1M;
SA6P2C=SA6P2M;
SA6P3C=SA6P3M;
SA6P4C=SA6P4M;
SA6P5C=SA6P5M;
SA6P6C=SA6P6M;
SA6P7C=SA6P7M;
SA6P8C=SA6P8M;
SA6P9C=SA6P9M;

for i=1:lengthRTS

    SA6RTSC(i,4)=SA6RTSC(i,4)+RTSA6C(1,1);
    SA6RTSC(i,5)=SA6RTSC(i,5)+RTSA6C(1,2);
    SA6RTSC(i,6)=SA6RTSC(i,6)+RTSA6C(1,3);

    SA6P1C(i,4)=SA6P1C(i,4)+K2MCPC(1,2);
    SA6P1C(i,5)=SA6P1C(i,5)+K2MCPC(1,3);
    SA6P1C(i,6)=SA6P1C(i,6)+K2MCPC(1,4);

    SA6P2C(i,4)=SA6P2C(i,4)+K2MCPC(2,2);
    SA6P2C(i,5)=SA6P2C(i,5)+K2MCPC(2,3);
    SA6P2C(i,6)=SA6P2C(i,6)+K2MCPC(2,4);

    SA6P3C(i,4)=SA6P3C(i,4)+K2MCPC(3,2);
    SA6P3C(i,5)=SA6P3C(i,5)+K2MCPC(3,3);
    SA6P3C(i,6)=SA6P3C(i,6)+K2MCPC(3,4);

    SA6P4C(i,4)=SA6P4C(i,4)+K2MCPC(4,2);
    SA6P4C(i,5)=SA6P4C(i,5)+K2MCPC(4,3);
    SA6P4C(i,6)=SA6P4C(i,6)+K2MCPC(4,4);

    SA6P5C(i,4)=SA6P5C(i,4)+K2MCPC(5,2);
    SA6P5C(i,5)=SA6P5C(i,5)+K2MCPC(5,3);
    SA6P5C(i,6)=SA6P5C(i,6)+K2MCPC(5,4);

    SA6P6C(i,4)=SA6P6C(i,4)+K2MCPC(6,2);
    SA6P6C(i,5)=SA6P6C(i,5)+K2MCPC(6,3);
    SA6P6C(i,6)=SA6P6C(i,6)+K2MCPC(6,4);

    SA6P7C(i,4)=SA6P7C(i,4)+K2MCPC(7,2);
    SA6P7C(i,5)=SA6P7C(i,5)+K2MCPC(7,3);
    SA6P7C(i,6)=SA6P7C(i,6)+K2MCPC(7,4);

    SA6P8C(i,4)=SA6P8C(i,4)+K2MCPC(8,2);
    SA6P8C(i,5)=SA6P8C(i,5)+K2MCPC(8,3);
    SA6P8C(i,6)=SA6P8C(i,6)+K2MCPC(8,4);

```

```

SA6P9C(i,4)=SA6P9C(i,4)+K2MCPC(9,2);
SA6P9C(i,5)=SA6P9C(i,5)+K2MCPC(9,3);
SA6P9C(i,6)=SA6P9C(i,6)+K2MCPC(9,4);

end

N=0;

for i=1:n
    for j=1:8

        N=N+1;

        %%%%%%%%%%%%%%%%%%%%%%%%%%%%%%%%%%%%%%%%%%%%%%%%%%%%%%%%%%%%%%%%%%%%%%%%% control point---No. 1
        DX1=SA6P1C(N,4)-SA6RTSC(N,4);
        DY1=SA6P1C(N,5)-SA6RTSC(N,5);
        DZ1=SA6P1C(N,6)-SA6RTSC(N,6);

        L1=sqrt(DX1.^2+DY1.^2+DZ1.^2);

        H1=atan(DX1/DY1);

        if DX1>0 && DY1>0
            H1=H1;
        end
        if DX1>0 && DY1<0
            H1=H1+pi;
        end
        if DX1<0 && DY1<0
            H1=H1+pi;
        end
        if DX1<0 && DY1>0
            H1=H1+2*pi;
        end

        V1=acos(DZ1/L1);

        %%%simulate observation data
        SOD(1,1)=1;
        SOD(1,2)=H1*200/pi;
        SOD(1,3)=V1*200/pi;
        SOD(1,4)=L1;

        %%%%%%%%%%%%%%%%%%%%%%%%%%%%%%%%%%%%%%%%%%%%%%%%%%%%%%%%%%%%%%%%%%%%%%%%% control point---No. 2
        DX2=SA6P2C(N,4)-SA6RTSC(N,4);
        DY2=SA6P2C(N,5)-SA6RTSC(N,5);
        DZ2=SA6P2C(N,6)-SA6RTSC(N,6);

        L2=sqrt(DX2*DX2+DY2*DY2+DZ2.^2);

        H2=atan(DX2/DY2);

        if DX2>0 && DY2>0
            H2=H2;
        end
        if DX2>0 && DY2<0
            H2=H2+pi;
        end
    end
end

```

```

end
if DX2<0 && DY2<0
    H2=H2+pi;
end
if DX2<0 && DY2>0
    H2=H2+2*pi;
end

V2=acos(DZ2/L2);

%%%simulate observation data
SOD(2,1)=2;
SOD(2,2)=H2*200/pi;
SOD(2,3)=V2*200/pi;
SOD(2,4)=L2;

%%%%%%%%%%%%% control point---No. 3
DX3=SA6P3C(N,4)-SA6RTSC(N,4);
DY3=SA6P3C(N,5)-SA6RTSC(N,5);
DZ3=SA6P3C(N,6)-SA6RTSC(N,6);

L3=sqrt(DX3*DX3+DY3*DY3+DZ3.^2);

H3=atan(DX3/DY3);

if DX3>0 && DY3>0
    H3=H3;
end
if DX3>0 && DY3<0
    H3=H3+pi;
end
if DX3<0 && DY3<0
    H3=H3+pi;
end
if DX3<0 && DY3>0
    H3=H3+2*pi;
end

V3=acos(DZ3/L3);

%%%simulate observation data
SOD(3,1)=3;
SOD(3,2)=H3*200/pi;
SOD(3,3)=V3*200/pi;
SOD(3,4)=L3;

%%%%%%%%%%%%% control point---No. 4
DX4=SA6P4C(N,4)-SA6RTSC(N,4);
DY4=SA6P4C(N,5)-SA6RTSC(N,5);
DZ4=SA6P4C(N,6)-SA6RTSC(N,6);

L4=sqrt(DX4*DX4+DY4*DY4+DZ4.^2);

H4=atan(DX4/DY4);

if DX4>0 && DY4>0
    H4=H4;
end
if DX4>0 && DY4<0

```

```

        H4=H4+pi;
    end
    if DX4<0 && DY4<0
        H4=H4+pi;
    end
    if DX4<0 && DY4>0
        H4=H4+2*pi;
    end

    V4=acos(DZ4/L4);

    %%simulate observation data
    SOD(4,1)=4;
    SOD(4,2)=H4*200/pi;
    SOD(4,3)=V4*200/pi;
    SOD(4,4)=L4;

    %%%%%%%%% control point---No. 5
    DX5=SA6P5C(N,4)-SA6RTSC(N,4);
    DY5=SA6P5C(N,5)-SA6RTSC(N,5);
    DZ5=SA6P5C(N,6)-SA6RTSC(N,6);

    L5=sqrt(DX5*DX5+DY5*DY5+DZ5.^2);

    H5=atan(DX5/DY5);

    if DX5>0 && DY5>0
        H5=H5;
    end
    if DX5>0 && DY5<0
        H5=H5+pi;
    end
    if DX5<0 && DY5<0
        H5=H5+pi;
    end
    if DX5<0 && DY5>0
        H5=H5+2*pi;
    end

    V5=acos(DZ5/L5);

    %%simulate observation data
    SOD(5,1)=5;
    SOD(5,2)=H5*200/pi;
    SOD(5,3)=V5*200/pi;
    SOD(5,4)=L5;

    %%%%%%%%% control point---No. 6
    DX6=SA6P6C(N,4)-SA6RTSC(N,4);
    DY6=SA6P6C(N,5)-SA6RTSC(N,5);
    DZ6=SA6P6C(N,6)-SA6RTSC(N,6);

    L6=sqrt(DX6*DX6+DY6*DY6+DZ6.^2);

    H6=atan(DX6/DY6);

    if DX6>0 && DY6>0
        H6=H6;
    end
end

```

```

if DX6>0 && DY6<0
    H6=H6+pi;
end
if DX6<0 && DY6<0
    H6=H6+pi;
end
if DX6<0 && DY6>0
    H6=H6+2*pi;
end

V6=acos(DZ6/L6);

%%simulate observation data
SOD(6,1)=6;
SOD(6,2)=H6*200/pi;
SOD(6,3)=V6*200/pi;
SOD(6,4)=L6;

%%%%%%%%%%%% control point---No. 7
DX7=SA6P7C(N,4)-SA6RTSC(N,4);
DY7=SA6P7C(N,5)-SA6RTSC(N,5);
DZ7=SA6P7C(N,6)-SA6RTSC(N,6);

L7=sqrt(DX7*DX7+DY7*DY7+DZ7.^2);

H7=atan(DX7/DY7);

if DX7>0 && DY7>0
    H7=H7;
end
if DX7>0 && DY7<0
    H7=H7+pi;
end
if DX7<0 && DY7<0
    H7=H7+pi;
end
if DX7<0 && DY7>0
    H7=H7+2*pi;
end

V7=acos(DZ7/L7);

%%simulate observation data
SOD(7,1)=7;
SOD(7,2)=H7*200/pi;
SOD(7,3)=V7*200/pi;
SOD(7,4)=L7;

%%%%%%%%%%%% control point---No. 8
DX8=SA6P8C(N,4)-SA6RTSC(N,4);
DY8=SA6P8C(N,5)-SA6RTSC(N,5);
DZ8=SA6P8C(N,6)-SA6RTSC(N,6);

L8=sqrt(DX8*DX8+DY8*DY8+DZ8.^2);

H8=atan(DX8/DY8);

if DX8>0 && DY8>0
    H8=H8;

```

```

end
if DX8>0 && DY8<0
    H8=H8+pi;
end
if DX8<0 && DY8<0
    H8=H8+pi;
end
if DX8<0 && DY8>0
    H8=H8+2*pi;
end

V8=acos(DZ8/L8);

%%%simulate observation data
SOD(8,1)=8;
SOD(8,2)=H8*200/pi;
SOD(8,3)=V8*200/pi;
SOD(8,4)=L8;

%%%%%%%%%%%%% control point---No. 9
DX9=SA6P9C(N,4)-SA6RTSC(N,4);
DY9=SA6P9C(N,5)-SA6RTSC(N,5);
DZ9=SA6P9C(N,6)-SA6RTSC(N,6);

L9=sqrt(DX9*DX9+DY9*DY9+DZ9.^2);

H9=atan(DX9/DY9);

if DX9>0 && DY9>0
    H9=H9;
end
if DX9>0 && DY9<0
    H9=H9+pi;
end
if DX9<0 && DY9<0
    H9=H9+pi;
end
if DX9<0 && DY9>0
    H9=H9+2*pi;
end

V9=acos(DZ9/L9);

%%%simulate observation data
SOD(9,1)=9;
SOD(9,2)=H9*200/pi;
SOD(9,3)=V9*200/pi;
SOD(9,4)=L9;

%%output the data
s1=strcat('c:\Model-
Data\SimulateControlPointsObservationData-withK2M\CPO-
',int2str(mon),'-',int2str(i),'-',int2str(j),'.txt');
fidl=fopen(s1,'w');
for ii=1:9
    for jj=1:4
        fprintf(fidl,'%0.6f\t',SOD(ii,jj));
        if rem(jj,4)==0
            fprintf(fidl,'\r\n');
        end
    end
end

```

```

        end
    end
end
fclose(fid1);

end
end

Tscp=toc    %%%record the running time

```

XI.7.2 Without the influence of thermal movement of K2M

```

tic

clear all

%%input the month and days
mon=10;
n=15;

%%load the coordinates
RTSA6C=load('c:\Model-Data\A6-RTS-Coordinates.txt'); %RTS-A6-
Coordinates

K2MCPC=load('c:\Model-Data\K2M-A6-CPC.txt'); %K2M-A6-Control Points
Coordinates

%%load the simulate movement of the control points and the RTS which
are
%%relates to A6

%%%%%%%%%-----A6--RTS
sa6=strcat('c:\Inputdata\A6-SRP\NodeMovement-',int2str(mon),'-Node-
196-A6.txt');
SA6RTSM=load(sa6);

%%simulate observation data
SOD=[];

lengthRTS=size(SA6RTSM,1);

SA6RTSC=SA6RTSM;

for i=1:lengthRTS

    SA6RTSC(i,4)=SA6RTSC(i,4)+RTSA6C(1,1);
    SA6RTSC(i,5)=SA6RTSC(i,5)+RTSA6C(1,2);
    SA6RTSC(i,6)=SA6RTSC(i,6)+RTSA6C(1,3);

    SA6P1C(i,4)=K2MCPC(1,2);
    SA6P1C(i,5)=K2MCPC(1,3);
    SA6P1C(i,6)=K2MCPC(1,4);

    SA6P2C(i,4)=K2MCPC(2,2);

```

```
SA6P2C(i,5)=K2MCPC(2,3);
SA6P2C(i,6)=K2MCPC(2,4);
```

```
SA6P3C(i,4)=K2MCPC(3,2);
SA6P3C(i,5)=K2MCPC(3,3);
SA6P3C(i,6)=K2MCPC(3,4);
```

```
SA6P4C(i,4)=K2MCPC(4,2);
SA6P4C(i,5)=K2MCPC(4,3);
SA6P4C(i,6)=K2MCPC(4,4);
```

```
SA6P5C(i,4)=K2MCPC(5,2);
SA6P5C(i,5)=K2MCPC(5,3);
SA6P5C(i,6)=K2MCPC(5,4);
```

```
SA6P6C(i,4)=K2MCPC(6,2);
SA6P6C(i,5)=K2MCPC(6,3);
SA6P6C(i,6)=K2MCPC(6,4);
```

```
SA6P7C(i,4)=K2MCPC(7,2);
SA6P7C(i,5)=K2MCPC(7,3);
SA6P7C(i,6)=K2MCPC(7,4);
```

```
SA6P8C(i,4)=K2MCPC(8,2);
SA6P8C(i,5)=K2MCPC(8,3);
SA6P8C(i,6)=K2MCPC(8,4);
```

```
SA6P9C(i,4)=K2MCPC(9,2);
SA6P9C(i,5)=K2MCPC(9,3);
SA6P9C(i,6)=K2MCPC(9,4);
```

```
end
```

```
N=0;
```

```
for i=1:n
    for j=1:8
```

```
        N=N+1;
```

```
        %%%%%%%%%%% control point---No. 1
```

```
        DX1=SA6P1C(N,4)-SA6RTSC(N,4);
```

```
        DY1=SA6P1C(N,5)-SA6RTSC(N,5);
```

```
        DZ1=SA6P1C(N,6)-SA6RTSC(N,6);
```

```
        L1=sqrt(DX1.^2+DY1.^2+DZ1.^2);
```

```
        H1=atan(DX1/DY1);
```

```
        if DX1>0 && DY1>0
            H1=H1;
```

```
        end
```

```
        if DX1>0 && DY1<0
            H1=H1+pi;
```

```
        end
```

```
        if DX1<0 && DY1<0
            H1=H1+pi;
```

```
        end
```

```

if DX1<0 && DY1>0
    H1=H1+2*pi;
end

V1=acos(DZ1/L1);

%%%simulate observation data
SOD(1,1)=1;
SOD(1,2)=H1*200/pi;
SOD(1,3)=V1*200/pi;
SOD(1,4)=L1;

%%%%%%%%%%%%%%%%%%%%%%%%%%%%%%%%%%%%%%%%%%%%%%%%%%%%%%%%%%%%%%%%%%%%%%%% control point---No. 2
DX2=SA6P2C(N,4)-SA6RTSC(N,4);
DY2=SA6P2C(N,5)-SA6RTSC(N,5);
DZ2=SA6P2C(N,6)-SA6RTSC(N,6);

L2=sqrt(DX2*DX2+DY2*DY2+DZ2.^2);

H2=atan(DX2/DY2);

if DX2>0 && DY2>0
    H2=H2;
end
if DX2>0 && DY2<0
    H2=H2+pi;
end
if DX2<0 && DY2<0
    H2=H2+pi;
end
if DX2<0 && DY2>0
    H2=H2+2*pi;
end

V2=acos(DZ2/L2);

%%%simulate observation data
SOD(2,1)=2;
SOD(2,2)=H2*200/pi;
SOD(2,3)=V2*200/pi;
SOD(2,4)=L2;

%%%%%%%%%%%%%%%%%%%%%%%%%%%%%%%%%%%%%%%%%%%%%%%%%%%%%%%%%%%%%%%%%%%%%%%% control point---No. 3
DX3=SA6P3C(N,4)-SA6RTSC(N,4);
DY3=SA6P3C(N,5)-SA6RTSC(N,5);
DZ3=SA6P3C(N,6)-SA6RTSC(N,6);

L3=sqrt(DX3*DX3+DY3*DY3+DZ3.^2);

H3=atan(DX3/DY3);

if DX3>0 && DY3>0
    H3=H3;
end
if DX3>0 && DY3<0
    H3=H3+pi;
end
if DX3<0 && DY3<0
    H3=H3+pi;
end

```

```

end
if DX3<0 && DY3>0
    H3=H3+2*pi;
end

V3=acos(DZ3/L3);

%%%simulate observation data
SOD(3,1)=3;
SOD(3,2)=H3*200/pi;
SOD(3,3)=V3*200/pi;
SOD(3,4)=L3;

%%%%%%%%%%%%% control point---No. 4
DX4=SA6P4C(N,4)-SA6RTSC(N,4);
DY4=SA6P4C(N,5)-SA6RTSC(N,5);
DZ4=SA6P4C(N,6)-SA6RTSC(N,6);

L4=sqrt(DX4*DX4+DY4*DY4+DZ4.^2);

H4=atan(DX4/DY4);

if DX4>0 && DY4>0
    H4=H4;
end
if DX4>0 && DY4<0
    H4=H4+pi;
end
if DX4<0 && DY4<0
    H4=H4+pi;
end
if DX4<0 && DY4>0
    H4=H4+2*pi;
end

V4=acos(DZ4/L4);

%%%simulate observation data
SOD(4,1)=4;
SOD(4,2)=H4*200/pi;
SOD(4,3)=V4*200/pi;
SOD(4,4)=L4;

%%%%%%%%%%%%% control point---No. 5
DX5=SA6P5C(N,4)-SA6RTSC(N,4);
DY5=SA6P5C(N,5)-SA6RTSC(N,5);
DZ5=SA6P5C(N,6)-SA6RTSC(N,6);

L5=sqrt(DX5*DX5+DY5*DY5+DZ5.^2);

H5=atan(DX5/DY5);

if DX5>0 && DY5>0
    H5=H5;
end
if DX5>0 && DY5<0
    H5=H5+pi;
end
if DX5<0 && DY5<0

```

```

        H5=H5+pi;
    end
    if DX5<0 && DY5>0
        H5=H5+2*pi;
    end

    V5=acos(DZ5/L5);

    %%simulate observation data
    SOD(5,1)=5;
    SOD(5,2)=H5*200/pi;
    SOD(5,3)=V5*200/pi;
    SOD(5,4)=L5;

    %%%%%%%%%%% control point---No. 6
    DX6=SA6P6C(N,4)-SA6RTSC(N,4);
    DY6=SA6P6C(N,5)-SA6RTSC(N,5);
    DZ6=SA6P6C(N,6)-SA6RTSC(N,6);

    L6=sqrt(DX6*DX6+DY6*DY6+DZ6.^2);

    H6=atan(DX6/DY6);

    if DX6>0 && DY6>0
        H6=H6;
    end
    if DX6>0 && DY6<0
        H6=H6+pi;
    end
    if DX6<0 && DY6<0
        H6=H6+pi;
    end
    if DX6<0 && DY6>0
        H6=H6+2*pi;
    end

    V6=acos(DZ6/L6);

    %%simulate observation data
    SOD(6,1)=6;
    SOD(6,2)=H6*200/pi;
    SOD(6,3)=V6*200/pi;
    SOD(6,4)=L6;

    %%%%%%%%%%% control point---No. 7
    DX7=SA6P7C(N,4)-SA6RTSC(N,4);
    DY7=SA6P7C(N,5)-SA6RTSC(N,5);
    DZ7=SA6P7C(N,6)-SA6RTSC(N,6);

    L7=sqrt(DX7*DX7+DY7*DY7+DZ7.^2);

    H7=atan(DX7/DY7);

    if DX7>0 && DY7>0
        H7=H7;
    end
    if DX7>0 && DY7<0
        H7=H7+pi;
    end
end

```

```

if DX7<0 && DY7<0
    H7=H7+pi;
end
if DX7<0 && DY7>0
    H7=H7+2*pi;
end

V7=acos(DZ7/L7);

%%%simulate observation data
SOD(7,1)=7;
SOD(7,2)=H7*200/pi;
SOD(7,3)=V7*200/pi;
SOD(7,4)=L7;

%%%%%%%%%%%% control point---No. 8
DX8=SA6P8C(N,4)-SA6RTSC(N,4);
DY8=SA6P8C(N,5)-SA6RTSC(N,5);
DZ8=SA6P8C(N,6)-SA6RTSC(N,6);

L8=sqrt(DX8*DX8+DY8*DY8+DZ8.^2);

H8=atan(DX8/DY8);

if DX8>0 && DY8>0
    H8=H8;
end
if DX8>0 && DY8<0
    H8=H8+pi;
end
if DX8<0 && DY8<0
    H8=H8+pi;
end
if DX8<0 && DY8>0
    H8=H8+2*pi;
end

V8=acos(DZ8/L8);

%%%simulate observation data
SOD(8,1)=8;
SOD(8,2)=H8*200/pi;
SOD(8,3)=V8*200/pi;
SOD(8,4)=L8;

%%%%%%%%%%%% control point---No. 9
DX9=SA6P9C(N,4)-SA6RTSC(N,4);
DY9=SA6P9C(N,5)-SA6RTSC(N,5);
DZ9=SA6P9C(N,6)-SA6RTSC(N,6);

L9=sqrt(DX9*DX9+DY9*DY9+DZ9.^2);

H9=atan(DX9/DY9);

if DX9>0 && DY9>0
    H9=H9;
end
if DX9>0 && DY9<0
    H9=H9+pi;
end

```

```
end
if DX9<0 && DY9<0
    H9=H9+pi;
end
if DX9<0 && DY9>0
    H9=H9+2*pi;
end

V9=acos(DZ9/L9);

%%simulate observation data
SOD(9,1)=9;
SOD(9,2)=H9*200/pi;
SOD(9,3)=V9*200/pi;
SOD(9,4)=L9;

%%output the data
s1=strcat('c:\Model-
Data\SimulateControlPointsObservationData-WithoutK2M\CPO-
',int2str(mon),'-',int2str(i),'-',int2str(j),'.txt');
fid1=fopen(s1,'w');
for ii=1:9
    for jj=1:4
        fprintf(fid1,'% .6f\t',SOD(ii,jj));
        if rem(jj,4)==0
            fprintf(fid1,'\r\n');
        end
    end
end
fclose(fid1);

end
end

Tscp=toc    %%%record the running time
```